

# **WEATHER ROUTING OF (SAIL-ASSISTED) MOTOR VESSELS**

**HIDEKI HAGIWARA**

442778  
217 9236  
TR diss 1764

## **WEATHER ROUTING OF (SAIL-ASSISTED) MOTOR VESSELS**



# WEATHER ROUTING OF (SAIL-ASSISTED) MOTOR VESSELS

Proefschrift ter verkrijging van de graad van doctor aan de Technische Universiteit Delft, op gezag van de Rector Magnificus, prof.drs. P.A. Schenck, in het openbaar te verdedigen ten overstaan van een commissie aangewezen door het College van Dekanen op dinsdag 7 november 1989 te 16.00 uur

door

**HIDEKI HAGIWARA**

geboren te Tokyo

Master of Mercantile Marine Science



Dit Proefschrift is goedgekeurd door de promotor:

**Prof. ir. J. A. Spaans**

# WEERROUTEREN VAN MOTORSCHEPEN ( MET HULPZEILVERMOGEN )

## SAMENVATTING

Sinds de jaren vijftig heeft een groot aantal schepen met succes gebruik gemaakt van weerroutering voor oceaanoversteken. De recentelijke introductie van motorschepen met hulpzeilvermogen, die de wind gebruiken als onderdeel van hun voortstuwing, heeft het belang van weerrouteren nog vergroot. Weerroutering is echter een nog onderontwikkelde technologie. Het doel van deze studie is, een geavanceerde methode voor weerroutering vast te stellen, die voldoende en nauwkeurige informatie kan verschaffen aan de gezagvoerder/reder voor de selectie van een (sub)optimale route voor een oceaanoversteek.

Allereerst wordt de probleemstelling van het weerrouteren geformuleerd en wordt er een algoritme voor de minimum-tijd route voorgesteld, die de "modified isochrone method" wordt genoemd. Vanuit een praktisch oogpunt wordt deze methode toegepast op het probleem van minimum-brandstof/kosten routeren en stochastisch routeren. Voor stochastisch routeren wordt een methode ontwikkeld om de standaard afwijkingen van passagetijsd en brandstof-verbruik te schatten.

Vervolgens wordt een geavanceerde methode beschreven om de scheepssnelheid, drifthoek, roerhoek, helling en motorvermogen te voorspellen gebaseerd op de evenwichtsvergelijkingen voor krachten en momenten die werken op een schip in zeegang. Als mathematisch modelschip wordt een 40,000 DWT produkttanker gebruikt met een hulpzeiloppervlak van 808 m<sup>2</sup>; de scheepsprestaties van dit schip worden voor een aantal wind- en zeecondities getoond. Aanvullend wordt de kans op het overnemen van groen water bij de boeg berekend als één van de maatstaven voor mogelijke schade in hoge golven.

Voor het uitvoeren van simulaties wordt een databestand gebruikt

van geanalyseerde en voorspelde wind-, golf- en stroomgegevens van het FNOC ( Fleet Numerical Oceanography Center ) van de U.S. Navy en een bestand van gegevens van oceaanstromen van het U.K. Meteorological Office. Voor stochastisch routeren worden de covariantie- en correlatiematrices van de voorspelde wind- en golfgegevens bepaald uit het FNOC-bestand, terwijl de covariantiematrices van de oceaanstromen verkregen worden uit het bestand van het U.K. Metoffice. De modellen voor wind en golven die gebruikt worden na de periode van numerieke voorspellingen worden eveneens beschreven.

Na een analyse van de nauwkeurigheid van de "modified isochrone method" worden uitvoerige simulaties met de methode uitgevoerd waarbij gebruik wordt gemaakt van de voorspellingsmethode van de scheepssnelheid en scheepsbewegingen van het bovengenoemde modelschip. Bij deterministisch routeren worden de voordelen van weerrouteren en het gebruik van hulpzeilen onderzocht door middel van minimum-tijd/brandstof/kosten routeringen. Bij stochastisch routeren wordt gerouteerd volgens minimum tijd en minimum brandstof; hierbij wordt een verzameling routes berekend met elk aanvullend de standaard afwijking van passagetijd en brandstofverbruik. Uit deze verzameling routes met de bijbehorende kenmerken kan de gezagvoerder of reder zijn toegesneden keuze maken.

Uit de resultaten van de simulaties kan worden geconcludeerd dat de voorgestelde methode van weerroutering voldoende nauwkeurig en praktisch is om de reder/gezagvoerder nuttige informatie te verschaffen.



## SUMMARY

Since the 1950's, a large number of vessels have been successfully operated in ocean-crossing voyages with the help of ship weather routing. In recent years, the advent of sail-assisted motor vessels which utilize the wind as a part of their propulsive power has enhanced the importance of weather routing. Weather routing is, however, an under developed technology. The aim of this study is to establish an advanced method of weather routing which can offer accurate and sufficient information to the shipmaster/owner in selecting a (sub) optimum ocean-crossing route.

First, the ship routing problem is formulated, and an algorithm to calculate the minimum time route is proposed, which is called the modified isochrone method. From a practical point of view, the modified isochrone method is applied to minimum fuel/cost routing and to stochastic routing as well. In order to perform stochastic routing, a method of estimating the standard deviations of passage time and fuel consumption is developed.

Next, a sophisticated method to predict the ship's speed, drift angle, rudder angle, heel angle and engine power is described based on the equilibrium equations for the forces and moments acting on a ship in a seaway. Using a 40,000 DWT product tanker with 808 m<sup>2</sup> sail area as a mathematical model ship, the ship performance is demonstrated for some environmental conditions. In addition, the probability of shipping green water at the bow, which is one of the measures of possible damage in rough seas, is calculated for the model ship.

In simulations, the analyzed and forecasted wind/wave data and ocean current data published by FNOG ( Fleet Numerical Oceanography Center ) of the U.S. Navy as well as the ocean current data by the U.K. Meteorological Office are used. For stochastic routing, the covariance and correlation matrices of the forecasted wind and waves are determined using the data of the FNOG, whereas the covariance matrices of the ocean currents are obtained from the data of the Meteorological Office. The wind/wave models to be used after the

period covered by the numerical forecasts are also described.

After an analysis on the accuracy of the modified isochrone method, comprehensive weather routing simulations are executed, using the modified isochrone method and the prediction method of speed and seakeeping performance of the mathematical model ship mentioned above. In deterministic routing, the advantages of weather routing and sail-assisted operations are investigated by minimum time/fuel/cost routing. In stochastic routing, minimum time/fuel routing is performed, calculating a set of routes each with additionally the standard deviations of passage time and fuel consumption in order that the shipmaster/owner may make his own choice.

As a result of the simulations, it can be concluded that the proposed method of weather routing is accurate and practical enough to provide profitable information to the shipmaster/owner.

# CONTENTS

1. INTRODUCTION	1
2. THE MODIFIED ISOCHRONE METHOD FOR THE PROBLEM OF SHIP ROUTING	
2.1 Introduction	7
2.2 Formulation of the ship routing problem	8
2.2.1 Formulation as a continuous optimization problem	8
2.2.2 Formulation as a discrete optimization problem	12
2.2.3 Review of the methods for solving the ship routing problem	15
2.3 The modified isochrone method for deterministic routing	19
2.3.1 Minimum time routing	19
2.3.2 Minimum fuel routing	26
2.3.3 Minimum cost routing	30
2.4 The modified isochrone method for stochastic routing	34
2.4.1 Estimation of the standard deviations of passage time and fuel consumption	35
2.4.2 Stochastic minimum time routing	47
2.4.3 Stochastic minimum fuel routing	49
2.5 General form of the objective function for the modified isochrone method	52
3. PREDICTION OF SPEED AND SEAKEEPING PERFORMANCE OF A ( SAIL-ASSISTED ) MOTOR VESSEL IN A SEAWAY	
3.1 Introduction	55
3.2 Description of the mathematical model ship	58
3.3 Equilibrium equations for the forces and moments acting on the ship	60
3.4 Calculation methods of forces and moments	62
3.5 Prediction of speed, drift angle, rudder angle and heel angle	76
3.6 Prediction of engine power	80



3.7	Calculation of speed, drift angle, rudder angle, heel angle and engine power of the model ship	82
3.8	Prediction of ship's motions in a seaway	99
3.9	Ship operation criteria in rough seas	101
3.10	Prediction of shipping green water at the bow of the model ship	103
4.	ENVIRONMENTAL DATA USED IN THE WEATHER ROUTING SIMULATIONS	
4.1	Introduction	106
4.2	Analyzed wind, sea and swell data	108
4.3	Forecasted wind and wave data	114
4.3.1	Forecasted wind and wave charts	114
4.3.2	Mean errors and covariance matrices of forecasted wind/wave data	121
4.3.3	Correlations between errors in forecasted wind/wave data	129
4.4	5-day mean wind and wave distribution models classified by the zonal index (ZI)	138
4.4.1	5-day mean zonal index as a measure of circulation pattern of the upper-air westerlies	138
4.4.2	5-day mean wind and wave distribution models classified by ZI	143
4.4.3	Mean errors and covariance matrices of the 5-day mean wind/wave models classified by ZI	154
4.4.4	Correlations between errors in the 5-day mean wind/wave models classified by ZI	159
4.5	1-month mean wind and wave data	165
4.5.1	1-month mean wind and wave charts	165
4.5.2	Mean errors and covariance matrices of the 1-month mean wind/wave data	170
4.5.3	Correlations between errors in the 1-month mean wind/wave data	172
4.6	Monthly ocean current data published by FNOG	176
4.7	Monthly ocean current data published by the Meteorological Office	179
4.7.1	Monthly mean value charts of the ocean currents	179
4.7.2	Monthly covariance ( 39% error ellipse ) charts of the ocean currents	180



4.8	Interpolation scheme for the environmental data for weather routing	185
4.9	Other hazardous environments to be considered in weather routing	190
5. ANALYSIS ON THE ACCURACY OF THE MODIFIED ISOCHRONE METHOD		
5.1	Introduction	191
5.2	Sensitivity of the solution to the time-interval between successive isochrones	192
5.3	Sensitivity of the solution to the sub-time-interval for calculating ship's speed, drift angle, etc.	195
5.4	Sensitivity of the solution to the increment of ship's heading for constructing the isochrones	197
5.5	Sensitivity of the solution to the resolution of the isochrone	199
5.6	Sensitivity of the solution to the increment in numerical differentiation for calculating the partial derivatives	201
6. WEATHER ROUTING SIMULATIONS OF A SAIL-ASSISTED/EQUIVALENT MOTOR VESSEL		
6.1	Introduction	207
6.2	Simulations of deterministic routing	209
6.2.1	Minimum time routing	211
6.2.2	Minimum fuel routing	225
6.2.3	Minimum cost routing	237
6.3	Simulations of stochastic routing	241
6.3.1	Minimum time routing using forecasted wind/wave data followed by the 5-day mean wind/wave models classified by ZI	242
6.3.2	Minimum time routing using forecasted wind/wave data followed by the 1-month mean wind/wave data	271
6.3.3	Minimum fuel routing using forecasted wind/wave data followed by the 5-day mean wind/wave models classified by ZI	278
6.3.4	Minimum fuel routing using forecasted wind/wave	

data followed by the 1-month mean wind/wave data	298
7. REVIEW, CONCLUSIONS AND SUGGESTIONS	303
APPENDICES	
Appendix 1 Accuracy of arrival latitude	310
Appendix 2 Accuracy of rhumbline distance	312
Appendix 3 Comparison of geodetic distance with great circle distance	313
Appendix 4 Reason for existence of the alternative route with a possibility to provide less fuel consumption	315
Appendix 5 Calculation method of the great circle route	316
Appendix 6 Calculation method of 39% error ellipse of the ship's position	317
REFERENCES	320
NOMENCLATURE	326
ACKNOWLEDGEMENTS	337
CURRICULUM VITAE	338

## 1. INTRODUCTION

Ship weather routing is defined as a procedure to determine an optimum route based on the forecasted environments and the ship speed and seakeeping performance for a particular transit. In view of the determination of an optimum route, weather routing is also called optimum routing.

For commercial operations, the term optimum is used to mean:

- minimum passage time
- minimum fuel consumption within specified passage time
- minimum damage to ship and ( deck ) cargo
- maximum comfort to passengers
- a combination of the above criteria

Since the 1950's, many weather routing bureaus have been providing weather routing services for a great number of ocean-crossing vessels with successful results. Before the oil crisis in the mid 1970's, minimum time routes were almost exclusively recommended. After that, however, since the saving of fuel oil became a major concern of the shipping companies, minimum fuel routes became a matter of great interest for those companies.

At present, for most commercial operations, the minimum time route is initially recommended although the approximate arrival time is scheduled. During the voyage, a new minimum time route is recommended whenever adverse weather is forecasted on the last recommended route. In the last part of the voyage, the shipmaster adjusts the ship's speed in order to get the ship to arrive at the destination at the scheduled arrival time.

In order to perform an effective weather routing, the following requirements should be fulfilled:

- (i) accurate forecasts of environmental conditions ( wind, sea, swell and ocean currents ) for a sufficient forecast period
- (ii) good predictions of ship's speed, engine power and drift



angle ( leeway ) as well as ship's motions and accompanying phenomena for the particular vessel for various conditions of draught, trim and environment

(iii) practical computation of a (sub) optimum route for various demands of shipmaster/owner

Requirement (i) is not fully met in practice, although the accuracy of forecasts has been improved and the forecast period has been extended steadily. In general, the waves are a principal disturbance which affects the ship's speed in the ocean-crossing voyage.

At present, the period of wave forecasts is limited up to 2 or 3 days ahead on the operational basis. Since it takes more than 10 days for example to cross the North Pacific Ocean, such a forecast period apparently does not meet the requirement for an effective weather routing. The 1-month mean wave data or other wave models have been used in weather routing bureaus for the period beyond 2 or 3 days from the starting time of the routing procedure.

Concerning requirement (ii), a number of theories based on physical laws have been developed to predict the ship speed and seakeeping performance in a seaway. Those theories, however, usually need detailed information on the waves, hull and superstructure, propeller, etc.. Particularly, the information on the ( directional ) wave spectra is essential for calculating the ship's speed and motions.

Because of the complexities of those theories and the lack of information to be used for them, most of the weather routing bureaus have adopted a simplified method based on statistical analysis of data from the ship's log book to predict the ship's speed in a seaway. That simplified method provides us so-called speed performance curves in which the ship's speed is represented as a function of significant wave height and wave direction ( or Beaufort scale and wind direction ) as well as the engine power. Such a speed performance curve, of course, does not satisfy requirement (ii).

In particular, the advent of sail-assisted motor vessels which utilize the wind as part of their propulsive power has posed

difficulties to the use of conventional speed performance curves. For sail-assisted motor vessels, the wind speed/direction, wave height/direction/period and engine power ( or number of propeller revolutions ) are at least necessary to calculate the ship's speed.

For requirement (iii), a number of algorithms have been proposed for the computation of a (sub) optimum route. Although the algorithms based on the calculus of variations seem elegant in their mathematical approach, they have many difficulties in the application to the actual problem. The algorithms based on dynamic programming are powerful and flexible enough for practical applications. However, since they need a lot of calculation time and memory space for objective functions other than minimizing passage time, they have only been used for minimum time routing in some weather routing bureaus.

The algorithms based on the isochrone method which was originally proposed by R.W. James<sup>(1)</sup> have been used for a long time in many weather routing bureaus as a practical ( hand ) method to obtain the minimum time route. The isochrone method proposed by James, however, does not give the correct isochrones in a strict sense, and it is less suitable for computerization.

In the actual weather routing, because the environmental forecasts inevitably involve forecast errors, the predicted passage time, fuel consumption, etc. on the optimum route will also include errors. Up to now, no algorithm for the determination and evaluation of an optimum route which takes into account the stochastic nature of environmental forecasts has been developed.

Until now, the above-mentioned requirements have not been satisfied simultaneously and effective weather routing of ( sail-assisted ) motor vessels has not yet been established.

During the academic year 1985 - 1986, the author conducted a joint project on practical weather routing of sail-assisted motor vessels with Prof. ir. J.A. Spaans at the Hydronautics section of the Department of Maritime Technology, Delft University of Technology. The aim of that project was to establish practical methods to



predict the speed performance of a sail-assisted motor vessel in a seaway as well as to compute a (sub) optimum route for various demands of the shipmaster/owner.

Mainly based on the studies developed at the Hydronautics section, the author proposed a method to predict the ship's speed, drift angle and engine power based on the equilibrium equations for the longitudinal and lateral forces acting on the ship.<sup>(2)</sup> The practical method to calculate a minimum time/fuel route - which was called the modified isochrone method by the author - was also proposed.

Since the academic year 1985 - 1986, that joint project has been continued. The yawing moments and heeling moments have been incorporated into the equilibrium equations to calculate the rudder angle and heel angle.

In order to take into account the uncertainties of environmental forecasts in determining the optimum route, a method of estimating the standard deviations of passage time and fuel consumption as well as the covariance matrices of ship's positions was developed. By combining that estimation method with the modified isochrone method, the algorithm to compute the optimum route from a stochastic point of view has been developed.

The interim results of the project were presented to the International Congress of the Institutes of Navigation held at Sydney in February, 1988.<sup>(3)</sup>

In this thesis, the methods which meet the requirements (ii) and (iii) are proposed and their usefulness are verified by comprehensive simulations. Although the fulfilment of requirement (i) mainly depends on the progress of meteorology and oceanography, wind/wave models to be used after the numerical forecasts are described and used in the simulations.

This thesis is organized as follows.

In Chapter 2, the methods for solving the ship routing problem

are mentioned. First, the ship routing is formulated as a continuous/discrete optimization problem. After the review of the methods to solve the ship routing problem, the modified isochrone method is proposed to perform the deterministic minimum time/fuel/cost routing.

Then the method of estimating the standard deviations of passage time and fuel consumption is described, and the modified isochrone method is extended to cope with the stochastic minimum time/fuel routing. The general form of the objective function for the modified isochrone method is also proposed.

Chapter 3 describes the methods to predict the ship speed and seakeeping performance in a seaway. After the description of the mathematical model ship, the methods to predict the ship's speed, drift angle, rudder angle, heel angle and engine power are proposed based on the equilibrium equations for the forces and moments acting on the ship in a seaway.

Using that model ship, the ship speed performance is demonstrated for various environmental conditions. Then the method to predict the ship's motions and accompanying phenomena in waves and ship operation criteria in rough seas are simply mentioned. For some wave conditions, the probabilities of shipping green water at the bow of the model ship are calculated.

Chapter 4 states the environmental data used for the weather routing simulations. First, the analyzed wind, sea and swell data of the North Pacific Ocean published by FNOC ( Fleet Numerical Oceanography Center ) of the U.S. Navy are shown as the data used for deterministic routing. Next, for stochastic routing, three kinds of wind/wave data of the North Pacific Ocean are described, namely, the forecasted wind/wave data by FNOC, the 5-day mean wind/wave models classified by zonal index and the 1-month mean wind/wave data.

In each kind of wind/wave data for the stochastic routing, the methods to compute the mean errors, covariance matrices and correlation matrices are proposed, and some computed results are shown. Concerning the ocean currents, the monthly ocean current



data of the North Pacific Ocean published by FNOG and the U.K. Meteorological Office are described, which are used for deterministic routing and stochastic routing, respectively. Using the covariance data provided by the Meteorological Office, the covariance ( 39% error ellipse ) charts are produced. The interpolation scheme for the environmental data as well as other hazardous environments to be considered in weather routing are also shown.

In Chapter 5, the accuracy of the modified isochrone method is investigated. Changing the increments to discretize the problem ( e.g. increment of ship's heading, resolution of isochrone, etc. ), the sensitivities of solutions to the sizes of increments of the various parameters used in the modified isochrone method are analyzed.

In Chapter 6, comprehensive weather routing simulations are executed using the modified isochrone method, the prediction method of ship speed and seakeeping performance as well as the mathematical model ship and the environmental data mentioned in previous chapters. In deterministic routing, the advantages of weather routing and sail-assisted operation are investigated for the minimum time/fuel/cost routing.

By stochastic routing, the minimum time and fuel routing are carried out, computing a set of routes each with the standard deviations of passage time and fuel consumption, and the methods to determine and evaluate the optimum route from a stochastic point of view are fully demonstrated. In addition, the advantages of recalculating the optimum route during a voyage based on the information of updated forecasts are also demonstrated.

Finally, Chapter 7 gives the review, conclusions and suggestions.



## 2. THE MODIFIED ISOCHRONE METHOD FOR THE PROBLEM OF SHIP ROUTING

### 2.1 INTRODUCTION

In order to perform an effective weather routing procedure utilizing the huge amount of forecasted environmental data and the ship speed and seakeeping performance data, the computation of the optimum route by a computer is indispensable. For carrying out weather routing simulations, we have to formulate the ship routing problem, i.e. the transition of the position of the ship, the objects to be optimized, etc. should be expressed by numerical formulae.

After formulating the problem, it is necessary to establish the solution. The optimization methods such as calculus of variations, dynamic programming and isochrone method can be used to solve the problem. According to the algorithm of solution, computer programs are set up to execute the weather routing simulations.

In this chapter, the ship routing problem is formulated as a continuous/discrete optimization problem. Reviewing the several methods for the ship routing problem, the modified isochrone method is proposed as a practical method to solve the problem. The modified isochrone method is applied to both the deterministic and stochastic routing problem.

In deterministic routing, the algorithms of the modified isochrone method are proposed to perform minimum time/fuel/cost routing. In stochastic routing, using the method to estimate the standard deviations of passage time and fuel consumption, the modified isochrone method is applied to minimum time/fuel routing. The general form of an objective function is also proposed in order to treat the various objects by the modified isochrone method.

## 2.2 FORMULATION OF THE SHIP ROUTING PROBLEM

### 2.2.1 Formulation as a continuous optimization problem

Let us define the following vectors:

$$\text{Ship's position vector : } \underline{X} = [ \phi \quad \lambda ]^T$$

where  $\phi$  : latitude  
 $\lambda$  : longitude

$$\text{Ship's control vector : } \underline{U} = [ \theta \quad n ]^T$$

where  $\theta$  : ship's heading  
 $n$  : number of propeller revolutions

$$\text{Ship's motion vector : } \underline{M} = [ a \quad b \quad \text{----} ]^T$$

where  $a, b, \text{----}$  : standard deviations of ship's  
motions and probabilities of  
shipping green water, slamming, etc.

In the above notation, the underbar  $\underline{\phantom{x}}$  denotes a vector and the superscript  $^T$  denotes the transpose of a vector.

The engine power may also be used as one of the ship's control variables instead of the number of propeller revolutions. However, since the diesel engines are equipped with governors which keep the number of revolutions constant within the range of normal engine loading, it seems practical for ships with diesel engines to adopt the number of propeller revolutions as a control variable.

The vectors  $\underline{X}$ ,  $\underline{U}$  and  $\underline{M}$  are subject to the following constraints:

$$\underline{X} \in \underline{X}_A \tag{2.1}$$

$$\underline{U} \in \underline{U}_A \tag{2.2}$$

$$\underline{M} \in \underline{M}_A \tag{2.3}$$

where  $\underline{X}_A$  : admissible position vector  
 ( i.e. navigable area for a ship )  
 $\underline{U}_A$  : admissible control vector  
 ( i.e. admissible ranges of controls )  
 $\underline{M}_A$  : admissible motion vector  
 ( i.e. admissible ranges of ship's motions )

The constraint (2.1) denotes that a ship should be navigated avoiding dangers such as areas of shallow water, sea ice or icebergs, military practice, etc.. The constraint (2.2) means that a ship's heading directing a ship extremely diverging from the destination can not be adopted and the number of propeller revolutions should be controlled between normal lower and upper limit without imposing excessive loading on the engine.

The constraint (2.3) indicates that in rough seas, it is not admissible to damage the hull, cargo, engine, etc. due to excessive ship's motions and accompanying phenomena such as shipping green water, slamming, propeller racing, etc..

The differentiation of the ship's position with respect to the time  $d\underline{X}/dt$  is a function of the environmental conditions ( i.e. wind, sea, swell and ocean currents ) and the ship's control vector  $\underline{U}$ . Provided the environmental conditions during a voyage can be predicted by specifying the time and position,  $d\underline{X}/dt$  can be expressed by a function of the ship's position  $\underline{X}$ , ship's control  $\underline{U}$  and time  $t$ :

$$d\underline{X}/dt = \underline{f}(\underline{X}, \underline{U}, t) \quad (2.4)$$

where  $\underline{f}$  is a two-dimensional vector function. The components of the vectors on both sides of equation (2.4) are given as follows:<sup>(1)</sup>

$$d\underline{X}/dt = [ d\phi/dt \quad d\lambda/dt ]^T \quad (2.5)$$

$$\underline{f}(\underline{X}, \underline{U}, t) = \begin{bmatrix} \{ V \cos(\theta + \alpha) + N \} / R_M(\phi) \\ \{ V \sin(\theta + \alpha) + E \} / R_P(\phi) \end{bmatrix} \quad (2.6)$$

where  $V = V(\underline{X}, \underline{U}, t)$  : ship's speed through the water



$\alpha = \alpha(\underline{X}, \underline{U}, t)$  : drift angle ( leeway caused by wind )  
of a ship

$N = N(\underline{X}, t)$  : northerly component of ocean current

$E = E(\underline{X}, t)$  : easterly component of ocean current

$R_M(\phi)$  : local radius of meridian of the earth

$R_P(\phi)$  : local radius of parallel of latitude of the earth

Using the standard spheroid defined by WGS-72 to represent the shape of the earth,  $R_M(\phi)$  and  $R_P(\phi)$  are given by

$$R_M(\phi) = a (1 - e^2) (1 - e^2 \sin^2 \phi)^{-3/2} \quad (2.7)$$

$$R_P(\phi) = a \cos \phi (1 - e^2 \sin^2 \phi)^{-1/2} \quad (2.8)$$

where  $a$  : radius of equator of the earth ( = 6,378,135 m )

$e$  : eccentricity of meridian of the earth ( = 0.08181881 )

Given the wind/wave conditions and the ship's control  $\underline{U}$  at the ship's position  $\underline{X}$  at time  $t$ , the speed through the water  $V$  and the drift angle  $\alpha$  as well as the ship's motions  $\underline{M}$  can be calculated by the methods mentioned in Chapter 3.

Now, we suppose a ship leaving departure point  $\underline{X}_0$  at time  $t_0$  for the destination  $\underline{X}_f$ , and consider the following objective function  $J$ :

$$J = \int_{t_0}^{t_f} A(\underline{X}, \underline{U}, t) dt + B(t_f, t_s) \quad (2.9)$$

where  $A(\underline{X}, \underline{U}, t)$  : quantity per unit time evaluated during the voyage

$B(t_f, t_s)$  : quantity evaluated at the destination

$t_f$  : actual arrival time at the destination ( unknown )

$t_s$  : scheduled arrival time at the destination given by  
a shipmaster/owner

Regarding the ship's position  $\underline{X}$  and control  $\underline{U}$  as functions of time  $t$ , we call the control  $\underline{U}^*(t)$  which minimizes  $J$  the 'optimum control' and the route  $\underline{X}^*(t)$  determined by  $\underline{U}^*(t)$  the 'optimum route'.

The  $A(\underline{X}, \underline{U}, t)$  represents the object to be minimized such as

passage time, fuel consumption, ship's motions, etc.. Its typical forms are shown below:

$$A(\underline{X}, \underline{U}, t) = 1 \quad \text{for minimizing passage time}$$

$$A(\underline{X}, \underline{U}, t) = [\text{fuel consumption per unit time}] \quad \text{for minimizing fuel consumption}$$

$$A(\underline{X}, \underline{U}, t) = [\text{fuel cost per unit time plus manning, maintenance, insurance and all other fixed running costs per unit time}] \quad \text{for minimizing total cost}$$

In towing operations, the motions of a ship, barge, oil rig, etc. per unit time may be used as  $A(\underline{X}, \underline{U}, t)$ . In addition, it is possible to use the sum of several weighted quantities having different units for  $A(\underline{X}, \underline{U}, t)$ .

On the other hand, the quantity evaluated at the destination  $B(t_f, t_s)$  is a function of the difference between actual arrival time  $t_f$  and scheduled arrival time  $t_s$ . In general,

$$B(t_f, t_s) \geq 0 \quad \text{if } t_f \geq t_s \quad (\text{delay penalty})$$

$$B(t_f, t_s) \leq 0 \quad \text{if } t_f \leq t_s \quad (\text{dispatch reward})$$

The  $B(t_f, t_s)$  is set to zero in the case of minimizing passage time, whereas for the other cases, the shipmaster/owner may give the appropriate functional forms to  $B(t_f, t_s)$ . For example, the following functional form may be given:

$$\begin{aligned} B(t_f, t_s) &= w (t_f - t_s)^2 & \text{if } t_f \geq t_s \\ B(t_f, t_s) &= 0 & \text{if } t_f \leq t_s \end{aligned} \quad (2.10)$$

where  $w$  is a constant representing the degree of delay penalty.

In the case of minimizing fuel oil, the passage time  $t_f - t_0$  is usually specified by letting  $t_f = t_s$  and  $B(t_f, t_s)$  is set to zero.

From the above-mentioned considerations, the continuous optimization problem of finding an optimum route  $\underline{X}^*(t)$  ( $t_0 \leq t \leq t_f$ ) can be reduced to determining an optimum control  $\underline{U}^*(t)$  ( $t_0 \leq t \leq t_f$ )

which minimizes the objective function  $J$  given by (2.9) following the ship's transition equation (2.4) under the constraints (2.1), (2.2) and (2.3). ( Fig.2.1 )

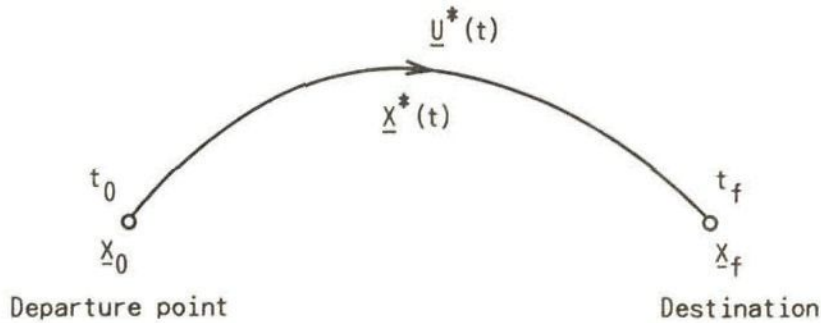


Fig. 2.1 Formulation of ship routing as a continuous optimization problem

### 2.2.2 Formulation as a discrete optimization problem

Although the ship's heading and the number of propeller revolutions are controlled continuously in the continuous optimization problem, it is normal for ocean-crossing vessels to change them once or twice a day. Besides, in order to perform weather routing simulations by a computer, it is more convenient to treat the problem as a multistage decision process by discretizing the time  $t$ . In this subsection, ship routing is formulated as a discrete optimization problem.

Since the arrival time  $t_f$  is unknown before the actual arrival at the destination, we set a suitable time  $t_n$  which will certainly be less than the arrival time  $t_f$  and be as close to  $t_f$  as possible.

Dividing the period from  $t_0$  to  $t_n$  into  $n$  time-intervals, we have the following discretized times:

$$t_i = t_0 + i \Delta t \quad (2.11)$$

$$\text{where } \Delta t = (t_n - t_0) / n \quad (2.12)$$



Representing the ship's position at time  $t_i$  and the control from  $t_i$  to  $t_{i+1}$  as  $\underline{X}_i$  and  $\underline{U}_i$  respectively (  $\underline{U}_i$  is constant from  $t_i$  to  $t_{i+1}$  ), and using Mercator's sailing to navigate a ship for  $\Delta t$  hours from the position  $\underline{X}_i$  with the control  $\underline{U}_i$ , the ship's position at  $t_{i+1}$  can be written as

$$\underline{X}_{i+1} = \underline{f}(\underline{X}_i, \underline{U}_i, t_i) \quad (i = 0, 1, \dots, n-1) \quad (2.13)$$

The components of the vectors on both sides of equation (2.13) are given as follows: <sup>(1)</sup>

$$\underline{X}_{i+1} = [ \phi_{i+1} \quad \lambda_{i+1} ]^T \quad (2.14)$$

$$\underline{f}(\underline{X}_i, \underline{U}_i, t_i) = \begin{bmatrix} \phi_i + \{ V_i \cos(\theta_i + \alpha_i) + N_i \} \Delta t / R_M(\phi_i) \\ \lambda_i + \{ mp(\phi_{i+1}) - mp(\phi_i) \} \frac{V_i \sin(\theta_i + \alpha_i) + E_i}{V_i \cos(\theta_i + \alpha_i) + N_i} \end{bmatrix} \quad (2.15)$$

where  $mp(\phi_i)$  represent the meridional parts from equator to latitude  $\phi_i$  ( unit : radian ), which is given by <sup>(1)</sup>

$$mp(\phi_i) = \ell n \{ \tan(\pi/4 + \phi_i/2) \} - \frac{e}{2} \ell n \left\{ \frac{1 + e \sin \phi_i}{1 - e \sin \phi_i} \right\} \quad (2.16)$$

where  $\ell n$  and  $e$  denote the natural logarithms and the eccentricity of meridian of the earth, respectively. ( Concerning the accuracy of the arrival latitude  $\phi_{i+1}$ , see Appendix 1. )

Using the time  $t_n$ , we rewrite the objective function  $J$  as follows:

$$J = \int_{t_0}^{t_n} A(\underline{X}, \underline{U}, t) dt + \int_{t_n}^{t_f} A(\underline{X}, \underline{U}, t) dt + B(t_f, t_s) \quad (2.17)$$

Representing the second integral by  $A'(\underline{X}_n, \underline{U}_n, t_n)$ ,  $J$  may be written discretely as

$$J = \sum_{i=0}^{n-1} A(\underline{X}_i, \underline{U}_i, t_i) \Delta t + A'(\underline{X}_n, \underline{U}_n, t_n) + B(t_f, t_s) \quad (2.18)$$

The  $A'(\underline{X}_n, \underline{U}_n, t_n)$  denotes the quantity evaluated during the period from  $t_n$  to  $t_f$  in which a ship is sailed along the rhumbline from  $\underline{X}_n$  to  $\underline{X}_f$  with the control  $\underline{U}_n$ . Hence concerning the control  $\underline{U}_n$ , only the number of propeller revolutions becomes the variable to be controlled.

We call the sequence of controls  $\underline{U}^*_i$  ( $i = 0, 1, \dots, n$ ) which minimizes  $J$  in (2.18) the 'optimum control' and the sequence of ship's positions  $\underline{X}^*_i$  ( $i = 1, 2, \dots, n$ ) determined by  $\underline{U}^*_i$  the 'optimum route'.

Thus the discrete optimization problem of finding an optimum route  $\underline{X}^*_i$  ( $i = 1, 2, \dots, n$ ) can be reduced to determining an optimum control  $\underline{U}^*_i$  ( $i = 0, 1, \dots, n$ ) which minimizes the objective function  $J$  given by (2.18) following the ship's transition equation (2.13) under the constraints (2.1), (2.2) and (2.3). ( Fig.2.2 )

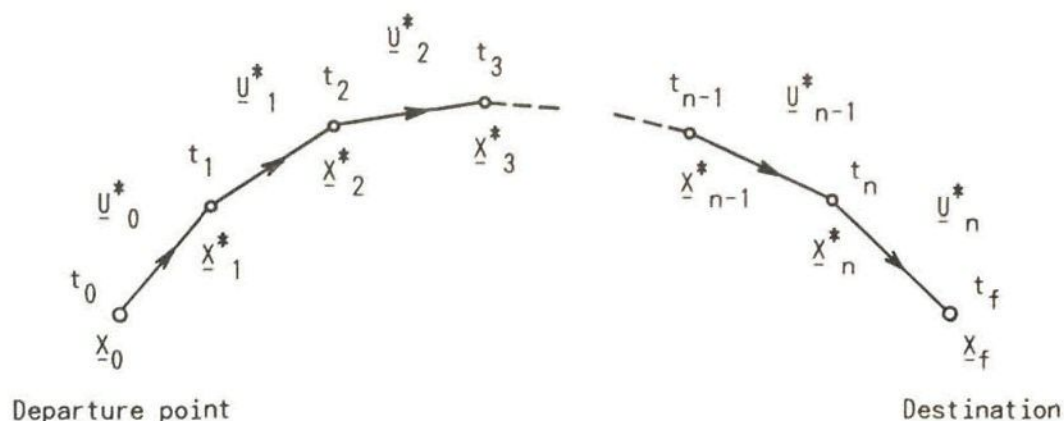


Fig. 2.2 Formulation of ship routing as a discrete optimization problem



In subsections 2.2.1 and 2.2.2, the ship routing was formulated as a deterministic optimization problem assuming the environmental conditions and the ship speed performance can be determined without uncertainties. In the actual weather routing, however, the forecasted wind, wave and ocean current data are used, which inevitably involve forecast errors. Furthermore, even if the forecasted values are accurate enough, the calculated ship's speed, drift angle, engine power, etc. are also accompanied by errors due to an imperfect mathematical modelling.

Therefore, in mathematical treatments, it is more strict to regard the ship's speed, drift angle and ocean current speed in (2.6) and (2.15) as random variables, and formulate the ship routing as a stochastic optimization problem.

In that case, the ship's transition equations (2.4) and (2.13) become stochastic differential equations and stochastic difference equations, respectively. Concerning the objective functions, the expected values of  $J$  in (2.9) and (2.18) can be used, and additionally, the uncertainties of evaluated quantities ( e.g. standard deviations ) may be added to  $J$  as penalties.

### 2.2.3 Review of the methods for solving the ship routing problem

A number of methods have been proposed for solving the ship routing problem formulated in subsections 2.2.1 and 2.2.2. Those methods can be classified into three categories:

- (a) calculus of variations ( or Pontryagin's maximum principle ) <sup>(2)</sup>.  
<sup>(3)</sup>. <sup>(4)</sup>. <sup>(5)</sup>
- (b) dynamic programming <sup>(6)</sup>. <sup>(7)</sup>. <sup>(8)</sup>
- (c) isochrone method <sup>(9)</sup>. <sup>(10)</sup>. <sup>(11)</sup>

(a) The method of calculus of variations treats the ship routing as a continuous optimization problem, and it seems elegant in the mathematical approach. For relatively simple objective functions, the optimal control laws on the ship's heading and the number of propeller revolutions can be derived from calculus of variations

as analytical forms.

Those optimal control laws, however, contain the partial derivatives of ship's speed, drift angle, etc. with respect to latitude, longitude and time, which should be calculated by numerical differentiation. In severe environmental conditions, such numerical differentiation may cause degradation of the accuracy of the solution.<sup>(6)</sup>

Since optimal control laws are merely necessary conditions to give a local extreme to an objective function  $J$ , we have to compute a number of routes for various initial ship's headings and initial number of propeller revolutions to find the solution giving the global minimum to  $J$ . In addition, it is often difficult to converge on a route to the destination, and very cumbersome to take into account the constraints (2.1), (2.2) and (2.3) in the routing algorithm.<sup>(6)</sup>

The calculus of variations can hardly treat ship routing as a stochastic optimization problem.<sup>(6)</sup> These drawbacks make the calculus of variations an impractical method for ship weather routing.

(b) Dynamic programming is a very powerful method for solving various kinds of optimization problems. Based on the Bellman's principle of optimality, it gives the functional recursion equation to solve the ship routing problem formulated as a discrete optimization problem.

Dynamic programming can provide the solution giving the global minimum to an objective function  $J$ , and can easily incorporate the constraints (2.1), (2.2) and (2.3) into the routing algorithm. Besides, since a set of optimum routes from the grid points covering the navigable area to the destination can be obtained, we can easily carry out a sensitivity analysis of the solution.

The accuracy of the solution by dynamic programming, however, largely depends on the fineness of the grid system used for the computation. Therefore it needs many grid points for the search routine to obtain an accurate solution, and it uses a lot of calculation time and memory space.<sup>(6)</sup>



For the stochastic routing problem, the dynamic programming provides an algorithm which minimizes the expected values of the objective function. However, since that algorithm requires a huge amount of calculations, a drastic simplification of the problem is necessary to obtain a solution.<sup>(6)</sup>

(c) The isochrone method, since it was proposed by R.W. James,<sup>(9)</sup> has been used in many weather routing facilities as a practical ( hand ) method to get the minimum time route. It treats the ship routing as a discrete optimization problem. The minimum time route is obtained by repeatedly computing an isochrone ( or time front ) which is defined as an outer boundary of the attainable region from the departure point after a certain time.

James constructed a number of tracks perpendicular to the isochrone and determined the next isochrone by navigating a ship along those tracks for a certain time-interval. Although the method proposed by James is convenient to obtain the isochrones by hand, it does not give the correct isochrones in a strict sense and it is less suitable for computerization. ( According to the Pontryagin's maximum principle, the ship has to be navigated along the track on which the projection of ship's speed on the isochrone's normal becomes maximum.<sup>(3)</sup> )

Hagiwara improved the isochrone method so as to make it suitable for computerization, and performed simulations of minimum time routing for a sailing ship.<sup>(10)</sup> During the academic year 1985 - 1986, Hagiwara and Spaans conducted a study on the practical weather routing of sail-assisted motor vessels.<sup>(11)</sup> In that study, the isochrone method improved by Hagiwara was used, and it was named 'modified isochrone method'. The modified isochrone method was slightly amended later<sup>(12)</sup> and adopted as the optimization method in this thesis.

The algorithm of the modified isochrone method is straightforward and very suitable for computerization. The modified isochrone method can determine the correct isochrones; thus it can calculate the accurate minimum time route. In addition, it can easily take into consideration the constraints (2.1), (2.2) and (2.3). Besides, since the method is based on normal navigation routines, it can

easily be understood by navigators, which makes acceptance easier.

From a practical point of view, the modified isochrone method can be applied to minimum fuel/cost routing. Furthermore, it can be extended to stochastic routing by incorporating the stochastic nature of the environmental forecasts into the routing algorithm.

In Sections 2.3 and 2.4, the modified isochrone method is explained in detail.

## 2.3 THE MODIFIED ISOCHRONE METHOD FOR DETERMINISTIC ROUTING

In this section, assuming the forecasted environmental conditions are strictly correct and the ship's speed, drift angle, engine power, etc. for the given environments can be accurately predicted, the algorithms of the modified isochrone method to solve the deterministic ship routing problem are stated.

### 2.3.1 Minimum time routing

We suppose a ship leaving the departure point  $\underline{X}_0$  at time  $t_0$  and sailing to the destination  $\underline{X}_f$  with maximum ( constant ) number of propeller revolutions. Since the object to be minimized is the passage time, the quantities in (2.18) become as follows:

$$\begin{aligned} A(\underline{X}_i, \underline{U}_i, t_i) &= 1 \\ A'(\underline{X}_n, \underline{U}_n, t_n) &= [ \text{passage time between } \underline{X}_n \text{ and } \underline{X}_f \text{ when a ship} \\ &\quad \text{is navigated along rhumbline from } \underline{X}_n \text{ to } \underline{X}_f ] \\ B(t_f, t_s) &= 0 \end{aligned}$$

Representing  $A'(\underline{X}_n, \underline{U}_n, t_n)$  by  $T_n$ , the passage time  $T$  between  $\underline{X}_0$  and  $\underline{X}_f$  is given as

$$T = n \Delta t + T_n \quad (2.19)$$

The problem is to determine the optimum headings  $\theta^*_i$  (  $i = 0, 1, \dots, n-1$  ) and the minimum time route via  $\underline{X}^*_i$  (  $i = 1, 2, \dots, n$  ) which minimize  $T$  in (2.19).

In 2.2.2, the time  $t_n$  was set up first for the discretization, and the time-interval  $\Delta t$  was defined later by (2.12). On the other hand, in the modified isochrone method, the time-interval  $\Delta t$  is set up first, and the time  $t_n$  is determined in the calculation depending on the minimum distance from the isochrone to the destination.

The time-interval  $\Delta t$  is divided into several sub-time-intervals  $\Delta t'$  in order to increase the accuracy of the solution:



$$\Delta t = q \Delta t' \quad (2.20)$$

where  $q$  : integer greater than 1

The ship is navigated for  $\Delta t'$  hours with constant ship's speed, drift angle, engine power, etc..

The algorithm of the modified isochrone method is as follows.

(i) Simulate the navigation of a ship for  $\Delta t$  hours from departure point  $\underline{X}_0$ , following discretized headings  $C_0 \pm i\Delta C$  ( $i = 0, 1, \dots, m$ ), where  $C_0$  is the initial course of the great circle route from  $\underline{X}_0$  to  $\underline{X}_1$  and  $\Delta C$  is the increment of heading.

In each heading, the ship's speed through the water, drift angle by wind, engine power, etc. are computed every  $\Delta t'$  hours based on the environmental forecasts, ship's heading and number of propeller revolutions; the ocean current speed is also taken from the data base every  $\Delta t'$  hours. The ship's positions at  $t_0 + \Delta t'$ ,  $t_0 + 2\Delta t'$ , ...,  $t_0 + q\Delta t'$  ( $= t_0 + \Delta t = t_1$ ) are calculated by transition equation (2.13) using  $\Delta t'$  instead of  $\Delta t$ .

The calculated arrival points at time  $t_1$  are represented by  $\underline{X}_1(i)$  ( $i = 1, 2, \dots, 2m+1$ ). The set  $\{\underline{X}_1(i)\}$  defines the isochrone at  $t_1$ . At each  $\underline{X}_1(i)$ , the ship's heading from  $\underline{X}_0$  to  $\underline{X}_1(i)$  is memorized. (Although it is not necessary for the optimization procedure to memorize the headings, it is extra information for the shipmaster.)

(ii) Let  $\underline{X}_1(i)$  be the departure points at  $t_1$ . Navigate the ship for  $\Delta t$  hours from each  $\underline{X}_1(i)$ , following discretized headings  $C_1 \pm j\Delta C$  ( $j = 0, 1, \dots, m$ ), where  $C_1$  is the arrival course of the great circle route from  $\underline{X}_0$  to each  $\underline{X}_1(i)$ .

In each heading, the ship's positions at  $t_1 + \Delta t'$ ,  $t_1 + 2\Delta t'$ , ...,  $t_1 + q\Delta t'$  ( $= t_1 + \Delta t = t_2$ ) are calculated by (2.13) using  $\Delta t'$  instead of  $\Delta t$ . The calculated arrival points at  $t_2$  are represented by  $\underline{X}_2(i, j)$  ( $i, j = 1, 2, \dots, 2m+1$ ). Then compute the initial courses  $C_2(i, j)$  and great circle distances  $D_2(i, j)$  of the great circle routes from  $\underline{X}_0$  to  $\underline{X}_2(i, j)$ .

Now, define a sub-sector set  $\{S_2(k)\}$  centered around the great circle route from  $\underline{X}_0$  to  $\underline{X}_f$ . ( Fig.2.3 )

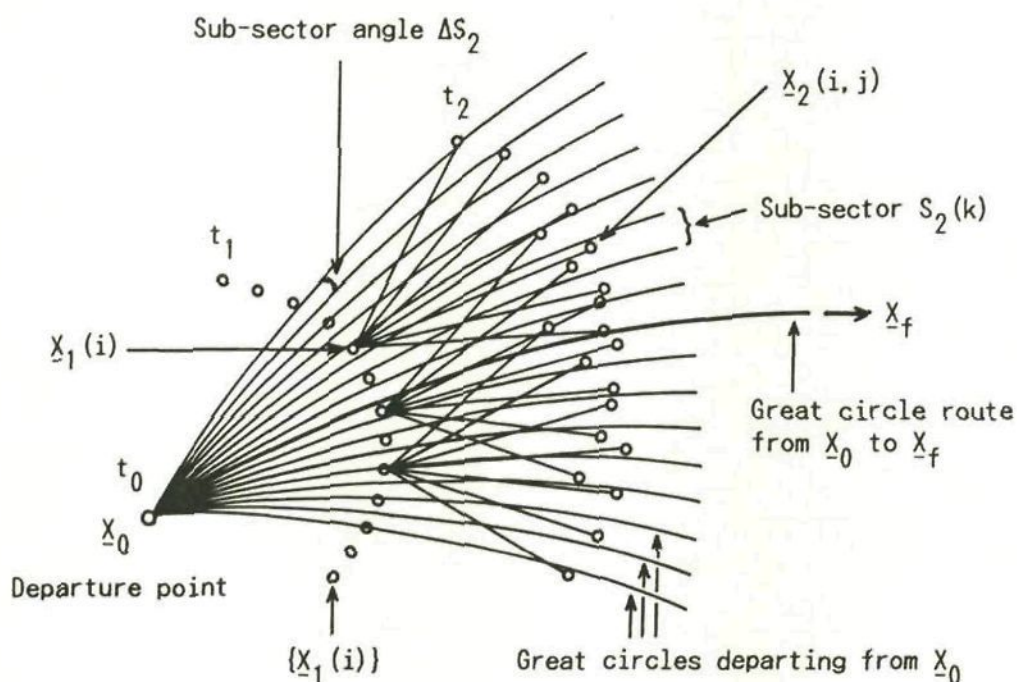


Fig. 2.3 Calculation of isochrone  $\{\underline{X}_2(k)\}$  at time  $t_2$

Each sub-sector  $S_2(k)$  represents the area surrounded by two great circles departing from  $\underline{X}_0$ , the initial courses of which are  $C_0 + (k-p-1)\Delta S_2$  and  $C_0 + (k-p)\Delta S_2$  ( $k = 1, 2, \dots, 2p$ ), where  $C_0$  is the initial course of the great circle route from  $\underline{X}_0$  to  $\underline{X}_f$  and  $\Delta S_2$  is the sub-sector angle, i.e. the increment of the initial course. The sub-sector angle  $\Delta S_2$  in radian is defined by

$$\Delta S_2 = c \Delta d / \sin( c d_2 ) \quad (2.21)$$

where  $c = \pi / ( 60 \times 180 )$

$d_2$  : expected travelled distance in n.m. after  $2\Delta t$  hours

$d_2 \approx 2 \Delta t V_s$  ( $V_s$  : service speed in knots )

$\Delta d$  : predetermined local sub-sector width ( i.e. resolution of the isochrone )



The number of sub-sectors  $2p$  is decided so that the set of sub-sectors covers the appropriate area to be searched. The initial course  $C_2(i,j)$  of the great circle route from  $\underline{X}_0$  to each  $\underline{X}_2(i,j)$  identifies the sub-sector  $S_2(k)$  to be assigned to each  $\underline{X}_2(i,j)$ .

From all  $\underline{X}_2(i,j)$  included in each sub-sector  $S_2(k)$ , the arrival point  $\underline{X}_2(k)$  is selected with maximum  $D_2(i,j)$ . The set  $\{\underline{X}_2(k)\}$  ( $k = 1, 2, \dots, 2p$ ) defines the isochrone at  $t_2$ . At each  $\underline{X}_2(k)$ , the departure point from which the ship arrived at  $\underline{X}_2(k)$  and the ship's heading from that departure point to  $\underline{X}_2(k)$  are memorized. ( Although it is not necessary for the optimization procedure to memorize the headings, it is extra information for the shipmaster. )

(iii) Changing the argument from  $k$  to  $i$ , let  $\underline{X}_2(i)$  be the departure points at  $t_2$ . Navigate the ship for  $\Delta t$  hours from each  $\underline{X}_2(i)$ , following discretized headings  $C_i \pm j\Delta C$  ( $j = 0, 1, \dots, m$ ), where  $C_i$  is the arrival course of the great circle route from  $\underline{X}_0$  to  $\underline{X}_2(i)$ .

In each heading, the ship's positions at  $t_2 + \Delta t'$ ,  $t_2 + 2\Delta t'$ , ...,  $t_2 + q\Delta t'$  ( $= t_2 + \Delta t = t_3$ ) are calculated by (2.13) using  $\Delta t'$  instead of  $\Delta t$ . The calculated arrival points at  $t_3$  are represented by  $\underline{X}_3(i,j)$  ( $i = 1, 2, \dots, 2p$ ;  $j = 1, 2, \dots, 2m+1$ ). In the same way as stated in (ii), compute  $C_3(i,j)$  and  $D_3(i,j)$  for all  $\underline{X}_3(i,j)$ .

Then define a new sub-sector set  $\{S_3(k)\}$  centered around the great circle route from  $\underline{X}_0$  to  $\underline{X}_t$ . The sub-sector angle  $\Delta S_3$  is computed by (2.21) using a constant value of  $\Delta d$  and  $d_3$  being the expected travelled distance after  $3\Delta t$  hours. The initial course  $C_3(i,j)$  identifies the sub-sector  $S_3(k)$  to be assigned to each  $\underline{X}_3(i,j)$ .

Comparing  $D_3(i,j)$  of all  $\underline{X}_3(i,j)$  included in each sub-sector  $S_3(k)$ , find  $\underline{X}_3(i,j)$  having maximum  $D_3(i,j)$  and represent it by  $\underline{X}_3(k)$ . The set  $\{\underline{X}_3(k)\}$  ( $k = 1, 2, \dots, 2p$ ) defines the isochrone at  $t_3$ . At each  $\underline{X}_3(k)$ , the departure point from which the ship arrived at  $\underline{X}_3(k)$  and the ship's heading from that departure point to  $\underline{X}_3(k)$  are memorized.

(iv) Repeating the procedures in (iii), compute the isochrones



$\{X_4(k)\}, \{X_5(k)\}, \dots$  at time  $t_4, t_5, \dots$ .

(v) When the isochrone  $\{X_n(k)\}$  at  $t_n (= t_0 + n\Delta t)$  approaches the destination  $X_f$  sufficiently, navigate the ship along rhumb lines from  $X_n(k)$  to  $X_f$  and calculate the passage times  $T_n(k)$  between  $X_n(k)$  and  $X_f$ .

In order to obtain each  $T_n(k)$ , the ship's positions at  $t_n + \Delta t'$ ,  $t_n + 2\Delta t'$ , --- along the rhumb line from  $X_n(k)$  to  $X_f$  are calculated by transition equation (2.13) using  $\Delta t'$  instead of  $\Delta t$ . We represent the ship's position at  $t_n + i\Delta t'$  as  $X_{ni}$  ( $i = 1, 2, \dots$ ). When the rhumb line distance between  $X_{nr}$  and  $X_f$  becomes less than  $V_{og}\Delta t'$ , where  $V_{og}$  is the ship's speed over the ground at  $t_n + r\Delta t'$ , the passage time  $T_n(k)$  between  $X_n(k)$  and  $X_f$  is computed by

$$T_n(k) = r \Delta t' + D_r / V_{og} \quad (2.22)$$

where  $D_r$  : rhumb line distance between  $X_{nr}$  and  $X_f$

Denoting the quantities at  $X_{nr}$  and  $X_f$  by the subscripts  $nr$  and  $f$  respectively,  $D_r$  and  $V_{og}$  are given as follows: <sup>(1)</sup>

$$D_r = R_M(\phi_m) (\phi_f - \phi_{nr}) \sec \theta_{nr} \quad (2.23)$$

where  $\phi_m = (\phi_{nr} + \phi_f) / 2$

$R_M(\phi_m)$  : local radius of meridian of the earth

( Concerning the accuracy of  $D_r$ , see Appendix 2. )

$$V_{og} = \{ [ V_{nr} \cos(\theta_{nr} + \alpha_{nr}) + N_{nr} ]^2 + [ V_{nr} \sin(\theta_{nr} + \alpha_{nr}) + E_{nr} ]^2 \}^{1/2} \quad (2.24)$$

The ship's heading  $\theta_{nr}$  from  $X_{nr}$  to  $X_f$  is calculated by <sup>(1)</sup>

$$\theta_{nr} = \tan^{-1} \{ (\lambda_f - \lambda_{nr}) / [ mp(\phi_f) - mp(\phi_{nr}) ] \} \quad (2.25)$$

where  $mp(\phi_{nr})$  and  $mp(\phi_f)$  : meridional parts from equator to latitude  $\phi_{nr}$  and  $\phi_f$

The minimum passage time  $T_{min}$  between  $X_0$  and  $X_f$  is given by

$$T_{min} = \min_k \{ n \Delta t + T_n(k) \} \quad (2.26)$$

Represent  $\underline{X}_n(k)$  giving that  $T_{min}$  by  $\underline{X}_n^*$ .

(vi) Find the departure point at  $t_{n-1}$  from which the ship arrived at  $\underline{X}_n^*$  and the ship's heading from that departure point to  $\underline{X}_n^*$ , and represent them by  $\underline{X}_{n-1}^*$  and  $\theta_{n-1}^*$ , respectively. Then find the departure point at  $t_{n-2}$  from which the ship arrived at  $\underline{X}_{n-1}^*$  and the ship's heading from that departure point to  $\underline{X}_{n-1}^*$ , and represent them by  $\underline{X}_{n-2}^*$  and  $\theta_{n-2}^*$ , respectively.

Repeating this tracing procedure to the departure point  $\underline{X}_0$ , the minimum time route  $\underline{X}_f, \underline{X}_n^*, \underline{X}_{n-1}^*, \dots, \underline{X}_1^*, \underline{X}_0$  and the optimum headings  $\theta_{n-1}^*, \theta_{n-2}^*, \dots, \theta_1^*, \theta_0^*$  are obtained.

( Fig.2.4 )

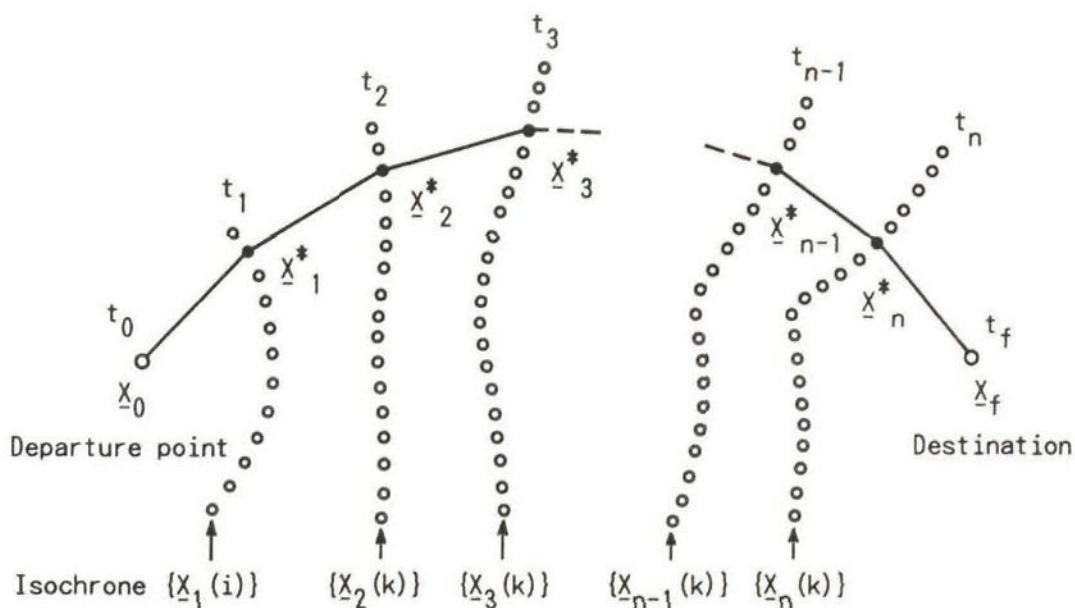


Fig. 2.4 Determination of minimum time route by tracing the points of the isochrones

The accuracy of this modified isochrone method can be increased by decreasing the predetermined local sub-sector width  $\Delta d$ . The

sub-sector angle  $\Delta S_i$  ( rad ) at time  $t_i$  is calculated as in (2.21). Fig.2.5 gives the sub-sector angle  $\Delta S_i$  as a function of the number of days underway for  $\Delta d = 45$  n.m. and a service speed of 14 knots.

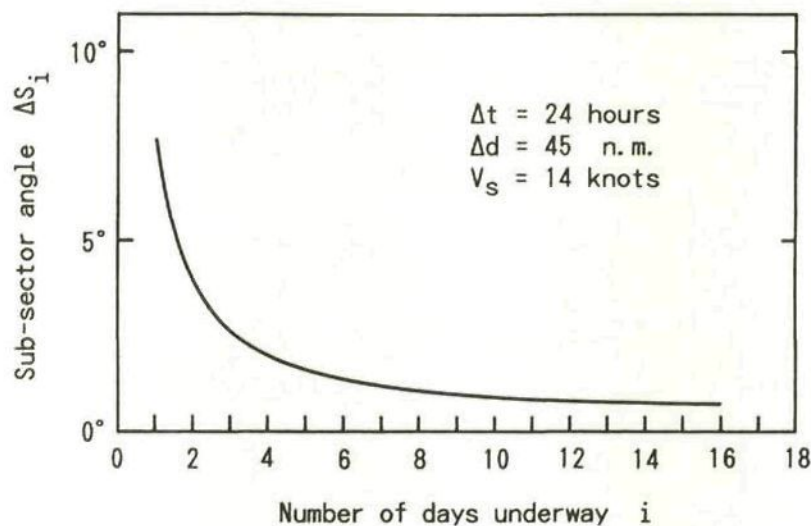


Fig. 2.5 Sub-sector angle  $\Delta S_i$  as a function of the number of days underway (  $\Delta d = 45$  n.m.,  $V_s = 14$  knots )

Since the number of arrival points constructing an isochrone after each time-interval  $\Delta t$  does not exceed  $2p$ , the amount of calculations is always kept within a certain feasible limit. In addition, this method can easily take into account the constraint (2.1), (2.2) and (2.3).

In the modified isochrone method, the isochrones are computed based on the definition of the isochrone, i.e. the outer boundary of the attainable region from the departure point after a certain time. Therefore, strictly correct isochrones can be obtained by letting the predetermined local width of sub-sector  $\Delta d$  be sufficiently small.

Since the spheroid defined by WGS-72 was adopted to represent a shape of the earth in the modified isochrone method, geodetic lines should be used instead of great circles for setting up the sub-sectors and determining the distances, initial courses, etc..



However, as the eccentricity of the meridian is very small, the distances, initial courses, etc. of the great circles are not very different from those of the geodetic lines. In addition, for determining the isochrones, not the absolute distances but the relative distances ( i.e. differences of distances ) between departure point and arrival points are important. The relative distances of the great circles for nearby arrival points almost coincide with those of the geodetic lines; see Appendix 3. Thus, in order to save computing time, great circles are used as substitutes for geodetic lines.

In actual minimum time routing, since the environmental forecasts are updated every 12 or 24 hours, it is necessary to recalculate the minimum time route by using the updated forecasts and ship's position at each updating time as a new departure point.

### 2.3.2 Minimum fuel routing

Consider a ship leaving departure point  $\underline{X}_0$  at time  $t_0$  and arriving at destination  $\underline{X}_f$  at time  $t_f$ , and let us minimize the total fuel consumption during the voyage. In this problem, it is assumed that the arrival time  $t_f$  is specified as  $t_s$  and the passage time  $T$  (  $= t_f - t_0$  ) is fixed as  $T_s$  (  $= t_s - t_0$  ).

From the mathematical point of view, as ship's heading and the number of propeller revolutions ( or engine power ) have to be controlled simultaneously in minimum fuel routing, the problem becomes more complicated than in minimum time routing. In actual ocean-crossing voyages, however, it has been found by simulations based on the calculus of variations that the control of ship's course is far more effective than the control of engine power to minimize the total fuel consumption.<sup>(5)</sup>

Provided the engine power is kept constant during the voyage, the minimum time route reaching  $\underline{X}_f$  at the specified arrival time  $t_s$  will give a sub-optimum solution from a mathematical point of view. In practice, as the number of propeller revolutions is kept constant, it is proposed to consider the minimum time route reaching  $\underline{X}_f$  at  $t_s$ .

with a constant number of propeller revolutions to be the sub-optimum minimum fuel route.

The following two kinds of algorithms for the minimum fuel routing based on the modified isochrone method are proposed.

#### Algorithm (I)

(i) Set up the following objective function J:

$$J = F + w \quad (2.27)$$

where F : total fuel consumption during the voyage

w : delay penalty

$$w = \infty \quad \text{if } t_f > t_s$$

$$w = 0 \quad \text{if } t_f \leq t_s$$

$t_f$  : actual arrival time

$t_s$  : specified arrival time

(ii) Setting a suitable number of propeller revolutions  $n_0$ , calculate the isochrones by using the modified isochrone method described in subsection 2.3.1. Then compute J given by (2.27) for all the routes reaching  $\underline{X}_f$  from  $\underline{X}_0$  via  $\underline{X}_n(k)$  ( $k = 1, 2, \dots, 2p$ ) of the final isochrone  $\{\underline{X}_n(k)\}$ , and represent them by  $J(k)$ . ( Those routes can be determined by tracing the isochrones memorized in the computer backwards from  $\underline{X}_n(k)$ . )

In each route, the total fuel consumption F is calculated as the sum of the fuel consumptions for sub-time-intervals  $\Delta t'$ . ( The method to compute the fuel consumption as a function of the number of propeller revolutions and the ship's speed through the water is stated in Section 3.6. )

Find the minimum value of  $J(k)$ , and represent it by  $J^*(n_0)$  as a function of the number of propeller revolutions:

$$J^*(n_0) = \min_k \{ J(k) \} \quad (2.28)$$

(iii) Calculate  $J^*(n)$  for various propeller revolutions  $n$ , i.e.  $n = n_0 \pm j\Delta n$  ( $j = 1, 2, \dots$ ) where  $\Delta n$  is the increment of the number of propeller revolutions. ( If  $J^*(n_0) = \infty$ , calculate  $J^*(n)$  for the greater  $n$  than  $n_0$ , i.e.  $n = n_0 + j\Delta n$ . )

Find the number of propeller revolutions  $n$  which minimizes  $J^*(n)$  and the minimum value of  $J^*(n)$ , and represent them by  $n^*$  and  $J^*_{min}$ , respectively:

$$J^*_{min} = \min_n \{ J^*(n) \} \quad (2.29)$$

(iv) Adopt  $n^*$  and the route giving  $J^*_{min}$  as the optimal number of propeller revolutions and the minimum fuel route for a specified passage time  $T_s$ , respectively. ( Fig.2.6 )

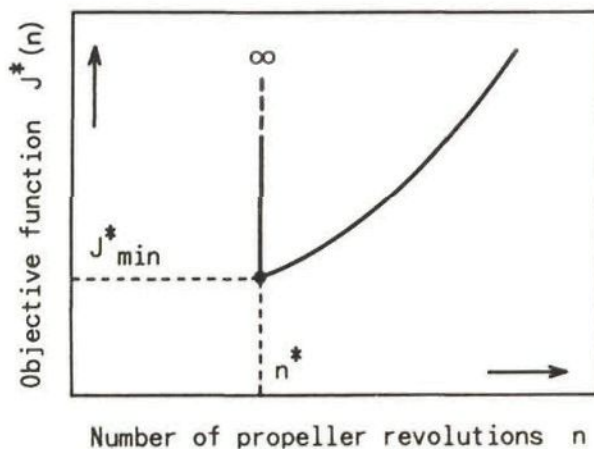


Fig. 2.6 Determination of minimum fuel route by the Algorithm (I)

In this algorithm, since it is necessary to decrease the increment  $\Delta n$  in the vicinity of the minimum value of the objective function in order to obtain the accurate  $n^*$  and  $J^*_{min}$ , a considerable amount of computing time is needed. Thus, for saving computing time, an alternative algorithm, having an iterative procedure, is proposed as follows.



### Algorithm (II)

(i) Setting a suitable number of propeller revolutions  $n_0$ , calculate the minimum time route and minimum passage time  $T_{min}$  by using the modified isochrone method. The total fuel consumption  $F$  on that minimum time route is also computed as a sum of the fuel consumptions for the sub-time-intervals  $\Delta t'$ .

(ii) Correct the number of propeller revolutions  $n_0$  so as to get  $T_{min}$  close to the specified passage time  $T_s$ . Using the corrected number of propeller revolutions  $n_1$ , recalculate the minimum time route and minimum passage time  $T_{min}$  as well as the total fuel consumption  $F$ .

(iii) If  $|T_s - T_{min}|$  becomes small enough, stop the calculation, and represent  $n_1$  and  $F$  as  $n^*$  and  $F^*$  respectively. Otherwise, letting  $n_1$  be  $n_0$ , repeat the procedures in (ii) and (iii).

(iv) Adopt the calculated minimum time route as the minimum fuel route for a specified passage time  $T_s$ . The  $n^*$  and  $F^*$  are regarded as the optimal number of propeller revolutions and the minimum fuel consumption.

Newton's method or regula-falsi method can be used for the correction of the number of propeller revolutions.

This Algorithm (II) has the advantage that if the initial number of propeller revolutions  $n_0$  is comparatively close to  $n^*$ ,  $T_{min}$  converges rapidly to  $T_s$ ; thus we can save computing time. With the Algorithm (II), however, care should be taken in the following case.

When the weather around the great circle route from  $\underline{X}_0$  to  $\underline{X}_f$  is extremely severe, the final isochrone may bend backwards sharply near the destination. Such a sharp bending point of the isochrone is usually called 'double point', because in this point two different tangent lines exist.

In that case, there is a possibility that a route passing through

the other side of the great circle route from  $\underline{X}_0$  to the double point of the final isochrone provides less fuel consumption with a bit larger number of propeller revolutions than the calculated minimum fuel route. Therefore, to check the fuel consumption of that alternative route, it is necessary to apply the algorithm again for only the other side of the great circle route from  $\underline{X}_0$  to the double point. The reason for the existence of that alternative route is given in Appendix 4.

On the other hand, the Algorithm (I) can always find the correct minimum fuel route by searching the number of propeller revolutions even if the final isochrone has a double point near the destination.

In the actual minimum fuel routing, it is necessary to recalculate the minimum fuel route whenever the environmental forecasts are updated.

### 2.3.3 Minimum cost routing

Suppose a ship leaving departure point  $\underline{X}_0$  at time  $t_0$  and reaching destination at time  $t_f$ , and let us minimize the total cost. In this case, it is assumed that the arrival time  $t_f$  is scheduled as  $t_s$  by a shipmaster/owner and the delay penalty given by (2.10) is imposed if  $t_f$  becomes larger than  $t_s$ .

In minimum cost routing, the same as mentioned in minimum fuel routing, as the ship's heading and the number of propeller revolutions have to be controlled simultaneously, the mathematical treatment becomes more complicated than in minimum time routing. However, since the ocean environments affect almost only the fuel cost ( i.e. fuel consumption ) per unit time during the voyage in normal ship operation, the sub-optimum solution for the minimum cost routing can be obtained by using the modified isochrone method in the same way as described in minimum fuel routing.

In minimum cost routing, we should find the optimal arrival time in order that a sum of the costs during the voyage and delay penalty cost at the destination will be minimized. Therefore, an iterative



algorithm using a fixed arrival time such as the Algorithm (II) in minimum fuel routing can not be applied to the minimum cost routing.

The algorithm of minimum cost routing based on the modified isochrone method is proposed as follows.

(i) Set up the following objective function J:

$$J = C + w ( t_f - t_s )^2 \quad (2.30)$$

where J : total cost

C : sum of the costs during the voyage, i.e. sum of the fuel cost, manning cost, insurance cost, etc. between  $\underline{X}_0$  and  $\underline{X}_f$

$w ( t_f - t_s )^2$  : delay penalty cost at the destination  $\underline{X}_f$

$t_f$  : actual arrival time

$t_s$  : scheduled arrival time

w : weighting coefficient for delay penalty

$w > 0$  if  $t_f > t_s$

$w = 0$  if  $t_f \leq t_s$

(ii) Setting a suitable number of propeller revolutions  $n_0$ , calculate the isochrones using the modified isochrone method. Then compute J given by (2.30) for all the routes reaching  $\underline{X}_f$  from  $\underline{X}_0$  via  $\underline{X}_n(k)$  ( $k = 1, 2, \dots, 2p$ ) of the final isochrone  $\{\underline{X}_n(k)\}$ , and represent them by J(k).

In each route, the costs for the sub-time-interval  $\Delta t'$  are calculated as functions of the environmental conditions, ship's heading and number of propeller revolutions. The summation of those costs over the voyage makes the sum of the costs C in (2.30).

Find the minimum value of J(k), and represent it by  $J^*(n_0)$  as a function of the number of propeller revolutions:

$$J^*(n_0) = \min_k \{ J(k) \} \quad (2.31)$$

(iii) Calculate  $J^*(n)$  for various propeller revolutions n, i.e.



$n = n_0 \pm j\Delta n$  (  $j = 1, 2, \dots$  ) where  $\Delta n$  is the increment of the number of propeller revolutions.

Find the number of propeller revolutions  $n$  which minimizes  $J^*(n)$ , the arrival time  $t_f$  for that  $n$  and the minimum value of  $J^*(n)$ , and represent them by  $n^*$ ,  $t_f^*$  and  $J_{min}^*$ , respectively:

$$J_{min}^* = \min_n \{ J^*(n) \} \quad (2.32)$$

(iv) Adopt the route giving  $J_{min}^*$  as the minimum cost route for a scheduled passage time  $T_s$ . The optimal number of propeller revolutions and the optimal arrival time are given by  $n^*$  and  $t_f^*$ , respectively. ( Fig.2.7 )

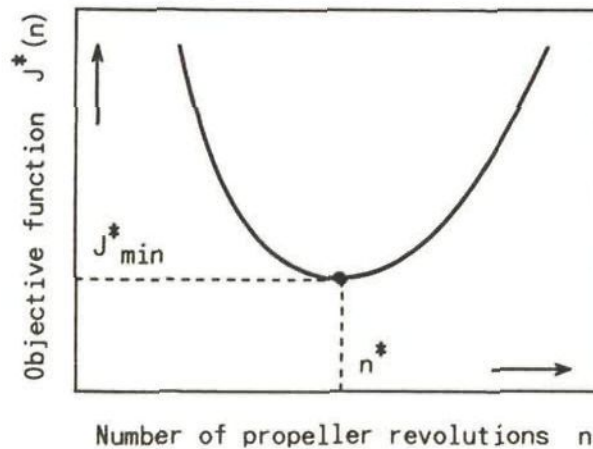


Fig. 2.7 Determination of minimum cost route

In order to obtain the accurate  $n^*$  and  $J_{min}^*$ , it is necessary to decrease the increment  $\Delta n$  in the vicinity of the minimum value of the objective function; or alternatively, approximating  $J^*(n)$  by a polynomial function of  $n$  near the minimum value of the objective function, the minimum of that polynomial function has to be calculated.

The weighting coefficient for delay penalty  $w$  changes with the operation schedule of a berth at the destination, the degree of reduction of the benefit due to late arrival, etc.. When the ship has to obey an operation schedule strictly, a considerably large value is taken for  $w$  and the minimum cost routing becomes almost equivalent to the minimum fuel routing.

In the actual minimum cost routing, it is necessary to recalculate the minimum cost route whenever the environmental forecasts are updated.

#### 2.4 THE MODIFIED ISOCHRONE METHOD FOR STOCHASTIC ROUTING

In actual weather routing, the forecasted environmental data inevitably involve forecast errors, and even if the environments are forecasted accurately, the predicted ship's speed, drift angle, engine power, etc. are accompanied by errors caused by an imperfect mathematical modelling. Therefore, the predicted passage time, fuel consumption, etc. on a certain route also contain prediction errors.

Regarding the errors of forecasted environments, information on the forecast errors can be obtained as mean errors ( or statistical biases ), covariance matrices and correlation matrices by comparing the forecasted data with the analyzed data for a long period. ( In this comparison, the values of analyzed data are regarded as the actual values or true values. )

On the other hand, concerning the errors of the predicted ship's speed, drift angle, engine power, etc., since it is difficult to measure those actual values and the wind/wave conditions precisely on board of ships, reliable error models for these quantities have not yet been available.

If these prediction errors and the wind/wave conditions can be measured accurately, the mathematical model can be improved so as to remove these errors. Consequently, it is assumed in this study that the ship's speed, drift angle, engine power, etc. predicted by the mathematical model are the expected values of these parameters.

In carrying out ship weather routing, it is very useful when the standard deviations or 95% (99%) confidence intervals of passage time and fuel consumption on a certain route can be estimated at the departure time or during the voyage. By means of those standard deviations, the degree of uncertainties of the arrival time and fuel consumption can be shown quantitatively, which makes it easy to plan the operation schedule of a ship and to determine a margin for fuel oil to be loaded. In addition, it is possible to incorporate those standard deviations into the objective functions in determining an optimum route from a stochastic point of view.



In this section, the method to estimate the standard deviations of passage time and fuel consumption as well as the covariance matrices of ship's positions are worked out using the information on the errors of forecasted environments. Then combining that method with the modified isochrone method, practical algorithms for stochastic minimum time and fuel routing are established.

#### 2.4.1 Estimation of the standard deviations of passage time and fuel consumption

- (I) Estimation of the covariance matrix of ship's position and the variance of accumulated fuel consumption

Consider a ship leaving departure point  $\underline{X}_0$  at time  $t_0$  and sailing to the destination  $\underline{X}_r$ . As mentioned in subsection 2.3.1, the ship's speed, drift angle, engine power, etc. are calculated at  $\Delta t'$  hours sub-time-intervals. In this subsection, the subscript  $i$  is used to represent the quantities at time  $t_0 + i\Delta t'$ .

We rewrite the discretized transition equation of a ship (2.13) as follows:

$$\underline{X}_{i+1} = \underline{f}(\underline{X}_i, \underline{S}_i, \underline{W}_i, \theta_i) \quad (2.33)$$

where  $\underline{X}_i = [\phi_i \ \lambda_i]^T$  : ship's position vector at  $t_0 + i\Delta t' = t_i$   
 $\underline{S}_i = [V_i \ \alpha_i]^T$  : vector comprised of ship's speed through the water  $V_i$  and drift angle  $\alpha_i$  at  $t_i$   
 $\underline{W}_i = [N_i \ E_i]^T$  : ocean current vector at  $t_i$   
 $\theta_i$  : ship's heading between  $t_i$  and  $t_{i+1}$

The two-dimensional vector function  $\underline{f}$  is given by

$$\underline{f}(\underline{X}_i, \underline{S}_i, \underline{W}_i, \theta_i) = \begin{bmatrix} \phi_i + \{ V_i \cos(\theta_i + \alpha_i) + N_i \} \Delta t' / R_M(\phi_i) \\ \lambda_i + \{ mp(\phi_{i+1}) - mp(\phi_i) \} \frac{V_i \sin(\theta_i + \alpha_i) + E_i}{V_i \cos(\theta_i + \alpha_i) + N_i} \end{bmatrix} \quad (2.34)$$

where  $R_M(\phi_i)$  : local radius of meridian of the earth  
 $mp(\phi_i)$  : meridional parts from equator to latitude  $\phi_i$

The vector  $\underline{S}_i$  is a function of the ship's heading  $\theta_i$ , number of propeller revolutions  $n_i$  and wind/wave conditions at the ship's position  $\underline{X}_i$  at time  $t_i$ . Compared with equation (2.13), equation (2.33) describes the ship's transition more precisely by using the vector  $\underline{S}_i$  depending on the wind/wave conditions and the ocean current vector  $\underline{W}_i$ .

Representing the wind/wave conditions by vector  $\underline{C}_i$ , the vector  $\underline{S}_i$  can be written as

$$\underline{S}_i = \underline{S}(\underline{C}_i, \theta_i, n_i) \quad (2.35)$$

where the components of  $\underline{C}_i$  are as follows:

$$\underline{C}_i = [ S_{WI} \ D_{WI} \ H_{SE} \ D_{SE} \ T_{SE} \ H_{SW} \ D_{SW} \ T_{SW} ]^T \quad (2.36)$$

The components  $S_{WI}, D_{WI}, H_{SE}, D_{SE}, T_{SE}, H_{SW}, D_{SW}$  and  $T_{SW}$  denote the wind speed, wind direction, significant sea height, predominant sea direction, average sea period, significant swell height, predominant swell direction and average swell period at the ship's position  $\underline{X}_i$  at time  $t_i$ , respectively.

As will be mentioned in Section 3.6, since the fuel consumption per unit time is a function of the ship's speed through the water and the number of propeller revolutions, the fuel consumption  $G_i$  for  $\Delta t'$  hours between  $t_i$  and  $t_{i+1}$  is represented as

$$G_i = G(V_i, n_i) \quad (2.37)$$

where  $V_i$  : ship's speed through the water at  $t_i$   
 $n_i$  : number of propeller revolutions between  $t_i$  and  $t_{i+1}$

Therefore, the accumulated fuel consumption  $F_{i+1}$  from  $t_0$  to  $t_{i+1}$  is given by

$$F_{i+1} = F_i + G(V_i, n_i) \quad (2.38)$$

In (2.33), (2.35) and (2.38), the vectors  $\underline{C}_i$  and  $\underline{W}_i$  are the actual ( i.e. true ) values of wind/wave conditions and ocean current respectively, each of which may be represented as the sum of the forecasted value by the numerical forecast model ( or other statistical models ) and the forecast error:

$$\underline{C}_i = \hat{\underline{C}}_i + \Delta\hat{\underline{C}}_i \quad (2.39)$$

$$\underline{W}_i = \hat{\underline{W}}_i + \Delta\hat{\underline{W}}_i \quad (2.40)$$

where  $\underline{C}_i$  : actual ( true ) value of wind/wave condition vector

$\underline{W}_i$  : actual ( true ) value of ocean current vector

$\hat{\underline{C}}_i$  : forecasted value of wind/wave condition vector

$\hat{\underline{W}}_i$  : forecasted value of ocean current vector

$\Delta\hat{\underline{C}}_i$  : error of forecasted wind /wave condition vector

$\Delta\hat{\underline{W}}_i$  : error of forecasted ocean current vector

Since the forecast errors  $\Delta\hat{\underline{C}}_i$  and  $\Delta\hat{\underline{W}}_i$  may be regarded as Gaussian random vectors, (2.33) and (2.38) become stochastic difference equations. The statistical characteristics of  $\Delta\hat{\underline{C}}_i$  and  $\Delta\hat{\underline{W}}_i$  are determined by their mean values and covariance matrices.

The mean values ( i.e. expected values ) of  $\Delta\hat{\underline{C}}_i$  and  $\Delta\hat{\underline{W}}_i$  are usually called the mean errors, which denote the statistical biases of the forecasted values against the actual values:

$$E[\Delta\hat{\underline{C}}_i] = E[ \underline{C}_i - \hat{\underline{C}}_i ] \quad (2.41)$$

$$E[\Delta\hat{\underline{W}}_i] = E[ \underline{W}_i - \hat{\underline{W}}_i ] \quad (2.42)$$

where  $E[\Delta\hat{\underline{C}}_i]$  : mean error of forecasted wind/wave condition vector

$E[\Delta\hat{\underline{W}}_i]$  : mean error of forecasted ocean current vector

where  $E$  is an operator representing the expected value ( i.e. ensemble average ).

Thus the unbiased forecast values ( i.e. mean values ) of wind/wave condition vector and ocean current vector are given by



$$\underline{\bar{C}}_i = \underline{\hat{C}}_i + E[\Delta \underline{\hat{C}}_i] \quad (2.43)$$

$$\underline{\bar{W}}_i = \underline{\hat{W}}_i + E[\Delta \underline{\hat{W}}_i] \quad (2.44)$$

where  $\underline{\bar{C}}_i$  : unbiased forecast value of wind/wave condition vector  
 $\underline{\bar{W}}_i$  : unbiased forecast value of ocean current vector

In the weather routing simulations in this thesis, the unbiased forecast values  $\underline{\bar{C}}_i$  and  $\underline{\bar{W}}_i$  are used instead of the biased forecast values  $\underline{\hat{C}}_i$  and  $\underline{\hat{W}}_i$ . Hereafter, we call  $\underline{\bar{C}}_i$  and  $\underline{\bar{W}}_i$  the unbiased wind/wave forecast vector and the unbiased ocean current forecast vector, respectively.

Using the unbiased forecasts  $\underline{\bar{C}}_i$  and  $\underline{\bar{W}}_i$  and their errors, the actual values  $\underline{C}_i$  and  $\underline{W}_i$  can be written as

$$\underline{C}_i = \underline{\bar{C}}_i + \Delta \underline{C}_i \quad (2.45)$$

$$\underline{W}_i = \underline{\bar{W}}_i + \Delta \underline{W}_i \quad (2.46)$$

where  $\Delta \underline{C}_i$  : error of unbiased wind/wave forecast vector  
 $\Delta \underline{W}_i$  : error of unbiased ocean current forecast vector

The errors  $\Delta \underline{C}_i$  and  $\Delta \underline{W}_i$  are considered to be Gaussian random vectors with zero mean values. The covariance matrices of  $\Delta \underline{C}_i$  and  $\Delta \underline{W}_i$  are given as

$$P_c(i) = E[ \Delta \underline{C}_i \Delta \underline{C}_i^T ] \quad (2.47)$$

$$P_w(i) = E[ \Delta \underline{W}_i \Delta \underline{W}_i^T ] \quad (2.48)$$

where  $P_c(i)$  : covariance matrix of the error of the unbiased wind/wave forecast vector  
 $P_w(i)$  : covariance matrix of the error of the unbiased ocean current forecast vector

The mean errors of forecasted wind/wave and ocean current vector as well as the covariance matrices of the errors of the unbiased wind/wave and ocean current forecast vector are functions of the forecast period and location in the ocean. Those values can be

calculated at each grid point for the forecasts by comparing the forecasted values with the actual ( true or analyzed ) values over a long period.

Then using (2.43), (2.44) and the interpolation procedure, the unbiased forecasts  $\bar{C}_i$ ,  $\bar{W}_i$  and the covariance matrices  $P_c(i)$ ,  $P_w(i)$  at the ship's position at time  $t_i$  can be obtained.

Now, representing each variable in (2.33), (2.35) and (2.38) as the sum of the predicted value ( i.e. expected value or mean value ) and its error, and expanding the functions  $f$ ,  $S$  and  $G$  in a Taylor series around the predicted values, then retaining terms only of first order, we have

$$\bar{X}_{i+1} + \Delta X_{i+1} = f(\bar{X}_i, \bar{S}_i, \bar{W}_i, \theta_i) + f_x \Delta X_i + f_s \Delta S_i + f_w \Delta W_i \quad (2.49)$$

$$\bar{S}_i + \Delta S_i = S(\bar{C}_i, \theta_i, n_i) + S_c \Delta C_i \quad (2.50)$$

$$\bar{F}_{i+1} + \Delta F_{i+1} = \bar{F}_i + \Delta F_i + G(\bar{V}_i, n_i) + G_v \Delta V_i \quad (2.51)$$

where  $\bar{X}_i$ ,  $\bar{X}_{i+1}$ ,  $\bar{S}_i$ ,  $\bar{F}_i$  and  $\bar{F}_{i+1}$  denote the predicted values, and  $\Delta X_i$ ,  $\Delta X_{i+1}$ ,  $\Delta S_i$ ,  $\Delta F_i$  and  $\Delta F_{i+1}$  denote the errors of predicted values which have Gaussian distributions with zero mean values. The partial derivatives  $f_x$ ,  $f_s$ ,  $f_w$ ,  $S_c$  and  $G_v$  ( i.e.  $\partial f / \partial X_i$ ,  $\partial f / \partial S_i$ ,  $\partial f / \partial W_i$ ,  $\partial S / \partial C_i$  and  $\partial G / \partial V_i$  ) are calculated using the predicted values at time  $t_i$ .

Taking expectations on both sides of (2.49), (2.50) and (2.51) yields

$$\bar{X}_{i+1} = f(\bar{X}_i, \bar{S}_i, \bar{W}_i, \theta_i) \quad (2.52)$$

$$\bar{S}_i = S(\bar{C}_i, \theta_i, n_i) \quad (2.53)$$

$$\bar{F}_{i+1} = \bar{F}_i + G(\bar{V}_i, n_i) \quad (2.54)$$

From (2.52), (2.53) and (2.54), the predicted ship's position  $\bar{X}_i$  at  $t_i$  (  $i = 0, 1, \dots$  ) and the predicted value of accumulated fuel consumption  $\bar{F}_i$  between  $t_0$  and  $t_i$  (  $i = 0, 1, \dots$  ) can be obtained.

Next, substituting (2.52), (2.53) and (2.54) into (2.49), (2.50) and (2.51), we have the following error equations:

$$\Delta \underline{X}_{i+1} = f_x \Delta \underline{X}_i + f_s \Delta \underline{S}_i + f_w \Delta \underline{W}_i \quad (2.55)$$

$$\Delta \underline{S}_i = S_c \Delta \underline{C}_i \quad (2.56)$$

$$\Delta \underline{F}_{i+1} = \Delta \underline{F}_i + G_v \Delta \underline{V}_i \quad (2.57)$$

In general, there exists a correlation between the error of the wind/wave conditions  $\Delta \underline{C}_i$  and  $\Delta \underline{C}_{i+1}$ , and between the error of the ocean current  $\Delta \underline{W}_i$  and  $\Delta \underline{W}_{i+1}$ . Thus we regard  $\Delta \underline{C}_i$  and  $\Delta \underline{W}_i$  ( $i = 0, 1, \dots$ ) as Gauss-Markov random sequences produced by the following shaping filters:

$$\Delta \underline{C}_{i+1} = \Phi_c(i) \Delta \underline{C}_i + \Delta \underline{C}_{i+1}^* \quad (2.58)$$

$$\Delta \underline{W}_{i+1} = \Phi_w(i) \Delta \underline{W}_i + \Delta \underline{W}_{i+1}^* \quad (2.59)$$

where  $\Delta \underline{C}_{i+1}^*$  and  $\Delta \underline{W}_{i+1}^*$  ( $i = 0, 1, \dots$ ) are Gaussian purely random sequences (i.e. Gaussian white sequences) with zero mean values;  $\Phi_c(i)$  and  $\Phi_w(i)$  are normalized correlation matrices representing the degree of correlation.

In the above shaping filters,  $\Phi_c(i)$  and  $\Phi_w(i)$  are assumed to be diagonal matrices. The diagonal terms of  $\Phi_c(i)$  and  $\Phi_w(i)$  are calculated by

$$\Phi_c(i)_j = E[ \Delta \underline{C}_{i+1} \Delta \underline{C}_i^T ]_j / P_c(i)_j \quad (j = 1, 2, \dots, 8) \quad (2.60)$$

$$\Phi_w(i)_j = E[ \Delta \underline{W}_{i+1} \Delta \underline{W}_i^T ]_j / P_w(i)_j \quad (j = 1, 2) \quad (2.61)$$

where subscript  $j$  denotes the  $j$ -th diagonal term of a matrix.

The correlation matrices are functions of the forecast period, ship's position, ship's course and travelled distance during  $\Delta t'$  hours. They can be calculated at each grid point for the forecasts by comparing the forecasted values with the actual (analyzed) values over a long period.

Then carrying out interpolation, the correlation matrices  $\Phi_c(i)$



and  $\Phi_w(i)$  for the predicted ship's position at time  $t_i$ , ship's course and predicted travelled distance between  $t_i$  and  $t_{i+1}$  can be obtained.

Combining equations (2.55) through (2.59), we have the following error equation in vector form:

$$\begin{bmatrix} \Delta \underline{X}_{i+1} \\ \Delta \underline{F}_{i+1} \\ \Delta \underline{C}_{i+1} \\ \Delta \underline{W}_{i+1} \end{bmatrix} = \begin{bmatrix} f_x & 0 & f_s S_c & f_w \\ 0 & 1 & G_v V_c & 0 \\ 0 & 0 & \Phi_c(i) & 0 \\ 0 & 0 & 0 & \Phi_w(i) \end{bmatrix} \begin{bmatrix} \Delta \underline{X}_i \\ \Delta \underline{F}_i \\ \Delta \underline{C}_i \\ \Delta \underline{W}_i \end{bmatrix} + \begin{bmatrix} 0 & 0 \\ 0 & 0 \\ I & 0 \\ 0 & I \end{bmatrix} \begin{bmatrix} \Delta \underline{C}^*_{i+1} \\ \Delta \underline{W}^*_{i+1} \end{bmatrix} \quad (2.62)$$

where  $I$  denotes an identity matrix.

Using the error vectors and matrices having augmented dimensions, we simply write (2.62) as

$$\Delta \underline{Y}_{i+1} = A_i \Delta \underline{Y}_i + B \Delta \underline{Z}^*_{i+1} \quad (2.63)$$

where  $\Delta \underline{Y}_i = [ \Delta \underline{X}_i^T \quad \Delta \underline{F}_i \quad \Delta \underline{C}_i^T \quad \Delta \underline{W}_i^T ]^T$

$$\Delta \underline{Z}^*_{i+1} = [ \Delta \underline{C}^*_{i+1}^T \quad \Delta \underline{W}^*_{i+1}^T ]^T$$

$A_i$  :  $13 \times 13$  matrix comprised of the partial derivatives  
and the correlation matrices

$B$  :  $13 \times 10$  constant matrix

The covariance matrix  $P_{i+1}$  of the error vector  $\Delta \underline{Y}_{i+1}$  is given by

$$P_{i+1} = A_i P_i A_i^T + B Q_{i+1} B^T \quad (i = 0, 1, \dots) \quad (2.64)$$

where  $P_i$  and  $Q_{i+1}$  are the covariance matrices of  $\Delta \underline{Y}_i$  and  $\Delta \underline{Z}^*_{i+1}$ , respectively;  $Q_{i+1}$  is calculated as

$$Q_{i+1} = \begin{bmatrix} P_c(i+1) - \Phi_c(i) P_c(i) \Phi_c(i)^T & 0 \\ 0 & P_w(i+1) - \Phi_w(i) P_w(i) \Phi_w(i)^T \end{bmatrix} \quad (i = 0, 1, \dots) \quad (2.65)$$

The covariance matrices  $P_c(i)$ ,  $P_w(i)$  and the correlation matrices  $\Phi_c(i)$ ,  $\Phi_w(i)$  (  $i = 0, 1, \dots$  ) are calculated at the predicted ship's position  $\bar{X}_i$  determined by (2.52). In formula (2.64), the initial covariance matrix  $P_0$  is given at the departure point.

The upper-left  $2 \times 2$  partitioned matrix of  $P_{i+1}$  represents the covariance matrix of the ship's position  $\bar{X}_{i+1}$ , and the third diagonal term of  $P_{i+1}$  represents the variance of accumulated fuel consumption  $F_{i+1}$ .

Thus we can determine the covariance matrix of a ship's position  $P_x(i)$  at time  $t_i$  (  $i = 0, 1, \dots$  ) and the variance of the accumulated fuel consumption  $\sigma_F(i)^2$  between  $t_0$  and  $t_i$  (  $i = 0, 1, \dots$  ). In addition, the standard error ellipse of a ship's position  $\bar{X}_i$  can be obtained by calculating the eigenvalues and eigenvectors of  $P_x(i)$ ; see Appendix 6.

## (II) Estimation of the standard deviations of passage time and total fuel consumption

Suppose that the predicted ship's position  $\bar{X}_n$  at time  $t_n$  (  $= t_0 + n\Delta t'$  ) approaches the destination  $\bar{X}_f$  sufficiently. ( These  $\bar{X}_n$  and  $t_n$  correspond to  $\bar{X}_{nr}$  and  $t_n + r\Delta t'$  mentioned in subsection 2.3.1. )

The passage time  $T_n$  between  $\bar{X}_n$  and  $\bar{X}_f$  is given by

$$T_n = D_r / V_{og} \quad (2.66)$$

where  $D_r$  : rhumbline distance between  $\bar{X}_n$  and  $\bar{X}_f$   
 $V_{og}$  : ship's speed over the ground at  $t_n$

$D_r$  and  $V_{og}$  can be calculated with Mercator's sailing as shown in (2.23), (2.24) and (2.25).

From (2.23), (2.24) and (2.25), it is found that  $T_n$  is a function of the vectors  $\bar{X}_n$ ,  $\bar{S}_n$  and  $\bar{W}_n$ ; thus  $T_n$  may be written as

$$T_n = T(\bar{X}_n, \bar{S}_n, \bar{W}_n) \quad (2.67)$$

Therefore, the passage time  $T$  between departure point  $\underline{X}_0$  and destination  $\underline{X}_f$  is represented as

$$T = n \Delta t' + T(\underline{X}_n, \underline{S}_n, \underline{W}_n) \quad (2.68)$$

where  $n \Delta t'$  is a deterministic quantity, whereas  $\underline{X}_n$ ,  $\underline{S}_n$  and  $\underline{W}_n$  are Gaussian random vectors.

Next, the fuel consumption  $G_n$  between  $\underline{X}_n$  and  $\underline{X}_f$  may be written as

$$G_n = G(V_n, n_n, T_n) \quad (2.69)$$

Hence the total fuel consumption  $F$  between  $\underline{X}_0$  and  $\underline{X}_f$  is given by

$$F = F_n + G(V_n, n_n, T_n) \quad (2.70)$$

where the number of propeller revolutions  $n_n$  is a deterministic control variable, whereas  $V_n$ ,  $T_n$  and  $F_n$  are random variables.

Now, representing each variable in (2.68) and (2.70) as the sum of the predicted value ( i.e. mean value ) and its error, and expanding the functions  $T(\underline{X}_n, \underline{S}_n, \underline{W}_n)$  and  $G(V_n, n_n, T_n)$  in a Taylor series around the predicted values, then retaining terms only of first order, we have

$$\bar{T} + \Delta T = n \Delta t' + T(\bar{\underline{X}}_n, \bar{\underline{S}}_n, \bar{\underline{W}}_n) + T_x \Delta \underline{X}_n + T_s \Delta \underline{S}_n + T_w \Delta \underline{W}_n \quad (2.71)$$

$$\bar{F} + \Delta F = \bar{F}_n + \Delta F_n + G(\bar{V}_n, n_n, \bar{T}_n) + G_v \Delta V_n + G_T \Delta T_n \quad (2.72)$$

where  $\bar{\underline{X}}_n$ ,  $\bar{\underline{S}}_n$ ,  $\bar{\underline{W}}_n$ ,  $\bar{T}_n$ ,  $\bar{T}$ ,  $\bar{F}_n$  and  $\bar{F}$  denote the predicted values, and  $\Delta \underline{X}_n$ ,  $\Delta \underline{S}_n$ ,  $\Delta \underline{W}_n$ ,  $\Delta T_n$ ,  $\Delta T$ ,  $\Delta F_n$  and  $\Delta F$  denote the errors of the predicted values which have Gaussian distributions with zero mean values; it should be noted that  $\Delta T_n = \Delta T$ . The partial derivatives  $T_x$ ,  $T_s$ ,  $T_w$ ,  $G_v$  and  $G_T$  ( i.e.  $\partial T / \partial \underline{X}_n$ ,  $\partial T / \partial \underline{S}_n$ ,  $\partial T / \partial \underline{W}_n$ ,  $\partial G / \partial V_n$  and  $\partial G / \partial T_n$  ) are calculated using the predicted values at time  $t_n$ .

Taking expectations on both sides of (2.71) and (2.72) yields



$$\bar{T} = n \Delta t' + T(\bar{X}_n, \bar{S}_n, \bar{W}_n) \quad (2.73)$$

$$\bar{F} = \bar{F}_n + G(\bar{V}_n, n_n, \bar{T}_n) \quad (2.74)$$

From (2.73) and (2.74), the predicted passage time  $\bar{T}$  and the predicted total fuel consumption  $\bar{F}$  can be determined.

Next, substituting (2.73) and (2.74) into (2.71) and (2.72), we have the following error equations:

$$\Delta T = T_x \Delta X_n + T_s \Delta S_n + T_w \Delta W_n \quad (2.75)$$

$$\Delta F = \Delta F_n + G_v \Delta V_n + G_T \Delta T \quad (2.76)$$

Representing the errors of predicted wind/wave conditions and predicted ocean current at the destination as  $\Delta C_f$  and  $\Delta W_f$ , respectively, we regard them as the outputs of the following shaping filters:

$$\Delta C_f = \Phi_c(n) \Delta C_n + \Delta C^*_f \quad (2.77)$$

$$\Delta W_f = \Phi_w(n) \Delta W_n + \Delta W^*_f \quad (2.78)$$

Combining the error equations (2.75) and (2.76) with the shaping filters (2.77) and (2.78), we have the following error equation in vector form:

$$\begin{bmatrix} \Delta T \\ \Delta F \\ \Delta C_f \\ \Delta W_f \end{bmatrix} = \begin{bmatrix} T_x & 0 & T_s S_c & T_w \\ G_T T_x & 1 & G_v V_c + G_T T_s S_c & G_T T_w \\ 0 & 0 & \Phi_c(n) & 0 \\ 0 & 0 & 0 & \Phi_w(n) \end{bmatrix} \begin{bmatrix} \Delta X_n \\ \Delta F_n \\ \Delta C_n \\ \Delta W_n \end{bmatrix} + \begin{bmatrix} 0 & 0 \\ 0 & 0 \\ I & 0 \\ 0 & I \end{bmatrix} \begin{bmatrix} \Delta C^*_f \\ \Delta W^*_f \end{bmatrix} \quad (2.79)$$

Using the error vectors and matrices having augmented dimensions, we simply write (2.79) as

$$\Delta Y_f = A_n \Delta Y_n + B \Delta Z^*_f \quad (2.80)$$

where

$$\Delta \underline{Y}_f = [ \Delta T \quad \Delta F \quad \Delta \underline{C}_f^T \quad \Delta \underline{W}_f^T ]^T$$

$$\Delta \underline{Y}_n = [ \Delta \underline{X}_n^T \quad \Delta F_n \quad \Delta \underline{C}_n^T \quad \Delta \underline{W}_n^T ]^T$$

$$\Delta \underline{Z}_f^* = [ \Delta \underline{C}_f^{*T} \quad \Delta \underline{W}_f^{*T} ]^T$$

$A_n$  :  $12 \times 13$  matrix comprised of the partial derivatives  
and the correlation matrices  
 $B$  :  $12 \times 10$  constant matrix

Note that  $\Delta \underline{Y}_n$  is a 13-dimensional vector, whereas  $\Delta \underline{Y}_f$  is a 12-dimensional vector.

The covariance matrix  $P_f$  of the error vector  $\Delta \underline{Y}_f$  is given by

$$P_f = A_n P_n A_n^T + B Q_f B^T \quad (2.81)$$

where  $P_n$  and  $Q_f$  are the covariance matrices of  $\Delta \underline{Y}_n$  and  $\Delta \underline{Z}_f^*$ , respectively;  $Q_f$  is calculated as

$$Q_f = \begin{bmatrix} P_c(f) - \Phi_c(n) P_c(n) \Phi_c(n)^T & 0 \\ 0 & P_w(f) - \Phi_w(n) P_w(n) \Phi_w(n)^T \end{bmatrix} \quad (2.82)$$

From equation (2.81), the variance of the passage time  $\sigma_T^2$  and the variance of the total fuel consumption  $\sigma_F^2$  are obtained as the first and the second diagonal term of the covariance matrix  $P_f$ , respectively.

Based on the above-mentioned procedure, we can estimate the predicted passage time  $\bar{T}$  and its standard deviation  $\sigma_T$  as well as the predicted total fuel consumption  $\bar{F}$  and its standard deviation  $\sigma_F$ .

Since the errors of passage time and total fuel consumption have Gaussian distributions in the above derivation, their 95% (99%) confidence intervals are given as 3.92 (5.16) times their standard deviations.

(III) Estimation of the standard deviation of average speed

In weather routing simulations, the average speed for the voyage is often calculated to evaluate the average encountered environmental conditions. The average speed  $V$  is calculated as

$$V = D / T \quad (2.83)$$

where  $D$  : total travelled distance

$T$  : passage time

The total travelled distance  $D$  can be obtained by accumulating the travelled distance for sub-time-interval  $\Delta t'$ .

Now, representing each variable in (2.83) as the sum of the predicted value ( i.e. mean value ) and its error, and expanding the right-hand side of (2.83) in a Taylor series around the predicted values, then retaining terms only of first order, we have

$$\bar{V} + \Delta V = \bar{D} / \bar{T} + \Delta D / \bar{T} - \Delta T \bar{D} / \bar{T}^2 \quad (2.84)$$

where  $\bar{D}$ ,  $\bar{T}$  and  $\bar{V}$  denote the predicted values, and  $\Delta D$ ,  $\Delta T$  and  $\Delta V$  denote the errors of the predicted values which have Gaussian distributions with zero mean values.

Taking expectations on both sides of (2.84) yields

$$\bar{V} = \bar{D} / \bar{T} \quad (2.85)$$

From (2.85), the predicted average speed  $\bar{V}$  can be determined.

Substituting (2.85) into (2.84), we have the following error equation:

$$\Delta V = \Delta D / \bar{T} - \Delta T \bar{D} / \bar{T}^2 \quad (2.86)$$

When the ship is navigated following the given sequences of the ship's headings  $\theta_i$  and the number of propeller revolutions  $n_i$  (  $i = 0, 1, \dots, n$  ), the first term on the right-hand side of (2.86) is, in



general, considerably smaller than the second term. This is because the difference in distance is generally smaller than the difference in passage time on tracks near the optimum track.

Therefore, neglecting the first term of (2.86) from a practical viewpoint, the standard deviation of average speed is computed by the following formula:

$$\sigma_v = \sigma_T \bar{D} / \bar{T}^2 \quad (2.87)$$

where  $\sigma_v$  : standard deviation of average speed  
 $\sigma_T$  : standard deviation of passage time

#### 2.4.2 Stochastic minimum time routing

In carrying out minimum time routing taking into account the uncertainties of environmental forecasts, not only the predicted passage time  $\bar{T}$  but also its standard deviation  $\sigma_T$  becomes an important factor to determine the optimum route.

That is, we sometimes meet the case that a route passing through a high wave area provides the minimum  $\bar{T}$  but a large  $\sigma_T$ , whereas an alternative route passing through a calm area ( but making a large detour ) provides a slightly larger  $\bar{T}$  but a considerably smaller  $\sigma_T$ . Such a situation often occurs when a sharp bending point ( double point ) of the final isochrone is located near the destination. In that case, most shipmasters will adopt the latter route as an optimum route by reason of good predictability of the arrival time.

In this subsection, the algorithm of minimum time routing by the modified isochrone method mentioned in 2.3.1 is combined with the algorithm to estimate the standard deviation of passage time stated in 2.4.1. Then, taking into consideration both the predicted passage time and its standard deviation, the algorithm to determine the minimum time route from a stochastic point of view is proposed.

Consider a ship leaving departure point  $\underline{X}_0$  at time  $t_0$  and sailing to destination  $\underline{X}_f$  with maximum ( constant ) number of propeller revolutions.

The proposed algorithm of the stochastic minimum time routing is as follows.

(i) Set up the following objective function  $J$ :

$$J = \bar{T} + w \sigma_T \quad (2.88)$$

where  $\bar{T}$  : predicted passage time

$\sigma_T$  : standard deviation of passage time

$w$  : weighting coefficient for the uncertainty of passage time

(ii) Calculate the isochrones  $\{\underline{X}_i(k)\}$  (  $i = 1, 2, \dots, n$  ) using the modified isochrone method. Then, based on the algorithm to estimate  $\bar{T}$ ,  $\sigma_T$ , etc. described in subsection 2.4.1, compute  $J$  given by (2.88) for all the routes reaching  $\underline{X}_f$  from  $\underline{X}_0$  via  $\underline{X}_n(k)$  (  $k = 1, 2, \dots, 2p$  ) of the final isochrone  $\{\underline{X}_n(k)\}$ , and represent them by  $J(k)$ .

Find the minimum value of  $J(k)$ , and represent it by  $J^*_{min}$ :

$$J^*_{min} = \min_k \{ J(k) \} \quad (2.89)$$

(iii) Adopt the route giving  $J^*_{min}$  as a minimum time route in the stochastic sense.

The value of the weighting coefficient  $w$  for  $\sigma_T$  depends how much penalty the shipmaster assigns to the uncertainty of the arrival time.

### 2.4.3 Stochastic minimum fuel routing

The same way as mentioned in stochastic minimum time routing, not only the predicted fuel consumption  $\bar{F}$  but also its standard deviation  $\sigma_F$  becomes an important factor to find the optimum solution for the stochastic minimum fuel routing.

That is, it may occur that a certain route provides the minimum  $\bar{F}$  but a large  $\sigma_F$  for the specified passage time, whereas an alternative route provides a slightly larger  $\bar{F}$  but a considerably smaller  $\sigma_F$ . In such a case, it may be wiser to adopt the latter as an optimum route from the viewpoint of good predictability of fuel consumption, because this will reduce the amount of bunkers to be loaded.

In this subsection, combining the algorithm of minimum fuel routing by the modified isochrone method described in 2.3.2 with the algorithm to estimate the standard deviations of the passage time and fuel consumption described in 2.4.1, the algorithm to determine the minimum fuel route from a stochastic standpoint is proposed.

Suppose a ship leaving departure point  $X_0$  at time  $t_0$  and arriving at destination  $X_f$  at time  $t_f$ . The arrival time  $t_f$  is specified as  $t_s$ .

In the actual voyage, however, the ship may not reach the destination at the specified arrival time  $t_s$  because of the uncertainties of the environmental forecasts. Therefore, it is reasonable to introduce the finite penalty for the expected delay of arrival into the objective function.

The algorithm of stochastic minimum fuel routing is as follows.

(i) Set up the following objective function J:

$$J = \bar{F} + w_1 \sigma_F + w_2 (\bar{t}_f - t_s)^2 \quad (2.90)$$

where  $\bar{F}$  : predicted total fuel consumption



$\sigma_F$  : standard deviation of total fuel consumption

$w_1$  : weighting coefficient for the uncertainty of fuel consumption

$\bar{t}_f$  : predicted arrival time

$t_s$  : specified arrival time

$w_2 (\bar{t}_f - t_s)^2$  : delay penalty

$w_2$  : weighting coefficient for delay penalty

$$w_2 > 0 \quad \text{if } \bar{t}_f > t_s$$

$$w_2 = 0 \quad \text{if } \bar{t}_f \leq t_s$$

(ii) Setting a suitable number of propeller revolutions  $n_0$ , calculate the isochrones  $\{\underline{X}_i(k)\}$  ( $i = 1, 2, \dots, n$ ) by using the modified isochrone method. Then, based on the algorithm to estimate  $\bar{T}$ ,  $\sigma_T$ ,  $\bar{F}$  and  $\sigma_F$ , compute  $J$  given by (2.90) for all the routes reaching  $\underline{X}_f$  from  $\underline{X}_0$  via  $\underline{X}_n(k)$  ( $k = 1, 2, \dots, 2p$ ) of the final isochrone  $\{\underline{X}_n(k)\}$ , and represent them by  $J(k)$ .

Find the minimum value of  $J(k)$ , and represent it by  $J^*(n_0)$  as a function of the number of propeller revolutions:

$$J^*(n_0) = \min_k \{ J(k) \} \quad (2.91)$$

(iii) Calculate  $J^*(n)$  for the various number of propeller revolutions  $n$ , i.e.  $n = n_0 \pm j\Delta n$  ( $j = 1, 2, \dots$ ) where  $\Delta n$  is the increment of the number of propeller revolutions.

Find the number of propeller revolutions  $n$  which minimizes  $J^*(n)$  and the minimum value of  $J^*(n)$ , and represent them by  $n^*$  and  $J^*_{min}$ , respectively:

$$J^*_{min} = \min_n \{ J^*(n) \} \quad (2.92)$$

(iv) Adopt  $n^*$  and the route giving  $J^*_{min}$  as the optimal number of propeller revolutions and the minimum fuel route in the stochastic sense, respectively.

The values of weighting coefficients  $w_1$  and  $w_2$  depend how much penalty the shipmaster assigns to the uncertainty of fuel consumption and the expected delay of arrival.

The above-mentioned algorithm for the stochastic minimum fuel routing is similar to the Algorithm (I) described in subsection 2.3.2. In order to obtain the accurate  $n^*$  and  $J^*_{min}$ , the number of propeller revolutions has to be searched finely by decreasing the increment  $\Delta n$  in the vicinity of the minimum value of the objective function.

## 2.5 GENERAL FORM OF THE OBJECTIVE FUNCTION FOR THE MODIFIED ISOCHRONE METHOD

The algorithms of the deterministic minimum time, fuel and cost routing based on the modified isochrone method were proposed in Section 2.3. Then those algorithms were extended so as to cope with the stochastic nature of environmental forecasts, and the algorithms of stochastic minimum time and fuel routing were proposed in Section 2.4.

In those algorithms, the values of the objective function  $J$  are computed for all the routes reaching the destination  $\underline{X}_f$  from the departure point  $\underline{X}_0$  via  $\underline{X}_n(k)$  (  $k = 1, 2, \dots, 2p$  ) of the final isochrone  $\{\underline{X}_n(k)\}$ , and the route giving minimum  $J$  is adopted as the optimum route.

In this section, the general form of the objective function for the modified isochrone is described taking into account all forementioned elements as well as the period of exposure to excessive ship's motions, shipping green water, slamming, etc..

The general form of the objective function  $J$  for the modified isochrone method is given as follows:

$$J = w_1 T + w_2 \sigma_T + w_3 F + w_4 \sigma_F + w_5 T_0 + w_6 (t_f - t_s)^2 \quad (2.93)$$

where  $T$  : ( predicted ) passage time  
 $\sigma_T$  : standard deviation of passage time  
 $F$  : ( predicted ) fuel consumption  
 $\sigma_F$  : standard deviation of fuel consumption  
 $T_0$  : ( predicted ) period of exposure to excessive ship's motions, shipping green water, slamming, etc.  
 $t_f$  : ( predicted ) arrival time  
 $t_s$  : specified ( or scheduled ) arrival time  
 $w_i$  : weighting coefficients (  $i = 1, 2, \dots, 6$  )

The weighting coefficients  $w_2$  and  $w_4$  are set to zero in deterministic routing, whereas appropriate values are used in stochastic routing based on the shipmaster's evaluation for the



uncertainties of arrival time and fuel consumption.

The weighting coefficient  $w_5$  represents how much the risk of damage due to rough seas is evaluated, and its value depends on the size and type of vessel, presence of deck cargo, risk appreciation of the shipmaster, etc..

The weighting coefficient  $w_6$  denotes how much the delay of arrival is evaluated, and its value is affected by the operation schedule of a berth at the destination, the degree of reduction of the benefit due to late arrival, etc..

By setting appropriate values to the weighting coefficients  $w_i$ , we can produce the objective functions for various kinds of ship routing as described below.

(i) Deterministic minimum time routing

$$J = T + w_5 T_D \quad (2.94)$$

where  $w_5$  : weighting coefficient for penalty of damage exposure

(ii) Deterministic minimum fuel routing

$$J = F + w_5 T_D + w_6 (t_f - t_s)^2 \quad (2.95)$$

$$w_6 = \infty \quad \text{if } t_f > t_s$$

$$w_6 = 0 \quad \text{if } t_f \leq t_s$$

(iii) Deterministic minimum cost routing

$$J = w_1 T + w_3 F + w_5 T_D + w_6 (t_f - t_s)^2 \quad (2.96)$$

where  $w_1$  : sum of the manning cost, insurance cost and all other fixed running cost per unit time

$w_3$  : fuel cost per unit weight

$w_6$  : delay penalty cost per unit time squared

$$w_6 > 0 \quad \text{if } t_f > t_s$$

$$w_6 = 0 \quad \text{if } t_f \leq t_s$$

(iv) Stochastic minimum time routing

$$J = T + w_2 \sigma_T + w_5 T_D \quad (2.97)$$

(v) Stochastic minimum fuel routing

$$J = F + w_4 \sigma_F + w_5 T_D + w_6 (t_f - t_s)^2 \quad (2.98)$$

$$\begin{aligned} w_6 &> 0 && \text{if } t_f > t_s \\ w_6 &= 0 && \text{if } t_f \leq t_s \end{aligned}$$

(vi) Stochastic minimum cost routing

The objective function  $J$  may have the form of (2.93).

As mentioned above, since the weighting coefficients  $w_i$  depend upon a number of factors, it may be difficult to determine the appropriate values of  $w_i$  for a particular voyage.

In practice, it is therefore proposed to calculate the values of  $T, \sigma_T, F, \sigma_F$  and  $T_D$  for all the routes reaching  $\underline{X}_f$  from  $\underline{X}_0$  via  $\underline{X}_n(k)$  of the final isochrone  $\{\underline{X}_n(k)\}$  and tabulate those values. Those tabulated data certainly provide valuable information to the shipmaster in order to make his own decision.

### 3. PREDICTION OF SPEED AND SEAKEEPING PERFORMANCE OF A (SAIL-ASSISTED) MOTOR VESSEL IN A SEAWAY

#### 3.1 INTRODUCTION

In order to perform an effective weather routing, accurate prediction of ship performance, i.e. the ship's speed, drift angle, engine power, etc. in a seaway, is essential.

Until now, for carrying out weather routing simulations, the ship's speed in waves has been represented by regression curves whose parameters are significant wave height, wave direction from the bow and engine power ( or number of propeller revolutions ). Those regression curves have been called speed performance curves, which can be obtained by theoretical calculations, towing tank tests or statistical analysis of the ships' log books.

In most speed performance curves, the ship's speed is represented as a function of only wave height and direction, and the effect of wind is not taken into account explicitly. Such a simplified representation of the ship's speed is considered acceptable in practice for conventional vessels because the added resistance due to waves is considerably larger than the wind resistance particularly in rough seas.

On sail-assisted motor vessels, however, since they utilize the wind as a part of the propulsive power by means of sails, the wind has to be considered as one of the essential environmental factors. ( The wind may also become an essential environmental factor for vessels which have large volumes above the water such as tankers in ballast condition, container ships with deck containers, pure car carriers, LNG ships, etc.. )

Furthermore, the wave period is usually not taken into account in the speed performance curves. However, since the added



resistance due to waves is largely affected by the encounter period of a ship to waves, the wave period has to be considered to predict the ship's speed accurately.<sup>(1)</sup>

Thus, in order to predict the speed of a sail-assisted motor vessel in a seaway accurately, we have to take into consideration the wind speed and wind direction as well as the significant wave height, predominant wave direction and average wave period as the environmental parameters. In case such many environmental parameters have to be considered, it becomes impossible to represent the ship's speed in the form of regression curves.

To meet the requirement for accurate prediction of the ship's speed performance, sophisticated methods have been developed mainly based on the studies of the Hydronautics section of the Department of Maritime Technology, Delft University of Technology. By using these methods, the ship's speed, drift angle ( leeway ), rudder angle, heel angle and engine power can be predicted based on the equilibrium equations for the forces and moments acting on the sail-assisted motor vessel in a seaway.

Because these prediction methods are repeatedly used several ten thousands of times in the weather routing simulation, not only the predicted values should be accurate but also the calculation speed should be sufficiently fast.

In this chapter, using a 40,000 DWT sail-assisted product tanker with 808 m<sup>2</sup> sail area as a mathematical model ship, the methods to predict the ship speed performance with sufficient accuracy and calculation speed are described, and some calculation results are shown.

Next, in the weather routing simulations, it is also necessary to predict the ship seakeeping performance, namely, the standard deviations of ship's motions in waves and probabilities of occurrence of accompanying phenomena such as shipping green water, slamming, propeller racing, etc.. ( These quantities were represented as the ship's motion vector M in 2.2.1. )

When those standard deviations or probabilities of occurrence

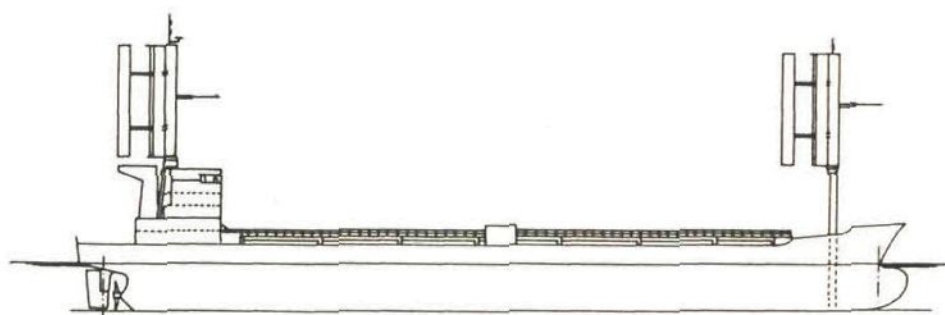
exceed critical values, the number of propeller revolutions ( or engine power ) has to be reduced to retain the safety of hull, cargo and crew. This intentional speed reduction for the safety of a ship is called voluntary speed reduction. ( On the other hand, the speed reduction caused by added resistance due to wind and waves is called natural speed reduction. )

The methods to predict the ship seakeeping performance and the ship operation criteria in rough seas for deciding voluntary speed reduction are also described in this chapter.

It has been pointed out that in calculating the ship's motions and speed of a sail-assisted motor vessel in a seaway, the sails have an effect to damp the ship's motions and consequently to reduce the added resistance due to waves. The quantitative studies on this phenomenon, however, have been hardly performed, and it is beyond the scope of this thesis to analyze this phenomenon in detail. Therefore the damping of the ship's motions and resultant reduction of added resistance due to waves by the use of sails are neglected in this thesis.

### 3.2 DESCRIPTION OF THE MATHEMATICAL MODEL SHIP

The mathematical model ship used for the weather routing simulations in this study is a 40,000 DWT sail-assisted product tanker with 808 m<sup>2</sup> sail area. A profile and main dimensions of this model ship are shown in Fig.3.1. Hereafter, the model ship is assumed to be in full loaded conditions, i.e. draught = 11.5 m, and even keel.



MAIN DIMENSIONS OF THE MODEL SHIP

Dead weight -----	40,000 t	Max. engine power ---	10,000 kW
Length between perp. ---	185.0 m	Total sail area -----	808 m <sup>2</sup>
Design draught -----	11.4 m	( Two tri-plane wingsails )	
Breadth moulded -----	32.0 m	Service speed -----	14 kn

Fig. 3.1 Profile and main dimensions of the model ship

As is found in Fig.3.1, the tri-plane wingsails are installed on the forecastle and the bridge of the model ship. These wingsails were provided by the Walker Wingsail Systems Ltd in England. <sup>(2)</sup>

This tri-plane wingsail consists of three wingsails and one tail vane which are mainly made of reinforced plastics, and its sail area is 404 m<sup>2</sup>. Each wingsail is constructed by a short chord leading section, i.e. a wing, a longer chord flap and an air director. When this wingsail receives wind, the flap and air director are adjusted as shown in Fig.3.2 so as to generate the large lift. The tri-plane wingsail possesses a lift coefficient of 3.3 and drag



coefficient 0.8.

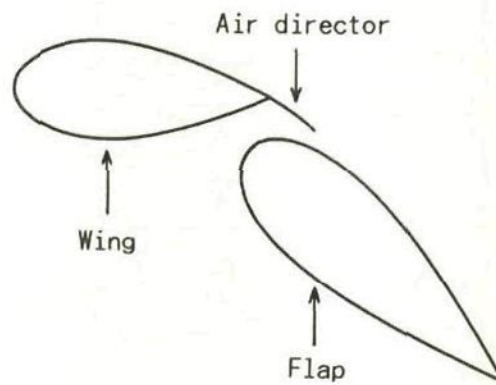


Fig. 3.2 Construction of wingsail

The two tri-plane wingsails on the forecastle and the bridge are controlled by a computer so that the maximum thrust may be obtained. The total performance of these two tri-plane wingsails is described in Section 3.4.

### 3.3 EQUILIBRIUM EQUATIONS FOR THE FORCES AND MOMENTS ACTING ON THE SHIP

For a sail-assisted motor vessel proceeding in a seaway at constant speed, the longitudinal forces, lateral forces, yawing moments and heeling moments acting on the ship should be balanced.

Representing the longitudinal forces, lateral forces, yawing moments and heeling moments about the center of gravity as  $X$ ,  $Y$ ,  $M$  and  $L$  respectively, the equilibrium equations for these forces and moments are given as follows: <sup>(1)</sup>, <sup>(3)</sup>, <sup>(4)</sup> ( Fig.3.3 )

$$X_S + X_A + X_H + X_R + X_W + X_P = 0 \quad (3.1)$$

$$Y_S + Y_A + Y_H + Y_R = 0 \quad (3.2)$$

$$M_S + M_A + M_H + M_R = 0 \quad (3.3)$$

$$L_S + L_A + L_H + L_R + L_B = 0 \quad (3.4)$$

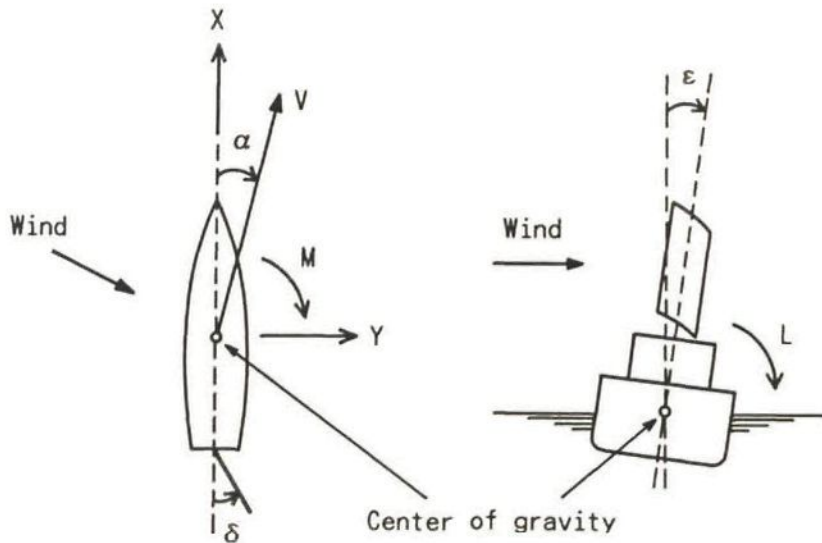


Fig. 3.3 Definitions of forces  $X$ ,  $Y$  and moments  $M$ ,  $L$  as well as ship's speed  $V$ , drift angle  $\alpha$ , rudder angle  $\delta$  and heel angle  $\epsilon$

where

$X_S, Y_S, M_S, L_S$  : aerodynamic forces and moments generated by sails

$X_A, Y_A, M_A, L_A$  : aerodynamic forces and moments due to hull and superstructure

$X_H, Y_H, M_H, L_H$  : hydrodynamic forces and moments due to hull

$X_R, Y_R, M_R, L_R$  : hydrodynamic forces and moments induced by rudder

$X_W$  : added resistance due to waves

$X_P$  : propeller thrust

$L_B$  : hydrostatic righting moment due to heel of hull

The signs of  $X, Y, M$  and  $L$  are defined as follows.

- \* The longitudinal force  $X$  is considered positive when directed from stern to bow.
- \* The lateral force  $Y$  is considered positive when directed away from the wind.
- \* The yawing moment  $M$  is considered positive when tending to turn the bow away from the wind.
- \* The heeling moment  $L$  is considered positive when tending to heel the hull leeward.

In the equilibrium equations (3.1) through (3.4), when the ship's heading, number of propeller revolutions, draught, trim and wind/wave conditions are given, each force and moment becomes a function of ship's speed through the water  $V$ , drift angle (leeway)  $\alpha$ , rudder angle  $\delta$ , and heel angle  $\varepsilon$ .

Therefore we can predict the ship's speed, drift angle, rudder angle and heel angle in a seaway by finding  $V, \alpha, \delta$  and  $\varepsilon$  which satisfy (3.1) through (3.4) simultaneously.

The signs of  $\alpha, \delta$  and  $\varepsilon$  are defined as follows.

- \* The drift angle  $\alpha$  is considered positive when the ship drifts leeward.
- \* The rudder angle  $\delta$  is considered positive when the rudder turns the bow away from the wind.
- \* The heel angle  $\varepsilon$  is considered positive when the hull heels leeward.



### 3.4 CALCULATION METHODS OF FORCES AND MOMENTS

Each force and moment in equilibrium equations (3.1) through (3.4) can be calculated by the following formulae.

#### (1) Aerodynamic forces and moments generated by the sails

The sail thrust  $X_s$ , sail lateral force  $Y_s$ , sail yawing moment  $M_s$  and sail heeling moment  $L_s$  are given by

$$X_s \approx 1/2 \rho_A C_{Xs} A_{sT} U_A^2 \quad (3.5)$$

$$Y_s \approx 1/2 \rho_A C_{Ys} A_{sT} U_A^2 \quad (3.6)$$

$$M_s \approx 1/2 \rho_A C_{Ys} \left\{ \sum_{i=1}^n A_s(i) D_s(i) \right\} U_A^2 \quad (3.7)$$

$$L_s \approx 1/2 \rho_A C_{Ys} \left\{ \sum_{i=1}^n A_s(i) H_s(i) \right\} U_A^2 \quad (3.8)$$

where  $\rho_A$  : density of air ( 1.22 kg/m<sup>3</sup> )

$C_{Xs}$  : sail thrust coefficient

$C_{Ys}$  : sail lateral force coefficient

$A_{sT}$  : total sail area

$U_A$  : apparent wind speed

$n$  : number of sails

$A_s(i)$  : area of i-th sail  $\sum_{i=1}^n A_s(i) = A_{sT}$

$D_s(i)$  : horizontal distance from the center of gravity to the center of effort of i-th sail

$H_s(i)$  : vertical distance from the center of gravity to the center of effort of i-th sail

The mathematical model ship shown in Fig.3.1 has the following values.

$$A_{sT} = 808.00 \text{ m}^2$$

$n = 2$                        $A_s(1) = A_s(2) = 404.00 \text{ m}^2$   
 Fore wingsail :  $D_s(1) = 80.27 \text{ m}$        $H_s(1) = 34.15 \text{ m}$   
 Aft wingsail :  $D_s(2) = -77.55 \text{ m}$        $H_s(2) = 36.55 \text{ m}$

The sail thrust coefficient  $C_{Xs}$  and sail lateral force coefficient  $C_{Ys}$  are functions of apparent wind direction from the bow  $\beta_A$ . The  $C_{Xs}$  and  $C_{Ys}$  versus  $\beta_A$  curves of the model ship are shown in Fig.3.4. In these curves, the interaction between sails and hull as well as the interaction between fore wingsail and aft wingsail are taken into account.

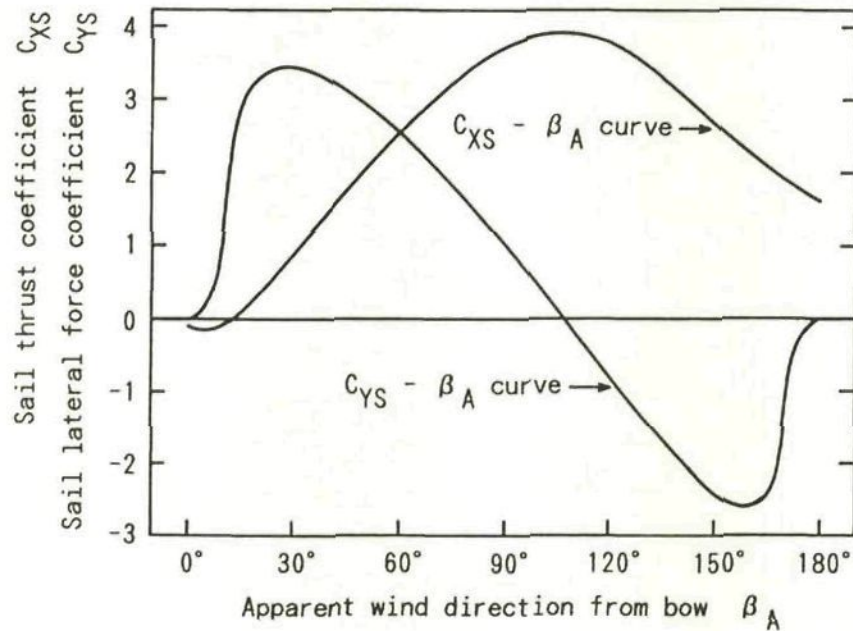


Fig. 3.4 Sail thrust coefficient and sail lateral force coefficient versus apparent wind direction from bow

The maximum value of  $C_{Xs}$  reaches 3.9 at  $\beta_A = 105^\circ$ . As the maximum value of  $C_{Xs}$  of a conventional rigid square sail with laminar sections used for the Japanese sail-assisted motor vessels is about 1.7, it is found that the tri-plane wingsail installed on the model ship possesses a remarkably high performance.

Because the wingsail maintains an approximately constant attack angle to the wind ( $\approx 15^\circ$ ) for  $\beta_A$  between  $15^\circ$  and  $160^\circ$ , the sign

of  $C_{Y_S}$  becomes negative for  $\beta_A$  greater than  $105^\circ$ . For  $\beta_A \doteq 180^\circ$ , since the wingsail takes the attack angle of  $90^\circ$ ,  $C_{Y_S}$  becomes zero.

In stormy weather, it is necessary to protect the sails against an excessive aerodynamic force by reducing the attack angle of sail to the wind. In formulae (3.5) through (3.8), when  $U_A$  exceeds 20 m/sec,  $X_S$ ,  $Y_S$ ,  $M_S$  and  $L_S$  are assumed to be equal to the values for  $U_A = 20$  m/sec.

## (2) Aerodynamic forces and moments due to hull and superstructure

The aerodynamic resistance  $X_A$ , lateral force  $Y_A$ , yawing moment  $M_A$  and heeling moment  $L_A$  due to hull and superstructure are given by

$$X_A = -1/2 \rho_A C_{XA} A_T U_A^2 \quad (3.9)$$

$$Y_A = 1/2 \rho_A C_{YA} A_L U_A^2 \quad (3.10)$$

$$M_A = 1/2 \rho_A C_{MA} A_L L_{OA} U_A^2 \quad (3.11)$$

$$L_A = Y_A H_A \quad (3.12)$$

where  $\rho_A$  : density of air  
 $C_{XA}$  : fore and aft wind force coefficient  
 $C_{YA}$  : lateral wind force coefficient  
 $C_{MA}$  : yawing moment coefficient

$A_T$  : transverse projected area of the above-water part  
 ( excluding sails )  
 $A_L$  : lateral projected area of the above-water part  
 ( excluding sails )  
 $L_{OA}$  : length overall of ship  
 $U_A$  : apparent wind speed  
 $H_A$  : vertical distance from the center of gravity to the  
 center of lateral projected area of the above-water  
 part excluding sails

The mathematical model ship has the following values.



$$A_T = 560.00 \text{ m}^2$$

$$A_L = 1400.0 \text{ m}^2$$

$$L_{OA} = 197.00 \text{ m}$$

$$H_A = 3.02 \text{ m}$$

The coefficients  $C_{XA}$ ,  $C_{YA}$  and  $C_{MA}$  are functions of the apparent wind direction from the bow  $\beta_A$ , and were calculated based on the Isherwood method.<sup>(5)</sup> The  $C_{XA}$ ,  $C_{YA}$  and  $C_{MA}$  versus  $\beta_A$  curves of the model ship are shown in Fig.3.5.

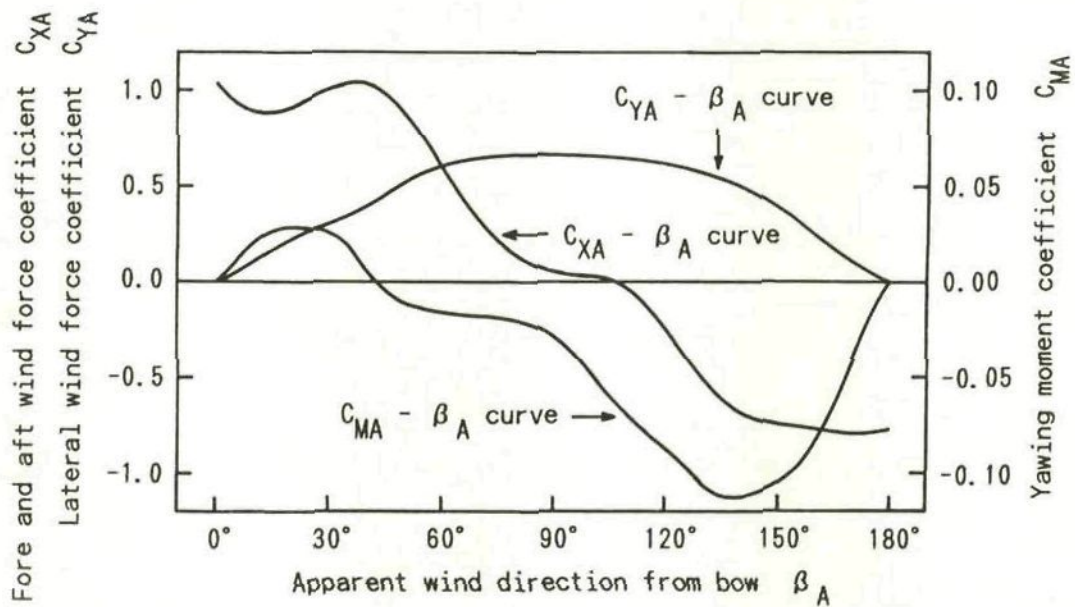


Fig. 3.5 Fore and aft wind force coefficient, lateral wind force coefficient and yawing moment coefficient versus apparent wind direction from bow

### (3) Hydrodynamic forces and moments due to the hull

The hydrodynamic resistance  $X_H$ , lateral force  $Y_H$ , yawing moment  $M_H$  and heeling moment  $L_H$  due to the hull under water are given as <sup>(6)</sup>

$$X_H = -1/2 \rho_w \{ C_v S + C_{XH} L d \} V^2 \quad (3.13)$$

$$Y_H = -1/2 \rho_w C_{YH} L d V^2 \quad (3.14)$$

$$M_H = -1/2 \rho_w C_{MH} L^2 d V^2 \quad (3.15)$$

$$L_H = Y_H H_H \quad (3.16)$$

where  $\rho_w$  : density of sea water ( 1025.0 kg/m<sup>3</sup> )  
 $C_v$  : still water resistance coefficient ( for no drift )  
 $C_{xH}$  : added resistance coefficient for drift  
 $C_{yH}$  : hydrodynamic lateral force coefficient  
 $C_{MH}$  : hydrodynamic yawing moment coefficient

$S$  : wetted surface of ship's hull  
 $L$  : waterline length of ship  
 $d$  : draught of ship  
 $H_H$  : vertical distance from the center of gravity to the  
center of water pressure acting on the hull

The model ship has the following values.

$$\begin{aligned} S &= 8598.00 \text{ m}^2 \\ L &= 187.31 \text{ m} \quad d = 11.50 \text{ m} \\ H_H &= -6.47 \text{ m} \end{aligned}$$

The still water resistance coefficient  $C_v$  consists of the coefficients representing the frictional resistance, residuary resistance, etc., and is a function of ship's speed, draught and trim. Fig.3.6 shows the still water resistance of the model ship as a function of ship's speed.

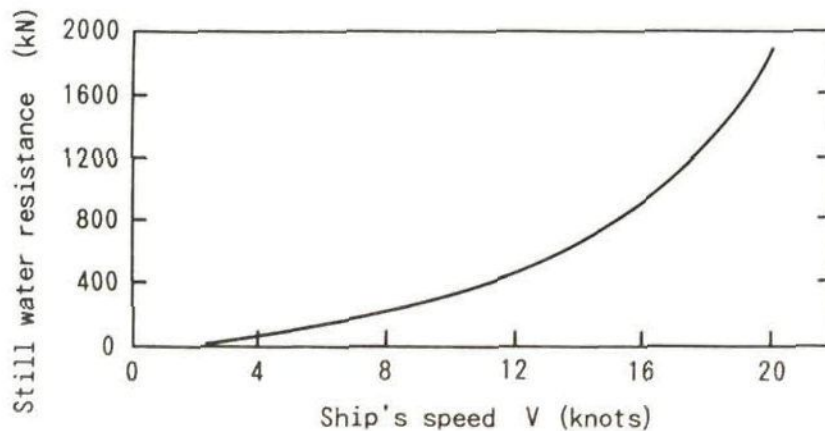


Fig. 3.6 Still water resistance versus ship's speed

The added resistance coefficient for drift  $C_{XH}$  of the model ship, i.e. tanker type ship, may be expressed as a function of the drift angle  $\alpha$  (radian) as follows: <sup>(7)</sup>

$$C_{XH} = 0.044 \alpha^2 \quad (3.17)$$

The coefficients  $C_{YH}$  and  $C_{MH}$  are also functions of drift angle  $\alpha$  (radian), and can be approximated by <sup>(8)</sup>

$$C_{YH} = K_1 \alpha + K_2 \alpha |\alpha| \quad (3.18)$$

$$C_{MH} = \frac{2d}{L} \alpha \quad (3.19)$$

where

$$K_1 = \frac{\pi d}{L} + 1.4 C_B \frac{B}{L} \quad (3.20)$$

$$K_2 = 6.6 (1 - C_B) \frac{d}{B} - 0.08 \quad (3.21)$$

where  $C_B$  : block coefficient  
 $B$  : breadth of ship

$C_B$  and  $B$  of the model ship are 0.79 and 32.00 m, respectively.

#### (4) Hydrodynamic forces and moments induced by the rudder

The hydrodynamic resistance  $X_R$ , lateral force  $Y_R$ , yawing moment  $M_R$  and heeling moment  $L_R$  induced by the rudder are given as follows: <sup>(6)</sup>

$$X_R = - F_N \sin \delta \quad (3.22)$$

$$Y_R = - (1 + a_H) F_N \cos \delta \quad (3.23)$$

$$M_R = - (D_R + a_H D_{HR}) F_N \cos \delta \quad (3.24)$$

$$L_R = - (H_R + a_H H_{HR}) F_N \cos \delta \quad (3.25)$$

where  $\delta$  : rudder angle  
 $F_N$  : rudder normal force  
 $D_R$  : horizontal distance from the center of gravity to the



center of water pressure acting on the rudder  
 $H_R$  : vertical distance from the center of gravity to the  
 center of water pressure acting on the rudder

$D_R$  and  $H_R$  of the model ship are -93.06 m and -7.42 m, respectively.

The rudder normal force  $F_N$  can be approximated by <sup>(8)</sup>

$$F_N = \frac{1}{2} \rho_w \frac{6.13\Lambda}{\Lambda + 2.25} A_R V_R^2 \sin \delta^* \quad (3.26)$$

where  $\rho_w$  : density of sea water  
 $\Lambda$  : aspect ratio of rudder  
 $A_R$  : rudder area  
 $V_R$  : effective rudder inflow speed  
 $\delta^*$  : effective rudder inflow angle

$\Lambda$  and  $A_R$  of the model ship are 1.80 and 49.40 m<sup>2</sup>, respectively.  
 $\delta^*$  is assumed to be equal to rudder angle  $\delta$ .

The effective rudder inflow speed  $V_R$  can be approximated by <sup>(9)</sup>

$$V_R = V (1 - w) (1 + 3.6 S^{1.5})^{1/2} \quad (3.27)$$

where  $V$  : ship's speed  
 $w$  : wake fraction  
 $S$  : propeller slip ratio

The wake fraction  $w$  largely depends on the draught and trim, but is hardly affected by the ship's speed. The  $w$  versus  $V$  curve of the model ship is shown in Fig.3.7.

The propeller slip ratio  $S$  is given by

$$S = 1 - \frac{V (1 - w)}{n p} \quad (3.28)$$

where  $V$  : ship's speed through the water  
 $w$  : wake fraction

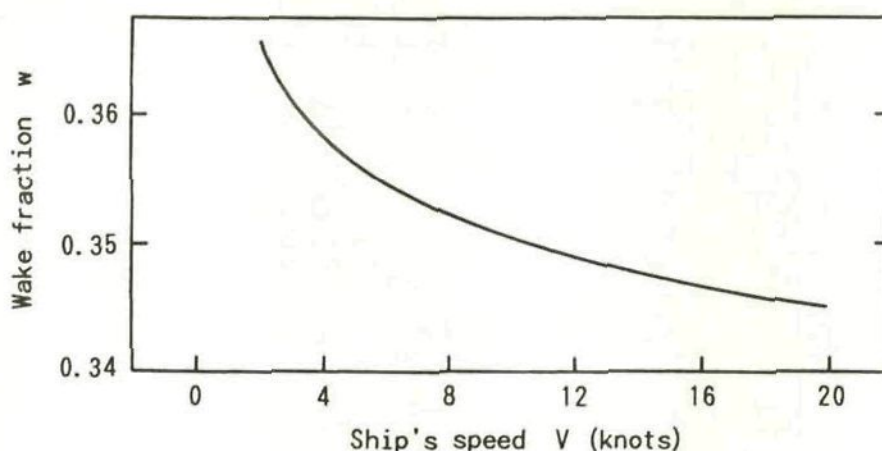


Fig. 3.7 Wake fraction versus ship's speed

$n$  : number of propeller revolutions per second

$p$  : propeller pitch

The propeller pitch  $p$  of the model ship is 6.00 m.

In formulae (3.23), (3.24) and (3.25),  $a_H$  denotes the ratio of lateral force induced on the hull by rudder action to the rudder lateral force, which means the hydrodynamic interaction between rudder and hull. The term  $-a_H F_N \cos \delta$  represents the hydrodynamic lateral force induced on the hull by rudder action.

The factor  $a_H$  may be regarded as a function of the block coefficient  $C_B$ ,<sup>(10)</sup> and is assumed to be 0.35 for the model ship.

In (3.24),  $D_{HR}$  represents the horizontal distance from the center of gravity to the point on which the lateral force induced on the hull by rudder action acts. For the model ship,  $D_{HR}$  is assumed as follows:<sup>(9)</sup>

$$D_{HR} = -0.45 \times (\text{waterline length}) = -84.29 \text{ m}$$

In (3.25),  $H_{HR}$  represents the vertical distance from the center of gravity to the point on which the lateral force induced on the hull by rudder action acts, which is assumed to be equal to  $H_H$  in (3.16) for the model ship.

(5) Added resistance due to waves

In general, the mean ( i.e. time-averaged ) added resistance in irregular waves  $R_{WAVE}$  is given by <sup>(1)</sup> ( Fig.3.8 )

$$R_{WAVE} = 2 \int_0^{2\pi} \int_0^{\infty} \{ R_w(\omega, V, \mu) / A_w^2 \} S(\omega, \chi) d\omega d\chi \quad (3.29)$$

where  $\omega$  : angular frequency of component wave

$\chi$  : direction of component wave from the north

$\mu$  : direction of component wave from the bow

$$\mu = \chi - \theta \quad \theta : \text{ship's heading}$$

$V$  : ship's speed

$A_w$  : amplitude of component wave

$\{ R_w(\omega, V, \mu) / A_w^2 \}$  : transfer function of added resistance

( i.e. added resistance per unit wave amplitude squared in regular waves )

$S(\omega, \chi)$  : directional spectrum of irregular waves

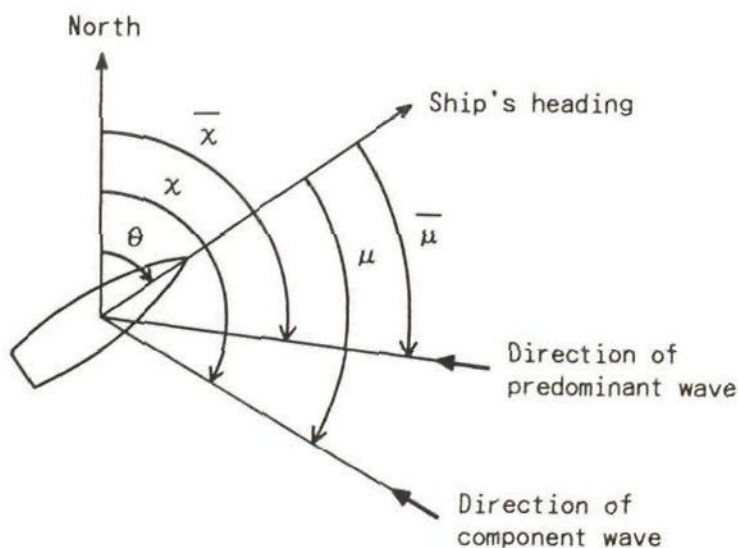


Fig. 3.8 Definitions of wave directions  $\chi$ ,  $\bar{\chi}$ ,  $\mu$  and  $\bar{\mu}$



Using the directional wave spectrum and the precalculated transfer function, the added resistance due to waves for the given ship's heading and ship's speed can be calculated by formula (3.29).

In actual weather routing, however, it is not practical to use formula (3.29) directly in the routing algorithm, because a huge amount of memory space is needed to store the directional wave spectra forecasted at the grid points covering the ocean, and in addition the period of wave forecasts in the form of directional spectra is limited up to 2 or 3 days ahead at present.

Thus we assume that the ocean waves consist of two ideal wave systems, namely, sea ( wind wave ) and swell which have the following wave spectra:<sup>(1)</sup>

$$\begin{aligned} \text{Sea : } S(\omega, \chi) &= S(\omega) \{ 2/\pi \cos^2(\chi - \bar{\chi}) \} & \text{if } |\chi - \bar{\chi}| \leq \pi/2 \\ S(\omega, \chi) &= 0 & \text{if } |\chi - \bar{\chi}| > \pi/2 \end{aligned} \quad (3.30)$$

$$\begin{aligned} \text{Swell : } S(\omega, \chi) &= S(\omega) & \text{if } \chi = \bar{\chi} \\ S(\omega, \chi) &= 0 & \text{if } \chi \neq \bar{\chi} \end{aligned} \quad (3.31)$$

where  $\bar{\chi}$  : predominant wave ( sea or swell ) direction  
 $S(\omega)$  : Bretschneider spectrum

$$S(\omega) = A \omega^{-5} \exp(-B \omega^{-4}) \quad (3.32)$$

where  $B = 691 T_w^{-4}$

$$A = B (0.5 H_w)^2$$

$T_w$  : average wave period

$$T_w = 2\pi m_0 / m_1$$

$H_w$  : significant wave height

$$H_w = 4 \sqrt{m_0}$$

$$m_n = \int_0^{\infty} \omega^n S(\omega) d\omega$$

In order to calculate the added resistance due to waves, the computer program was developed at the Hydronautics section of the

Department of Maritime Technology, Delft University of Technology. Based on the radiated energy method of Gerritsma-Beukelman for head to beam waves and the integrated pressure method of Boese for beam to following waves, the computer program calculates the transfer function of the added resistance.<sup>(11)</sup>

Then using formula (3.29), (3.30) and (3.31), the added resistances per unit significant wave height squared for sea and swell are computed as functions of average wave period  $T_w$ , ship's speed  $V$  and predominant wave direction from the bow  $\bar{\mu}$ .

We represent these added resistances per unit significant wave height squared for sea and swell as  $(R_{SEA}/H_{SEA}^2)$  and  $(R_{SWELL}/H_{SWELL}^2)$ , respectively. The added resistance due to sea  $R_{SEA}$  and added resistance due to swell  $R_{SWELL}$  are given by

$$R_{SEA} = (R_{SEA}/H_{SEA}^2) H_{SEA}^2 \quad (3.33)$$

$$R_{SWELL} = (R_{SWELL}/H_{SWELL}^2) H_{SWELL}^2 \quad (3.34)$$

where  $H_{SEA}$  : significant sea height

$H_{SWELL}$  : significant swell height

In order to reduce the data size, the computer program approximates the added resistance per unit significant wave height squared as a combination of linear expressions of average wave period for various ship's speeds and predominant wave directions from the bow.

In the model ship,  $(R_{SEA}/H_{SEA}^2)$  and  $(R_{SWELL}/H_{SWELL}^2)$  were calculated as a combination of linear expressions of average wave period for the ship's speed of 2, 5, 8, ---, 20 knots, and predominant wave direction from the bow of  $0^\circ, 20^\circ, 40^\circ, ---, 180^\circ$ .  $(R_{SEA}/H_{SEA}^2)$  and  $(R_{SWELL}/H_{SWELL}^2)$  for the ship's speed of 14 knots are shown in Fig. 3.9 and Fig. 3.10, respectively.

It can be seen from Figs 3.9 and 3.10 that since the swell does not have a directional spreading of energy,  $(R_{SWELL}/H_{SWELL}^2)$  becomes somewhat larger than  $(R_{SEA}/H_{SEA}^2)$  except for the value for wave direction from the bow of  $120^\circ$ .

For an arbitrary ship's speed and wave direction,  $(R_{SEA}/H_{SEA}^2)$  and  $(R_{SWELL}/H_{SWELL}^2)$  are calculated by using quadratic interpolation.

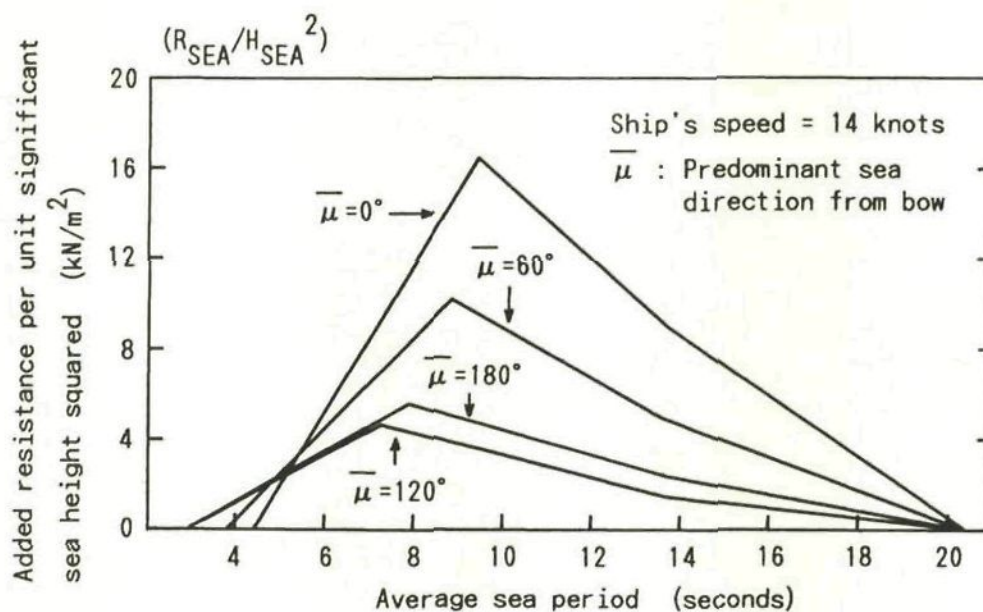


Fig. 3.9 Added resistance per unit significant sea height squared versus average sea period

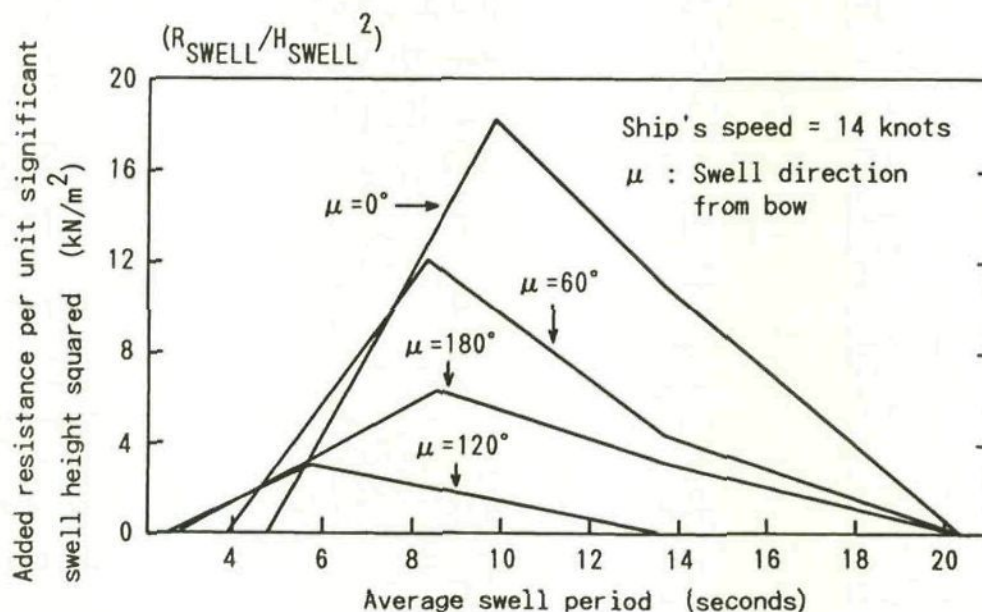


Fig. 3.10 Added resistance per unit significant swell height squared versus average swell period



The added resistance due to waves  $X_w$  is given as a sum of  $R_{SEA}$  and  $R_{SWELL}$ :

$$X_w = - ( R_{SEA} + R_{SWELL} ) \quad (3.35)$$

#### (6) Propeller thrust

The propeller thrust  $X_p$  is calculated by <sup>(1)</sup>

$$X_p = ( 1 - t ) K_T \rho_w D^4 n^2 \quad (3.36)$$

where  $t$  : thrust-deduction fraction

$K_T$  : thrust coefficient

$\rho_w$  : density of sea water

$D$  : propeller diameter

$n$  : number of propeller revolutions per second

The propeller diameter  $D$  of the model ship is 7.00 m.

When the number of propeller revolutions  $n$  is kept constant, thrust-deduction fraction  $t$  increases as the ship's speed increases ( i.e. as the loading of the propeller decreases );  $t$  changes also with draught and trim. The  $t$  versus  $V/n$  curve of the model ship is shown in Fig.3.11.

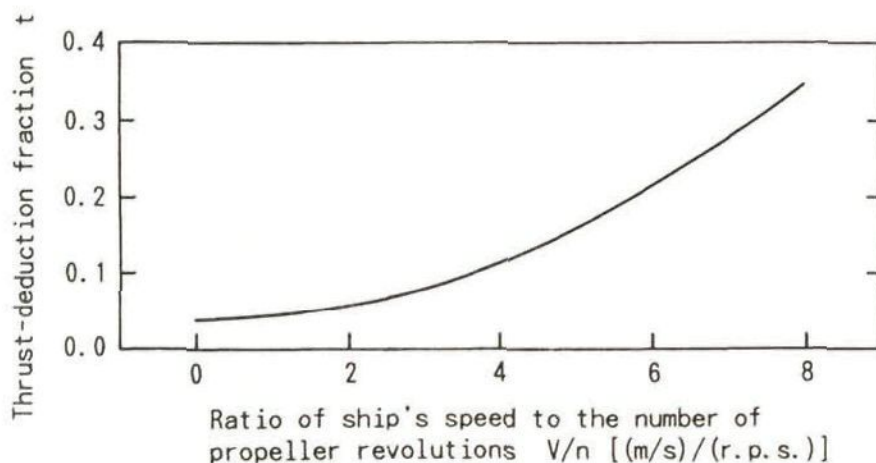


Fig. 3.11 Thrust-deduction fraction versus ratio of ship's speed to the number of propeller revolutions

The thrust coefficient  $K_T$  is a monotonically decreasing function of the advance ratio  $J$  which is defined by

$$J = \frac{V (1 - w)}{n D} \quad (3.37)$$

where  $V$  is the ship's speed and  $w$  is the wake fraction shown in Fig.3.7. The  $K_T$  versus  $J$  curve of the model ship is shown in Fig.3.12.

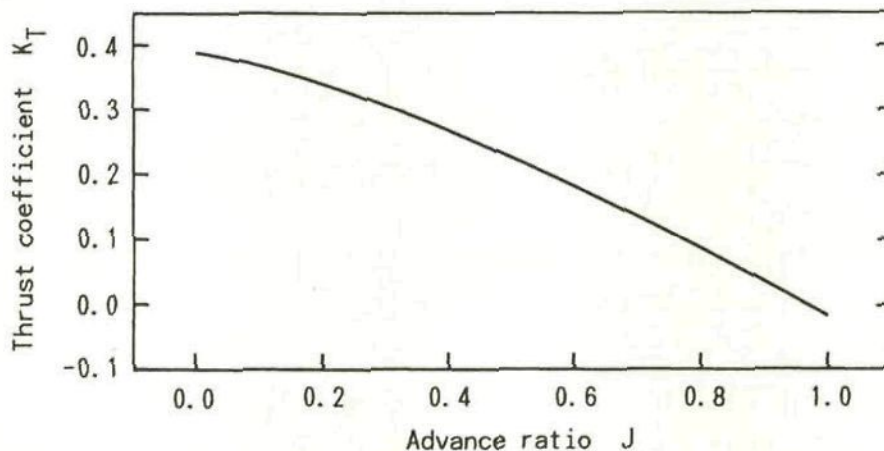


Fig. 3.12 Thrust coefficient versus advance ratio

#### (7) Hydrostatic righting moment due to heel of the hull

The hydrostatic righting moment due to heel of the hull  $L_B$  is given as

$$L_B = - W \rho_w g \overline{GM} \sin \varepsilon \quad (3.38)$$

where  $W$  : volume of displacement of the ship  
 $\rho_w$  : density of sea water  
 $g$  : acceleration of gravity ( = 9.80665 m/s<sup>2</sup> )  
 $\overline{GM}$  : metacentric height  
 $\varepsilon$  : heel angle

The volume of displacement and metacentric height of the model ship are 54,479 m<sup>3</sup> and 1.00 m, respectively.

### 3.5 PREDICTION OF SPEED, DRIFT ANGLE, RUDDER ANGLE AND HEEL ANGLE

As mentioned in Section 3.4, provided the ship's heading, number of propeller revolutions, draught, trim and wind/wave conditions are given, each force and moment in the equilibrium equations (3.1) through (3.4) becomes a function of four unknown variables, i.e. ship's speed through the water  $V$ , drift angle  $\alpha$ , rudder angle  $\delta$  and heel angle  $\varepsilon$ .

Now, we assume that  $\alpha$  is small enough and its influence on the apparent wind direction, apparent wind speed, wave direction from the bow, rudder force and propeller thrust can be neglected. Moreover, we assume that  $\varepsilon$  is also small and it affects the hydrostatic righting moment due to heel of the hull  $L_B$  only.

Then each term in (3.1) through (3.4) becomes a function of the following unknown variables.

$$\begin{aligned} X_S, Y_S, M_S, L_S, X_A, Y_A, M_A, L_A, X_W, X_P &: \text{function of } V \\ X_H, Y_H, M_H, L_H &: \text{function of } V \text{ and } \alpha \\ X_R, Y_R, M_R, L_R &: \text{function of } V \text{ and } \delta \\ L_B &: \text{function of } \varepsilon \end{aligned}$$

Four unknown variables  $V$ ,  $\alpha$ ,  $\delta$  and  $\varepsilon$  can be obtained by the following algorithm.<sup>(1), (3), (12)</sup>

(i) Set a suitable ship's speed  $V$ .

(ii) Using that ship's speed  $V$  and the formulae described in 3.4, the equilibrium equation for lateral forces (3.2) and yawing moments (3.3) can be written as

$$Y_S + Y_A - \frac{1}{2} \rho_w L d V^2 (k_1 \alpha + K_2 \alpha |\alpha|) - (1 + a_H) F_N \cos \delta = 0 \quad (3.39)$$

$$M_S + M_A - \frac{1}{2} \rho_w L^2 d V^2 \frac{2 d}{L} \alpha - (D_R + a_H D_{HR}) F_N \cos \delta = 0 \quad (3.40)$$



Eliminating  $F_N \cos \delta$  from (3.39) and (3.40), and collecting terms of the same order of  $\alpha$ , we have

$$\begin{aligned} & \left\{ \frac{1}{2} \rho_w L d V^2 (D_R + a_H D_{HR}) K_2 \right\} \alpha + \left\{ \frac{1}{2} \rho_w L d V^2 [(D_R + a_H D_{HR}) K_1 - 2 d (1 + a_H)] \right\} \alpha \\ & + \{ (1 + a_H) (M_S + M_A) - (Y_S + Y_A) (D_R + a_H D_{HR}) \} = 0 \quad (3.41) \end{aligned}$$

Since  $Y_S$ ,  $Y_A$ ,  $M_S$  and  $M_A$  can be calculated as a function of  $V$ , the drift angle  $\alpha$  may be determined as the proper root of the quadratic equation of  $\alpha$  (3.41).

Substituting that  $\alpha$  into (3.40), and letting  $F_N = F_N' \sin \delta$  based on the formula (3.26), equation (3.40) can be reduced as follows:

$$M_S + M_A - \rho_w L d^2 V^2 \alpha - (D_R + a_H D_{HR}) F_N' \sin \delta \cos \delta = 0 \quad (3.42)$$

where  $F_N'$  is a function of  $V$  and was already obtained in (3.26).

Thus the rudder angle  $\delta$  can be determined by

$$\delta = \frac{1}{2} \sin^{-1} \left\{ \frac{2}{(D_R + a_H D_{HR}) F_N'} (M_S + M_A - \rho_w L d^2 V^2 \alpha) \right\} \quad (3.43)$$

(iii) Calculate the left-hand side of (3.1) using  $V$  as well as  $\alpha$  and  $\delta$  determined in (ii). Then correct  $V$  so as to get the left-hand side of (3.1) close to zero.

(iv) Using the corrected  $V$ , repeat the procedures in (ii) and (iii). If the absolute value of the left-hand side of (3.1) becomes small enough, stop the calculation.

Those  $V$ ,  $\alpha$  and  $\delta$  may be regarded as the ship's speed, drift angle and rudder angle for the given ship's heading, number of propeller revolutions, draught, trim and wind/wave conditions.

(v) By calculating  $L_S$ ,  $L_A$ ,  $L_H$  and  $L_R$  in equation (3.4) using obtained  $V$ ,  $\alpha$  and  $\delta$ , we can determine the heel angle  $\varepsilon$  by

$$\varepsilon = \sin^{-1} \{ (L_S + L_A + L_H + L_R) / (W \rho_w g \overline{GM}) \} \quad (3.44)$$

In the above-mentioned algorithm, the calculation speed depends upon the iterative method to converge the left-hand side of (3.1) to zero. Because  $V$ ,  $\alpha$ ,  $\delta$  and  $\varepsilon$  have to be calculated several ten thousand times in the weather routing simulation, that iterative method should possess a high converging efficiency.

To meet the requirement on calculation speed, the following iterative method is proposed.

(i) Set a suitable initial ship's speed  $V_1$ , and calculate the drift angle  $\alpha_1$  and the rudder angle  $\delta_1$  based on (3.41) and (3.43) using  $V_1$ . Then compute the left-hand side of (3.1) using  $V_1$ ,  $\alpha_1$  and  $\delta_1$ , and represent it by  $X_1$ .

(ii) Correct the ship's speed as follows:

$$V_2 = V_1 + \Delta V \quad \text{if } X_1 > 0$$

$$V_2 = V_1 - \Delta V \quad \text{if } X_1 < 0$$

where  $\Delta V$  : increment of ship's speed

Calculate  $\alpha_2$  and  $\delta_2$  based on (3.41) and (3.43) using  $V_2$ . Then compute the left-hand side of (3.1) using  $V_2$ ,  $\alpha_2$  and  $\delta_2$ , and represent it by  $X_2$ .

(iii) Correct the ship's speed as follows:

$$V_3 = V_2 + \Delta V \quad \text{if } X_2 > 0$$

$$V_3 = V_2 - \Delta V \quad \text{if } X_2 < 0$$

In the same manner as mentioned in (ii), calculate  $\alpha_3$ ,  $\delta_3$  and  $X_3$ .

(iv) Repeat the procedure in (iii) until the product of  $X_k$  and  $X_{k+1}$  becomes negative. When that product becomes negative, calculate  $\alpha_{k+2}$ ,  $\delta_{k+2}$  and  $X_{k+2}$  by letting  $V_{k+2} = (V_k + V_{k+1})/2$ .

(v) Determine the ship's speed  $V^*$  as a V-coordinate of the intersection of the V-axis and the parabola passing through three points  $(V_k, X_k)$ ,  $(V_{k+1}, X_{k+1})$  and  $(V_{k+2}, X_{k+2})$ . ( Fig.3.13 )

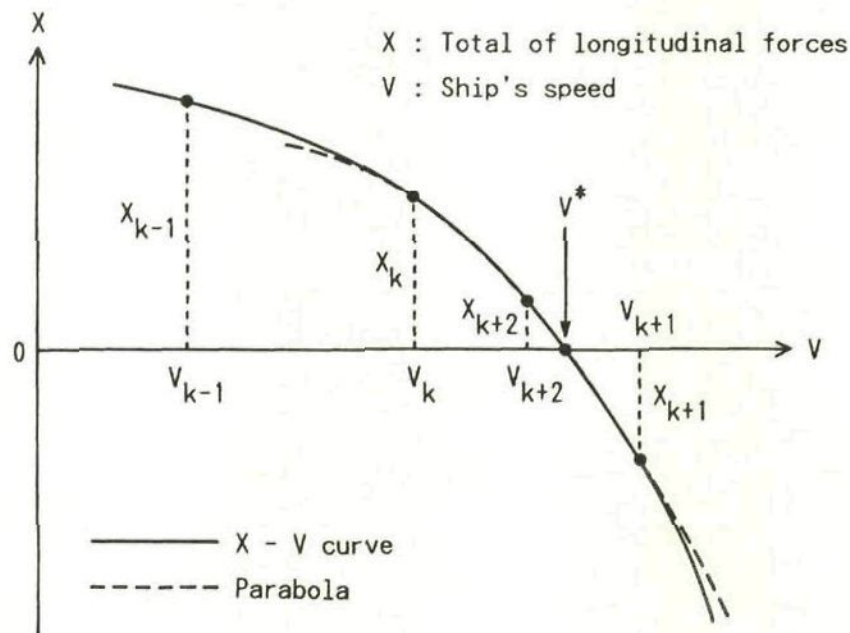


Fig. 3.13 Determination of ship's speed by parabolic approximation of X versus V curve

Then calculate the drift angle  $\alpha^*$  and the rudder angle  $\delta^*$  based on (3.41) and (3.43). Adopt  $V^*$ ,  $\alpha^*$  and  $\delta^*$  as the solutions for the equilibrium equations (3.1), (3.2) and (3.3).

In this iterative method, since the actual X versus V curve is approximated by a parabola in the vicinity of  $V^*$ , the accurate  $V^*$  may be obtained even if a large increment  $\Delta V$  is used. As a matter of course, as a large increment  $\Delta V$  reduces the number of iterations to obtain  $V^*$ , we can considerably save computing time for the weather routing simulations.

Although the value of the left-hand side of (3.1) for  $V^*$ ,  $\alpha^*$  and  $\delta^*$  is not checked in this method, it has been verified that it becomes small enough for practical use.



### 3.6 PREDICTION OF ENGINE POWER

When the ship's speed through the water  $V$  is obtained by the method described in 3.5, the engine power  $P$  can be predicted by <sup>(1)</sup>

$$P = 2\pi K_Q \rho_w D^5 n^3 / (\eta_R \eta_M) \quad (3.45)$$

where  $K_Q$  : torque coefficient  
 $\rho_w$  : density of sea water  
 $D$  : propeller diameter  
 $n$  : number of propeller revolutions per second  
 $\eta_R$  : relative rotative efficiency  
 $\eta_M$  : mechanical efficiency of shaft bearings

$\eta_R$  and  $\eta_M$  of the model ship are assumed to be 1.017 and 0.990, respectively.

The torque coefficient  $K_Q$  is a monotonically decreasing function of the advance ratio  $J$ . Thus, provided the number of propeller revolutions is kept constant, the engine power decreases as the ship's speed increases. The  $K_Q$  versus  $J$  curve of the model ship is shown in Fig.3.14.

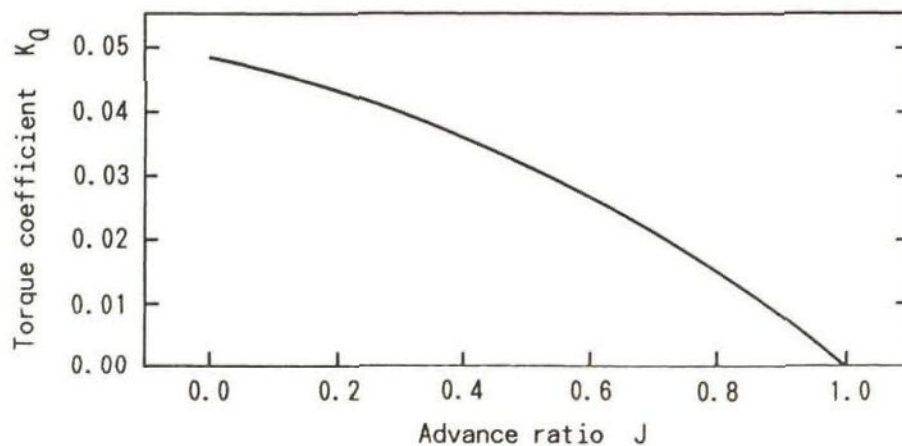


Fig. 3.14 Torque coefficient versus advance ratio

Given the engine power  $P$ , the fuel consumption per hour  $F$  can be calculated by

$$F = K P \quad (3.48)$$

where  $K$  is the specific fuel consumption.

$K$  of the model ship is assumed to be 0.21 kg/kW per hour.

### 3.7 CALCULATION OF SPEED, DRIFT ANGLE, RUDDER ANGLE, HEEL ANGLE AND ENGINE POWER OF THE MODEL SHIP

In this section, the ship's speed through the water, drift angle, rudder angle and heel angle of the model ship described in 3.2 are calculated for some environmental conditions based on the equilibrium equations (3.1) through (3.4) and the algorithm to solve them mentioned in 3.5. The engine power is also calculated for those environmental conditions based on formula (3.45).

In the iterative method proposed in 3.5, the initial ship's speed  $V_1$  and the increment of ship's speed  $\Delta V$  are set to 6.5 m/sec and 1.8 m/sec, respectively.

Hereafter, we call the mathematical model ship described in 3.2 'sail-assisted motor vessel' and the same ship without sails 'equivalent motor vessel'. For these vessels, we use the following abbreviations:

Sail-assisted motor vessel : S-A MV  
Equivalent motor vessel : EQ MV

First, the ship's speed, engine power, drift angle, rudder angle and heel angle of S-A MV and EQ MV were calculated for four kinds of wind/wave conditions with a constant number of propeller revolutions ( 75 r.p.m. ).

In Figs 3.15 - 3.18, the ship's speeds ( solid lines ) and the engine powers ( dashed lines ) of S-A MV and EQ MV are shown for four kinds of wind/wave conditions. The wind/wave conditions gradually become severer in Fig.3.15, 16, 17 and 18.

The circles and the triangles plotted every 10 degrees wind direction denote the calculated values for S-A MV and EQ MV, respectively. The solid lines and the dashed lines represent the regression curves based on the cubic spline function with least-squares fitting using the calculated values for every 1 degree wind direction. The meanings of the circles and the triangles as



well as the regression curves in Figs 3.19 - 3.34 are the same as mentioned here.

From Figs 3.15 - 3.18, it can be seen that for true wind directions larger than  $20^\circ$ , the S-A MV can sail faster with smaller engine power than EQ MV. Since the sails do not generate thrust for true wind directions between  $0^\circ$  and  $15^\circ$  and they increase the wind resistance, the speed of S-A MV becomes slightly less than that of EQ MV.

The differences of both speed and engine power between S-A MV and EQ MV increase as the wind speed increases. When the wind speed is 45 knots, those differences reach 3.7 knots and 1,500 kW for the true wind direction from the bow of  $120^\circ$ .

In Figs 3.19 - 3.22, the drift angles of S-A MV and EQ MV are shown for four kinds of wind/wave conditions. ( It should be noted that the scale of the ordinate in Fig.3.22 is half of those in Figs 3.19 - 3.21. )

From Figs 3.19 - 3.22, we can find that when the true wind direction from the bow is small, the drift angle of S-A MV becomes much larger than that of EQ MV because of the large sail lateral force. For the S-A MV, the wind direction which gives maximum drift angle approaches the bow as the wind speed increases.

For a quartering wind of 25, 35 and 45 knots, the drift angle of S-A MV becomes negative because the sail lateral force directed windward becomes larger than the lateral wind force due to hull and superstructure directed leeward.

In Figs 3.23 - 3.26, the rudder angles of S-A MV and EQ MV are shown for four kinds of wind/wave conditions. It is found from these figures that when the true wind direction from the bow is small, the S-A MV needs a considerably large rudder angle.

This results from the fact that the large hydrodynamic lateral force due to a comparatively large drift angle acts on the bow and it generates a large yawing moment to turn the bow close to the wind. Therefore, a large rudder angle to turn the bow away from the wind

becomes necessary so as to cancel that large yawing moment.

It is also found that for a quartering wind of 25, 35 and 45 knots, the S-A MV needs a rudder angle to turn the bow close to the wind in order to cancel the hydrodynamic yawing moment to turn the bow away from the wind caused by the negative drift angle.

In Figs 3.27 - 3.30, the heel angles of S-A MV and EQ MV are shown for four kinds of wind/wave conditions. Since the product tanker used here is in full loaded condition, the heel angle of EQ MV remains very small even for a wind speed of 45 knots. When the true wind direction from the bow is small, the heel angle of S-A MV becomes large because of the large sail heeling moment.

For true wind directions less than about  $90^\circ$ , the heel angle of S-A MV for a wind speed of 35 knots ( Fig.3.29 ) almost coincides with that for a wind speed of 45 knots ( Fig.3.30 ), showing a maximum heel angle of  $3.1^\circ$ . This is because since the apparent wind speed  $U_A$  exceeds 20 m/sec for that range of true wind directions, the sail lateral force is kept equal to that for  $U_A = 20$  m/sec by reducing the attack angle of sails to the wind.

It is found that for a quartering wind of 25, 35 and 45 knots, the S-A MV takes a negative heel angle as the wingsails which have a comparatively small attack angle to the wind generate a heeling moment to heel the hull windward.

Next, the ship's speed, engine power, etc. of S-A MV and EQ MV were calculated for two different swell directions. The ship's speed and engine power for head swell are shown in Fig.3.31, and those for following swell are shown in Fig.3.32.

From Figs 3.31 and 3.32, it can be seen that as a matter of course, the ship's speed for head swell is always smaller than that for following swell, whereas the engine power for head swell is always larger than that for following swell.

Furthermore, the ship's speed, engine power, etc. of S-A MV and



EQ MV were calculated for four kinds of numbers of propeller revolutions. The ship's speeds and engine powers for the number of propeller revolutions of 60, 65, 70 and 75 r.p.m. are shown in Fig.3.33 ( S-A MV ) and Fig.3.34 ( EQ MV ).

We can find from Fig.3.33 that for a beam wind, the differences between ship's speeds of S-A MV for 60, 65, 70 and 75 r.p.m. become comparatively small. This comes from the fact that the wingsails generate maximum sail thrust for beam wind and the contribution of sail thrust to the ship's speed increases as the number of propeller revolutions decreases.

From Figs 3.15 - 3.32, it is found that the ship's speeds, engine powers, drift angles, rudder angles and heel angles of S-A MV and EQ MV plotted every 10 degrees wind direction almost coincide with the regression curves based on the calculated values for every 1 degree wind direction. Therefore, it can be said that the ship's speed, engine power, etc. predicted by the proposed method are consistent for every true wind direction from the bow.



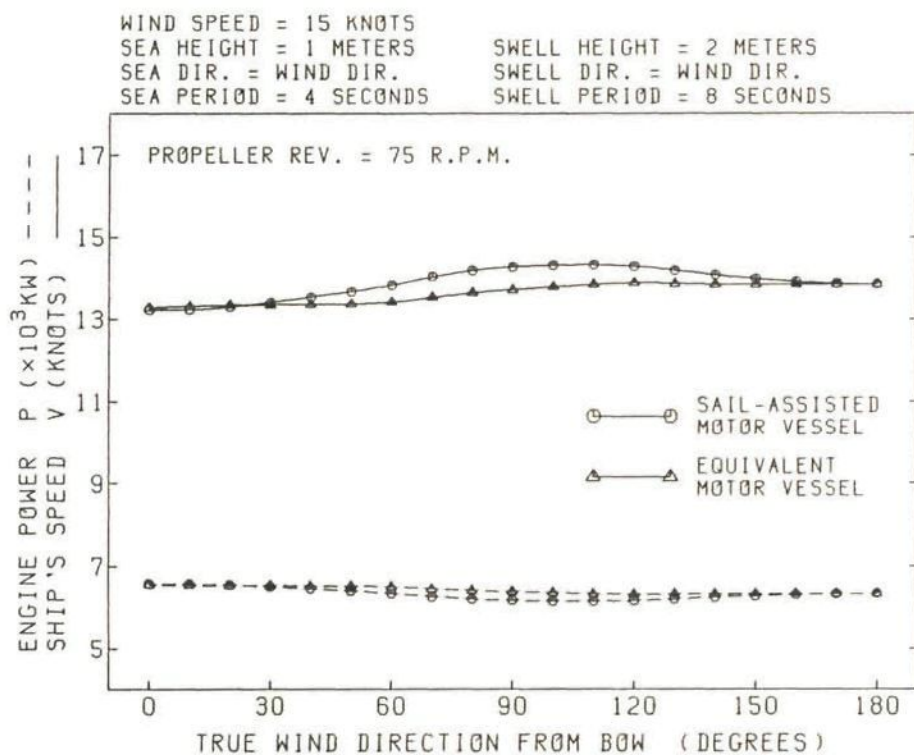


Fig. 3.15 Ship's speed and engine power versus true wind direction from bow ( wind speed = 15 knots )

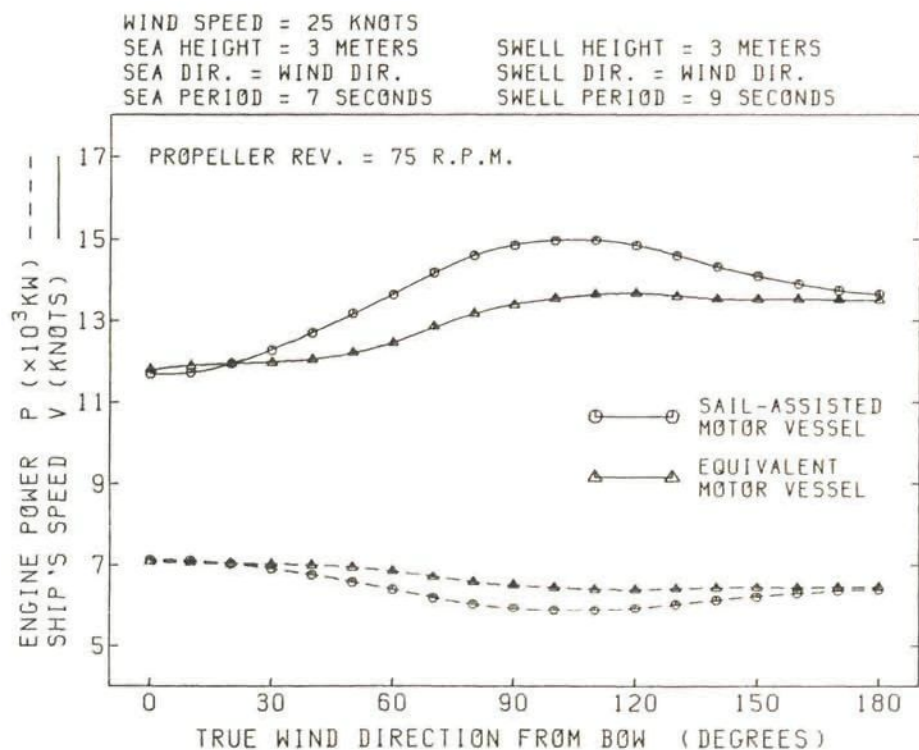


Fig. 3.16 Ship's speed and engine power versus true wind direction from bow ( wind speed = 25 knots )

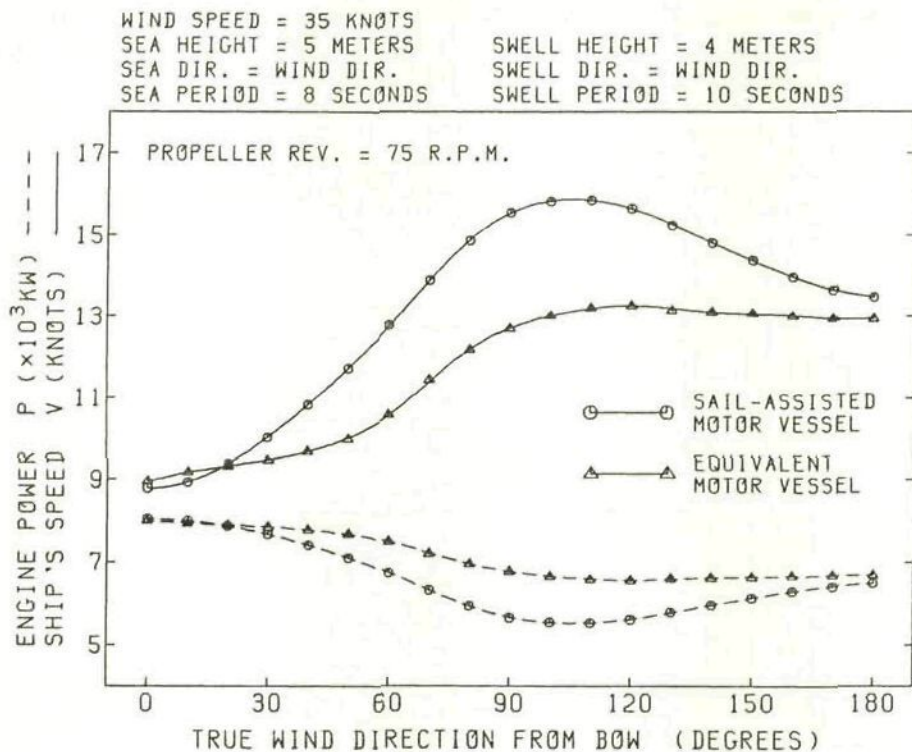


Fig. 3.17 Ship's speed and engine power versus true wind direction from bow ( wind speed = 35 knots )

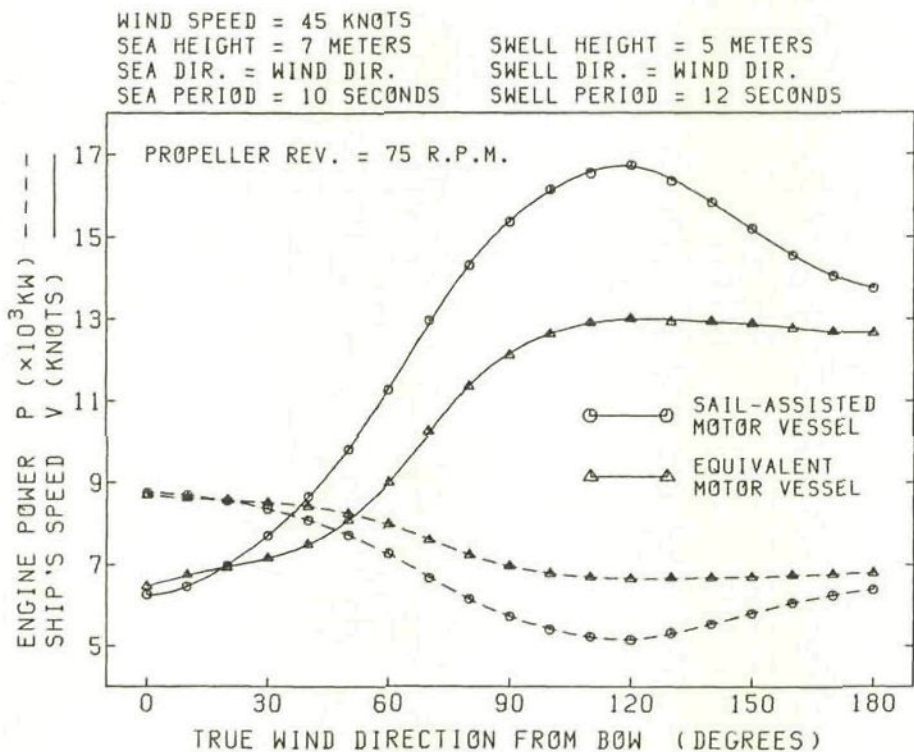


Fig. 3.18 Ship's speed and engine power versus true wind direction from bow ( wind speed = 45 knots )

WIND SPEED = 15 KNOTS  
 SEA HEIGHT = 1 METERS  
 SEA DIR. = WIND DIR.  
 SEA PERIOD = 4 SECONDS

SWELL HEIGHT = 2 METERS  
 SWELL DIR. = WIND DIR.  
 SWELL PERIOD = 8 SECONDS

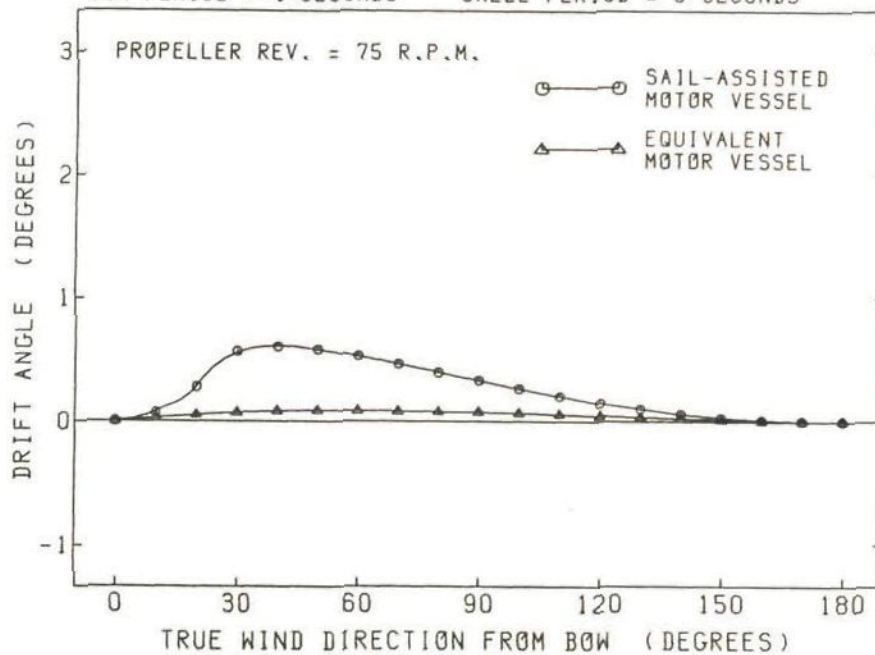


Fig. 3.19 Drift angle versus true wind direction from bow  
 ( wind speed = 15 knots )

WIND SPEED = 25 KNOTS  
 SEA HEIGHT = 3 METERS  
 SEA DIR. = WIND DIR.  
 SEA PERIOD = 7 SECONDS

SWELL HEIGHT = 3 METERS  
 SWELL DIR. = WIND DIR.  
 SWELL PERIOD = 9 SECONDS

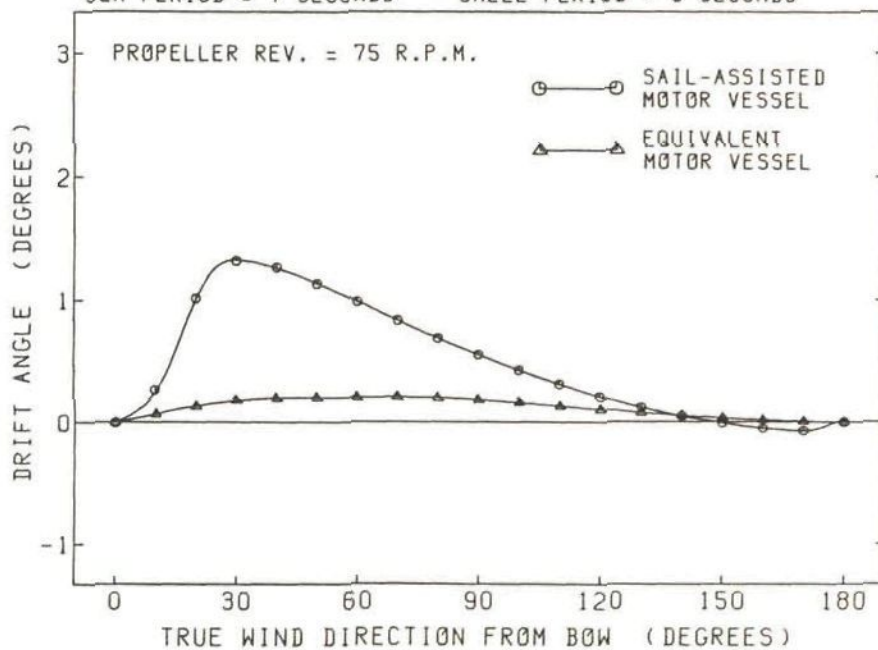


Fig. 3.20 Drift angle versus true wind direction from bow  
 ( wind speed = 25 knots )



WIND SPEED = 35 KNOTS  
 SEA HEIGHT = 5 METERS  
 SEA DIR. = WIND DIR.  
 SEA PERIOD = 8 SECONDS

SWELL HEIGHT = 4 METERS  
 SWELL DIR. = WIND DIR.  
 SWELL PERIOD = 10 SECONDS

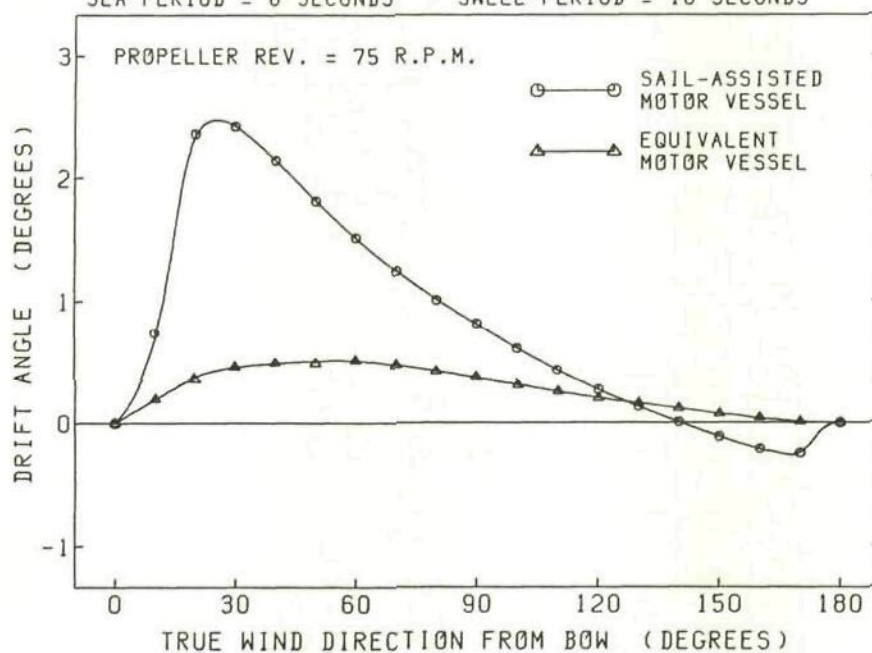


Fig. 3.21 Drift angle versus true wind direction from bow  
 ( wind speed = 35 knots )

WIND SPEED = 45 KNOTS  
 SEA HEIGHT = 7 METERS  
 SEA DIR. = WIND DIR.  
 SEA PERIOD = 10 SECONDS

SWELL HEIGHT = 5 METERS  
 SWELL DIR. = WIND DIR.  
 SWELL PERIOD = 12 SECONDS

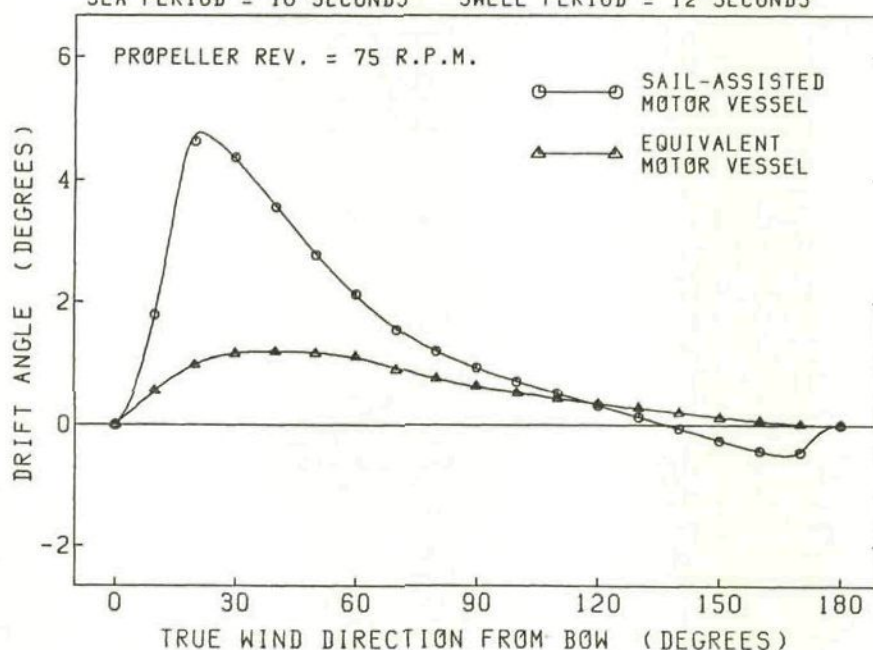


Fig. 3.22 Drift angle versus true wind direction from bow  
 ( wind speed = 45 knots )

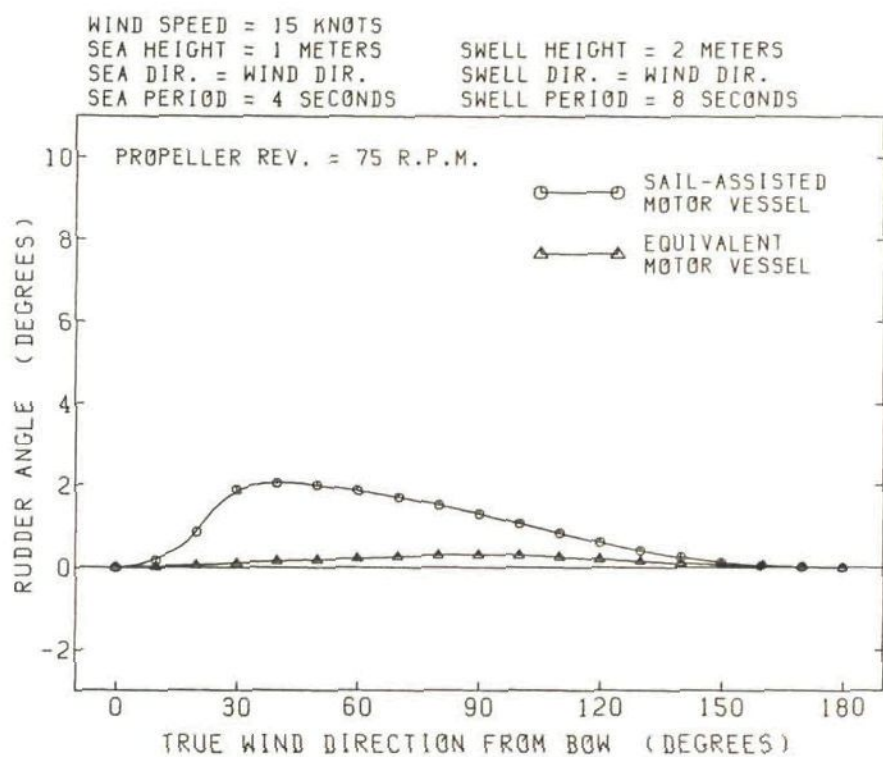


Fig. 3.23 Rudder angle versus true wind direction from bow  
( wind speed = 15 knots )

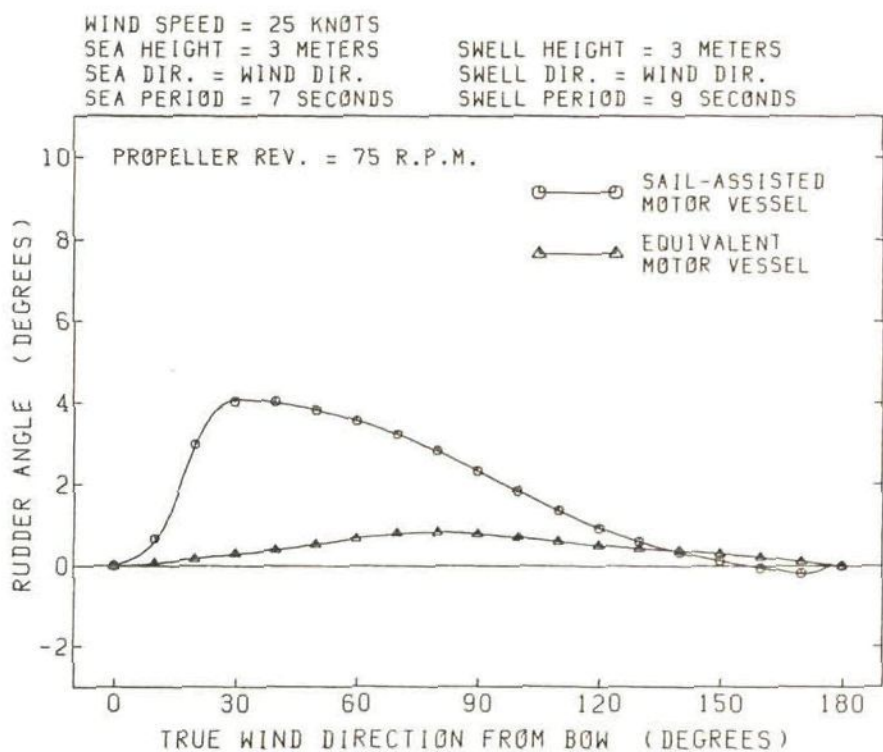


Fig. 3.24 Rudder angle versus true wind direction from bow  
( wind speed = 25 knots )

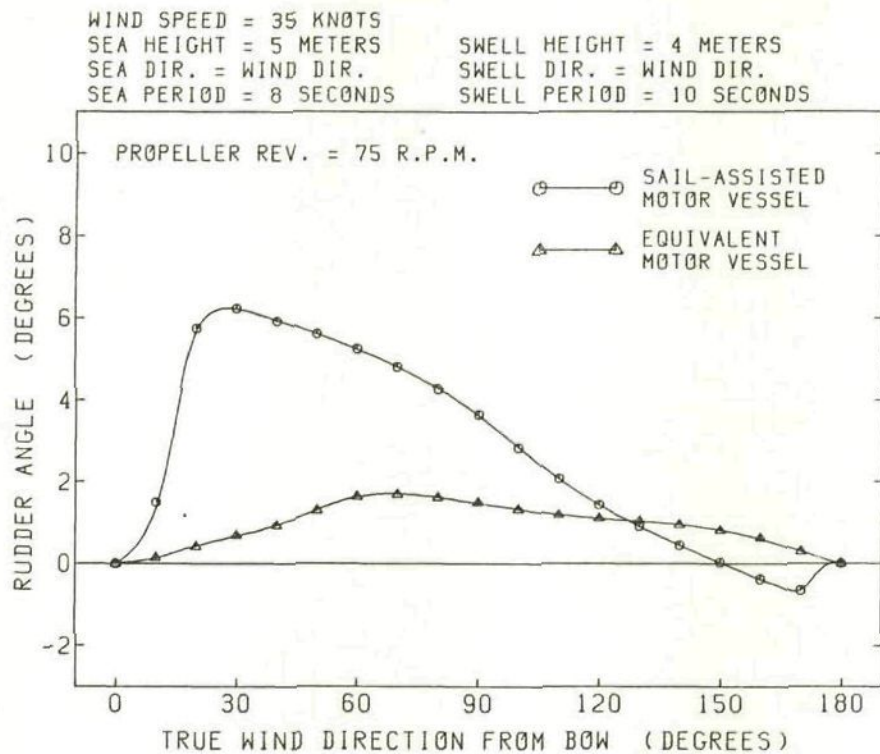


Fig. 3.25 Rudder angle versus true wind direction from bow  
( wind speed = 35 knots )

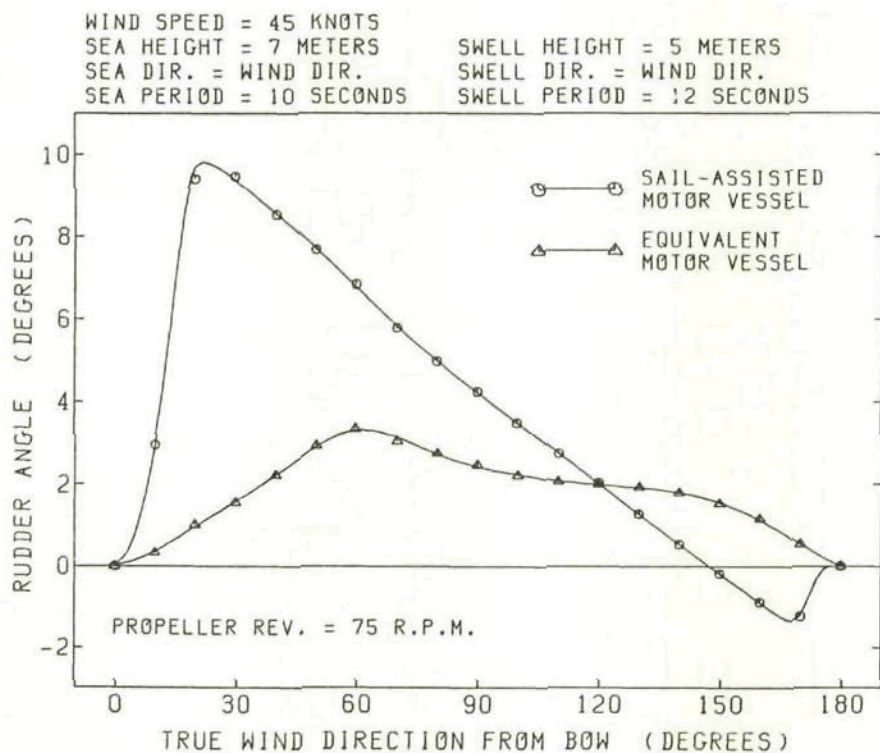


Fig. 3.26 Rudder angle versus true wind direction from bow  
( wind speed = 45 knots )



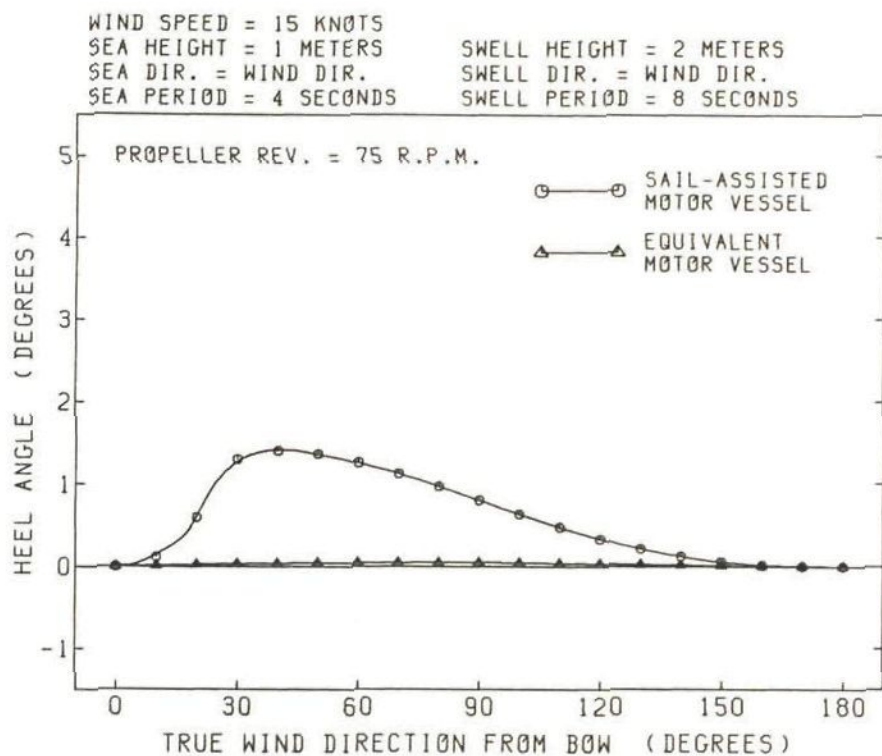


Fig. 3.27 Heel angle versus true wind direction from bow  
(wind speed = 15 knots )

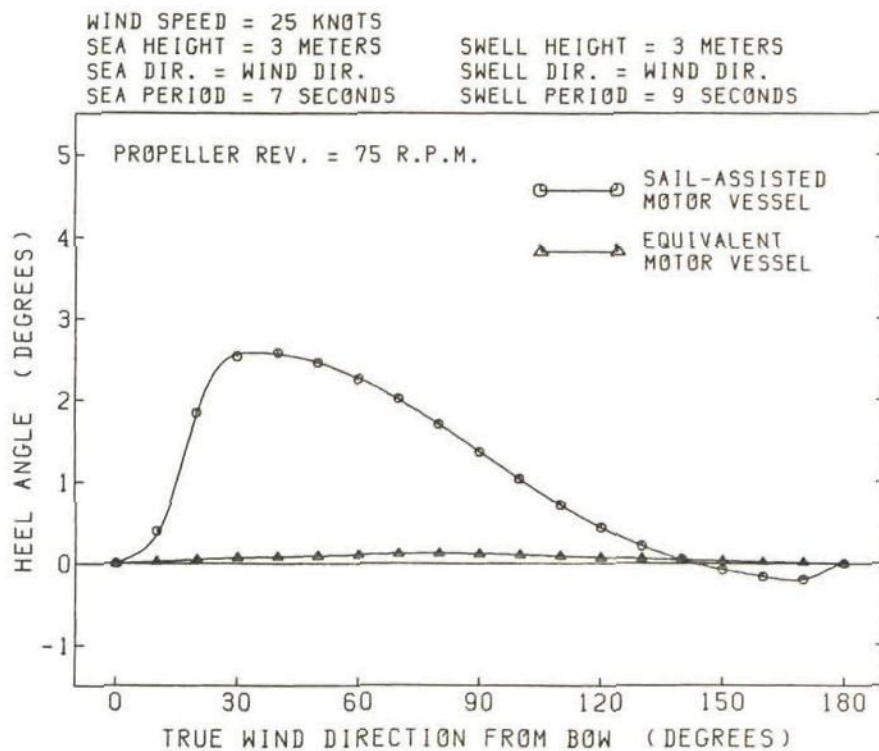


Fig. 3.28 Heel angle versus true wind direction from bow  
(wind speed = 25 knots )

WIND SPEED = 35 KNOTS  
 SEA HEIGHT = 5 METERS  
 SEA DIR. = WIND DIR.  
 SEA PERIOD = 8 SECONDS

SWELL HEIGHT = 4 METERS  
 SWELL DIR. = WIND DIR.  
 SWELL PERIOD = 10 SECONDS

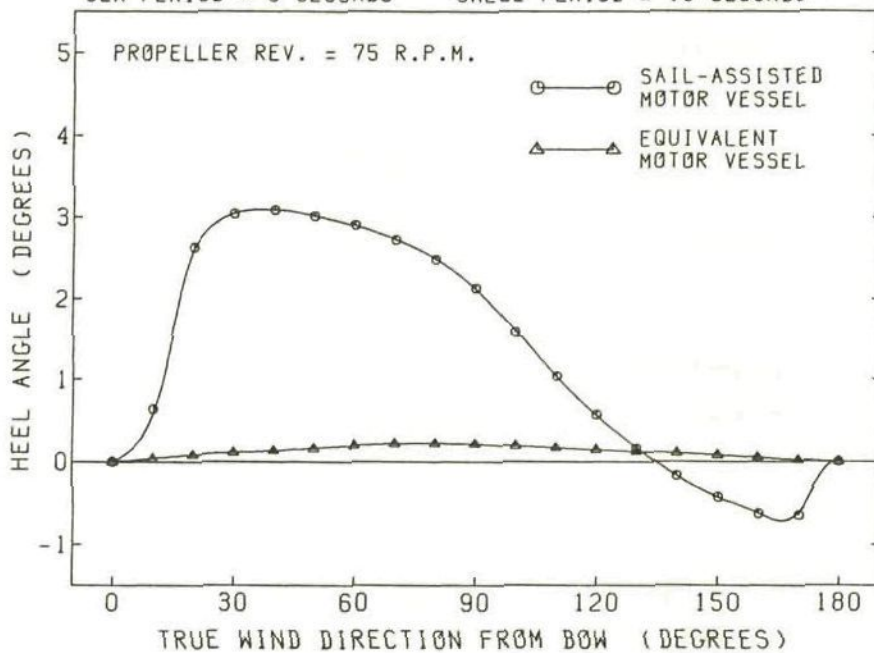


Fig. 3.29 Heel angle versus true wind direction from bow  
 ( wind speed = 35 knots )

WIND SPEED = 45 KNOTS  
 SEA HEIGHT = 7 METERS  
 SEA DIR. = WIND DIR.  
 SEA PERIOD = 10 SECONDS

SWELL HEIGHT = 5 METERS  
 SWELL DIR. = WIND DIR.  
 SWELL PERIOD = 12 SECONDS

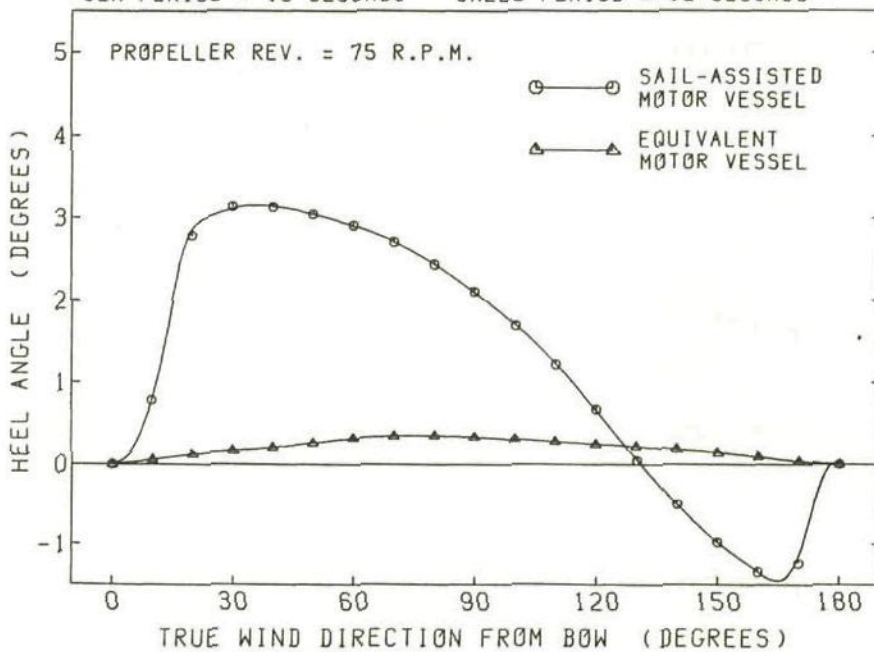


Fig. 3.30 Heel angle versus true wind direction from bow  
 ( wind speed = 45 knots )

The forces and moments acting on the S-A MV under the same wind/wave conditions as described in Figs 3.17, 3.21, 3.25 and 3.29 are shown in Table 3.1. From Table 3.1, the following facts can be observed.

(i) The wingsails installed on the S-A MV possess a remarkably high performance. They generate a sail thrust ( $X_s$ ) of 100.5 kN even for a true wind direction from the bow ( $\beta$ ) of  $30^\circ$ . For  $\beta = 90^\circ$ , the sail thrust  $X_s$  reaches 539.6 kN, which is greater than the propeller thrust  $X_p$ . The sail lateral force  $Y_s$  reaches 665.7 kN for  $\beta = 30^\circ$ , which causes the comparatively large drift angle.

(ii) For head waves ( $\beta = 0^\circ$  and  $30^\circ$ ), the absolute value of added resistance due to waves  $X_w$  is greater than that of still water resistance (including added resistance caused by drift)  $X_H$ .

Since the directional spreading of energy is not taken into account for the swell, the added resistance due to swell  $R_{SWELL}$  becomes considerably smaller than that due to sea  $R_{SEA}$  for  $\beta = 90^\circ$  and  $120^\circ$ .

(iii) Concerning the equilibrium for yawing moments, the balance between the hydrodynamic yawing moment due to the hull  $M_H$  and the hydrodynamic yawing moment induced by the rudder  $M_R$  is dominant for  $\beta = 30^\circ, 60^\circ, 90^\circ$  and  $120^\circ$ . For  $\beta = 150^\circ$ , the balance between the aerodynamic yawing moment due to the hull and the superstructure  $M_A$  and  $M_H$  becomes dominant.

(iv) Regarding the equilibrium for the heeling moment, the balance between the sail heeling moment  $L_s$  and the hydrostatic righting moment due to heel of the hull  $L_B$  is dominant for every wind direction.

(v) The total of the longitudinal forces  $X$  (i.e. the error in longitudinal equilibrium) is very small for  $\beta = 0^\circ, 30^\circ, 60^\circ, 150^\circ$  and  $180^\circ$ . For  $\beta = 90^\circ$  and  $120^\circ$ , however, it becomes a bit large value; i.e. 15.0 kN for  $\beta = 90^\circ$  and 13.1 kN for  $\beta = 120^\circ$ .

In order to check the accuracy of ship's speed  $V$  and engine power  $P$  for  $\beta = 90^\circ$  and  $120^\circ$ , the exact  $V$  and  $P$  were calculated by letting the increment of ship's speed  $\Delta V$  be 0.1 m/sec. Those exact values are as follows:



Exact ship's speed :	15.62 knots	for $\beta = 90^\circ$
	15.71 knots	for $\beta = 120^\circ$
Exact engine power :	5626 kW	for $\beta = 90^\circ$
	5588 kW	for $\beta = 120^\circ$

By comparing V and P in Table 3.1 with these exact V and P, the errors of ship's speed and engine power are given as follows:

Error of ship's speed :	0.07 knots ( 0.45% )	for $\beta = 90^\circ$
	0.06 knots ( 0.38% )	for $\beta = 120^\circ$
Error of engine power :	-29 kW ( -0.52% )	for $\beta = 90^\circ$
	-24 kW ( -0.43% )	for $\beta = 120^\circ$

The above errors of the ship's speed and engine power may be considered to be small enough from a practical point of view. Thus it can be said that in spite of a considerably large increment  $\Delta V$ , the proposed iterative method provides the accurate ship's speed and engine power.

When the initial ship's speed and increment of ship's speed are set to 6.5 m/sec and 1.8 m/sec respectively, the proposed iterative method can determine the ship's speed, engine power, etc. within six iterations, which is a great advantage for saving computing time.

In practice, the value of increment  $\Delta V$  may be determined by the trade-off between accuracy of solution and computing time. For the weather routing simulations performed in this study, the initial ship's speed  $V_1$  and the increment of ship's speed  $\Delta V$  are set to the same values used here, i.e. 6.5 m/sec and 1.8 m/sec.

Table 3.1 Forces and moments acting on the sail-assisted motor vessel in a seaway

True wind speed = 35 knots  
 Significant sea height = 5 meters  
 Predominant sea direction = wind direction  
 Average sea period = 8 seconds  
 Significant swell height = 4 meters  
 Swell direction = wind direction  
 Average swell period = 10 seconds

V : Ship's speed through the water  
 P : Engine power  
 $\alpha$  : Drift angle  
 $\delta$  : Rudder angle  
 $\varepsilon$  : Heel angle

Number of propeller revolutions = 75 r.p.m.

X : Longitudinal force (kN)  
 Y : Lateral force (kN)  
 M : Yawing moment (kN-m)  
 L : Heeling moment (kN-m)  
 $R_{SEA}$  : Added resistance due to sea  
 $R_{SWELL}$  : Added resistance due to swell

Meaning of subscript  
 S : generated by sails  
 A : due to hull and superstructure  
 H : due to hull under water  
 R : induced by rudder  
 W : due to waves  
 P : generated by propeller

True wind dir. from bow $\beta$ :	0°	30°	60°	90°	120°	150°	180°
$X_S$	-22.5	100.5	341.4	539.6	456.7	247.3	96.8
$X_A$	-182.1	-164.4	-160.1	-56.3	-3.8	27.9	32.3
$X_H$	-250.4	-321.9	-515.4	-811.3	-826.0	-685.3	-580.6
$X_R$	0.0	-22.6	-21.3	-12.3	-1.8	0.0	0.0
$(R_{SEA})$	(319.2)	(285.1)	(216.8)	(145.4)	(108.1)	(123.0)	(136.0)
$(R_{SWELL})$	(219.6)	(215.4)	(150.1)	(28.2)	(25.7)	(76.6)	(84.4)
$X_W$	-538.8	-500.5	-366.9	-173.6	-133.8	-199.6	-220.4
$X_P$	993.5	912.7	723.2	528.9	521.8	609.5	674.9
Total of X	-0.3	3.8	0.9	15.0	13.1	-0.2	3.0
$Y_S$	0.0	665.7	614.9	436.2	96.8	-114.0	0.0
$Y_A$	0.0	111.1	193.1	212.2	136.8	70.7	0.0
$Y_H$	0.0	-497.1	-495.4	-389.3	-131.6	45.0	0.0
$Y_R$	0.0	-279.7	-312.6	-259.1	-102.0	-1.7	0.0
Total of Y	0.0	0.0	0.0	0.0	0.0	0.0	0.0
$M_S$	0	905	836	593	132	-155	0
$M_A$	0	2313	-228	-1039	-1503	-2713	0
$M_H$	0	-28607	-28990	-23080	-7885	2706	0
$M_R$	0	25389	28382	23526	9256	162	0
Total of M	0	0	0	0	0	0	0
$L_S$	0	23533	21737	15419	3421	-4030	0
$L_A$	0	335	583	641	413	214	0
$L_H$	0	3216	3205	2519	852	-291	0
$L_R$	0	2006	2243	1859	731	13	0
$L_B$	0	-29090	-27768	-20438	-5417	4094	0
Total of L	0	0	0	0	0	0	0
V (knots)	8.79	10.03	12.78	15.55	15.65	14.40	13.47
P (kW)	8049	7673	6737	5655	5612	6123	6482
$\alpha$ (deg.)	0.00	2.43	1.51	0.81	0.27	-0.11	0.00
$\delta$ (deg.)	0.00	6.23	5.25	3.66	1.43	0.03	0.00
$\varepsilon$ (deg.)	0.00	3.05	2.91	2.14	0.57	-0.43	0.00



### 3.8 PREDICTION OF SHIP'S MOTIONS IN A SEAWAY

In carrying out weather routing simulations, it becomes important to predict the ship's motions and the probabilities of occurrence of accompanying phenomena such as shipping green water, slamming, propeller racing, etc. in rough seas so as to secure the safety of hull, cargo and crew.

Based on the linear superposition theory developed by St. Denis and Pierson,<sup>(13)</sup> the ship's motions in irregular waves can be predicted by superimposing the ship's motion for each component wave. That is, the variance of ship's motion in irregular waves can be calculated by integrating the product of the response amplitude operator squared for regular waves and the directional wave spectrum:

$$\sigma_z^2 = \int_0^{2\pi} \int_0^\infty \{ \text{RAO}(\omega, V, \mu) \}^2 S(\omega, \chi) d\omega d\chi \quad (3.47)$$

where  $\sigma_z^2$  : variance of ship's motion  $z(t)$

$\omega$  : angular frequency of component wave

$\chi$  : direction of component wave from the north

$\mu$  : direction of component wave from the bow

$\mu = \chi - \theta$                        $\theta$  : ship's heading

$V$  : ship's speed

$\text{RAO}(\omega, V, \mu)$  : response amplitude operator of ship's motion in regular waves ( i.e. amplitude of ship's motion per unit wave amplitude in regular waves )

$S(\omega, \chi)$  : directional spectrum of the ocean waves

For the same reason as mentioned for formula (3.29), it is not practical to use formula (3.47) directly in the routing algorithm for the prediction of ship's motions. Thus, following the manner taken for the calculation of added resistance due to waves, we assume that the ocean waves consist of two ideal wave systems, namely, sea and swell which have wave spectra given by (3.30) and (3.31).



By substituting the sea spectrum (3.30) or swell spectrum (3.31) into (3.47), we can calculate the variance of ship's motion due to sea  $\sigma_{SEA}^2$  or the variance of ship's motion due to swell  $\sigma_{SWELL}^2$ . The variance of ship's motion  $\sigma_z^2$  in ocean waves comprised of sea and swell is given by

$$\sigma_z^2 = \sigma_{SEA}^2 + \sigma_{SWELL}^2 \quad (3.48)$$

In general, the ship's motion  $z(t)$  in irregular waves may be regarded as a Gaussian random process, and its amplitude  $z_A$  follows a Rayleigh distribution.<sup>(14)</sup> When the amplitude of ship's motion  $z_A$  has a Rayleigh distribution, its mean value  $\bar{z}_A$ , 1/3 highest mean (significant amplitude)  $\bar{z}_{A1/3}$  and 1/10 highest mean  $\bar{z}_{A1/10}$  are given by<sup>(15)</sup>

$$\bar{z}_A = 1.25 \sigma_z \quad (3.49)$$

$$\bar{z}_{A1/3} = 2.00 \sigma_z \quad (3.50)$$

$$\bar{z}_{A1/10} = 2.55 \sigma_z \quad (3.51)$$

The formulae (3.49), (3.50) and (3.51) can be used to predict the heel/pitch angle, vertical/lateral acceleration, bending moment, etc..

The probability that the amplitude of ship's motion  $z_A$  exceeds a critical value  $z_{AC}$  can be calculated by<sup>(16)</sup>

$$P(z_A > z_{AC}) = \exp\{ -z_{AC}^2 / ( 2 \sigma_z^2 ) \} \quad (3.52)$$

The formula (3.52) can be used to predict the probabilities of occurrence of shipping green water, slamming, propeller racing, etc..

### 3.9 SHIP OPERATION CRITERIA IN ROUGH SEAS

In rough seas, when the ship's motions or the probabilities of occurrence of shipping green water, slamming, etc. exceed the critical limits ( i.e. thresholds ), the shipmaster usually reduces the ship's speed for the safety of hull, cargo and crew. In order to execute such voluntary speed reduction properly, the appropriate operation criteria of a ship in rough seas have to be established.

By investigating a number of voyage records, Lewis<sup>(17)</sup> and Aertssen<sup>(18)</sup> proposed critical values and thresholds of probability for the limit of ship operation shown in Table 3.2.

Table 3.2 Critical values and thresholds of probability for the limit of ship operation

$Z_{AC}$  : Critical value  
 $P(Z_A > Z_{AC})$  : Threshold of probability

	Vertical acceleration			Slamming	Shipping green water	Whipping stress
		$Z_{AC}$	$P(Z_A > Z_{AC})$	$P(Z_A > Z_{AC})$	$P(Z_A > Z_{AC})$	$Z_{AC}$
Lewis	Passengers' room	0.2 g	0.04	0.01	0.02	
	Crew's quarter	0.4 g	0.04			
	Working section	0.4 g	0.04			
Aertssen	Tanker	0.5 g	} at bow	0.03	0.05	2.0 kg/mm <sup>2</sup>
	Bulk carrier	0.5 g		0.03	0.05	2.0 kg/mm <sup>2</sup>
	Cargo ship	0.9 g		0.04	0.05	0.6 kg/mm <sup>2</sup>
	Ferry	1.0 g		0.05	0.05	0.4 kg/mm <sup>2</sup>
	Trawler	1.4 g		0.06	0.05	0.9 kg/mm <sup>2</sup>

Kitazawa, et al. established critical values and thresholds of probability shown in Table 3.3 for a container ship (  $L_{PP} = 175$  meters, service speed = 22.5 knots ), and calculated the critical ship's speed in rough seas.<sup>(19)</sup>

Table 3.3 Critical values and thresholds of probability used for calculating the critical speed of a container ship

	Critical value	Threshold of probability
Vertical acceleration at F.P.	0.8 g	$1 \times 10^{-3}$
Slamming	—	$1 \times 10^{-2}$
Shipping green water at F.P.	—	$2 \times 10^{-2}$
Vertical wave bending moment at midship	$7 \times 10^4$ t-m	$1 \times 10^{-5}$
Propeller racing	—	$1 \times 10^{-1}$
Lateral acceleration at S.S. 8 1/2	0.6 g	$1 \times 10^{-3}$
Rolling	$22.2^\circ - 25.8^\circ$	$1 \times 10^{-3}$

In general, the following phenomena may cause voluntary speed reduction in rough seas:

- (i) Vertical acceleration at the bow, slamming and shipping green water at the bow for head seas
- (ii) Propeller racing and a vertical wave bending moment at midship for head seas and following seas
- (iii) Lateral acceleration and rolling for beam seas or quartering seas

Particularly, slamming and shipping green water for head seas are the most dominant phenomena. In practice, it can be said that voluntary speed reduction is caused by slamming for ballast condition and by shipping green water at the bow for loaded condition.

In weather routing simulations, setting an appropriate critical value  $z_{AC}$  to detect the occurrence of slamming or shipping green water, the probability of occurrence  $P(z_A > z_{AC})$  is calculated based on formulae (3.47) and (3.52) for the given ship's heading and the number of propeller revolutions.

If  $P(z_A > z_{AC})$  exceeds the predetermined threshold of probability such as shown in Tables 3.2 and 3.3, that particular part of the route is omitted or as mentioned in 2.5, the penalty for the risk of damage is added to the objective function.



### 3.10 PREDICTION OF SHIPPING GREEN WATER AT THE BOW OF THE MODEL SHIP

The mathematical model ship described in section 3.2 is used for weather routing simulations in this study. Since this model ship is assumed to be in full loaded condition, shipping green water at the bow has to be considered as a dangerous phenomenon.

Thus the probabilities of occurrence of shipping green water at the bow of the model ship were calculated for various wave conditions and ship's speeds. These calculations were carried out by using the program developed at the Hydronautics section of the Department of Maritime Technology, Delft University of Technology.<sup>(20)</sup>

In order to predict the probability of occurrence of shipping green water, the relative vertical displacement of the bow to the local wave surface was taken as the quantity of the ship's motion  $z(t)$ . ( Fig.3.35 )

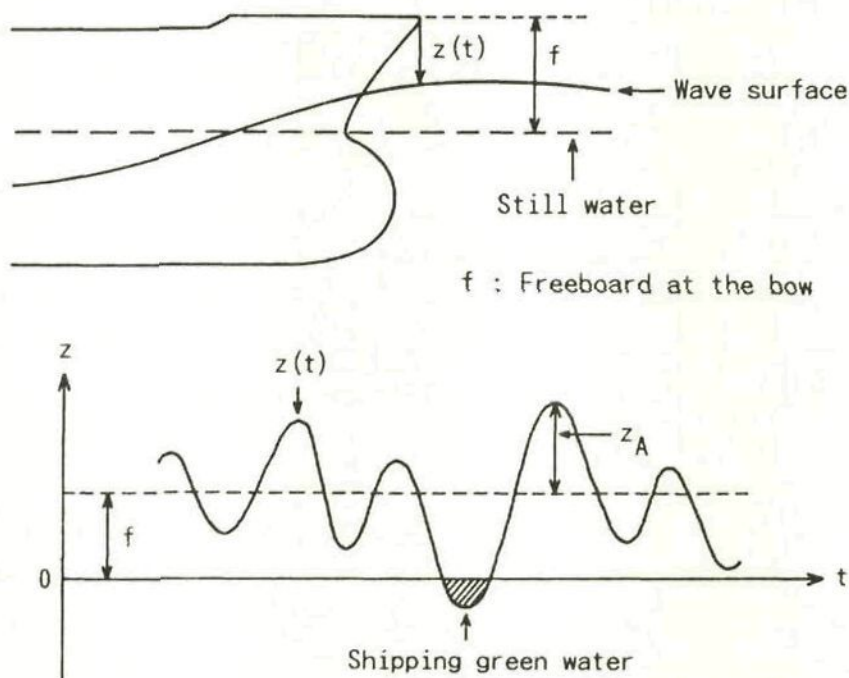


Fig. 3.35 Definitions of  $z(t)$ ,  $z_A$  and  $f$  in the model to predict the probability of occurrence of shipping green water at the bow

The relative vertical displacement  $z(t)$  is measured from the bow downward, and when  $z(t)$  becomes negative, shipping green water occurs.

The amplitude  $z_A$  of  $z(t)$  has a Rayleigh distribution. Letting the critical value of  $z_A$  be the freeboard at the bow  $f$ , the probability that  $z_A$  exceeds  $f$ , i.e. shipping green water occurs, is given by

$$P(z_A > f) = \exp\{ -f^2 / ( 2 \sigma_z^2 ) \} \quad (3.53)$$

where  $\sigma_z^2$  is the variance of  $z(t)$ .

In formula (3.53), the static and dynamic swell up of the wave surface under the bow are not taken into consideration. The freeboard at the bow  $f$  of the model ship is 10.2 meters.

In order to calculate the variance  $\sigma_z^2$  in (3.53), the unidirectional wave spectrum (3.31) was used for  $S(\omega, \chi)$  in formula (3.47). Based on formulae (3.47) and (3.53), the probabilities of occurrence of shipping green water at the bow  $P(z_A > f)$  of the model ship were calculated for the ship's speed of 3, 6, 9, 12, 15 knots, significant wave height of 4, 6, 8, 10, 12, 14 meters, wave direction from the bow of  $0^\circ, 25^\circ, 50^\circ, 75^\circ$  and average wave period of 6, 8, 10, 12, 14, 16 seconds.

Fig.3.36 shows those  $P(z_A > f)$  for a ship's speed of 12 knots and a significant wave height of 8 meters. From Fig.3.36, it is found that for an average wave period greater than 10 seconds,  $P(z_A > f)$  decreases as the wave direction from the bow  $\mu$  increases. For  $\mu = 75^\circ$ ,  $P(z_A > f)$  was zero for every average wave period.

In all results of calculations, when the ship's speed and significant wave height are given,  $P(z_A > f)$  decreased as  $\mu$  increased for an average wave period greater than 10 seconds. For average wave periods of 6 and 8 seconds,  $P(z_A > f)$  became maximum at  $\mu$  other than  $0^\circ$  depending on the encounter period of the ship to the waves.

In addition, as a matter of course,  $P(z_A > f)$  increased rapidly as the significant wave height increased. For example, when the ship's speed, wave direction from the bow and average wave period

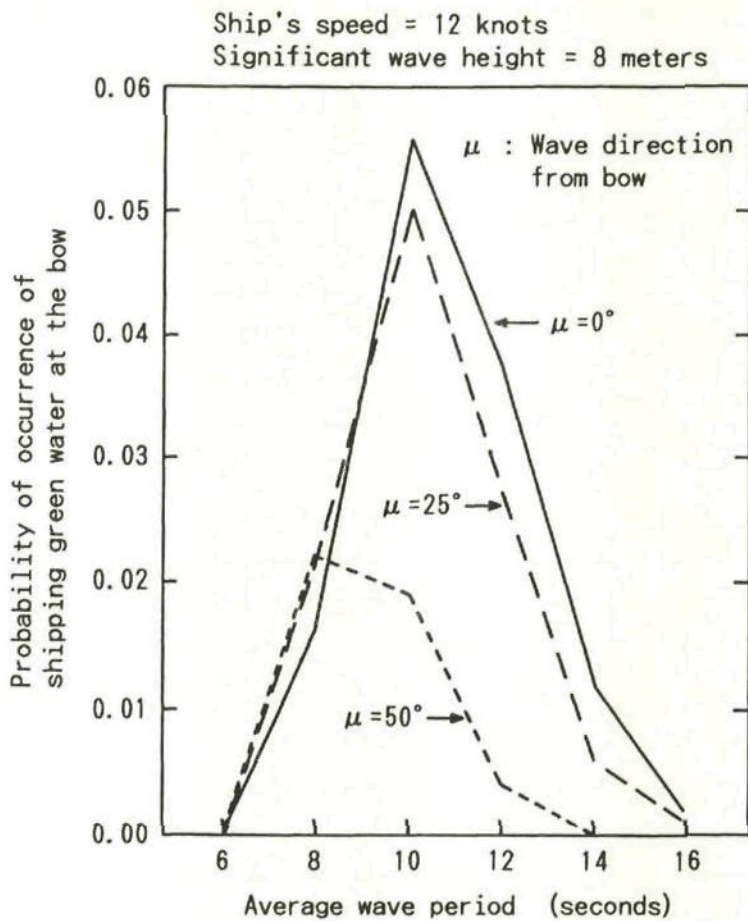


Fig. 3.36 Probability of occurrence of shipping green water at the bow versus average wave period

were 12 knots,  $0^\circ$  and 10 seconds,  $P(z_A > f)$  became 0.056, 0.158, 0.277 and 0.390 for the significant wave height of 8, 10, 12 and 14 meters.

In weather routing simulations performed in Chapter 6, when  $P(z_A > f)$  exceeds 0.04, it is assumed that the model ship has a risk of damage due to shipping green water. Thus the period in which  $P(z_A > f)$  exceeds 0.04 is accumulated during the voyage, and its total  $T_D$  is shown as one of various information for the shipmaster to determine the optimum route.



## 4. ENVIRONMENTAL DATA USED IN THE WEATHER ROUTING SIMULATIONS

### 4.1 INTRODUCTION

Many kinds of actual ( analyzed ) and/or predicted environmental data are used in the weather routing simulations for this thesis.

In the simulations of deterministic routing performed in Sections 5.2 through 5.5 and 6.2, the analyzed wind/sea/swell data and monthly ocean current data are used, which were prepared from the global-band data set published on magnetic tape by FNOC ( Fleet Numerical Oceanography Center ) of the U.S. Navy. Those analyzed wind/sea/swell data and ocean current data are described in 4.2 and 4.6, respectively.

On the other hand, in the simulations of stochastic routing carried out in Sections 5.6 and 6.3, various kinds of predicted wind, wave and ocean current data are used.

Concerning the wind and waves, the forecasted data by the numerical forecast models of FNOC are used for the period up to 72 hours ahead. At present, FNOC provides the longest period of wave forecasts on an operational basis, namely, 72 hours.

In recent years, ECMWF ( European Centre for Medium Range Weather Forecasts ) has been developing a new third generation model of wave forecasts. The test runs of global wave forecasting up to 5 days were already performed, but the daily operation of that new model has not yet been started.<sup>(1)</sup> Thus the forecasted wind/wave data by FNOC were chosen as the best data available now. The examples of those forecasted wind/wave data are shown in 4.3.

As mentioned in 2.4.1, the mean errors, covariance matrices and correlation matrices of forecasted wind/wave data are also necessary in stochastic routing to estimate the standard deviations of passage time and fuel consumption. The methods to calculate those mean

errors, covariance matrices and correlation matrices as well as their examples are described in 4.3.

In the simulations, the model ship is navigated in the North Pacific Ocean, and it takes more than two weeks for voyages between Tokyo and San Francisco. Therefore, it is necessary to use statistical wind/wave data or other wind/wave models as the predicted data for the period beyond 72 hours from the departure time in which the numerical forecasts are available. For those wind/wave data, the 5-day mean wind/wave models classified by the zonal index and the 1-month mean wind/wave data are used in this thesis.

In 4.4, the 5-day mean zonal index as a measure of circulation pattern of the upper-air westerlies is explained, and the 5-day mean wind/wave models classified by the zonal index are described. The methods to calculate the mean errors, covariance matrices and correlation matrices of those models as well as their examples are also shown in 4.4.

The 1-month mean wind/wave data as well as the examples of mean errors, covariance matrices and correlation matrices of those data are shown in 4.5.

Concerning the ocean currents for stochastic routing, the monthly ocean current data published on magnetic tape by the U.K. Meteorological Office are used as the predicted data. The mean value charts and covariance charts of those ocean current data are described in 4.7.

All wind/wave data and ocean current data mentioned above are memorized in a random-access file to be used in the simulations.

When the above-mentioned data are used in the simulations, interpolations over time and space are necessary to obtain the data for intermediate points. The interpolation scheme for the environmental data is described in 4.8. In addition, other hazardous environments to be considered in weather routing are stated in 4.9.



#### 4.2 ANALYZED WIND, SEA AND SWELL DATA

The analyzed wind, sea and swell data used for deterministic routing are taken from the outputs of the numerical forecast models of FNOC.

The weather forecast model 'NOGAPS' ( Navy Operational Global Atmospheric Prediction System ) computes the analyzed and forecasted global weather conditions up to 5 days at 12-hour intervals.<sup>(2)</sup> The wind speed and direction at 19.5 meters above the sea surface are obtained at each grid point as one of the outputs of NOGAPS.<sup>(3)</sup> In deterministic routing, the analyzed values of those wind speed and direction are used.

( In a surface boundary layer, the wind speed increases as the height above the sea surface increases, according to a logarithmic law. For the model ship, the height of the center of effort of the sails is about 35 meters, whereas that of the center of wind pressure necessary for calculating the wind resistance, etc. is about 13 meters. The wind speeds at these two points will be about 105% and 96% of the wind speed at a height of 19.5 meters. In the actual voyage, however, the sail performance will deteriorate in some degree because of the ship's motions. In addition, since the model ship is in full loaded conditions, wind resistance, etc. due to hull and superstructure are comparatively small. Thus, all aerodynamic forces and moments are calculated using the wind speed at a height of 19.5 meters in this thesis. )

Using the wind data provided by NOGAPS, the wave forecast model 'SOWM' ( Spectral Ocean Wave Model ) computes the analyzed and forecasted wave conditions for the Northern Hemisphere up to 3 days at 12-hour intervals as a form of directional wave spectrum ( 15 frequency bands and 12 direction bands ).<sup>(3)</sup>

Then, based on that directional wave spectrum, two ideal wave systems, i.e. sea and swell, are calculated at each grid point, the data form of which is significant height, predominant direction and average period. In deterministic routing, the analyzed values of those sea and swell data are used.



( Since April in 1983, the form of the output data of SOWM has been changed to significant wave height, primary wave direction/period and secondary wave direction/period. Furthermore, since 1985, SOWM has been extended so as to cover also the Southern Hemisphere, and has been renamed 'GSOWM' ( Global Spectral Ocean Wave Model ). )

In order to execute deterministic routing, the analyzed wind/sea/swell data for the North Pacific Ocean at 00 and 12 hours GMT for November and December in 1980 were selected from the output data set of NOGAPS and SOWM. The number of grid points for those data is 1,500 (  $25 \times 60$  ), and the intervals between grid points are  $1.87^\circ$  ( on average ) for latitudinal direction and  $2.50^\circ$  for longitudinal direction. Table 4.1 shows the latitudes and longitudes of those grid points.

Table 4.1 Table of latitudes and longitudes of  $25 \times 60$  grid points in the North Pacific Ocean

Grid number	Latitude	Grid number	Longitude
1	$59.745^\circ$ N	1	$120.0^\circ$ E
2	$58.462^\circ$ N	2	$122.5^\circ$ E
3	$57.131^\circ$ N	3	$125.0^\circ$ E
4	$55.750^\circ$ N	.	.
5	$54.318^\circ$ N	.	.
6	$52.835^\circ$ N	.	.
7	$51.300^\circ$ N	58	$97.5^\circ$ W
8	$49.711^\circ$ N	59	$95.0^\circ$ W
9	$48.069^\circ$ N	60	$92.5^\circ$ W
10	$46.372^\circ$ N		
11	$44.621^\circ$ N		
12	$42.816^\circ$ N		
13	$40.956^\circ$ N		
14	$39.042^\circ$ N		
15	$37.076^\circ$ N		
16	$35.056^\circ$ N		
17	$32.986^\circ$ N		
18	$30.866^\circ$ N		
19	$28.698^\circ$ N		
20	$26.484^\circ$ N		
21	$24.226^\circ$ N		
22	$21.928^\circ$ N		
23	$19.593^\circ$ N		
24	$17.222^\circ$ N		
25	$14.821^\circ$ N		

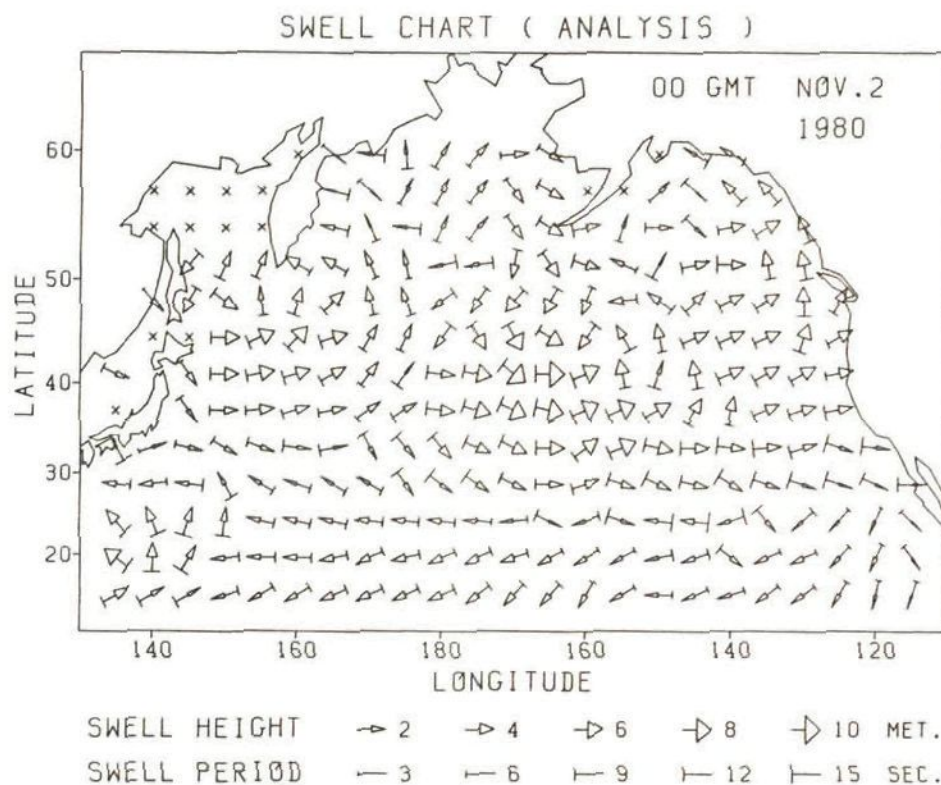


Fig. 4.1 (c) Example of analyzed swell data  
( 00 hours GMT 2 November 1980 )

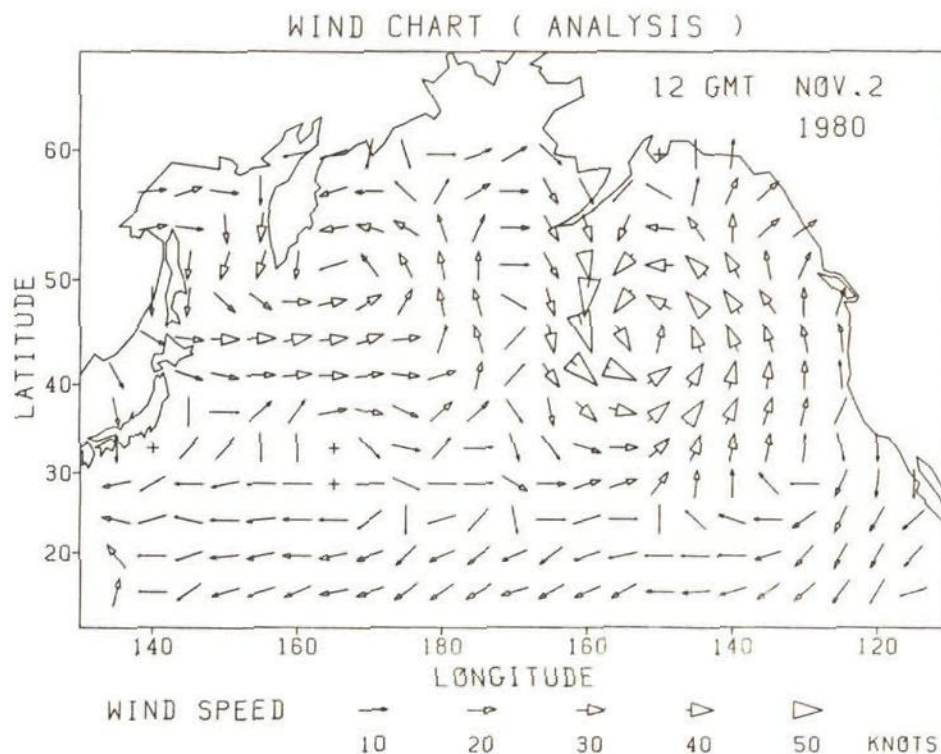


Fig. 4.2 (a) Example of analyzed wind data  
( 12 hours GMT 2 November 1980 )

# SEA CHART ( ANALYSIS )

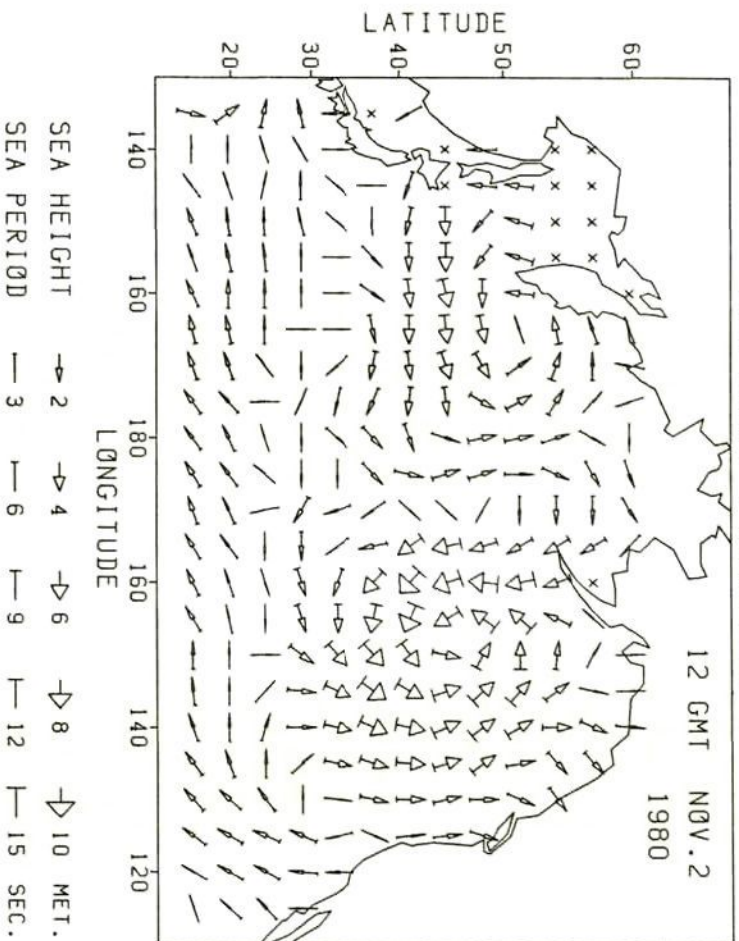


Fig. 4.2 (b) Example of analyzed sea data  
( 12 hours GMT 2 November 1980 )

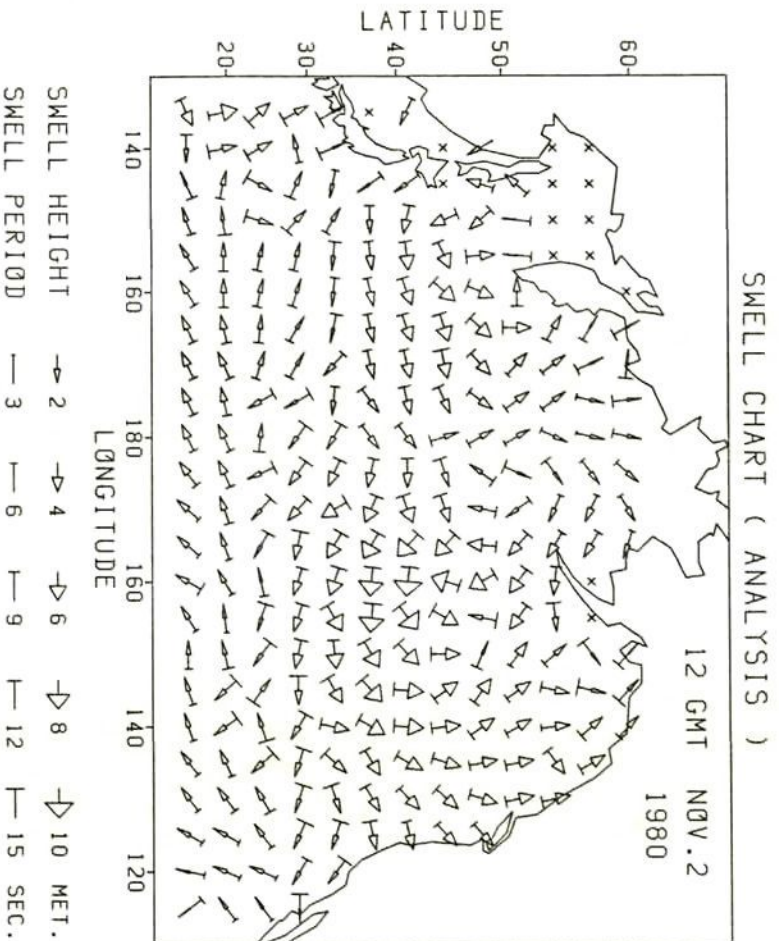


Fig. 4.2 (c) Example of analyzed swell data  
( 12 hours GMT 2 November 1980 )



### 4.3 FORECASTED WIND AND WAVE DATA

#### 4.3.1 Forecasted wind and wave charts

For stochastic routing, the analyzed wind/wave data and the forecasted wind/wave data for 12, 24, 36, 48, 60 and 72-hour forecasts are taken from the outputs of NOGAPS and GSOWM.

Concerning the wave data, as mentioned in 4.2, the parameters of the output data of GSOWM are the significant wave height, primary wave direction/period and secondary wave direction/period. Since we do not have a reasonable way to separate the significant wave height into the heights of primary and secondary wave systems, only the significant wave height and primary wave direction/period are adopted as the parameters to represent the wave conditions.

In order to perform stochastic routing, the analyzed and forecasted wind/wave data for the North Pacific Ocean at 00 and 12 hours GMT for February in 1985 were selected from the output data set of NOGAPS and GSOWM. ( In addition, the analyzed wind/wave data for the first half of March in 1985 were also selected. )

The analyzed and forecasted wind/wave data for 00 hours GMT on 14 February in 1985 issued 00, 12, 24, 36, 48 and 72 hours before are shown in Fig.4.3 through Fig.4.8. As the 60-hour and 72-hour forecasts are issued only at 00 hours GMT every day, there is no 60-hour forecast for 00 hours GMT.

By comparing Fig.4.3 with Figs 4.4 - 4.8, it is found that the depressions located to the east of Japan and in the Gulf of Alaska could be predicted properly in some degree.

To remove the statistical biases from the forecasted data mentioned above, the mean errors are added to the forecasted data. Then those unbiased wind/wave forecast data are used in the stochastic routing.

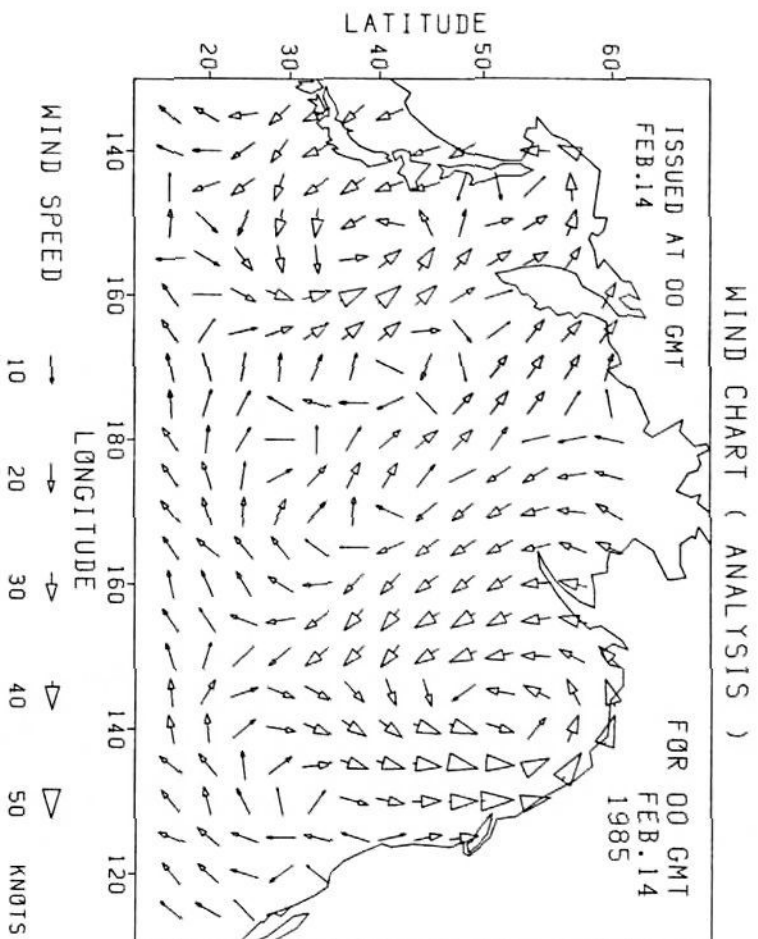


Fig. 4.3 (a) Example of analyzed wind data  
( 00 hours GMT 14 February 1985 )

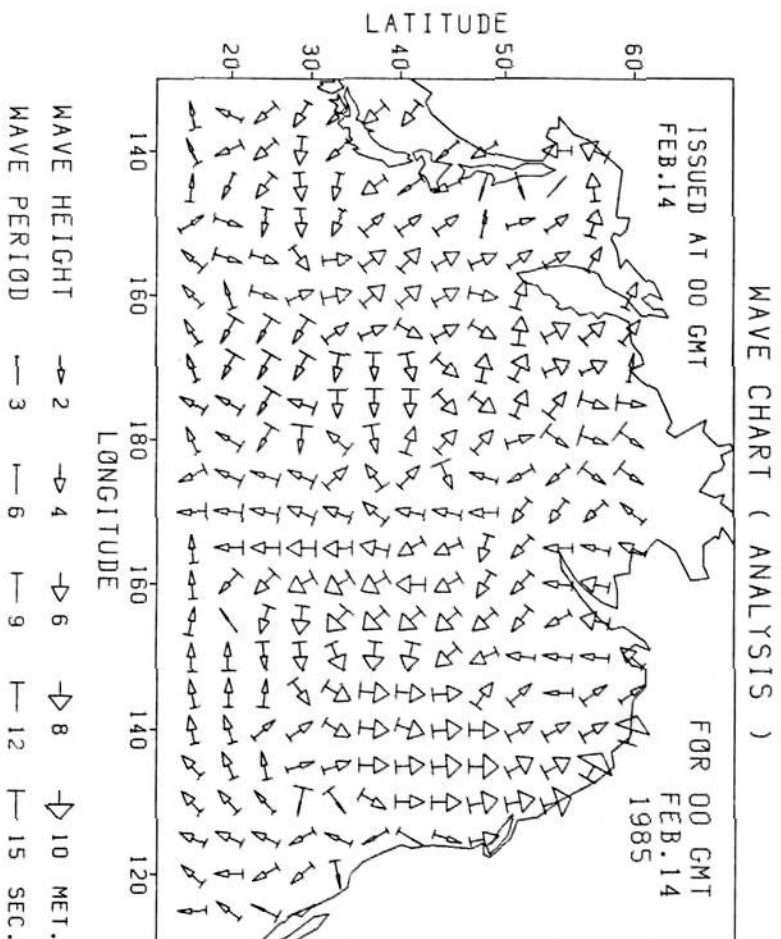


Fig. 4.3 (b) Example of analyzed wave data  
( 00 hours GMT 14 February 1985 )

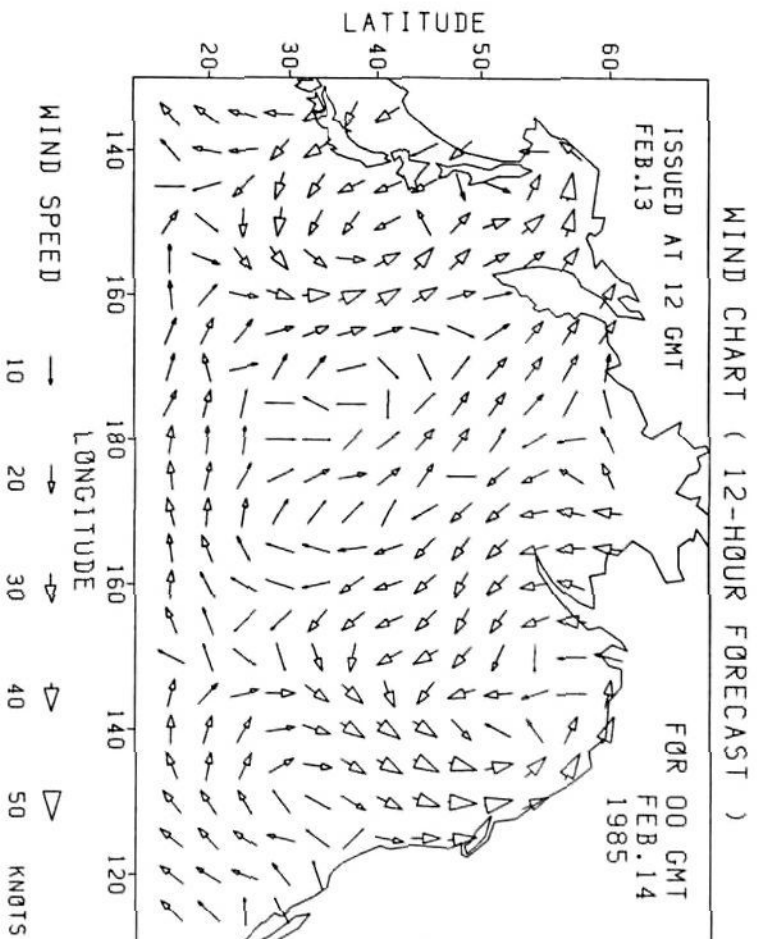


Fig. 4.4 (a)    Example of forecasted wind data  
 ( 12-hour forecast for 00 hours GMT 14 February 1985 )

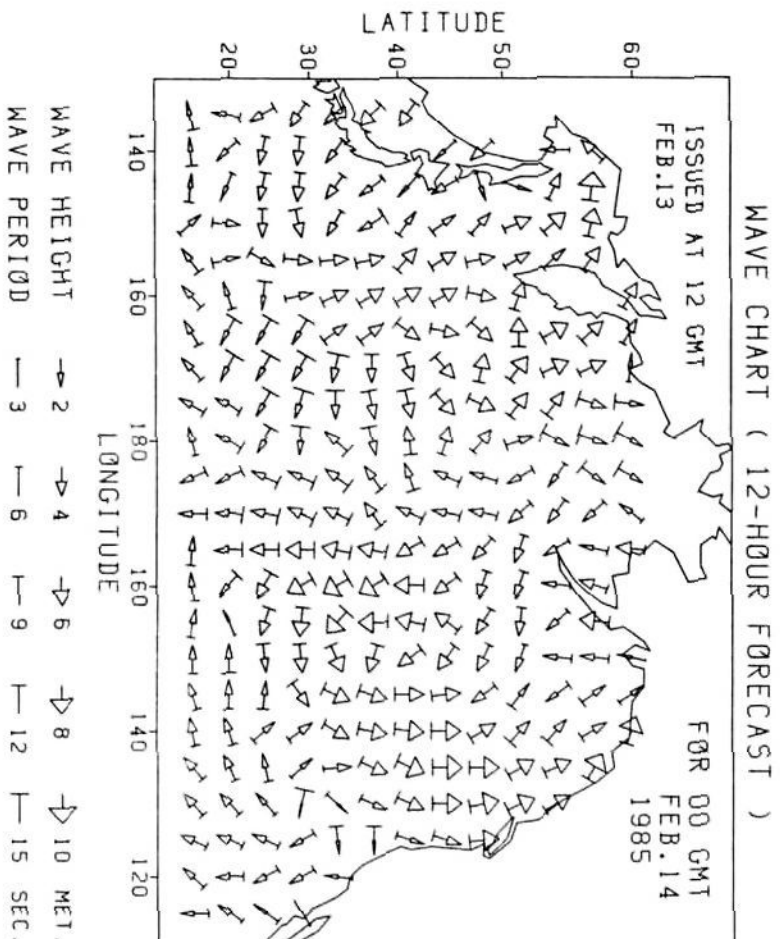


Fig. 4.4 (b)    Example of forecasted wave data  
 ( 12-hour forecast for 00 hours GMT 14 February 1985 )



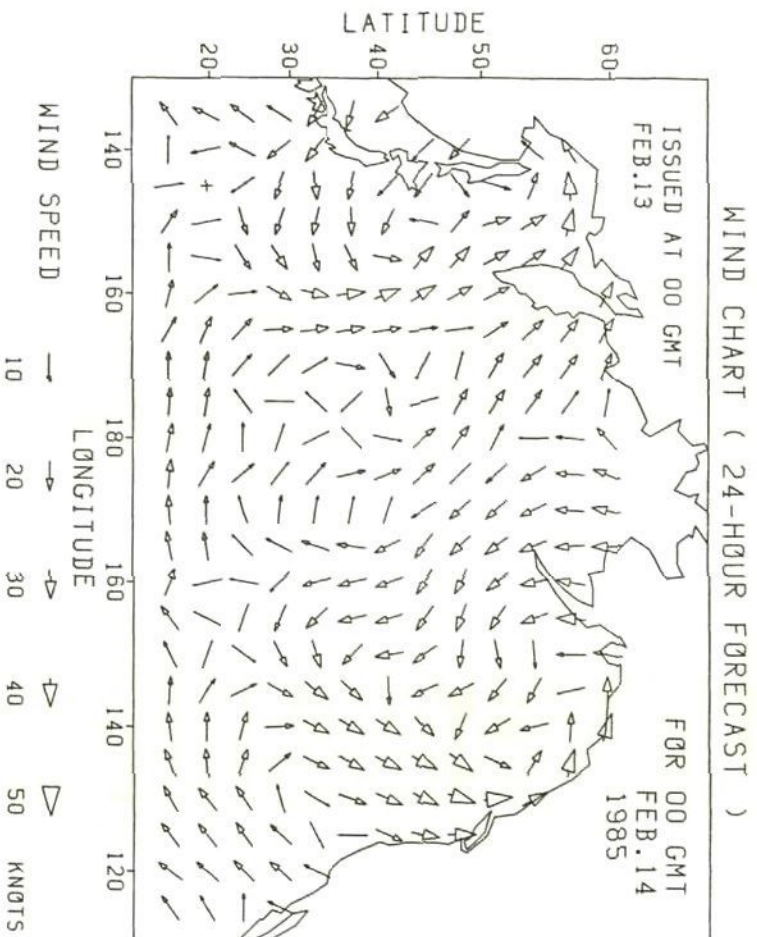


Fig. 4.5 (a) Example of forecasted wind data  
( 24-hour forecast for 00 hours GMT 14 February 1985 )

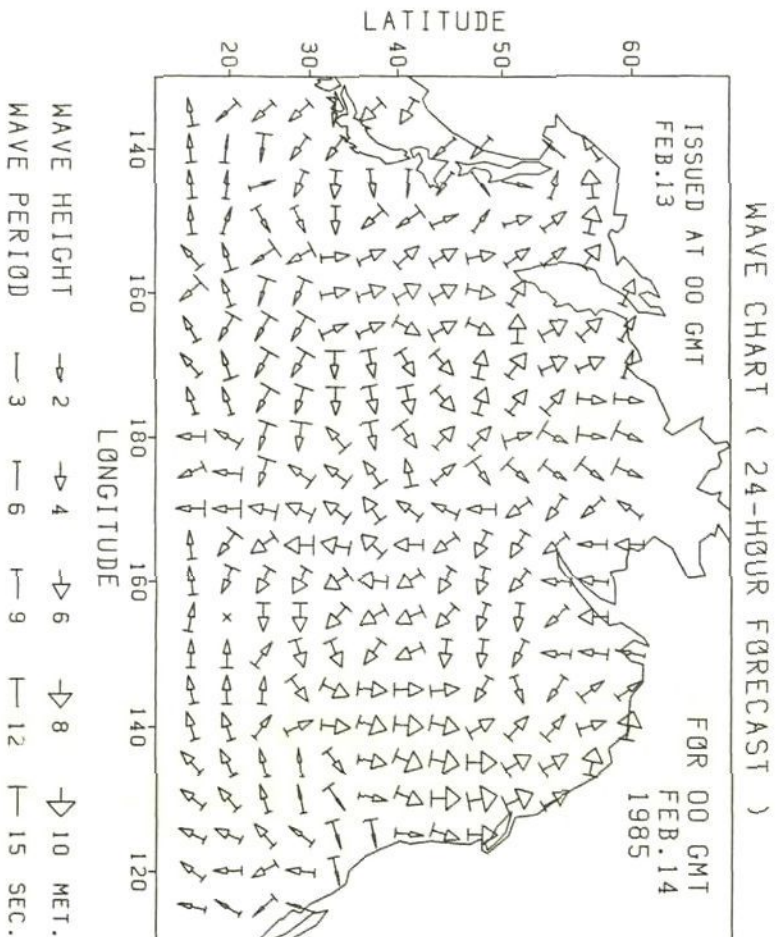


Fig. 4.5 (b) Example of forecasted wave data  
( 24-hour forecast for 00 hours GMT 14 February 1985 )

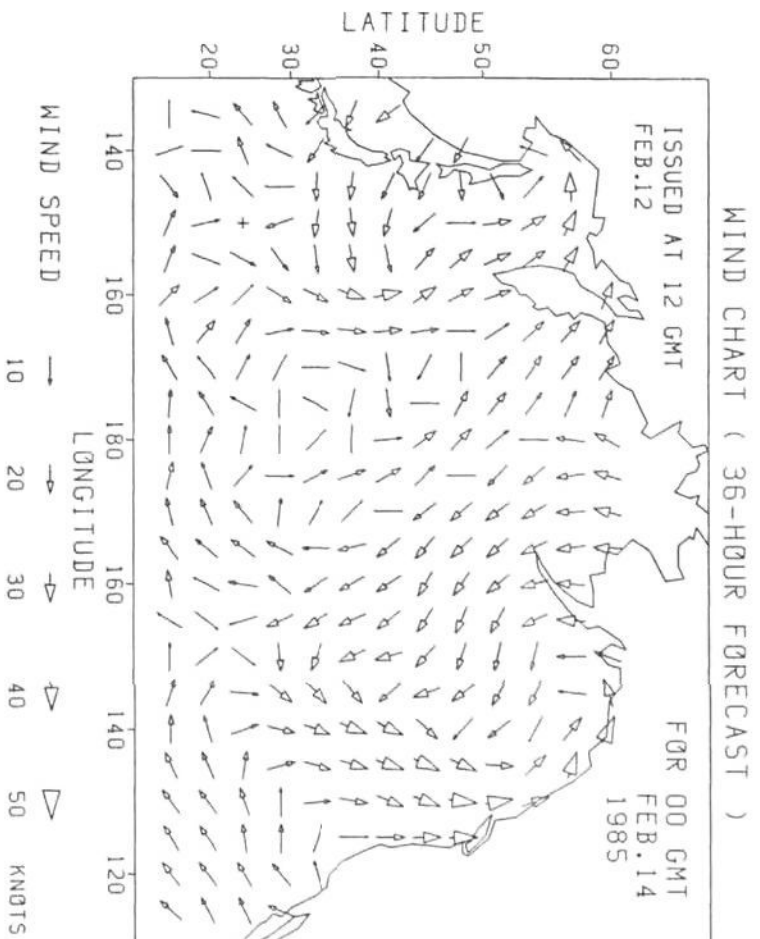


Fig. 4.6 (a)      Example of forecasted wind data  
 ( 36-hour forecast for 00 hours GMT 14 February 1985 )

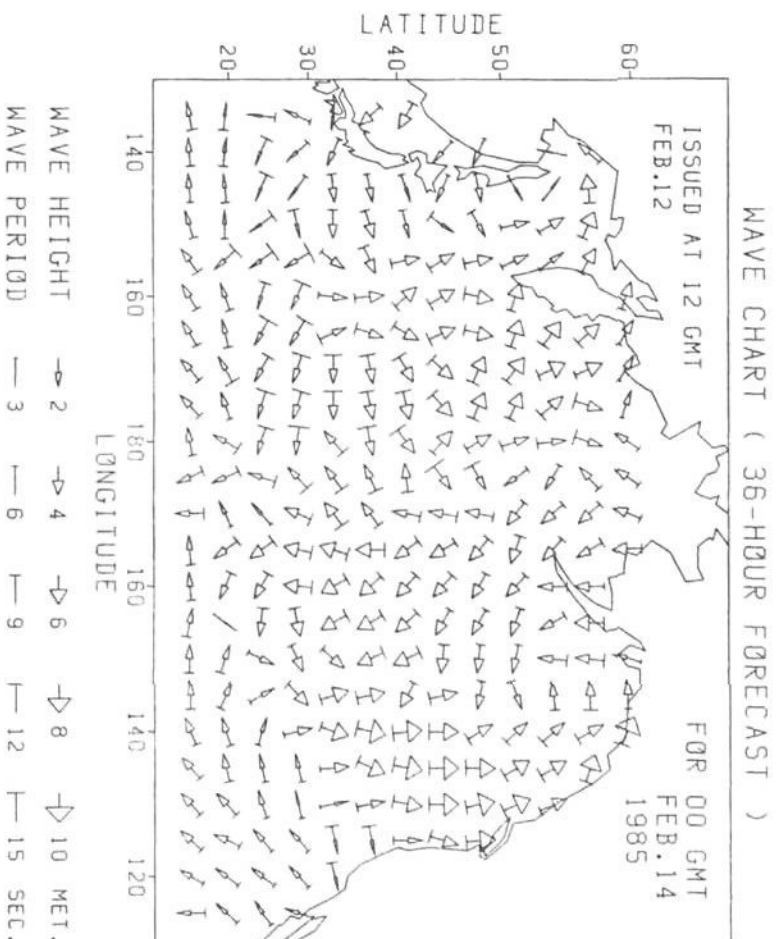


Fig. 4.6 (b)      Example of forecasted wave data  
 ( 36-hour forecast for 00 hours GMT 14 February 1985 )

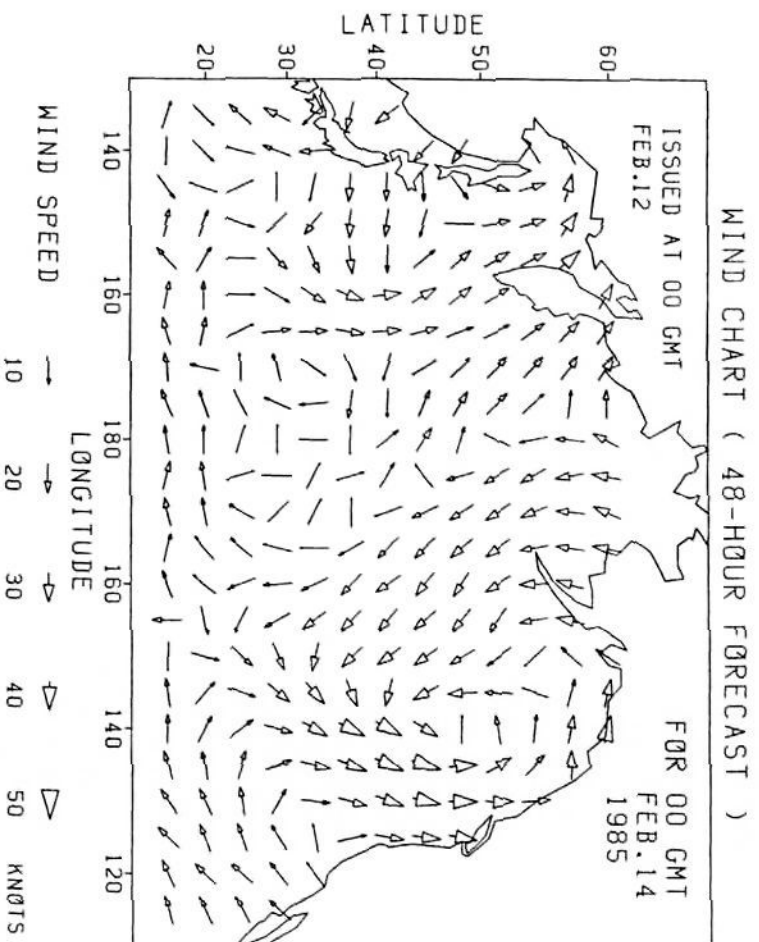


Fig. 4.7 (a) Example of forecasted wind data  
( 48-hour forecast for 00 hours GMT 14 February 1985 )

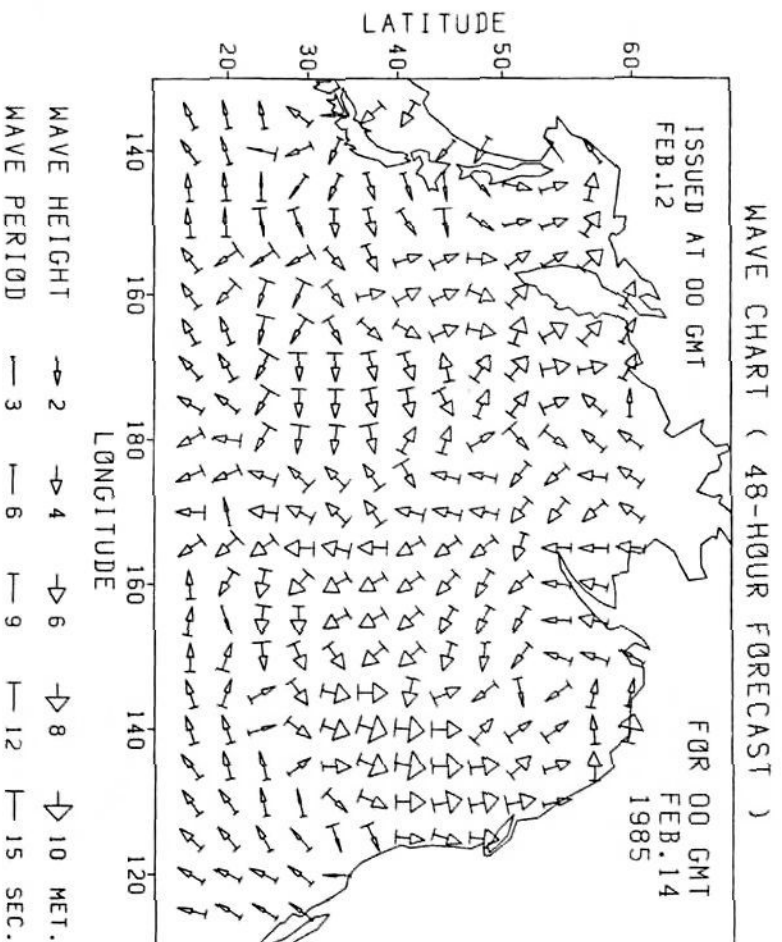


Fig. 4.7 (b) Example of forecasted wave data  
( 48-hour forecast for 00 hours GMT 14 February 1985 )



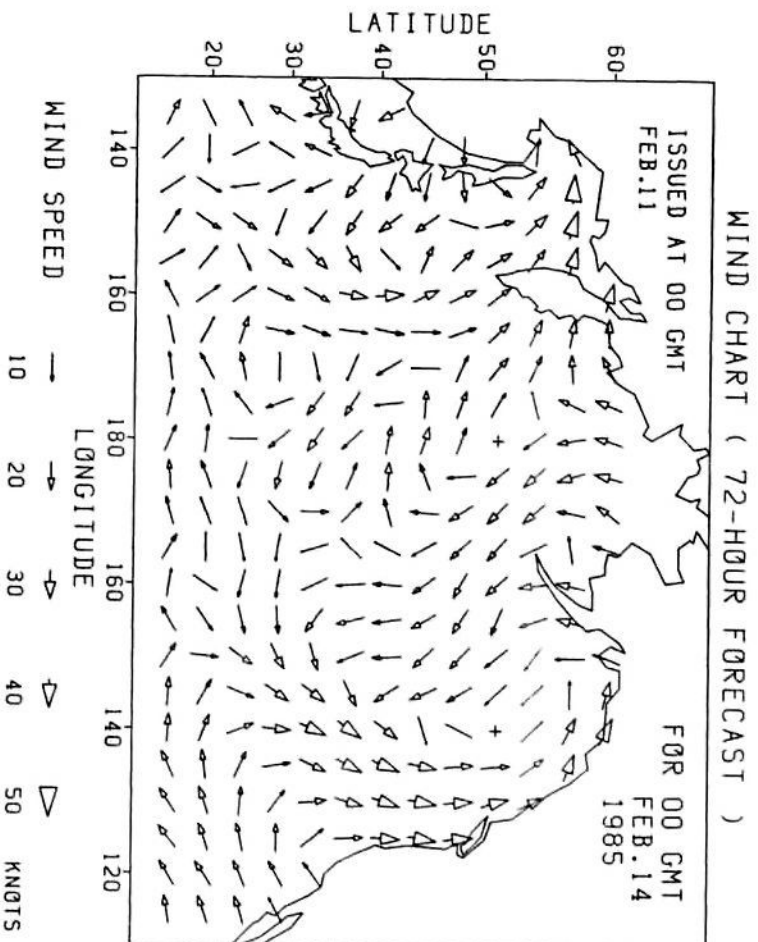


Fig. 4.8 (a) Example of forecasted wind data  
( 72-hour forecast for 00 hours GMT 14 February 1985 )

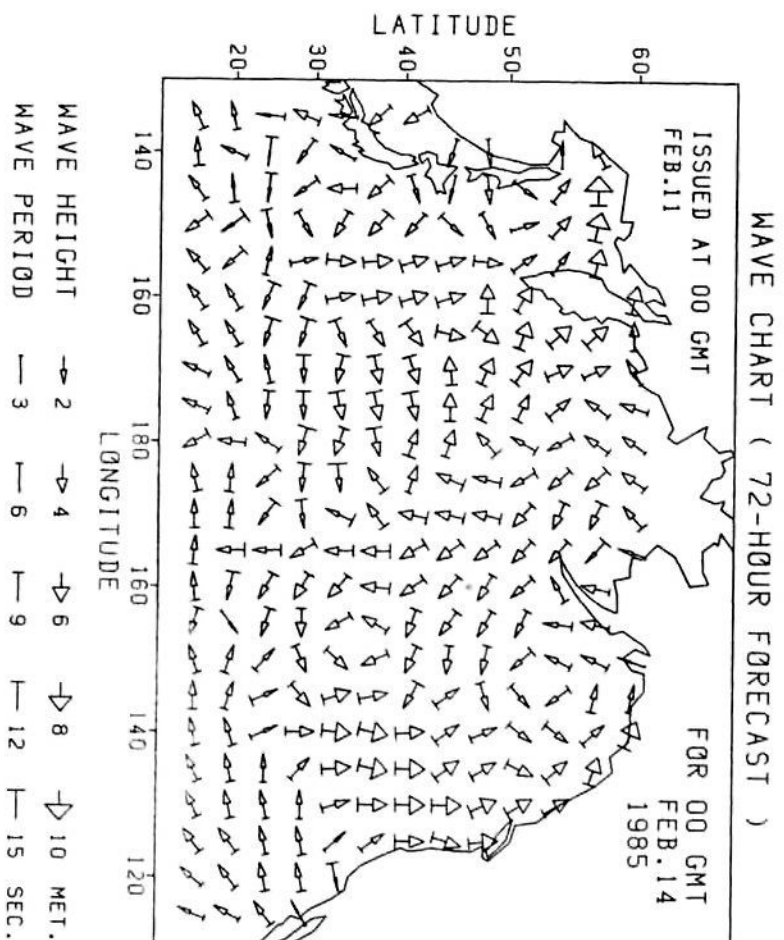


Fig. 4.8 (b) Example of forecasted wave data  
( 72-hour forecast for 00 hours GMT 14 February 1985 )

#### 4.3.2 Mean errors and covariance matrices of forecasted wind/wave data

As stated in 2.4.1, for carrying out stochastic routing, it is necessary to obtain the unbiased wind/wave forecast data  $\bar{C}_i$  and the covariance matrix  $P_c(i)$  of their errors  $\Delta C_i$ .

First, at each grid point of NOGAPS and GSOWM shown in Table 4.1, the mean errors of forecasted wind/wave data were calculated by averaging the differences between analyzed data and forecasted data at 00 and 12 hours GMT for February in 1985:

$$E[\Delta \hat{C}(m,n,t)] = E[ \underline{C}(m,n) - \hat{C}(m,n,t) ] \quad (4.1)$$

where  $m,n$  : grid point number in the North Pacific Ocean

(  $m = 1,2,---,25$  ;  $n = 1,2,---,60$  )

$t$  : time of forecasts (  $t = 12,24,36,48,60$  and  $72$  hours )

$\underline{C}(m,n)$  : analyzed wind/wave data

$\hat{C}(m,n,t)$  : forecasted wind/wave data

$E[\Delta \hat{C}(m,n,t)]$  : mean errors of forecasted wind/wave data

The components of vector  $\underline{C}(m,n)$  and  $\hat{C}(m,n,t)$  are as follows:

$$\underline{C}(m,n) = [ S_w \ D_w \ H_s \ D_p \ T_p ]^T \quad (4.2)$$

$$\hat{C}(m,n,t) = [ \hat{S}_w \ \hat{D}_w \ \hat{H}_s \ \hat{D}_p \ \hat{T}_p ]^T \quad (4.3)$$

where  $S_w$ ,  $D_w$ ,  $H_s$ ,  $D_p$  and  $T_p$  are analyzed wind speed, wind direction, significant wave height, primary wave direction and primary wave period, respectively at grid point  $(m,n)$  ;

$\hat{S}_w$ ,  $\hat{D}_w$ ,  $\hat{H}_s$ ,  $\hat{D}_p$  and  $\hat{T}_p$  are forecasted wind speed, wind direction, significant wave height, primary wave direction and primary wave period, respectively at grid point  $(m,n)$  for  $t$ -hour forecast.

Then, by adding the mean errors to the forecasted wind/wave data at each grid point, the unbiased wind/wave forecast data were calculated:

$$\bar{C}(m,n,t) = \hat{C}(m,n,t) + E[\Delta\hat{C}(m,n,t)] \quad (4.4)$$

where  $\bar{C}(m,n,t)$  : unbiased wind/wave forecast data ( i.e. mean values of wind/wave data ) at grid point (m,n) for t-hour forecast

In the simulations, the unbiased wind/wave forecast data  $\bar{C}_i$  at the given time  $t_i$  and predicted ship's position  $\bar{X}_i$  are calculated by linear interpolations over time and space using  $\bar{C}(m,n,t)$ .

Next, the errors of the unbiased wind/wave forecast data at each grid point were defined as

$$\Delta C(m,n,t) = C(m,n) - \bar{C}(m,n,t) \quad (4.5)$$

where  $\Delta C(m,n,t)$  : errors of unbiased wind/wave forecast data

Multiplying the error vector  $\Delta C(m,n,t)$  by its transpose and taking its average over February in 1985, the covariance matrix  $P_c(m,n,t)$  of the errors in the unbiased wind/wave forecast data were calculated at each grid point:

$$P_c(m,n,t) = E[ \Delta C(m,n,t) \Delta C(m,n,t)^T ] \quad (4.6)$$

It is not practical to use  $P_c(m,n,t)$  directly in the routing algorithm, because a huge amount of memory space is needed to store  $P_c(m,n,t)$  (  $5 \times 5$  matrix ) at  $25 \times 60$  grid points for  $t = 12, 24, \dots, 72$  hours. Moreover, since the period for averaging was only one month ( i.e. February in 1985 ), the values of  $P_c(m,n,t)$  varied considerably even in a small area.

Thus, in order to overcome such problems, the whole area of the North Pacific Ocean to be considered in the simulations was divided into sub-areas as shown in Fig.4.9. The size of each sub-area is  $7.4^\circ$  ( on average ) in latitude and  $10.0^\circ$  in longitude, and it contains 16 (  $4 \times 4$  ) grid points.



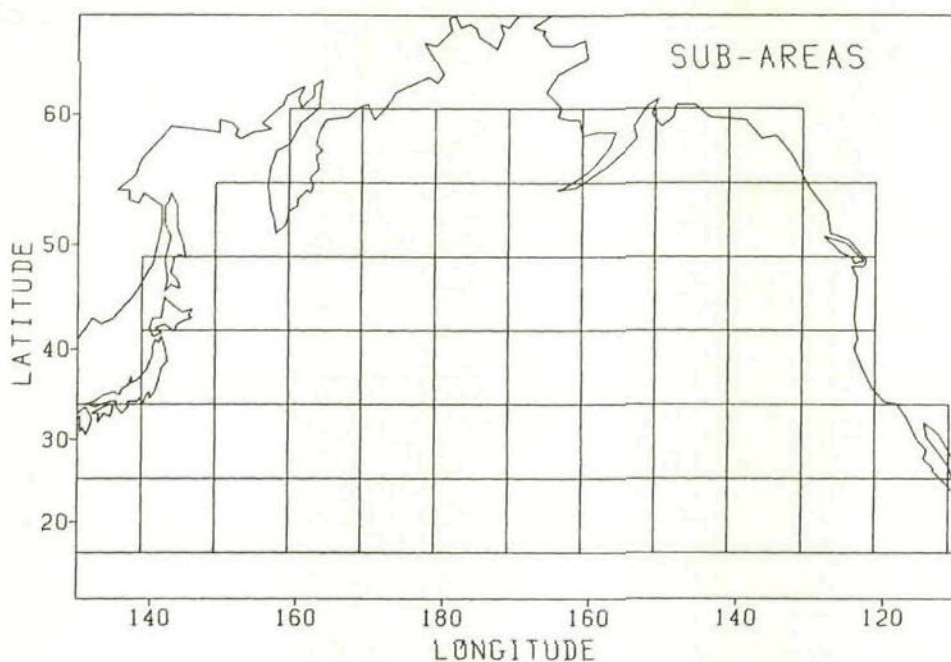


Fig. 4.9 Sub-areas for averaging covariance matrices and correlation coefficients

Averaging the covariance matrices  $P_c(m,n,t)$  at all grid points included in each sub-area, the averaged covariance matrix  $\bar{P}_c(m',n',t)$  was calculated and memorized at the central point of each sub-area, where  $m'$  and  $n'$  denote the sub-area number. ( In this averaging,  $P_c(m,n,t)$  at the grid points on the land were excluded. ) By using  $\bar{P}_c(m',n',t)$  instead of  $P_c(m,n,t)$ , we can save memory space and improve the confidence of the covariance matrix.

In the simulations, the covariance matrix  $P_c(i)$  of the errors in the unbiased wind/wave forecast data at the given time  $t_i$  and predicted ship's position  $\bar{X}_i$  is calculated by linear interpolations over time and space using the averaged covariance matrices  $\bar{P}_c(m',n',t)$  memorized at the central points of the sub-areas.

Examples of the mean errors of forecasted wind/wave data and the covariance matrix of the errors in the unbiased wind/wave forecast data are described below. In these examples, the simplified term 'covariance matrix ( or standard deviations ) of forecasted wind/wave data' is used in the same meaning as 'covariance matrix

( or standard deviations ) of the errors in the unbiased wind/wave forecast data'.

Table 4.2 shows the mean errors and covariance matrices of forecasted wind/wave data averaged over 16 grid points in sub-area (  $41.89^{\circ}\text{N}$  -  $48.89^{\circ}\text{N}$ ,  $178.75^{\circ}\text{E}$  -  $171.25^{\circ}\text{W}$  ) for the time of forecasts  $t = 12, 24, 36, 48, 60$  and  $72$  hours.

The diagonal terms in each covariance matrix represent the variances of errors in forecasted wind speed, wind direction, significant wave height, primary wave direction and primary wave period. It can be seen that those variances increase as the time of forecasts increases.

The mean errors and standard deviations of forecasted wind/wave data averaged over all the North Pacific Ocean versus time of forecasts are shown in Fig.4.10 (a)-(e). ( In this averaging, the sub-areas which have more than 6 grid points on the land were excluded. )

From Fig.4.10, it is found that as a matter of course, the standard deviations of forecasted wind/wave data increase as the time of forecasts increases. Furthermore, we can find that the mean errors of wind speed, wave height and wave period increase with the time of forecasts.

Table 4.2 Mean errors and covariance matrices of forecasted wind/wave data averaged over 16 grid points in sub-area ( 41.89°N - 48.89°N, 178.75°E - 171.25°W ) for 12, 24, 36, 48, 60 and 72-hour forecasts

\*\*\*\*\* TIME OF FORECASTS = 12 HOURS \*\*\*\*\*

(1) MEAN ERRORS OF FORECASTED WIND/WAVE DATA

WIND SPEED = 1.048 KNOTS  
WIND DIRECTION = 0.094 DEGREES  
WAVE HEIGHT = 0.270 METERS  
WAVE DIRECTION = -0.467 DEGREES  
WAVE PERIOD = 0.156 SECONDS

(2) COVARIANCE MATRIX OF FORECASTED WIND/WAVE DATA

	WIND SPE.	WIND DIR.	WAVE HEI.	WAVE DIR.	WAVE PER.
WIND SPEED (KNOTS)	42.68	-7.93	0.94	-1.36	0.70
WIND DIRECTION (DEGREES)	-7.93	793.10	0.64	54.89	1.89
WAVE HEIGHT (METERS)	0.94	0.64	0.25	0.74	0.15
WAVE DIRECTION (DEGREES)	-1.36	54.89	0.74	685.70	0.07
WAVE PERIOD (SECONDS)	0.70	1.89	0.15	0.07	1.63

\*\*\*\*\* TIME OF FORECASTS = 24 HOURS \*\*\*\*\*

(1) MEAN ERRORS OF FORECASTED WIND/WAVE DATA

WIND SPEED = 4.157 KNOTS  
WIND DIRECTION = 0.390 DEGREES  
WAVE HEIGHT = 0.468 METERS  
WAVE DIRECTION = 2.123 DEGREES  
WAVE PERIOD = 0.403 SECONDS

(2) COVARIANCE MATRIX OF FORECASTED WIND/WAVE DATA

	WIND SPE.	WIND DIR.	WAVE HEI.	WAVE DIR.	WAVE PER.
WIND SPEED (KNOTS)	56.28	-14.94	2.87	-24.02	0.59
WIND DIRECTION (DEGREES)	-14.94	1687.69	-2.49	182.22	-2.41
WAVE HEIGHT (METERS)	2.87	-2.49	0.68	-4.49	0.47
WAVE DIRECTION (DEGREES)	-24.02	182.22	-4.49	1498.85	-8.75
WAVE PERIOD (SECONDS)	0.59	-2.41	0.47	-8.75	3.32

\*\*\*\*\* TIME OF FORECASTS = 36 HOURS \*\*\*\*\*

(1) MEAN ERRORS OF FORECASTED WIND/WAVE DATA

WIND SPEED = 3.731 KNOTS  
WIND DIRECTION = 1.088 DEGREES  
WAVE HEIGHT = 0.621 METERS  
WAVE DIRECTION = 3.439 DEGREES  
WAVE PERIOD = 0.366 SECONDS

(2) COVARIANCE MATRIX OF FORECASTED WIND/WAVE DATA

	WIND SPE.	WIND DIR.	WAVE HEI.	WAVE DIR.	WAVE PER.
WIND SPEED (KNOTS)	88.12	-0.17	5.64	-82.67	3.73
WIND DIRECTION (DEGREES)	-0.17	2128.12	-1.16	400.90	-3.06
WAVE HEIGHT (METERS)	5.64	-1.16	1.13	-10.67	0.93
WAVE DIRECTION (DEGREES)	-82.67	400.90	-10.67	2195.39	-14.72
WAVE PERIOD (SECONDS)	3.73	-3.06	0.93	-14.72	4.52



\*\*\*\*\* TIME OF FORECASTS = 48 HOURS \*\*\*\*\*

(1) MEAN ERRORS OF FORECASTED WIND/WAVE DATA

WIND SPEED = 2.136 KNOTS  
WIND DIRECTION = 2.950 DEGREES  
WAVE HEIGHT = 0.651 METERS  
WAVE DIRECTION = 3.835 DEGREES  
WAVE PERIOD = 0.507 SECONDS

(2) COVARIANCE MATRIX OF FORECASTED WIND/WAVE DATA

	WIND SPE.	WIND DIR.	WAVE HEI.	WAVE DIR.	WAVE PER.
WIND SPEED (KNOTS)	92.82	23.35	6.50	-61.81	1.39
WIND DIRECTION (DEGREES)	23.35	2447.18	1.06	645.80	-9.74
WAVE HEIGHT (METERS)	6.50	1.06	1.42	-6.24	0.90
WAVE DIRECTION (DEGREES)	-61.81	645.80	-6.24	2783.02	-13.87
WAVE PERIOD (SECONDS)	1.39	-9.74	0.90	-13.87	4.58

\*\*\*\*\* TIME OF FORECASTS = 60 HOURS \*\*\*\*\*

(1) MEAN ERRORS OF FORECASTED WIND/WAVE DATA

WIND SPEED = 2.464 KNOTS  
WIND DIRECTION = 0.745 DEGREES  
WAVE HEIGHT = 0.642 METERS  
WAVE DIRECTION = 3.808 DEGREES  
WAVE PERIOD = 0.471 SECONDS

(2) COVARIANCE MATRIX OF FORECASTED WIND/WAVE DATA

	WIND SPE.	WIND DIR.	WAVE HEI.	WAVE DIR.	WAVE PER.
WIND SPEED (KNOTS)	104.10	50.36	5.65	-27.99	1.08
WIND DIRECTION (DEGREES)	50.36	3813.03	8.57	942.28	-12.30
WAVE HEIGHT (METERS)	5.65	8.57	1.37	4.22	0.61
WAVE DIRECTION (DEGREES)	-27.99	942.28	4.22	2950.35	-18.81
WAVE PERIOD (SECONDS)	1.08	-12.30	0.61	-18.81	3.79

\*\*\*\*\* TIME OF FORECASTS = 72 HOURS \*\*\*\*\*

(1) MEAN ERRORS OF FORECASTED WIND/WAVE DATA

WIND SPEED = 1.959 KNOTS  
WIND DIRECTION = -16.038 DEGREES  
WAVE HEIGHT = 0.705 METERS  
WAVE DIRECTION = 0.952 DEGREES  
WAVE PERIOD = 0.760 SECONDS

(2) COVARIANCE MATRIX OF FORECASTED WIND/WAVE DATA

	WIND SPE.	WIND DIR.	WAVE HEI.	WAVE DIR.	WAVE PER.
WIND SPEED (KNOTS)	100.94	0.96	7.43	46.34	2.15
WIND DIRECTION (DEGREES)	0.96	4064.81	15.62	734.43	-5.63
WAVE HEIGHT (METERS)	7.43	15.62	1.67	9.36	1.03
WAVE DIRECTION (DEGREES)	46.34	734.43	9.36	3584.98	-2.58
WAVE PERIOD (SECONDS)	2.15	-5.63	1.03	-2.58	5.03

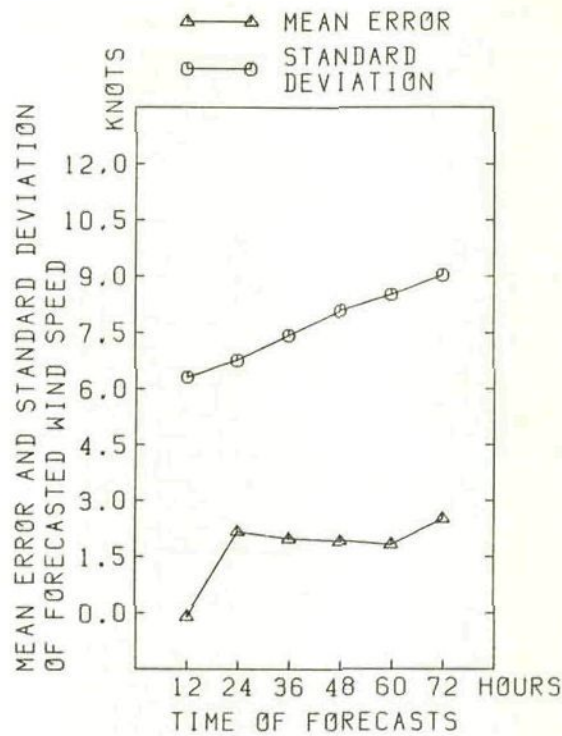


Fig. 4.10 (a) Mean error and standard deviation of forecasted wind speed averaged over all the North Pacific Ocean versus the time of forecasts

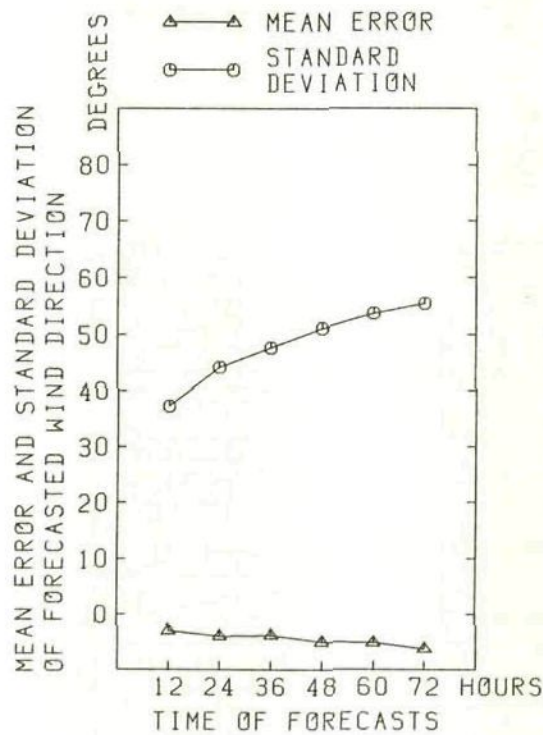


Fig. 4.10 (b) Mean error and standard deviation of forecasted wind direction averaged over all the North Pacific Ocean versus the time of forecasts

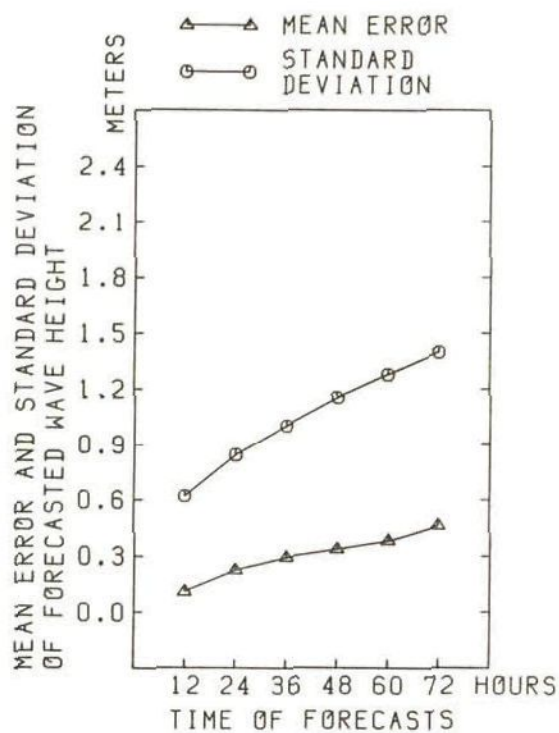


Fig. 4.10 (c) Mean error and standard deviation of forecasted wave height averaged over all the North Pacific Ocean versus the time of forecasts

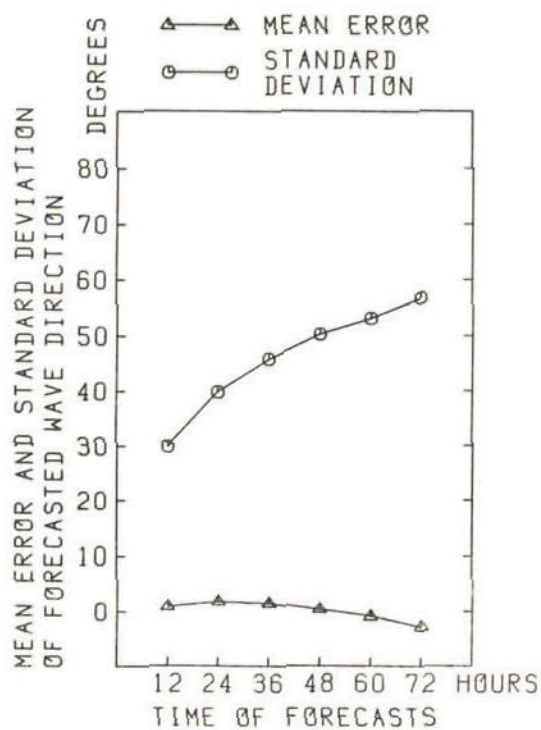


Fig. 4.10 (d) Mean error and standard deviation of forecasted wave direction averaged over all the North Pacific Ocean versus the time of forecasts



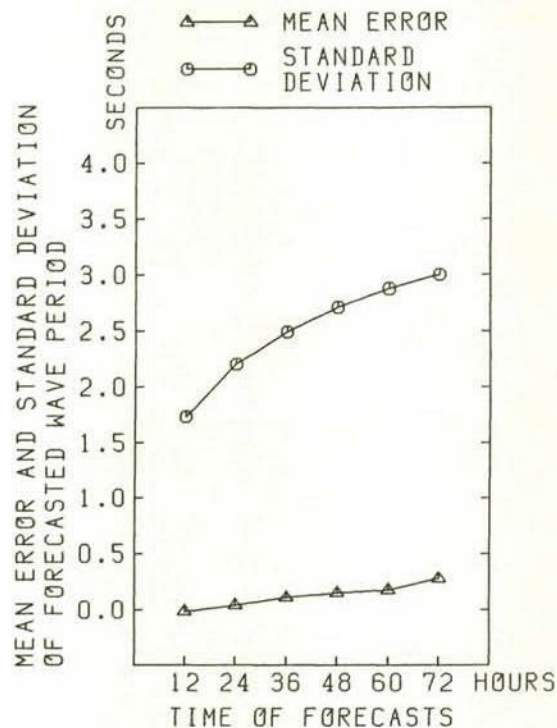


Fig. 4.10 (e) Mean error and standard deviation of forecasted wave period averaged over all the North Pacific Ocean versus the time of forecasts

#### 4.3.3 Correlations between errors in forecasted wind/wave data

For executing stochastic routing, as described in 2.4.1, it is also necessary to obtain the normalized correlation matrix  $\Phi_c(i)$  between errors of unbiased wind/wave forecast data.

In the simulations performed in Chapter 5 and 6, since the sub-time-interval  $\Delta t'$  for computing the ship's speed, engine power, drift angle, etc. is set to 12 hours, the correlation matrix  $\Phi_c(i)$  for a 12-hour sub-time-interval has to be calculated.

As the correlation matrix  $\Phi_c(i)$  is applied to the moving ship, it depends on not only the time of forecasts and the ship's position but also on the ship's course and the travelled distance for 12 hours. Thus, at each grid point of NOGAPS and GSOWM, the following

correlation coefficients were calculated using the errors of the unbiased wind/wave forecast data:

$$K_{SW}(m,n,\Delta m,\Delta n,t) = E[\Delta S_W(m+\Delta m,n+\Delta n,t+12)\Delta S_W(m,n,t)] / E[\Delta S_W(m,n,t)^2] \quad (4.7)$$

$$K_{DW}(m,n,\Delta m,\Delta n,t) = E[\Delta D_W(m+\Delta m,n+\Delta n,t+12)\Delta D_W(m,n,t)] / E[\Delta D_W(m,n,t)^2] \quad (4.8)$$

$$K_{HS}(m,n,\Delta m,\Delta n,t) = E[\Delta H_S(m+\Delta m,n+\Delta n,t+12)\Delta H_S(m,n,t)] / E[\Delta H_S(m,n,t)^2] \quad (4.9)$$

$$K_{DP}(m,n,\Delta m,\Delta n,t) = E[\Delta D_P(m+\Delta m,n+\Delta n,t+12)\Delta D_P(m,n,t)] / E[\Delta D_P(m,n,t)^2] \quad (4.10)$$

$$K_{TP}(m,n,\Delta m,\Delta n,t) = E[\Delta T_P(m+\Delta m,n+\Delta n,t+12)\Delta T_P(m,n,t)] / E[\Delta T_P(m,n,t)^2] \quad (4.11)$$

where the expectation was taken for the data at 00 and 12 hours GMT during February in 1985;

$m,n$  : grid point number in the North Pacific Ocean

$\Delta m,\Delta n$  : increment of grid point number ( $\Delta m,\Delta n = 0,\pm 1,\pm 2,\pm 3$ )

$t$  : time of forecasts at the departure grid point

( $t = 12,24,36,48$  and 60 hours)

$K_{SW}(m,n,\Delta m,\Delta n,t)$  : correlation coefficient between errors in the unbiased forecasts of wind speed

$K_{DW}(m,n,\Delta m,\Delta n,t)$  : correlation coefficient between errors in the unbiased forecasts of wind direction

$K_{HS}(m,n,\Delta m,\Delta n,t)$  : correlation coefficient between errors in the unbiased forecasts of wave height

$K_{DP}(m,n,\Delta m,\Delta n,t)$  : correlation coefficient between errors in the unbiased forecasts of wave direction

$K_{TP}(m,n,\Delta m,\Delta n,t)$  : correlation coefficient between errors in the unbiased forecasts of wave period

$\Delta S_W(m,n,t)$  : error in the unbiased forecast of the wind speed

$\Delta D_W(m,n,t)$  : error in the unbiased forecast of the wind direction

$\Delta H_S(m,n,t)$  : error in the unbiased forecast of the wave height

$\Delta D_P(m,n,t)$  : error in the unbiased forecast of the wave direction

$\Delta T_P(m,n,t)$  : error in the unbiased forecast of the wave period

In formulae (4.7) through (4.11), it is assumed that the ship departs from the grid point  $(m,n)$  and arrives at the grid point

$(m+\Delta m, n+\Delta n)$  after 12 hours. ( Fig.4.11 )

( The distance between successive grid points changes with latitude in the grid system of NOGAPS and GSOWM as shown in Table 4.1. )

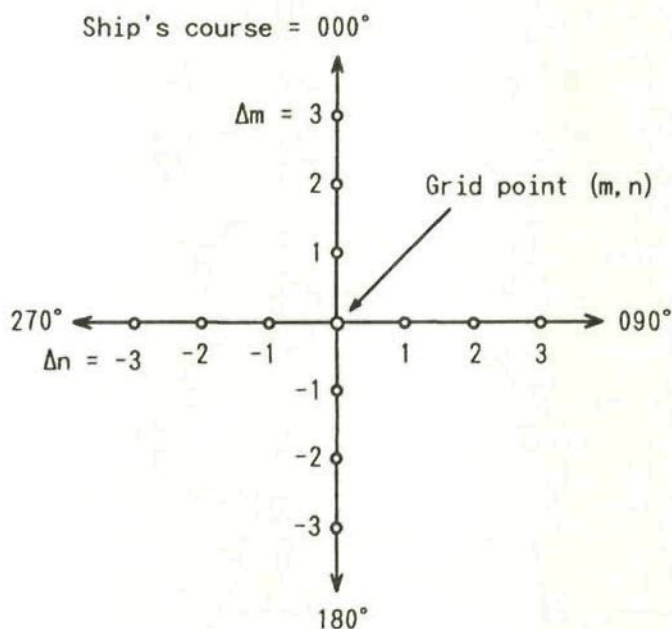


Fig. 4.11 Grid points for calculating correlation coefficients

It is not practical to use the above-mentioned correlation coefficients calculated at each grid point directly in the routing algorithm, because a huge amount of memory space is needed to store them and their spatial variations become large due to the lack of period for averaging.

Then, averaging the correlation coefficients  $K_{sw}(m,n,\Delta m,\Delta n,t)$ , ---,  $K_{TP}(m,n,\Delta m,\Delta n,t)$  at all grid points included in each sub-area shown in Fig.4.9, the averaged correlation coefficients  $\bar{K}_{sw}(m',n',\Delta m,\Delta n,t)$ , ---,  $\bar{K}_{TP}(m',n',\Delta m,\Delta n,t)$  were calculated and memorized at the central point of each sub-area, where  $m'$  and  $n'$  denote the sub-area number.

In the simulations, the correlation coefficients  $K_{sw}(i)$ , ---,  $K_{TP}(i)$  between the errors of unbiased wind/wave forecast data for the given



time  $t_i$ , predicted ship's position  $\bar{X}_i$ , ship's course and travelled distance for 12 hours are calculated by linear interpolations over time, space, course and distance using averaged correlation coefficients  $\bar{K}_{SW}(m', n', \Delta m, \Delta n, t)$ , ---,  $\bar{K}_{TP}(m', n', \Delta m, \Delta n, t)$  memorized at the central points of the sub-areas.

The correlation coefficients  $K_{SW}(i)$ , ---,  $K_{TP}(i)$  constitute the diagonal terms of the normalized diagonal correlation matrix  $\Phi_c(i)$ :

$$\Phi_c(i) = \begin{bmatrix} K_{SW}(i) & & & & \\ & K_{DW}(i) & & & 0 \\ & & K_{HS}(i) & & \\ & 0 & & K_{DP}(i) & \\ & & & & K_{TP}(i) \end{bmatrix} \quad (4.12)$$

Examples of the correlation coefficients between the errors of unbiased wind/wave forecast data are described below. In these examples, the simplified term 'correlations between the errors of forecasted wind/wave data' is used in the same meaning as 'correlation coefficients between the errors of unbiased wind/wave forecast data'.

Table 4.3 shows the correlations between the errors of forecasted wind/wave data averaged over 16 grid points in sub-area (  $41.89^\circ\text{N} - 48.89^\circ\text{N}$ ,  $178.75^\circ\text{E} - 171.25^\circ\text{W}$  ) for the time of forecasts being 12 and 24 hours. In Table 4.3, the grid point number indicates an absolute value of  $\Delta m$  or  $\Delta n$  shown in Fig.4.11, and the grid point number 0 corresponds to the central point of sub-area (  $45.39^\circ\text{N}$ ,  $176.25^\circ\text{W}$  ).

From Table 4.3, it is found that the correlations between the errors of forecasted wind speeds and those of forecasted wave heights are particularly large in this sub-area.

The correlations between the errors of forecasted wind/wave data averaged over all the North Pacific Ocean versus the time of forecasts are shown in Fig.4.12 (a)-(e). In Fig.4.12, the grid number denotes an absolute value of increment  $\Delta m$  or  $\Delta n$ .

It can be seen from Fig.4.12 that the correlations between the errors of forecasted wind/wave data on the ship's course  $090^\circ$  are larger than those on the other ship's courses. Concerning the correlations between the errors of forecasted wind speeds/directions on the ship's course  $090^\circ$  ( Fig.4.12 (a) and (b) ), they take maximum values at grid point number 1.

This may result from the fact that most of the depressions move eastwards in middle latitudes, and the forecasts of wind and waves on those depressions tend to keep similar errors for any time of the forecasts. It is noteworthy that the correlations between errors of forecasted wave heights are considerably larger than those of other factors of forecasted wind/wave conditions.

In subsection 2.4.1, the shaping filter (2.77) was set up to represent the correlation between error vector  $\Delta \underline{C}_n$  at the predicted ship's position  $\bar{\underline{X}}_n$  and error vector  $\Delta \underline{C}_f$  at the destination  $\underline{X}_f$ . Since the predicted passage time between  $\bar{\underline{X}}_n$  and  $\underline{X}_f$  is, in general, not equal to the sub-time-interval  $\Delta t'$  ( = 12 hours ), the correlation matrix  $\Phi_c(n)$  can not be computed by the method mentioned here.

The shaping filter (2.77), however, does not affect the upper-left  $2 \times 2$  matrix of the covariance matrix  $P_f$  in (2.81); i.e. the correlation matrix  $\Phi_c(n)$  does not influence the variances of passage time and fuel consumption. Therefore, for only computing the variances of passage time and fuel consumption, the correlation matrix  $\Phi_c(n)$  is not necessary ( or it may be assumed to be zero ).

Table 4.3 Correlations between errors of forecasted wind/wave data averaged over 16 grid points in sub-area ( 41.89°N - 48.89°N, 178.75°E - 171.25°W ) for 12-hour and 24-hour forecasts

\*\*\*\*\* TIME OF FORECASTS = 12 AND 24 HOURS \*\*\*\*\*

(1) CORRELATION BETWEEN ERRORS OF FORECASTED WIND SPEEDS

		GRID POINT NUMBER			
		0	1	2	3
SHIP'S COURSE	000 DEGREES	0.4247	0.3198	0.2344	0.1519
SHIP'S COURSE	090 DEGREES	0.4247	0.4114	0.3057	0.1681
SHIP'S COURSE	180 DEGREES	0.4247	0.3863	0.2872	0.2084
SHIP'S COURSE	270 DEGREES	0.4247	0.3014	0.1822	0.1378

(2) CORRELATION BETWEEN ERRORS OF FORECASTED WIND DIRECTIONS

		GRID POINT NUMBER			
		0	1	2	3
SHIP'S COURSE	000 DEGREES	0.1297	0.0157	-0.0792	-0.1324
SHIP'S COURSE	090 DEGREES	0.1297	0.1247	-0.0480	0.0257
SHIP'S COURSE	180 DEGREES	0.1297	0.0114	-0.0480	0.0562
SHIP'S COURSE	270 DEGREES	0.1297	-0.0904	-0.1191	-0.1022

(3) CORRELATION BETWEEN ERRORS OF FORECASTED WAVE HEIGHTS

		GRID POINT NUMBER			
		0	1	2	3
SHIP'S COURSE	000 DEGREES	0.7553	0.6002	0.3606	0.0869
SHIP'S COURSE	090 DEGREES	0.7553	0.6776	0.5266	0.3598
SHIP'S COURSE	180 DEGREES	0.7553	0.8184	0.8318	0.7894
SHIP'S COURSE	270 DEGREES	0.7553	0.6895	0.5226	0.2984

(4) CORRELATION BETWEEN ERRORS OF FORECASTED WAVE DIRECTIONS

		GRID POINT NUMBER			
		0	1	2	3
SHIP'S COURSE	000 DEGREES	0.1948	0.1886	0.0427	-0.0500
SHIP'S COURSE	090 DEGREES	0.1948	0.2182	0.1829	0.0614
SHIP'S COURSE	180 DEGREES	0.1948	0.2355	-0.0183	-0.0099
SHIP'S COURSE	270 DEGREES	0.1948	-0.0471	-0.2379	-0.1419

(5) CORRELATION BETWEEN ERRORS OF FORECASTED WAVE PERIODS

		GRID POINT NUMBER			
		0	1	2	3
SHIP'S COURSE	000 DEGREES	0.1566	0.0951	-0.0590	-0.1121
SHIP'S COURSE	090 DEGREES	0.1566	0.2396	0.1643	0.0523
SHIP'S COURSE	180 DEGREES	0.1566	0.2280	0.2651	0.2763
SHIP'S COURSE	270 DEGREES	0.1566	0.0963	0.0953	0.1061



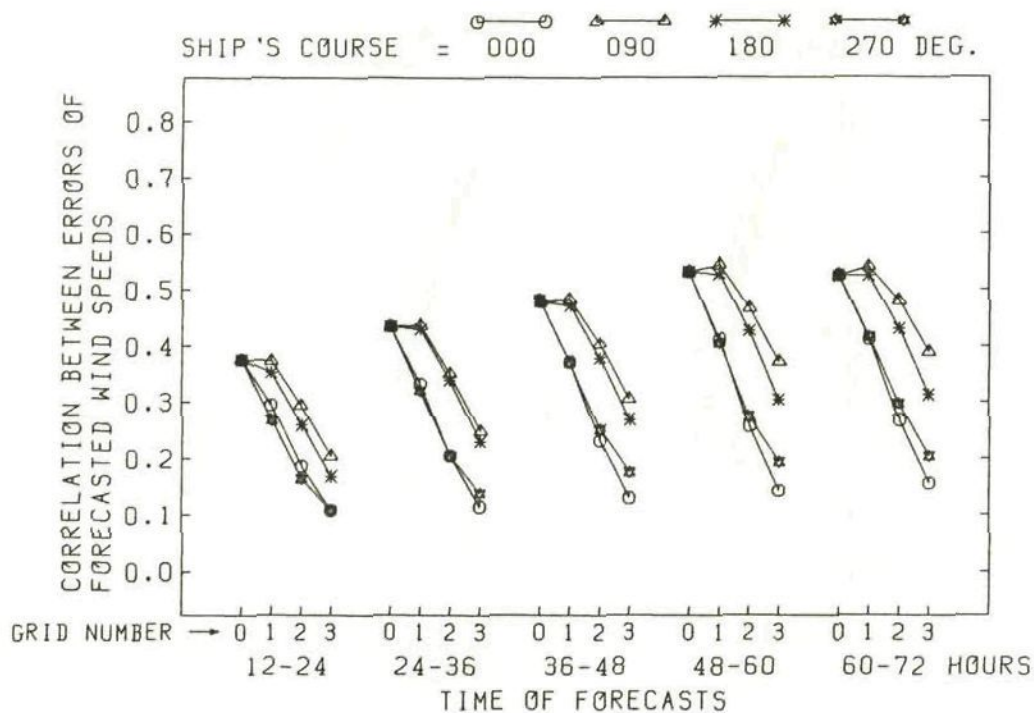


Fig. 4.12 (a) Correlation between errors of forecasted wind speeds averaged over all the North Pacific Ocean versus the time of forecasts

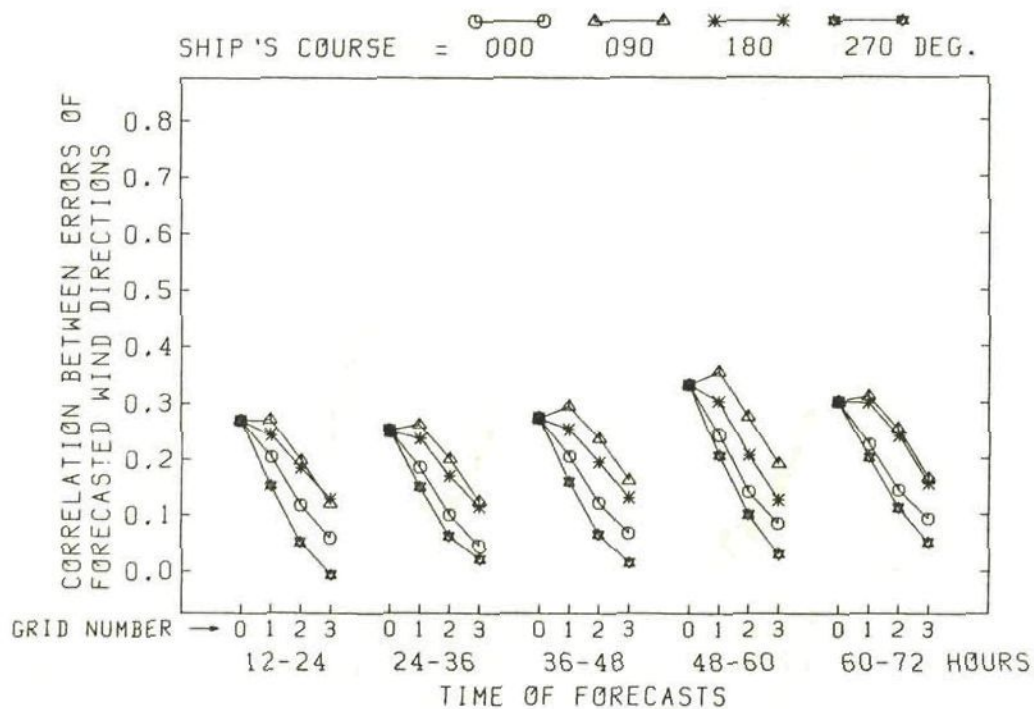


Fig. 4.12 (b) Correlation between errors of forecasted wind directions averaged over all the North Pacific Ocean versus the time of forecasts

#### 4.4 5-DAY MEAN WIND AND WAVE DISTRIBUTION MODELS CLASSIFIED BY THE ZONAL INDEX (ZI)

In order to perform effective weather routing, it is essential to use reliable wind and wave data for the period beyond 72 hours from the departure time in which the numerical forecasts are available.

The research group on ship weather routing established in Tokyo University of Mercantile Marine has found that the 5-day mean wind/wave distribution over the North Pacific in the winter is closely related with the corresponding 5-day mean upper-air circulation pattern.

They have used the 'zonal index' to represent the pattern of upper-air circulation, and constructed the 5-day mean wind/wave distribution models classified by the zonal index. Furthermore, using those models as the predicted wind/wave data, they have proposed strategic weather routing based on the mean upper-air circulation. (4), (5), (6), (7), (8), (9)

In the stochastic routing of this study, those 5-day mean wind/wave distribution models classified by the zonal index are used after the forecasted wind/wave data by NOGAPS and GSOWM. The details of those models are mentioned in this section.

##### 4.4.1 5-day mean zonal index as a measure of circulation pattern of the upper-air westerlies

The upper-air westerlies in the Northern Hemisphere flows around the North Pole with a north-south oscillation. This oscillating shape of the upper-air westerlies is called the westerly waves.

The zonal index is known as a useful measure to represent the pattern of westerly waves, which can be calculated as follows.

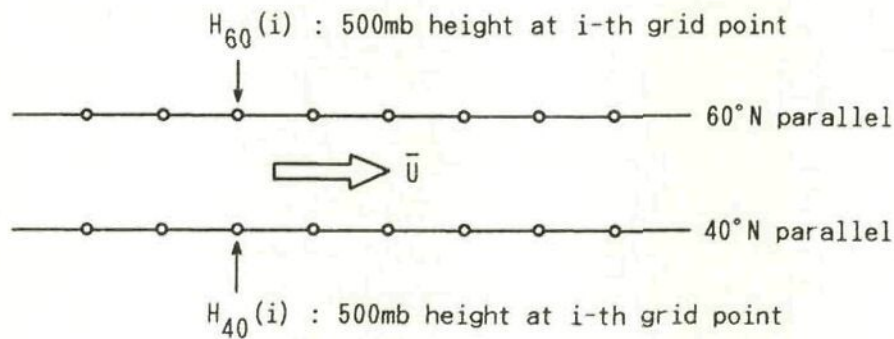
(i) On the mean 500mb chart for a certain period, read the heights of the 500mb isobaric surface along the 40°N parallel for every 10 degrees of longitude in an appropriate longitudinal range.

(ii) Averaging those 500mb heights, obtain the zonal mean 500mb height  $\bar{H}_{40}$  for the 40°N parallel.

(iii) In the same way, calculate the zonal mean 500mb height  $\bar{H}_{60}$  for the 60°N parallel.

(iv) The difference (  $\bar{H}_{40} - \bar{H}_{60}$  ) gives the zonal index (ZI):

$$ZI = \bar{H}_{40} - \bar{H}_{60} \quad (4.13)$$



$$\bar{H}_{40} = \left\{ \sum_{i=1}^n H_{40}(i) \right\} / n \quad \bar{H}_{60} = \left\{ \sum_{i=1}^n H_{60}(i) \right\} / n$$

$$ZI = \bar{H}_{40} - \bar{H}_{60}$$

Fig. 4.13 Calculation method of the zonal index

The above-mentioned zonal index is proportional to the mean easterly component of the velocity of the upper-air westerlies between 40°N and 60°N parallel according to the geostrophic wind equation (4.14):

$$\begin{aligned} \bar{U} &= g ( \bar{H}_{40} - \bar{H}_{60} ) / ( 2 \omega D \sin \phi ) \\ &= g ZI / ( 2 \omega D \sin \phi ) \end{aligned} \quad (4.14)$$



where  $\bar{U}$  : mean easterly component of the velocity of the upper-air westerlies between  $40^\circ\text{N}$  and  $60^\circ\text{N}$  parallel  
 $g$  : acceleration of gravity  
 $\bar{H}_{40}$  : zonal mean 500mb height for  $40^\circ\text{N}$  parallel  
 $\bar{H}_{60}$  : zonal mean 500mb height for  $60^\circ\text{N}$  parallel  
 $ZI$  : zonal index  
 $\omega$  : angular velocity of rotation of the earth  
 $D$  : distance between  $40^\circ\text{N}$  and  $60^\circ\text{N}$  parallel  
 $\phi$  : latitude ( =  $50^\circ\text{N}$  )

When the zonal index ( $ZI$ ) is large ( or the mean easterly component of the velocity of upper-air westerlies  $\bar{U}$  is large ), the amplitude of the westerly waves is small and the strong wind zone of upper-air westerlies is located in high latitudes. ( Fig.4.14 (a) )

As  $ZI$  ( or  $\bar{U}$  ) decreases, the amplitude of the westerly waves increases. ( Fig.4.14 (b) )

When  $ZI$  ( or  $\bar{U}$  ) becomes very small, the tip of the upper-air ridge is cut off in high latitudes and it forms the cut-off high ( blocking high ), whereas the tip of the upper-air trough is cut off in low latitudes and it forms the cut-off low. ( Fig.4.14 (c) )

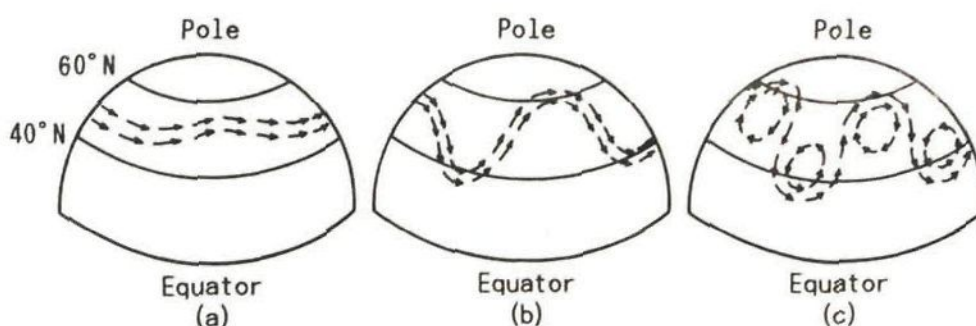


Fig. 4.14 Relation between zonal index and flow of the upper-air westerlies  
 ( The amplitude of westerly waves increases as the zonal index decreases in the order of (a), (b) and (c). )

As mentioned above, ZI is a very useful index to represent the upper-air circulation pattern. For representing the upper-air circulation pattern over the North Pacific by ZI, it seems appropriate to take the longitudinal range for calculating ZI from the west end to the east end of the North Pacific, i.e. from  $140^{\circ}\text{E}$  to  $110^{\circ}\text{W}$ . In addition, ZI based on the 5-day mean 500mb chart is suitable for investigating the variation of upper-air westerlies during the transpacific voyage which usually needs 10 - 20 days.

Hereafter, the zonal index (ZI) denotes the quantity calculated by (4.13) for the longitudinal range from  $140^{\circ}\text{E}$  to  $110^{\circ}\text{W}$  on the 5-day mean 500mb chart.

The changes of ZI in five winters of 1978 - 1983 are shown in Fig.4.15. From Fig.4.15, it can be seen that ZI changes its value with a quasiperiodicity of several weeks called the 'index cycle'. The period of one index cycle depends on the velocity of the upper-air westerlies as well as the quantity of sensible heat transported northwards by anticyclones and depressions.

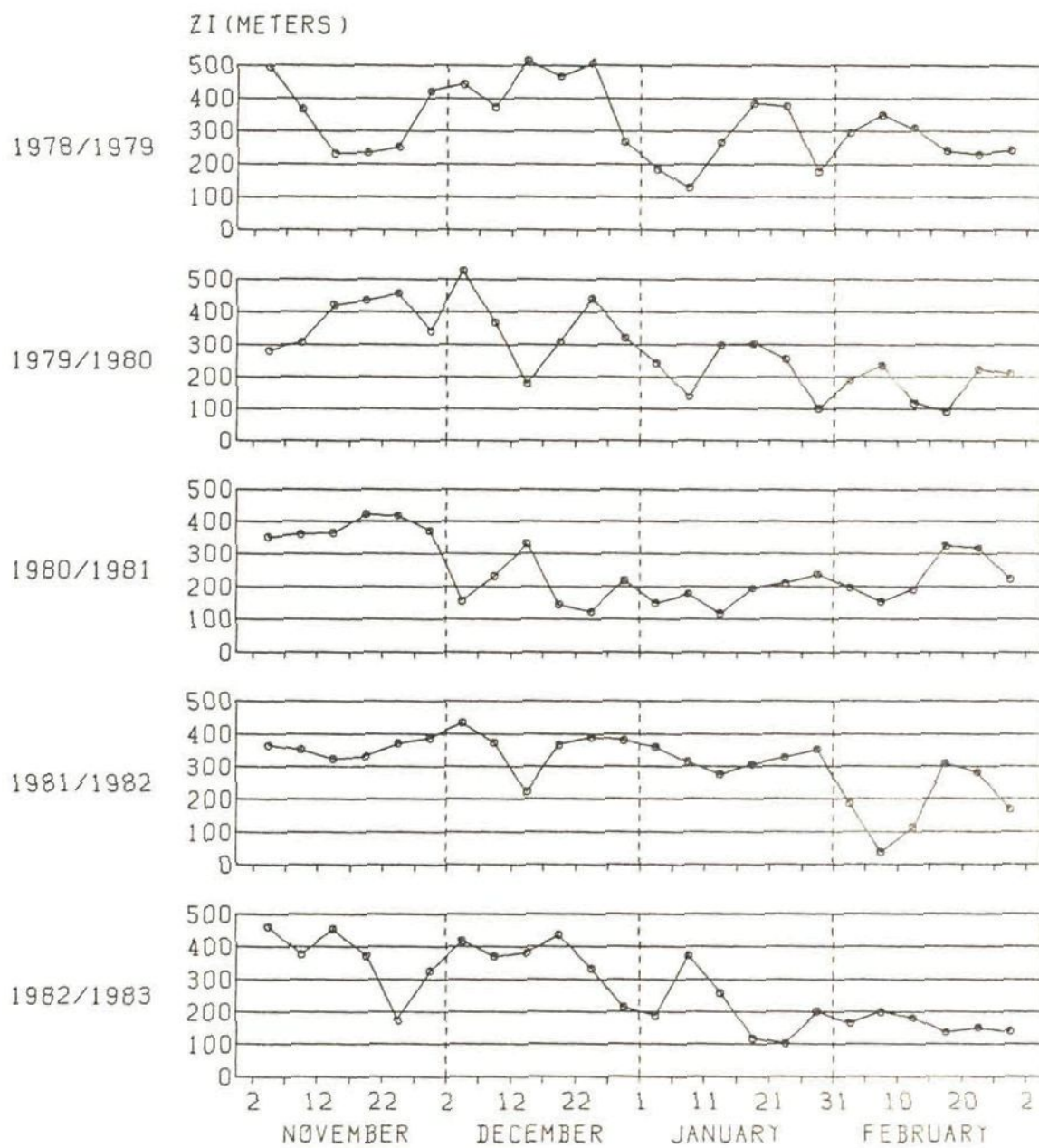


Fig. 4.15 Change of the 5-day mean zonal index for the North Pacific Ocean in five winters ( 1978 - 1983 )



#### 4.4.2 5-day mean wind and wave distribution models classified by ZI

In general, the 5-day mean wind/wave distribution over the North Pacific in the winter is determined by the paths and developments of the surface depression. As a well known fact in the meteorology, those paths and developments are largely influenced by the upper-air westerlies. Since ZI is a quantity to represent the circulation pattern of upper-air westerlies, there should be a close relationship between ZI and the 5-day mean wind/wave distribution.

In order to investigate that relationship, the 5-day mean wind/wave charts in five winters ( Nov., Dec., Jan., Feb. ) of 1978 - 1983 were constructed following the procedure mentioned below.

(i) At each grid point, using the output data of SOWM, calculate the significant wave height  $H_s$ , primary wave direction  $D_p$  and primary wave period  $T_p$  at 00 and 12 hours GMT in five winters of 1978 - 1983. ( In this period, the parameters of output data by SOWM are significant sea/swell height, predominant sea/swell direction and average sea/swell period. )

$$H_s = ( H_{SEA}^2 + H_{SWELL}^2 )^{1/2} \quad (4.15)$$

where  $H_{SEA}$  : significant sea height  
 $H_{SWELL}$  : significant swell height

$$\left\{ \begin{array}{ll} D_p = \text{predominant sea direction} & \text{if } H_{SEA} \geq H_{SWELL} \\ D_p = \text{predominant swell direction} & \text{if } H_{SEA} < H_{SWELL} \end{array} \right. \quad (4.16)$$

$$\left\{ \begin{array}{ll} T_p = \text{average sea period} & \text{if } H_{SEA} \geq H_{SWELL} \\ T_p = \text{average swell period} & \text{if } H_{SEA} < H_{SWELL} \end{array} \right. \quad (4.17)$$

(ii) Then calculate the 5-day mean wind speed  $\bar{S}_w$ , wind direction  $\bar{D}_w$ , significant wave height  $\bar{H}_s$ , primary wave direction  $\bar{D}_p$  and primary wave period  $\bar{T}_p$  by the following formulae:

$$\bar{S}_w = \{ \sum_{i=1}^{10} S_w(i) \} / 10 \quad (4.18)$$

$$\bar{D}_w = \tan^{-1} \{ [ \sum_{i=1}^{10} \sin D_w(i) ] / [ \sum_{i=1}^{10} \cos D_w(i) ] \} \quad (4.19)$$

$$\bar{H}_s = \{ \sum_{i=1}^{10} H_s(i) \} / 10 \quad (4.20)$$

$$\bar{D}_p = \tan^{-1} \{ [ \sum_{i=1}^{10} \sin D_p(i) ] / [ \sum_{i=1}^{10} \cos D_p(i) ] \} \quad (4.21)$$

$$\bar{T}_p = \{ \sum_{i=1}^{10} T_p(i) \} / 10 \quad (4.22)$$

where  $S_w(i)$ ,  $D_w(i)$ ,  $H_s(i)$ ,  $D_p(i)$  and  $T_p(i)$  ( $i = 1, 2, \dots, 10$ ) denote the wind speed, wind direction, significant wave height, primary wave direction and primary wave period at 00 and 12 hours GMT in five days.

Comparing a number of 5-day mean wind/wave charts with the corresponding 5-day mean 500mb charts, it was verified that the 5-day mean wind/wave distribution over the North Pacific in the winter was closely related to the upper-air circulation pattern, i.e. ZI.

Thus, classifying ZI into 8 classes with 50-meter intervals, and averaging the 5-day mean wind/wave charts included in each class over five winters (1978 - 1983), the 5-day mean wind/wave distribution models were constructed. Figs 4.16 - 4.23 show those 5-day mean wind/wave distribution models.

From Figs 4.16 - 4.23, it can be seen that the 5-day mean wind/wave distribution pattern changes very systematically according to the change of ZI. That is, the south limit of the westerly wind/waves is located at about 40°N for ZI greater than 450 m, and gradually shifts southwards as ZI decreases; it reaches about 25°N for ZI less than 150 m.

On the other hand, the north limit of the westerly wind/waves is located in the north of the Bering Sea when ZI is large, and moves

gradually southwards as ZI decreases. The easterly wind/waves covers the whole Bering Sea for  $ZI = 300 - 350$  m, and it becomes dominant to the north of about  $45^{\circ}N$  for ZI less than 150 m.

The cyclonic wind/wave circulation appears in the northwest of the Bering Sea for  $ZI = 350 - 400$  m, and shifts gradually southeastwards; its center reaches about  $45^{\circ}N$ ,  $160^{\circ}W$  for ZI less than 150 m.

If the successive ZI classes during the voyage can be predicted correctly, the above-mentioned 5-day mean wind/wave distribution models may be used as reliable wind/wave data to follow the numerical forecasts. In the stochastic routing, after the statistical biases are removed, these models are used as the predicted data for the period beyond the time of 72-hour forecasts by NOGAPS and GSOWM.

Concerning the predictability of ZI, the prediction of the 5-day mean 500mb height over the North Pacific which is necessary to calculate ZI seems much easier than the prediction of the daily wind/wave conditions. For example, since August in 1979, ECMWF has provided global weather forecasts ( including 500mb height ) up to 10 days on a daily basis. The research group in Tokyo University of Mercantile Marine also proposed a method to predict ZI directly based on multiple regression analysis.<sup>(4)</sup>

In this study, however, the predictability of ZI is not taken into consideration, and it is assumed that ZI during the voyage can be predicted correctly.



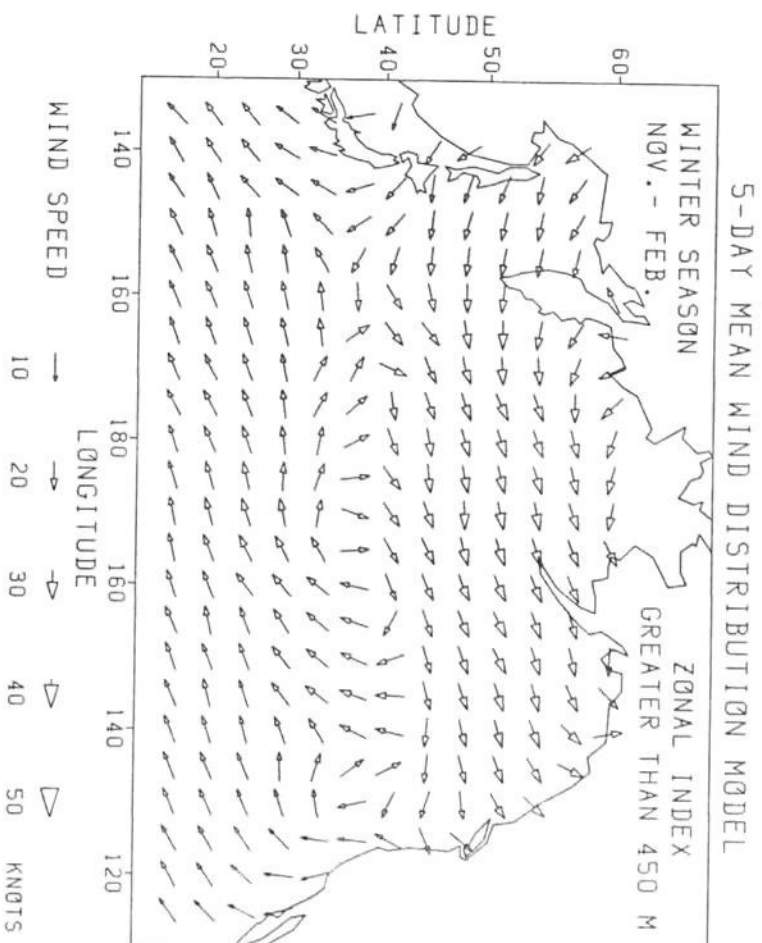


Fig. 4.16 (a) 5-day mean wind distribution model  
(ZI greater than 450 meters )

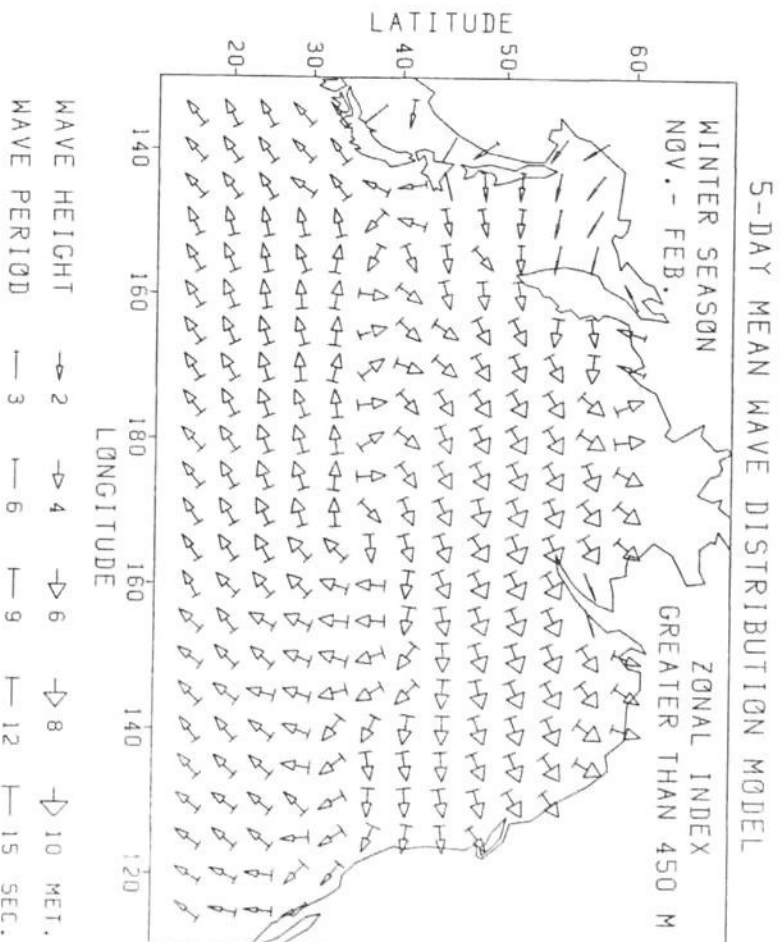


Fig. 4.16 (b) 5-day mean wave distribution model  
(ZI greater than 450 meters )

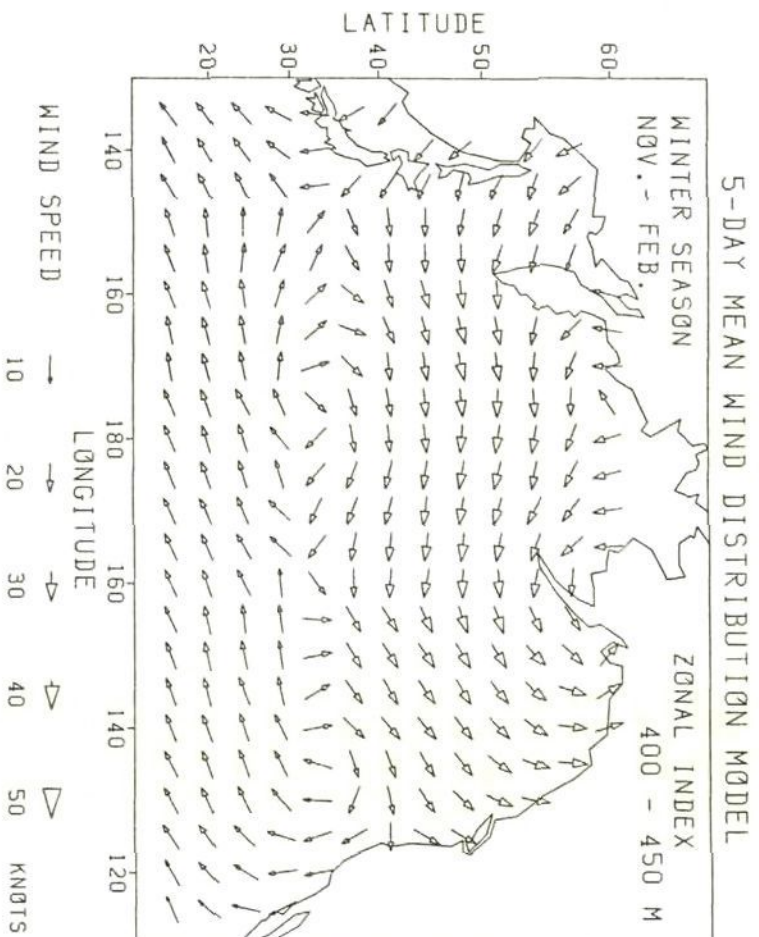


Fig. 4.17 (a) 5-day mean wind distribution model  
( ZI = 400 - 450 meters )

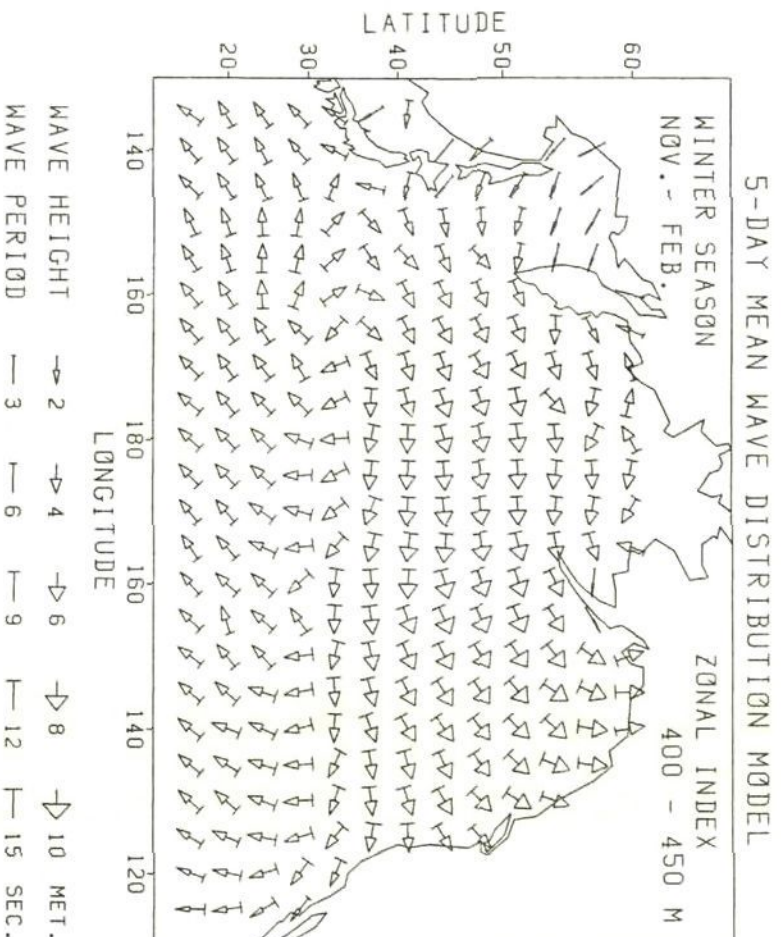


Fig. 4.17 (b) 5-day mean wave distribution model  
( ZI = 400 - 450 meters )

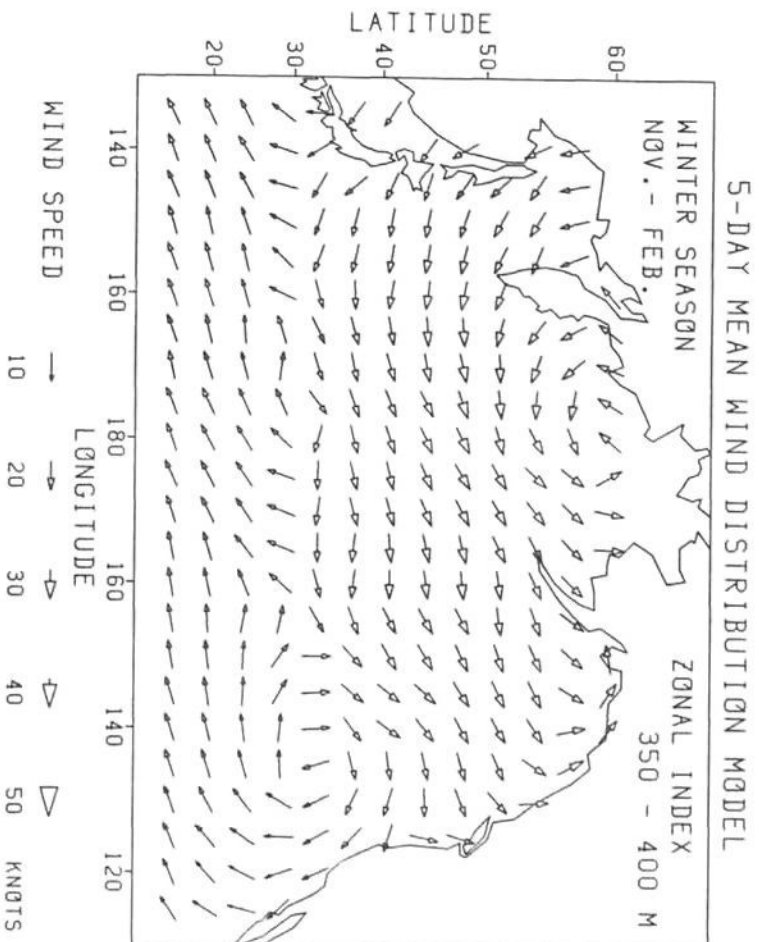


Fig. 4.18 (a) 5-day mean wind distribution model  
( ZI = 350 - 400 meters )

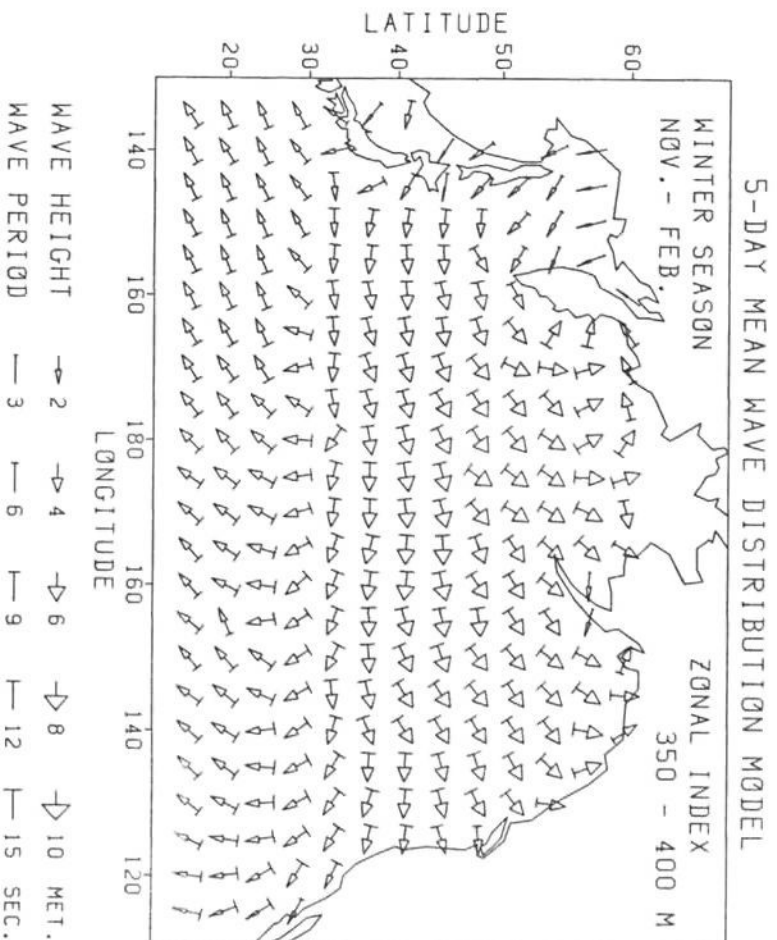


Fig. 4.18 (b) 5-day mean wave distribution model  
( ZI = 350 - 400 meters )



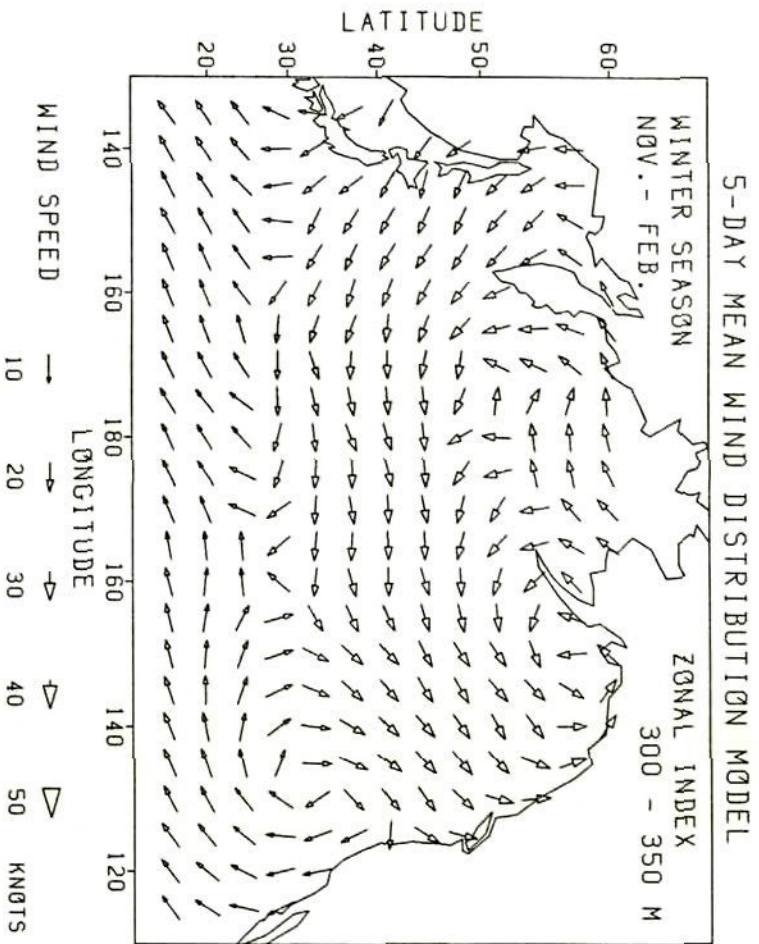


Fig. 4.19 (a) 5-day mean wind distribution model  
( ZI = 300 - 350 meters )

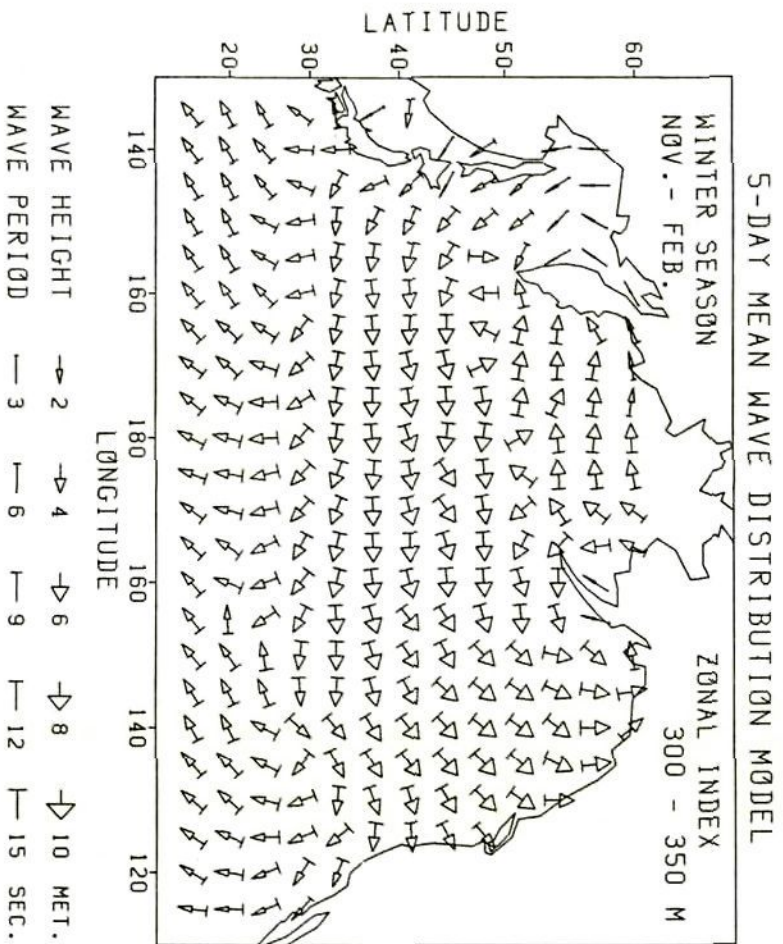


Fig. 4.19 (b) 5-day mean wave distribution model  
( ZI = 300 - 350 meters )

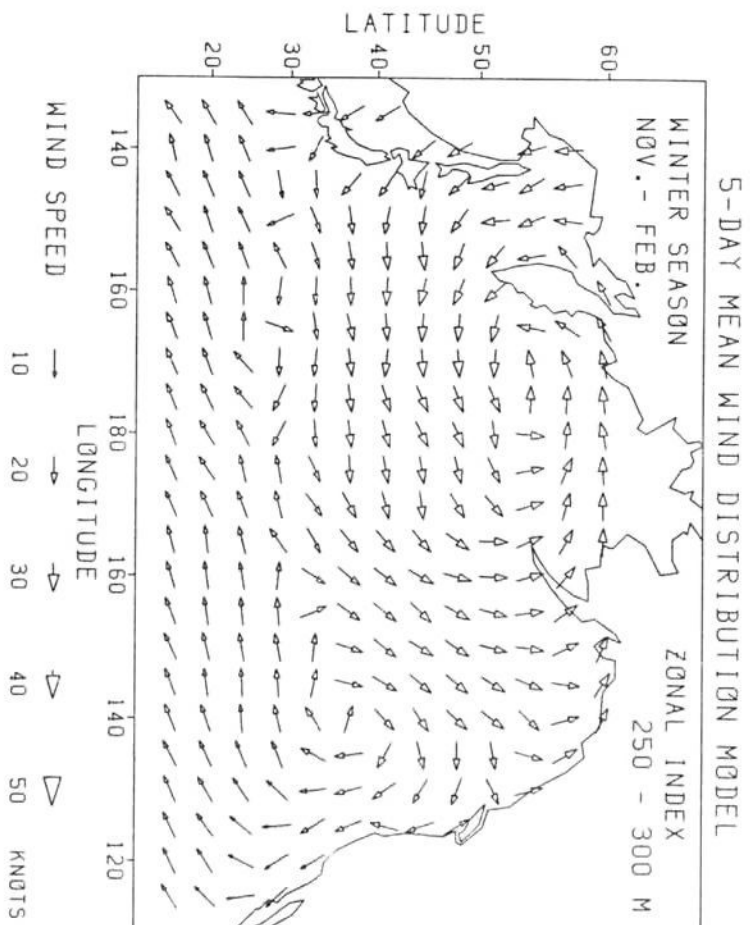


Fig. 4.20 (a) 5-day mean wind distribution model  
( ZI = 250 - 300 meters )

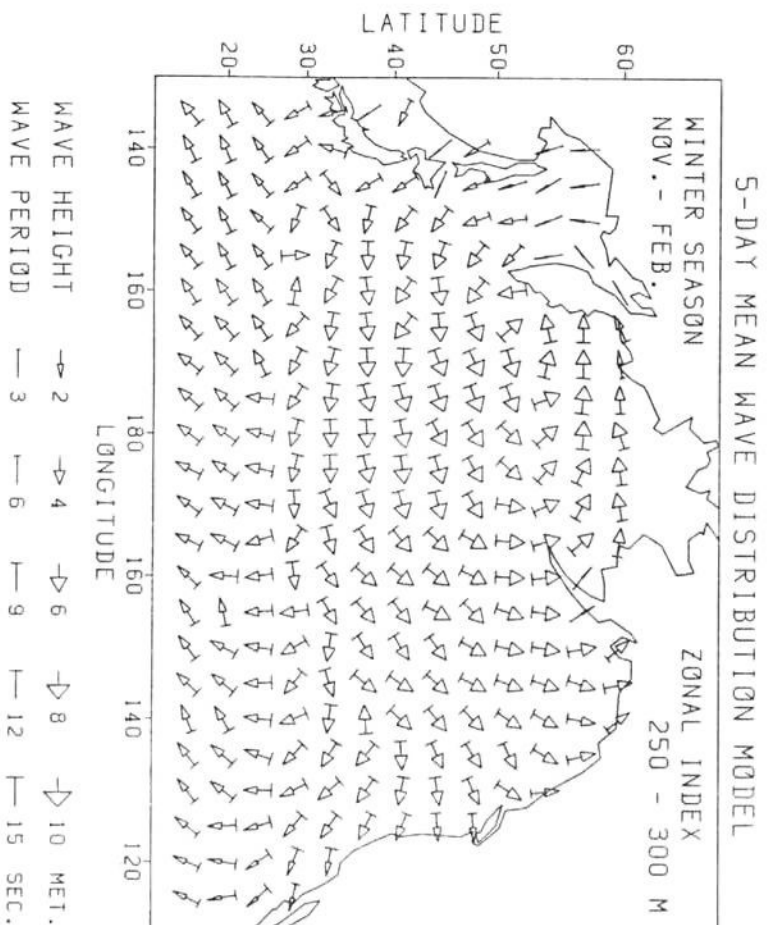


Fig. 4.20 (b) 5-day mean wave distribution model  
( ZI = 250 - 300 meters )

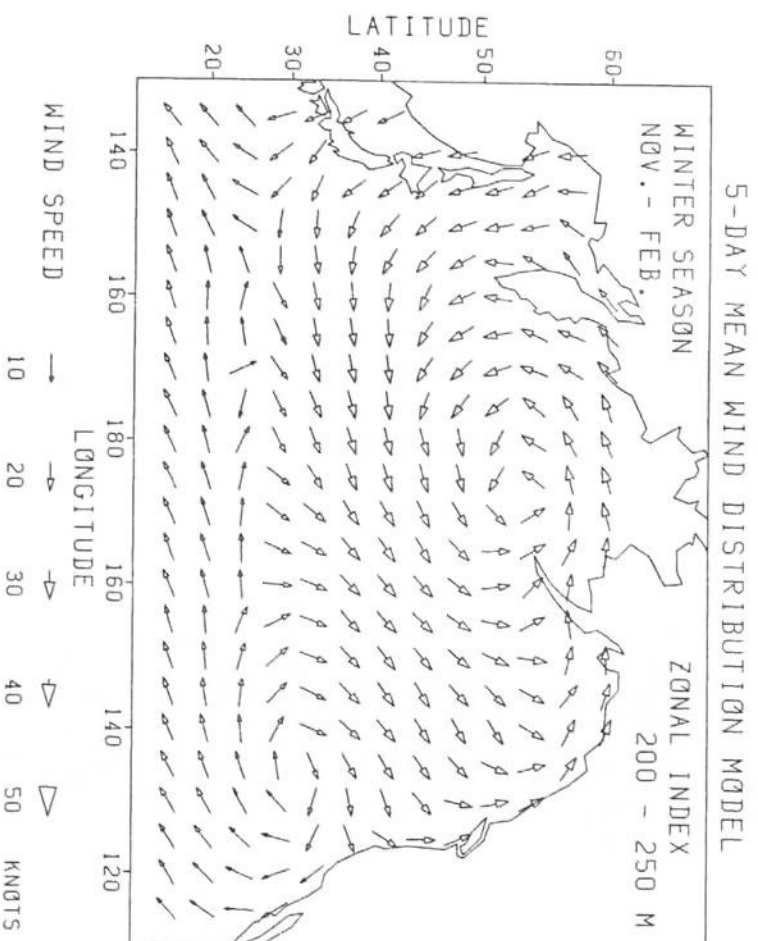


Fig. 4.21 (a) 5-day mean wind distribution model  
( ZI = 200 - 250 meters )

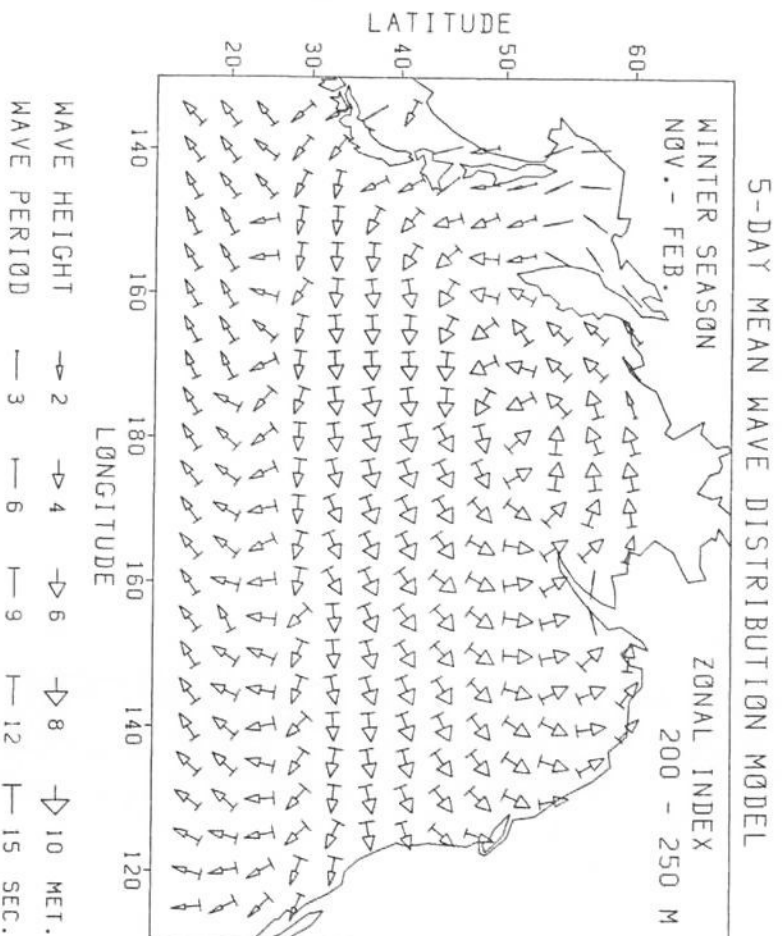


Fig. 4.21 (b) 5-day mean wave distribution model  
( ZI = 200 - 250 meters )



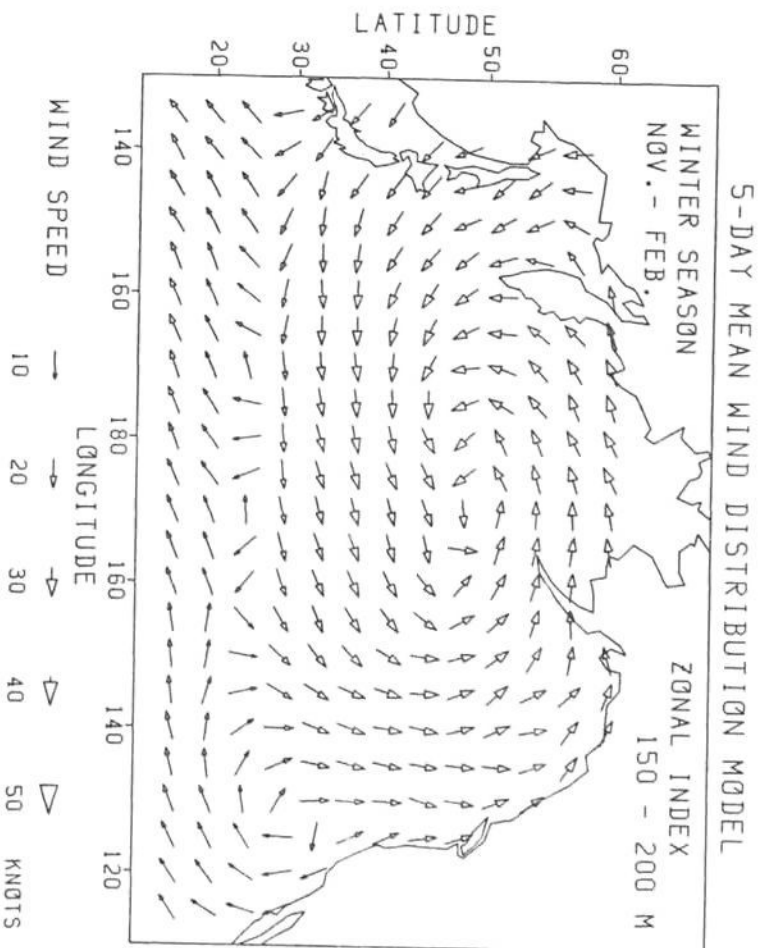


Fig. 4.22 (a) 5-day mean wind distribution model  
( ZI = 150 - 200 meters )

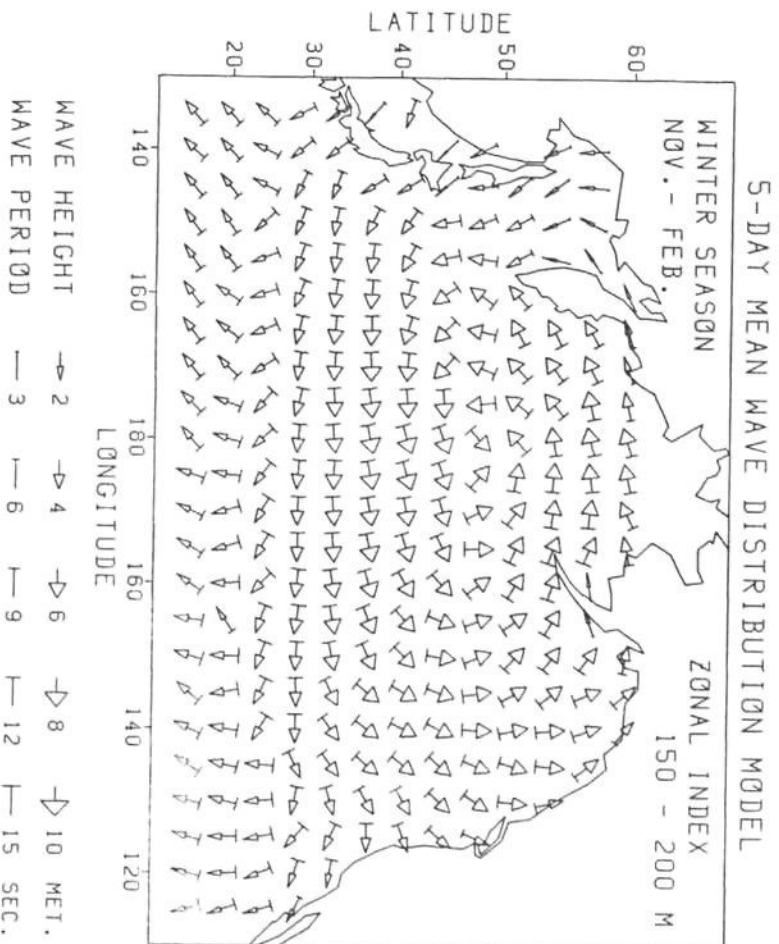


Fig. 4.22 (b) 5-day mean wave distribution model  
( ZI = 150 - 200 meters )

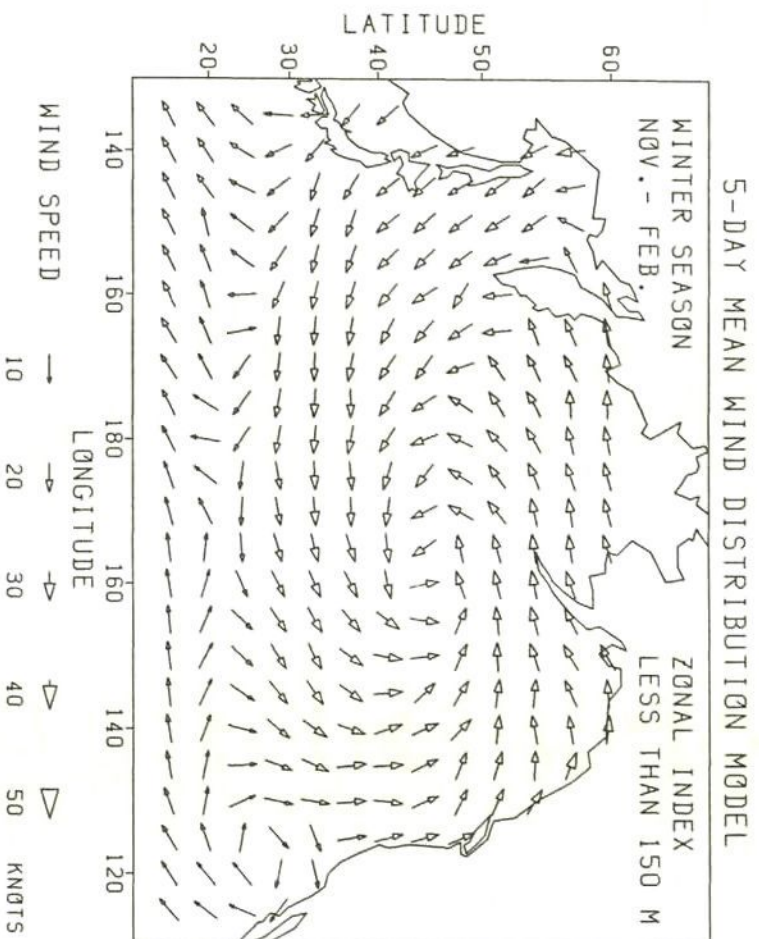


Fig. 4.23 (a) 5-day mean wind distribution model  
(ZI less than 150 meters)

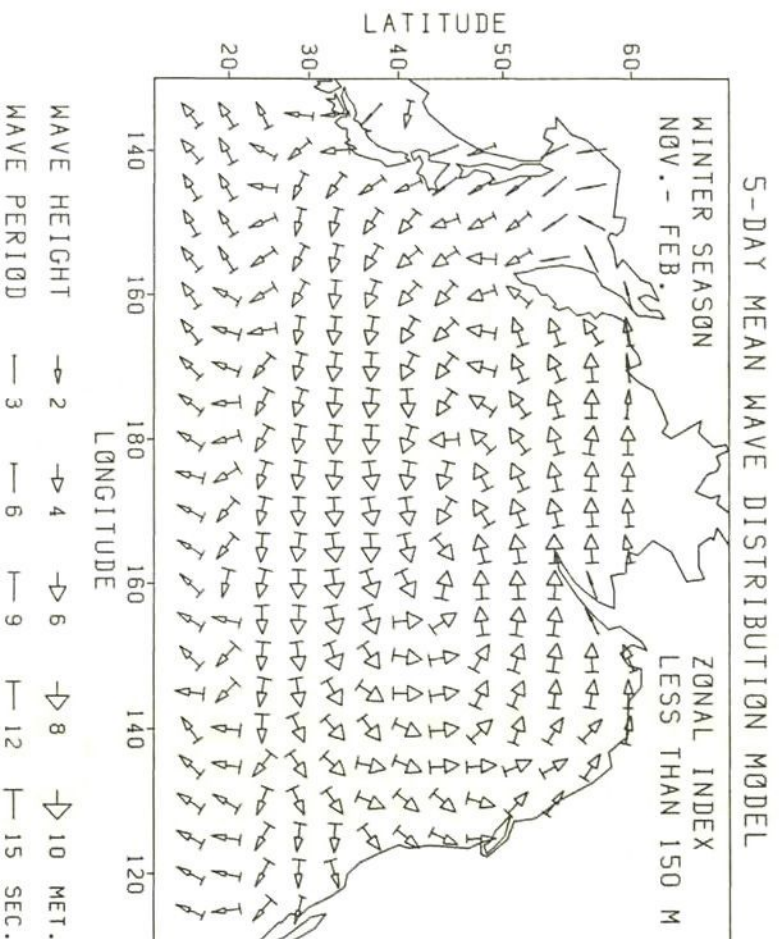


Fig. 4.23 (b) 5-day mean wave distribution model  
(ZI less than 150 meters)

#### 4.4.3 Mean errors and covariance matrices of the 5-day mean wind/wave models classified by ZI

When the 5-day mean wind/wave models classified by ZI are used as the predicted data in stochastic routing, it is necessary to obtain their unbiased values and covariance matrices.

In the same manner as explained in 4.3.2, comparing each 5-day mean wind/wave model classified by ZI with the analyzed data at 00 and 12 hours GMT for the corresponding periods in five winters, the mean errors and covariance matrix were calculated at each grid point. Then the averaged covariance matrix was calculated in each sub-area shown in Fig.4.9.

In the simulations, the mean errors are added to the data of the 5-day mean wind/wave model at each grid point, and the resultant unbiased data are used to calculate the unbiased wind/wave data  $\bar{C}_i$ . The averaged covariance matrices memorized at the central points of the sub-areas are used to calculate the covariance matrix  $P_c(i)$ .

The mean errors and standard deviations of the 5-day mean wind/wave models classified by ZI averaged over all the North Pacific Ocean are shown in Fig.4.24 (a)-(e). In Fig.4.24, the class of zonal index denotes the following range of zonal index.

Class of zonal index	Range of zonal index
1	greater than 450 m
2	400 m - 450 m
3	350 m - 400 m
4	300 m - 350 m
5	250 m - 300 m
6	200 m - 250 m
7	150 m - 200 m
8	less than 150 m

Concerning the mean errors, as the 5-day mean wind/wave models classified by ZI were constructed by averaging 5-day mean wind/wave charts for the corresponding periods, they should not have biases, i.e. their mean errors should be zero, from the mathematical



interpretation.

The number of analyzed wind/wave data to construct each 5-day mean wind/wave charts was, however, not always 10 in formulae (4.18) through (4.22) due to the operational trouble of NOGAPS and SOWM, and the variation of that number was not taken into account for the averaging calculation to obtain the 5-day mean wind/wave models. In addition, the 5-day mean wind/wave direction was determined as a direction of the resultant vector of 10 vectors each with a unit length and analyzed wind/wave direction as described by formulae (4.19) and (4.21).

Therefore the 5-day mean wind/wave models are not the mean values of the analyzed wind/wave data in a strict sense, thus they have small mean errors as shown in Fig.4.24.

Next, it is found that the standard deviations of the 5-day mean wind/wave models classified by ZI in Fig.4.24 are a bit larger than those of the forecasted wind/wave data for 72-hour forecasts in Fig.4.10. Particularly, for the significant wave height, the standard deviations of the 5-day mean wind/wave models become about 0.6 meters (40%) larger than those of the 72-hour forecasts.

It should be noted, however, that the period for investigating the standard deviations of forecasted wind/wave data is only one month, i.e. February in 1985, whereas that of 5-day mean wind/wave models is five winters, i.e. Nov., Dec., Jan. and Feb. in 1978 - 1983.

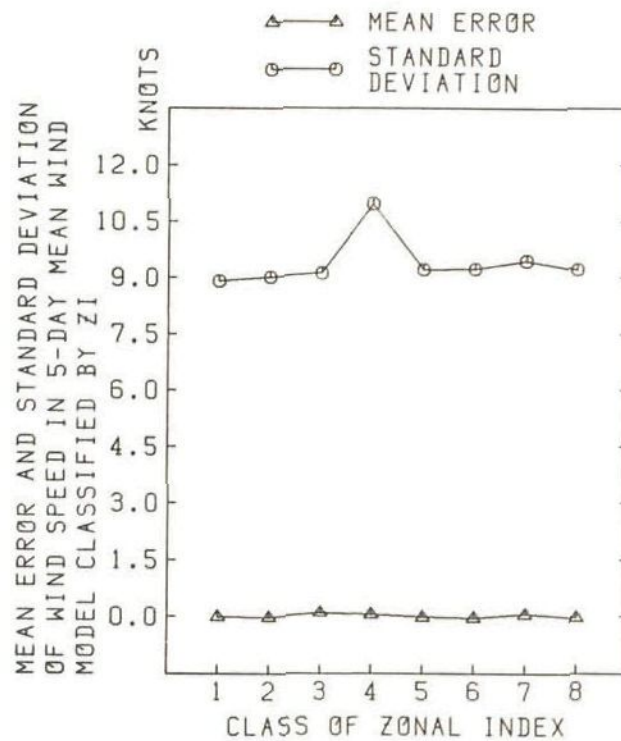


Fig. 4.24 (a) Mean error and standard deviation of wind speed in each 5-day mean wind model classified by ZI averaged over all the North Pacific Ocean

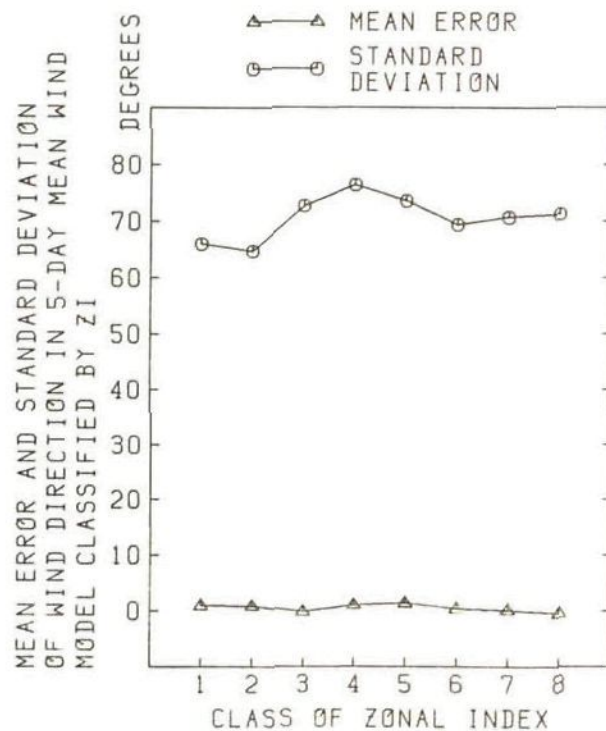


Fig. 4.24 (b) Mean error and standard deviation of wind direction in each 5-day mean wind model classified by ZI averaged over all the North Pacific Ocean

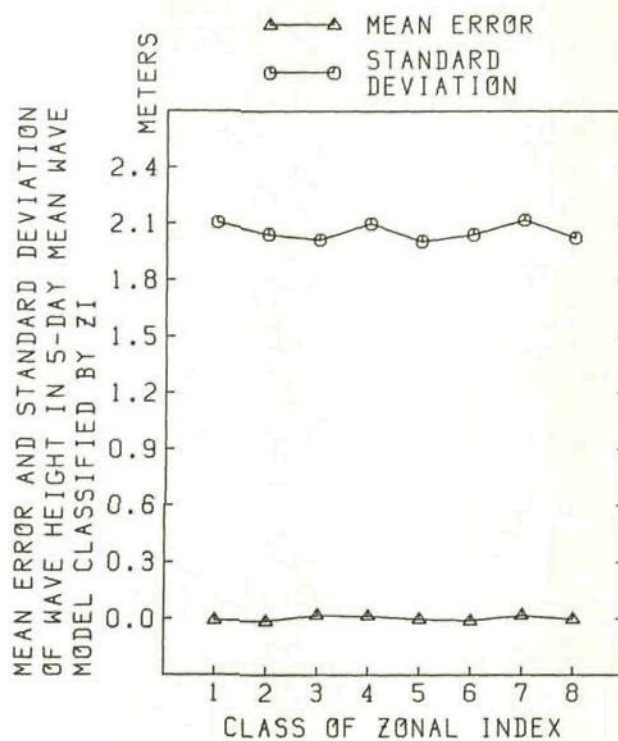


Fig. 4.24 (c) Mean error and standard deviation of wave height in each 5-day mean wave model classified by ZI averaged over all the North Pacific Ocean

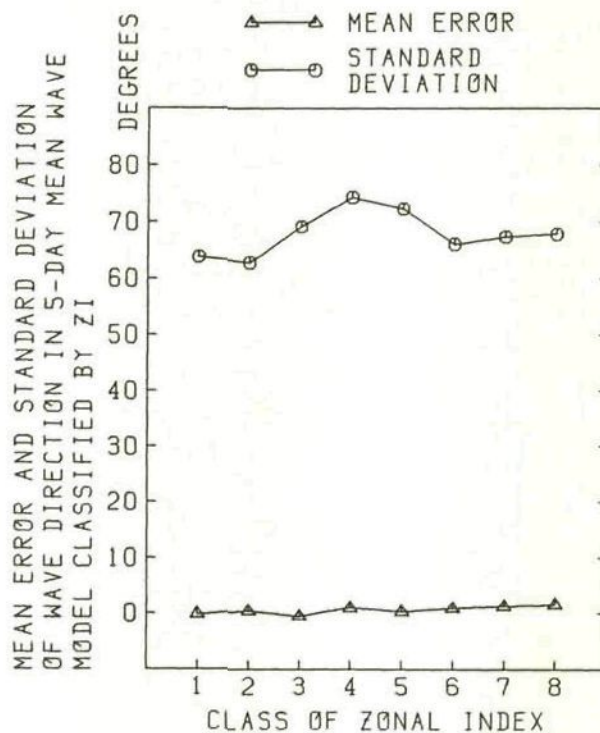


Fig. 4.24 (d) Mean error and standard deviation of wave direction in each 5-day mean wave model classified by ZI averaged over all the North Pacific Ocean



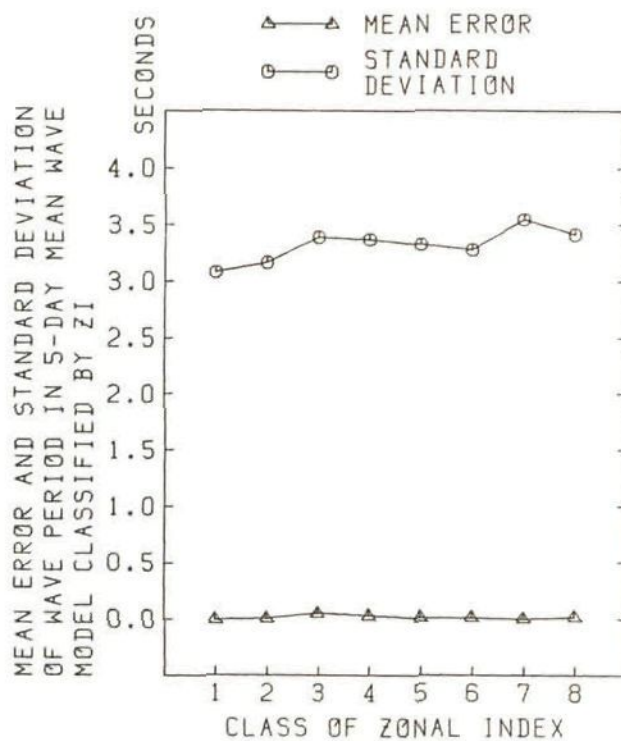


Fig. 4.24 (e) Mean error and standard deviation of wave period in each 5-day mean wave model classified by ZI averaged over all the North Pacific Ocean

#### 4.4.4 Correlations between errors in the 5-day mean wind/wave models classified by ZI

When the 5-day mean wind/wave models classified by ZI are used for stochastic routing, it is also necessary to obtain the correlations between errors in those models.

In the same manner as mentioned in 4.3.3, comparing each 5-day mean wind/wave model classified by ZI with the analyzed data at 00 and 12 hours GMT for the corresponding periods in five winters, the correlations ( correlation coefficients ) between errors in the 5-day mean wind/wave model for 12-hour sub-time-interval were computed at each grid point, and then they were averaged in each sub-area.

In the simulations, the averaged correlations memorized at the central points of the sub-areas are used to calculate the correlation matrix  $\Phi_c(i)$ .

The correlations between errors in the 5-day mean wind/wave models averaged over all the North Pacific Ocean are shown in Fig.4.25 (a)-(e). It can be seen that the correlations between errors of wind speeds/directions and wave directions/periods in the 5-day mean wind/wave models in Fig.4.25 are larger than those in the forecasted wind/wave data in Fig.4.12.

It is also found from Fig.4.25 that the correlations on the ship's course 090° become considerably larger than those on the other ship's courses. This tendency is more conspicuous in Fig.4.25 than in Fig.4.12. This results from the fact that since the 5-day mean wind/wave models are static ( time-invariant ), those models tend to keep similar errors for the disturbances, i.e. the depressions, which generally move eastwards in middle latitudes.

We can also find that the correlations between errors of the wave heights in the 5-day mean wind/wave models are considerably larger than those of other factors in the 5-day mean wind/wave models.

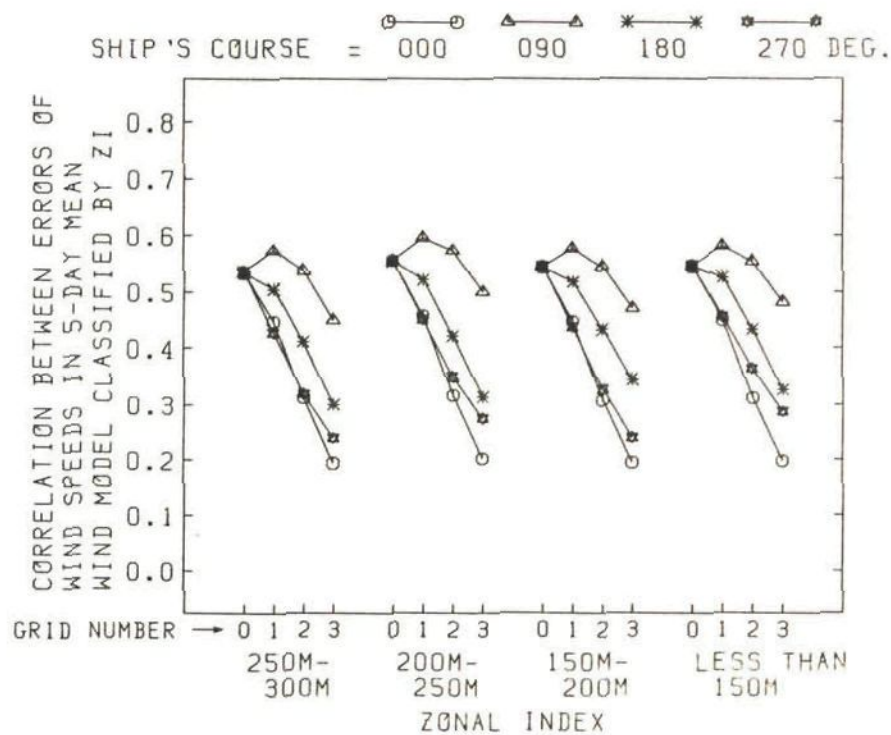
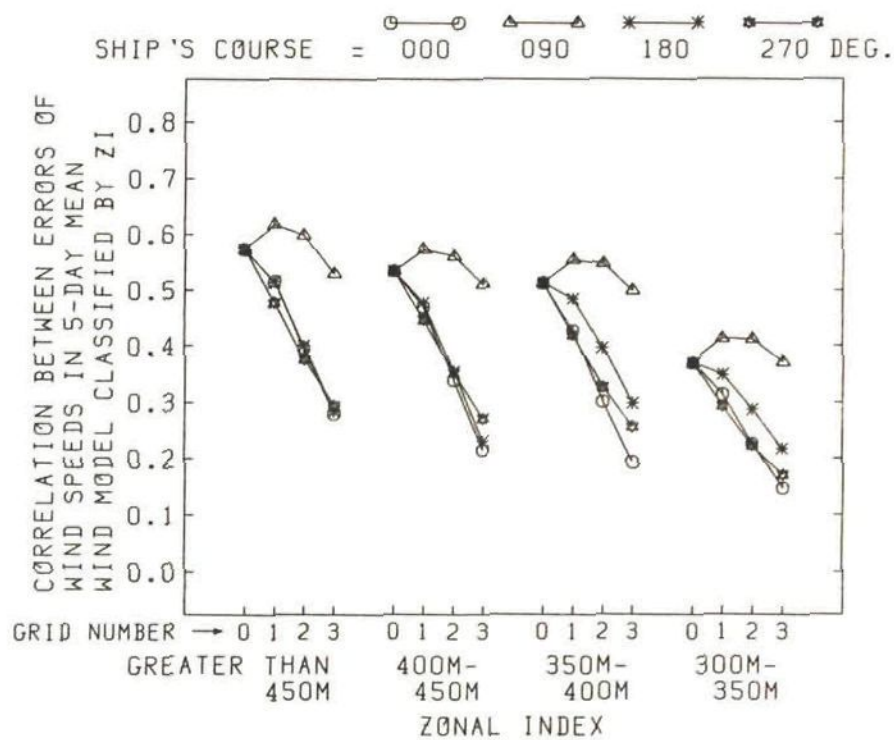


Fig. 4.25 (a) Correlation between errors of wind speeds in each 5-day mean wind model classified by ZI averaged over all the North Pacific Ocean



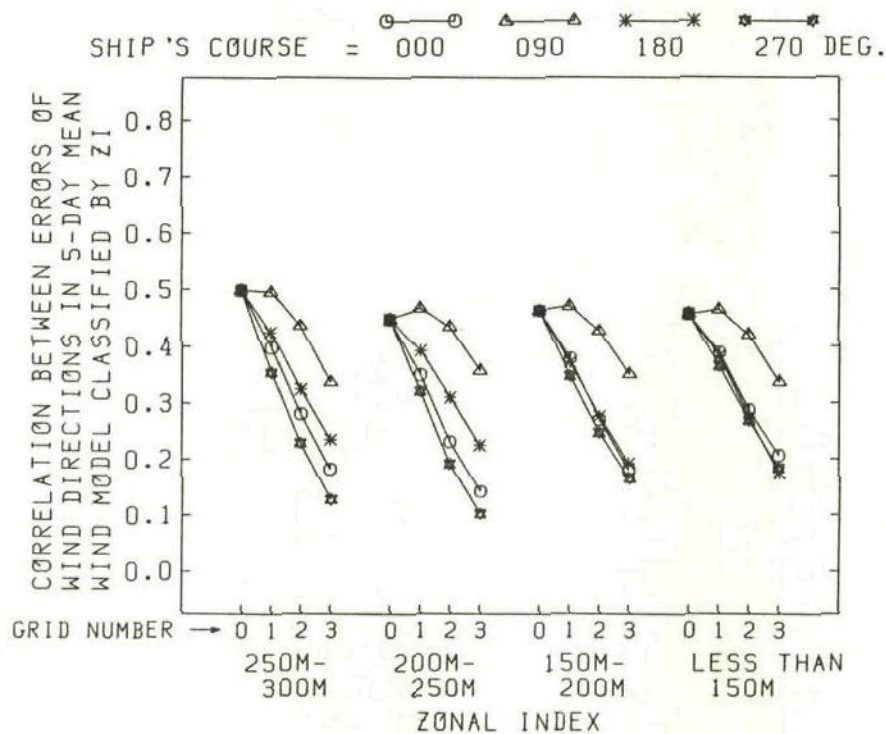
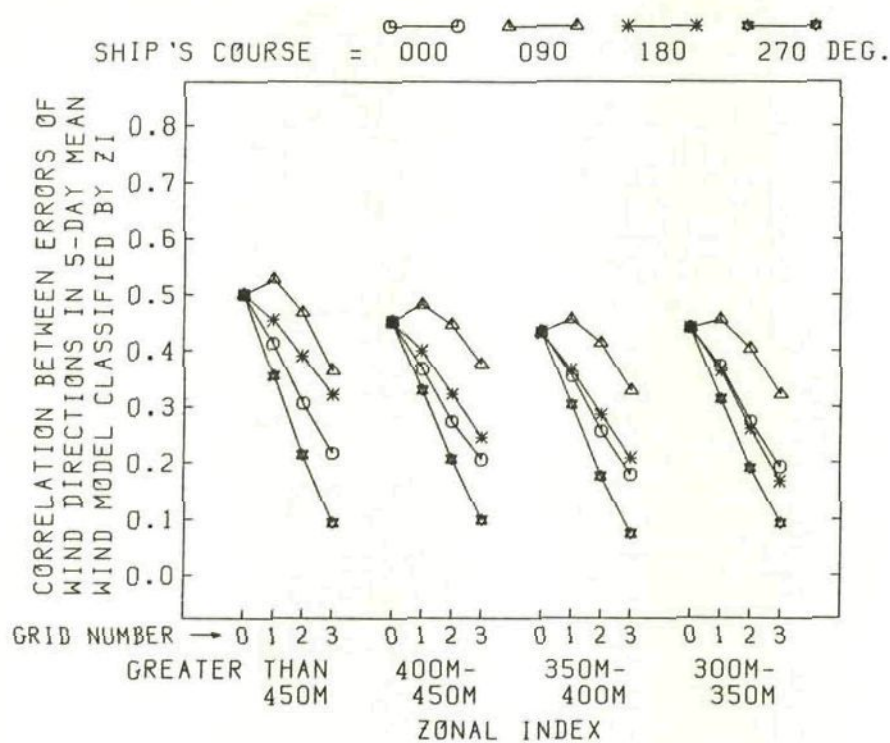


Fig. 4.25 (b) Correlation between errors of wind directions in each 5-day mean wind model classified by ZI averaged over all the North Pacific Ocean

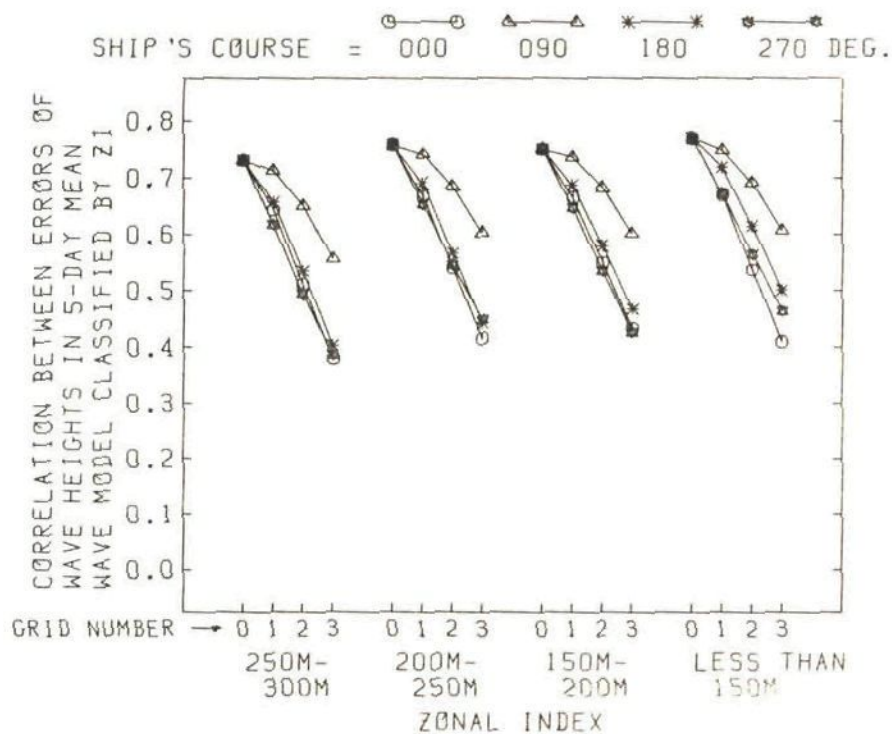
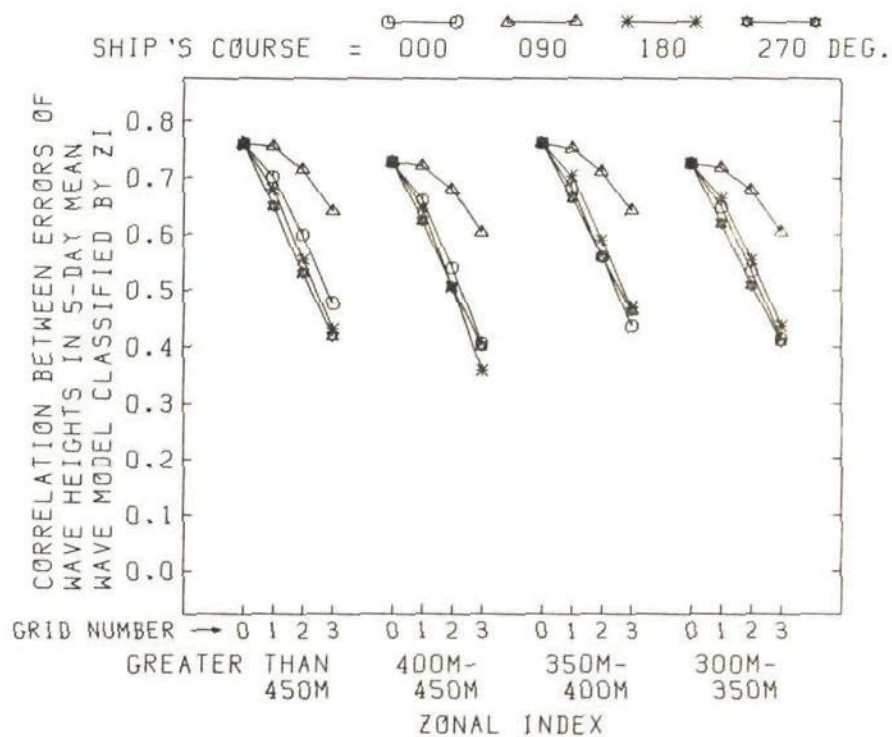


Fig. 4.25 (c) Correlation between errors of wave heights in each 5-day mean wave model classified by ZI averaged over all the North Pacific Ocean

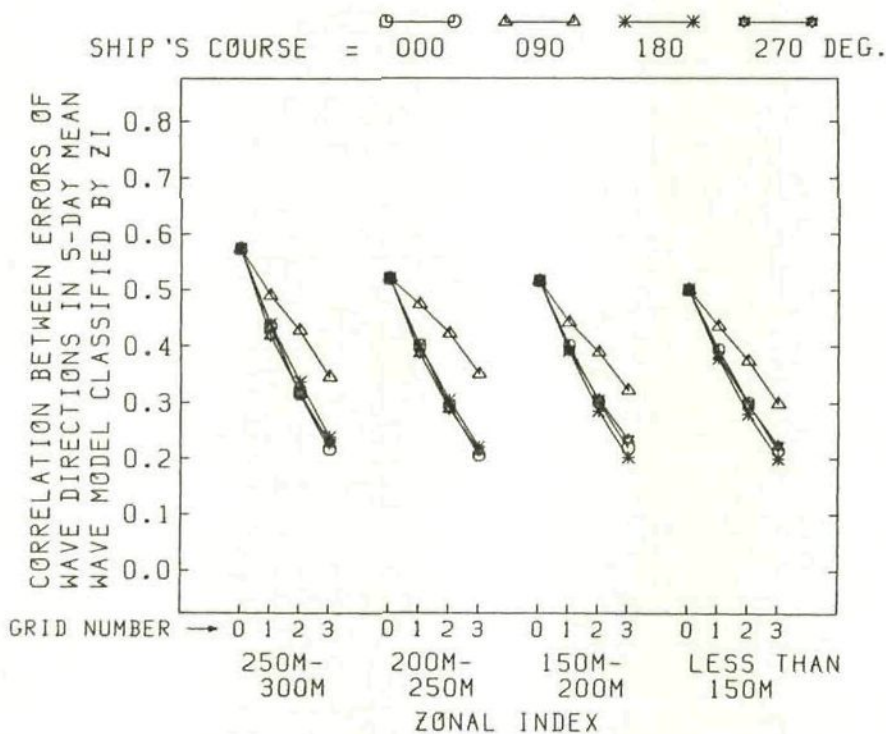
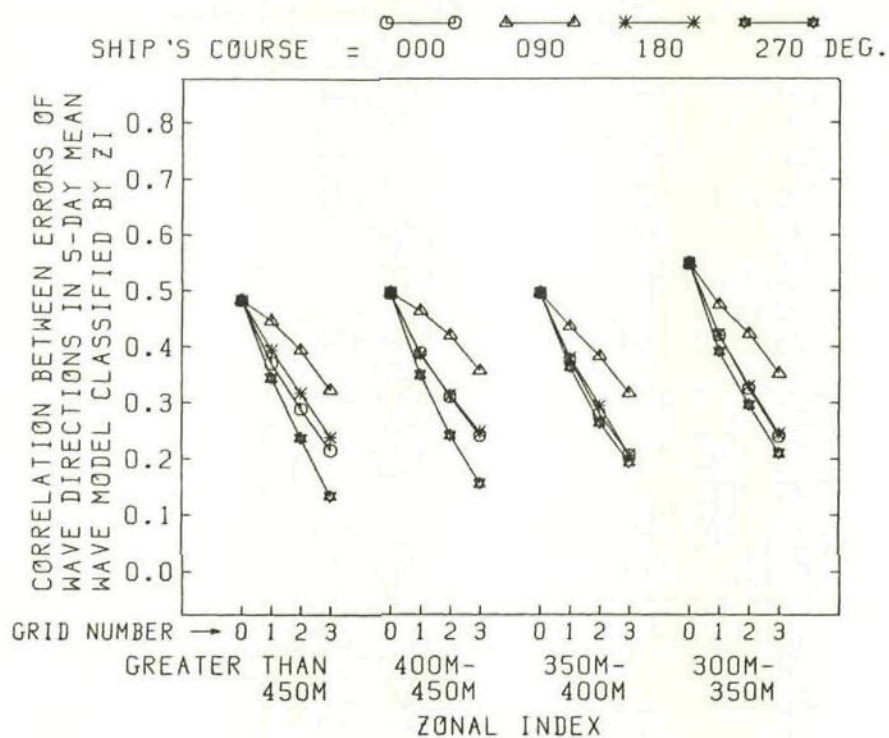


Fig. 4.25 (d) Correlation between errors of wave directions in each 5-day mean wave model classified by ZI averaged over all the North Pacific Ocean



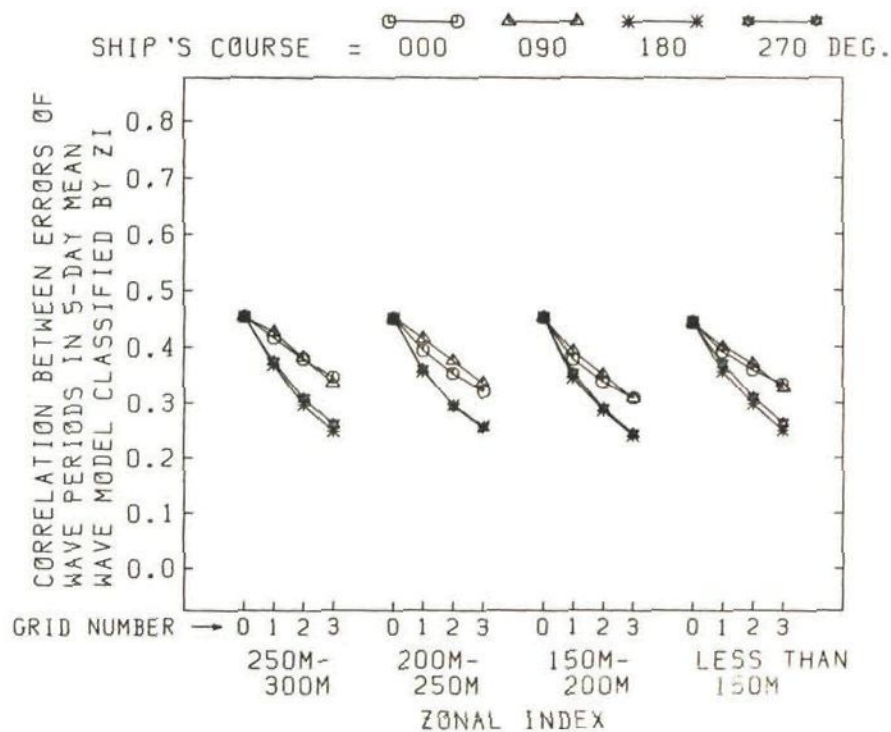
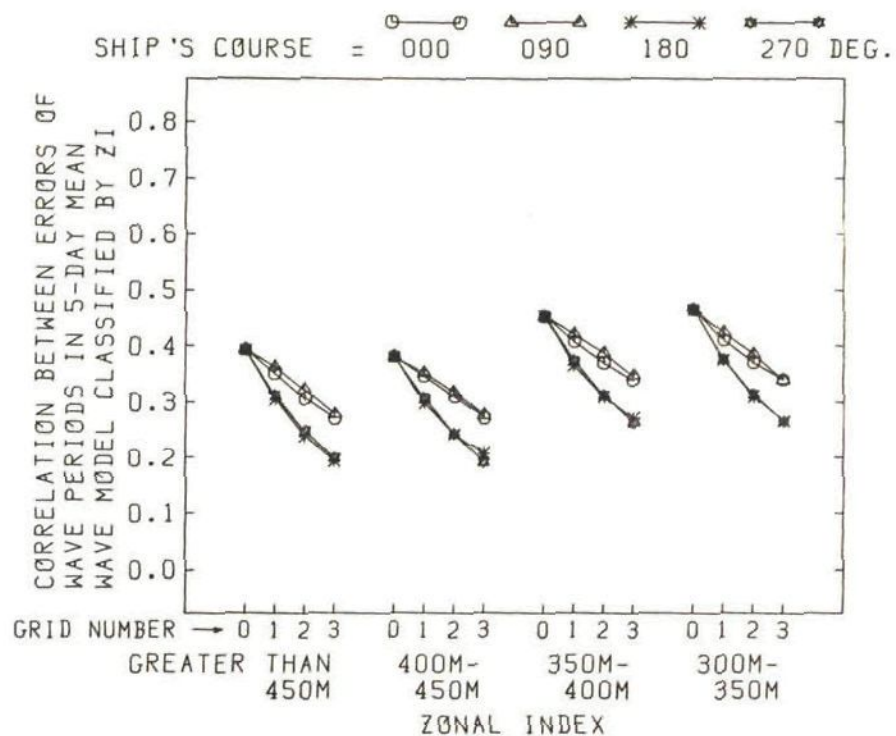


Fig. 4.25 (e) Correlation between errors of wave periods in each 5-day mean wave model classified by ZI averaged over all the North Pacific Ocean

#### 4.5 1-MONTH MEAN WIND AND WAVE DATA

In the stochastic routing simulations, not only the 5-day mean wind/wave models classified by ZI but also the 1-month mean wind/wave data are used to follow the forecasted wind/wave data. Those 1-month mean wind/wave data are described in this section.

##### 4.5.1 1-month mean wind and wave charts

In the same way as mentioned in 4.4.2, averaging the 5-day mean wind/wave charts involved in each month ( Nov., Dec., Jan., Feb. ) over five winters of 1978 - 1983, the 1-month mean wind and wave charts were constructed, which are shown in Figs 4.26 - 4.29.

From Figs 4.26 - 4.29, it is found that the pattern of 1-month mean wind/wave distribution changes systematically in some degree. This is because the zonal index decreases gradually from November to February on the average; the zonal indexes of November, December, January and February averaged over five winters are 361 m, 341 m, 237 m and 207 m, respectively. The 1-month mean wind/wave data of November, December and January/February resemble the 5-day mean wind/wave models for ZI = 350 m - 400 m ( Fig.4.18 ), ZI = 300 m - 350 m ( Fig.4.19 ) and ZI = 200 m - 250 m ( Fig.4.21 ), respectively.

In the stochastic routing simulations, after the statistical biases are removed, these 1-month mean wind/wave data are used as the predicted data for the period beyond the time of 72-hour forecasts by NOGAPS and GSOWM.

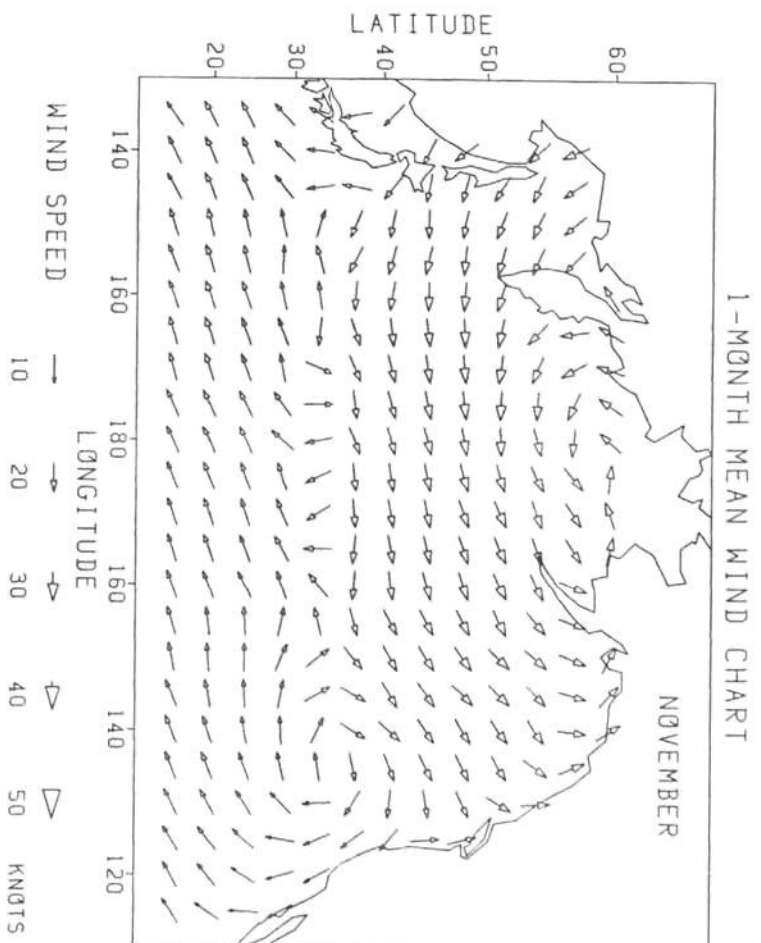


Fig. 4.26 (a) 1-month mean wind chart ( November )

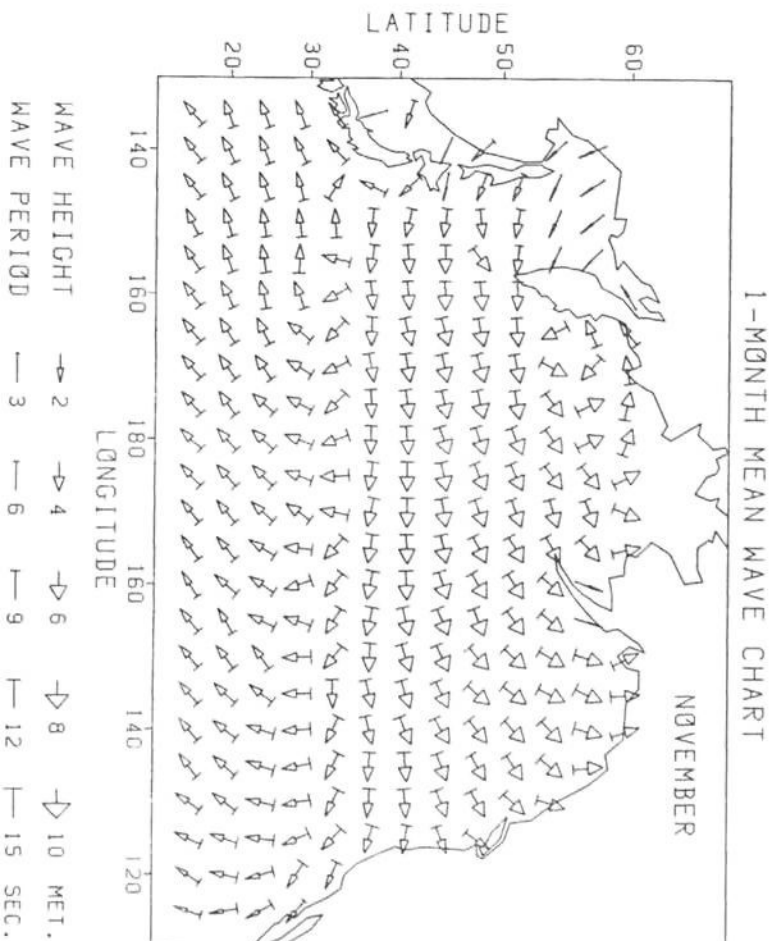


Fig. 4.26 (b) 1-month mean wave chart ( November )



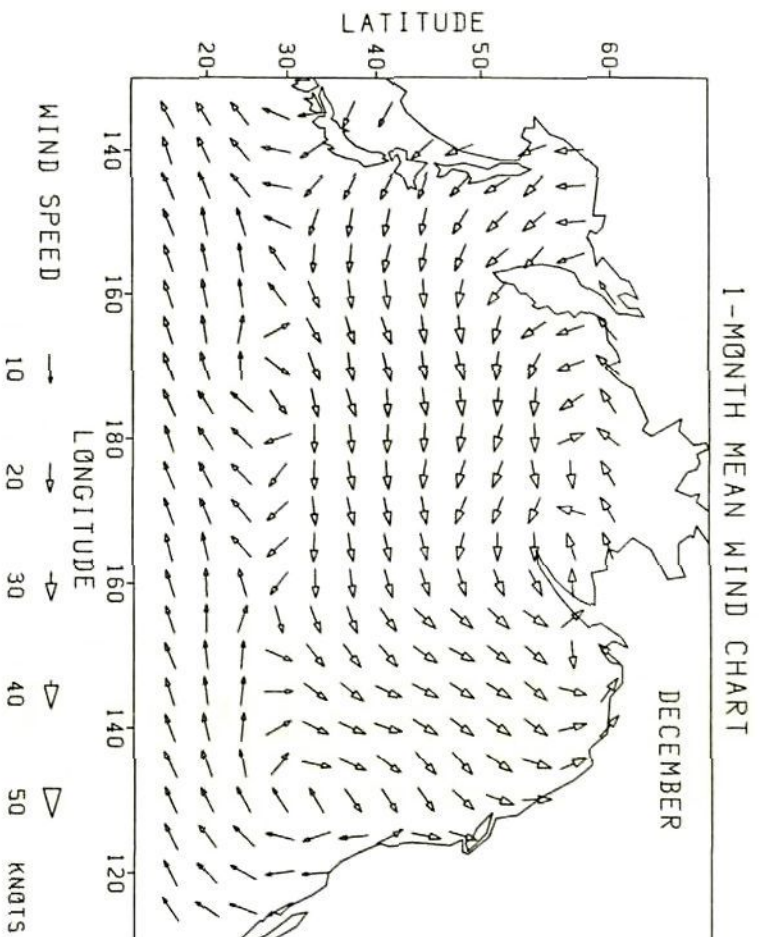


Fig. 4.27 (a) 1-month mean wind chart ( December )

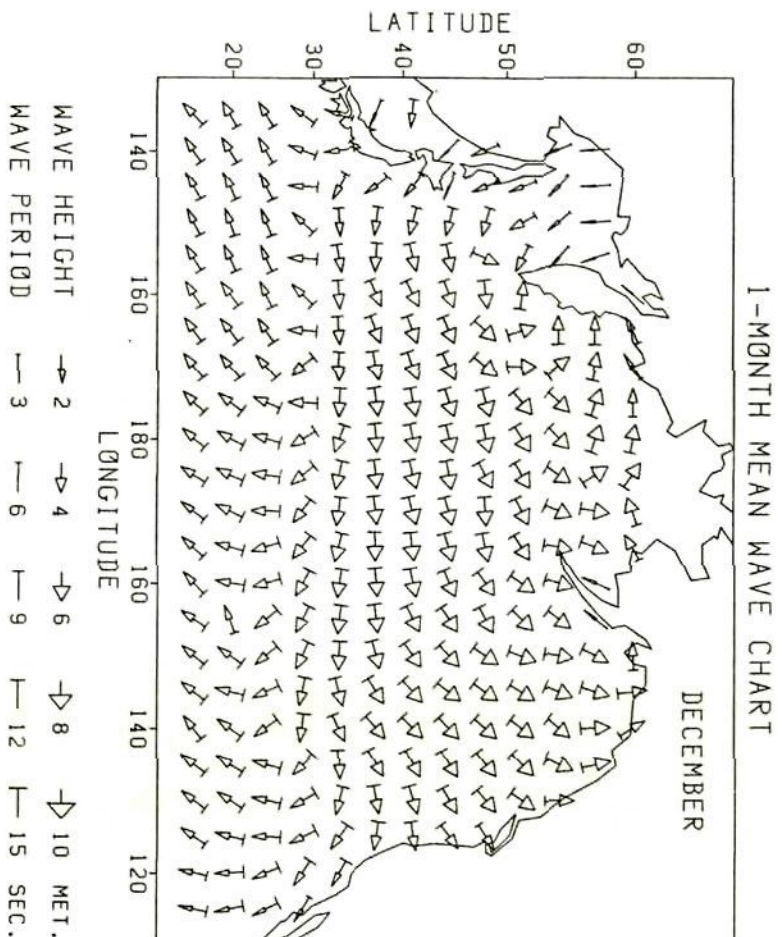


Fig. 4.27 (b) 1-month mean wave chart ( December )

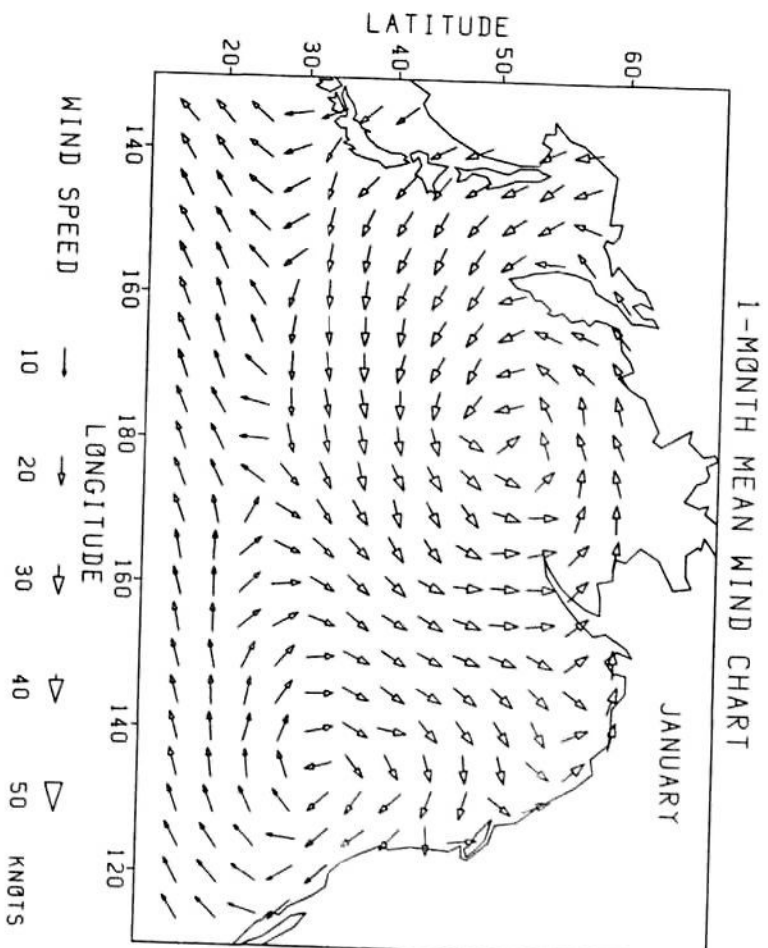


Fig. 4.28 (a) 1-month mean wind chart ( January )

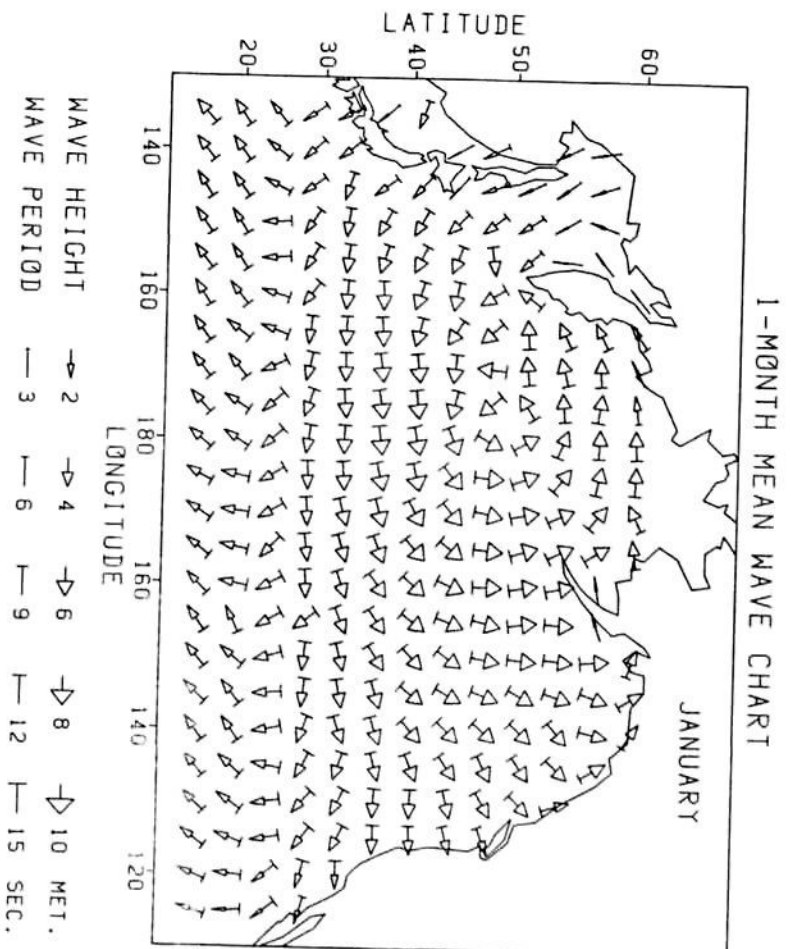


Fig. 4.28 (b) 1-month mean wave chart ( January )

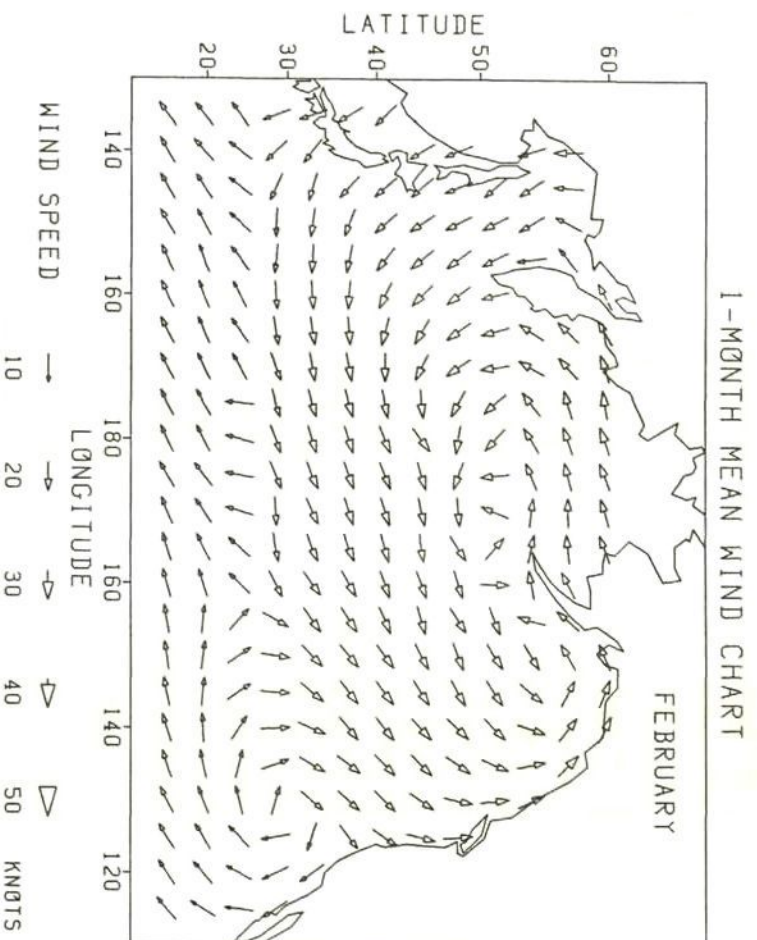


Fig. 4.29 (a) 1-month mean wind chart ( February )

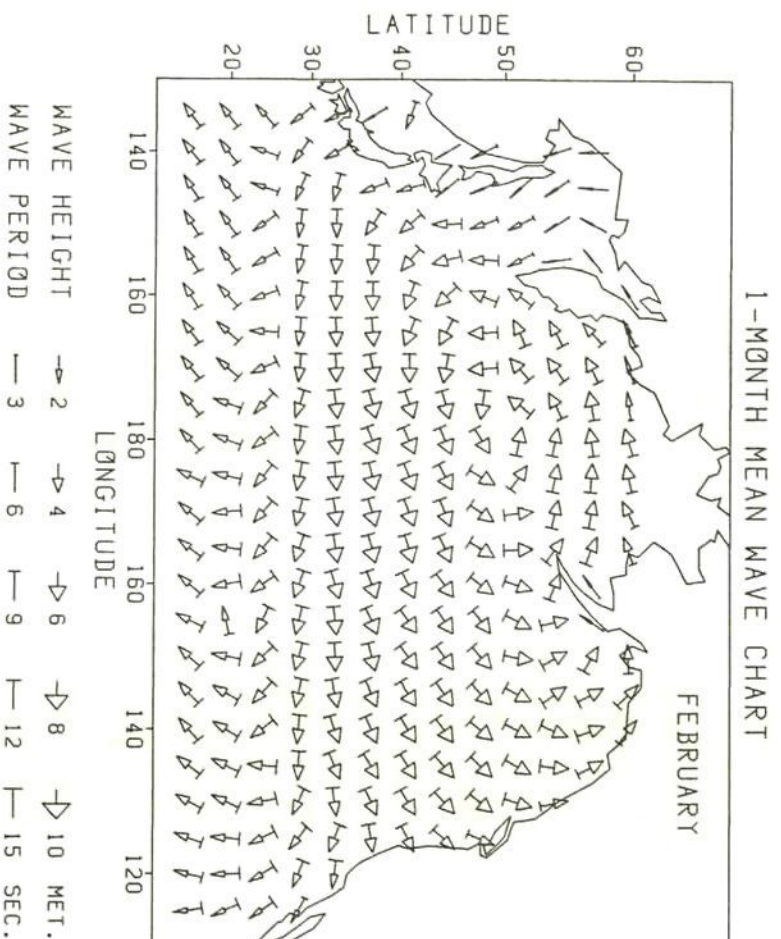


Fig. 4.29 (b) 1-month mean wave chart ( February )



#### 4.5.2 Mean errors and covariance matrices of the 1-month mean wind/wave data

When the 1-month mean wind/wave data are used as the predicted data in stochastic routing, it is necessary to obtain their unbiased values and covariance matrices.

In the same way as mentioned in 4.3.2, comparing each 1-month mean wind/wave data with the analyzed data at 00 and 12 hours GMT for the corresponding month in five winters, the mean errors and covariance matrix of 1-month mean wind/wave data were calculated at each grid point. Then the covariance matrices were averaged in each sub-area.

In the simulations, the mean errors are added to the 1-month mean wind/wave data at each grid point, and the resultant unbiased data are used to calculate the unbiased wind/wave data  $\bar{C}_i$ . The averaged covariance matrices memorized at the central points of the sub-areas are used to calculate the covariance matrix  $P_c(i)$ .

Averaging the mean errors and standard deviations of 1-month mean wind/wave data over all the North Pacific Ocean, Fig.4.30 (a)-(e) were obtained. It is found from Fig.4.30 that for the same reason as mentioned in 4.4.3, the 1-month mean wind/wave data have small mean errors. The standard deviations of the 1-month mean wind/wave data are almost equal to those of the 5-day mean wind/wave models classified by ZI in Fig.4.24.

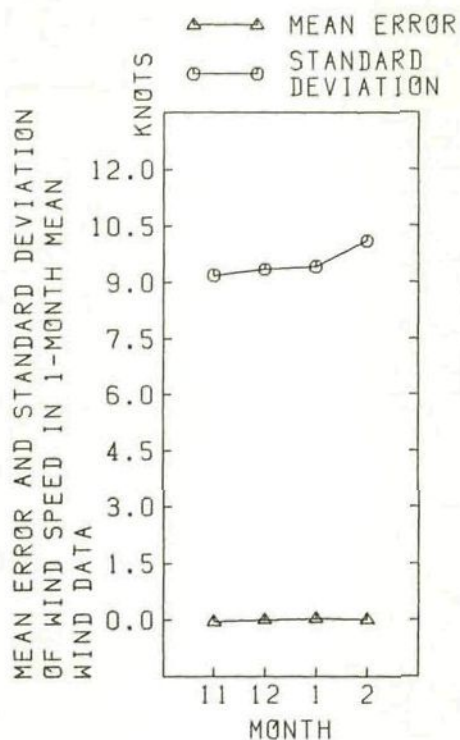


Fig. 4.30 (a) Mean error and standard deviation of wind speed in each 1-month mean wind data averaged over all the North Pacific Ocean

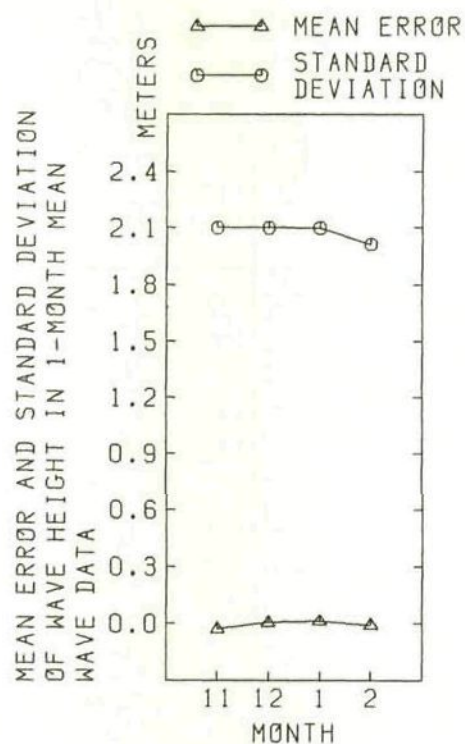


Fig. 4.30 (c) Mean error and standard deviation of wave height in each 1-month mean wave data averaged over all the North Pacific Ocean

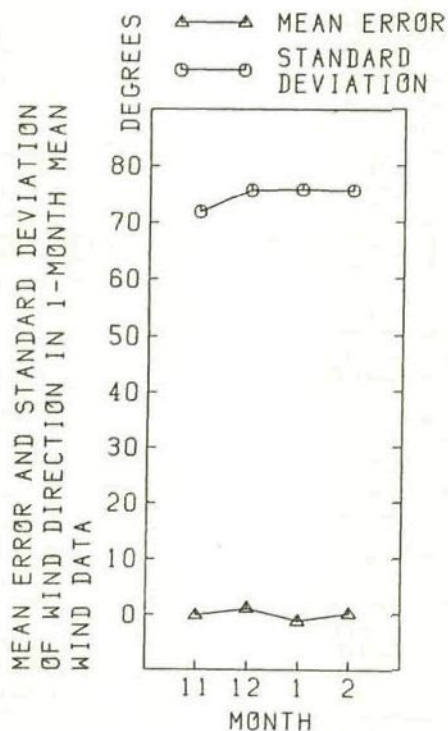


Fig. 4.30 (b) Mean error and standard deviation of wind direction in each 1-month mean wind data averaged over all the North Pacific Ocean

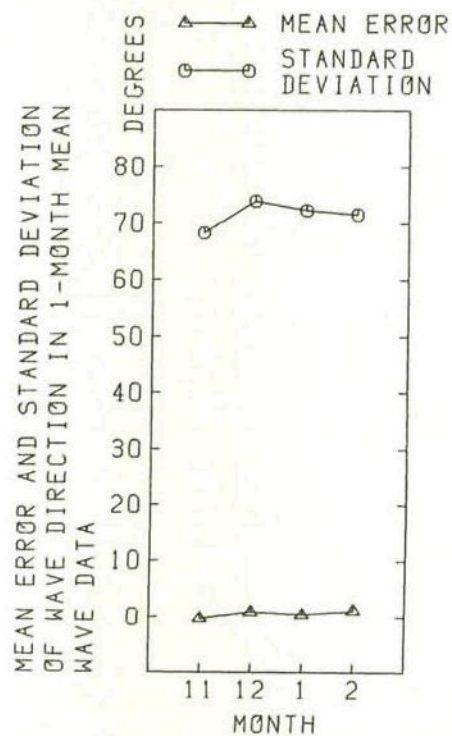


Fig. 4.30 (d) Mean error and standard deviation of wave direction in each 1-month mean wave data averaged over all the North Pacific Ocean

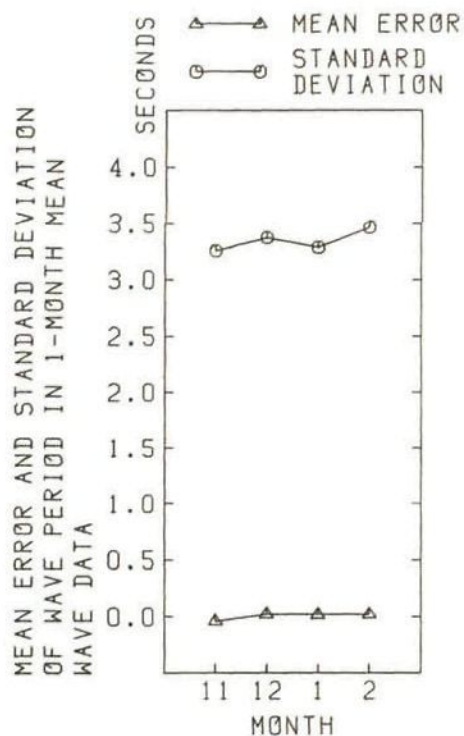


Fig. 4.30 (e) Mean error and standard deviation of wave period in each 1-month mean wave data averaged over all the North Pacific Ocean

#### 4.5.3 Correlations between errors in the 1-month mean wind/wave data

When the 1-month mean wind/wave data are used for stochastic routing, it is also necessary to obtain the correlations between errors in those data.

In the same manner as mentioned in 4.3.3, comparing each 1-month mean wind/wave data with the analyzed data at 00 and 12 hours GMT for the corresponding month in five winters, the correlations ( correlation coefficients ) between errors in the 1-month mean wind/wave data for 12-hour sub-time-interval were computed at each grid point, and then they were averaged in each sub-area.

In the simulations, the averaged correlations memorized at the central points of the sub-areas are used to calculate the correlation matrix  $\Phi_c(i)$ .



Averaging the correlations between errors in the 1-month mean wind/wave data over all the North Pacific Ocean, Fig.4.31 (a)-(e) were obtained. It is found from Fig.4.31 that the correlations between errors in the 1-month mean wind/wave data are very similar to those in the 5-day mean wind/wave models in Fig.4.25.

The correlations on the ship's course 090° are considerably larger than those on the other ship's courses for the same reason as explained in 4.4.4. It is also found that the correlations between errors of the wave heights in the 1-month mean wind/wave data are larger than those of other factors in the 1-month mean wind/wave data.

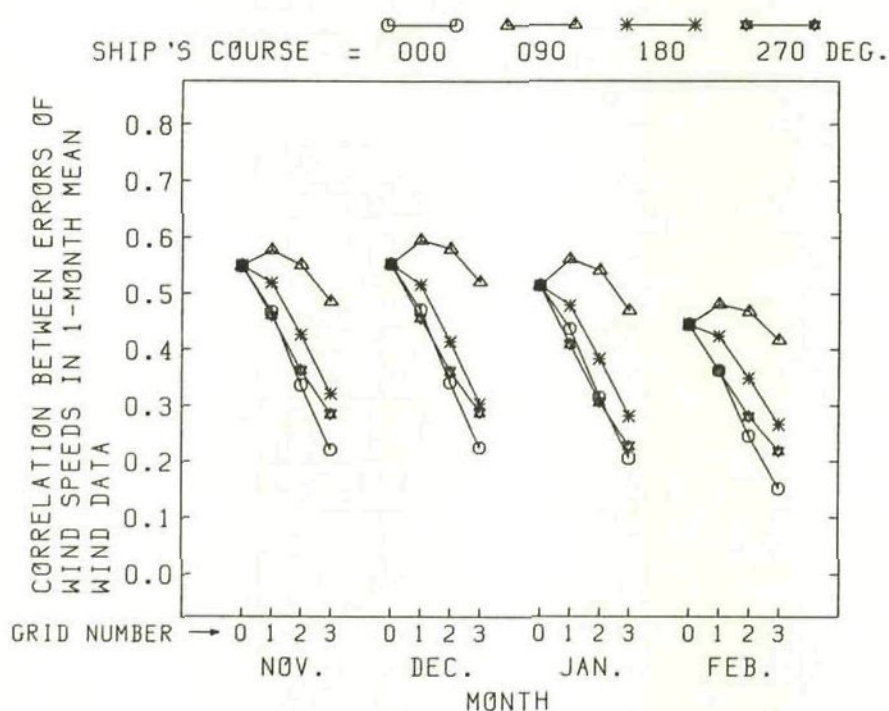


Fig. 4.31 (a) Correlation between errors of wind speeds in each 1-month mean wind data averaged over all the North Pacific Ocean

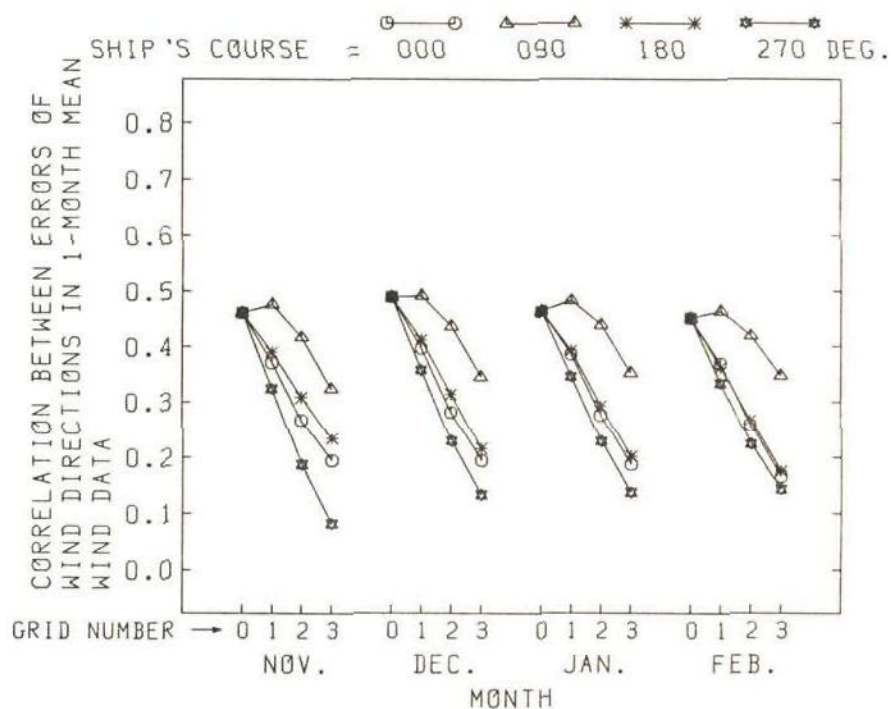


Fig. 4.31 (b) Correlation between errors of wind directions in each 1-month mean wind data averaged over all the North Pacific Ocean

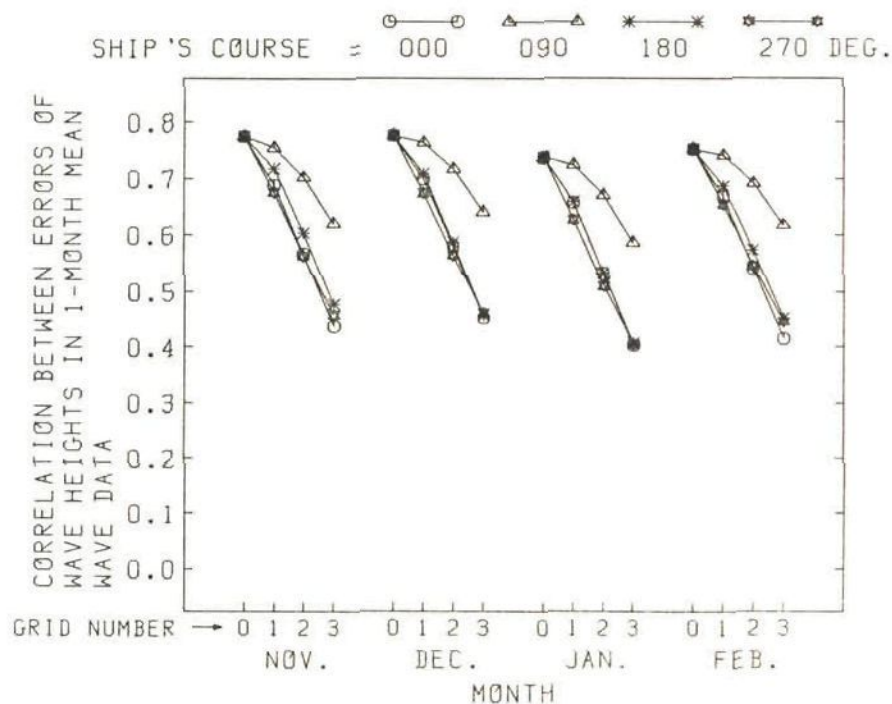


Fig. 4.31 (c) Correlation between errors of wave heights in each 1-month mean wave data averaged over all the North Pacific Ocean

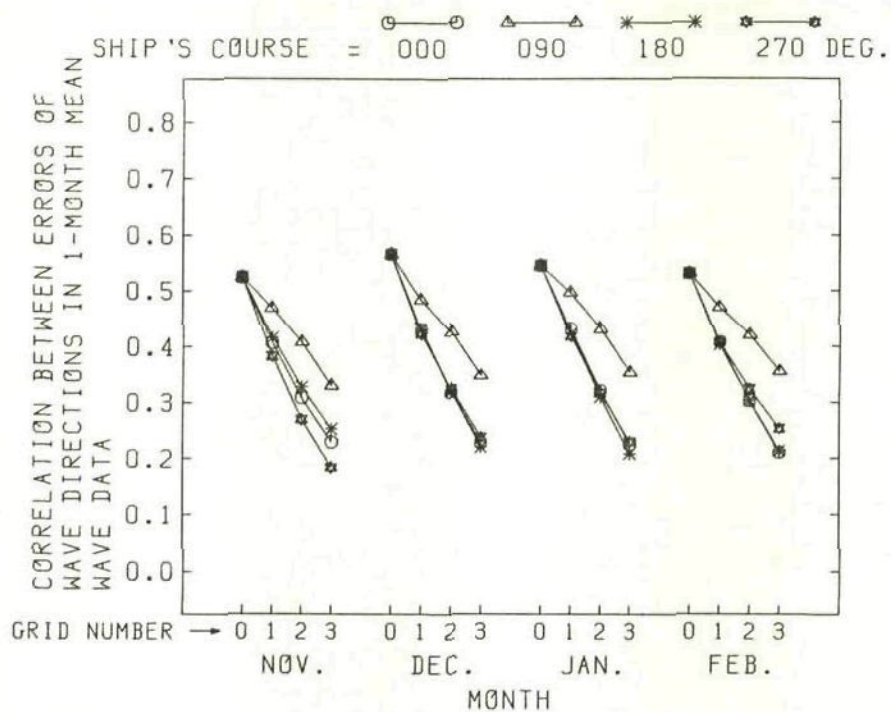


Fig. 4.31 (d) Correlation between errors of wave directions in each 1-month mean wave data averaged over all the North Pacific Ocean

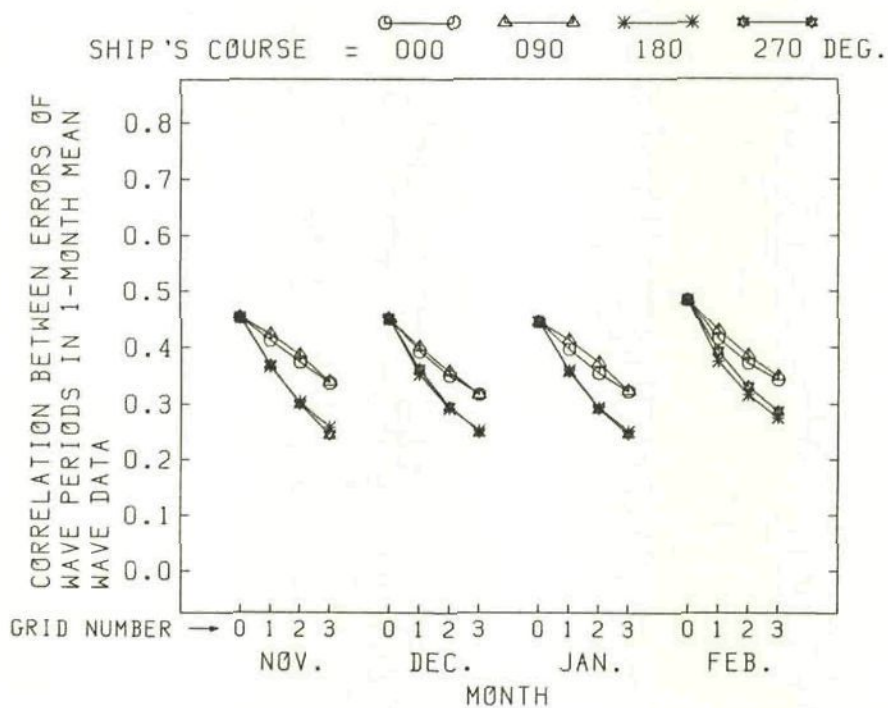


Fig. 4.31 (e) Correlation between errors of wave periods in each 1-month mean wave data averaged over all the North Pacific Ocean



#### 4.6 MONTHLY OCEAN CURRENT DATA PUBLISHED BY FNOC

In the deterministic routing, the monthly ocean current data published by FNOC are used, which were produced from the Pilot Charts of the U.S. Defense Mapping Agency. The grid system used for the ocean current data is the same as that for the wind/wave data shown in Table 4.1.

The monthly ocean current charts of November, December, January and February are shown in Figs 4.32 - 4.35. It can be seen from Figs 4.32 - 4.35 that the monthly ocean current data by FNOC are well harmonized in both speed and direction.

In the simulations, the ocean current data  $\underline{W}_i$  at the ship's position  $\underline{X}_i$  are computed by linear interpolation over space.

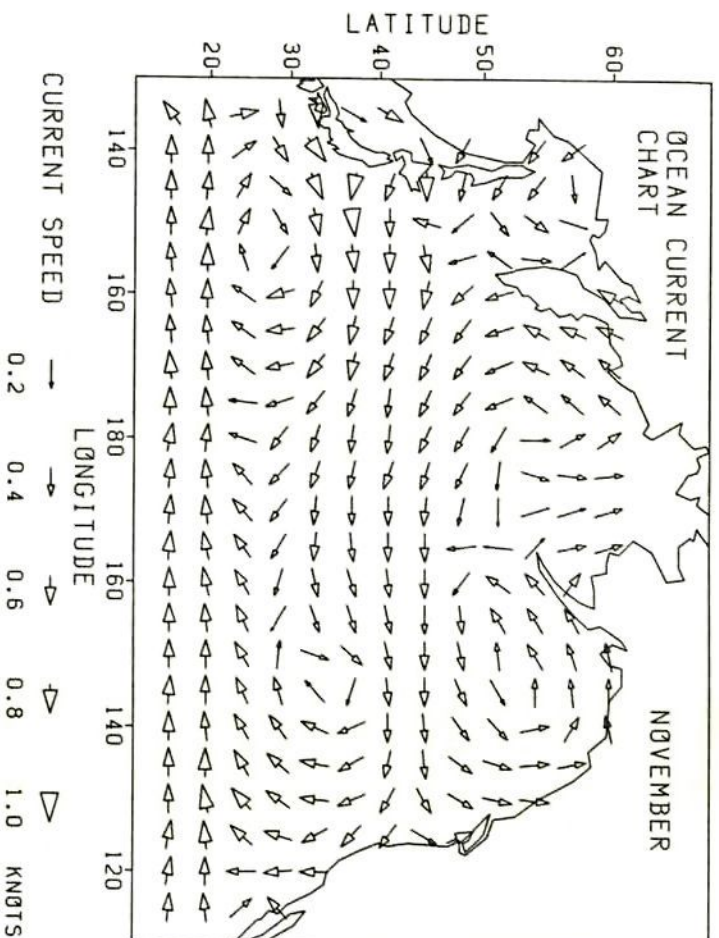


Fig. 4.32 Monthly ocean current chart ( November )

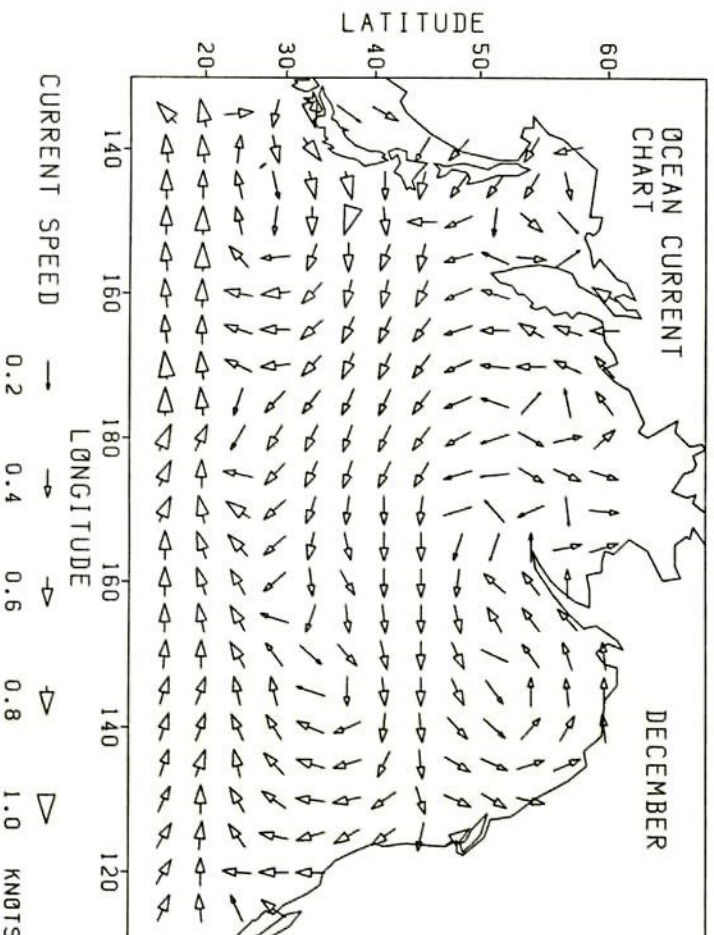


Fig. 4.33 Monthly ocean current chart ( December )

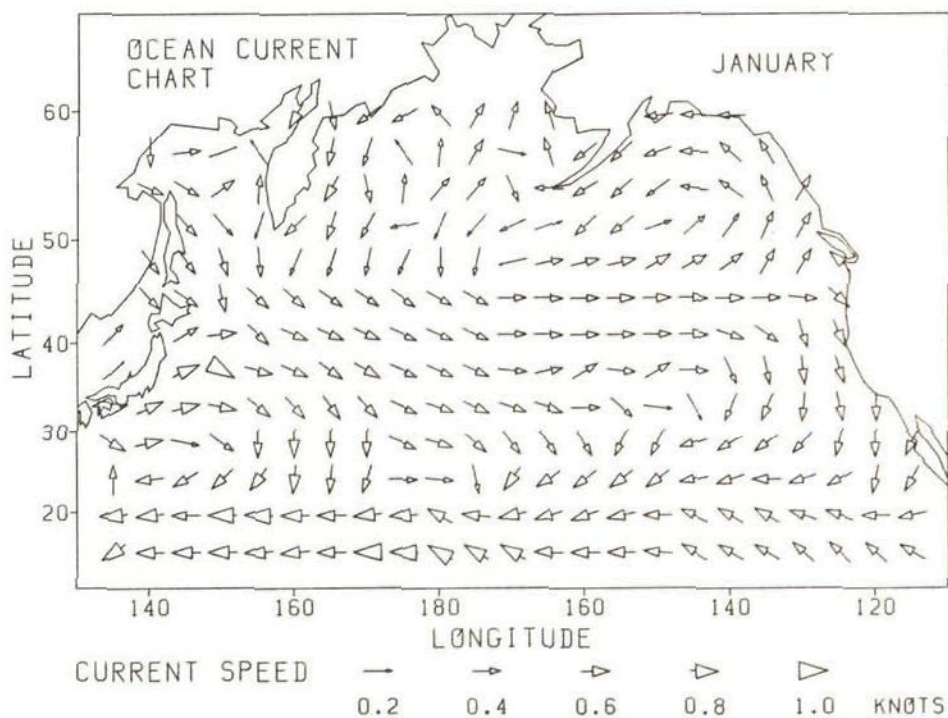


Fig. 4.34 Monthly ocean current chart ( January )

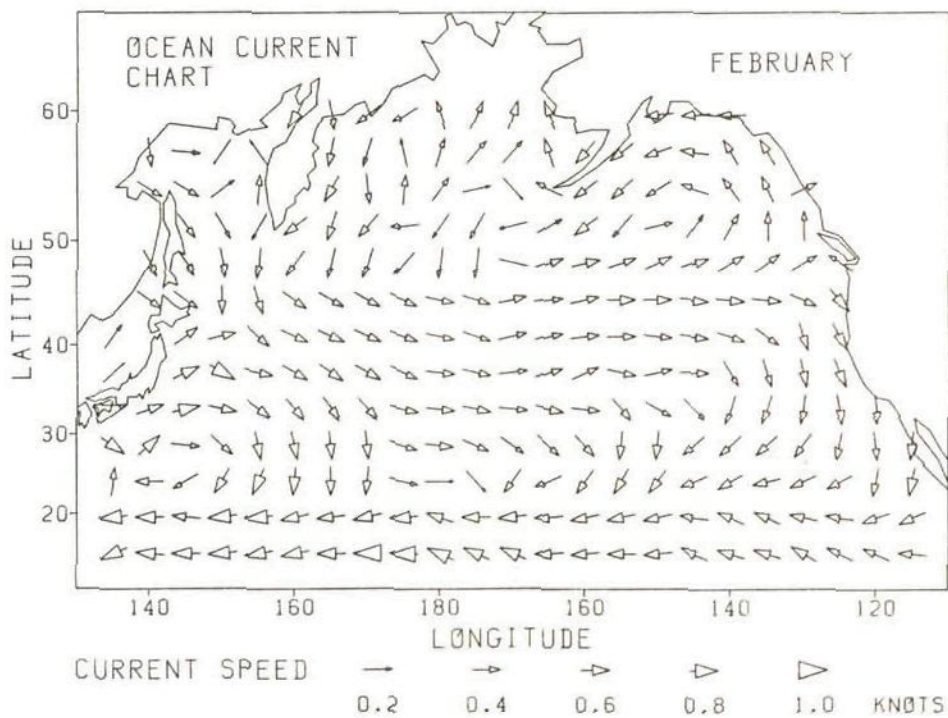


Fig. 4.35 Monthly ocean current chart ( February )



#### 4.7 MONTHLY OCEAN CURRENT DATA PUBLISHED BY THE METEOROLOGICAL OFFICE

In the stochastic routing, the monthly ocean current data published by the U.K. Meteorological Office are used. The details of those data are described below.

##### 4.7.1 Monthly mean value charts of the ocean currents

For this study, the monthly mean values of the ocean currents, i.e. the mean northerly component  $\bar{N}$  and the mean easterly component  $\bar{E}$  in each  $5^\circ \times 5^\circ$  sub-area over the North Pacific and North Atlantic Ocean, were calculated by the Meteorological Office using a data base of about five million current observations by ships gathered world-wide since 1853:

$$\bar{N} = \left\{ \sum_{i=1}^n N(i) \right\} / n \quad (4.23)$$

$$\bar{E} = \left\{ \sum_{i=1}^n E(i) \right\} / n \quad (4.24)$$

where  $N(i)$  and  $E(i)$  : observed northerly and easterly component of the ocean current in each  $5^\circ \times 5^\circ$  sub-area in each month

$n$  : number of observations

The mean values  $\bar{N}$  and  $\bar{E}$  were memorized at the central point of each sub-area.

The monthly mean value charts of the ocean currents for the North Pacific Ocean are shown in Fig.4.36 (a) ( January ) and Fig.4.37 (a) ( February ). Note that in these charts, the sizes of the arrows are doubled compared with those in the monthly ocean current charts by FNOC.

The total number of observations used for drawing Fig.4.36 (a)

and Fig.4.37 (a) is 34,133 and 29,581, respectively. The observations were sparse in the middle of the North Pacific and dense off Japan and the West Coast of North America.

From Fig.4.36 (a) and Fig.4.37 (a), the mean values of the ocean currents seem too small except those of the North Equatorial Current and Kuroshio, and in addition, there are some inconsistent mean values. Those unreasonable mean values result from inaccurate observations.

Although the mean values of the ocean currents calculated by the Meteorological Office have a problem in their accuracies, they are used as the unbiased predicted data in the stochastic routing simulations to obtain the unbiased predicted value of ocean current  $\bar{W}_i$ .

#### 4.7.2 Monthly covariance ( 39% error ellipse ) charts of the ocean currents

When the monthly ocean current data described in 4.7.1 are used as the predicted data in stochastic routing, it is necessary to obtain their covariance matrices.

Monthly variances and covariance of the ocean current, i.e. the variance of northerly component  $P_{NN}$ , the variance of easterly component  $P_{EE}$  and the covariance between northerly component and easterly component  $P_{NE}$  in each  $5^\circ \times 5^\circ$  sub-area, were computed by the Meteorological Office as follows:

$$P_{NN} = \left\{ \sum_{i=1}^n [ N(i) - \bar{N} ]^2 \right\} / n \quad (4.25)$$

$$P_{EE} = \left\{ \sum_{i=1}^n [ E(i) - \bar{E} ]^2 \right\} / n \quad (4.26)$$

$$P_{NE} = \left\{ \sum_{i=1}^n [ N(i) - \bar{N} ] [ E(i) - \bar{E} ] \right\} / n \quad (4.27)$$

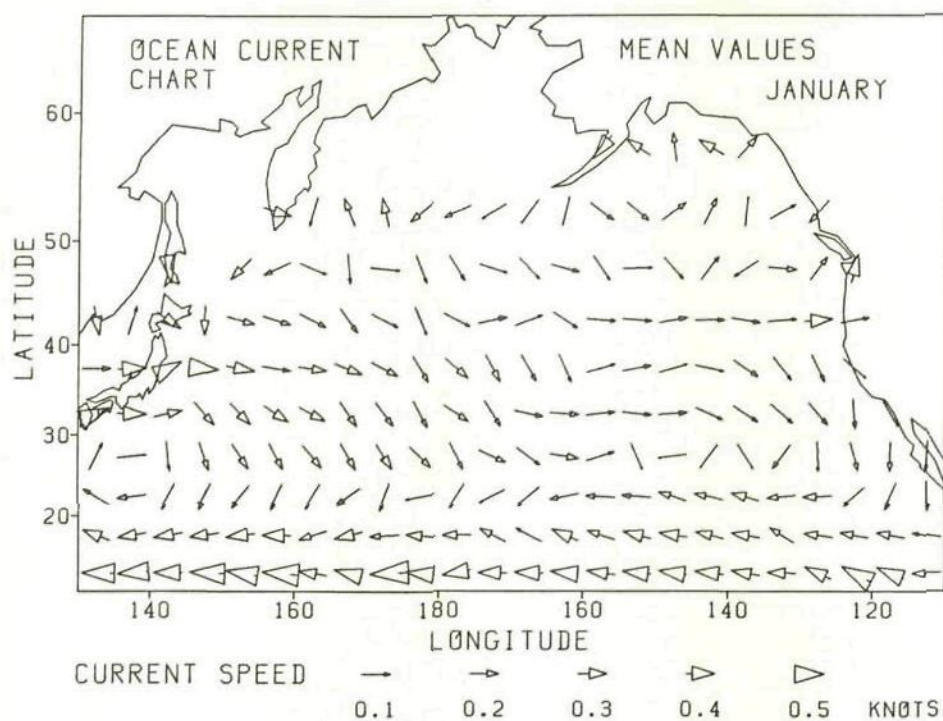


Fig. 4.36 (a) Monthly mean value chart of the ocean currents ( January )

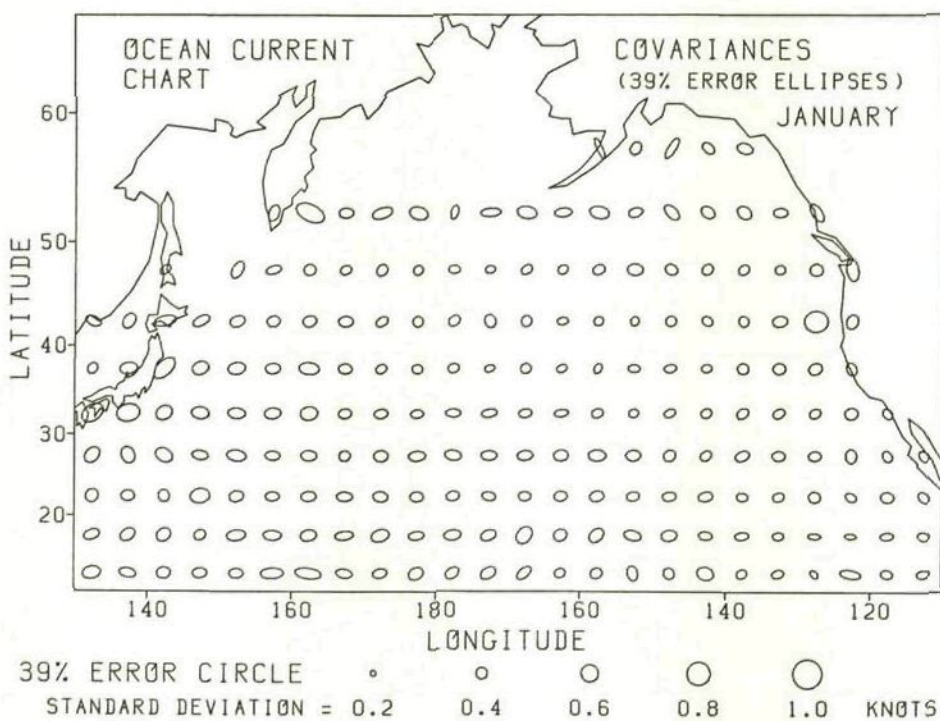


Fig. 4.36 (b) Monthly covariance ( 39% error ellipse ) chart of the ocean currents ( January )



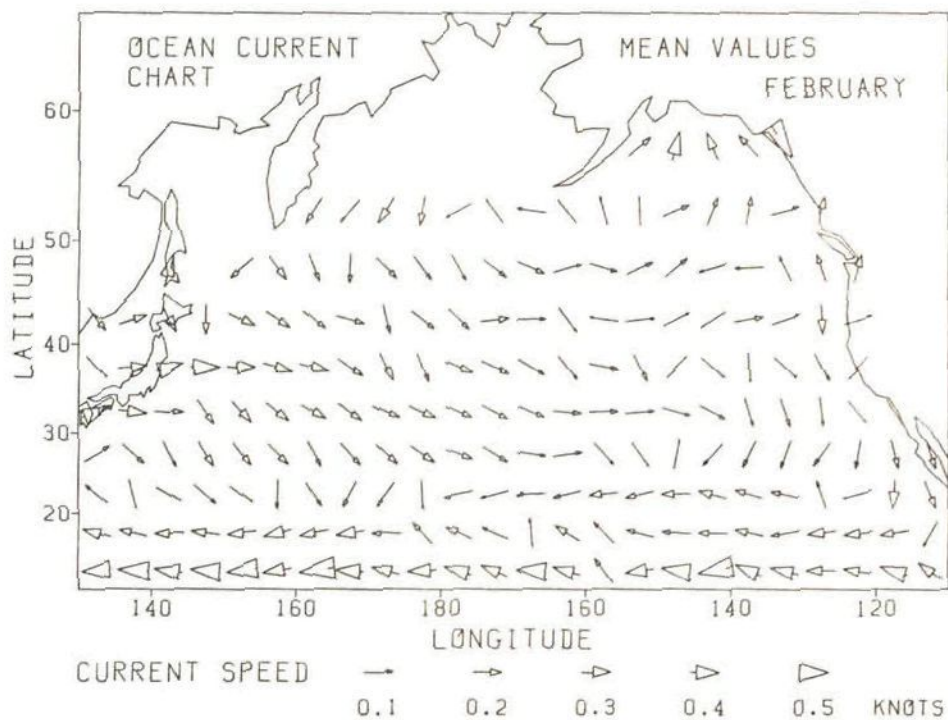


Fig. 4.37 (a) Monthly mean value chart of the ocean currents (February)

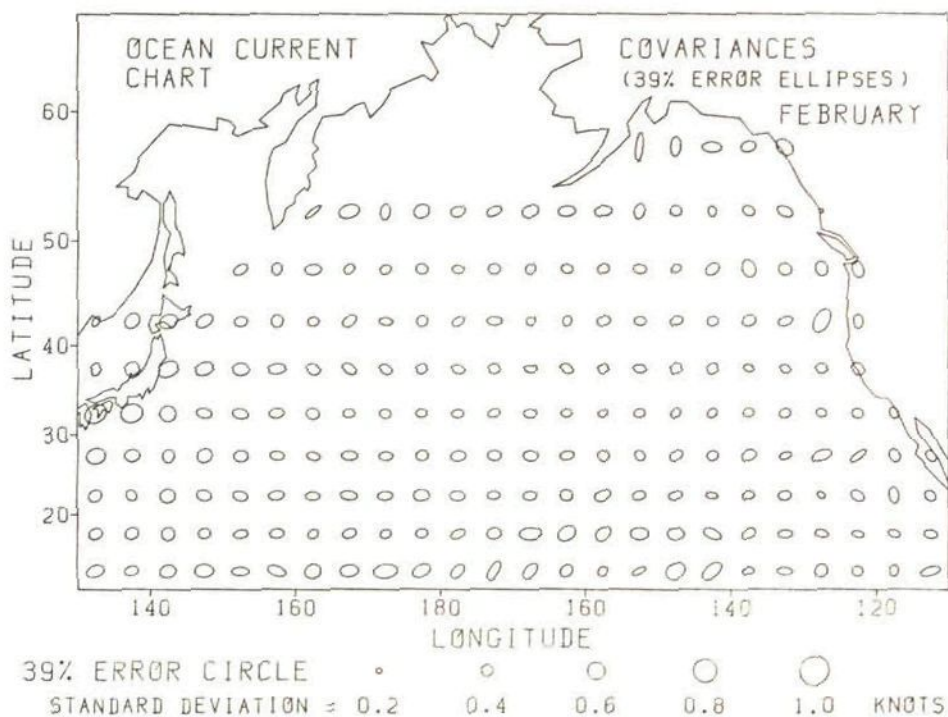


Fig. 4.37 (b) Monthly covariance (39% error ellipse) chart of the ocean currents (February)

The  $P_{NN}$ ,  $P_{EE}$  and  $P_{NE}$  constitute the covariance matrix of the ocean current, which is memorized at the central point of each sub-area.

Assuming that the ocean current vector has a two-dimensional Gaussian distribution, the covariance ( 39% error ellipse ) charts were constructed by computing the eigenvalues and eigenvectors of the covariance matrices of the ocean currents. The probability of finding the end of the ocean current vector inside the 39% error ellipse is 0.39347 [  $= 1 - \exp(-0.5)$  ]. ( Fig.4.38 )

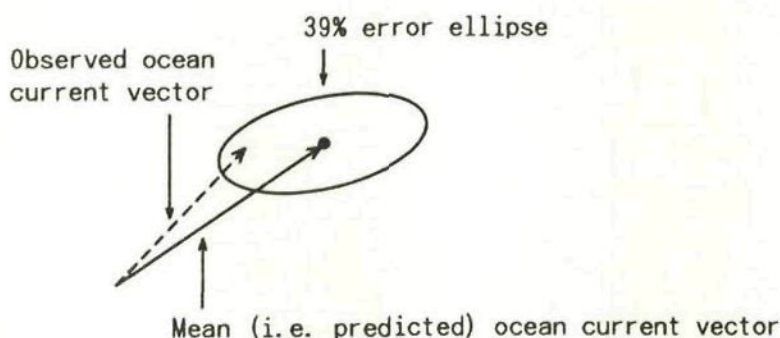


Fig. 4.38 39% error ellipse of the ocean current vector

The monthly covariance ( 39% error ellipse ) charts of the ocean currents for the North Pacific Ocean are shown in Fig.4.36 (b) and Fig.4.37 (b). The sizes of the 39% error circles are shown below those charts. For example, the 39% error circle for standard deviation of 1.0 knots means that when the standard deviations of northerly and easterly components of the ocean current are 1.0 knots and there is no covariance, the probability of finding the end of the ocean current vector inside that circle is 0.39347.

Compared with the mean value charts ( Fig.4.36 (a) and Fig.4.37 (a) ), a number of 39% error ellipses seem too large. For example, in the mean value chart and covariance chart for January, averaging the mean values and standard deviations of the North Pacific Current along  $42.5^{\circ}\text{N}$  parallel for the longitudinal range between  $160^{\circ}\text{E}$  and

140°W, we have the following averaged values:

Averaged northerly component = -0.021 knots

Averaged easterly component = 0.088 knots

Averaged standard deviation of northerly component = 0.356 knots

Averaged standard deviation of easterly component = 0.392 knots

These too small mean values and too large standard deviations result from the inaccurate observations performed on board the ships.

Although there is a problem with the accuracy of covariance matrices of the ocean currents calculated by the Meteorological Office, they are used in the stochastic routing simulations to obtain the covariance matrix  $P_w(i)$ .

Concerning the correlations between errors of the ocean currents, since the observed data were taken at various times during a long period, it was not possible to extract information on the correlations.

Makishima calculated the correlation between errors of the ocean currents based on the data observed by a tanker which navigated off Florida at about 15 knots, and indicated that the correlation decreases rapidly as the time-interval for computing the correlation increases.<sup>(10)</sup> He represented the correlation coefficient for time-interval  $\tau$  ( hours ) as  $\exp(-\tau/0.9)$ .

In the stochastic routing, since the sub-time-interval to calculate the correlations is 12 hours, it is expected that the correlations between errors of the ocean currents become very small values. Therefore, in the simulations, the correlation matrix  $\Phi_w(i)$  is assumed to be zero, i.e. the errors of the ocean currents are regarded as a white sequence.

In the future, the numerical forecasts of the ocean currents will be performed on a daily basis, which will provide us information to compute the correlations.



#### 4.8 INTERPOLATION SCHEME FOR THE ENVIRONMENTAL DATA FOR WEATHER ROUTING

In the deterministic routing, it is necessary to obtain the wind/sea/swell and ocean current conditions at the given time  $t_i$  and ship's position  $\underline{X}_i$  using the wind/sea/swell and ocean current data memorized at  $25 \times 60$  grid points shown in Table 4.1.

In the stochastic routing, it is necessary to obtain the predicted wind/wave and ocean current conditions at the given time  $t_i$  and predicted ship's position  $\bar{\underline{X}}_i$  using the wind/wave data memorized at  $25 \times 60$  grid points and the ocean current data memorized at the central points of the sub-areas. Besides, it becomes necessary to obtain the covariance matrix and correlation matrix for the given time  $t_i$  and predicted ship's position  $\bar{\underline{X}}_i$  ( as well as ship's course and travelled distance for 12 hours ) using the covariance matrices and correlation matrices memorized at the central points of the sub-areas.

Numerical interpolations are used to calculate the above-mentioned environmental data in the routing algorithm. As numerous interpolations have to be carried out in the simulation, a simple linear interpolation scheme was adopted to save computing time.

The linear interpolation over space is performed by the following formula:

$$Z = Z_{31} + (Z_{32} - Z_{31})(\lambda - \lambda_1) / (\lambda_2 - \lambda_1) \quad (4.28)$$

$$\text{where } Z_{31} = Z_{11} + (Z_{21} - Z_{11})(\phi - \phi_1) / (\phi_2 - \phi_1)$$

$$Z_{32} = Z_{12} + (Z_{22} - Z_{12})(\phi - \phi_1) / (\phi_2 - \phi_1)$$

$Z$  : environmental condition at the ship's position  $(\phi, \lambda)$   
 $Z_{11}, Z_{12}, Z_{21}, Z_{22}$  : environmental data at the grid points  $(\phi_1, \lambda_1)$ ,  
 $(\phi_1, \lambda_2), (\phi_2, \lambda_1), (\phi_2, \lambda_2)$  surrounding the ship's  
position  $(\phi, \lambda)$

$$\phi_1 \leq \phi \leq \phi_2 \quad \lambda_1 \leq \lambda \leq \lambda_2$$

The linear interpolation over time is executed by

$$Z = Z_1 + (Z_2 - Z_1)(t - t_1) / (t_2 - t_1) \quad (4.29)$$

where  $Z$  : environmental condition at time  $t$

$Z_1, Z_2$  : environmental data at time  $t_1$  and  $t_2$

$t_1 = 00, t_2 = 12$  hours GMT

or  $t_1 = 12, t_2 = 00$  hours GMT

$$t_1 \leq t \leq t_2$$

For calculating the wind direction and sea/swell ( or primary wave ) direction by linear interpolation,  $Z_{32} - Z_{31}, Z_{21} - Z_{11}$  and  $Z_{22} - Z_{12}$  in (4.28) as well as  $Z_2 - Z_1$  in (4.29) are adjusted so that their absolute values will not exceed  $180^\circ$ ; i.e. when they become greater than  $180^\circ$ ,  $360^\circ$  is subtracted, whereas when they become less than  $-180^\circ$ ,  $360^\circ$  is added.

All environmental data and interpolation procedures used in the simulations are summarized in Fig.4.39 ( deterministic routing ) and Fig.4.40 ( stochastic routing ).

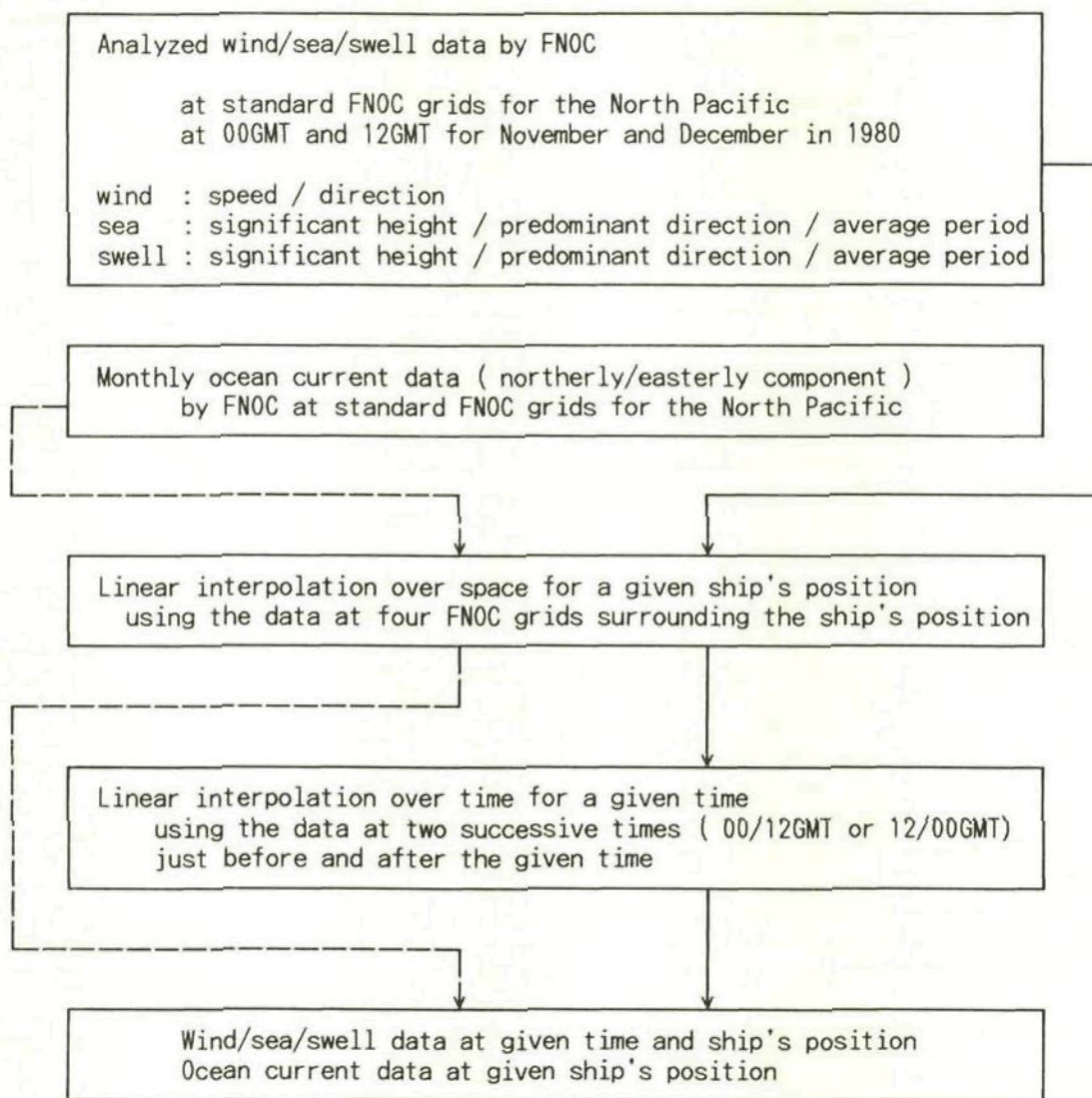


Fig. 4.39 Environmental data and interpolation procedure for the deterministic routing



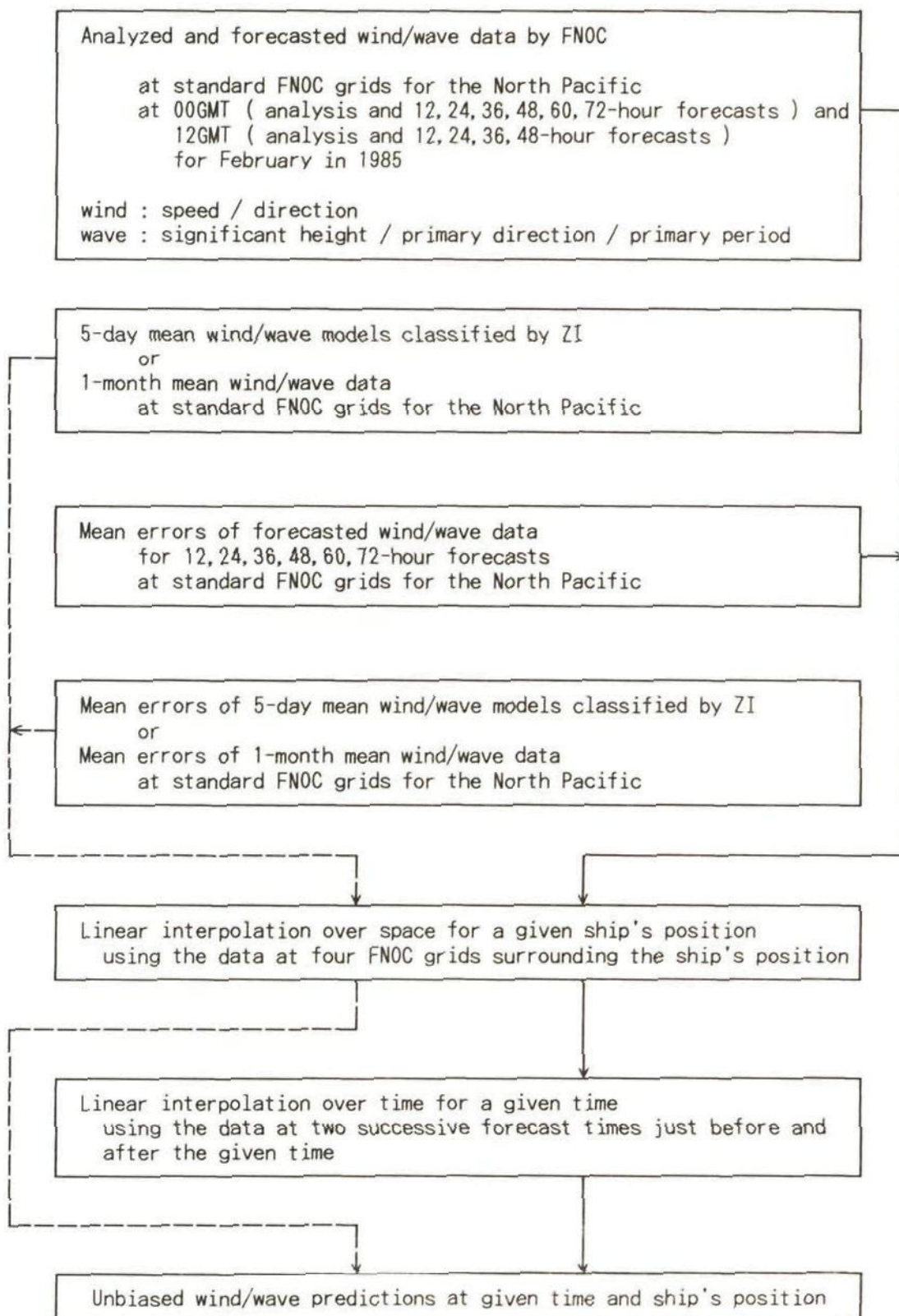
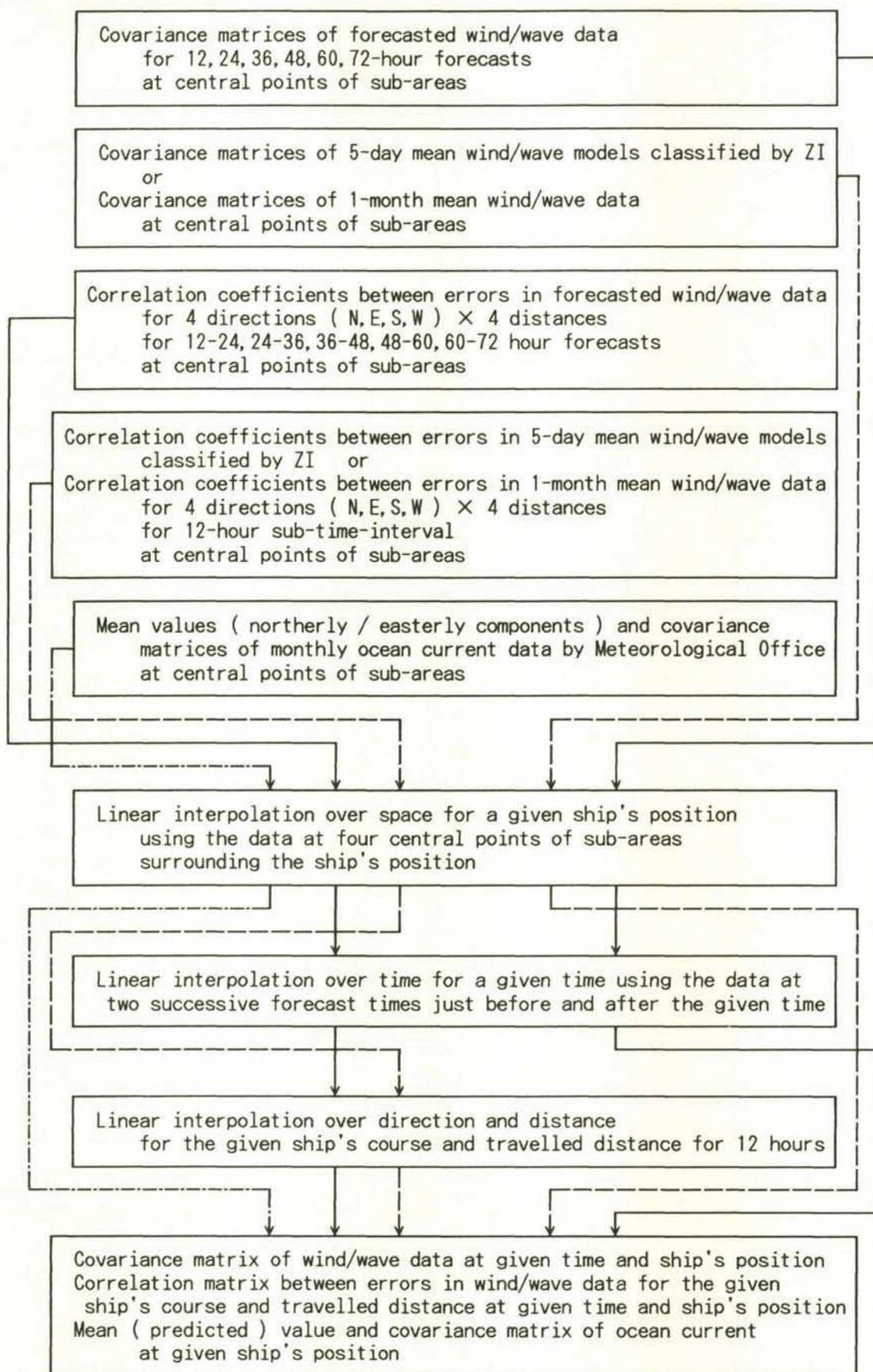


Fig. 4.40 Environmental data and interpolation procedure for the stochastic routing





#### 4.9 OTHER HAZARDOUS ENVIRONMENTS TO BE CONSIDERED IN WEATHER ROUTING

For executing weather routing, the following hazardous environments have to be considered in addition to the wind, wave and ocean current conditions.

- \* Sea ice ( packed ice ) or icebergs
- \* Icing
- \* Fog

Packed ice or icebergs can be observed by airplanes and meteorological satellites. Since their drifting speed is comparatively slow, the observed area plus a surrounding region as a safety margin may be specified as the unnavigable area in the routing algorithm.

Icing can be predicted as a function of the temperature and wind speed in some degree. In the North Pacific Ocean, it often occurs off the Kuril Islands in the winter. When an heavy icing is predicted for a certain area, we can regard such an area as an unnavigable area in the routing algorithm.

Although the fog itself does not affect the ship's speed, it may cause a speed reduction to avoid grounding or collision in an area where a lot of islands or fishing boats exist. In the North Pacific Ocean, a large-scale sea fog takes place in the North-west Pacific in the summer, and it lasts for a long period. In the routing algorithm, if necessary, some penalty may be imposed on the objective function when a ship navigates through the area covered by fog.

There are two methods to specify the unnavigable ( or unfavorable ) area due to hazardous environments. When the shape of the unnavigable area is comparatively simple, the unnavigable area can be specified by approximating the boundary of that area by a simple function of latitude and longitude. On the other hand, when the shape of the unnavigable area is complex, the unnavigable area is specified by giving a special code to the grid points of the FNOC grid system involved in that area.



## 5. ANALYSIS ON THE ACCURACY OF THE MODIFIED ISOCHRONE METHOD

### 5.1 INTRODUCTION

In the weather routing simulations performed in Chapter 6, the optimum routes are calculated based on the modified isochrone method described in Sections 2.3 and 2.4.

Since the modified isochrone method treats the ship routing problem as a discrete optimization problem, it becomes important to investigate how much the solution is affected by the sizes of the increments to discretize the problem. By changing the increments ( e.g. increment of ship's heading, resolution of isochrone, etc. ), the sensitivities of the solutions to the sizes of the increments of several parameters are analyzed in this chapter.

In addition, for the stochastic routing, the partial derivatives of the ship's speed through the water and drift angle with respect to the wind/wave conditions ( i.e.  $S_c$  ( =  $\partial S / \partial C_i$  ) in (2.50) ) are calculated by numerical differentiations. In that case, the appropriate increments of the wind/wave conditions for the numerical differentiations have to be chosen to obtain the correct partial derivatives  $\partial S / \partial C_i$ . Thus the sensitivity of the solution to the increment in the numerical differentiation is also investigated.

The computer used for the simulations of this study is a HITAC M-682H mainframe computer in the Computer Center of the University of Tokyo. Concerning the weather routing simulations, the calculation speed of the HITAC M-682H was about 4 times faster than that of the IBM 3083-JX1 mainframe computer in the Computer Center of the Delft University of Technology.

## 5.2 SENSITIVITY OF THE SOLUTION TO THE TIME-INTERVAL BETWEEN SUCCESSIVE ISOCHRONES

On the parameters used in the modified isochrone method, we set up the following standards of the increments:

- \* Time-interval between successive isochrones  $\Delta t = 24$  hours
- \* Sub-time interval for calculating ship's speed, drift angle, etc.  
 $\Delta t' = 12$  hours
- \* Increment of ship's heading for constructing the isochrones  
 $\Delta C = 10^\circ$
- \* Resolution of the isochrone ( i.e. local width of the sub-sector )  
 $\Delta d = 45$  n.m.

The service speed  $V_s$  to calculate the sub-sector angle in formula (2.21) is set to 14 knots.

Using the above increments, the minimum time routing of the model ship ( sail-assisted motor vessel ) described in Section 3.2 was performed for the voyage from San Francisco to Tokyo departing at 00 hours GMT on 11 November 1980. The analyzed wind/sea/swell data mentioned in 4.2 and the monthly ocean current data mentioned in 4.6 were used for this simulation.

Fig.5.1 shows the result of the simulation. In Fig.5.1, the solid line and dashed line denote the minimum time route and great circle route. ( See Appendix 5 for the method to calculate the great circle route. )

The tips, directions and lengths of the arrows attached to both routes represent the ship's positions, wind directions and wind speeds for every 24 hours, respectively. The isochrones at 1,3,5,--- days and 2,4,6,--- days after the departure time are shown by circle marks and cross marks, respectively.

In order to investigate the sensitivity of the solution to the time-interval  $\Delta t$  between successive isochrones, letting  $\Delta t'$ ,  $\Delta C$  and  $\Delta d$  be the aforementioned values, two simulations of minimum time routing were carried out using  $\Delta t$  of 12 hours and 36 hours.



Fig.5.2 (a) and (b) show the results of those simulations for  $\Delta t = 12$  hours and 36 hours, respectively. The time-interval between successive arrows attached to both minimum time route and great circle route is 12 hours in Fig.5.2 (a) and 36 hours in Fig.5.2 (b).

It is found that the shapes of minimum time routes and isochrones as well as the passage times in Fig.5.1 and Fig.5.2 (a),(b) hardly differ from each other. Thus it can be said that the accuracy of the solution is not largely influenced by the time-interval  $\Delta t$  between successive isochrones.

Computing times ( except compiling times ) were 16, 12 and 10 seconds for  $\Delta t = 12, 24$  and 36 hours, respectively.

In practice, provided  $\Delta t'$ ,  $\Delta C$  and  $\Delta d$  are sufficiently small, the time-interval  $\Delta t$  which gives about 10 - 15 isochrones between departure point and destination suffices for obtaining a sufficiently accurate solution.

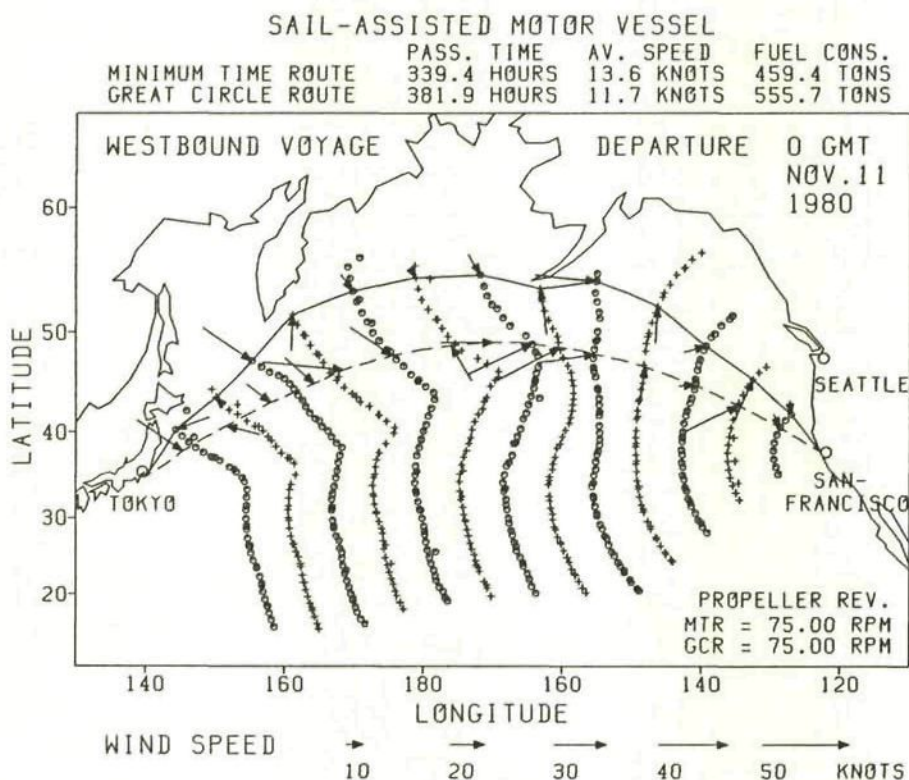


Fig. 5.1 Minimum time routing of the sail-assisted motor vessel  
(  $\Delta t = 24$  hours,  $\Delta t' = 12$  hours,  $\Delta C = 10^\circ$ ,  $\Delta d = 45$  n.m. )



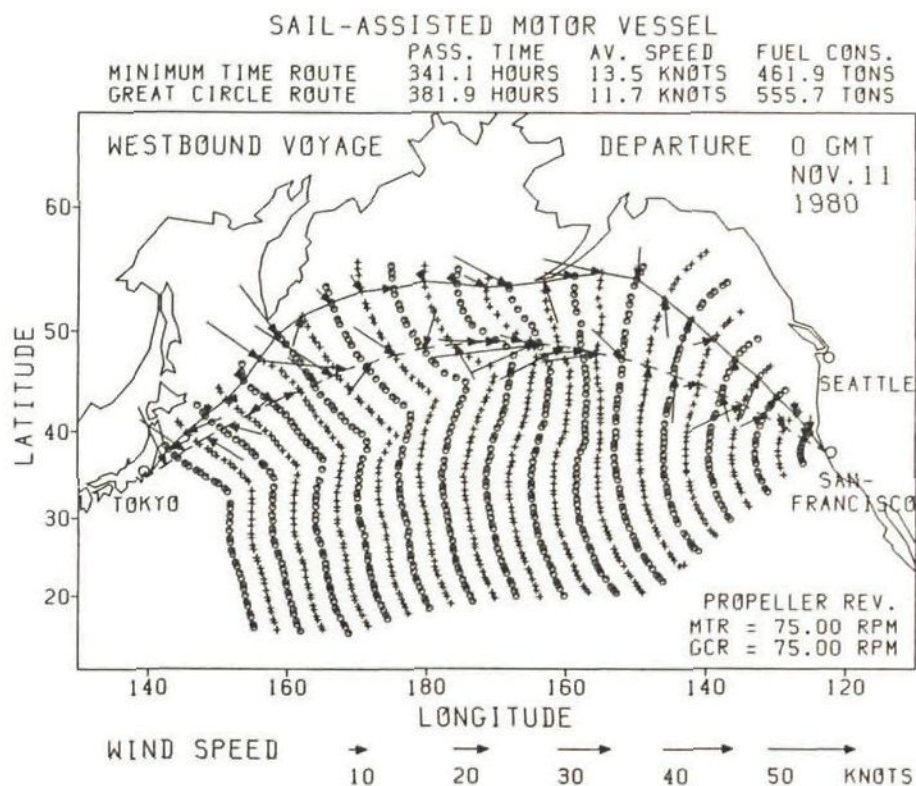


Fig. 5.2 (a) Minimum time routing of the sail-assisted motor vessel  
(  $\Delta t = 12$  hours,  $\Delta t' = 12$  hours,  $\Delta C = 10^\circ$ ,  $\Delta d = 45$  n.m. )

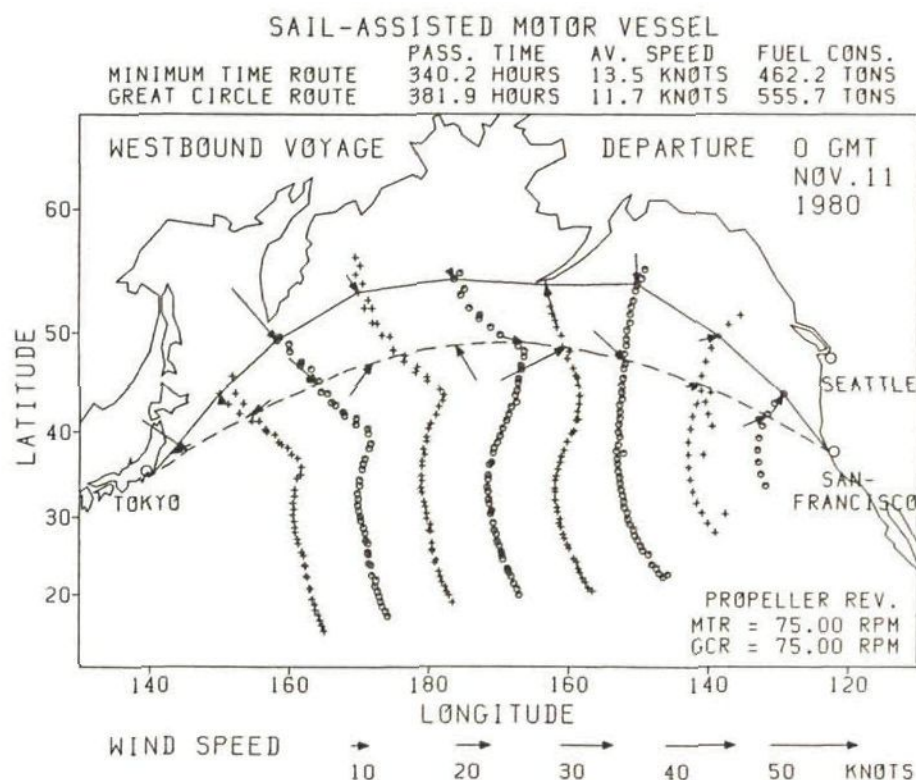


Fig. 5.2 (b) Minimum time routing of the sail-assisted motor vessel  
(  $\Delta t = 36$  hours,  $\Delta t' = 12$  hours,  $\Delta C = 10^\circ$ ,  $\Delta d = 45$  n.m. )

### 5.3 SENSITIVITY OF THE SOLUTION TO THE SUB-TIME-INTERVAL FOR CALCULATING SHIP'S SPEED, DRIFT ANGLE, ETC.

The sensitivity of the solution to the sub-time-interval  $\Delta t'$  for calculating ship's speed, drift angle, etc. is investigated in this section.

Letting  $\Delta t$ ,  $\Delta C$  and  $\Delta d$  be 24 hours,  $10^\circ$  and 45 n.m., two simulations of minimum time routing of the model ship were performed for the same voyage as stated in 5.2, using  $\Delta t'$  of 6 hours and 24 hours. The results of these simulations are shown in Fig.5.3 (a) ( $\Delta t' = 6$  hours) and Fig.5.3 (b) ( $\Delta t' = 24$  hours).

It is found that the shapes of the minimum time routes in Fig.5.1 ( $\Delta t' = 12$  hours) and Fig.5.3 (a),(b) almost coincide. We can find, however, that the shapes of the isochrones in Fig.5.1 and Fig.5.3 (a) are a bit different from those in Fig.5.3 (b). Particularly, the difference is apparent in the final isochrones (i.e. the closest isochrones to the destination).

The passage times on the minimum time routes for  $\Delta t' = 12$  hours and 24 hours became 2.6 hours (0.8%) and 4.6 hours (1.3%) smaller than that for  $\Delta t' = 6$  hours.

Computing times (except compiling times) were 21, 12 and 7 seconds for  $\Delta t' = 6, 12$  and 24 hours, respectively.

Since the small  $\Delta t'$  enables us to use the environmental data densely over time and space, the accuracy of the solution increases as  $\Delta t'$  decreases.

For the model ship with a service speed of 14 knots, it seems that the sub-time-interval  $\Delta t'$  should not be greater than 12 hours to obtain an accurate solution. For the faster ships, e.g. a container ship with service speed greater than 20 knots, it becomes necessary to use a smaller  $\Delta t'$  (e.g. 6 hours) for taking into account the larger variation of environments due to the longer travelled distance during  $\Delta t'$ .



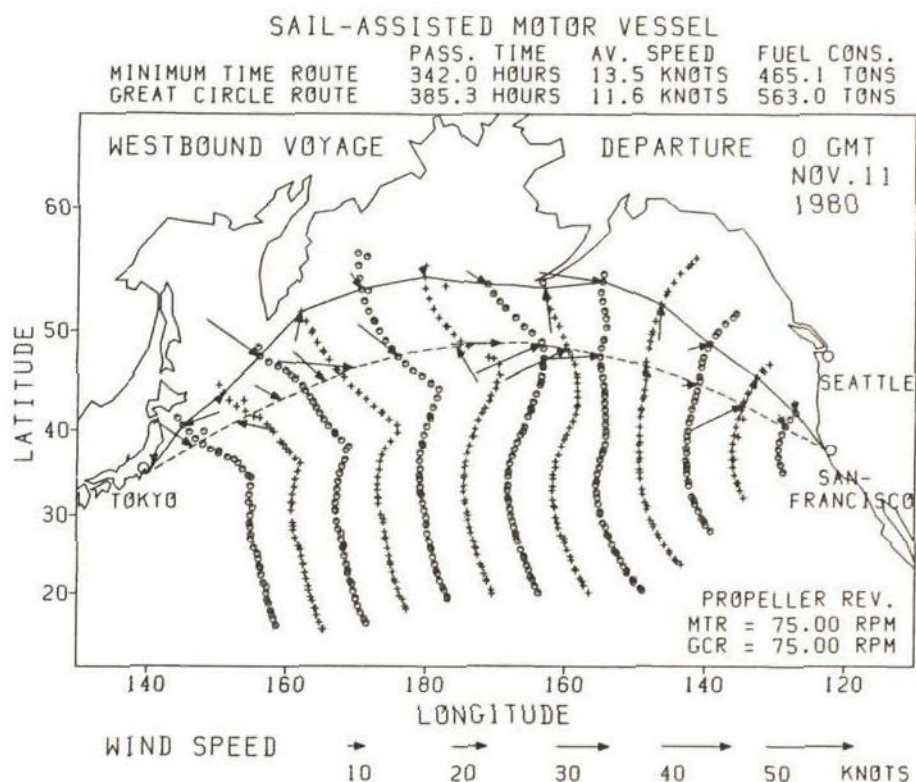


Fig. 5.3 (a) Minimum time routing of the sail-assisted motor vessel  
(  $\Delta t = 24$  hours,  $\Delta t' = 6$  hours,  $\Delta C = 10^\circ$ ,  $\Delta d = 45$  n.m. )

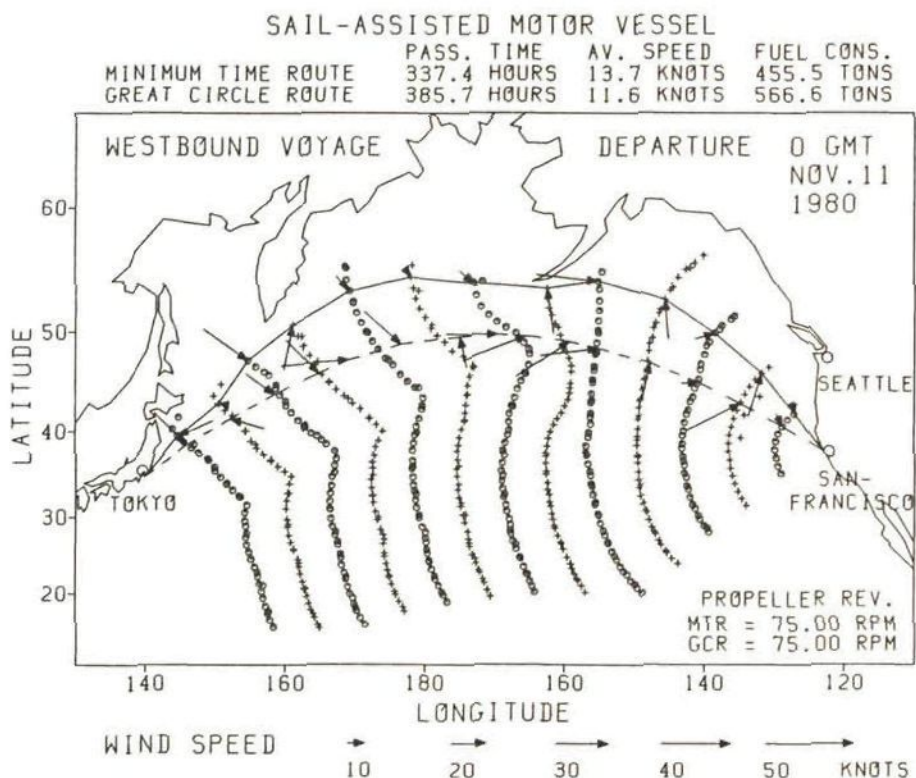


Fig. 5.3 (b) Minimum time routing of the sail-assisted motor vessel  
(  $\Delta t = 24$  hours,  $\Delta t' = 24$  hours,  $\Delta C = 10^\circ$ ,  $\Delta d = 45$  n.m. )



#### 5.4 SENSITIVITY OF THE SOLUTION TO THE INCREMENT OF SHIP'S HEADING FOR CONSTRUCTING THE ISOCHRONES

The sensitivity of the solution to the increment of ship's heading  $\Delta C$  for constructing the isochrones is investigated here.

Letting  $\Delta t$ ,  $\Delta t'$  and  $\Delta d$  be 24 hours, 12 hours and 45 n.m., two simulations of minimum time routing of the model ship were carried out for the same voyage as mentioned in 5.2, using  $\Delta C$  of  $5^\circ$  and  $15^\circ$ . The results of these simulations are shown in Fig.5.4 (a) ( $\Delta C = 5^\circ$ ) and Fig.5.4 (b) ( $\Delta C = 15^\circ$ ). We can find that the shapes of the minimum time routes and the passage times in Fig.5.1 and Fig.5.4 (a),(b) are hardly different from each other.

As a matter of course, the shapes of the isochrones become rough as  $\Delta C$  increases. The isochrones in Fig.5.4 (a) ( $\Delta C = 5^\circ$ ) may be regarded as smooth curves, whereas those in Fig.5.4 (b) ( $\Delta C = 15^\circ$ ) become far from smooth curves.

Computing times ( except compiling times ) were 21, 12 and 10 seconds for  $\Delta C = 5^\circ$ ,  $10^\circ$  and  $15^\circ$ , respectively.

In practice, it seems necessary to use the increment of ship's heading  $\Delta C$  being not greater than  $10^\circ$  to obtain a sufficiently accurate solution.

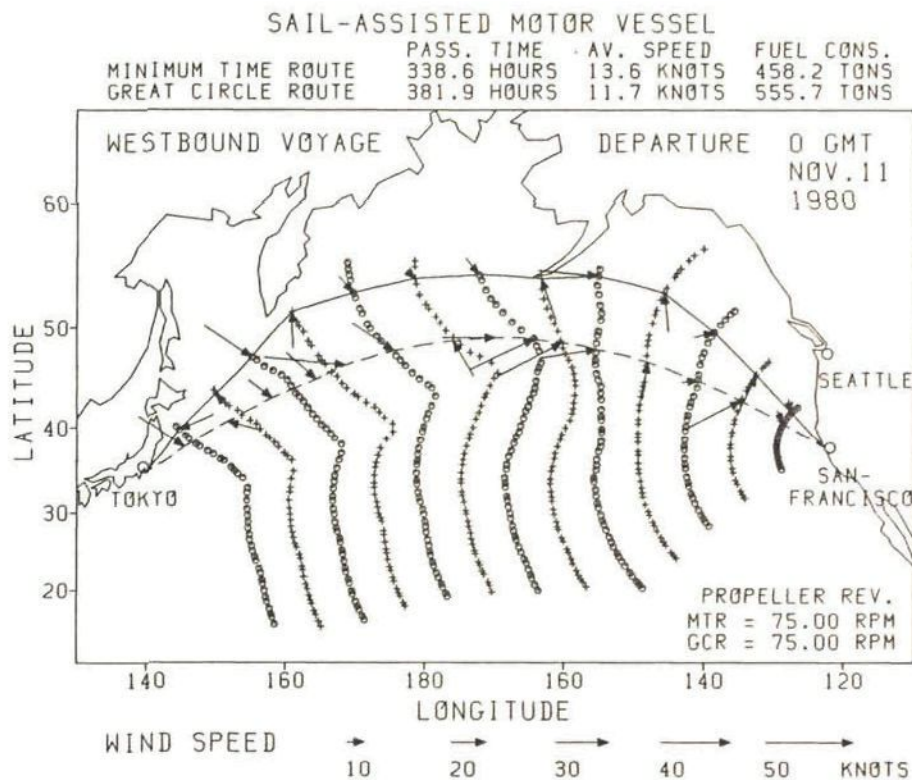


Fig. 5.4 (a) Minimum time routing of the sail-assisted motor vessel  
(  $\Delta t = 24$  hours,  $\Delta t' = 12$  hours,  $\Delta C = 5^\circ$ ,  $\Delta d = 45$  n.m. )

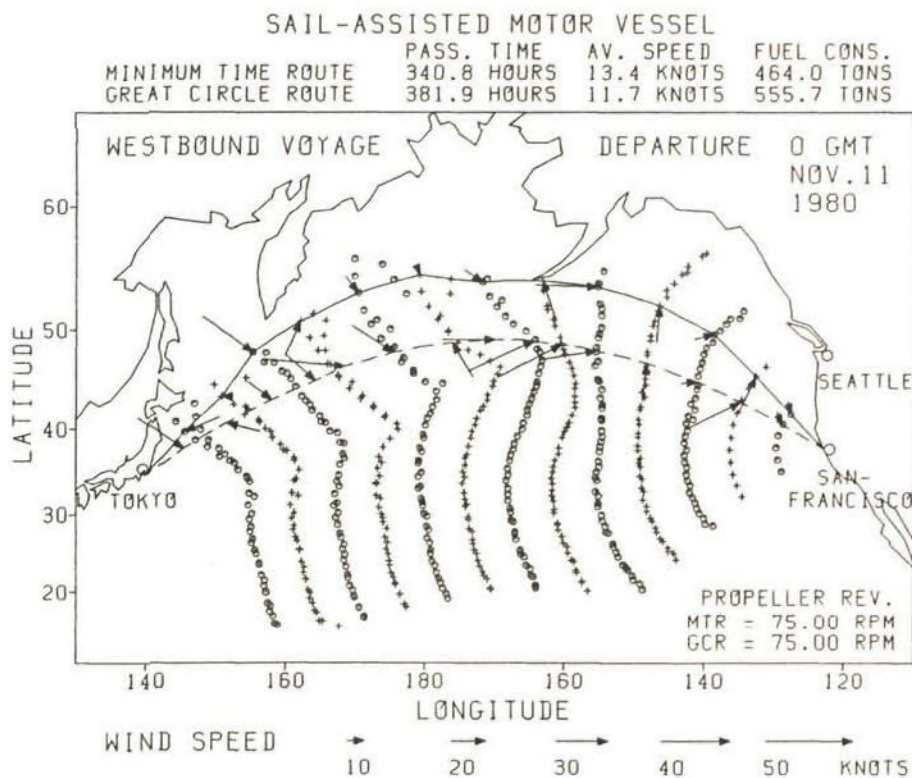


Fig. 5.4 (b) Minimum time routing of the sail-assisted motor vessel  
(  $\Delta t = 24$  hours,  $\Delta t' = 12$  hours,  $\Delta C = 15^\circ$ ,  $\Delta d = 45$  n.m. )



## 5.5 SENSITIVITY OF THE SOLUTION TO THE RESOLUTION OF THE ISOCHRONE

The sensitivity of the solution to the resolution of the isochrone, i.e. the local width of the sub-sector  $\Delta d$  is investigated here.

Letting  $\Delta t$ ,  $\Delta t'$  and  $\Delta C$  be 24 hours, 12 hours and  $10^\circ$ , two simulations of minimum time routing of the model ship were executed for the same voyage as stated in 5.2, using  $\Delta d$  of 30 n.m. and 90 n.m.. The results of these simulations are shown in Fig.5.5 (a) (  $\Delta d = 30$  n.m. ) and Fig.5.5 (b) (  $\Delta d = 90$  n.m. ).

We can find that compared with Fig.5.1 and Fig.5.5 (a), the shapes of the minimum time route in Fig.5.5 (b) becomes rather rough. It is also found from Fig.5.5 (a) that a few isochrones become rough to the north of the great circle route. This is because since  $\Delta d$  (  $= 30$  n.m. ) was too small compared with  $\Delta C$  (  $= 10^\circ$  ), many sub-sectors had few arrival points from the preceding isochrone.

The passage time on the minimum time route for  $\Delta d = 90$  n.m. was 5.7 hours ( 1.7% ) longer than that for  $\Delta d = 30$  n.m..

Computing times ( except compiling times ) were 17, 12 and 8 seconds for  $\Delta d = 30, 45$  and 90 n.m., respectively.

In general, the accuracy of the solution can be improved by decreasing the resolution of the isochrone  $\Delta d$ . It should be noted, however, that when  $\Delta d$  is decreased, the increment of ship's heading  $\Delta C$  should be also decreased to avoid getting the isochrones rough as shown in Fig.5.5 (a). In practice,  $\Delta d$  seems appropriate when it is a bit smaller than  $V_s \Delta t \sin(\Delta C)$ , where  $V_s$  is the service speed.



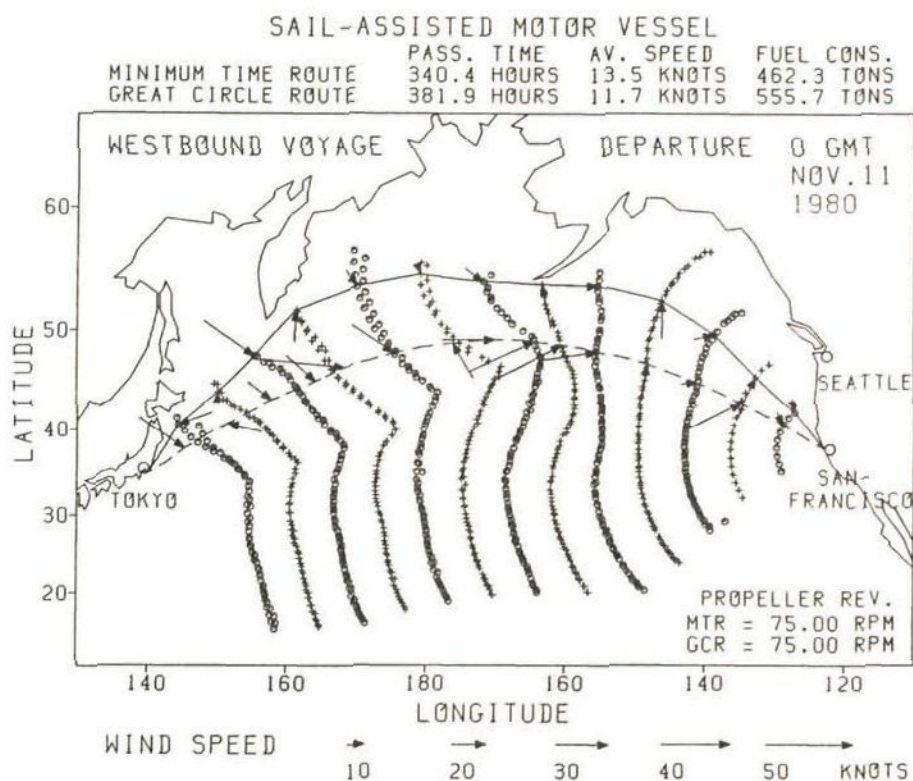


Fig. 5.5 (a) Minimum time routing of the sail-assisted motor vessel  
(  $\Delta t = 24$  hours,  $\Delta t' = 12$  hours,  $\Delta C = 10^\circ$ ,  $\Delta d = 30$  n.m. )

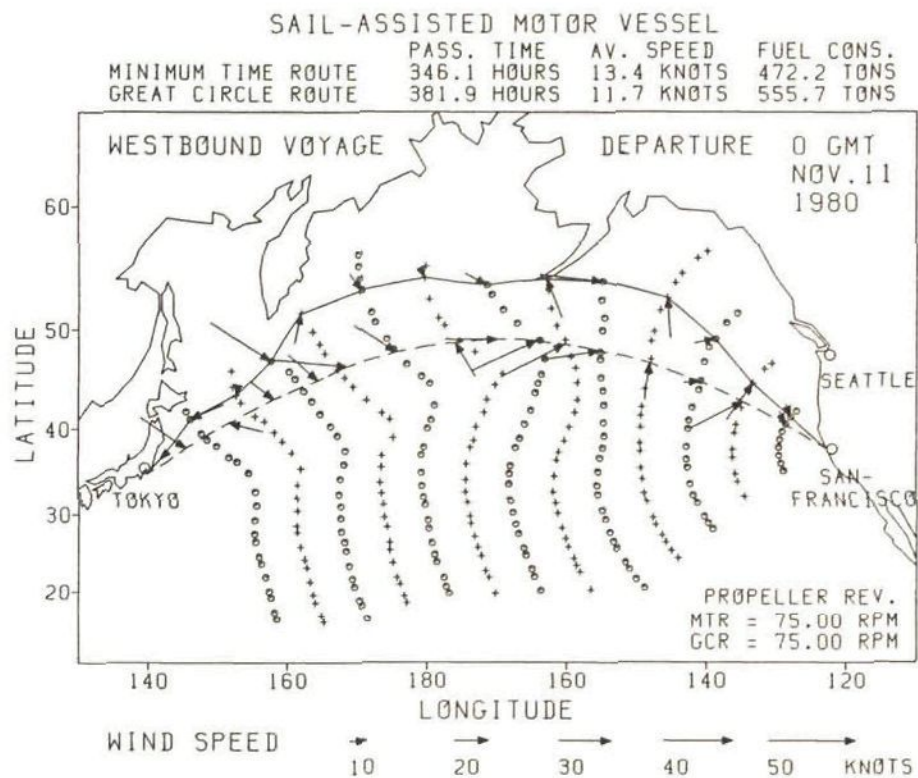


Fig. 5.5 (b) Minimum time routing of the sail-assisted motor vessel  
(  $\Delta t = 24$  hours,  $\Delta t' = 12$  hours,  $\Delta C = 10^\circ$ ,  $\Delta d = 90$  n.m. )

## 5.6 SENSITIVITY OF THE SOLUTION TO THE INCREMENT IN NUMERICAL DIFFERENTIATION FOR CALCULATING THE PARTIAL DERIVATIVES

For carrying out the stochastic routing, the partial derivatives of ship's speed through the water and drift angle with respect to wind/wave conditions at time  $t_i$  ( i.e.  $S_c = \partial \underline{S} / \partial \underline{C}_i$  in (2.50) ) have to be calculated. These partial derivatives affect the covariance matrices of ship's positions as well as the standard deviations of passage time and fuel consumption.

In (2.50), it was assumed that the ocean waves consisted of two ideal wave systems, namely, sea and swell; thus  $\underline{C}_i$  representing wind/wave conditions was a 8-dimensional vector as shown in (2.36), and  $\partial \underline{S} / \partial \underline{C}_i$  became a  $2 \times 8$  matrix. In the stochastic routing, however, since the wave conditions are represented as significant wave height and primary wave direction/period,  $\underline{C}_i$  becomes a 5-dimensional vector and  $\partial \underline{S} / \partial \underline{C}_i$  becomes the following  $2 \times 5$  matrix:

$$\partial \underline{S} / \partial \underline{C}_i = \begin{bmatrix} \partial V / \partial S_w & \partial V / \partial D_w & \partial V / \partial H_s & \partial V / \partial D_p & \partial V / \partial T_p \\ \partial \alpha / \partial S_w & \partial \alpha / \partial D_w & \partial \alpha / \partial H_s & \partial \alpha / \partial D_p & \partial \alpha / \partial T_p \end{bmatrix} \quad (5.1)$$

where  $\underline{S}_i = [ V_i \ \alpha_i ]^T = \underline{S}(\underline{C}_i, \theta_i, n_i)$  { See (2.33) and (2.35). }

$\underline{C}_i = [ S_w \ D_w \ H_s \ D_p \ T_p ]^T$

$V_i$  : ship's speed through the water at  $t_i$

$\alpha_i$  : drift angle at  $t_i$

$\theta_i$  : ship's heading between  $t_i$  and  $t_{i+1}$

$n_i$  : number of propeller revolutions between  $t_i$  and  $t_{i+1}$

$S_w$  : wind speed at  $t_i$

$D_w$  : wind direction at  $t_i$

$H_s$  : significant wave height at  $t_i$

$D_p$  : primary wave direction at  $t_i$

$T_p$  : primary wave period at  $t_i$

In (5.1), each partial derivative is calculated using the predicted wind/wave conditions at the predicted ship's position  $\bar{\underline{X}}_i$  at



time  $t_i$ .

Because  $V_i$  and  $\alpha_i$  are calculated based on the numerical iterative method proposed in 3.5, each partial derivative in (5.1) has to be computed by numerical differentiation. For given  $\theta_i$  and  $n_i$ , regarding  $V_i$  and  $\alpha_i$  as functions of  $S_w$ ,  $D_w$ ,  $H_s$ ,  $D_p$  and  $T_p$ , and writing them as  $V(S_w, D_w, H_s, D_p, T_p)$  and  $\alpha(S_w, D_w, H_s, D_p, T_p)$ , the partial derivatives are computed by

$$\partial V / \partial S_w = \{V(\bar{S}_w + \Delta S_w, \bar{D}_w, \bar{H}_s, \bar{D}_p, \bar{T}_p) - V(\bar{S}_w - \Delta S_w, \bar{D}_w, \bar{H}_s, \bar{D}_p, \bar{T}_p)\} / (2\Delta S_w) \quad (5.2)$$

$$\partial V / \partial D_w = \{V(\bar{S}_w, \bar{D}_w + \Delta D_w, \bar{H}_s, \bar{D}_p, \bar{T}_p) - V(\bar{S}_w, \bar{D}_w - \Delta D_w, \bar{H}_s, \bar{D}_p, \bar{T}_p)\} / (2\Delta D_w) \quad (5.3)$$

$$\partial V / \partial H_s = \{V(\bar{S}_w, \bar{D}_w, \bar{H}_s + \Delta H_s, \bar{D}_p, \bar{T}_p) - V(\bar{S}_w, \bar{D}_w, \bar{H}_s - \Delta H_s, \bar{D}_p, \bar{T}_p)\} / (2\Delta H_s) \quad (5.4)$$

$$\partial V / \partial D_p = \{V(\bar{S}_w, \bar{D}_w, \bar{H}_s, \bar{D}_p + \Delta D_p, \bar{T}_p) - V(\bar{S}_w, \bar{D}_w, \bar{H}_s, \bar{D}_p - \Delta D_p, \bar{T}_p)\} / (2\Delta D_p) \quad (5.5)$$

$$\partial V / \partial T_p = \{V(\bar{S}_w, \bar{D}_w, \bar{H}_s, \bar{D}_p, \bar{T}_p + \Delta T_p) - V(\bar{S}_w, \bar{D}_w, \bar{H}_s, \bar{D}_p, \bar{T}_p - \Delta T_p)\} / (2\Delta T_p) \quad (5.6)$$

$$\partial \alpha / \partial S_w = \{\alpha(\bar{S}_w + \Delta S_w, \bar{D}_w, \bar{H}_s, \bar{D}_p, \bar{T}_p) - \alpha(\bar{S}_w - \Delta S_w, \bar{D}_w, \bar{H}_s, \bar{D}_p, \bar{T}_p)\} / (2\Delta S_w) \quad (5.7)$$

$$\partial \alpha / \partial D_w = \{\alpha(\bar{S}_w, \bar{D}_w + \Delta D_w, \bar{H}_s, \bar{D}_p, \bar{T}_p) - \alpha(\bar{S}_w, \bar{D}_w - \Delta D_w, \bar{H}_s, \bar{D}_p, \bar{T}_p)\} / (2\Delta D_w) \quad (5.8)$$

$$\partial \alpha / \partial H_s = \{\alpha(\bar{S}_w, \bar{D}_w, \bar{H}_s + \Delta H_s, \bar{D}_p, \bar{T}_p) - \alpha(\bar{S}_w, \bar{D}_w, \bar{H}_s - \Delta H_s, \bar{D}_p, \bar{T}_p)\} / (2\Delta H_s) \quad (5.9)$$

$$\partial \alpha / \partial D_p = \{\alpha(\bar{S}_w, \bar{D}_w, \bar{H}_s, \bar{D}_p + \Delta D_p, \bar{T}_p) - \alpha(\bar{S}_w, \bar{D}_w, \bar{H}_s, \bar{D}_p - \Delta D_p, \bar{T}_p)\} / (2\Delta D_p) \quad (5.10)$$

$$\partial \alpha / \partial T_p = \{\alpha(\bar{S}_w, \bar{D}_w, \bar{H}_s, \bar{D}_p, \bar{T}_p + \Delta T_p) - \alpha(\bar{S}_w, \bar{D}_w, \bar{H}_s, \bar{D}_p, \bar{T}_p - \Delta T_p)\} / (2\Delta T_p) \quad (5.11)$$

where  $\bar{S}_w$ ,  $\bar{D}_w$ ,  $\bar{H}_s$ ,  $\bar{D}_p$  and  $\bar{T}_p$  denote the predicted values of  $S_w$ ,  $D_w$ ,  $H_s$ ,  $D_p$  and  $T_p$ , respectively;  $\Delta S_w$ ,  $\Delta D_w$ ,  $\Delta H_s$ ,  $\Delta D_p$  and  $\Delta T_p$  are the increments for calculating the partial derivatives.

In formulae (5.2) through (5.11), the values of the partial derivatives depend on the values of the increments. That is, when the increments are too small, the partial derivatives become inaccurate because of the errors in calculating the ship's speeds



and drift angles by the iterative method. On the other hand, when the increments are too large, the partial derivatives also become inaccurate in terms of the mathematical definition of partial derivative.

Thus the sensitivity of the solution to the increments  $\Delta S_w$ ,  $\Delta D_w$ ,  $\Delta H_s$ ,  $\Delta D_p$  and  $\Delta T_p$  was investigated by simulations. Letting  $\Delta t$ ,  $\Delta t'$ ,  $\Delta C$  and  $\Delta d$  be 24 hours, 12 hours,  $10^\circ$  and 45 n.m. respectively, four simulations of stochastic minimum time routing of the model ship were performed for the voyage from San Francisco to Tokyo departing at 00 hours GMT on 1 February 1985, using four sets of  $\Delta S_w$ ,  $\Delta D_w$ ,  $\Delta H_s$ ,  $\Delta D_p$  and  $\Delta T_p$  as mentioned in Figs 5.6 (a)-(d).

In these simulations, the forecasted wind/wave data published by FNOG described in 4.3 were used for the period up to 3 days from the departure time, and after that, the 1-month mean wind/wave data described in 4.5 were used. The monthly ocean current data published by the U.K. Meteorological Office mentioned in 4.7 were also used.

The results of these simulations are shown in Fig.5.6 (a)-(d). In Fig.5.6, the isochrones at 1,2,3,--- days after the departure time are represented as the 39% error ellipses of ship's positions. The 39% error ellipse denotes the isopleth of the probability density of ship's position error; the probability of finding the ship's position inside this ellipse is 0.39347 [ =  $1 - \exp(-0.5)$  ]. The predicted ship's position is located at the center of the 39% error ellipse. ( The method to calculate the 39% error ellipse is described in Appendix 6. )

Above each figure, the standard deviations of passage times, average speeds and fuel consumptions computed by the method mentioned in 2.4.1 are shown after  $\pm$  signs.

It is found that the sizes of the 39% error ellipses as well as the standard deviations in Fig.5.6 (a),(b),(c) are hardly different from each other. In Fig.5.6 (d), however, the standard deviations are a bit smaller than those in Fig.5.6 (a),(b),(c), since the accuracies of the partial derivatives were deteriorated to some extent because of the rather large increments.

From Fig.5.6 (a), it can be said that accurate partial derivatives could be calculated in spite of considerably small increments. This indirectly shows that the iterative method proposed in 3.5 could determine very accurate ship's speeds and drift angles.

Computing times ( except compiling times ) were 26 seconds for these simulations.

In practice, the following values of increments seem appropriate to obtain accurate partial derivatives.

$$\begin{aligned}\Delta S_w &= 0.25 - 0.5 \text{ m/sec} \\ \Delta D_w &= 2.5 - 5.0 \text{ degrees} \\ \Delta H_s &= 0.25 - 0.5 \text{ meters} \\ \Delta D_p &= 2.5 - 5.0 \text{ degrees} \\ \Delta T_p &= 0.25 - 0.5 \text{ seconds}\end{aligned}$$



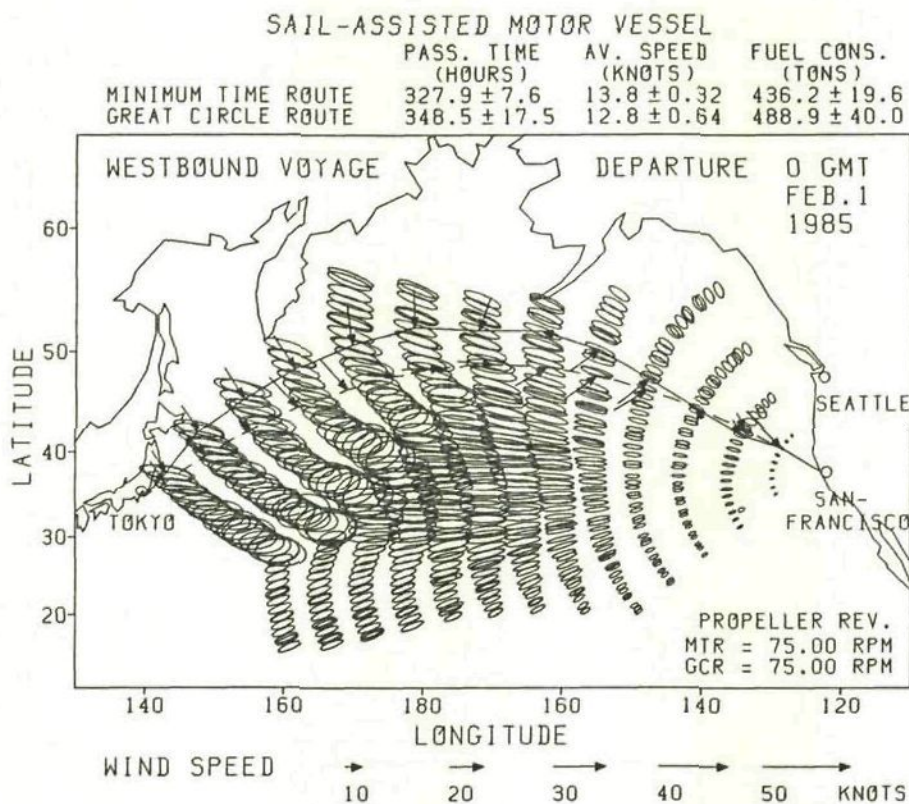


Fig. 5.6 (a) Stochastic minimum time routing of the sail-assisted motor vessel (  $\Delta S_w = 0.125$  m/sec,  $\Delta D_w = 1.25$  deg.,  $\Delta H_s = 0.125$  m,  $\Delta D_p = 1.25$  deg.,  $\Delta T_p = 0.125$  sec. )

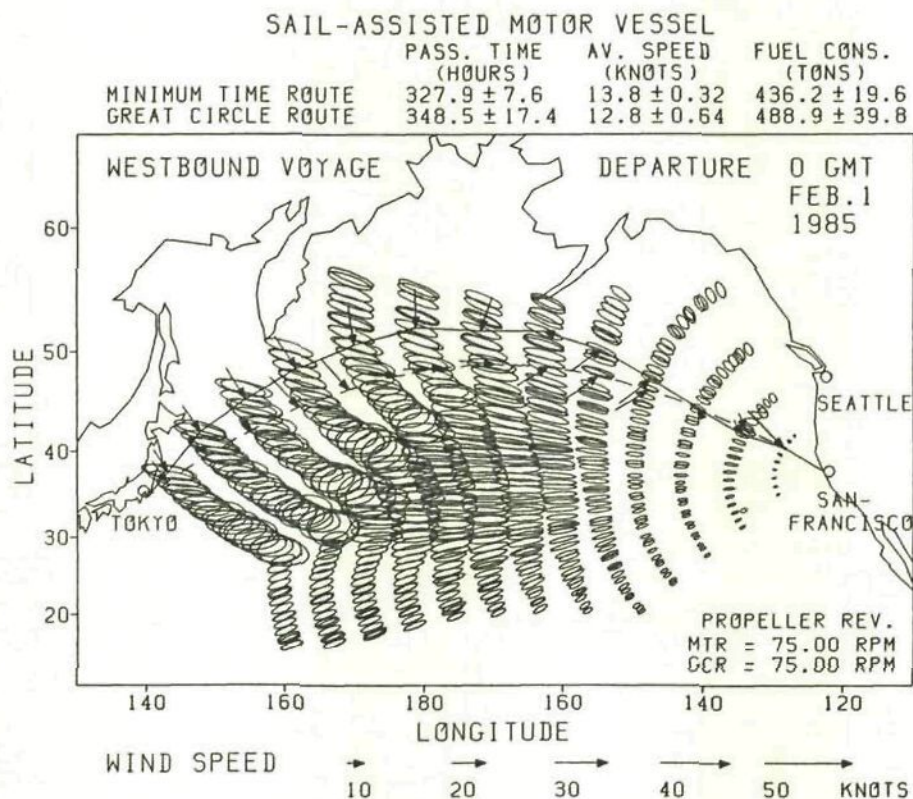


Fig. 5.6 (b) Stochastic minimum time routing of the sail-assisted motor vessel (  $\Delta S_w = 0.250$  m/sec,  $\Delta D_w = 2.50$  deg.,  $\Delta H_s = 0.250$  m,  $\Delta D_p = 2.50$  deg.,  $\Delta T_p = 0.250$  sec. )



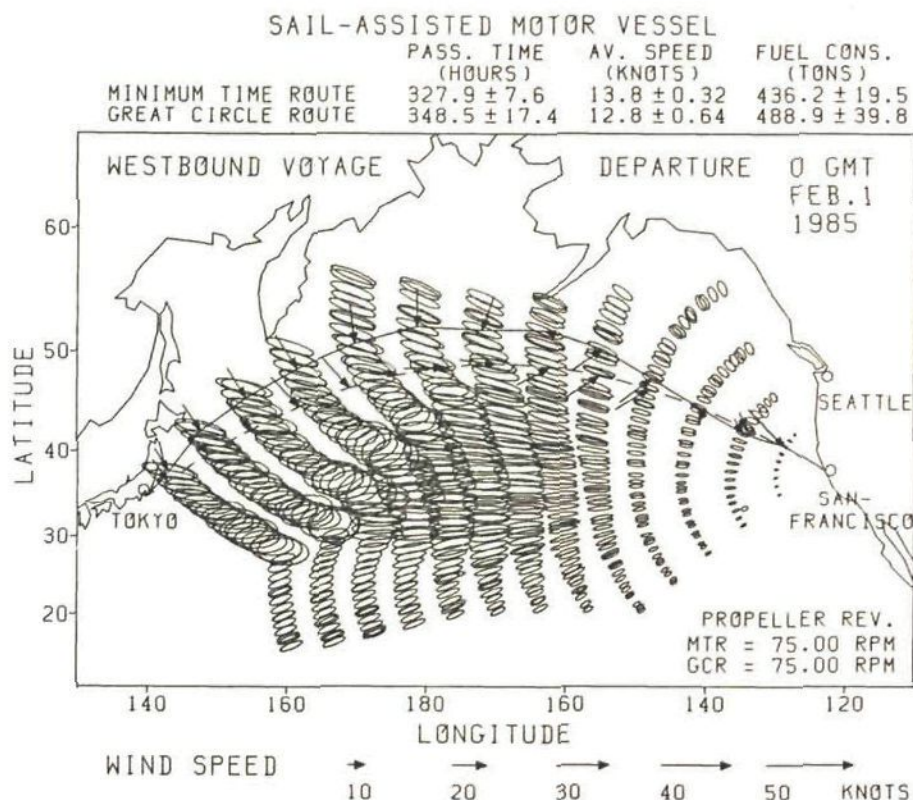


Fig. 5.6 (c) Stochastic minimum time routing of the sail-assisted motor vessel ( $\Delta S_w = 0.500$  m/sec,  $\Delta D_w = 5.00$  deg.,  $\Delta H_s = 0.500$  m,  $\Delta D_p = 5.00$  deg.,  $\Delta T_p = 0.500$  sec.)

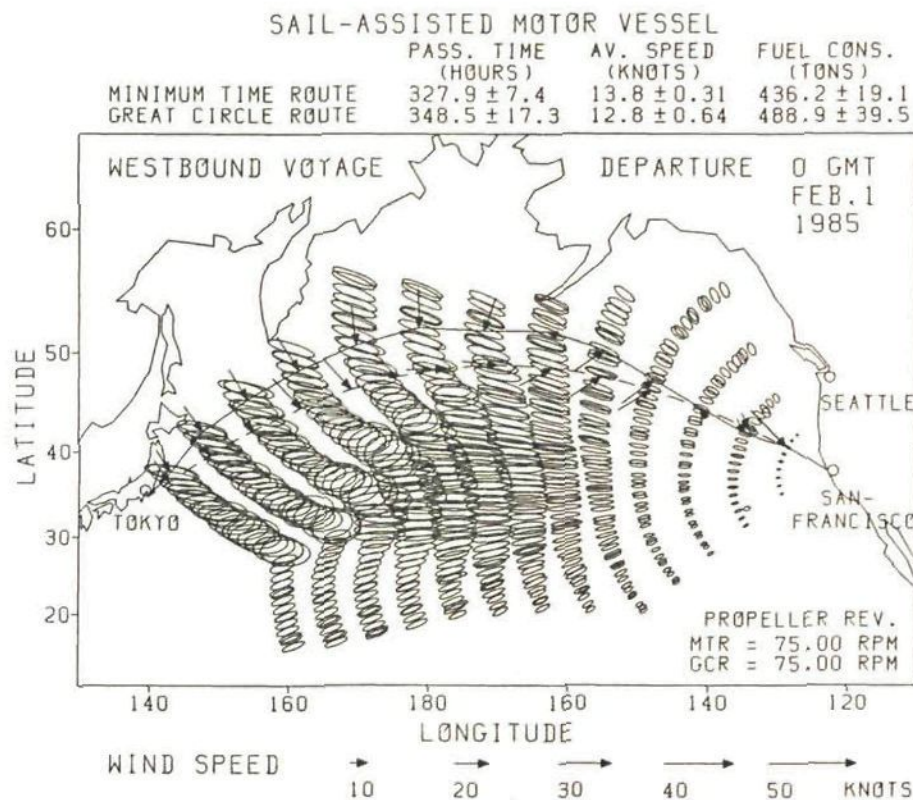


Fig. 5.6 (d) Stochastic minimum time routing of the sail-assisted motor vessel ( $\Delta S_w = 1.000$  m/sec,  $\Delta D_w = 10.0$  deg.,  $\Delta H_s = 1.000$  m,  $\Delta D_p = 10.0$  deg.,  $\Delta T_p = 1.000$  sec.)

## 6. WEATHER ROUTING SIMULATIONS OF A SAIL-ASSISTED/EQUIVALENT MOTOR VESSEL

### 6.1 INTRODUCTION

In this chapter, using the modified isochrone method described in Chapter 2 and the methods to predict the ship's speed and seakeeping performance mentioned in Chapter 3, comprehensive weather routing simulations are performed.

The mathematical model ship ( 40,000 DWT sail-assisted product tanker with 808 m<sup>2</sup> sail area ) described in Section 3.2 and the same vessel without sails are navigated in the simulations. As defined in Section 3.7, we call the former vessel 'sail-assisted motor vessel (S-A MV)' and the latter 'equivalent motor vessel (EQ MV)'. The specific fuel consumption of these vessels is assumed to be 0.21 kg/kW per hour as mentioned in Section 3.6.

In Section 6.2, the deterministic routing simulations are executed, using the analyzed wind/sea/swell data and the monthly ocean current data published by FNOG. In these simulations, the advantages of weather routing and sail-assisted operation are investigated for the minimum time/fuel/cost routing.

In Section 6.3, the simulations of stochastic minimum time/fuel routing are carried out, using the forecasted wind/wave data by FNOG followed by the 5-day mean wind/wave models classified by ZI or the 1-month mean wind/wave data and the monthly ocean current data published by the Meteorological Office. In both minimum time and minimum fuel routing, a set of routes each with the standard deviations of passage time and fuel consumption are calculated to provide information for deciding an optimum route from a stochastic point of view.

In addition, since the forecasted wind/wave data are updated every 12 hours, the simulations of recalculating the minimum

time/fuel route at every updating time of the forecasts are also executed.

Throughout the deterministic/stochastic routing simulations, the advantages of weather routing based on the modified isochrone method are fully demonstrated.



## 6.2 SIMULATIONS OF DETERMINISTIC ROUTING

In this section, the simulations of deterministic minimum time/fuel/cost routing are performed for voyages between Tokyo (  $34^{\circ}50'N$ ,  $140^{\circ}00'E$  ) and San Francisco (  $37^{\circ}50'N$ ,  $123^{\circ}00'W$  ).

The environmental data used for these simulations are shown in Fig.4.39. It is assumed that the sea and swell possess the wave spectrum (3.30) and (3.31), respectively.

Concerning the modified isochrone method, the increments for discretizing the problem are set as follows:

- \* Time-interval between successive isochrones  $\Delta t = 24$  hours
- \* Sub-time-interval for calculating ship's speed, drift angle, etc.  
 $\Delta t' = 12$  hours
- \* Increment of ship's heading for constructing the isochrones  
 $\Delta C = 10^{\circ}$
- \* Resolution of the isochrone ( i.e. local width of the sub-sector )  
 $\Delta d = 45$  n.m.

The number of ship's headings to be searched is 13; i.e. the ship is sailed for 24 hours from each point of the isochrone, following headings  $C_i \pm j \times 10^{\circ}$  (  $j = 0, 1, \dots, 8$  ), where  $C_i$  is the arrival course of the great circle route from departure point to each point of the isochrone. The service speed  $V_s$  of S-A MV and EQ MV is set to 14 knots.

The number of sub-sectors is 80; i.e. there are 40 sub-sectors on each side of the great circle route between Tokyo and San Francisco. The optimum route is searched in a lane of 3,600 n.m. width centered on the great circle route between Tokyo and San Francisco. The isochrone is regarded as a final one when the shortest rhumbline distance from that isochrone to the destination becomes less than  $1.5 V_s \Delta t$  ( = 504 n.m. ).

The navigable area, i.e.  $X_A$  in (2.1), is set up as shown in Fig.6.1. In Fig.6.1, the boundaries of the navigable area were defined by linear functions of latitude and longitude. The

boundaries in the Bering Sea, off the Kamchatka and off the Kuril Islands were determined so as to coincide with the maximum extent of sea ice described in the U.S. Pilot Charts for the winter season.

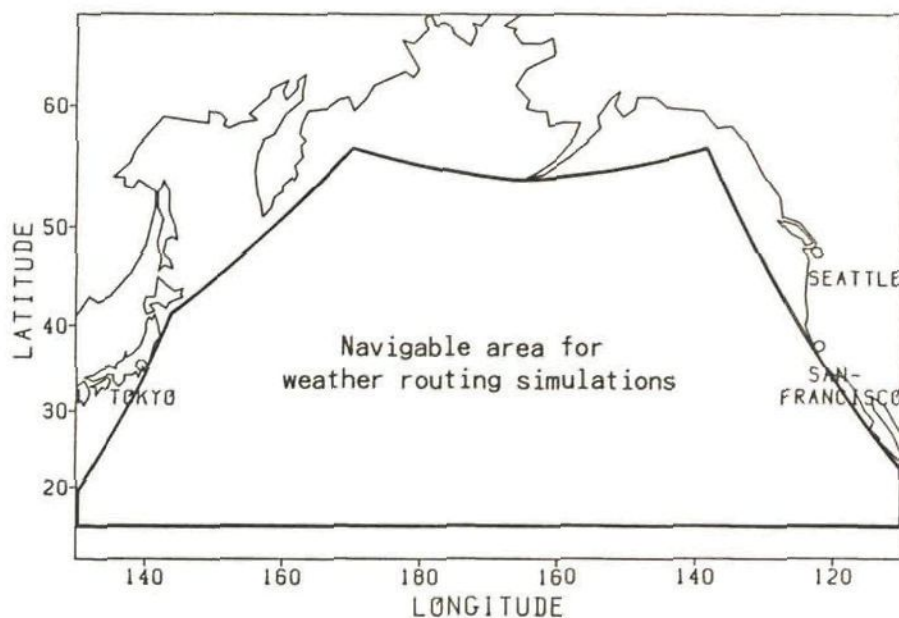


Fig. 6.1 Navigable area for weather routing simulations

The probability of occurrence of shipping green water at the bow  $P(z_A > f)$  is calculated every 12 hours by the method stated in Section 3.10. When  $P(z_A > f)$  exceeds 0.04, it is considered that the S-A MV/EQ MV has a risk of damage due to shipping green water. Thus the period in which  $P(z_A > f)$  exceeds 0.04 is accumulated during the voyage, and its total period is shown as one of the various information to determine the optimum route.

( In Section 3.10, the unidirectional Bretschneider spectrum was used to calculate  $P(z_A > f)$ . Therefore, using sea and swell data, the significant wave height and primary wave direction/period are computed by (4.15), (4.16) and (4.17). Assuming that the computed primary wave system possesses the unidirectional Bretschneider spectrum,  $P(z_A > f)$  is calculated. )

In the simulations, the shapes, passage times, fuel consumptions,



etc. of the optimum routes are compared with those of the great circle routes. The great circle routes are calculated based on the method described in Appendix 5 with sub-time-interval  $\Delta t'$  of 12 hours.

Hereafter, we use the following abbreviations:

Minimum time route : MTR  
Minimum fuel route : MFR  
Minimum cost route : MCR  
Great circle route : GCR

#### 6.2.1 Minimum time routing

Using the algorithm described in 2.3.1, the simulations of minimum time routing were carried out.

The S-A MV and EQ MV were sailed between Tokyo and San Francisco with a constant ( maximum ) number of propeller revolutions ( 75 r.p.m. ) departing from both points at 00 hours GMT on 1, 6, 11, 16, 21 and 26 November and 1, 6, 11 and 16 December in 1980.

In each voyage, the following quantities were calculated for all the routes reaching the destination from the departure point via points of the final isochrone, and they were tabulated.

- \* Passage time
- \* Travelled distance
- \* Average speed
- \* Fuel consumption
- \* Period in which the probability of shipping green water exceeded 0.04

From those routes, the route giving minimum passage time was adopted as a minimum time route.

The tracks of MTR and GCR in the westbound voyage ( San Francisco → Tokyo ) departing at 00 hours GMT on 6 November 1980 are shown in Fig.6.2 ( S-A MV ) and Fig.6.3 ( EQ MV ). In Figs 6.2 and 6.3, the



solid lines and dashed lines denote the MTR and GCR.

The tips, directions and lengths of the arrows attached to both routes represent the ship's positions, wind directions and wind speeds for every 24 hours, respectively. The isochrones at 1,3,5,--- days and 2,4,6,--- days after the departure time are shown by circle marks and cross marks respectively.

From Figs 6.2 and 6.3, it can be seen that the MTR of S-A MV and EQ MV are completely different from each other in this westbound voyage, i.e. the MTR of S-A MV passes through the Bering Sea, whereas that of EQ MV passes along about the 34°N parallel.

The isochrones bend backwards sharply around the GCR west of 170°W. This is because a westerly gale prevailed in that area and westbound vessels received strong head winds and high head waves.

To investigate these sharp bends of the isochrones in detail, all minimum time routes reaching each isochrone are depicted in Fig.6.4 ( S-A MV ) and Fig.6.5 ( EQ MV ); the thick lines indicate the MTR from San Francisco to Tokyo. From Figs 6.4 and 6.5, it is found that two minimum time routes ( i.e. northern MTR and southern MTR ) exist from San Francisco to the sharp bending points of the isochrones.

These bending points are, as mentioned in 2.3.2, usually called 'double points'. In a case where the destination corresponds to a double point, two minimum time routes from the departure point to the destination exist. In such a case, no matter which minimum time route is chosen, a ship should deviate considerably from the great circle route.

All minimum time routes of S-A MV reaching the final isochrone are shown in Fig.6.6; the thick line indicates the MTR from San Francisco to Tokyo. On the routes depicted in Fig.6.6, the positions of the points of the final isochrone as well as the passage times, travelled distances, average speeds, fuel consumptions and periods in which the probability of shipping green water exceeded 0.04 between San Francisco and Tokyo are shown in Table 6.1 below FINAL ISOCHRONE, PASS. TIME, DISTANCE, AV. SPEED,

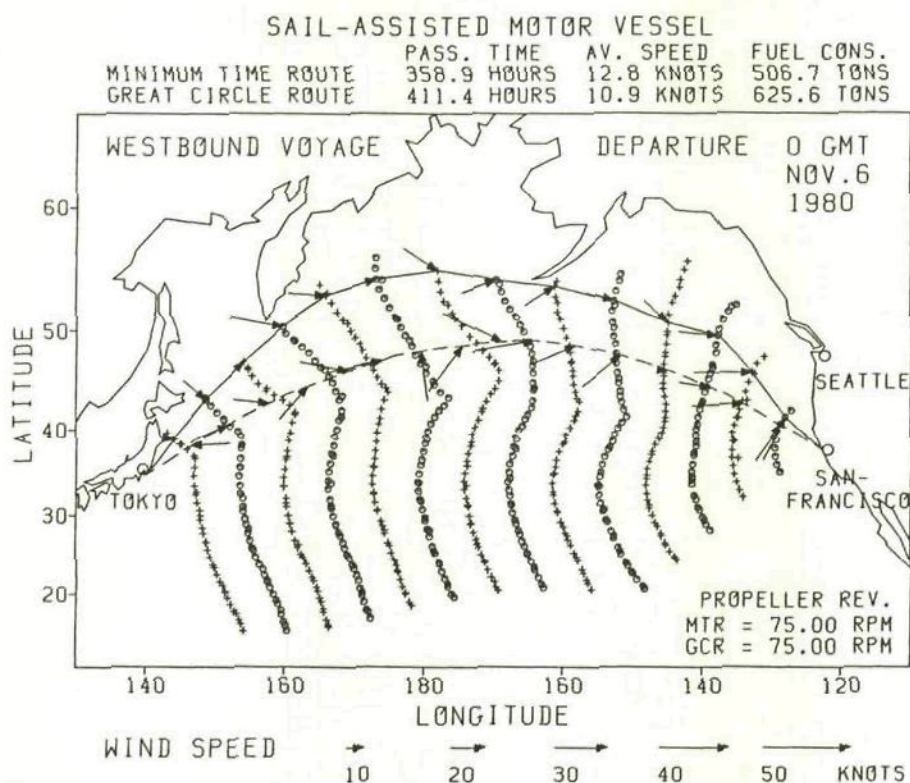


Fig. 6.2 Minimum time route and great circle route of the sail-assisted motor vessel ( westbound voyage )

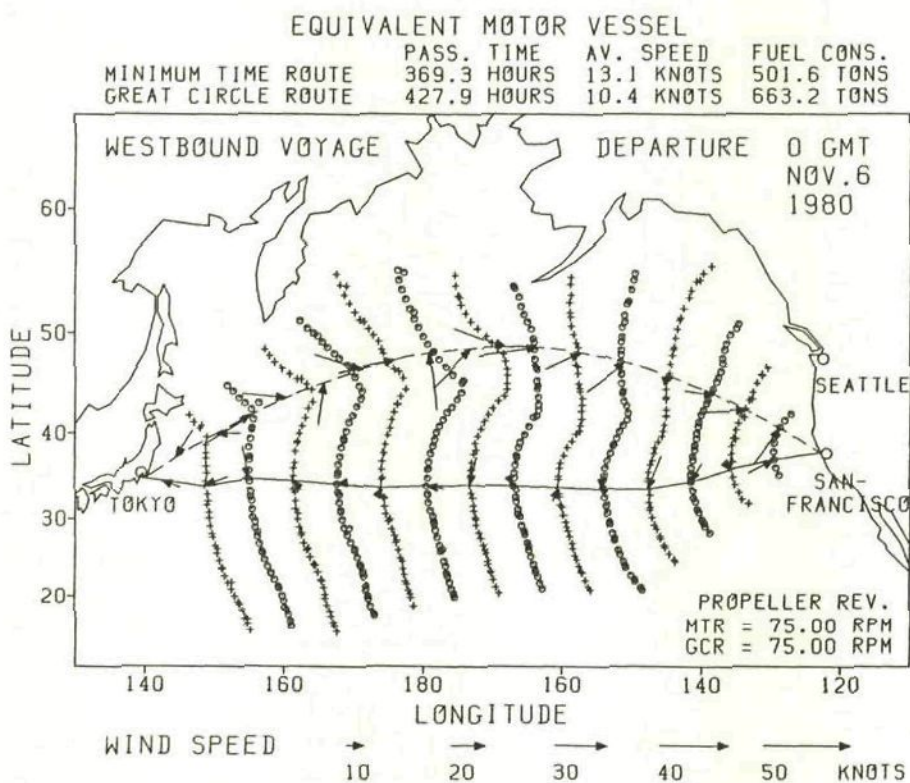


Fig. 6.3 Minimum time route and great circle route of the equivalent motor vessel ( westbound voyage )



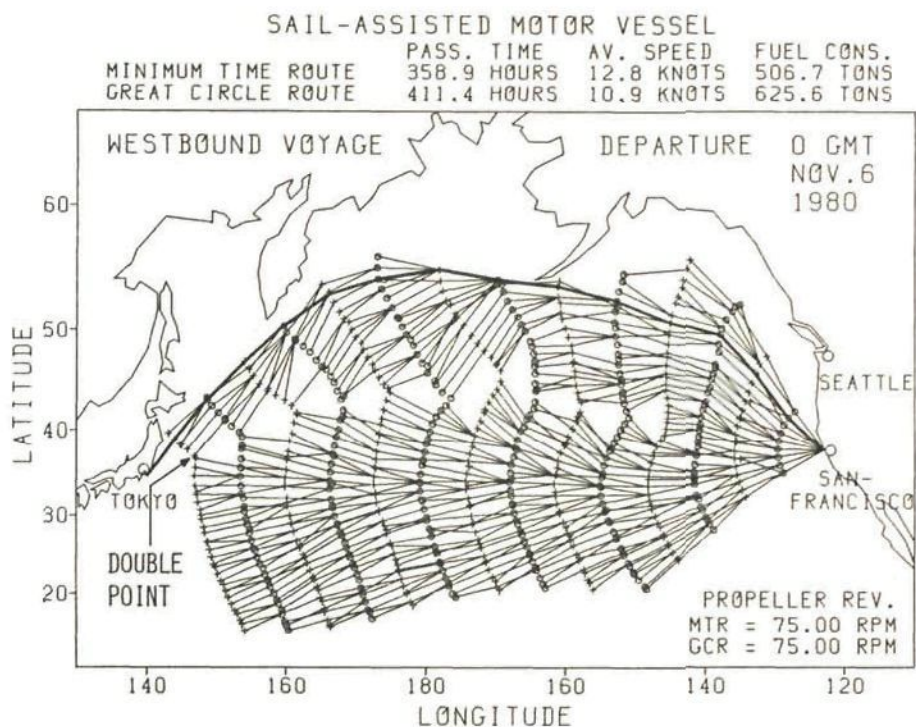


Fig. 6.4 All minimum time routes of the sail-assisted motor vessel reaching each isochrone ( westbound voyage )

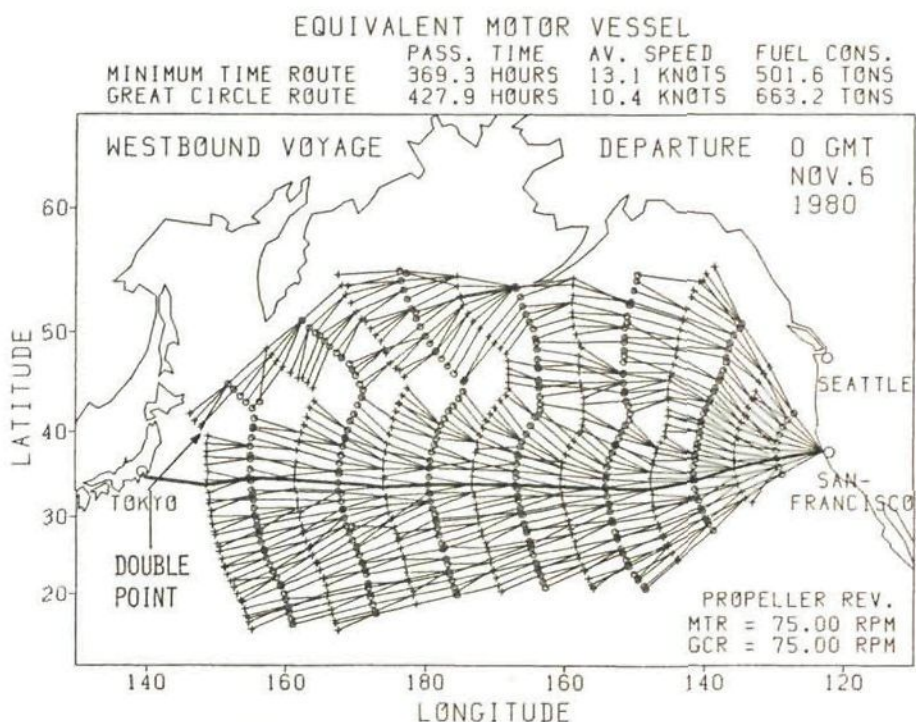


Fig. 6.5 All minimum time routes of the equivalent motor vessel reaching each isochrone ( westbound voyage )



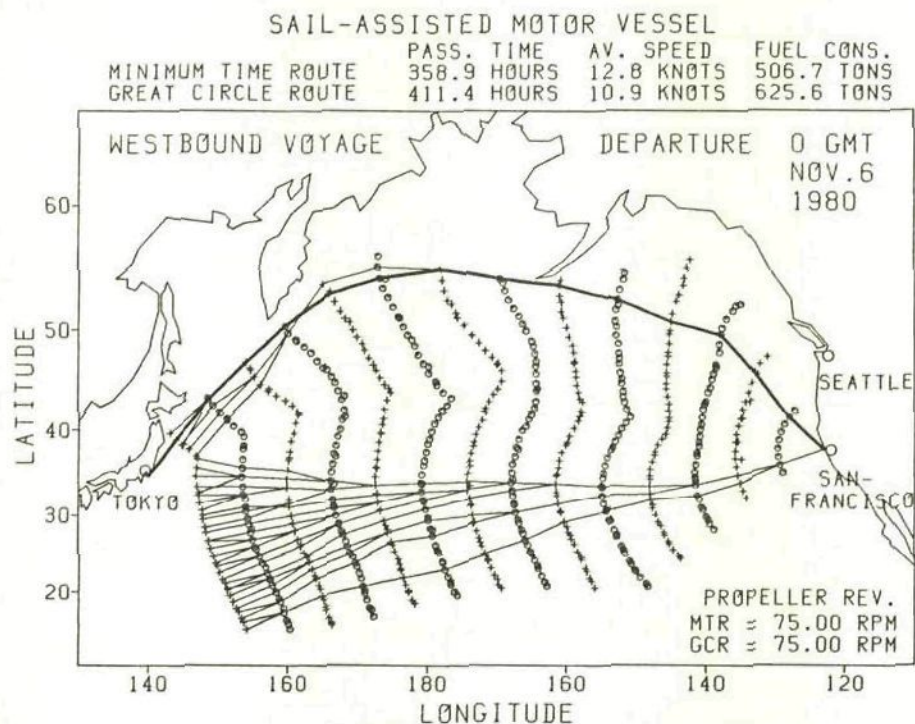


Fig. 6.6 All minimum time routes of the sail-assisted motor vessel reaching the final isochrone (westbound voyage)

Table 6.1 Information on the routes reaching Tokyo from San Francisco via points of the final isochrone

SUBJECT.NO.	FINAL ISOCHRONE		PASS. TIME	DISTANCE	AV. SPEED	FUEL CONS.	PER OF SGW
	LATI (DEG)	LONG (DEG)	(HR)	(NM)	(KN)	(TN)	(HR)
15	19.521	151.724	413.284	5697.48	13.786	552.758	0.0
16	20.259	151.387	410.219	5633.55	13.733	549.302	0.0
17	20.420	151.373	409.629	5641.99	13.773	547.910	0.0
18	21.162	151.036	406.216	5577.90	13.731	543.765	0.0
19	21.645	150.637	403.613	5542.95	13.733	539.680	0.0
20	22.575	150.186	399.633	5474.93	13.700	534.741	0.0
21	23.494	149.848	395.860	5418.91	13.689	529.739	0.0
22	23.816	149.634	394.166	5394.45	13.686	526.776	0.0
23	24.730	149.298	390.271	5339.33	13.681	521.437	0.0
24	25.686	148.988	386.644	5278.49	13.652	516.769	0.0
25	26.635	148.806	383.315	5229.54	13.643	512.220	0.0
26	26.681	148.665	382.751	5215.38	13.626	511.477	0.0
27	27.762	148.341	378.788	5147.42	13.589	506.140	0.0
28	28.473	148.199	376.531	5097.49	13.538	503.223	0.0
29	29.427	147.875	373.291	5042.79	13.509	499.027	0.0
30	29.964	147.851	371.945	5025.41	13.511	497.190	0.0
31	30.619	147.745	370.131	4982.69	13.462	494.808	0.0
32	31.552	147.369	367.156	4937.70	13.449	490.991	0.0
33	32.528	147.186	365.001	4904.70	13.437	488.156	0.0
34	32.798	147.314	365.115	4899.52	13.419	487.910	0.0
35	33.538	146.992	363.180	4876.20	13.426	485.534	0.0
36	34.743	146.852	362.056	4851.16	13.399	483.917	0.0
37	35.720	146.961	362.734	4857.11	13.390	484.956	0.0
38	36.777	147.030	363.973	4869.73	13.379	486.712	0.0
39	37.049	146.865	363.752	4698.73	12.917	507.813	0.0
40	37.817	145.810	361.317	4654.76	12.883	506.408	0.0
41	38.370	145.041	360.181	4608.32	12.794	508.186	0.0
42	38.432	144.798	359.630	4644.75	12.915	503.813	0.0
43	38.949	143.991	358.941	4595.87	12.804	506.713	0.0
44	39.674	143.111	359.657	4605.39	12.805	507.893	0.0

FUEL CONS. and PER OF SGW, respectively.

( In Table 6.1, the passage times, travelled distances, etc. were calculated by additionally navigating the S-A MV along rhumb lines from the points of the final isochrone to Tokyo. ) The routes on which the passage times from the final isochrone to the destination exceeded about 3 days were excluded from Table 6.1.

In Table 6.1, we represent the route which reaches Tokyo from San Francisco via the point of the final isochrone having sub-sector number k by 'route (k)'. The route (43) is the MTR. The routes (15)-(38) are the southern routes passing south of the latitude of San Francisco, whereas the routes (39)-(44) are the northern routes passing through the Bering Sea.

A double point exists between points of the final isochrone having sub-sector number 38 and 39. It is found that compared with the route (39), although the route (38) provides almost the same passage time, its travelled distance and average speed are considerably larger and its fuel consumption is considerably smaller. This is because compared with the route (39) ( northern route ), the route (38) ( southern route ) passed through a lower wind speed/wave height area by making a larger detour.

In Table 6.1, since the periods in which the probability of shipping green water exceeded 0.04 are 0 hours for all the routes, it can be seen that all minimum time routes reaching the final isochrone avoided the area of high head waves.

The details of the MTR of S-A MV are shown in Table 6.2. In Table 6.2 are shown the times, latitudes, longitudes, wind speeds, wind directions, sea heights, sea periods, swell heights, swell directions, swell periods, ship's headings, speeds through the water, drift angles, rudder angles, heel angles, northerly/easterly components of ocean current, courses/speeds over the ground, engine powers and probabilities of shipping green water for every 12 hours.

The periods in which the probability of shipping green water exceeded 0.04 were 12, 0 and 24 hours on the GCR of S-A MV, MTR of EQ MV and GCR of EQ MV, respectively.



Table 6.2 Details of the minimum time route of the sail-assisted motor vessel ( westbound voyage )

\*\*\*\*\* MINIMUM TIME ROUTE \*\*\*\*\*

SAIL-ASSISTED MOTOR VESSEL

WESTBOUND VOYAGE

TIME INTERVAL FOR CALCULATION OF ISOCHRONE = 24 HOURS  
TIME INTERVAL FOR CALCULATION OF SHIP'S SPEED = 12 HOURS

NUMBER OF SUB-SECTORS = 80  
RESOLUTION OF ISOCHRONE = 45 MILES

DEPARTURE TIME = 0 GMT NOV. 6 1980

DEPARTURE POINT = 37 50 N 123 0 W  
DESTINATION = 34 50 N 140 0 E

TIME (DAY)	LATI (DEG)	LONG (DEG)	WISP (KN)	WIDI (DEG)	SEHE (MET)	SEPE (SEC)	SWHE (MET)	SWDI (DEG)	SWPE (SEC)	HEAD (DEG)	SPTW (KN)	DRIF (DEG)	RUDD (DEG)	HEEL (DEG)	CUNO (KN)	CUEA (KN)	COOG (DEG)	SPOG (KN)	PENG (KW)	PROB
6.00	37.83	237.00	7.1	318.4	0.51	1.1	1.05	289.4	10.0	312.2	13.63	-0.01	0.03	0.02	-0.11	0.08	312.1	13.49	6422.1	.0
6.50	39.64	234.44	7.0	248.4	0.65	1.2	3.09	256.7	10.7	312.2	13.40	0.27	0.89	0.61	-0.30	0.37	312.5	12.92	6508.3	.0
7.00	41.39	231.94	27.6	207.7	4.37	7.8	6.09	247.0	14.5	320.8	14.75	0.31	1.37	0.67	-0.00	0.23	321.8	14.60	5982.9	.0
7.50	43.69	229.50	35.5	240.7	6.49	10.3	8.65	245.6	14.6	320.8	14.22	1.09	4.40	2.45	0.16	0.37	323.4	14.12	6193.6	.0
8.00	45.96	227.13	33.8	270.7	6.03	9.8	8.62	237.1	14.7	314.5	11.08	2.03	5.81	3.06	0.20	0.21	318.0	11.09	7329.9	.0
8.50	47.60	224.97	18.8	263.9	2.60	5.3	6.34	237.4	14.0	314.5	13.64	0.76	2.59	1.76	0.28	0.23	316.8	13.69	6415.5	.0
9.00	49.60	222.15	22.7	275.3	3.29	6.0	3.72	273.8	9.9	282.2	11.37	0.10	0.21	0.12	0.34	0.16	284.2	11.29	7233.7	.002
9.50	50.15	218.76	14.0	274.7	1.76	3.8	3.33	275.2	11.0	282.2	12.58	0.04	0.10	0.06	0.22	0.29	283.5	12.34	6808.1	.0
10.00	50.73	215.01	18.4	312.4	2.39	4.9	3.55	259.2	10.7	291.1	12.44	-0.57	1.72	1.11	0.13	0.26	291.6	12.24	6859.8	.000
10.50	51.63	211.39	21.6	222.1	3.05	6.0	3.73	237.4	10.9	291.1	13.57	0.74	2.69	1.64	0.07	-0.04	292.1	13.63	6444.9	.000
11.00	52.65	207.29	16.3	284.9	1.92	4.2	4.69	222.0	12.0	283.9	12.69	-0.01	0.02	0.01	-0.05	-0.21	283.4	12.88	6771.2	.0
11.50	53.25	203.15	21.4	207.9	3.05	6.0	5.63	224.3	12.0	283.9	13.27	0.68	2.48	1.42	-0.18	-0.29	283.5	13.51	6554.5	.001
12.00	53.88	198.74	19.9	237.2	2.80	5.4	6.46	239.7	15.0	275.9	12.11	1.00	3.03	1.85	-0.28	-0.33	275.5	12.41	6976.0	.001
12.50	54.11	194.56	19.3	231.8	2.67	5.3	6.10	232.5	14.0	275.9	12.38	0.92	2.85	1.77	0.06	-0.13	277.0	12.52	6879.5	.001
13.00	54.42	190.32	20.8	249.9	2.83	5.7	6.32	240.0	13.9	278.3	11.63	1.07	3.10	1.85	0.06	-0.05	279.6	11.69	7143.9	.002
13.50	54.81	186.35	18.5	334.3	2.45	5.1	3.33	276.8	10.0	278.3	12.98	-0.75	2.48	1.57	0.21	0.01	278.5	13.01	6662.0	.000
14.00	55.19	181.88	23.2	303.1	3.43	6.3	4.25	281.9	11.4	261.8	12.09	-1.22	3.70	2.24	0.26	-0.00	261.8	12.05	6984.0	.002
14.50	54.85	177.74	26.5	181.7	4.04	7.3	4.40	228.0	11.8	261.8	13.42	0.83	3.10	1.72	-0.21	-0.15	261.9	13.60	6498.5	.002
15.00	54.46	173.10	23.1	253.6	3.39	6.2	5.44	198.0	12.0	254.1	11.36	0.01	0.02	0.01	-0.30	-0.18	252.9	11.62	7235.0	.001
15.50	53.78	169.33	26.2	240.6	4.11	7.5	4.99	198.0	11.1	254.1	10.61	0.60	1.46	0.79	-0.43	-0.14	252.7	10.87	7485.4	.002
16.00	53.13	165.86	21.5	273.1	3.00	5.8	4.03	209.8	10.0	237.6	12.05	-1.12	3.36	2.05	-0.44	-0.11	235.1	12.39	6997.1	.002
16.50	51.72	162.54	38.5	276.0	4.03	11.2	4.03	216.0	10.0	237.6	11.12	-2.11	5.85	3.12	-0.39	0.00	233.9	11.34	7318.1	.001
17.00	50.38	159.63	31.0	279.8	3.62	9.0	3.62	258.0	8.9	231.5	12.24	-1.63	5.17	3.04	-0.34	0.20	228.1	12.31	6931.8	.001
17.50	48.74	156.82	31.6	289.6	3.80	8.9	3.80	257.3	9.5	231.5	12.61	-1.51	5.09	2.92	-0.29	0.13	228.6	12.71	6797.0	.003
18.00	47.06	153.99	11.7	222.9	1.23	3.2	2.31	246.5	7.2	226.1	13.31	0.01	0.03	0.02	-0.15	0.22	225.0	13.26	6540.9	.0
18.50	45.18	151.29	20.1	260.5	2.19	5.5	2.39	222.4	6.7	226.1	13.39	-0.88	2.94	2.01	-0.30	0.05	224.1	13.57	6509.9	.0
19.00	43.24	148.66	17.2	309.9	2.18	4.6	2.50	306.2	8.0	221.4	14.33	-0.39	1.55	0.94	-0.18	0.30	219.6	14.27	6151.9	.0
19.50	41.04	146.22	8.1	269.6	0.33	1.1	0.91	314.1	3.0	221.4	13.85	-0.30	1.04	0.74	0.01	0.54	219.4	13.50	6335.0	.0
20.00	38.95	143.99	2.2	278.5	0.30	0.0	0.56	77.3	7.4	217.9	13.85	-0.04	0.11	0.08	-0.24	0.27	216.4	13.88	6338.1	.0
20.50	36.71	141.91	3.4	139.1	0.37	0.4	0.90	101.0	6.8	219.7	13.88	0.11	0.39	0.28	0.14	0.63	218.1	13.37	6326.7	.0

PASSAGE TIME = 358.941 HOURS

TOTAL DISTANCE = 4595.86 MILES

AVERAGE SPEED = 12.804 KNOTS

TOTAL FUEL CONSUMPTION = 506.71 TONS

PROPELLER REVOLUTION PER MINUTE = 75.00 RPM

PERIOD IN WHICH THE PROBABILITY OF SHIPPING GREEN WATER EXCEEDS 0.04 = 0.0 HOURS



In this westbound voyage, compared with the GCR of EQ MV, the savings of passage time and fuel oil were 58.6 hours, 161.6 tons on the MTR of EQ MV, 16.5 hours, 37.6 tons on the GCR of S-A MV, and 69.0 hours, 156.5 tons on the MTR of S-A MV. These savings are regarded, respectively, as the benefits of weather routing for the MTR of EQ MV, benefits of sail-assisted operation for the GCR of S-A MV, and benefits of weather routing plus sail-assisted operation for the MTR of S-A MV. Hence, in this voyage, it can be said that the benefits of weather routing were greater than those of the sail-assisted operation.

It should be noted that the time saving on the MTR of EQ MV is less than that on the MTR of S-A MV, whereas fuel saving on the MTR of EQ MV is larger than that on the MTR of S-A MV. This is because the S-A MV made a comparatively small detour ( travelled distance = 4,596 n.m. ) for avoiding the severe weather in order to utilize the wind as a propulsive power, whereas the EQ MV made a large detour ( travelled distance = 4,850 n.m. ) and passed through the calm area with smaller engine power than the S-A MV.

Next, the tracks of MTR and GCR in an eastbound voyage ( Tokyo → San Francisco ) departing at 00 hours GMT on 6 November 1980 are shown in Fig.6.7 ( S-A MV ) and Fig.6.8 ( EQ MV ).

From Figs 6.7 and 6.8, it can be seen that concerning the MTR, the S-A MV sailed slightly north of the GCR receiving very strong following wind, whereas the EQ MV sailed south of the GCR receiving moderate following wind. It is also found that since the sharp backward bends of the isochrones are not observed, the area of strong head wind and high head waves did not exist in this eastbound voyage.

All minimum time routes reaching each isochrone are depicted in Fig.6.9 ( S-A MV ) and Fig.6.10 ( EQ MV ); the thick lines indicate the MTR from Tokyo to San Francisco. From Figs 6.9 and 6.10, it becomes clear that the sharp bending points of the isochrones, i.e. double points, do not exist and the tracks of the minimum time routes from Tokyo to the neighbouring points of each isochrone are not very different from each other.

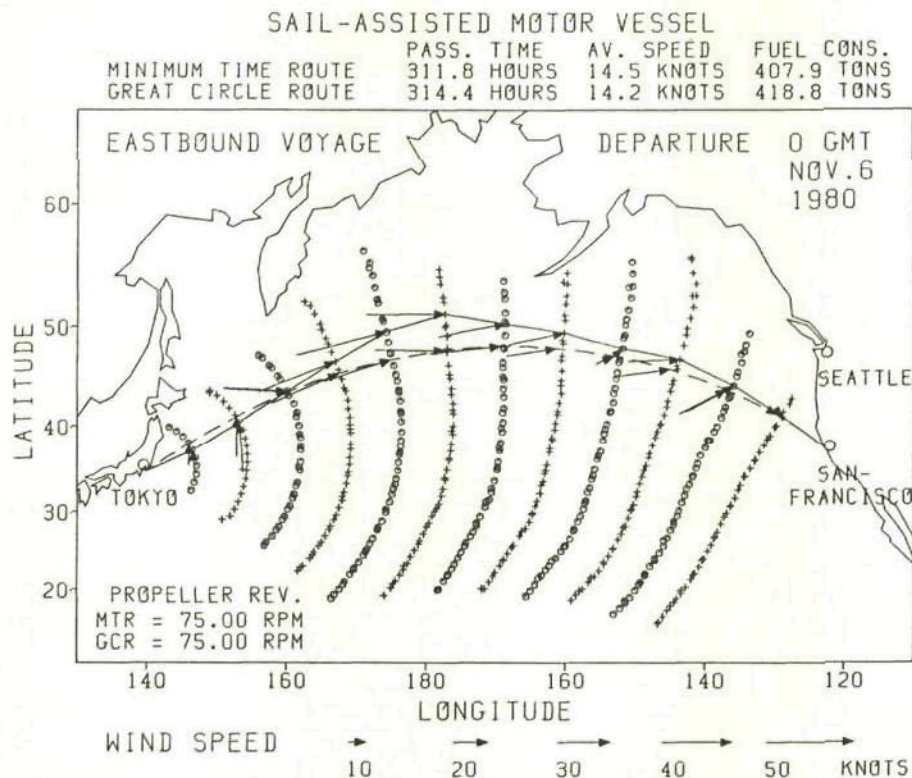


Fig. 6.7 Minimum time route and great circle route of the sail-assisted motor vessel ( eastbound voyage )

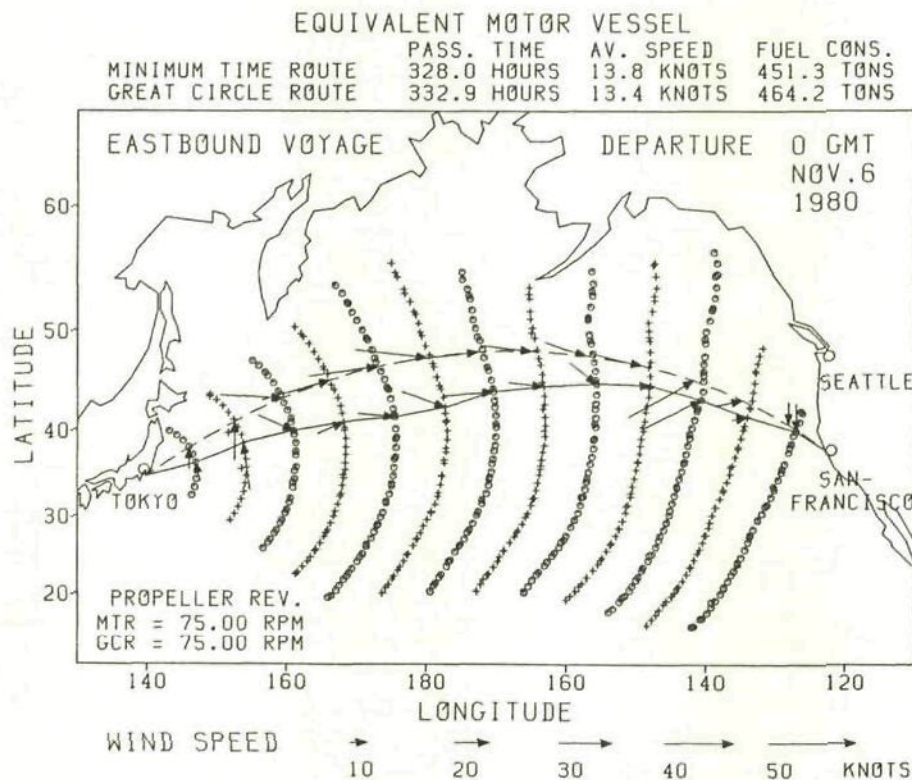


Fig. 6.8 Minimum time route and great circle route of the equivalent motor vessel ( eastbound voyage )



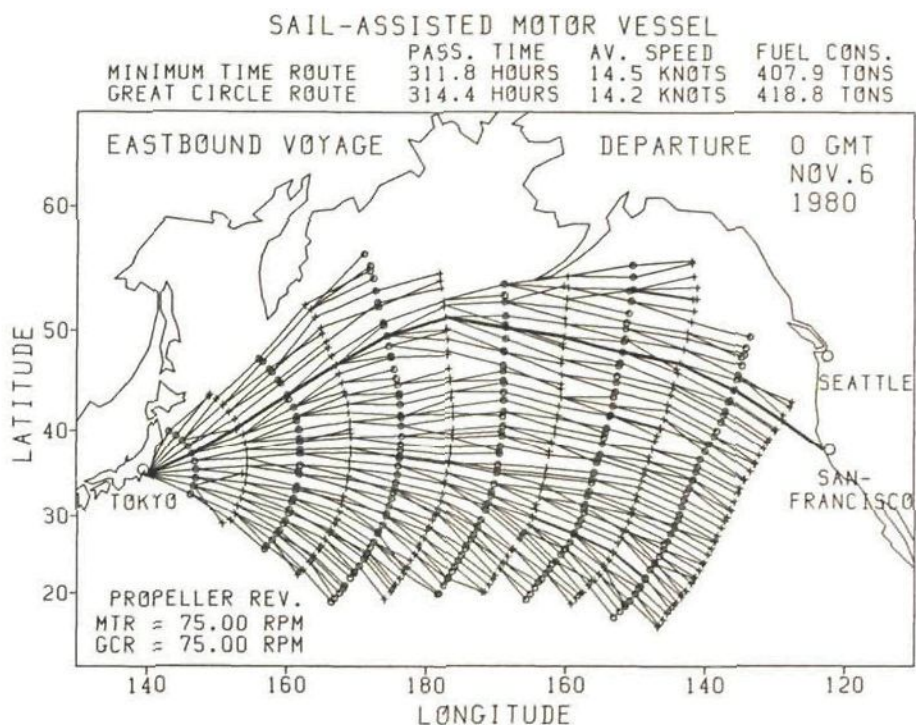


Fig. 6.9 All minimum time routes of the sail-assisted motor vessel reaching each isochrone ( eastbound voyage )

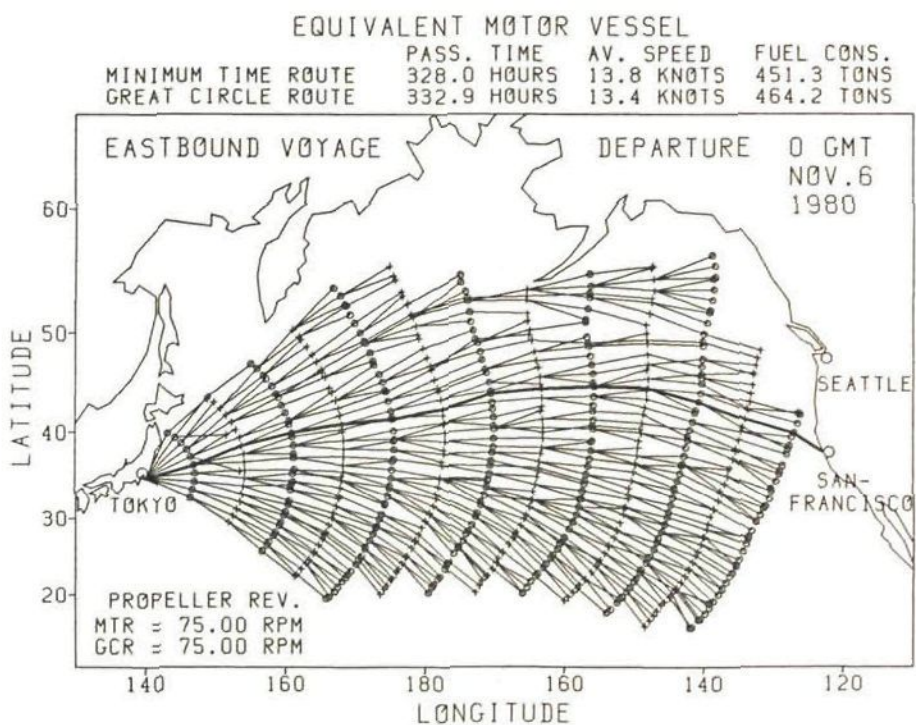


Fig. 6.10 All minimum time routes of the equivalent motor vessel reaching each isochrone ( eastbound voyage )



Compared with the GCR of EQ MV, the savings of passage time and fuel oil were 4.9 hours, 12.9 tons on the MTR of EQ MV, 18.5 hours, 45.4 tons on the GCR of S-A MV, and 21.1 hours, 56.3 tons on the MTR of S-A MV. Therefore, it can be said that the sail-assisted operation was more effective than weather routing for saving passage time and fuel oil in this eastbound voyage.

Passage times and fuel consumptions on the MTR and GCR of S-A MV and EQ MV for the voyages departing on 1, 6, 11, 16, 21 and 26 November and 1, 6, 11 and 16 December are shown in Fig.6.11 ( westbound voyages ) and Fig.6.12 ( eastbound voyages ).

These figures show that both value and variation of passage time and fuel consumption in westbound voyages are far larger than those in eastbound voyages. This comes from the fact that most of the depressions moved northeastwards from the vicinity of Japan in this period and they caused larger speed reduction and larger deviations from the GCR in westbound voyages than in eastbound voyages.

The mean values of travelled distances, average speeds, passage times and fuel consumptions as well as the number of voyages in which the probability of shipping green water exceeded 0.04 in ten voyages departing every 5 days are shown in Table 6.3 ( westbound voyages ) and Table 6.4 ( eastbound voyages ).

In these tables, the time savings and fuel savings are related to the passage time and fuel consumption of the EQ MV on the GCR. From the tables, it can be seen that, as a general rule, the MTR of S-A MV yielded the largest time and fuel savings.

In westbound voyages, since the time and fuel savings on the MTR of EQ MV are 1.3 times larger than those on the GCR of S-A MV, it can be said that weather routing was, on the average, a bit more effective than sail-assisted operation. On the other hand, in eastbound voyages, as the time and fuel savings on the GCR of S-A MV are 1.9 times larger than those on the MTR of EQ MV, it is found that sail-assisted operation was more effective than weather routing on the average.

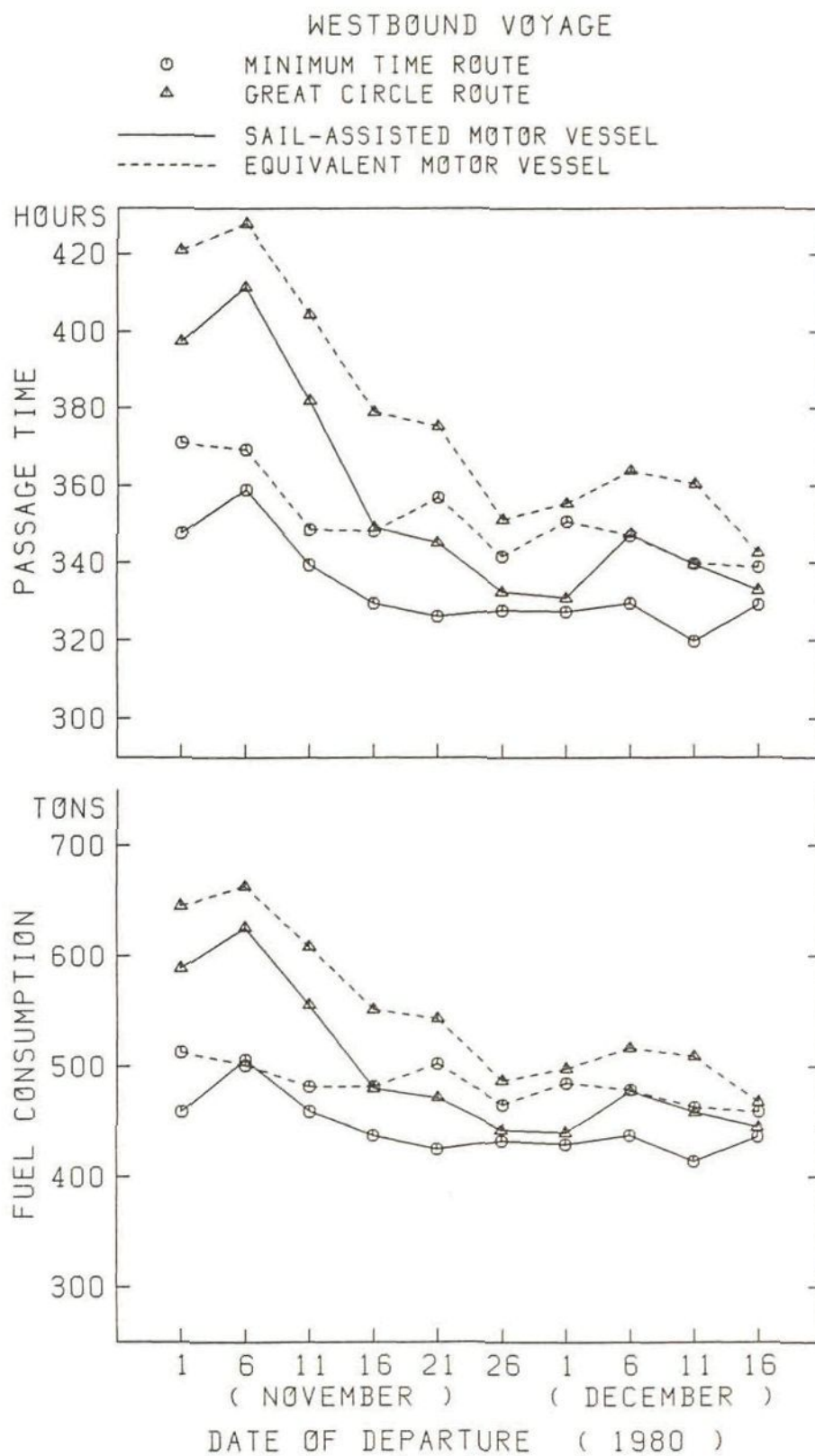


Fig. 6.11 Passage times and fuel consumptions for each date of departure ( westbound voyage )

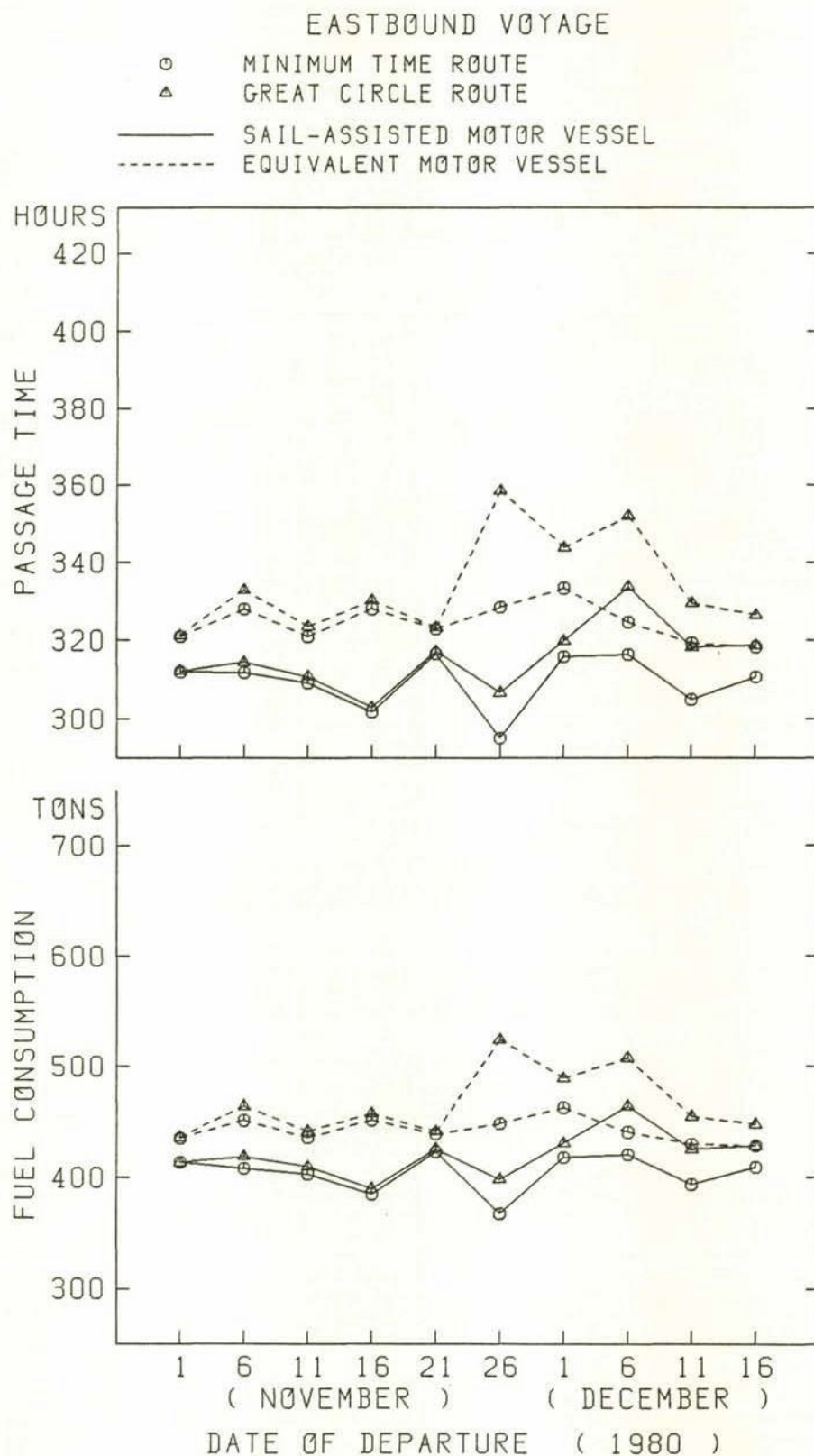


Fig. 6.12 Passage times and fuel consumptions for each date of departure ( eastbound voyage )



Table 6.3 Mean values of 10 westbound voyages

Minimum time routing  
Propeller rev. = 75 r.p.m.

	Sail-assisted MV		Equivalent MV	
	MTR	GCR	MTR	GCR
Distance (n.m.)	4575	4471	4605	4470
Average speed (knots)	13.73	12.60	13.12	11.89
Passage time (hours)	333.5	356.8	351.1	378.0
Time saving (hours)	44.5	21.2	26.9	0.0
Time saving (%)	11.8	5.6	7.1	0.0
Fuel consumption (tons)	443.5	498.5	483.4	549.1
Fuel saving (tons)	105.6	50.6	65.7	0.0
Fuel saving (%)	19.2	9.2	12.0	0.0
Number of voyages in which the probability of shipping green water exceeded 0.04	0	5	0	5

Table 6.4 Mean values of 10 eastbound voyages

Minimum time routing  
Propeller rev. = 75 r.p.m.

	Sail-assisted MV		Equivalent MV	
	MTR	GCR	MTR	GCR
Distance (n.m.)	4508	4470	4517	4470
Average speed (knots)	14.58	14.18	13.92	13.39
Passage time (hours)	309.4	315.5	324.5	334.2
Time saving (hours)	24.8	18.7	9.7	0.0
Time saving (%)	7.4	5.6	2.9	0.0
Fuel consumption (tons)	404.1	420.6	442.4	466.6
Fuel saving (tons)	62.5	46.0	24.2	0.0
Fuel saving (%)	13.4	9.9	5.2	0.0
Number of voyages in which the probability of shipping green water exceeded 0.04	0	2	0	2

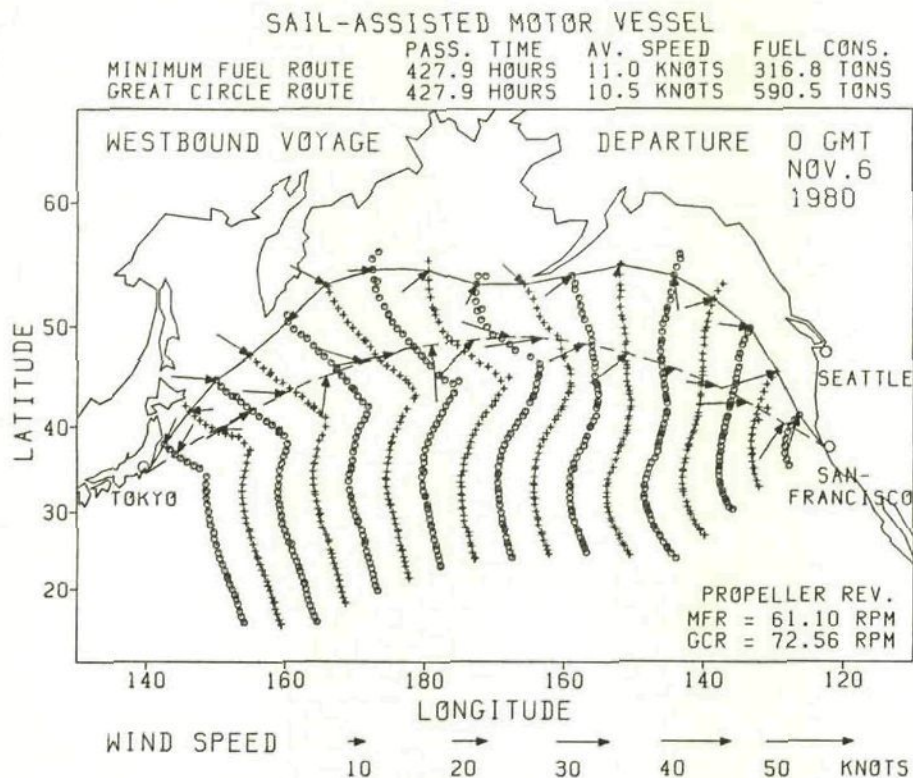


Fig. 6.13 Minimum fuel route and great circle route of the sail-assisted motor vessel ( westbound voyage )

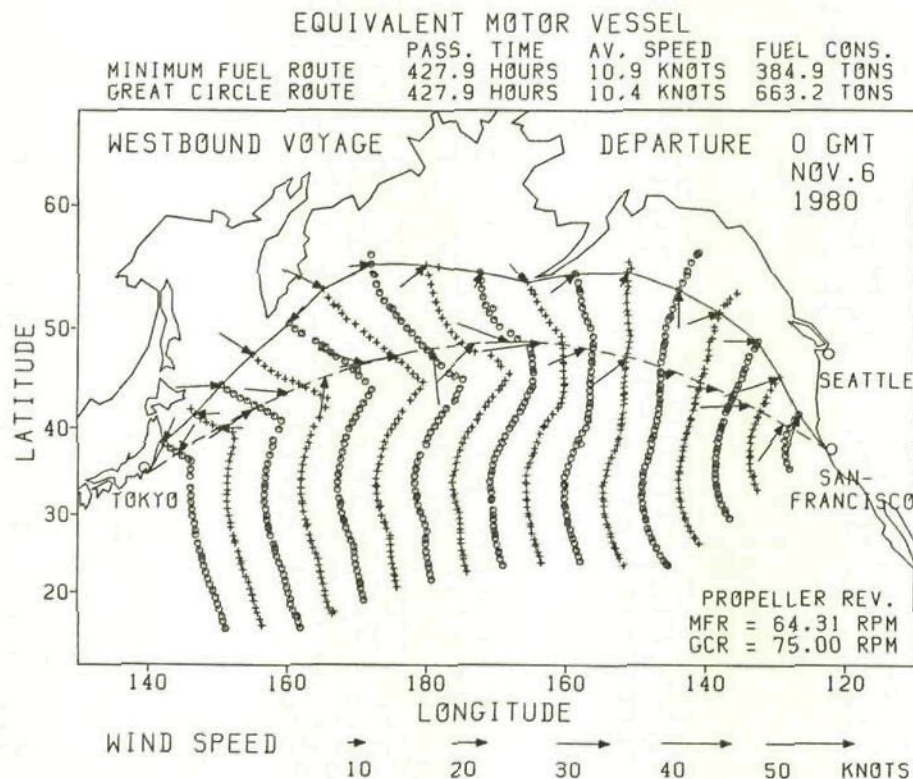


Fig. 6.14 Minimum fuel route and great circle route of the equivalent motor vessel ( westbound voyage )



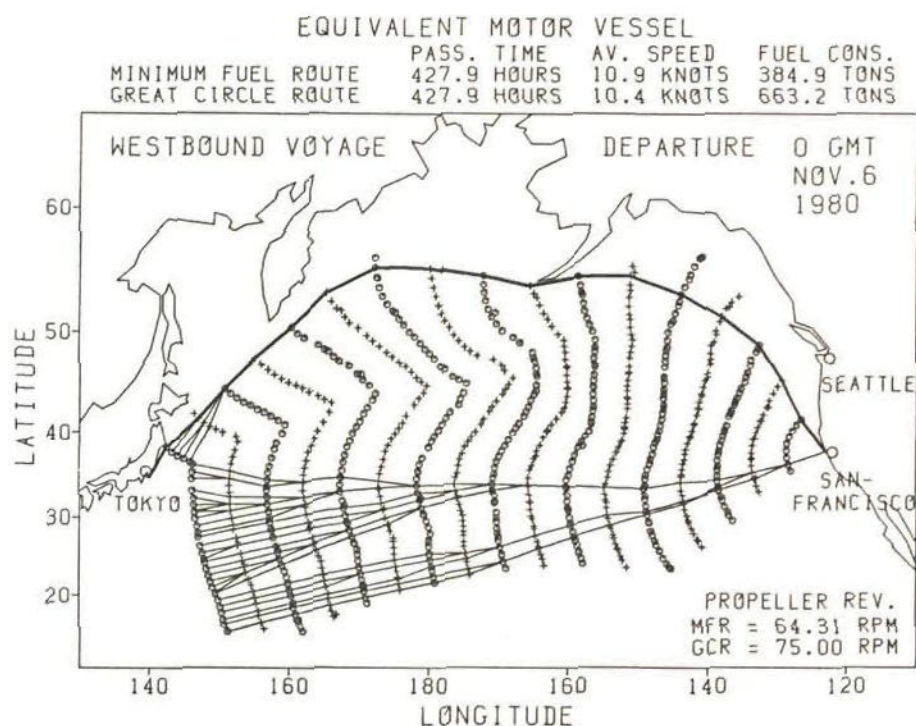


Fig. 6.15 All minimum time routes of the equivalent motor vessel reaching the final isochrone ( westbound voyage )

Table 6.5 Information on the routes reaching Tokyo from San Francisco via points of the final isochrone

SUBJECT.NO.	FINAL ISOCHRONE		PASS. TIME	DISTANCE	AV. SPEED	FUEL CONS.	PER OF SGW
	LATI	LONG	(HR)	(NM)	(KN)	(TN)	(HR)
	(DEG)	(DEG)					
21	22.631	148.437	483.192	5515.91	11.416	417.858	0.0
22	23.472	148.173	477.319	5459.18	11.437	411.746	0.0
23	24.342	147.954	471.557	5398.56	11.448	405.871	0.0
24	24.702	147.829	469.585	5367.21	11.430	403.994	0.0
25	25.476	147.542	465.329	5320.08	11.433	400.064	0.0
26	26.400	147.283	461.014	5257.12	11.403	396.265	0.0
27	27.463	146.920	455.792	5186.58	11.379	391.270	0.0
28	28.026	146.927	453.667	5144.19	11.339	389.538	0.0
29	28.897	146.752	450.081	5087.90	11.304	386.658	0.0
30	29.825	146.522	446.241	5030.01	11.272	383.415	0.0
31	30.628	146.384	443.266	4993.03	11.264	380.902	0.0
32	30.676	146.422	443.263	4988.91	11.255	380.968	0.0
33	31.480	146.244	440.390	4955.30	11.252	378.430	0.0
34	32.299	146.248	438.446	4932.33	11.250	376.680	0.0
35	33.206	146.203	436.678	4900.53	11.222	375.357	0.0
36	34.576	146.124	435.310	4861.26	11.167	374.230	0.0
37	35.402	146.160	435.730	4864.41	11.164	374.563	0.0
38	36.283	146.256	436.849	4864.89	11.136	376.003	0.0
39	36.529	145.849	435.449	4733.68	10.871	391.281	0.0
40	36.881	144.971	432.477	4700.31	10.868	388.959	0.0
41	37.335	144.051	429.764	4676.43	10.881	386.552	0.0
42	37.725	143.263	428.091	4664.34	10.896	385.094	0.0
43	38.302	142.458	427.914	4668.49	10.910	384.868	0.0



Hence, in order to check the existence of such a route, the Algorithm (II) was applied again for only the south of the double point.

The result of that simulation is shown in Fig.6.16. From Fig.6.16, it is found that the alternative route passing along about the  $34^{\circ}\text{N}$  parallel gives almost the same fuel consumption as that on the MFR in Fig.6.14. The number of propeller revolutions on that alternative route was 0.96 r.p.m. larger than that on the MFR in Fig.6.14.

As was shown in the above mentioned minimum fuel routing of the EQ MV, when using the Algorithm (II), care should be taken for the existence of an alternative MFR if the double point of the final isochrone is located near the destination.

The Algorithm (I) mentioned in 2.3.2 was also applied to the minimum fuel routing of the EQ MV. That is, letting the number of propeller revolutions  $n_0$  be 66.0 r.p.m. and using the objective function  $J$  defined by (2.27), the minimum value of objective function  $J^*(n_0)$  was selected from all  $J$  of the routes reaching Tokyo from San Francisco via points of the final isochrone.

Then reducing the number of propeller revolutions  $n$  by 0.1 r.p.m.,  $J^*(n)$  were computed for various numbers of propeller revolutions. Fig.6.17 shows the result of those computations.

In Fig.6.17, the northern routes passing through the Bering Sea give  $J^*(n)$  for  $n$  less than or equal to 65.2 r.p.m., whereas the southern routes passing along about  $34^{\circ}\text{N}$  parallel give  $J^*(n)$  for  $n$  greater than 65.2 r.p.m..

It can be seen that the passage time and the minimum value of the objective function for  $n = 65.2$  r.p.m. are largely different from those for  $n = 65.3$  r.p.m.. From Fig.6.17, we obtain a minimum fuel consumption of 384.1 tons for 65.3 r.p.m. ( southern route ), and the second minimum fuel consumption of 385.8 tons for 64.4 r.p.m. ( northern route ), which almost coincide with the results by the Algorithm (II).

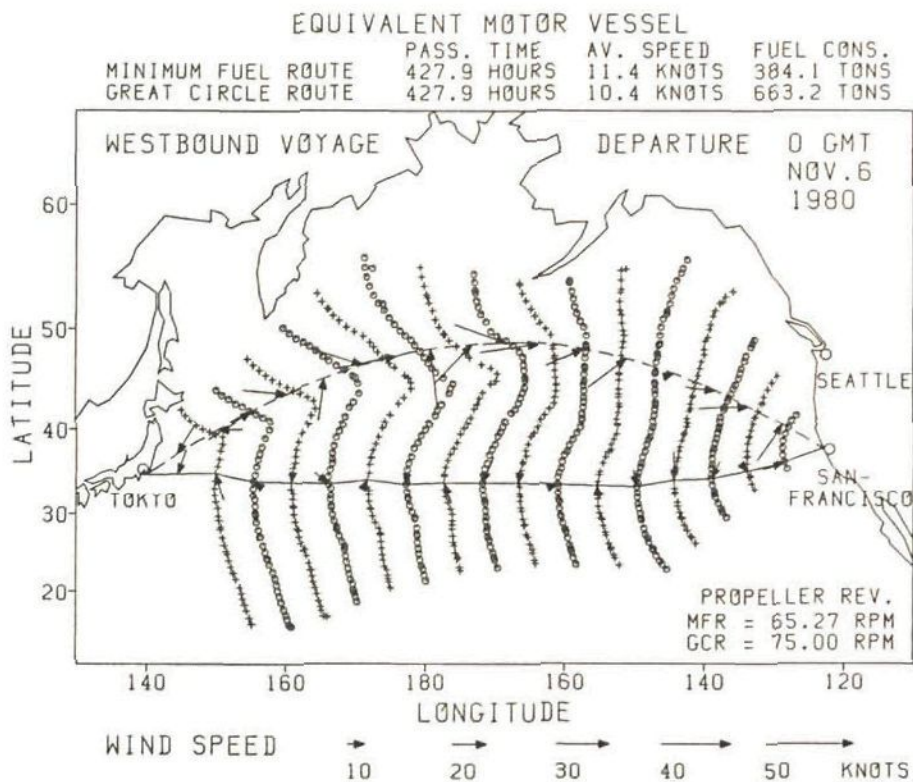


Fig. 6.16 ( Alternative ) minimum fuel route and great circle route of the equivalent motor vessel ( westbound voyage )

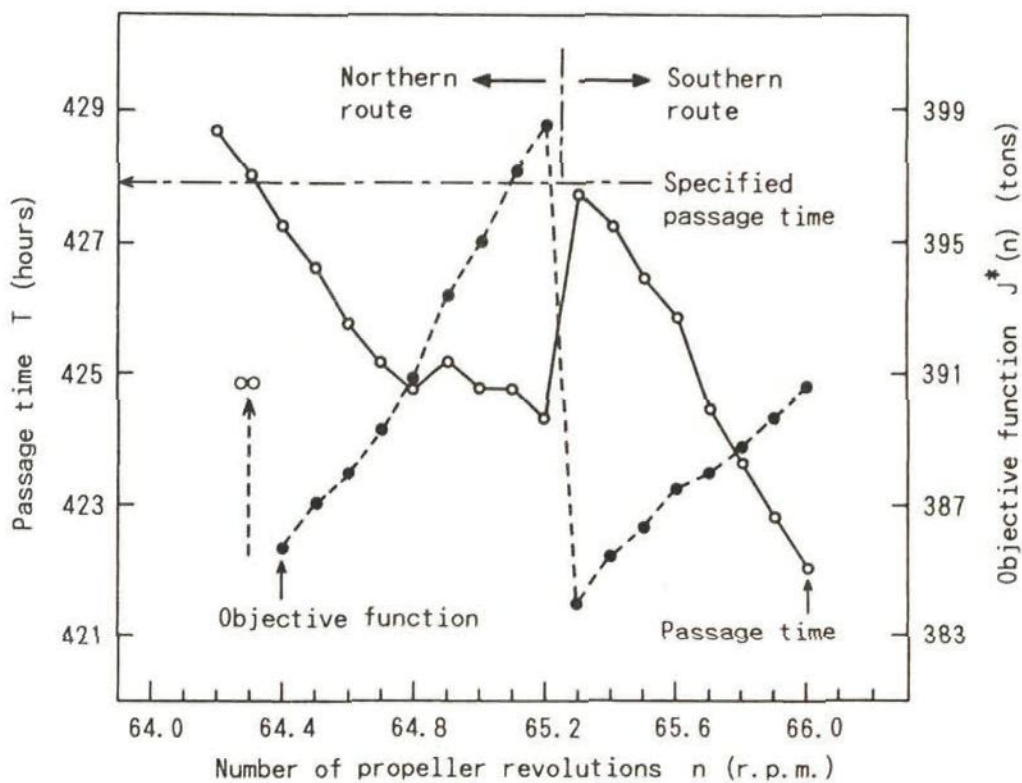


Fig. 6.17 Passage time and objective function versus number of propeller revolutions



As was seen in this simulation, although the Algorithm (I) needs a considerable computing time, it can always find the global minimum value of the objective function.

The passage times, travelled distances, average speeds, numbers of propeller revolutions and fuel consumptions as well as the periods in which the probability of shipping green water exceeded 0.04 on the MFR and GCR of S-A MV and EQ MV in this westbound voyage are shown in Table 6.6.

In Table 6.6, N.R. ( northern route ) and S.R. ( southern route ) denote the MFR in Fig.6.14 and the MFR in Fig.6.16, respectively. The fuel savings are related to the fuel consumption of the EQ MV on the GCR. From Table 6.6, it can be seen that more than half the amount of fuel oil consumed on the GCR of EQ MV was saved on the MFR of S-A MV in that particular period.

Table 6.6 Summary of minimum fuel routing ( Westbound voyage )

Departure : 00 hours GMT 6 November 1980  
Specified passage time = 427.9 hours

	Sail-assisted MV		Equivalent MV		
	MFR	GCR	MFR		GCR
			N. R.	S. R.	
Passage time (hours)	427.9	427.9	427.9	427.9	427.9
Distance (n.m.)	4701	4473	4668	4863	4470
Average speed (knots)	10.99	10.45	10.91	11.36	10.45
Propeller rev. (r.p.m.)	61.10	72.56	64.31	65.27	75.00
Fuel consumption (tons)	316.8	590.5	384.9	384.1	663.2
Fuel saving (tons)	346.4	72.7	278.3	279.1	0.0
Fuel saving (%)	52.2	11.0	42.0	42.1	0.0
Period in which the Probability of shipping green water exceeded 0.04 (hours)	0	36	0	0	24



As shown in Fig.6.2, since the passage time and fuel consumption were 358.9 hours and 506.7 tons on the MTR of S-A MV, it is found that 189.9 tons of fuel oil was saved by the 69.0 hours extension of the passage time on the MFR of S-A MV. Since the fuel saving on the MFR of EQ MV is 3.8 times larger than that on the GCR of S-A MV, it can be seen that weather routing was far more effective than sail-assisted operation to save fuel oil in this westbound voyage.

Concerning the period in which the probability of shipping green water exceeded 0.04, it is found that the S-A MV and EQ MV were exposed to high head waves on the GCR, whereas the MFR of both vessels avoided areas of such high head waves.

Next, the tracks of MFR and GCR in eastbound voyage are shown in Fig.6.18 ( S-A MV ) and Fig.6.19 ( EQ MV ).

By comparing Figs 6.18 and 6.19 with Figs 6.7 and 6.8, we can find that the tracks of the MFR of S-A MV and EQ MV almost coincide with those of the MTR of both vessels. It was already found in the simulations of the westbound voyage that the tracks of the MFR of S-A MV ( Fig.6.13 ) and EQ MV ( Fig.6.16 ) hardly differ from those of the MTR of S-A MV ( Fig.6.2 ) and EQ MV ( Fig.6.3 ). In addition, the shapes of the isochrones of the MFR closely resemble those of the MTR.

Hence it can be said that provided the specified passage time on the MFR does not differ largely from the passage time on the MTR, the track of the MFR almost coincides with that of the MTR. In other words, a ship following the track of the MTR with reduced number of propeller revolutions ( or engine power ) will have maximum fuel savings. This fact has been verified in other simulations by the author. <sup>(1)</sup>. <sup>(2)</sup>

The passage times, travelled distances, average speeds, numbers of propeller revolutions and fuel consumptions as well as the periods in which the probability of shipping green water exceeded 0.04 on the MFR and GCR of S-A MV and EQ MV in this eastbound voyage are shown in Table 6.7.

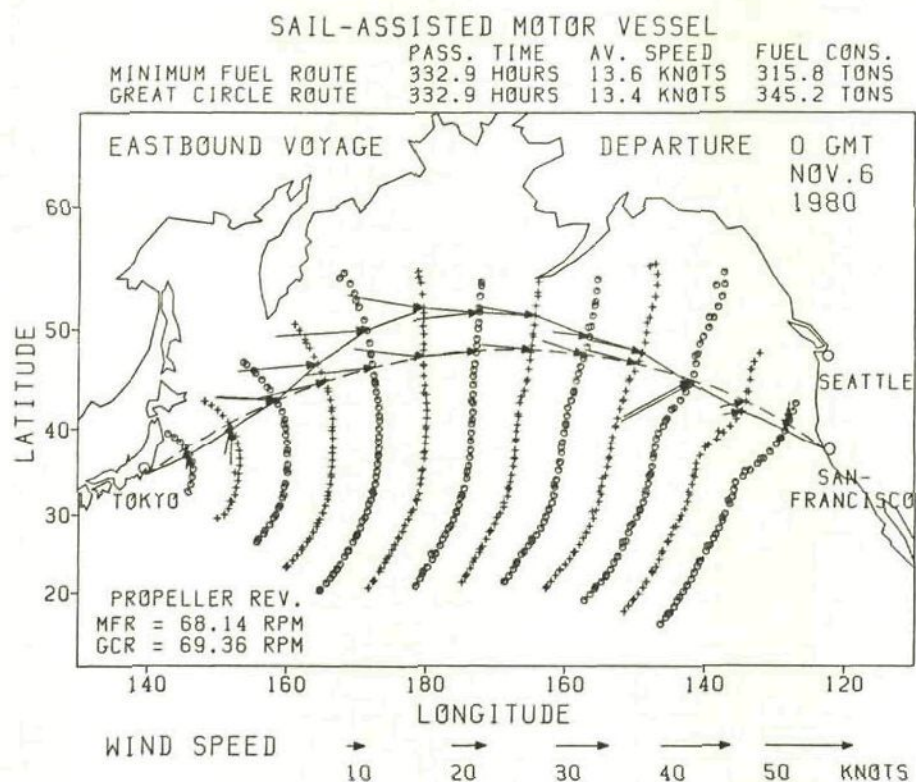


Fig. 6.18 Minimum fuel route and great circle route of the sail-assisted motor vessel ( eastbound voyage )

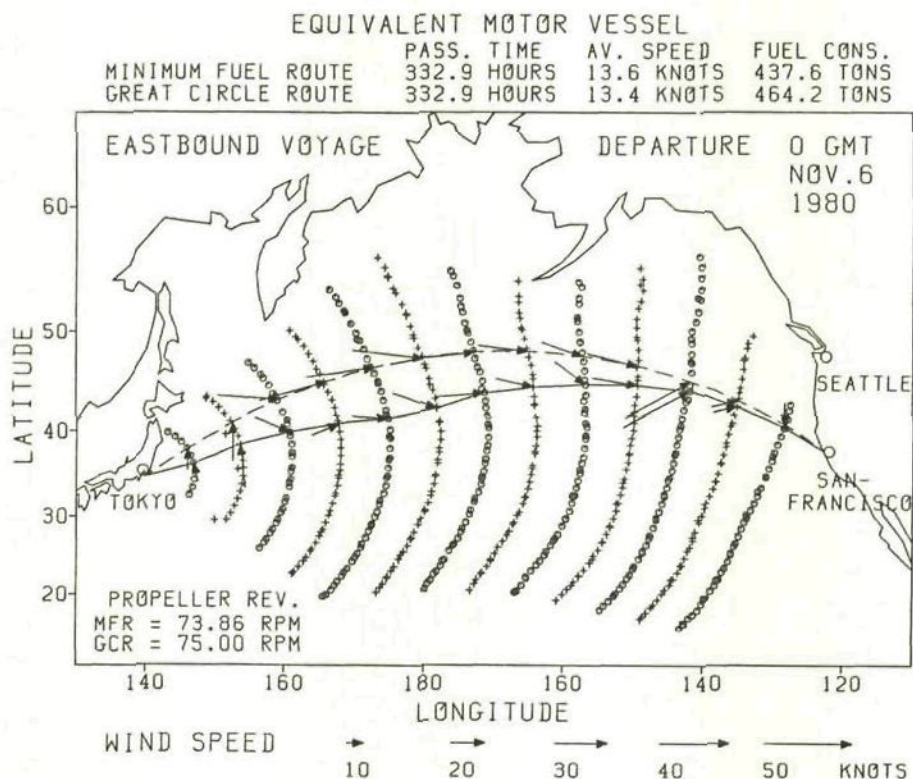


Fig. 6.19 Minimum fuel route and great circle route of the equivalent motor vessel ( eastbound voyage )



From Table 6.7, it is found that compared with the GCR of EQ MV, the S-A MV on the MFR could save fuel oil by 32% through the weather routing plus sail-assisted operation. Since the fuel saving on the GCR of S-A MV is 4.5 times larger than that on the MFR of EQ MV, it can be said that in this eastbound voyage, sail-assisted operation was far more effective than weather routing.

Table 6.7 Summary of minimum fuel routing ( Eastbound voyage )

Departure : 00 hours GMT 6 November 1980  
Specified passage time = 332.9 hours

	Sail-assisted MV		Equivalent MV	
	MFR	GCR	MFR	GCR
Passage time (hours)	332.9	332.9	332.9	332.9
Distance (n.m.)	4543	4470	4527	4470
Average speed (knots)	13.65	13.43	13.60	13.43
Propeller rev. (r.p.m.)	68.14	69.36	73.86	75.00
Fuel consumption (tons)	315.8	345.2	437.6	464.2
Fuel saving (tons)	148.4	119.0	26.6	0.0
Fuel saving (%)	32.0	25.6	5.7	0.0
Period in which the probability of shipping green water exceeded 0.04 (hours)	0	0	0	0

The simulations of the minimum fuel routing were performed also for a vessel which has half the sail area ( i.e. half the sail thrust and half the sail lateral force ) of the former S-A MV. The tracks of the MFR and the GCR of that vessel are shown in Fig.6.20 ( westbound voyage ) and Fig.6.21 ( eastbound voyage ).

As shown in Figs 6.20 and 6.21, it can be seen that the tracks of the MFR of that vessel are similar to those of the MFR of S-A MV in both westbound and eastbound voyages.



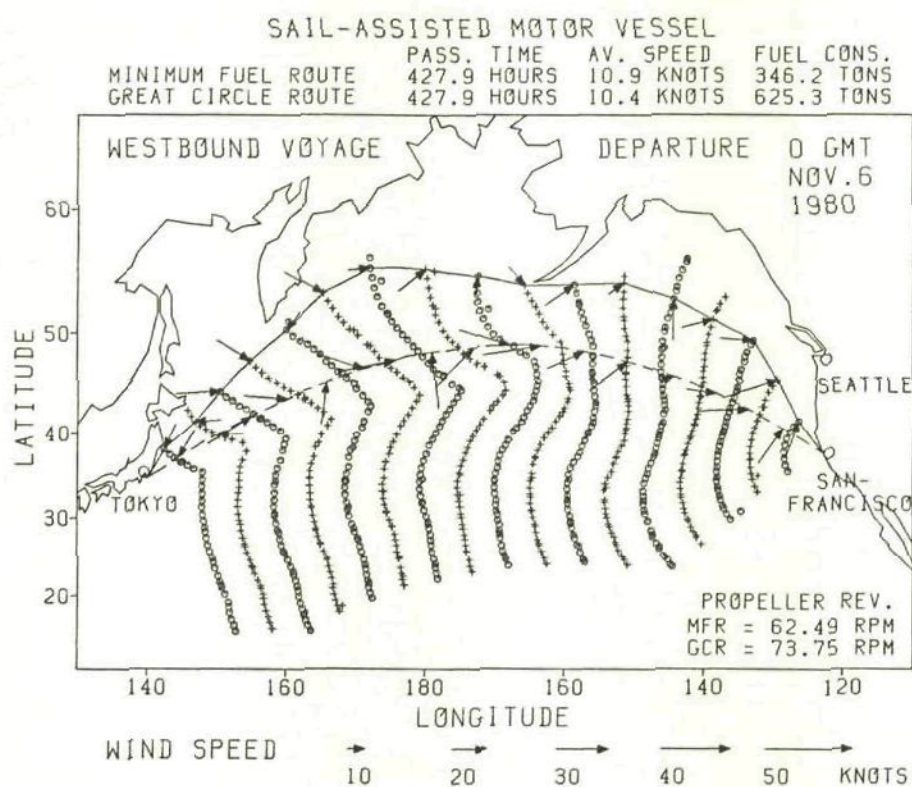


Fig. 6.20 Minimum fuel route and great circle route of the sail-assisted motor vessel ( 1/2 sail area; westbound voyage )

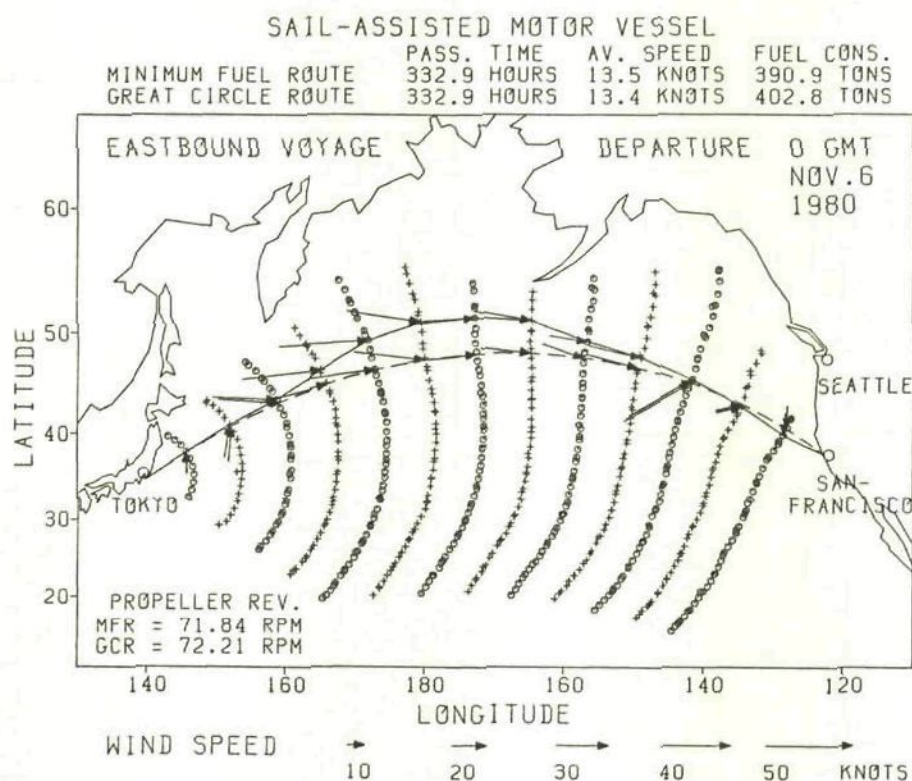


Fig. 6.21 Minimum fuel route and great circle route of the sail-assisted motor vessel ( 1/2 sail area; eastbound voyage )

The passage times, fuel consumptions, etc. on the MFR and GCR of the half-sail-area vessel are shown in Table 6.8. In Table 6.8, the fuel savings are related to the fuel consumption of the EQ MV on the GCR.

We can find from Tables 6.6, 6.7 and 6.8 that the fuel savings by the half-sail-area vessel on the GCR lie approximately halfway between those by the S-A MV and EQ MV. Therefore, it can be said that provided the passage time is specified, the fuel saving on a certain route is almost directly proportional to the sail area ( or sail thrust ) for relatively small sail areas.

Table 6.8 Summary of minimum fuel routing ( 1/2 sail area )

Departure : 00 hours GMT 6 November 1980  
 Specified passage time = 427.9 hours ( Westbound voyage )  
                               = 332.9 hours ( Eastbound voyage )

	Westbound voyage		Eastbound voyage	
	MFR	GCR	MFR	GCR
Passage time (hours)	427.9	427.9	332.9	332.9
Distance (n.m.)	4665	4471	4507	4470
Average speed (knots)	10.90	10.45	13.54	13.43
Propeller rev. (r.p.m.)	62.49	73.75	71.84	72.21
Fuel consumption (tons)	346.2	625.3	390.9	402.8
Fuel saving (tons)	317.0	37.9	73.3	61.4
Fuel saving (%)	47.8	5.7	15.8	13.2
Period in which the probability of shipping green water exceeded 0.04 (hours)	0	36	0	0



### 6.2.3 Minimum cost routing

Based on the algorithm mentioned in 2.3.3, simulations of minimum cost routing were performed for the westbound voyage of the S-A MV departing at 00 hours GMT on 6 November 1980.

In this simulation, taking into account only the fuel cost during the voyage, the following objective function J was set up:

$$J = \begin{cases} C F + w ( t_f - t_s )^2 & \text{if } t_f \geq t_s \\ C F & \text{if } t_f < t_s \end{cases} \quad (6.1)$$

where J : total cost ( dollars )  
F : total fuel consumption ( tons )  
C : fuel cost per unit weight = 85 ( dollars/ton )  
 $t_f$  : actual arrival time ( hours )  
 $t_s$  : scheduled arrival time ( hours )  
w : delay penalty cost per unit time squared = 10  
( dollars/hour<sup>2</sup> )

The scheduled passage time (  $t_s - t_0$  ) [  $t_0$  : departure time ] was set to 411.4 hours which was the passage time on the GCR of S-A MV with the number of propeller revolutions being 75 r.p.m. shown in Fig.6.2.

In the simulation, letting the number of propeller revolutions  $n_0$  be 70 r.p.m., the minimum value of the objective function  $J^*(n_0)$  was selected from all J of the routes reaching Tokyo from San Francisco via points of the final isochrone. Then reducing the number of propeller revolutions n by 1 r.p.m.,  $J^*(n)$  were computed for various numbers of propeller revolutions.

Fig.6.22 shows the result of those computations. In Fig.6.22, the northern routes passing through the Bering Sea give  $J^*(n)$  for n less than or equal to 65 r.p.m., whereas the southern routes passing along parallels between 32°N and 34°N give  $J^*(n)$  for n greater than 65 r.p.m..



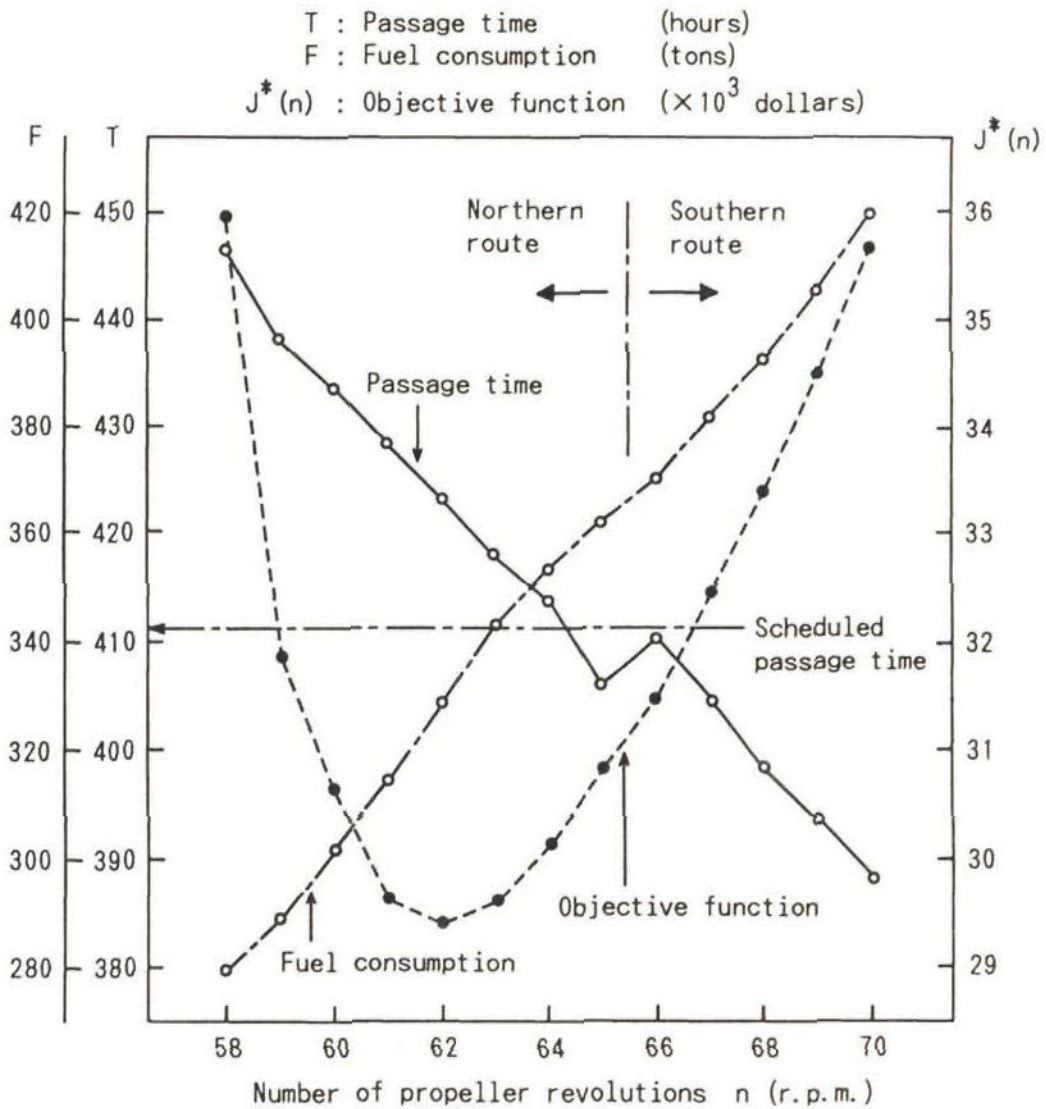


Fig. 6.22 Passage time, fuel consumption and objective function versus number of propeller revolutions

That is, for each number of propeller revolutions greater than 65 r.p.m., since the passage time on the southern route becomes smaller than the scheduled passage time, the delay penalty cost is not imposed on the objective function. Therefore,  $J^*(n)$  is provided by the southern route which passes through a calm area with smaller fuel consumption than that on the northern route.

On the other hand, for each number of propeller revolutions less than or equal to 65 r.p.m., as the passage time on the southern route exceeds the scheduled passage time, the delay penalty cost is

added to the fuel cost. Thus,  $J^*(n)$  is provided by the northern route which passes through a comparatively rough area with a bit larger fuel consumption but shorter passage time ( i.e. smaller delay penalty cost ) than those on the southern route.

In Fig.6.22, the minimum total cost  $J^*_{min}$  was determined as the minimum of the parabola passing through three points whose numbers of propeller revolutions were 61, 62 and 63 r.p.m.. The  $J^*_{min}$  became 29,400 dollars for the optimal number of propeller revolutions  $n^*$  being 62.01 r.p.m..

Concerning the GCR, reducing the number of propeller revolutions  $n$  by 1 r.p.m. from 75 r.p.m., the total costs were calculated and plotted for various numbers of propeller revolutions. Then the minimum total cost was determined as the minimum of the parabola passing through three points whose numbers of propeller revolutions were 73, 74 and 75 r.p.m.. The minimum total cost on the GCR became 52,272 dollars for  $n$  being 73.74 r.p.m..

The tracks of the MCR and GCR are shown in Fig.6.23. In Fig.6.23, the solid line and dashed line denote the MCR and GCR. From Fig.6.23, it is found that the track of the MCR almost coincides with that of the MFR for the specified passage time of 427.9 hours shown in Fig.6.13.

The passage times, fuel costs, delay penalty costs, total costs, etc. on the MCR and GCR of S-A MV are shown in Table 6.9. From Table 6.9, we can find that compared with the GCR, the cost saving on the MCR reaches 43.8%. It is also found that the fuel costs form respectively 95.2% and 98.7% of the total costs on the MCR and GCR for the given fuel cost per unit weight  $C$  and delay penalty cost per unit time squared  $w$ .

As stated in 2.3.3, the delay penalty cost per unit time squared  $w$  will change with the operation schedule of a berth at the destination, the degree of reduction of the benefit due to late arrival, etc.. It may be said that unless  $w$  is extremely small, the tracks of the MCR for the scheduled passage time (  $t_s - t_0$  ) almost coincides with that of the MFR for the same specified passage time as (  $t_s - t_0$  ).



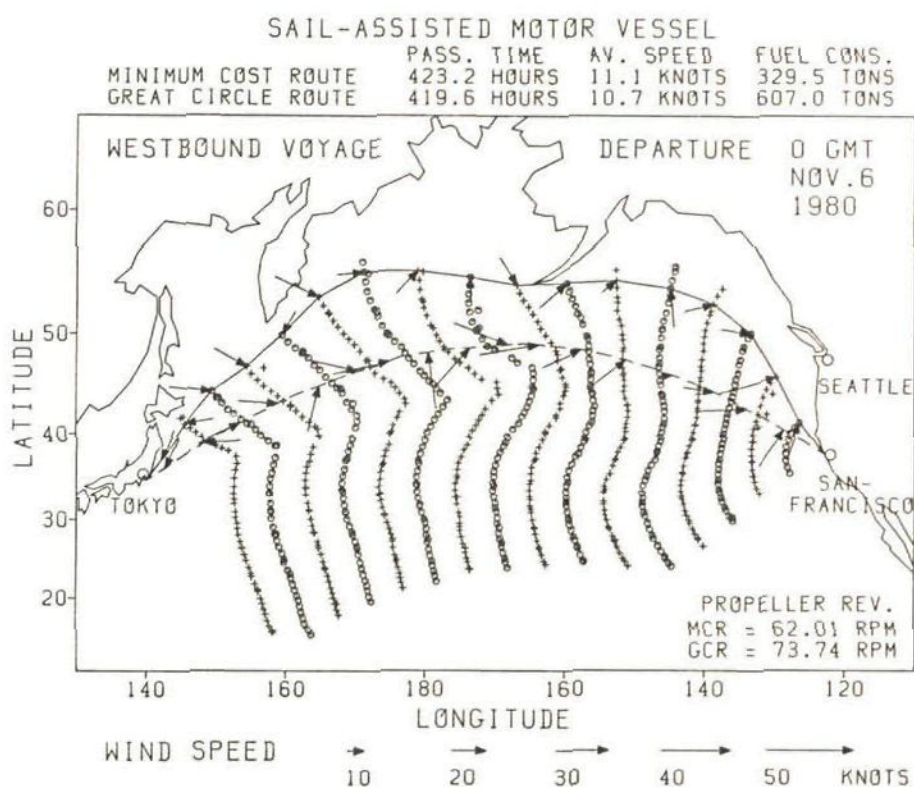


Fig. 6.23 Minimum cost route and great circle route of the sail-assisted motor vessel ( westbound voyage )

Table 6.9 Summary of minimum cost routing

Sail-assisted motor vessel ( Westbound voyage )  
Departure : 00 hours GMT 6 November 1980  
Scheduled passage time = 411.4 hours

		MCR	GCR
Passage time	(hours)	423.2	419.6
Distance	(n.m.)	4678	4473
Average speed	(knots)	11.05	10.66
Propeller rev.	(r.p.m.)	62.01	73.74
Fuel consumption	(tons)	329.5	607.0
Fuel cost	(dollars)	28003	51592
Delay penalty cost	(dollars)	1397	680
Total cost	(dollars)	29400	52272
Cost saving	(dollars)	22872	0
Cost saving	(%)	43.8	0.0
Period in which the probability of shipping green water exceeded 0.04 (hours)		0	36



### 6.3 SIMULATIONS OF STOCHASTIC ROUTING

In this section, the simulations of stochastic minimum time/fuel routing are executed for voyages between Tokyo and San Francisco.

The environmental data used for these simulations are shown in Fig.4.40. As mentioned in Sections 4.3, 4.4 and 4.5, the wave conditions are represented by three parameters in the stochastic routing, i.e. significant wave height, primary wave direction and primary wave period.

It is assumed that the wave system has a directional Bretschneider spectrum (3.30) for calculating the added resistance due to waves, whereas it has an unidirectional Bretschneider spectrum (3.31) for calculating the probability of shipping green water at the bow.

Concerning the modified isochrone method, the increments for discretizing the problem ( i.e.  $\Delta t$ ,  $\Delta t'$ ,  $\Delta C$  and  $\Delta d$  ), number of ship's headings, number of sub-sectors, service speed, etc. are set to the same values as used in Section 6.2. The navigable area is set up as shown in Fig.6.1.

In order to obtain the partial derivative  $\partial \underline{S} / \partial \underline{C}_i$  in (5.1), the following increments for numerical differentiation are adopted:

Increment of wind speed	$\Delta S_w = 0.5$ m/sec
Increment of wind direction	$\Delta D_w = 5.0$ degrees
Increment of significant wave height	$\Delta H_s = 0.5$ meters
Increment of primary wave direction	$\Delta D_p = 5.0$ degrees
Increment of primary wave period	$\Delta T_p = 0.5$ seconds

In the simulations, the shapes, predicted passage times/fuel consumptions, standard deviations of passage times/fuel consumptions, etc. of the optimum routes are compared with those of the great circle routes. The great circle routes are calculated based on the method described in Appendix 5 with sub-time-interval  $\Delta t'$  of 12 hours.

6.3.1 Minimum time routing using forecasted wind/wave data followed by the 5-day mean wind/wave models classified by ZI

In this subsection, using the forecasted wind/wave data followed by the 5-day mean wind/wave models classified by ZI, simulations of stochastic minimum time routing are performed.

Referring to the objective function for stochastic minimum time routing proposed in Section 2.5, the following objective function may be considered for the S-A MV and EQ MV:

$$J = \bar{T} + w_1 \sigma_T + w_2 \bar{T}_D \quad (6.2)$$

where  $\bar{T}$  : predicted passage time

$\sigma_T$  : standard deviation of passage time

$\bar{T}_D$  : predicted period in which the probability of shipping green water at the bow exceeds 0.04

$w_1$  : weighting coefficient for the uncertainty of passage time

$w_2$  : weighting coefficient for the risk of damage due to shipping green water

As mentioned in 2.5, the values of  $w_1$  and  $w_2$  depend on the evaluation of the shipmaster/shipowner for the uncertainty of arrival time and the risk of damage, respectively. Hence, it seems difficult to give appropriate values to  $w_1$  and  $w_2$  in the simulations.

Thus  $w_1$  and  $w_2$  were set to zero. That is, in the simulations,  $\bar{T}$ ,  $\sigma_T$  and  $\bar{T}_D$  as well as the following quantities were calculated for all the routes reaching the destination from the departure point via points of the final isochrone, and they were tabulated.

* Predicted travelled distance	$\bar{D}$
* Predicted average speed	$\bar{V}$
* Standard deviation of average speed	$\sigma_V$
* Predicted fuel consumption	$\bar{F}$
* Standard deviation of fuel consumption	$\sigma_F$

From those routes, the route giving minimum predicted passage time  $\bar{T}_{min}$  was adopted as a minimum time route. Although  $\sigma_T$  and  $\bar{T}_D$  were not taken into consideration in determining the minimum time route, those tabulated values were thoroughly investigated.

The 5-day mean zonal indexes for the period from 31 January to 11 March in 1985 are shown in Table 6.10.

Table 6.10 5-day mean zonal indexes for the period from 31 January to 11 March in 1985

Period	5-day mean zonal index
31 January - 4 February	242 meters
5 February - 9 February	213 meters
10 February - 14 February	225 meters
15 February - 19 February	291 meters
20 February - 24 February	313 meters
25 February - 1 March	386 meters
2 March - 6 March	388 meters
7 March - 11 March	470 meters

(I) Predicted minimum time routes calculated at the departure time

The S-A MV and EQ MV were sailed between Tokyo and San Francisco with a constant ( maximum ) number of propeller revolutions ( 75 r.p.m. ) departing from both points at 00 hours GMT on 1, 6, 11, 16 and 21 February in 1985.

The forecasted wind/wave data were used for the period up to 72 hours after the departure time, and after that period, the 5-day mean wind/wave models classified by ZI were used in each 5 days shown in Table 6.10.

In these simulations, the following abbreviations are used:

Predicted minimum time route calculated at the departure time based on the forecasted wind/wave data followed by the 5-day mean wind/wave models classified by ZI : PMTR



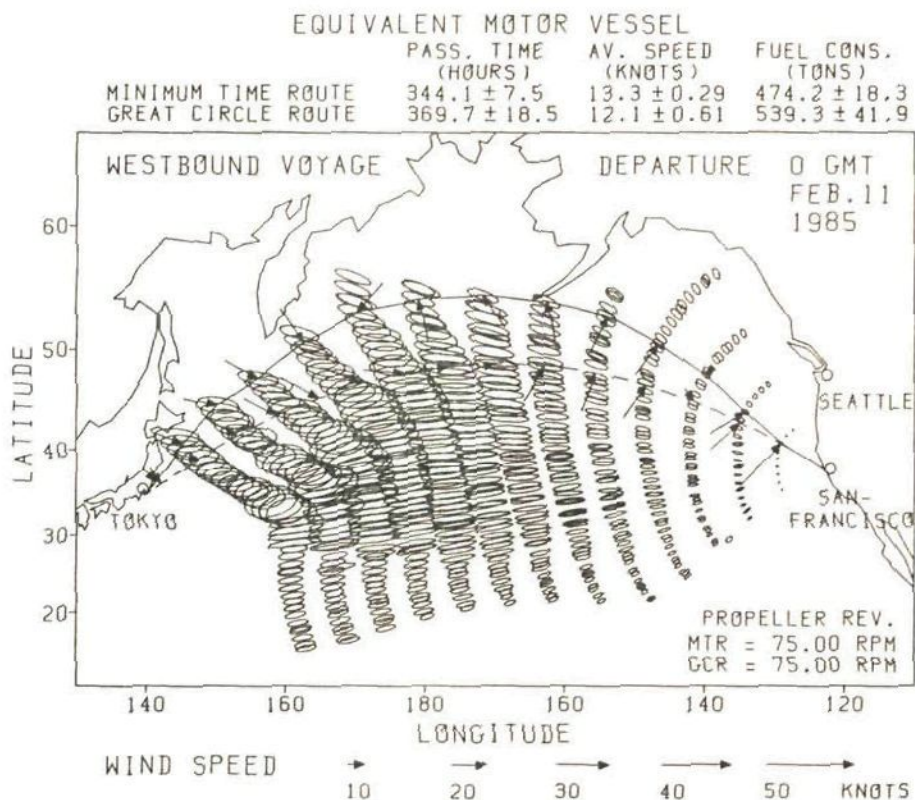


Fig. 6.26 Predicted minimum time route (PMTR) and great circle route (GCRF) of the equivalent motor vessel ( westbound voyage )

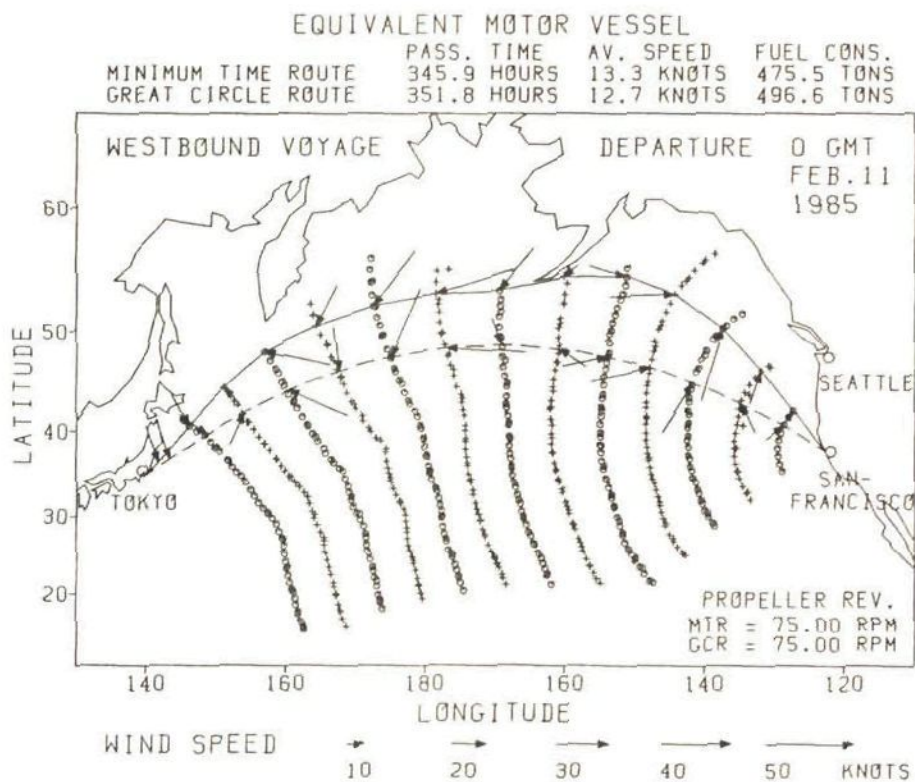


Fig. 6.27 True minimum time route (TMTR) and great circle route (GCRA) of the equivalent motor vessel ( westbound voyage )

Comparing Figs 6.24 and 6.26 with Figs 6.25 and 6.27, since the passage times on the GCRF are 17.9 hours longer than those on the GCRA, it can be seen that the wind/wave conditions of the 5-day mean wind/wave models classified by ZI were much severer than the actual ( analyzed ) wind/wave conditions for the westbound S-A MV and EQ MV sailed along the great circle route.

All predicted minimum time routes reaching the final isochrones in Figs 6.24 and 6.26 are shown in Fig.6.28 ( S-A MV ) and Fig.6.29 ( EQ MV ); the thick lines indicate PMTR from San Francisco to Tokyo.

From Figs 6.28 and 6.29, it can be seen that along the particular route, the 39% error ellipse increases as the vessel proceeds from San Francisco to Tokyo. Furthermore, we can find the discontinuities in the sizes and shapes of the 39% error ellipses at the double points of the final isochrones. ( We can also observe such discontinuities in Fig.5.6 (a)-(d). )

It is also found that near the double points of the final isochrones, the shapes of the 39% error ellipses of the northern routes are comparatively round since the ship's headings were changed largely on the northern routes, whereas those of the southern routes are comparatively slender because the changes of the ship's headings were not so large on the southern routes.

Another example of the westbound voyage is shown in Fig.6.30. In Fig.6.30, all predicted minimum time routes of the S-A MV reaching the final isochrone are depicted for the voyage departing at 00 hours GMT on 16 February 1985.

From Fig.6.30, we can find that the sizes of the 39% error ellipses of the northern routes are much larger than those of the southern routes.

On the routes depicted in Fig.6.30, the predicted positions of the points of the final isochrone as well as  $\bar{T}$ ,  $\bar{D}$ ,  $\bar{V}$ ,  $\bar{F}$ ,  $\bar{T}_D$ ,  $\sigma_T$ ,  $\sigma_V$  and  $\sigma_F$  are shown in Table 6.11 below FINAL ISOCHRONE, PASS. TIME, DISTANCE, AV. SPEED, FUEL CONS., PER OF SCW, TIME STD, AVSP STD and



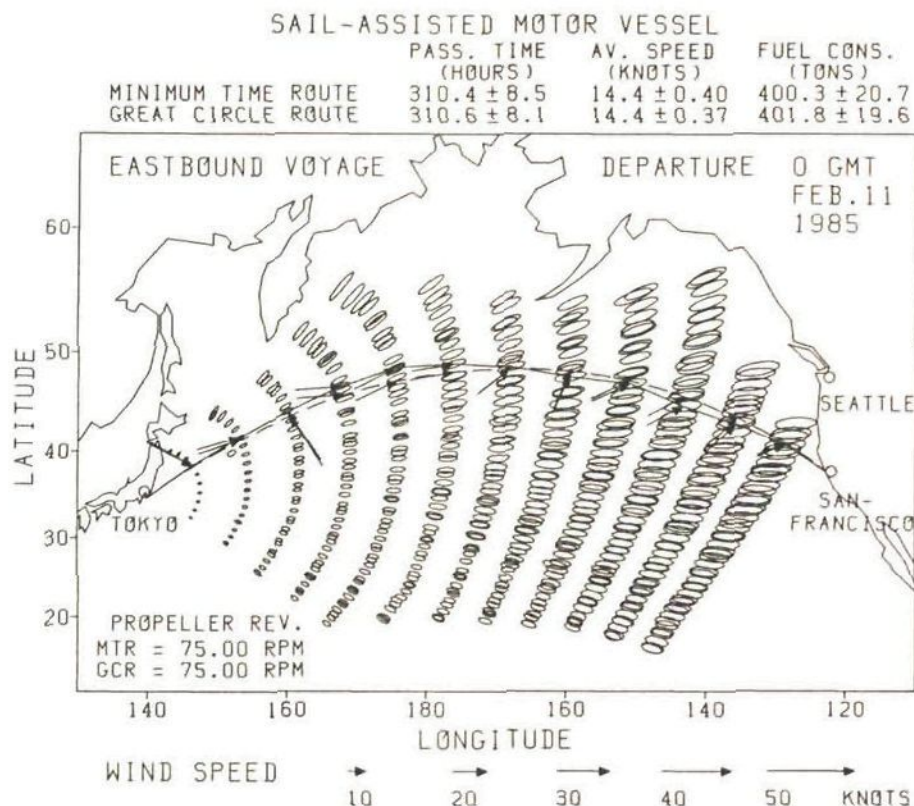


Fig. 6.31 Predicted minimum time route (PMTR) and great circle route (GCRF) of the sail-assisted motor vessel ( eastbound voyage )

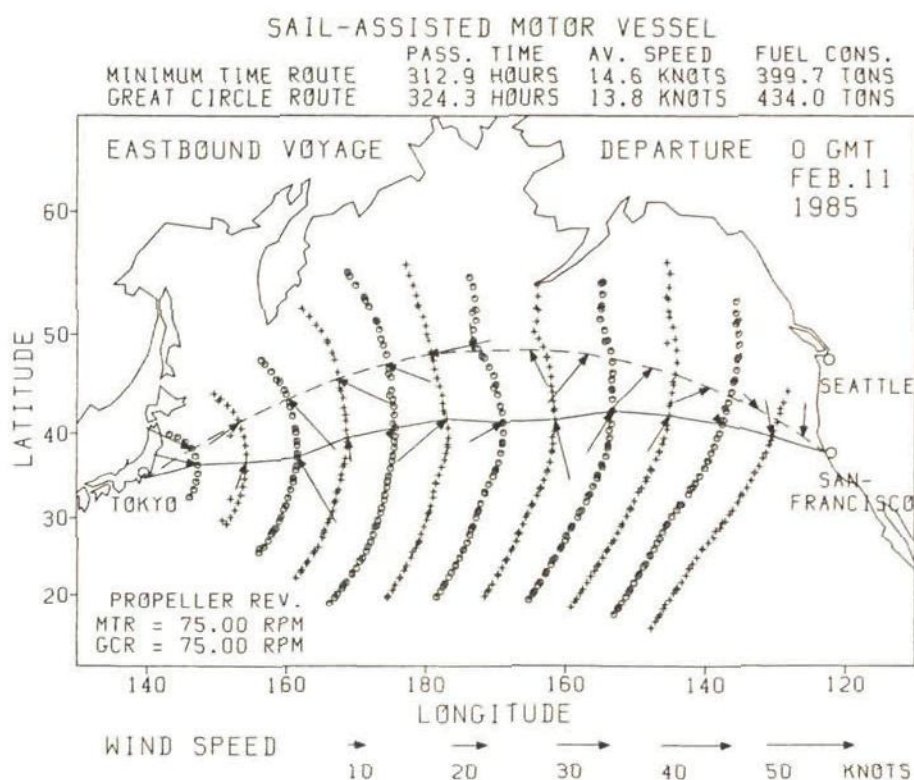


Fig. 6.32 True minimum time route (TMTR) and great circle route (GCRA) of the sail-assisted motor vessel ( eastbound voyage )



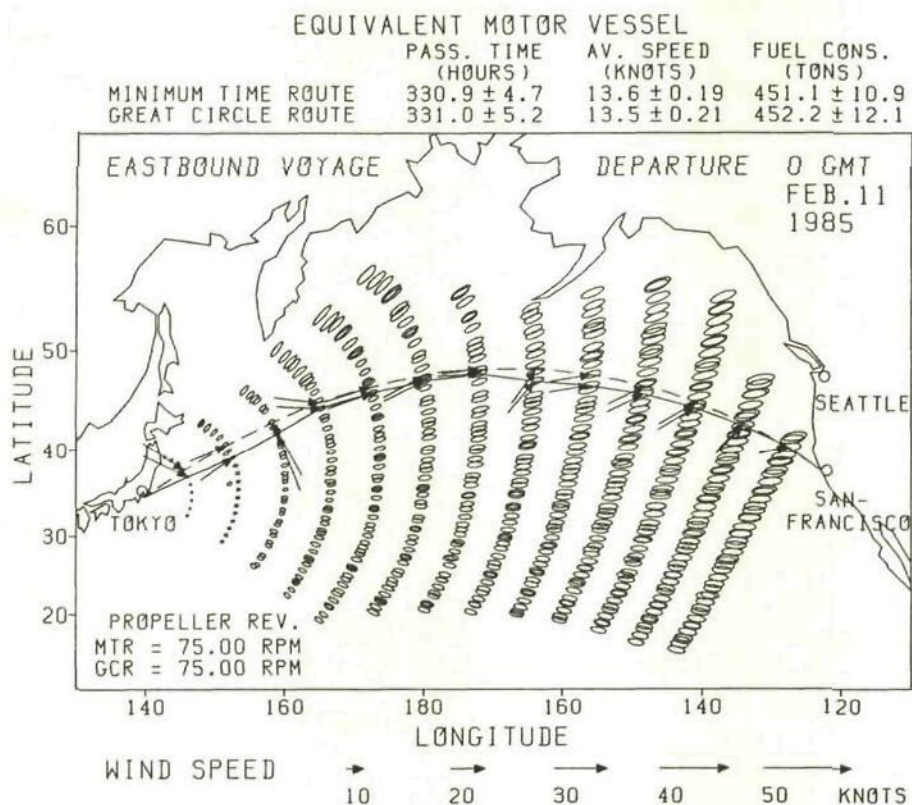


Fig. 6.33 Predicted minimum time route (PMTR) and great circle route (GCRF) of the equivalent motor vessel ( eastbound voyage )

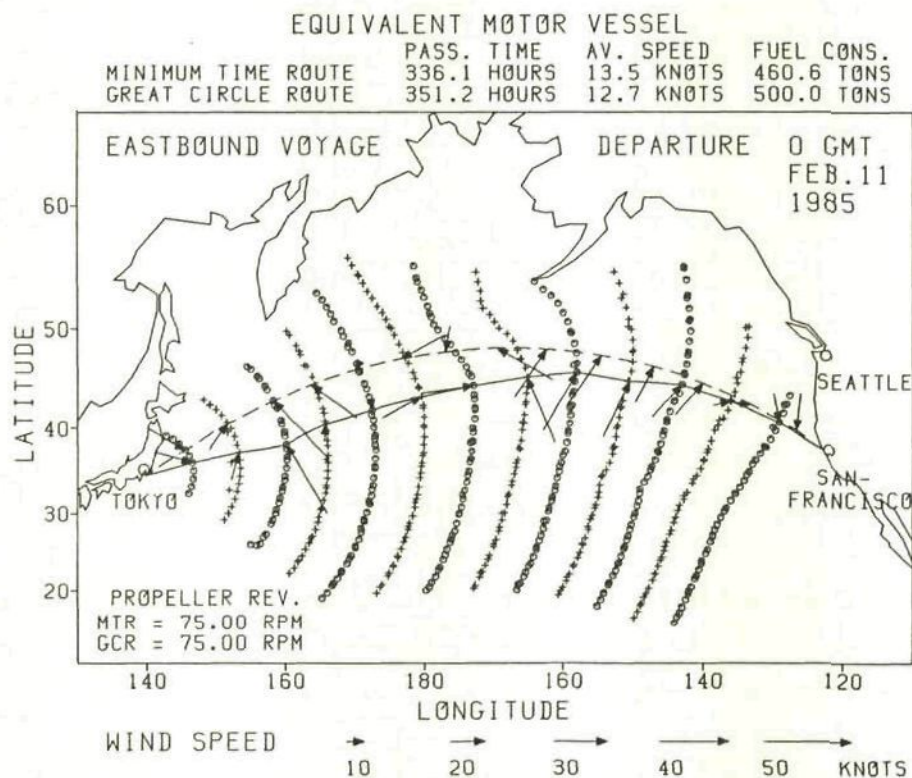


Fig. 6.34 True minimum time route (TMTR) and great circle route (GCRA) of the equivalent motor vessel ( eastbound voyage )

are much greater than those of the EQ MV. This is because the ship's speed of the S-A MV is much more sensitive than that of the EQ MV to the beam, quartering and following winds which are predominant in the eastbound voyage under the 5-day mean wind/wave models classified by ZI.

The passage times of the S-A MV and EQ MV on the GCRA are 13.7 hours and 20.2 hours longer than those on the GCRF. Thus it can be said that the actual ( analyzed ) wind/wave conditions were much more adverse than the wind/wave conditions of the 5-day mean wind/wave models classified by ZI for the eastbound vessels sailed along the great circle route.

All predicted minimum time routes reaching the final isochrones in Figs 6.31 and 6.33 are depicted in Fig.6.35 ( S-A MV ) and Fig.6.36 ( EQ MV ); the thick lines indicate PMTR from Tokyo to San Francisco.

From Figs 6.35 and 6.36, it can be seen that as no double points exist on the final isochrones in this eastbound voyage, the sizes and shapes of the 39% error ellipses change very smoothly on the final isochrones. In such a case, the standard deviation of passage time hardly becomes an important factor to determine the minimum time route.

## (II) Actual routes calculated at every updating time of the forecasts

The wind/wave forecasts by FNOG are updated every 12 hours. Thus the simulations of recalculating the minimum time route at every updating time of the forecasts were also carried out. In these simulations, the following abbreviation is used:

Actual route calculated every 12 hours based on the updated  
wind/wave forecasts followed by the 5-day mean wind/wave models  
classified by ZI : ARUF

On the ARUF, when the wind/wave forecasts were updated, a new minimum time route from the ship's position to the destination was calculated using the updated wind/wave forecasts followed by the



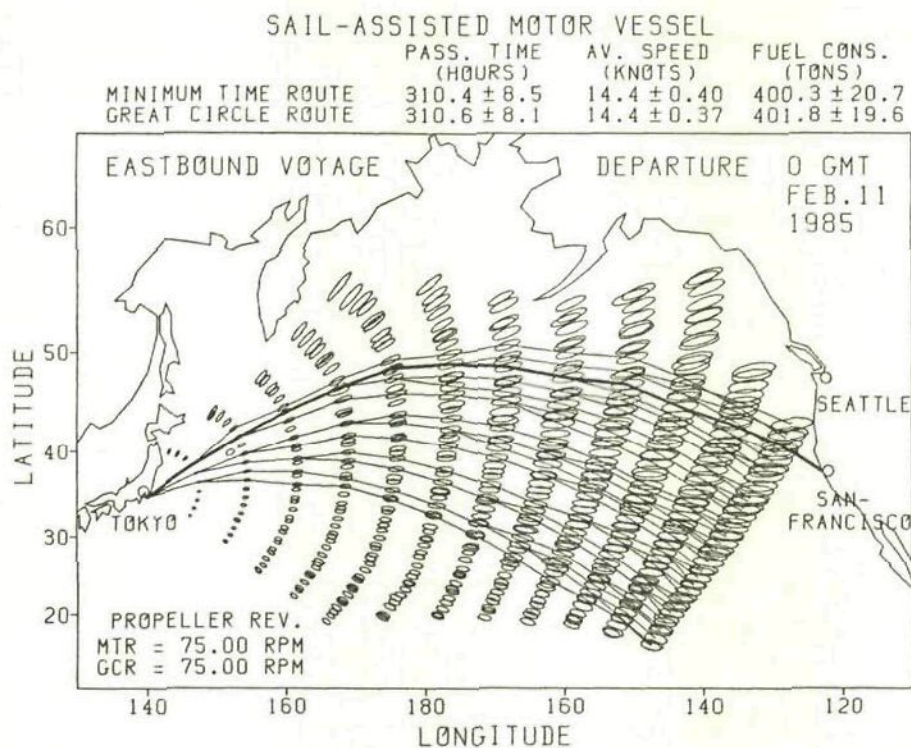


Fig. 6.35 All predicted minimum time routes of the sail-assisted motor vessel reaching the final isochrone ( eastbound voyage )

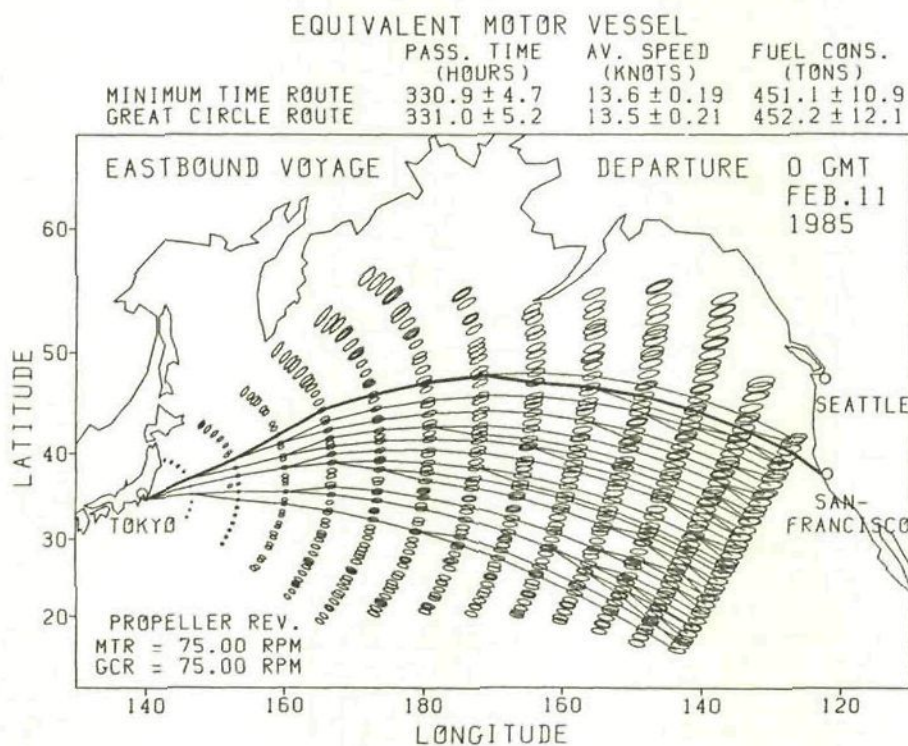


Fig. 6.36 All predicted minimum time routes of the equivalent motor vessel reaching the final isochrone ( eastbound voyage )



5-day mean wind/wave models classified by ZI. Then the ship was sailed for 12 hours under analyzed wind/wave conditions following the initial course of that minimum time route.

Since the forecasted wind/wave data for March in 1985 were not available, the ARUF were calculated for the voyages departing at 00 hours GMT on 1, 6 and 11 February in 1985.

The tracks of the ARUF and TMTR in the westbound voyage departing at 00 hours GMT on 11 February 1985 are shown in Fig.6.37 ( S-A MV ) and Fig.6.38 ( EQ MV ). In these figures, the dashed lines and solid lines denote the ARUF and TMTR, respectively. The isochrones were calculated using the analyzed wind/wave data, i.e. they are the same as those in Figs 6.25 and 6.27.

From Figs 6.37 and 6.38, it is found that although the tracks of the ARUF deviated from those of the TMTR in the first half of the voyage, they almost coincided in the latter half of the voyage. The passage times of the S-A MV and EQ MV on the ARUF were only 2.0 hours and 1.1 hours longer than those on the TMTR, respectively.

Next, the tracks of the ARUF and TMTR in the eastbound voyage departing at 00 hours GMT on 11 February 1985 are shown in Fig.6.39 ( S-A MV ) and Fig.6.40 ( EQ MV ).

From Figs 6.39 and 6.40, it can be seen that the ARUF of S-A MV and EQ MV altered their tracks southwards at about  $165^{\circ}\text{E}$  in order to avoid adverse weather on the great circle route according to information of the updated forecasts. The passage times of S-A MV and EQ MV on the ARUF were 6.8 hours and 3.8 hours longer than those on the TMTR, respectively.

Fig.6.41 shows the variations of predicted passage time and fuel consumption calculated every 12 hours on the ARUF of S-A MV in eastbound voyage shown in Fig.6.39. The variations of ship's speed and engine power are also shown in Fig.6.41.

The predicted passage time/fuel consumption represents the sum of the predicted value from the ship's position to the destination and

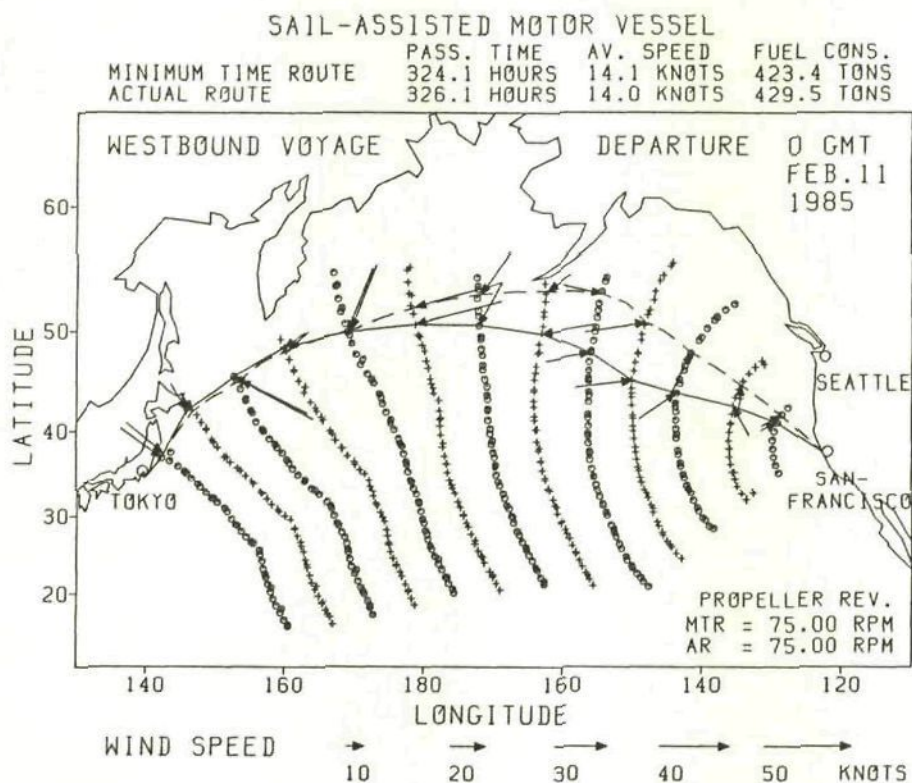


Fig. 6.37 Actual route (ARUF) [dashed line] and true minimum time route (TMTR) [solid line] of the sail-assisted motor vessel ( westbound voyage )

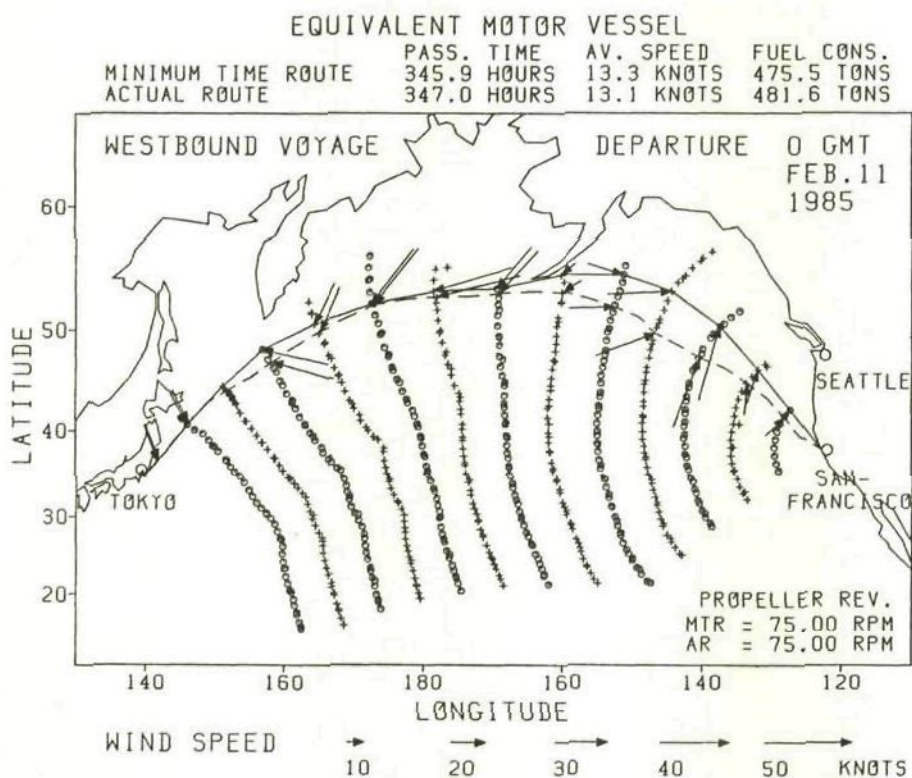


Fig. 6.38 Actual route (ARUF) [dashed line] and true minimum time route (TMTR) [solid line] of the equivalent motor vessel ( westbound voyage )



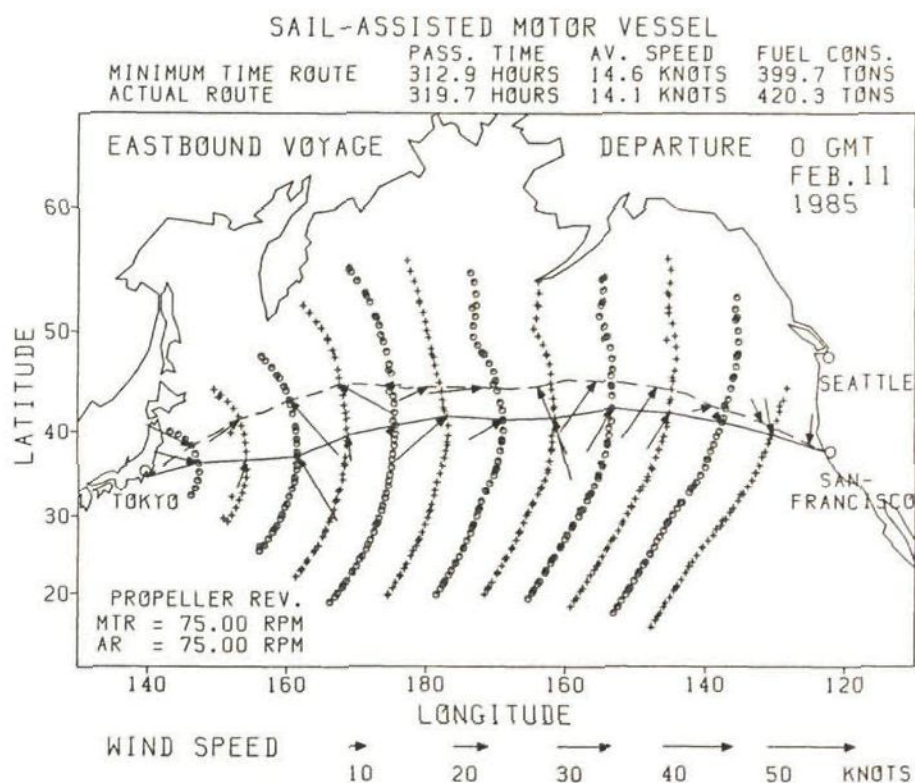


Fig. 6.39 Actual route (ARUF) [dashed line] and true minimum time route (TMTR) [solid line] of the sail-assisted motor vessel ( eastbound voyage )

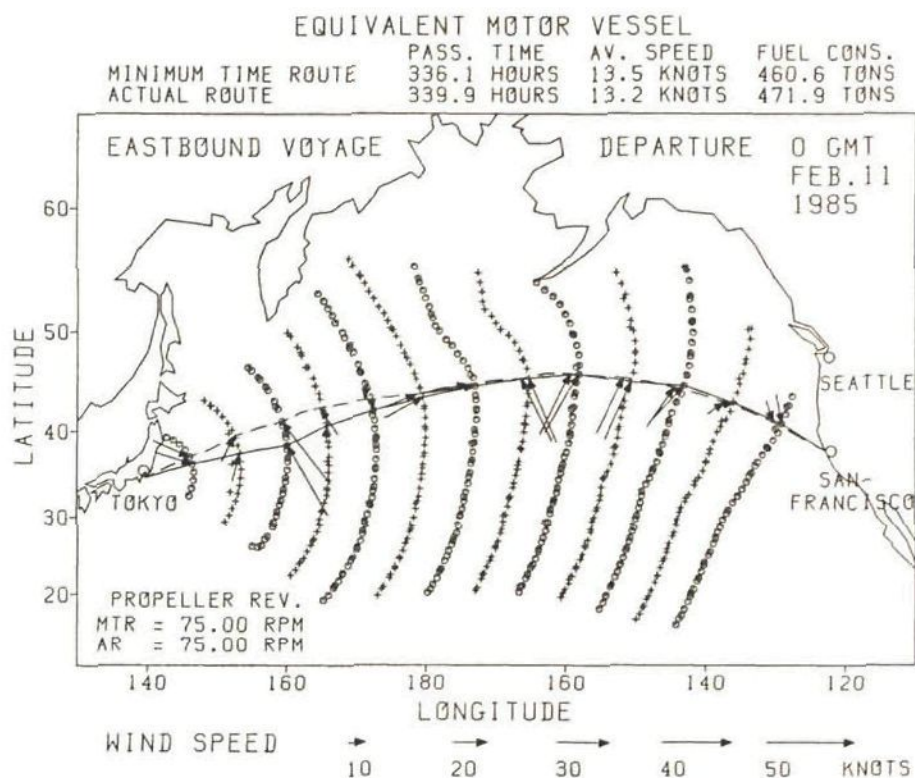


Fig. 6.40 Actual route (ARUF) [dashed line] and true minimum time route (TMTR) [solid line] of the equivalent motor vessel ( eastbound voyage )



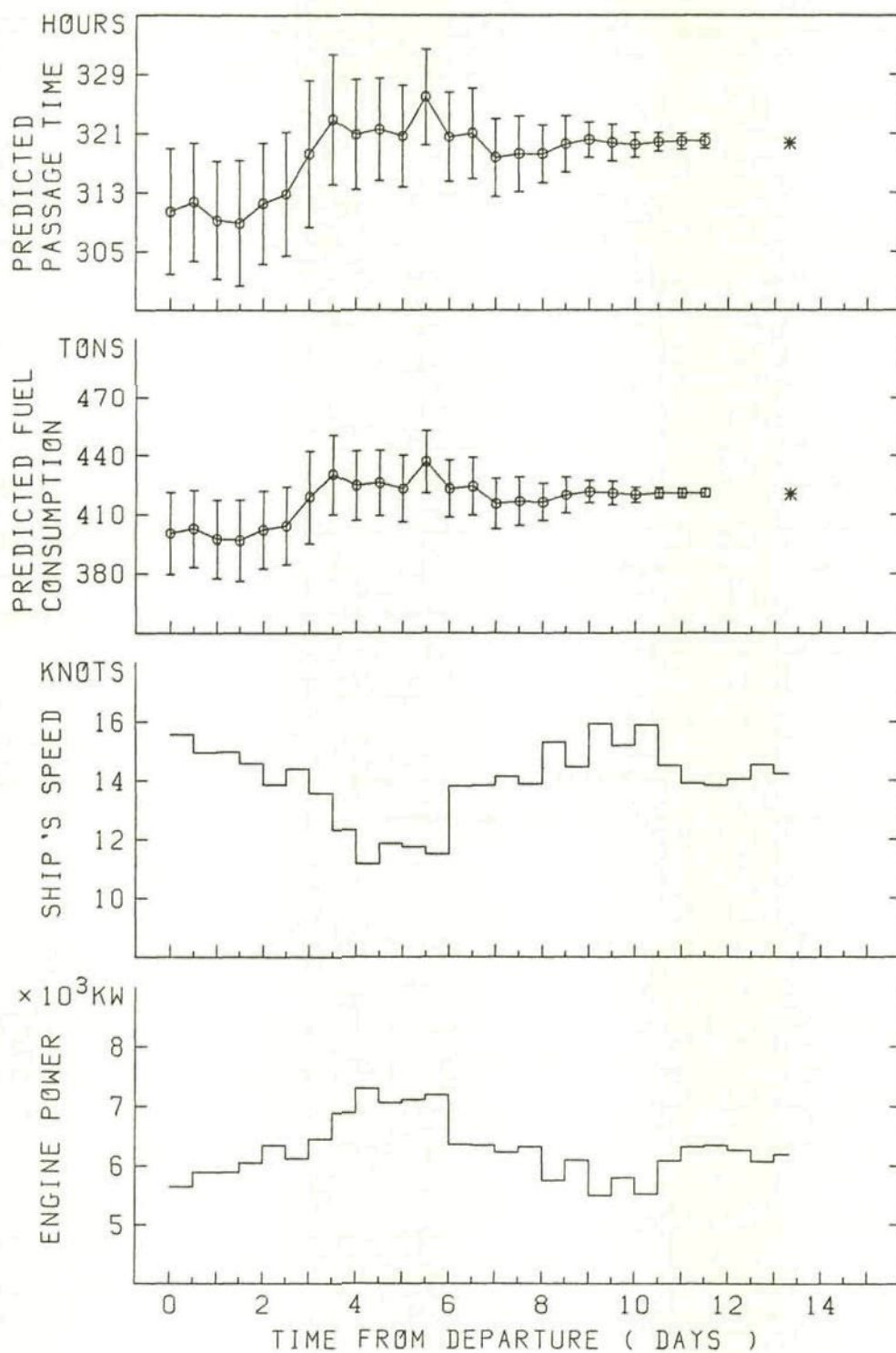


Fig. 6.41 Variations of predicted passage time and fuel consumption as well as ship's speed and engine power calculated every 12 hours on the actual route (ARUF) of the sail-assisted motor vessel ( eastbound voyage )  
( The length of the vertical segment indicates twice the standard deviation. )

the accumulated actual value from the departure point to the ship's position. The asterisks denote the actual passage time and fuel consumption.

The length of the vertical segment indicates twice the standard deviation. Since the passage time and fuel consumption are assumed to have Gaussian distributions as mentioned in 2.4.1, multiplying the length of the vertical segment by 1.96 gives the 95% confidence interval.

From Fig.6.41, it is found that the standard deviations of the passage time and fuel consumption gradually decrease as the S-A MV approaches the destination. It is also found that since rough weather was forecasted on the third and fourth day after the departure time, the predicted passage time and fuel consumption increased in those days.

In addition, it can be seen that as the number of propeller revolutions was kept constant during the voyage, the engine power increased when the ship's speed decreased, and vice versa.

### (III) Summary of minimum time routing simulations

The passage times and fuel consumptions on the PMTR, TMTR, ARUF, GCRF and GCRA of the S-A MV and EQ MV for the westbound voyages departing on 1, 6, 11, 16 and 21 February in 1985 are shown in Fig.6.42 ( passage times ) and Fig.6.43 ( fuel consumptions ).

The passage times and fuel consumptions on those routes for the eastbound voyages are shown in Fig.6.44 ( passage times ) and Fig.6.45 ( fuel consumptions ).

In Figs 6.42 - 6.45, the values on the PMTR, TMTR and ARUF are plotted on the left-hand sides, whereas the values on the GCRF and GCRA are plotted on the right-hand sides.

The length of each vertical segment indicates twice the standard deviation. The midpoint of that vertical segment ( circle or square mark ) represents the predicted passage time/fuel consumption

on the PMTR/GCRF. Multiplying the length of the vertical segment by 1.96 gives the 95% confidence interval.

On the left-hand sides in Figs 6.42 - 6.45, the passage times and fuel consumptions on the 'routes based on the predicted headings and analyzed wind/wave data' are also plotted. To represent that route, the following abbreviation is used:

Route based on the predicted headings and analyzed wind/wave data  
: RPHA

On the RPHA, the ship is sailed under the analyzed wind/wave conditions following the sequence of optimal headings predicted at the departure time using the forecasted wind/wave data followed by the 5-day mean wind/wave models classified by ZI. That is, on the RPHA, the ship follows the same sequence of headings as taken on the PMTR.

The mean values of passage times, fuel consumptions and their standard deviations in five westbound/eastbound voyages are shown in Table 6.12. ( On the ARUF, mean values in three voyages are shown. )

Concerning the westbound voyages ( Figs 6.42, 6.43 and Table 6.12 ), we can find the following facts.

(i) For both the S-A MV and EQ MV, the standard deviations of passage times and fuel consumptions on the PMTR are considerably smaller than those on the GCRF because of much better predicted wind/wave conditions.

(ii) Since the passage times and fuel consumptions on the GCRA are far smaller than those on the GCRF, it can be seen that compared with the analyzed wind/wave data, the 5-day mean wind/wave models classified by ZI were too severe for the westbound vessels sailed along the great circle route.

(iii) The passage times and fuel consumptions on the ARUF are always less than those on the RPHA. The differences of passage times and fuel consumptions between ARUF and RPHA may be regarded as



- PREDICTED MINIMUM TIME ROUTE BASED ON FORECAST DATA
- △---△ TRUE MINIMUM TIME ROUTE BASED ON ANALYSIS DATA
- \*---\* ROUTE BASED ON PREDICTED HEADINGS AND ANALYSIS DATA
- ✱-----✱ ACTUAL ROUTE BASED ON UPDATED FORECAST DATA
- GREAT CIRCLE ROUTE BASED ON FORECAST DATA
- ✱---✱ GREAT CIRCLE ROUTE BASED ON ANALYSIS DATA

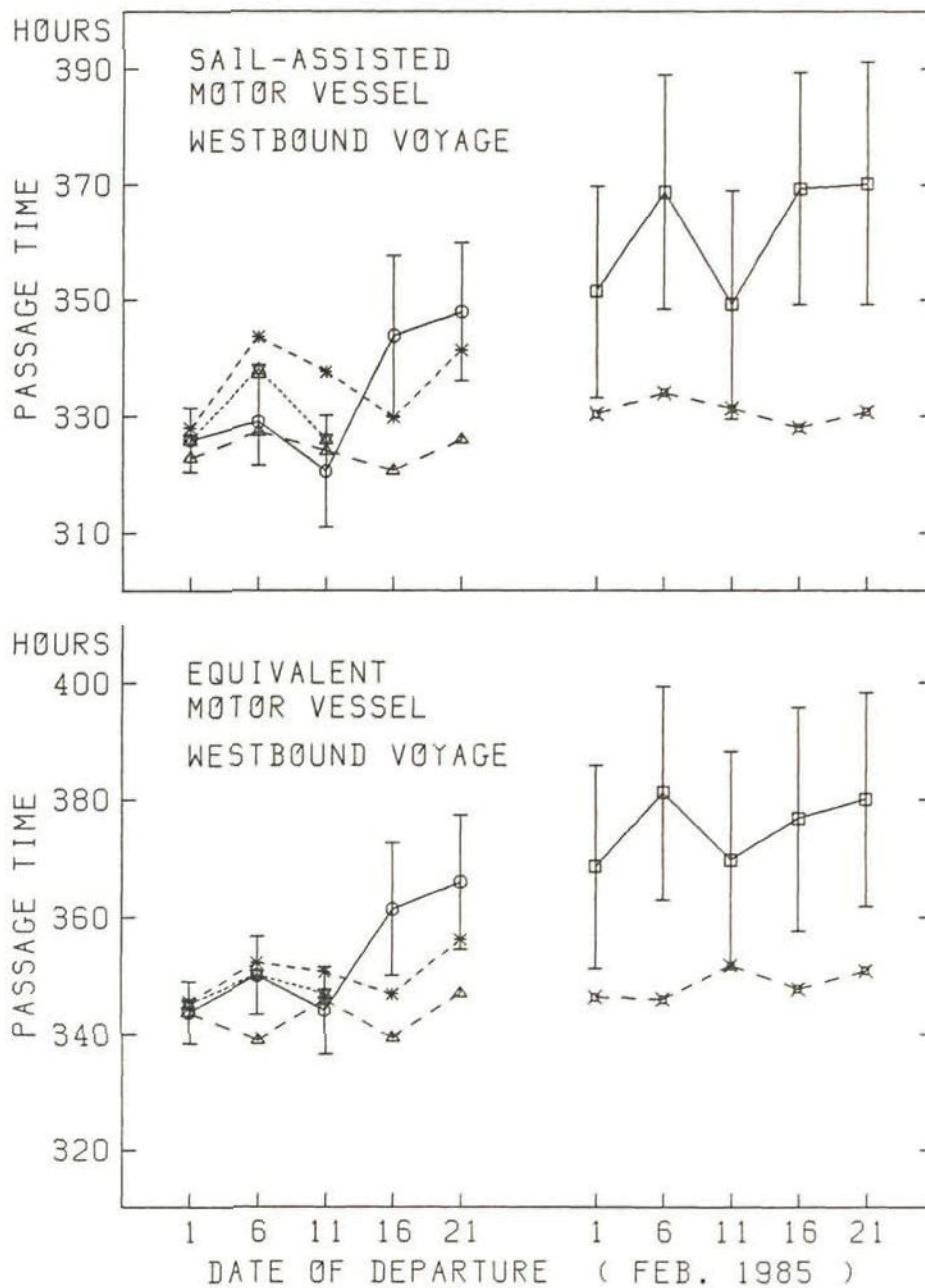


Fig. 6.42 Passage times and their standard deviations for each date of departure ( westbound voyage )

- PREDICTED MINIMUM TIME ROUTE BASED ON FORECAST DATA
- △---△ TRUE MINIMUM TIME ROUTE BASED ON ANALYSIS DATA
- \*---\* ROUTE BASED ON PREDICTED HEADINGS AND ANALYSIS DATA
- ☆---☆ ACTUAL ROUTE BASED ON UPDATED FORECAST DATA
- GREAT CIRCLE ROUTE BASED ON FORECAST DATA
- ×---× GREAT CIRCLE ROUTE BASED ON ANALYSIS DATA

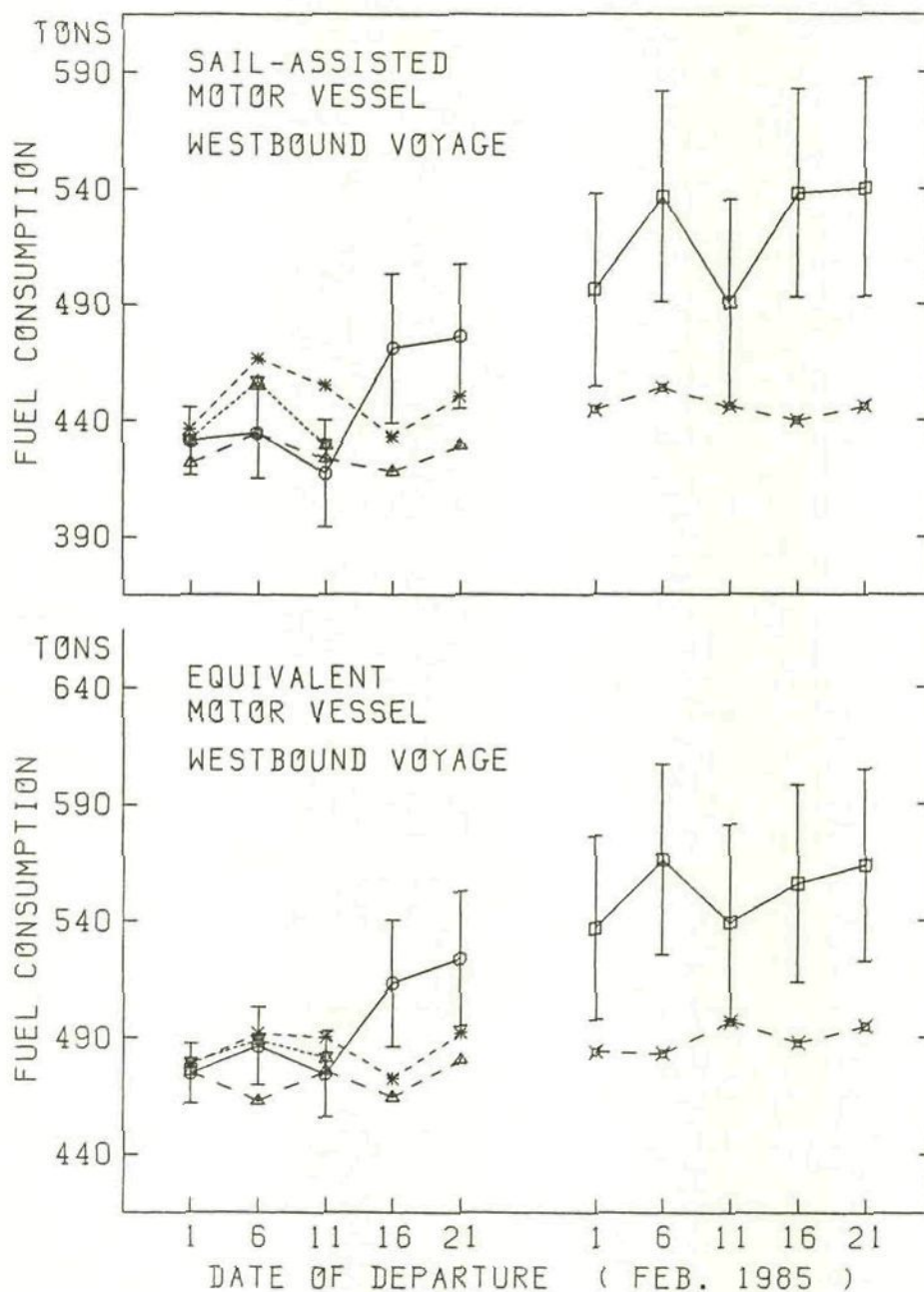


Fig. 6.43 Fuel consumptions and their standard deviations for each date of departure ( westbound voyage )

- PREDICTED MINIMUM TIME ROUTE BASED ON FORECAST DATA
- △---△ TRUE MINIMUM TIME ROUTE BASED ON ANALYSIS DATA
- \*---\* ROUTE BASED ON PREDICTED HEADINGS AND ANALYSIS DATA
- ✱-----✱ ACTUAL ROUTE BASED ON UPDATED FORECAST DATA
- GREAT CIRCLE ROUTE BASED ON FORECAST DATA
- ✕---✕ GREAT CIRCLE ROUTE BASED ON ANALYSIS DATA

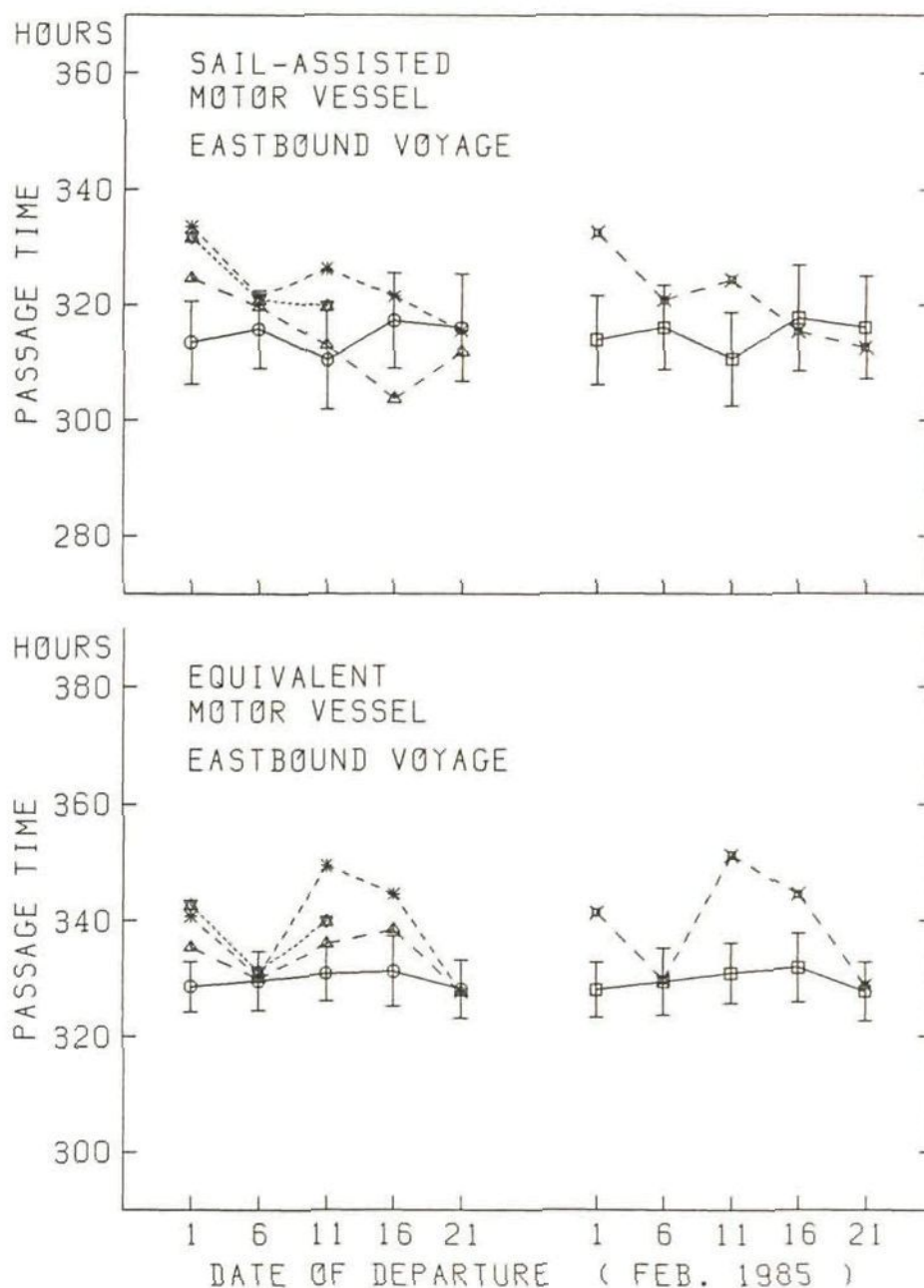


Fig. 6.44 Passage times and their standard deviations for each date of departure ( eastbound voyage )



- PREDICTED MINIMUM TIME ROUTE BASED ON FORECAST DATA
- △---△ TRUE MINIMUM TIME ROUTE BASED ON ANALYSIS DATA
- \*---\* ROUTE BASED ON PREDICTED HEADINGS AND ANALYSIS DATA
- ✱---✱ ACTUAL ROUTE BASED ON UPDATED FORECAST DATA
- GREAT CIRCLE ROUTE BASED ON FORECAST DATA
- ✱---✱ GREAT CIRCLE ROUTE BASED ON ANALYSIS DATA

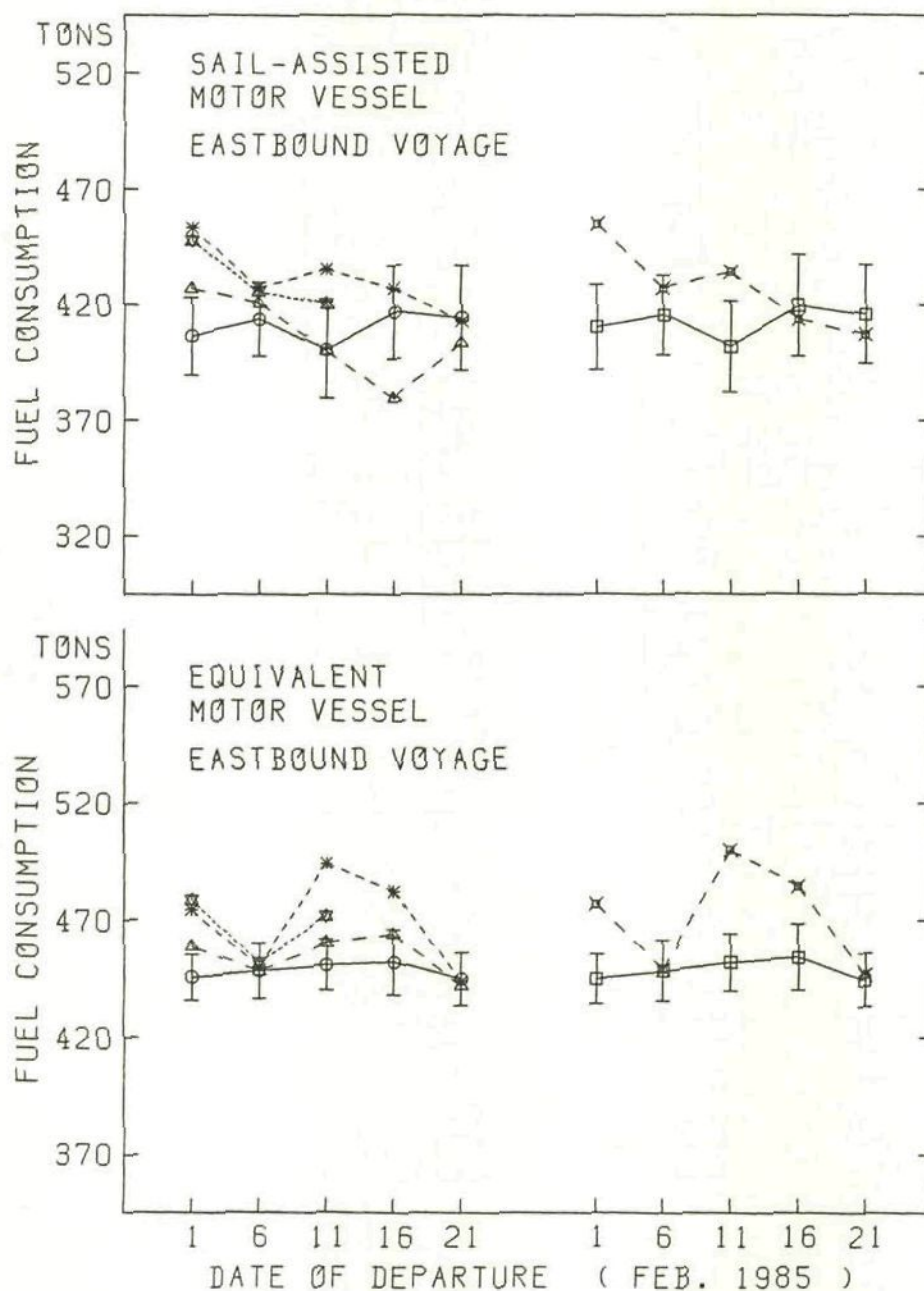


Fig. 6.45 Fuel consumptions and their standard deviations for each date of departure ( eastbound voyage )

Table 6.12 Mean values of passage times, fuel consumptions and their standard deviations in five voyages

Minimum time routing ( propeller rev. = 75 r.p.m. )

Wind/wave data : forecasted wind/wave data followed by the 5-day mean wind/wave models classified by ZI

Remarks : On the ARUF, mean values in three voyages are shown.  
S.D. means the standard deviation.

Westbound voyages

	PMTR	TMTR	RPHA	ARUF	GCRF	GCRA
<u>Sail-assisted motor vessel</u>						
Passage time (hours)	333.5	324.2	336.1	(330.0)	361.8	330.9
S.D. of pass. time (hours)	9.6	—	—	—	19.9	—
Fuel consumption (tons)	445.9	425.3	448.2	(439.3)	520.2	446.0
S.D. of fuel cons. (tons)	23.9	—	—	—	44.8	—
<u>Equivalent motor vessel</u>						
Passage time (hours)	353.1	343.0	350.3	(347.5)	375.3	348.6
S.D. of pass. time (hours)	8.4	—	—	—	18.3	—
Fuel consumption (tons)	494.4	471.6	484.9	(483.2)	552.4	489.2
S.D. of fuel cons. (tons)	20.9	—	—	—	41.1	—

Eastbound voyages

	PMTR	TMTR	RPHA	ARUF	GCRF	GCRA
<u>Sail-assisted motor vessel</u>						
Passage time (hours)	314.5	314.5	323.6	(324.1)	314.8	321.1
S.D. of pass. time (hours)	8.0	—	—	—	8.2	—
Fuel consumption (tons)	410.3	406.0	431.1	(431.1)	412.5	427.2
S.D. of fuel cons. (tons)	19.2	—	—	—	19.7	—
<u>Equivalent motor vessel</u>						
Passage time (hours)	329.8	333.4	338.6	(338.0)	329.7	339.2
S.D. of pass. time (hours)	5.0	—	—	—	5.4	—
Fuel consumption (tons)	448.6	454.9	469.2	(467.6)	449.0	471.6
S.D. of fuel cons. (tons)	11.5	—	—	—	12.3	—



the benefits by the use of information on the updated wind/wave forecasts. Particularly, in the voyage departing on 11 February, the passage time and fuel consumption of the S-A MV were saved by 11.5 hours and 25.5 tons on the ARUF compared with those on the RPHA.

Next, concerning the eastbound voyages ( Figs 6.44, 6.45 and Table 6.12 ), the following facts can be observed.

(i) Since the tracks of the PMTR almost coincided with those of the GCRF in all voyages, the predicted values/standard deviations of passage times/fuel consumptions on the PMTR and GCRF hardly differ from each other.

(ii) The standard deviations of passage times/fuel consumptions on the PMTR and GCRF of the S-A MV are larger than those of the EQ MV since the speed of the S-A MV is more sensitive than that of the EQ MV to the beam, quartering and following winds which are predominant in the eastbound voyages. On the PMTR, the standard deviations of passage time and fuel consumption of the S-A MV are 1.6 times and 1.7 times larger than those of the EQ MV on the average.

(iii) The standard deviations of passage times/fuel consumptions on the PMTR/GCRF in eastbound voyages are much smaller than those in westbound voyages because of much favorable predicted wind/wave conditions. Particularly, on the GCRF, the standard deviations of passage times in the westbound voyages are 2.4 times ( S-A MV ) and 3.4 times ( EQ MV ) larger than those in the eastbound voyages on the average.

(iv) Compared with the RPHA, the passage time and fuel oil could be saved on the ARUF except for the voyages of the EQ MV departing on 1 and 6 February. Especially, in the voyage of the EQ MV departing on 11 February, the savings of passage time and fuel oil reached 9.6 hours and 22.3 tons.

For all the routes of the S-A MV and EQ MV in all voyages, the probability of shipping green water at the bow did not exceed 0.04.



(IV) Effect of correlations between errors in wind/wave data on the standard deviations

In the aforementioned simulations of stochastic minimum time routing, the correlation coefficients calculated in 4.3.3 and 4.4.4 were used for the diagonal terms of the normalized correlation matrix  $\Phi_c(i)$ . In those simulations, we could not know how much the correlation matrix  $\Phi_c(i)$  affected the standard deviations of passage time and fuel consumption.

Thus, assuming dummy correlation coefficients for the diagonal terms of  $\Phi_c(i)$ , and changing the values of those coefficients, the effect of correlations between errors in wind/wave data on the standard deviations was investigated.

Letting all correlation coefficients in formula (4.12) be always 0.0, 0.3, 0.6 and 0.9, four simulations of stochastic minimum time routing were executed for the westbound voyage of the S-A MV departing at 00 hours GMT on 11 February 1985. The results of these simulations are shown in Figs 6.46 - 6.49.

In these simulations, the same forecasted wind/wave data, 5-day mean wind/wave models classified by ZI and their covariance matrices as used for the simulation shown in Fig.6.24 were used.

From Figs 6.46 - 6.49, it can be found that the standard deviations of passage time and fuel consumption as well as the 39% error ellipses of ship's positions increase as the correlation coefficients increase. Therefore, it can be said that the correlations between errors in wind/wave data increase the standard deviations of passage time and fuel consumption.

We can find that the standard deviations of passage time and fuel consumption in the simulation based on the actual correlation data ( Fig.6.24 ) are almost equal to those based on the correlation coefficients being 0.3 ( Fig.6.47 ).

In the simulations of this study, the correlation coefficients for the 12-hour sub-time-interval are used. When we adopt a smaller sub-time-interval ( e.g. 6 hours ), the correlation

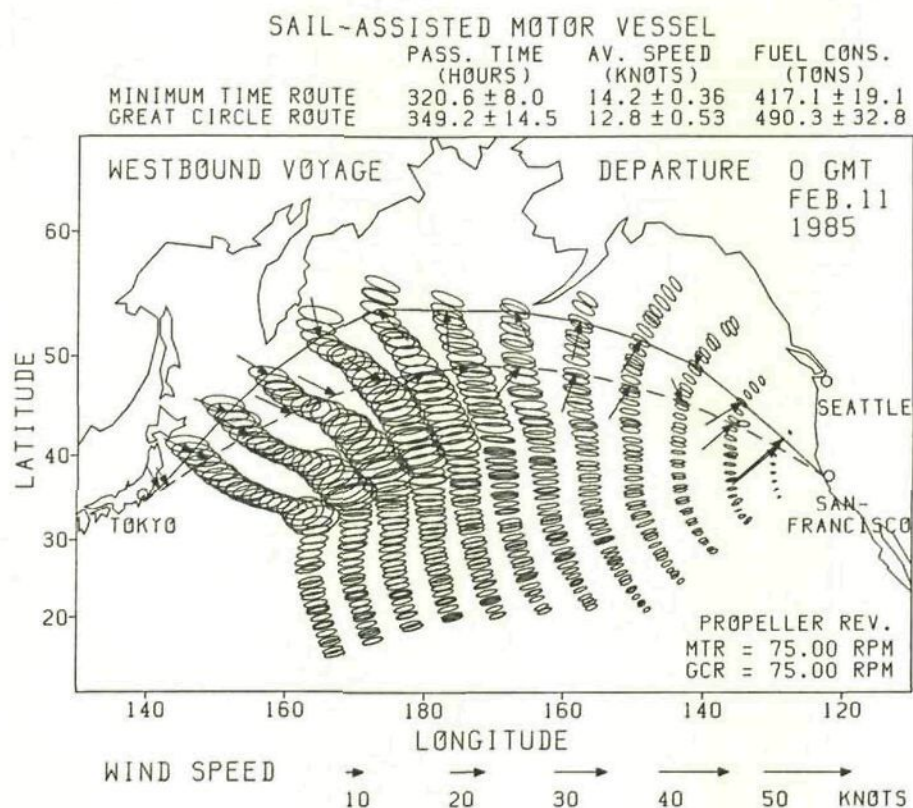


Fig. 6.46 Predicted minimum time route (PMTR) and great circle route (GCRF) of the sail-assisted motor vessel  
( correlation coefficients = 0.0; westbound voyage )

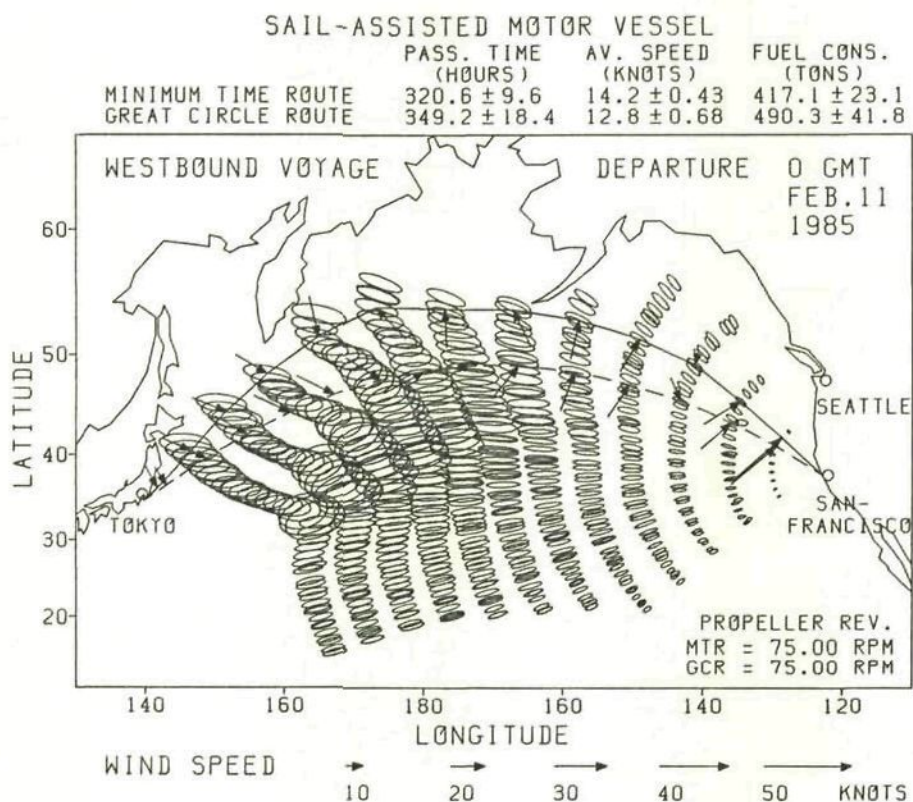


Fig. 6.47 Predicted minimum time route (PMTR) and great circle route (GCRF) of the sail-assisted motor vessel  
( correlation coefficients = 0.3; westbound voyage )



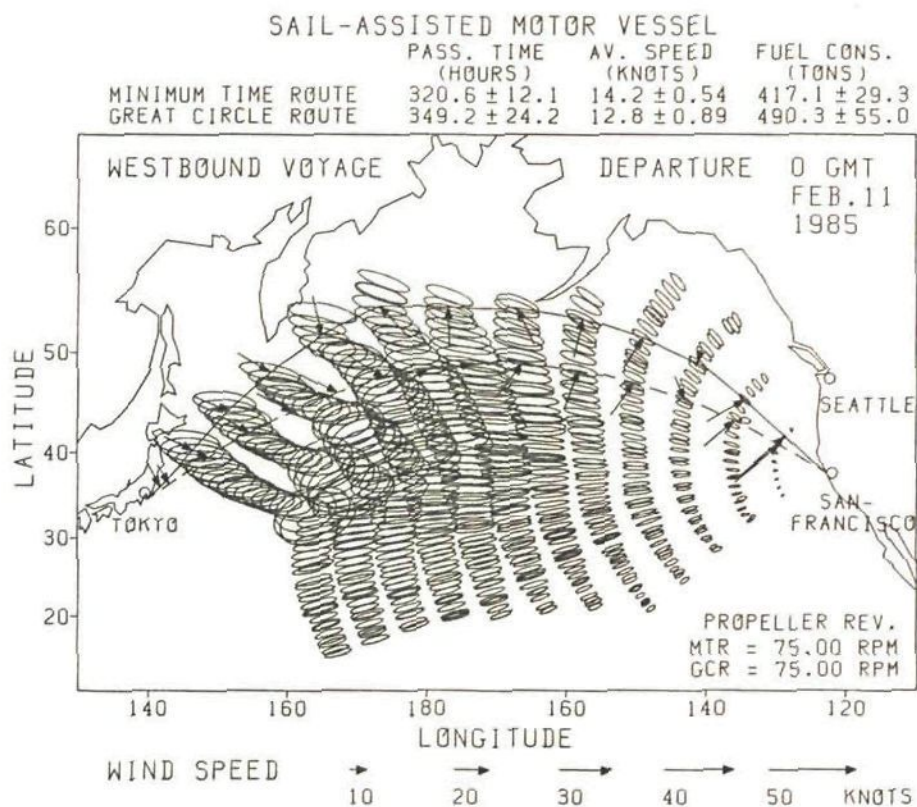


Fig. 6.48 Predicted minimum time route (PMTR) and great circle route (GCRF) of the sail-assisted motor vessel  
( correlation coefficients = 0.6; westbound voyage )

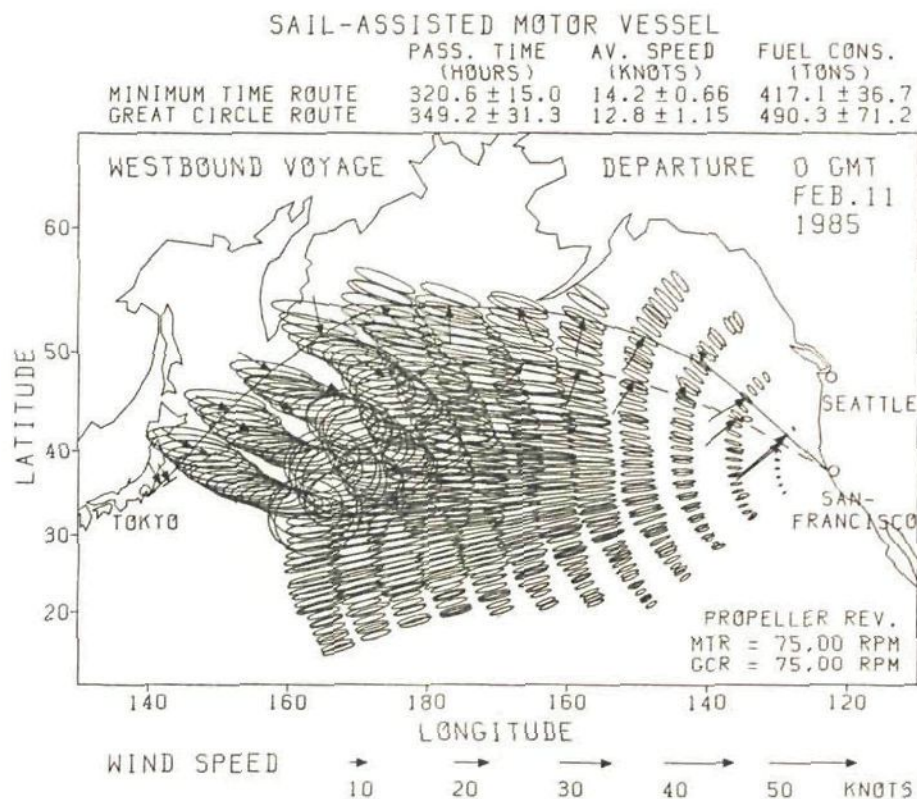


Fig. 6.49 Predicted minimum time route (PMTR) and great circle route (GCRF) of the sail-assisted motor vessel  
( correlation coefficients = 0.9; westbound voyage )



coefficients become larger as a matter of course. In that case, the standard deviations of passage time and fuel consumption calculated without taking into account the correlations will become considerably smaller than the correct standard deviations.

As was shown in the above simulations, it can be understood that the correlations between errors in wind/wave data play an important role in estimating the standard deviations of passage time and fuel consumption.

#### 6.3.2 Minimum time routing using forecasted wind/wave data followed by the 1-month mean wind/wave data

In this subsection, using the forecasted wind/wave data followed by the 1-month mean wind/wave data, the simulations of stochastic minimum time routing are carried out in the same manner as mentioned in subsection 6.3.1.

The S-A MV and EQ MV were sailed between Tokyo and San Francisco with a constant ( maximum ) number of propeller revolutions ( 75 r.p.m. ) departing from both points at 00 hours GMT on 1, 6, 11, 16 and 21 February in 1985. The 1-month mean wind/wave data for February shown in Fig.4.29 were used after the 72-hour wind/wave forecasts.

In these simulations, the following abbreviations are used:

Predicted minimum time route calculated at the departure time based on the forecasted wind/wave data followed by the 1-month mean wind/wave data : PMTR

Great circle route calculated at the departure time based on the forecasted wind/wave data followed by the 1-month mean wind/wave data : GCRF

Actual route calculated every 12 hours based on the updated wind/wave forecasts followed by the 1-month mean wind/wave data : ARUF

Route based on the predicted headings and analyzed wind/wave data  
: RPHA

As the results of the simulations on the PMTR, GCRF, ARUF and RPHA were not very different from those in subsection 6.3.1, the details of the simulations are omitted here.

The passage times and fuel consumptions on the PMTR, TMTR, RPHA, ARUF, GCRF and GCRA of the S-A MV and EQ MV for the westbound voyages departing on 1, 6, 11, 16 and 21 February in 1985 are shown in Fig.6.50 ( passage times ) and Fig.6.51 ( fuel consumptions ). The passage times and fuel consumptions on those routes for the eastbound voyages are shown in Fig.6.52 ( passage times ) and Fig.6.53 ( fuel consumptions ).

The mean values of passage times, fuel consumptions and their standard deviations in five westbound/eastbound voyages are shown in Table 6.13. ( On the ARUF, mean values in three voyages are shown. )

Regarding the westbound voyages ( Figs 6.50, 6.51 and Table 6.13 ), the following facts can be seen.

(i) For both the S-A MV and EQ MV, the standard deviations of passage times and fuel consumptions on the PMTR are much less than those on the GCRF because of much favorable predicted wind/wave conditions.

(ii) Compared with Figs 6.42 and 6.43, the predicted values and standard deviations of passage times and fuel consumptions on the PMTR/GCRF of S-A MV/EQ MV are considerably smaller in Figs 6.50 and 6.51 for most of the voyages. Hence, it can be seen that the wind/wave conditions of the 5-day mean wind/wave models classified by ZI used for the simulations were severer than those of the 1-month mean wind/wave data for the westbound vessels.

(iii) Since all passage times and fuel consumptions on the ARUF were less than those on the RPHA, it can be said that the use of updated forecasts was always effective to save passage time and fuel oil.



- PREDICTED MINIMUM TIME ROUTE BASED ON FORECAST DATA
- △---△ TRUE MINIMUM TIME ROUTE BASED ON ANALYSIS DATA
- \*---\* ROUTE BASED ON PREDICTED HEADINGS AND ANALYSIS DATA
- ☆---☆ ACTUAL ROUTE BASED ON UPDATED FORECAST DATA
- GREAT CIRCLE ROUTE BASED ON FORECAST DATA
- ×---× GREAT CIRCLE ROUTE BASED ON ANALYSIS DATA

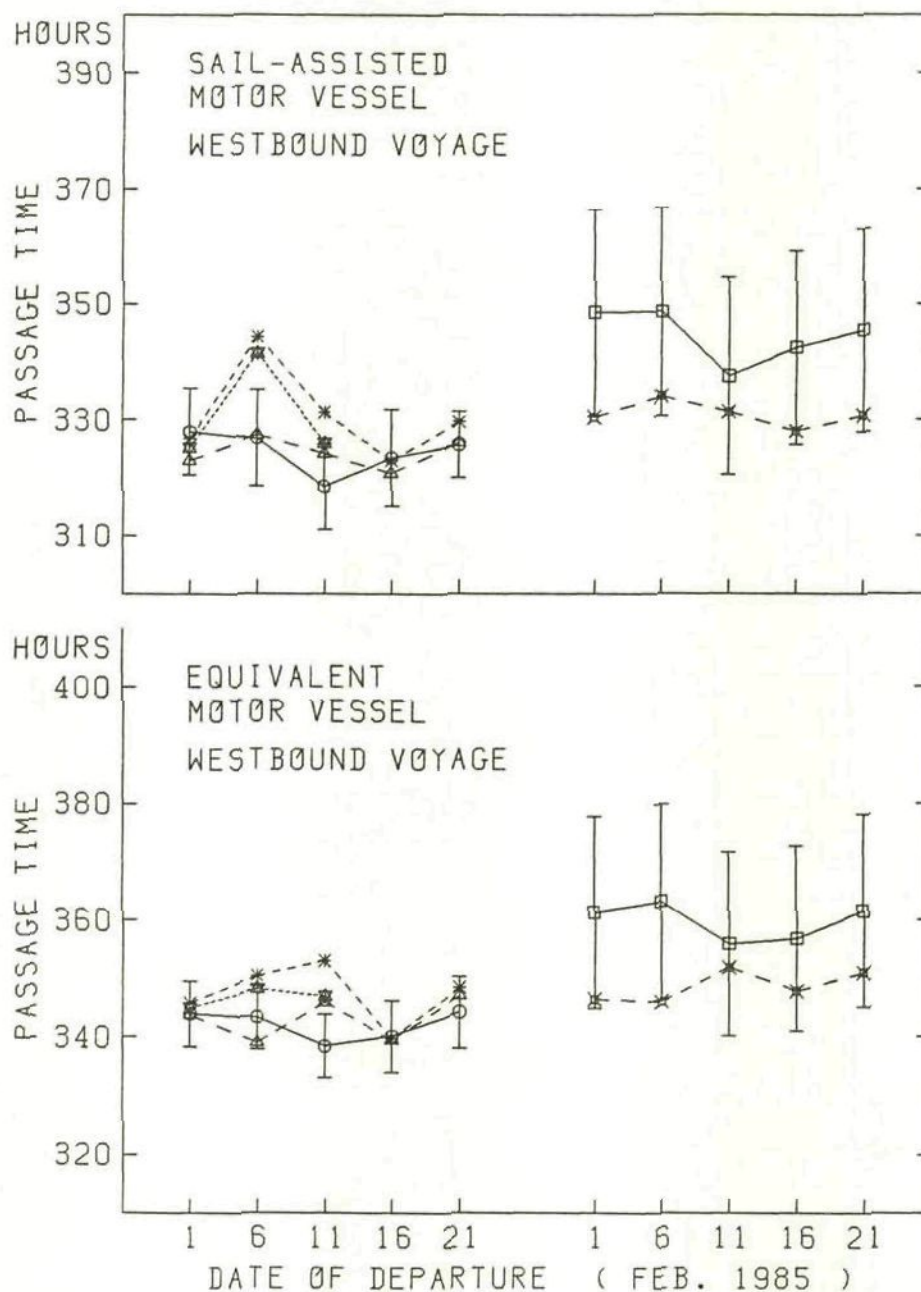


Fig. 6.50 Passage times and their standard deviations for each date of departure ( westbound voyage )



- PREDICTED MINIMUM TIME ROUTE BASED ON FORECAST DATA
- △---△ TRUE MINIMUM TIME ROUTE BASED ON ANALYSIS DATA
- \*---\* ROUTE BASED ON PREDICTED HEADINGS AND ANALYSIS DATA
- ×---× ACTUAL ROUTE BASED ON UPDATED FORECAST DATA
- GREAT CIRCLE ROUTE BASED ON FORECAST DATA
- ×---× GREAT CIRCLE ROUTE BASED ON ANALYSIS DATA

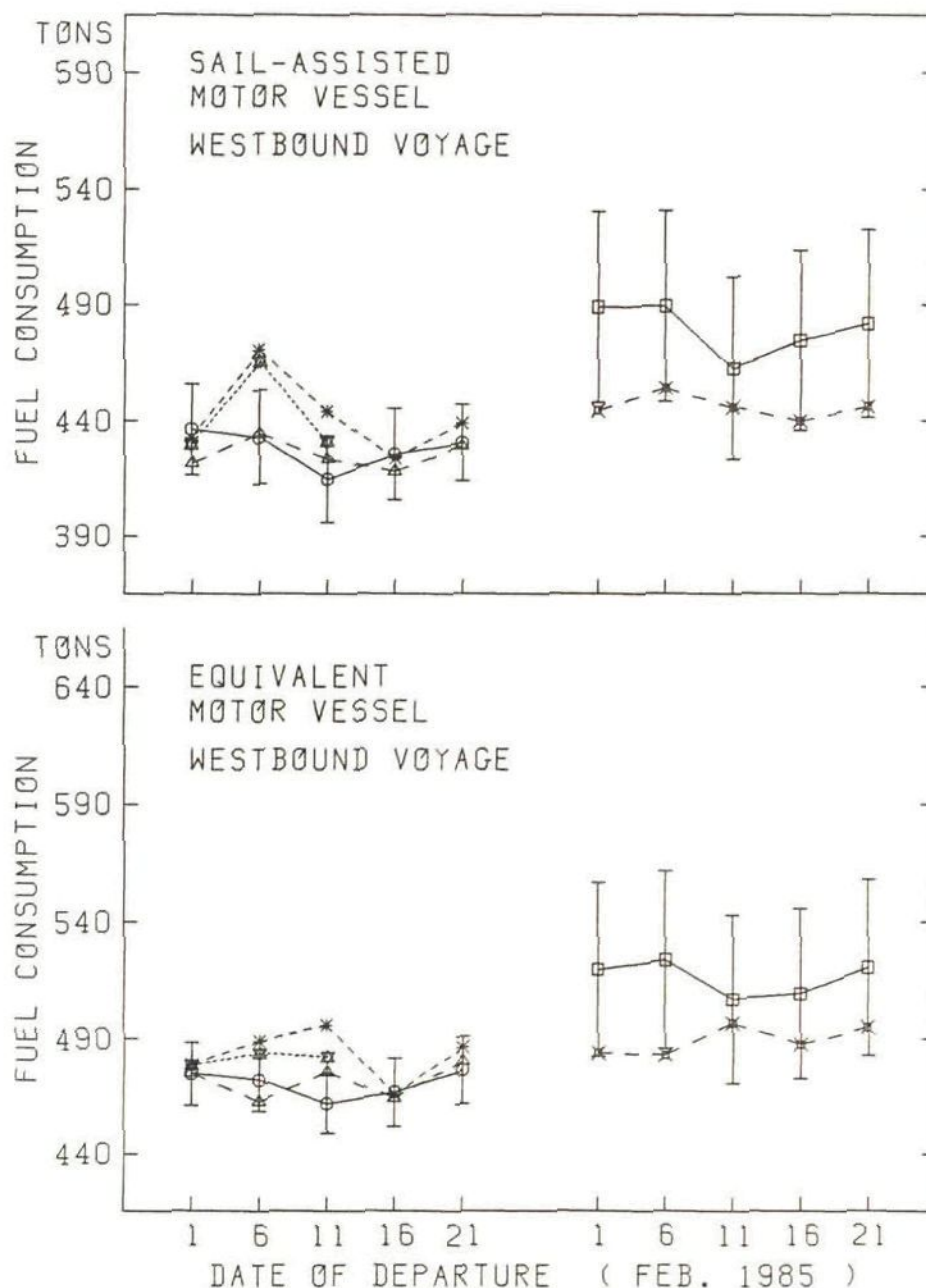


Fig. 6.51 Fuel consumptions and their standard deviations for each date of departure ( westbound voyage )

- PREDICTED MINIMUM TIME ROUTE BASED ON FORECAST DATA
- △---△ TRUE MINIMUM TIME ROUTE BASED ON ANALYSIS DATA
- \*---\* ROUTE BASED ON PREDICTED HEADINGS AND ANALYSIS DATA
- ✱---✱ ACTUAL ROUTE BASED ON UPDATED FORECAST DATA
- GREAT CIRCLE ROUTE BASED ON FORECAST DATA
- ✕---✕ GREAT CIRCLE ROUTE BASED ON ANALYSIS DATA

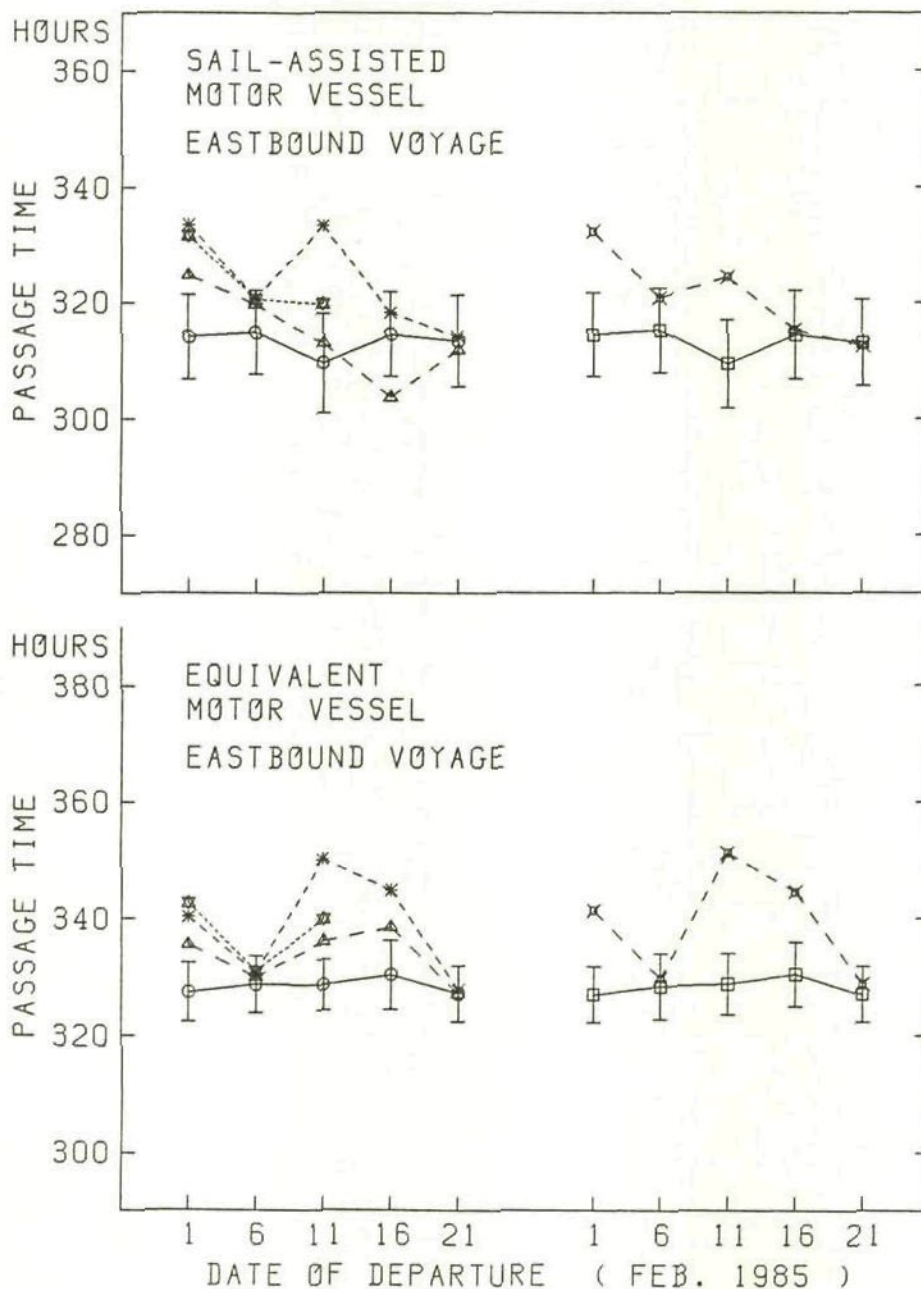


Fig. 6.52 Passage times and their standard deviations for each date of departure ( eastbound voyage )

- PREDICTED MINIMUM TIME ROUTE BASED ON FORECAST DATA
- △---△ TRUE MINIMUM TIME ROUTE BASED ON ANALYSIS DATA
- \*---\* ROUTE BASED ON PREDICTED HEADINGS AND ANALYSIS DATA
- ☆---☆ ACTUAL ROUTE BASED ON UPDATED FORECAST DATA
- GREAT CIRCLE ROUTE BASED ON FORECAST DATA
- ×---× GREAT CIRCLE ROUTE BASED ON ANALYSIS DATA

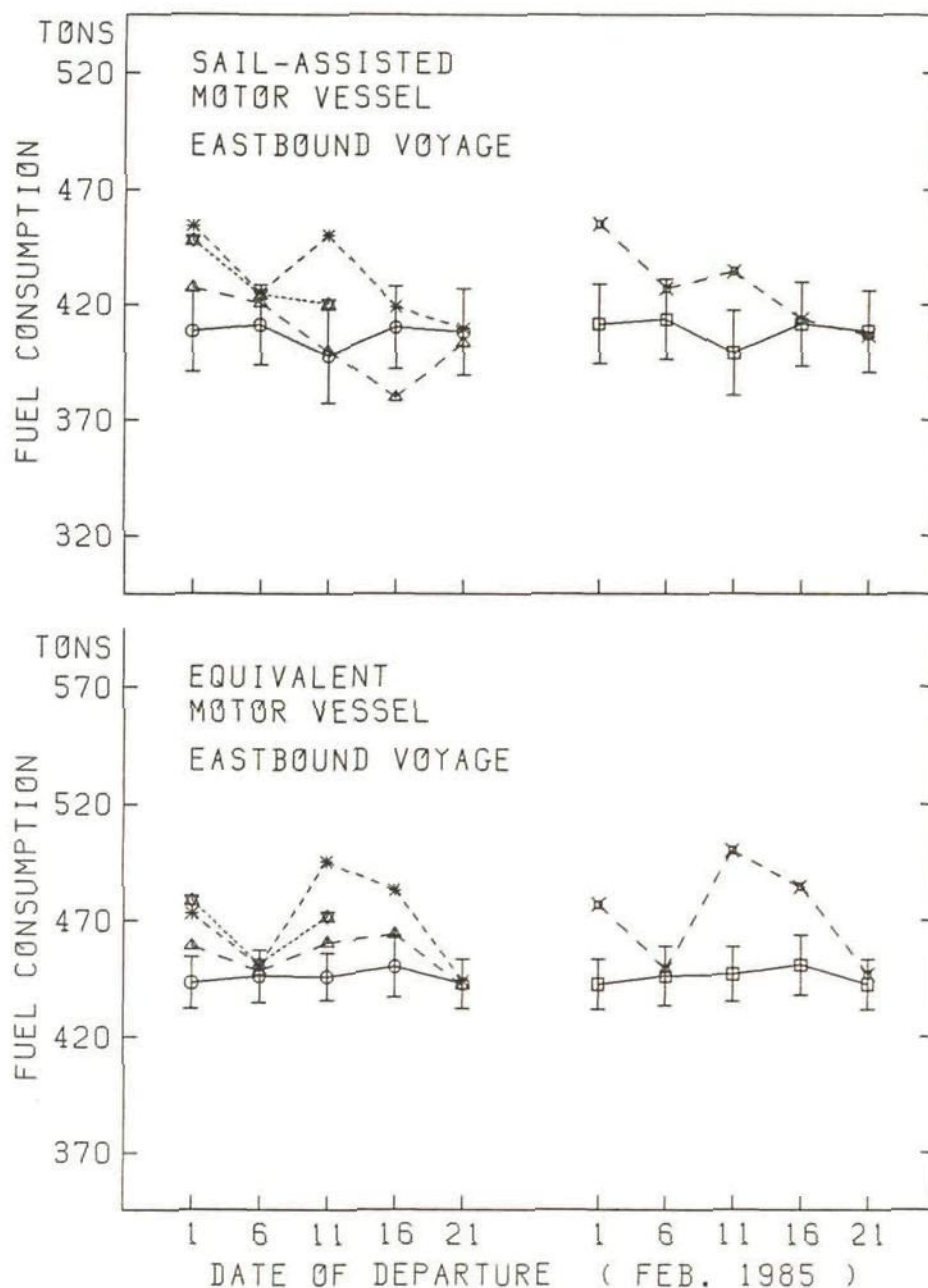


Fig. 6.53 Fuel consumptions and their standard deviations for each date of departure ( eastbound voyage )



Table 6.13 Mean values of passage times, fuel consumptions and their standard deviations in five voyages

Minimum time routing ( propeller rev. = 75 r.p.m. )

Wind/wave data : forecasted wind/wave data followed by the 1-month mean wind/wave data

Remarks : On the ARUF, mean values in three voyages are shown.  
S.D. means the standard deviation.

Westbound voyages

	PMTR	TMTR	RPHA	ARUF	GCRF	GCRA
<u>Sail-assisted motor vessel</u>						
Passage time (hours)	324.4	324.2	330.9	(330.9)	344.5	330.9
S.D. of pass. time (hours)	7.4	—	—	—	17.4	—
Fuel consumption (tons)	427.9	425.3	441.9	(441.9)	479.4	446.0
S.D. of fuel cons. (tons)	19.0	—	—	—	39.9	—
<u>Equivalent motor vessel</u>						
Passage time (hours)	342.0	343.0	347.5	(346.7)	359.7	348.6
S.D. of pass. time (hours)	5.7	—	—	—	16.3	—
Fuel consumption (tons)	470.4	471.6	483.2	(481.5)	516.0	489.2
S.D. of fuel cons. (tons)	13.8	—	—	—	37.1	—

Eastbound voyages

	PMTR	TMTR	RPHA	ARUF	GCRF	GCRA
<u>Sail-assisted motor vessel</u>						
Passage time (hours)	313.2	314.5	323.9	(323.9)	313.4	321.1
S.D. of pass. time (hours)	7.6	—	—	—	7.4	—
Fuel consumption (tons)	406.9	406.0	431.3	(430.7)	408.8	427.2
S.D. of fuel cons. (tons)	18.3	—	—	—	17.8	—
<u>Equivalent motor vessel</u>						
Passage time (hours)	328.5	333.4	338.8	(337.9)	328.3	339.2
S.D. of pass. time (hours)	5.0	—	—	—	5.2	—
Fuel consumption (tons)	445.7	454.9	469.3	(467.4)	445.8	471.6
S.D. of fuel cons. (tons)	11.3	—	—	—	11.8	—

Next, regarding the eastbound voyages ( Figs 6.52, 6.53 and Table 6.13 ), we can find the following facts.

(i) As the tracks of the PMTR almost coincide with those of GCRF in all voyages, the predicted values/standard deviations of passage times/fuel consumptions on both routes are hardly different from each other.

(ii) The standard deviations of passage times/fuel consumptions on the GCRF in eastbound voyages are much smaller than those in westbound voyages because of much better predicted wind/wave conditions.

(iii) The predicted values and standard deviations of passage times and fuel consumptions on the PMTR/GCRF of S-A MV/EQ MV are nearly the same as those in Figs 6.44 and 6.45. Therefore, it is found that the 1-month mean wind/wave data provided almost the same wind/wave conditions as the 5-day mean wind/wave models classified by ZI for the eastbound vessels.

(iv) The passage times and fuel consumptions on the ARUF are smaller than those on the RPHA except for the voyages of the EQ MV departing on 1 and 6 February. Particularly in the voyage departing on 11 February, compared with the RPHA, the savings of passage time and fuel oil on the ARUF reached 13.6 hours, 29.3 tons for the S-A MV and 10.3 hours, 23.4 tons for the EQ MV.

For all the routes of the S-A MV and EQ MV in all voyages, the probability of shipping green water at the bow did not exceed 0.04.

#### 6.3.3 Minimum fuel routing using forecasted wind/wave data followed by the 5-day mean wind/wave models classified by ZI

In this subsection, using the forecasted wind/wave data followed by the 5-day mean wind/wave models classified by ZI, simulations of stochastic minimum fuel routing are executed.



Referring to the objective function for stochastic minimum fuel routing proposed in Section 2.5, the following objective function may be considered for the S-A MV and EQ MV:

$$J = \bar{F} + w_1 \sigma_F + w_2 \bar{T}_D + w_3 (\bar{T} - T_s)^2 \quad (6.3)$$

where  $\bar{F}$  : predicted fuel consumption

$\sigma_F$  : standard deviation of fuel consumption

$\bar{T}_D$  : predicted period in which the probability of shipping green water at the bow exceeds 0.04

$\bar{T}$  : predicted passage time

$T_s$  : specified passage time

$w_1$  : weighting coefficient for the uncertainty of fuel consumption

$w_2$  : weighting coefficient for the risk of damage due to shipping green water

$w_3$  : weighting coefficient for the delay penalty

As stated in 2.5, the values of  $w_1$ ,  $w_2$  and  $w_3$  depend on the evaluation of the shipmaster/shipowner for the uncertainty of fuel consumption, risk of damage and loss due to delay, respectively. Hence, it seems difficult to give appropriate values to  $w_1$ ,  $w_2$  and  $w_3$  in the simulations.

Thus  $w_1$  and  $w_2$  were set to zeros, and  $w_3$  was assumed as follows.

$$w_3 = \infty \quad \text{if } \bar{T} > T_s$$

$$w_3 = 0 \quad \text{if } \bar{T} \leq T_s$$

In order to save computing time, the Algorithm (II) described in 2.3.2 was adopted. That is, a suitable number of propeller revolutions was set and then corrected so as to get the minimum predicted passage time  $\bar{T}_{min}$  as close as possible to the specified passage time  $T_s$ .

When  $|T_s - \bar{T}_{min}|$  became small enough, the calculation was stopped.

As mentioned in 6.3.1,  $\bar{T}$ ,  $\bar{D}$ ,  $\bar{V}$ ,  $\bar{F}$ ,  $\bar{T}_D$ ,  $\sigma_T$ ,  $\sigma_V$  and  $\sigma_F$  on all the routes reaching the destination from the departure point via points



of the final isochrone were computed and tabulated. Although  $\sigma_f$  and  $\bar{T}_0$  were not taken into account in determining the minimum fuel route, those tabulated values were thoroughly investigated.

(I) Predicted minimum fuel routes calculated at the departure time

The S-A MV and EQ MV were sailed between Tokyo and San Francisco departing from both points at 00 hours GMT on 11 February in 1985.

The passage times were specified as 369.7 hours and 351.2 hours in the westbound voyage and eastbound voyage respectively, which were equal to those of the EQ MV on the GCRF ( Fig.6.26 ) and GCRA ( Fig.6.34 ) with the number of propeller revolutions being 75 r.p.m.. The iterative calculations were stopped when  $\bar{T}_{min}$  converged to the range of  $T_s \pm 0.05$  hours.

In these simulations, the following abbreviations are used:

Predicted minimum fuel route calculated at the departure time based on the forecasted wind/wave data followed by the 5-day mean wind/wave models classified by ZI : PMFR

Great circle route calculated at the departure time based on the forecasted wind/wave data followed by the 5-day mean wind/wave models classified by ZI : GCRF

In order to compare the above PMFR and GCRF with the true minimum fuel routes and great circle routes based on the analyzed wind/wave data, the simulations of deterministic minimum fuel routing were also performed. Concerning the deterministic routing, we use the following abbreviations:

True minimum fuel route based on the analyzed wind/wave data : TMFR

Great circle route based on the analyzed wind/wave data : GCRA

The tracks of the PMFR and GCRF in the westbound voyage ( San

Francisco  $\rightarrow$  Tokyo ) are shown in Fig.6.54 ( S-A MV ) and Fig.6.56 ( EQ MV ). The tracks of the TMFR and GCRA for the same voyage are shown in Fig.6.55 ( S-A MV ) and Fig.6.57 ( EQ MV ).

The solid lines and dashed lines represent the PMFR and GCRF in Figs 6.54 and 6.56, whereas they represent the TMFR and GCRA in Figs 6.55 and 6.57.

Comparing Figs 6.54 and 6.56 with Figs 6.55 and 6.57, since the fuel consumptions on the GCRF are much larger than those on the GCRA, it is found that the wind/wave conditions of the 5-day mean wind/wave models classified by ZI were much severer than the actual ( analyzed ) wind/wave conditions for the westbound S-A MV and EQ MV sailed along the great circle route.

It should be noted that the standard deviation of passage time as well as the sizes of the 39% error ellipses on the PMFR of S-A MV in Fig.6.54 are considerably larger than those on the PMTR of S-A MV in Fig.6.24.

This results from the fact that when the ship's speed is low ( or the number of propeller revolutions is small ), the ratio of sail thrust to propeller thrust becomes large and the speed of the S-A MV becomes sensitive to a change of wind speed and direction. Thus the partial derivatives  $\partial V / \partial S_w$  and  $\partial V / \partial D_w$  in (5.1) become large, which leads to large 39% error ellipses and a large standard deviation of the passage time.

On the other hand, the standard deviation of fuel consumption on the PMFR of S-A MV in Fig.6.54 is a bit smaller than that on the PMTR of S-A MV in Fig.6.24. This is because when the ship's speed is low, the fuel consumption per unit time becomes insensitive to the change of ship's speed. Therefore the partial derivative  $G_v$  (  $= \partial G / \partial V_i$  ) in (2.51) becomes small, which cancels the above mentioned effect.

All predicted minimum time routes reaching the final isochrone in Fig.6.54 are shown in Fig.6.58; the thick line indicates the PMFR ( i.e. PMTR in this algorithm ) from San Francisco to Tokyo.



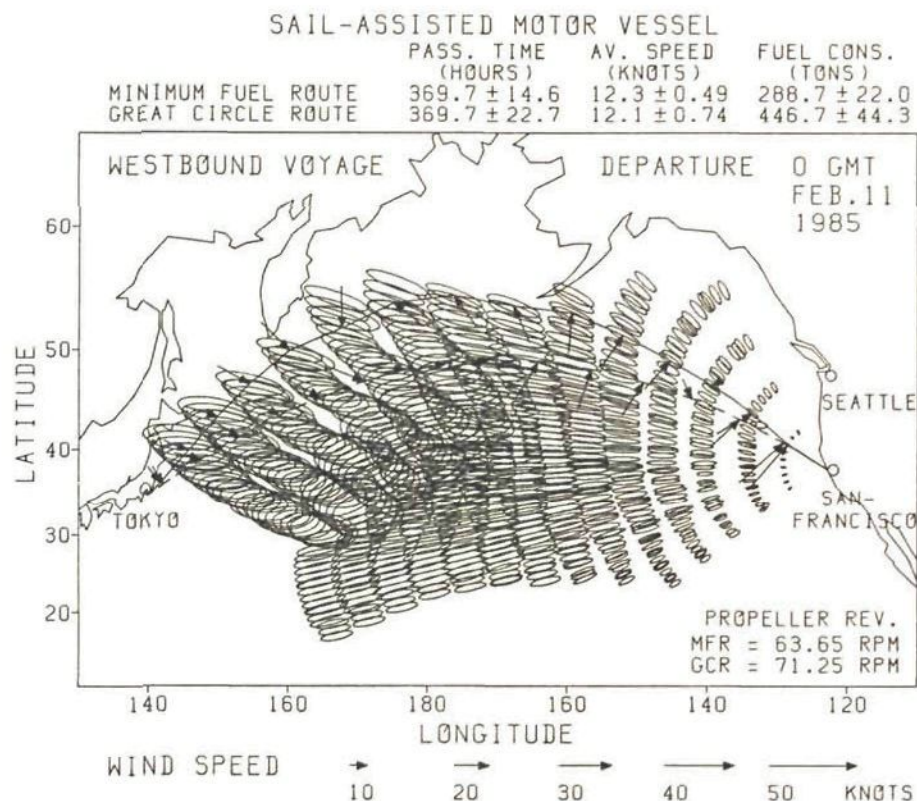


Fig. 6.54 Predicted minimum fuel route (PMFR) and great circle route (GCRF) of the sail-assisted motor vessel ( westbound voyage )

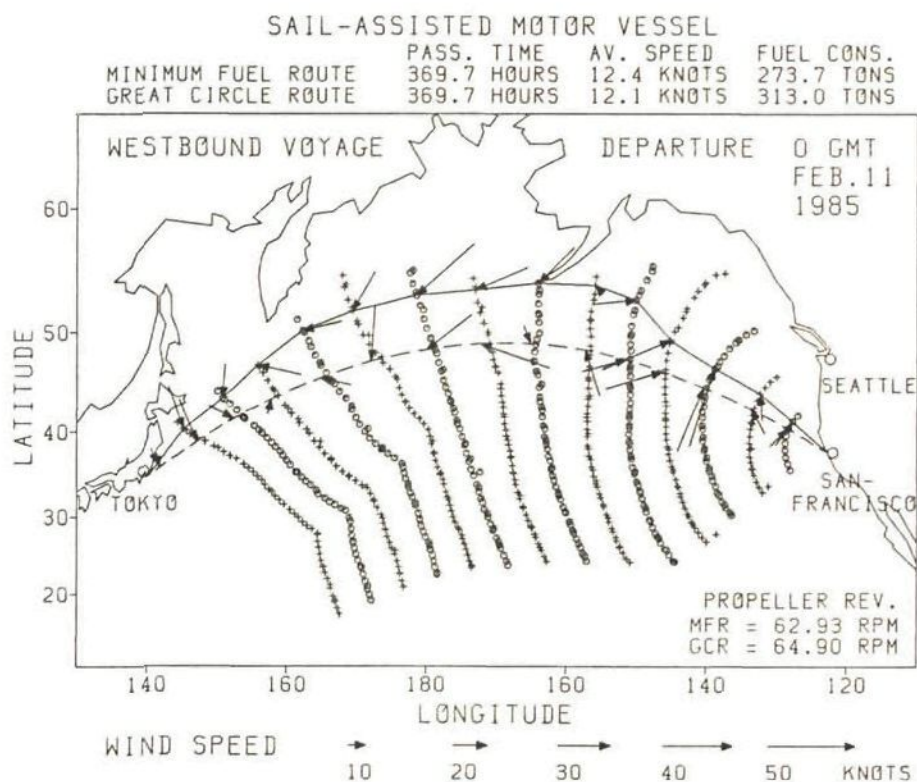


Fig. 6.55 True minimum fuel route (TMFR) and great circle route (GCRA) of the sail-assisted motor vessel ( westbound voyage )



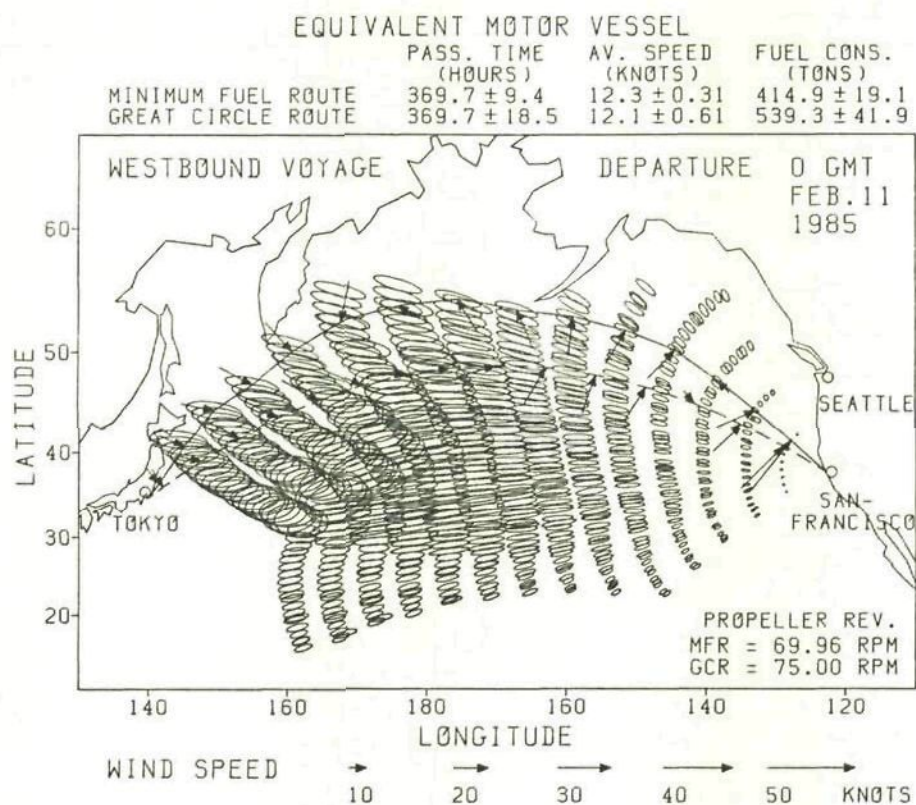


Fig. 6.56 Predicted minimum fuel route (PMFR) and great circle route (GCRF) of the equivalent motor vessel ( westbound voyage )

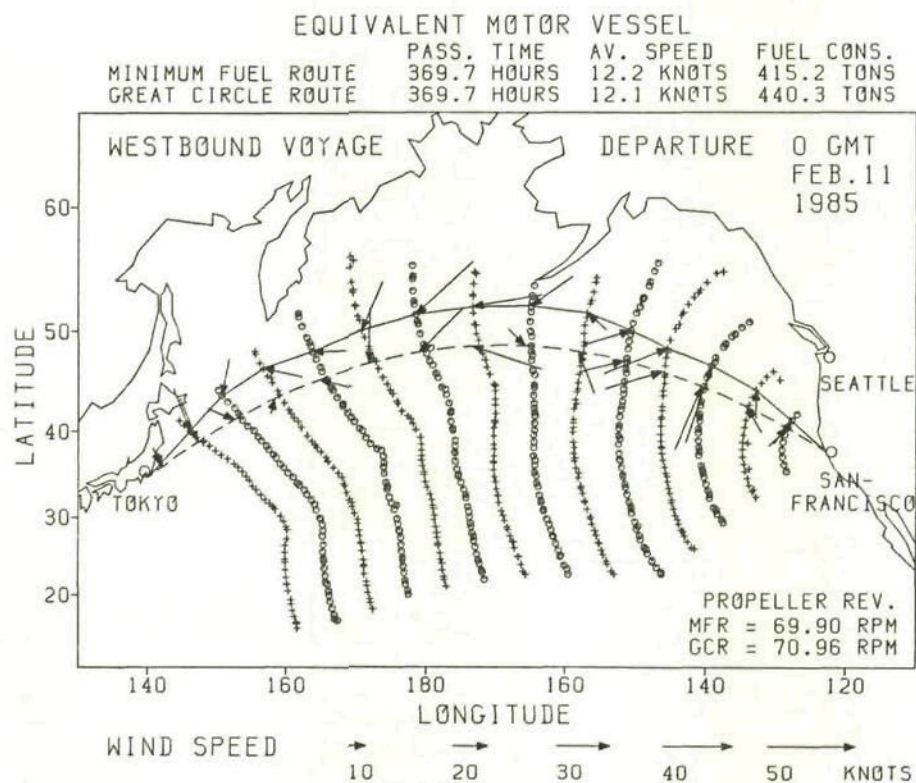


Fig. 6.57 True minimum fuel route (TMFR) and great circle route (GCRA) of the equivalent motor vessel ( westbound voyage )

On the routes depicted in Fig.6.58, the predicted positions of the points of the final isochrone as well as  $\bar{T}$ ,  $\bar{D}$ ,  $\bar{V}$ ,  $\bar{F}$ ,  $\bar{T}_D$ ,  $\sigma_T$ ,  $\sigma_V$  and  $\sigma_F$  are shown in Table 6.14. ( The quantities in Table 6.14 were computed by additionally navigating the S-A MV along rhumbines from the points of the final isochrone to Tokyo. )

The routes on which the passage times from the final isochrone to the destination exceeded about 3 days were excluded from Table 6.14.

In Table 6.14, we represent the route which reaches Tokyo from San Francisco via the point of the final isochrone having sub-sector number k by 'route (k)'. The route (43) is the PMFR.

We can find from Table 6.14 that  $\sigma_T$  and  $\sigma_F$  decrease gradually as the sub-sector number increases. As explained for Table 6.11, this comes from the fact that since the 39% error ellipses of ship's

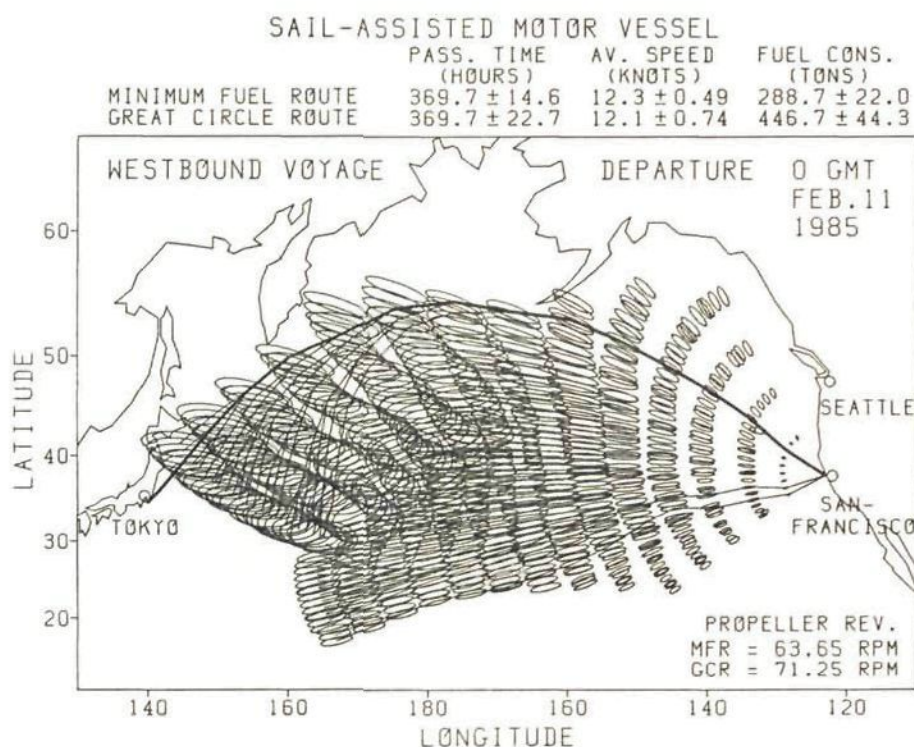


Fig. 6.58 All predicted minimum time routes of the sail-assisted motor vessel reaching the final isochrone ( westbound voyage )



Table 6.14 Information on the routes reaching Tokyo from  
San Francisco via points of the final isochrone

SUBSECT.NO.	FINAL LATI (DEG)	ISOCHRON LONG (DEG)	PASS. TIME (HR)	DISTANCE (NM)	AV. SPEED (KN)	FUEL CONS. (TN)	PER OF SGW (HR)	TIME STD (HR)	AVSP STD (KN)	FUEL STD (TN)
29	33.586	156.370	412.744	4960.51	12.018	328.874	0.0	22.731	0.662	29.525
30	34.235	155.119	406.096	4930.60	12.141	320.685	0.0	21.950	0.656	27.814
31	34.573	154.113	401.049	4874.96	12.156	316.358	0.0	22.244	0.674	28.479
32	34.929	153.153	396.033	4818.01	12.166	312.140	0.0	21.730	0.668	27.886
33	35.118	153.066	395.518	4831.09	12.215	310.641	0.0	21.601	0.667	27.367
34	35.454	152.074	390.626	4775.31	12.225	306.553	0.0	21.621	0.677	27.541
35	35.941	151.144	386.057	4725.34	12.240	302.613	0.0	21.247	0.674	27.335
36	36.649	150.088	381.415	4682.69	12.277	298.173	0.0	20.612	0.663	26.625
37	37.037	149.530	379.127	4638.55	12.235	297.204	0.0	20.619	0.665	27.112
38	37.124	149.173	377.575	4637.80	12.283	295.016	0.0	20.127	0.655	26.480
39	37.807	148.296	374.587	4603.52	12.290	292.640	0.0	19.138	0.628	25.608
40	38.594	147.322	372.193	4584.98	12.319	290.357	0.0	17.429	0.577	24.000
41	39.079	146.897	371.742	4563.88	12.277	290.785	0.0	16.991	0.561	24.073
42	39.186	146.514	370.588	4565.54	12.320	289.182	0.0	16.137	0.536	23.079
43	39.809	145.684	369.686	4554.07	12.319	288.708	0.0	14.648	0.488	21.987
44	40.483	145.030	370.203	4557.11	12.310	289.400	0.0	12.941	0.430	20.610
45	41.196	144.392	371.511	4567.06	12.293	290.944	0.0	11.254	0.372	19.215



positions constructing the final isochrone are much longer in longitudinal direction than in latitudinal direction, the variance of ship's position error along the rhumbline from the center of the 39% error ellipse to the destination decreases as the sub-sector number increases ( i.e. as the direction of that rhumbline approaches  $180^\circ$  ).

It is also found that since a double point does not exist in the range of the final isochrone shown in Table 6.14, the change of  $\sigma_F$  is comparatively smooth, and  $\sigma_F$  increases as  $\bar{F}$  increases except for the routes (44) and (45) in the neighborhood of route (43) ( PMFR ). Thus it can be said that in this westbound voyage, the standard deviation of fuel consumption would not be an important factor to determine the minimum fuel route.

Next, the tracks of the PMFR and GCRF in the eastbound voyage ( Tokyo  $\rightarrow$  San Francisco ) are shown in Fig.6.59 ( S-A MV ) and Fig.6.61 ( EQ MV ). The tracks of the TMFR and GCRA for the same voyage are shown in Fig.6.60 ( S-A MV ) and Fig.6.62 ( EQ MV ).

The solid lines and dashed lines represent the PMFR and GCRF in Figs 6.59 and 6.61, whereas they represent the TMFR and GCRA in Figs 6.60 and 6.62.

Comparing Figs 6.59 and 6.61 with Figs 6.60 and 6.62, since the fuel consumptions on the GCRA are much larger than those on the GCRF, it can be seen that the actual ( analyzed ) wind/wave conditions were much more adverse than the wind/wave conditions of the 5-day mean wind/wave models classified by ZI for the eastbound S-A MV and EQ MV sailed along the great circle route.

It is found that the standard deviations of passage time and fuel consumption of the S-A MV in Fig.6.59 are much greater than those of the EQ MV in Fig.6.61 because of the same reason as mentioned for Figs 6.31 and 6.33.

We can also find that for the same reason as stated for Fig.6.54, the standard deviation of passage time as well as the 39% error

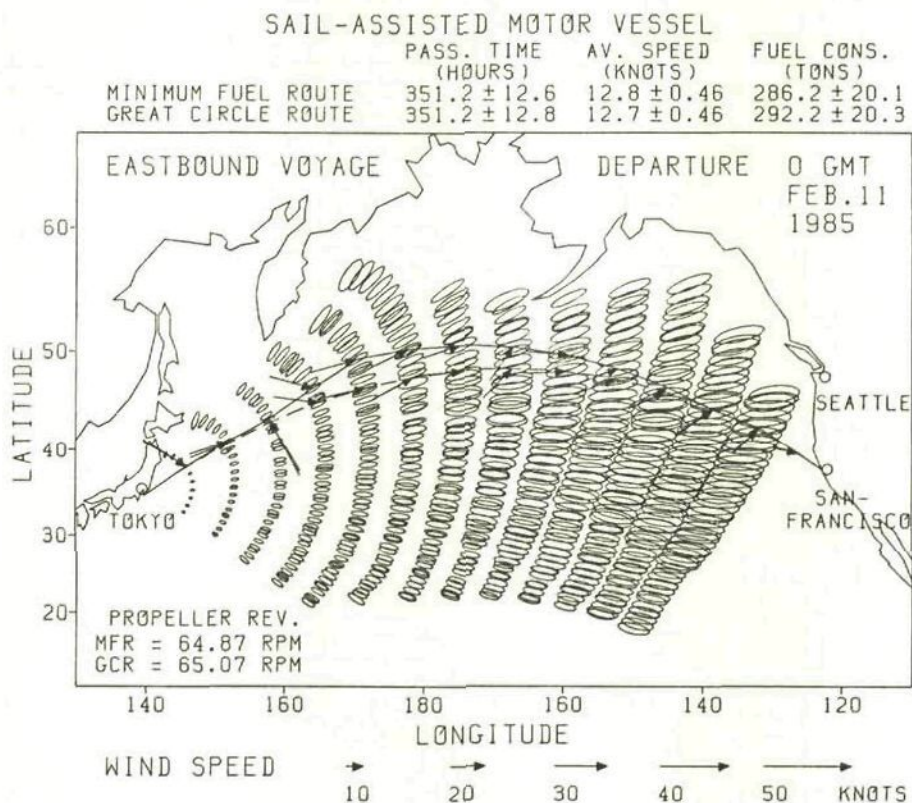


Fig. 6.59 Predicted minimum fuel route (PMFR) and great circle route (GCRF) of the sail-assisted motor vessel ( eastbound voyage )

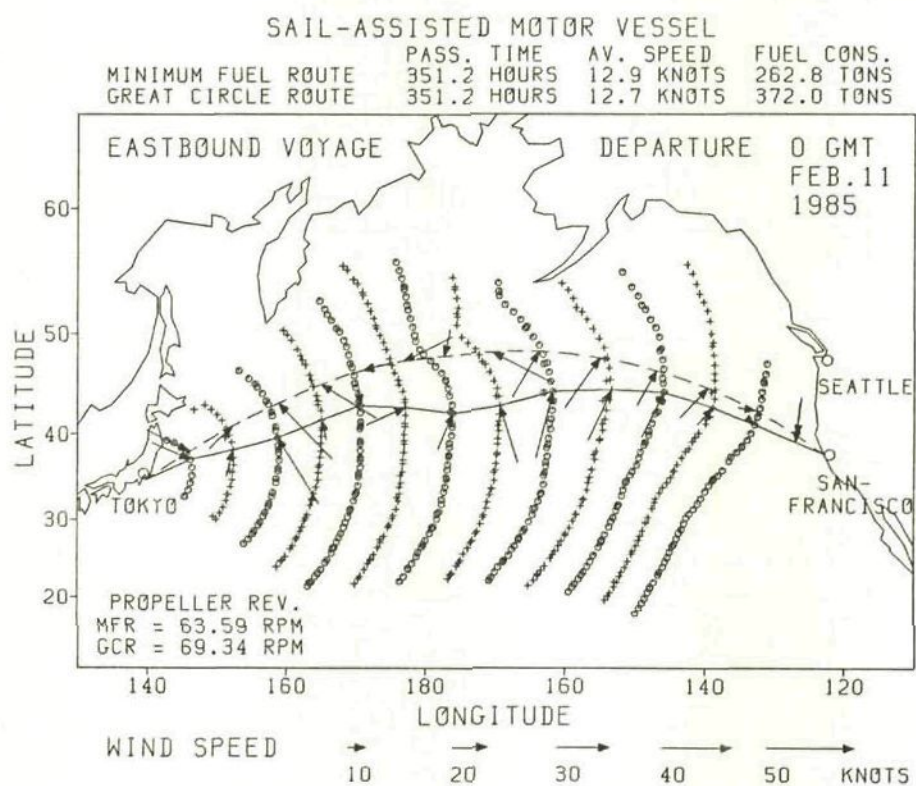


Fig. 6.60 True minimum fuel route (TMFR) and great circle route (GCRA) of the sail-assisted motor vessel ( eastbound voyage )



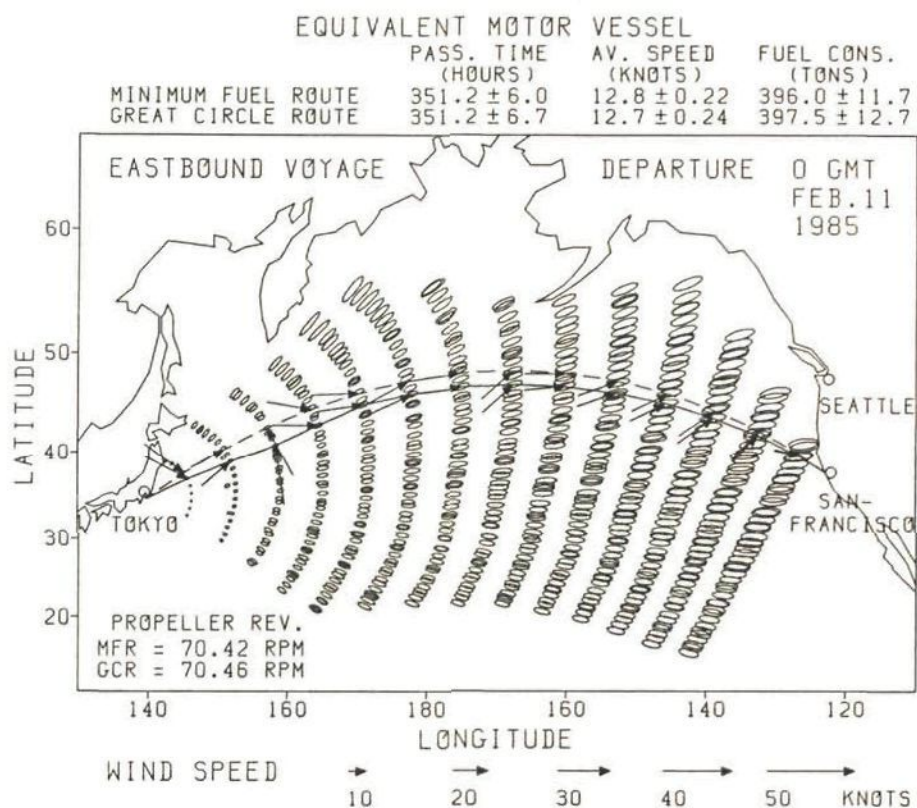


Fig. 6.61 Predicted minimum fuel route (PMFR) and great circle route (GCRF) of the equivalent motor vessel ( eastbound voyage )

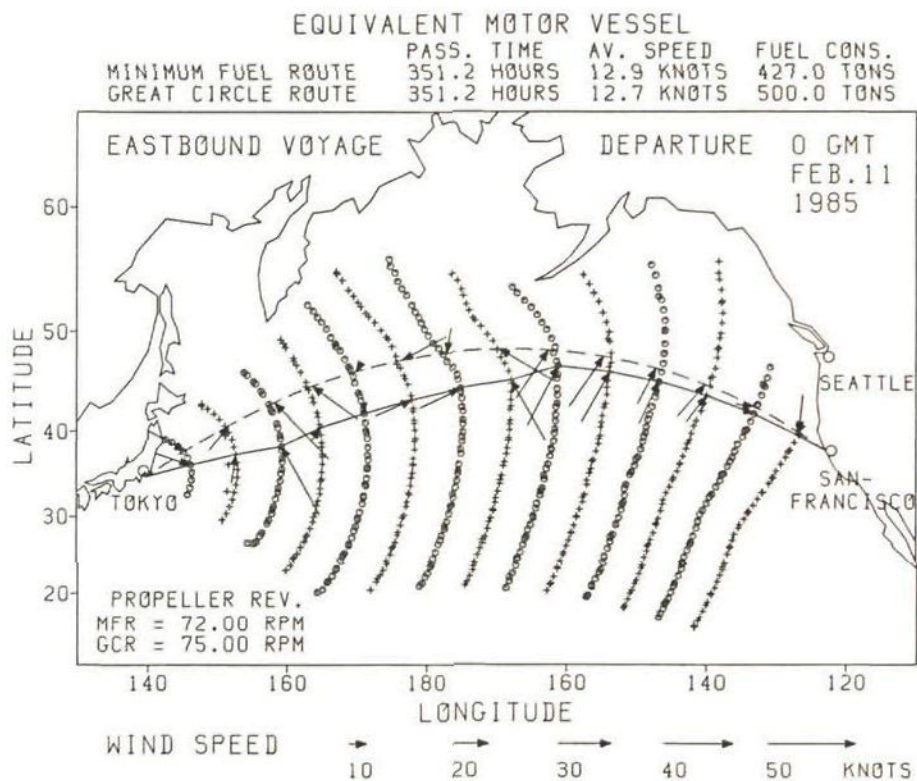


Fig. 6.62 True minimum fuel route (TMFR) and great circle route (GCRA) of the equivalent motor vessel ( eastbound voyage )



ellipses on the PMFR of S-A MV in Fig.6.59 are considerably larger than those on the PMTR of S-A MV in Fig.6.31.

In Figs 6.59 and 6.61, there are no remarkable discontinuities in the sizes and shapes of the 39% error ellipses constructing the final isochrone. Hence, it can be understood that the standard deviation of the fuel consumption would hardly influence the determination of minimum fuel route in this eastbound voyage.

(II) Actual routes calculated at every updating time of the forecasts

Since the wind/wave forecasts by FNOC are updated every 12 hours, simulations of recalculating the minimum fuel route at every updating time of the forecasts were also performed.

At each recalculation of the minimum fuel route, the number of propeller revolutions was adjusted so as to get the ship to reach the destination with the specified passage time  $T_s$ . As a number of minimum time routes had to be recalculated during the voyage, the iterative calculation for each minimum fuel route was stopped when the predicted minimum passage time between departure point and destination converged to the range of  $T_s \pm 2$  hours in order to save computing time.

In these simulations, the following abbreviation is used:

Actual route calculated every 12 hours based on the updated wind/wave forecasts followed by the 5-day mean wind/wave models classified by ZI : ARUF

On the ARUF, when the wind/wave forecasts were updated, a new minimum fuel route from the ship's position to the destination was calculated using the updated wind/wave forecasts followed by the 5-day mean wind/wave models classified by ZI. Then the ship was sailed for 12 hours under analyzed wind/wave conditions following the initial course and the number of propeller revolutions of that minimum fuel route.

The tracks of the ARUF and TMFR in the westbound voyage departing

at 00 hours GMT on 11 February-1985 are shown in Fig.6.63 ( S-A MV ) and Fig.6.64 ( EQ MV ).

In these figures, the dashed lines and solid lines denote the ARUF and TMFR, respectively. The isochrones were calculated based on the analyzed wind/wave data, i.e. they are the same as those in Figs 6.55 and 6.57.

From Figs 6.63 and 6.64, it is found that the tracks and the fuel consumptions of ARUF hardly differ from those of the TMFR. Therefore, it can be said that the recalculations of minimum fuel routes based on the updated wind/wave forecasts were effective to save fuel oil.

Next, the tracks of the ARUF and TMFR in the eastbound voyage departing at 00 hours GMT on 11 February 1985 are shown in Fig.6.65 ( S-A MV ) and Fig.6.66 ( EQ MV ).

From Figs 6.65 and 6.66, we can find that the ARUF of S-A MV and EQ MV changed their tracks southwards at about  $165^{\circ}\text{E}$  to avoid adverse weather on the great circle route according to information of the updated forecasts.

In Fig.6.67 are shown the variations of predicted passage time and fuel consumption calculated every 12 hours on the ARUF of S-A MV in the eastbound voyage shown in Fig.6.65. The variations of ship's speed and the number of propeller revolutions are also shown in Fig.6.67.

The predicted passage time/fuel consumption represents the sum of the predicted value from the ship's position to the destination and the accumulated actual value from the departure point to the ship's position. The length of the vertical segment indicates twice the standard deviation.

The asterisks denote the actual passage time and fuel consumption; the horizontal dashed line denotes the specified passage time ( = 351.2 hours ).



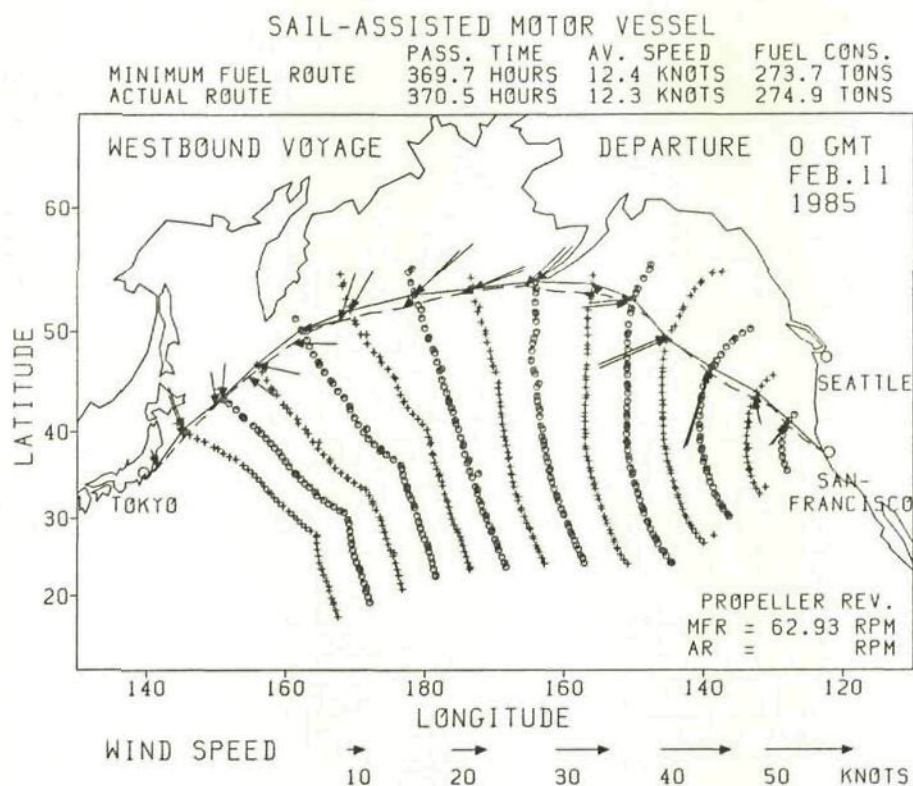


Fig. 6.63 Actual route (ARUF) [dashed line] and true minimum fuel route (TMFR) [solid line] of the sail-assisted motor vessel ( westbound voyage )

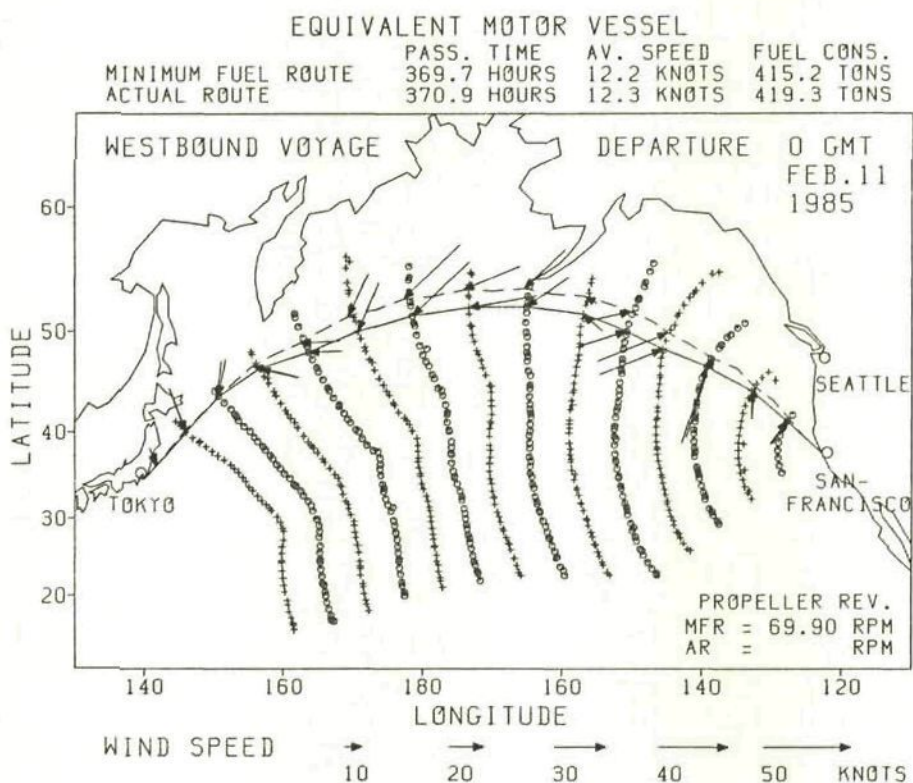


Fig. 6.64 Actual route (ARUF) [dashed line] and true minimum fuel route (TMFR) [solid line] of the equivalent motor vessel ( westbound voyage )



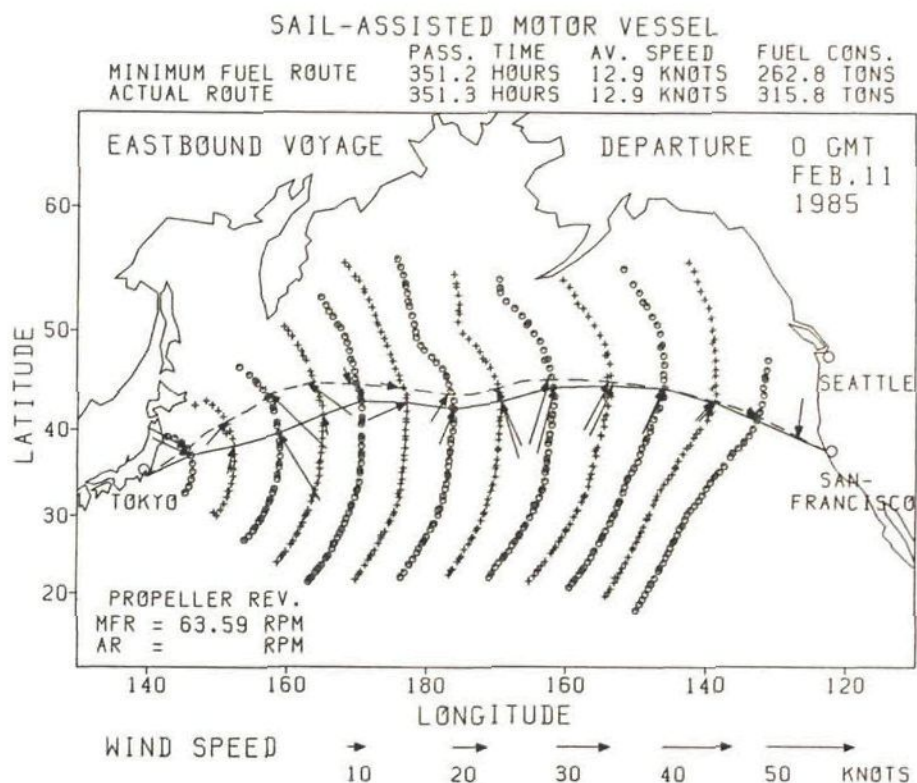


Fig. 6.65 Actual route (ARUF) [dashed line] and true minimum fuel route (TMFR) [solid line] of the sail-assisted motor vessel ( eastbound voyage )

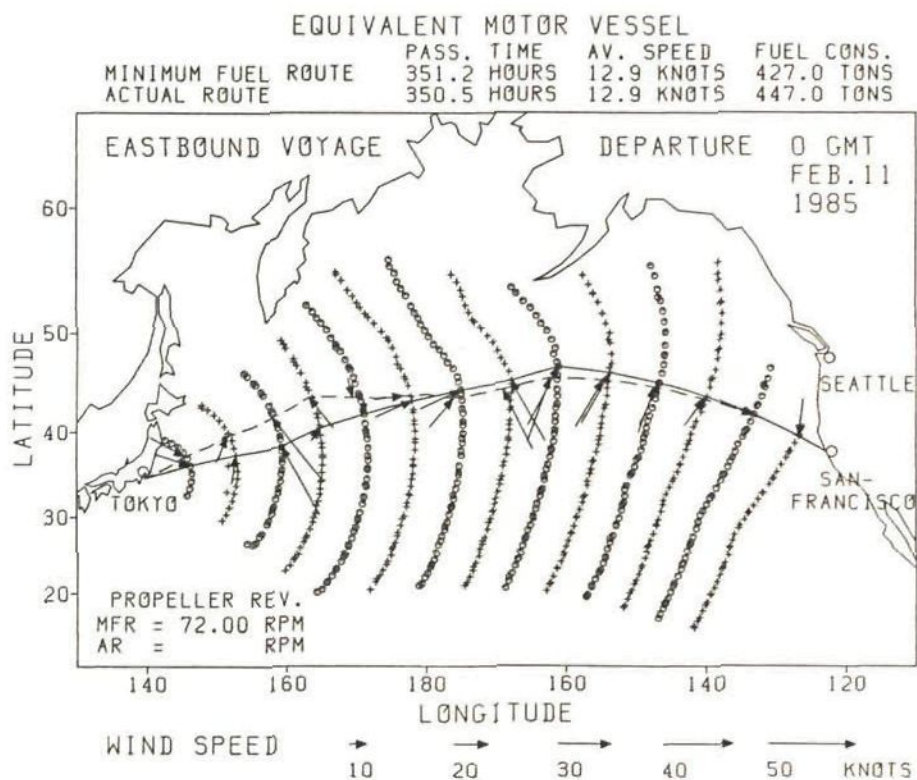


Fig. 6.66 Actual route (ARUF) [dashed line] and true minimum fuel route (TMFR) [solid line] of the equivalent motor vessel ( eastbound voyage )

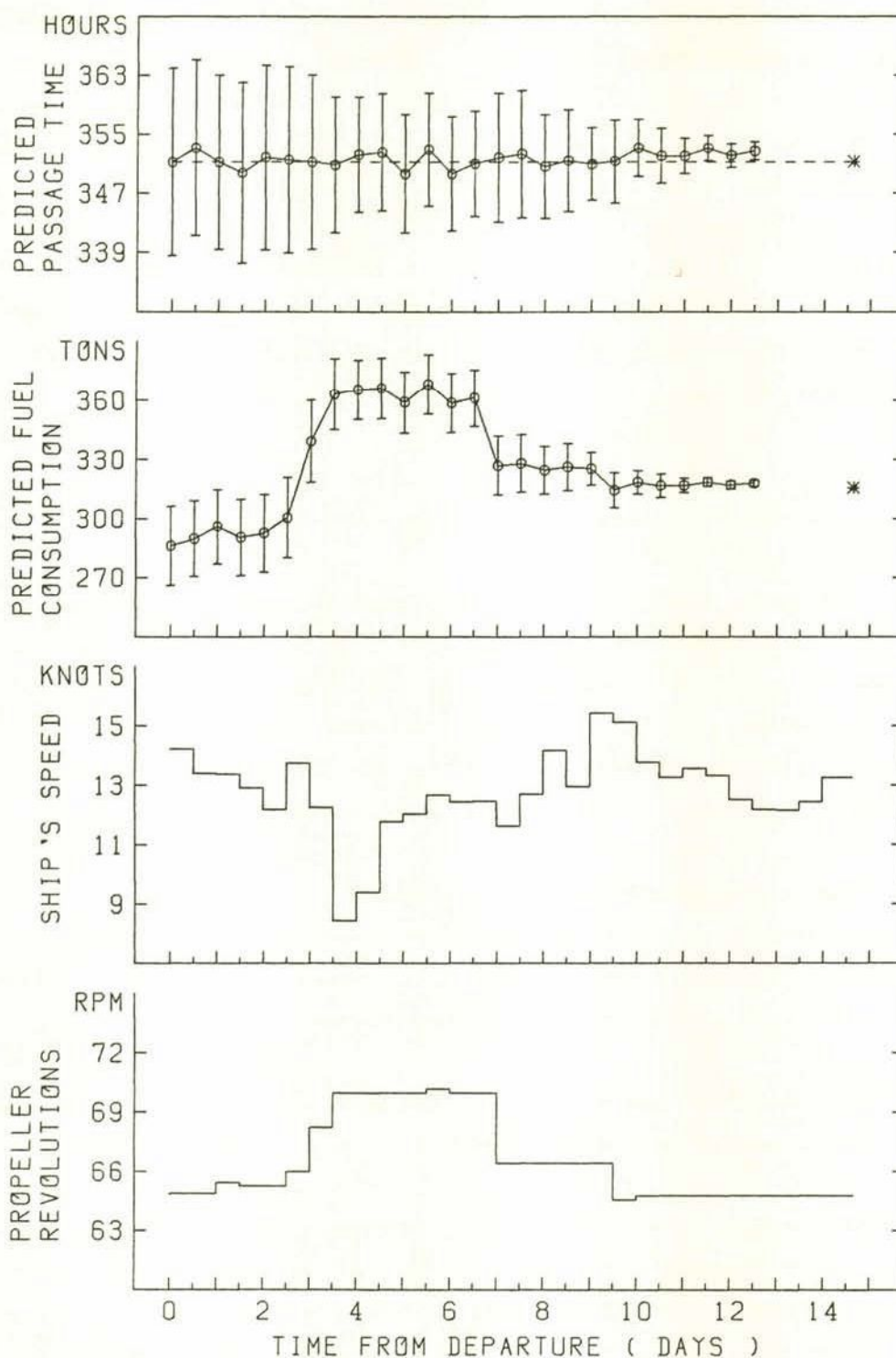


Fig. 6.67 Variations of predicted passage time and fuel consumption as well as ship's speed and number of propeller revolutions calculated every 12 hours on the actual route (ARUF) of the sail-assisted motor vessel ( eastbound voyage )  
( The length of the vertical segment indicates twice the standard deviation. )

From Fig.6.67, it can be seen that the number of propeller revolutions was controlled so as to keep the predicted passage time within the range of  $351.2 \pm 2.0$  hours. As a matter of course, the standard deviations of passage time and fuel consumption gradually decrease as the S-A MV approaches the destination.

We can also find that since severe weather was forecasted on the third and fourth day after the departure time, the number of propeller revolutions was increased and thus the predicted fuel consumption increased in those days.

### (III) Summary of minimum fuel routing simulations

The passage times, average speeds, fuel consumptions and their standard deviations as well as the travelled distances and the numbers of propeller revolutions on the PMFR, TMFR, ARUF, GCRF and GCRA are shown in Table 6.15 ( westbound voyage ) and Table 6.16 ( eastbound voyage ). For the ARUF, the maximum and minimum number of propeller revolutions during the voyage are shown.

In Tables 6.15 and 6.16, the above mentioned values on the 'route based on the predicted headings/propeller revolutions and analyzed wind/wave data' are also shown. The following abbreviation is used to represent that route:

Route based on the predicted headings/propeller revolutions and analyzed wind/wave data : RPHPA

On the RPHPA, the ship is sailed under the analyzed wind/wave conditions following both the sequence of optimal headings and the optimal number of propeller revolutions predicted at the departure time using the forecasted wind/wave data followed by the 5-day mean wind/wave models classified by ZI. That is, on the RPHPA, the ship follows the same sequence of headings and the number of propeller revolutions as taken on the PMFR.

In Tables 6.15 and 6.16, the fuel savings are related to the fuel consumption on the GCRA.



Table 6.15 Summary of stochastic minimum fuel routing ( Westbound voyage )

Departure : 00 hours GMT 11 February 1985

Specified passage time = 369.7 hours

Wind/wave data : forecasted wind/wave data followed by the  
5-day mean wind/wave models classified by ZI

Sail-assisted motor vessel

	PMFR	TMFR	RPHPA	ARUF	GCRF	GCRA
Passage time (hours)	369.7	369.7	376.0	370.5	369.7	369.7
S.D. of pass. time (hours)	14.6	—	—	—	22.7	—
Distance (n.m.)	4554	4578	4552	4561	4470	4471
Average speed (knots)	12.32	12.38	12.11	12.31	12.09	12.09
S.D. of av. speed (knots)	0.49	—	—	—	0.74	—
Max. propeller rev. (r.p.m.)	63.65	62.93	63.65	66.94	71.25	64.90
Min. propeller rev. (r.p.m.)	—	—	—	55.76	—	—
Fuel consumption (tons)	288.7	273.7	296.5	274.9	446.7	313.0
S.D. of fuel cons. (tons)	22.0	—	—	—	44.3	—
Fuel saving (tons)	—	39.3	—	38.1	—	0.0
Fuel saving (%)	—	12.6	—	12.2	—	0.0

Equivalent motor vessel

	PMFR	TMFR	RPHPA	ARUF	GCRF	GCRA
Passage time (hours)	369.7	369.7	372.5	370.9	369.7	369.7
S.D. of pass. time (hours)	9.4	—	—	—	18.5	—
Distance (n.m.)	4556	4516	4540	4545	4469	4469
Average speed (knots)	12.33	12.22	12.19	12.25	12.09	12.09
S.D. of av. speed (knots)	0.31	—	—	—	0.61	—
Max. propeller rev. (r.p.m.)	69.96	69.90	69.96	71.71	75.00	70.96
Min. propeller rev. (r.p.m.)	—	—	—	67.11	—	—
Fuel consumption (tons)	414.9	415.2	420.2	419.3	539.3	440.3
S.D. of fuel cons. (tons)	19.1	—	—	—	41.9	—
Fuel saving (tons)	—	25.1	—	21.0	—	0.0
Fuel saving (%)	—	5.7	—	4.8	—	0.0

Table 6.16 Summary of stochastic minimum fuel routing ( Eastbound voyage )

Departure : 00 hours GMT 11 February 1985  
 Specified passage time = 351.2 hours  
 Wind/wave data : forecasted wind/wave data followed by the  
 5-day mean wind/wave models classified by ZI

Sail-assisted motor vessel

	PMFR	TMFR	RPHPA	ARUF	GCRF	GCRA
Passage time (hours)	351.2	351.2	391.7	351.3	351.2	351.2
S.D. of pass. time (hours)	12.6	—	—	—	12.8	—
Distance (n.m.)	4497	4539	4554	4432	4469	4470
Average speed (knots)	12.81	12.92	11.63	12.90	12.73	12.73
S.D. of av. speed (knots)	0.46	—	—	—	0.46	—
Max. propeller rev. (r.p.m.)	64.87	63.59	64.87	70.15	65.07	69.34
Min. propeller rev. (r.p.m.)	—	—	—	64.55	—	—
Fuel consumption (tons)	286.2	262.8	345.0	315.8	292.2	372.0
S.D. of fuel cons. (tons)	20.1	—	—	—	20.3	—
Fuel saving (tons)	—	109.2	—	56.2	—	0.0
Fuel saving (%)	—	29.4	—	15.1	—	0.0

Equivalent motor vessel

	PMFR	TMFR	RPHPA	ARUF	GCRF	GCRA
Passage time (hours)	351.2	351.2	370.4	350.5	351.2	351.2
S.D. of pass. time (hours)	6.0	—	—	—	6.7	—
Distance (n.m.)	4482	4530	4504	4523	4469	4469
Average speed (knots)	12.76	12.90	12.16	12.91	12.72	12.73
S.D. of av. speed (knots)	0.22	—	—	—	0.24	—
Max. propeller rev. (r.p.m.)	70.42	72.00	70.42	74.34	70.46	75.00
Min. propeller rev. (r.p.m.)	—	—	—	70.42	—	—
Fuel consumption (tons)	396.0	427.0	432.3	447.0	397.5	500.0
S.D. of fuel cons. (tons)	11.7	—	—	—	12.7	—
Fuel saving (tons)	—	73.0	—	53.0	—	0.0
Fuel saving (%)	—	14.6	—	10.6	—	0.0



Concerning the westbound voyage ( Table 6.15 ), the following facts can be found.

(i) For both the S-A MV and EQ MV, since the fuel savings on the ARUF are not so different from those on the TMFR, it can be seen that the use of information on the updated wind/wave forecasts was effective for fuel saving. The passage time and fuel consumption of the S-A MV on the ARUF are 5.5 hours and 21.6 tons smaller than those on the RPHPA.

(ii) The passage times and fuel consumptions of the S-A MV and EQ MV on the RPHPA are comparatively close to those on the PMFR. Thus it can be said that the severity of actual ( analyzed ) wind/wave conditions on the RPHPA was not so different from that of forecasts and the 5-day mean wind/wave models classified by ZI on the PMFR on average.

(iii) On the ARUF, the number of propeller revolutions of the S-A MV was controlled in a larger range than for the EQ MV.

Next, concerning the eastbound voyage ( Table 6.16 ), the following facts can be observed.

(i) For both the S-A MV and EQ MV, the fuel savings on the ARUF reach more than 50 tons. Hence, it can be said that the use of information on the updated wind/wave forecasts was very effective for saving fuel oil.

(ii) The passage times and fuel consumptions of the S-A MV and EQ MV on the RPHPA are much larger than those on the PMFR. Therefore, it can be said that the actual ( analyzed ) wind/wave conditions on the RPHPA were much severer than the forecasts and the 5-day mean wind/wave models classified by ZI on the PMFR.

For this westbound/eastbound voyage, the probability of shipping green water at the bow did not exceed 0.04 on all the routes shown in Tables 6.15 and 6.16.



#### 6.3.4 Minimum fuel routing using forecasted wind/wave data followed by the 1-month mean wind/wave data

In this subsection, using the forecasted wind/wave data followed by the 1-month mean wind/wave data, the simulations of stochastic minimum fuel routing are carried out in the same way as described in subsection 6.3.3.

The S-A MV and EQ MV were sailed between Tokyo and San Francisco departing from both points at the same time as mentioned in 6.3.3, i.e. 00 hours GMT on 11 February in 1985. The passage times were specified as 369.7 hours and 351.2 hours in the westbound voyage and eastbound voyage respectively. The 1-month mean wind/wave data for February shown in Fig.4.29 were used after the 72-hour wind/wave forecasts.

In these simulations, the following abbreviations are used:

Predicted minimum fuel route calculated at the departure time based on the forecasted wind/wave data followed by the 1-month mean wind/wave data : PMFR

Great circle route calculated at the departure time based on the forecasted wind/wave data followed by the 1-month mean wind/wave data : GCRF

Actual route calculated every 12 hours based on the udated wind/wave forecasts followed by the 1-month mean wind/wave data : ARUF

Route based on the predicted headings/propeller revolutions and analyzed wind/wave data : RPHPA

Since the results of the simulations on the PMFR, GCRF, ARUF and RPHPA were not very different from those in subsection 6.3.3, the details of the simulations are omitted here.

The passage times, average speeds, fuel consumptions and their standard deviations as well as the travelled distances and the numbers of propeller revolutions on the PMFR, TMFR, RPHPA, ARUF,

GCRF and GCRA are shown in Table 6.17 ( westbound voyage ) and Table 6.18 ( eastbound voyage ).

The values on the TMFR and GCRA are the same as those in Tables 6.15 and 6.16. For the ARUF, the maximum and minimum number of propeller revolutions during the voyage are shown. The fuel savings are related to the fuel consumption on the GCRA.

Concerning the westbound voyage ( Table 6.17 ), the following facts can be seen.

(i) For both the S-A MV and EQ MV, as the fuel savings on the ARUF are close to those on the TMFR, it can be said that the use of information on the updated wind/wave forecasts was effective for fuel saving.

(ii) The predicted fuel consumptions of the S-A MV and EQ MV on the GCRF in Table 6.17 are much smaller than those in Table 6.15. Hence, it can be seen that the wind/wave conditions of the 5-day mean wind/wave models classified by ZI were much severer than those of the 1-month mean wind/wave data for the westbound vessels sailed on the great circle route.

(iii) On the ARUF of S-A MV and EQ MV, the ranges of the numbers of propeller revolutions ( i.e. differences between maxima and minima ) in Table 6.17 are smaller than those in Table 6.15. This comes from the fact that the unique 1-month mean wind/wave data for February were used for the voyage in Table 6.17, whereas four kinds of the 5-day mean wind/wave models classified by ZI shown in Table 6.10 were used for the voyage in Table 6.15.

Next, concerning the eastbound voyage ( Table 6.18 ), the following facts can be observed.

(i) Since the fuel savings on the ARUF of S-A MV and EQ MV reach 68.4 tons and 61.8 tons respectively, it can be said that the use of information on the updated wind/wave forecasts was very effective for saving fuel oil.



Table 6.17 Summary of stochastic minimum fuel routing ( Westbound voyage )

Departure : 00 hours GMT 11 February 1985  
 Specified passage time = 369.7 hours  
 Wind/wave data : forecasted wind/wave data followed by  
 the 1-month mean wind/wave data

Sail-assisted motor vessel

	PMFR	TMFR	RPHPA	ARUF	GCRF	GCRA
Passage time (hours)	369.7	369.7	378.5	370.3	369.7	369.7
S.D. of pass. time (hours)	13.2	—	—	—	22.0	—
Distance (n.m.)	4533	4578	4522	4551	4470	4471
Average speed (knots)	12.26	12.38	11.95	12.29	12.09	12.09
S.D. of av. speed (knots)	0.44	—	—	—	0.72	—
Max. propeller rev. (r.p.m.)	63.17	62.93	63.17	65.17	68.66	64.90
Min. propeller rev. (r.p.m.)	—	—	—	59.41	—	—
Fuel consumption (tons)	281.4	273.7	293.1	281.2	389.4	313.0
S.D. of fuel cons. (tons)	20.1	—	—	—	38.6	—
Fuel saving (tons)	—	39.3	—	31.8	—	0.0
Fuel saving (%)	—	12.6	—	10.2	—	0.0

Equivalent motor vessel

	PMFR	TMFR	RPHPA	ARUF	GCRF	GCRA
Passage time (hours)	369.7	369.7	380.8	369.0	369.7	369.7
S.D. of pass. time (hours)	6.5	—	—	—	17.4	—
Distance (n.m.)	4552	4516	4540	4543	4469	4469
Average speed (knots)	12.31	12.22	11.92	12.31	12.09	12.09
S.D. of av. speed (knots)	0.22	—	—	—	0.57	—
Max. propeller rev. (r.p.m.)	68.62	69.90	68.62	70.47	72.66	70.96
Min. propeller rev. (r.p.m.)	—	—	—	68.62	—	—
Fuel consumption (tons)	386.3	415.2	406.0	418.3	480.9	440.3
S.D. of fuel cons. (tons)	12.6	—	—	—	36.1	—
Fuel saving (tons)	—	25.1	—	22.0	—	0.0
Fuel saving (%)	—	5.7	—	5.0	—	0.0



Table 6.18 Summary of stochastic minimum fuel routing (Eastbound voyage)

Departure : 00 hours GMT 11 February 1985  
 Specified passage time = 351.2 hours  
 Wind/wave data : forecasted wind/wave data followed by  
 the 1-month mean wind/wave data

Sail-assisted motor vessel

	PMFR	TMFR	RPHPA	ARUF	GCRF	GCRA
Passage time (hours)	351.2	351.2	394.9	350.5	351.2	351.2
S.D. of pass. time (hours)	12.0	—	—	—	11.3	—
Distance (n.m.)	4480	4539	4536	4524	4469	4470
Average speed (knots)	12.76	12.92	11.49	12.91	12.72	12.73
S.D. of av. speed (knots)	0.44	—	—	—	0.41	—
Max. propeller rev. (r.p.m.)	63.84	63.59	63.84	69.58	64.12	69.34
Min. propeller rev. (r.p.m.)	—	—	—	63.84	—	—
Fuel consumption (tons)	270.0	262.8	331.0	303.6	275.8	372.0
S.D. of fuel cons. (tons)	18.2	—	—	—	17.3	—
Fuel saving (tons)	—	109.2	—	68.4	—	0.0
Fuel saving (%)	—	29.4	—	18.4	—	0.0

Equivalent motor vessel

	PMFR	TMFR	RPHPA	ARUF	GCRF	GCRA
Passage time (hours)	351.2	351.2	372.7	351.8	351.2	351.2
S.D. of pass. time (hours)	5.9	—	—	—	6.3	—
Distance (n.m.)	4482	4530	4496	4507	4469	4469
Average speed (knots)	12.76	12.90	12.06	12.81	12.73	12.73
S.D. of av. speed (knots)	0.21	—	—	—	0.23	—
Max. propeller rev. (r.p.m.)	69.86	72.00	69.86	73.50	69.92	75.00
Min. propeller rev. (r.p.m.)	—	—	—	69.86	—	—
Fuel consumption (tons)	384.4	427.0	424.7	439.2	386.0	500.0
S.D. of fuel cons. (tons)	10.9	—	—	—	11.6	—
Fuel saving (tons)	—	73.0	—	61.8	—	0.0
Fuel saving (%)	—	14.6	—	12.4	—	0.0

(ii) The passage times and fuel consumptions of the S-A MV and EQ MV on the RPHPA are much larger than those on the PMFR. Thus, it can be seen that the actual ( analyzed ) wind/wave conditions on the RPHPA were much severer than the forecasts and the 1-month mean wind/wave data on the PMFR.

For this westbound/eastbound voyage, the probability of shipping green water at the bow did not exceed 0.04 on all the routes shown in Tables B.17 and B.18.

## 7. REVIEW, CONCLUSIONS AND SUGGESTIONS

### 7.1 REVIEW

In this thesis, innovative methods to perform effective weather routing of ( sail-assisted ) motor vessels were proposed, and comprehensive simulations of weather routing were executed to verify the effectiveness of those proposed methods.

First, in Chapter 2, after formulating the ship routing problem, the modified isochrone method was proposed as a practical method to perform deterministic minimum time/fuel/cost routing. Then, taking into account the uncertainties of predicted environments, a method of estimating the standard deviations of passage time and fuel consumption on a particular route was proposed. By incorporating those standard deviations into the objective function, the modified isochrone method was applied to the stochastic routing problem.

Next, based on the equilibrium equations for the forces and moments acting on the ship, the methods to predict the ship's speed, drift angle, rudder angle, heel angle and engine power of a ( sail-assisted ) motor vessel in a seaway were proposed in Chapter 3. Using a 40,000 DWT product tanker with 808 m<sup>2</sup> sail area as a mathematical model ship, the ship's speed, drift angle, etc. were calculated by the proposed methods under various wind/wave conditions and numbers of propeller revolutions.

As a result, it was verified that the accuracy and computational efficiency of the proposed prediction methods sufficiently met the requirements for practical weather routing mentioned in Chapter 1. In addition, the methods to predict the ship's motions and accompanying phenomena in waves were described, and the probabilities of shipping green water at the bow of the model ship were calculated for some wave conditions.

In Chapter 4, the environmental data used in the weather routing



simulations were mentioned. The analyzed wind, sea and swell data as well as the monthly ocean current data of the North Pacific Ocean published by FNOC were described as the data for deterministic routing simulations.

For stochastic routing simulations, three kinds of wind/wave data were described, namely, the forecasted wind/wave data, the 5-day mean wind/wave models classified by ZI and the 1-month mean wind/wave data of the North Pacific Ocean. In each type of wind/wave data, the methods to calculate the mean errors, covariance matrices and correlation matrices were explained. Monthly ocean current data published by the Meteorological Office were also described as mean value charts and covariance charts.

The accuracy of the modified isochrone method was discussed in Chapter 5 by means of a sensitivity analysis. By changing the increments for discretization ( e.g. increment of ship's heading ), the sensitivities of the solutions to the sizes of the increments of various parameters used in the modified isochrone method were investigated. From the results of the investigations, suitable sizes of increments were suggested.

In Chapter 6, using the aforementioned methods, the environmental data of the North Pacific Ocean and the mathematical model ships ( i.e. sail-assisted motor vessel and equivalent motor vessel ), computer simulations were carried out for both deterministic routing and stochastic routing.

## 7.2 CONCLUSIONS

The principal results of the research are as follows.

### (I) Deterministic routing

(i) Using the minimum time route, compared with the great circle route of an equivalent motor vessel, the passage time of a sail-assisted motor vessel could on average be reduced by 11.8%.

( westbound voyage ) and 7.4% ( eastbound voyage ). At the same time, 19.2% ( westbound voyage ) and 13.4% ( eastbound voyage ) fuel saving could be achieved on average. These savings can be regarded as maximum benefits by the use of weather routing plus sail-assisted operation.

(ii) In the example of (sub) minimum fuel routing, fuel consumption could be reduced by 52.2% ( westbound voyage ) and 32.0% ( eastbound voyage ) on the minimum fuel route of a sail-assisted motor vessel compared with the great circle route of an equivalent motor vessel. In the westbound voyage of an equivalent motor vessel, the existence of an alternative minimum fuel route passing through the other side of the great circle route from the departure point to the double point of the final isochrone was clearly demonstrated. The proposed two kinds of algorithms ( i.e. Algorithm (I) and (II) ) showed the same fuel consumptions on the minimum fuel route and the alternative route.

(iii) Provided the specified passage time on the (sub) minimum fuel route does not differ largely from the passage time on the minimum time route, the former route almost coincides with the latter route.

(iv) On a sail-assisted motor vessel, when the passage time is specified, the fuel saving on a certain route is almost directly proportional to the sail area ( or sail thrust ) for relatively small sail areas.

(v) Concerning the minimum cost routing, unless the weighting coefficient for delay penalty is extremely small, the track of the minimum cost route for the scheduled passage time  $T_s$  hardly differs from that of the minimum fuel route for the same specified passage time  $T_s$ .

(vi) The probability of shipping green water at the bow did not exceed 0.04 during the voyages on all minimum time/fuel/cost routes. Thus it can be said that the optimum route calculated by the modified isochrone method automatically avoids areas of high head seas.

(vii) Deterministic routing simulation is a powerful tool to

determine time schedules and ship characteristics for a particular trade.

(viii) Deterministic routing simulation is also a powerful tool to determine sail performance and sail area to be provided for a particular sail-assisted motor vessel for a particular trade.

## (II) Stochastic routing

(i) In all westbound voyages, the standard deviations of the passage time and fuel consumption on the minimum time/fuel routes were much smaller than those on the great circle routes. On the other hand, in all eastbound voyages, the standard deviations on the minimum time/fuel routes were nearly equal to those on the great circle routes.

(ii) In all eastbound voyages, the standard deviations of the passage time and fuel consumption on the minimum time/fuel routes and the great circle routes of a sail-assisted motor vessel became considerably larger than those of an equivalent motor vessel. This comes from the fact that the ship's speed of a sail-assisted motor vessel is much more sensitive than that of an equivalent motor vessel to the beam, quartering and following winds which are predominant in the eastbound voyage.

(iii) On a sail-assisted motor vessel, the standard deviations of the passage time on the minimum fuel routes became much larger than those on the minimum time routes. This results from the fact that when the passage time is extended ( i.e. the ship's speed is reduced ), the ratio of sail thrust to propeller thrust increases and the speed of a sail-assisted motor vessel becomes sensitive to a change of wind speed and direction. Thus the partial derivatives of ship's speed with respect to wind speed and direction become large, which leads to a large standard deviation of the passage time.

(iv) In general, when the destination is located away from the double point of the final isochrone, the standard deviation of the passage time/fuel consumption is not such an important factor compared with the predicted value of passage time/fuel consumption.



in determining the minimum time/fuel route in the stochastic sense. On the other hand, when the destination is situated near the double point, the standard deviation becomes a major factor to determine the optimum route.

(v) The correlations between errors in the predicted environments play an important role in estimating the standard deviations of passage time and fuel consumption. That is, those standard deviations increase as the correlations increase.

(vi) By recalculating the minimum time/fuel route every 12 hours according to information on the updated wind/wave forecasts, the vessels could avoid adverse weather which had not been predicted at the departure time. Compared with the predicted minimum time/fuel route calculated at the departure time, considerable time and fuel savings were achieved on the route based on the updated forecasts.

(vii) In both minimum time and minimum fuel routing, the advantage of using the 5-day mean wind/wave models classified by ZI instead of the 1-month mean wind/wave data could not be observed. It should be noted, however, since the simulations were performed for only February in 1985, this result does not deny the usefulness of those models to be used after the numerical forecasts.

In the stochastic routing simulations, the table of predicted values and standard deviations of passage time and fuel consumption, etc. on all the routes reaching the destination from the departure point via points of the final isochrone provided valuable information in determining the optimum route from the stochastic point of view. Such information will certainly be a great help for the shipmaster/owner to make his own choice.

Using a HITAC M-882H mainframe computer, the calculation times (except compiling times) for the minimum time routes between Tokyo and San Francisco were around 12 seconds and 26 seconds in deterministic routing and stochastic routing respectively, which fully meet the requirement for practical weather routing.

Since the covariance and correlation matrices of forecasted

wind/wave conditions were calculated based on the data in a rather short period, i.e. February in 1985, the confidence level of those matrices is of course not sufficient. For the implementation of stochastic routing, those matrices should be determined based on the data over sufficiently long period. The new global model of wave forecasts which has been developed by ECMWF will clearly provide a good data base for that purpose.

Concerning the covariance and correlation matrices of the ocean currents, a reliable data base has not yet been established until now. In the future, a numerical forecast model of the ocean currents will be operated on a daily basis,<sup>(1)</sup> and it will produce a good data base for the calculation of those matrices.

### 7.3 SUGGESTIONS

In this thesis, advanced methods for determining an optimum route based on the forecasted environments ( i.e. strategic routing ) were described. Since a huge amount of environmental data has to be treated in strategic routing, it is commonly performed by a mainframe computer in the weather routing office.

In actual voyage, it often occurs that a ship is forced to navigate in rough seas owing to inaccurate forecasts of the environments. In such a case, determination of the optimum ship's speed and/or heading for avoiding damage to ship and cargo based on the existing environmental conditions ( i.e. tactical routing ) becomes essential.

Recently, in order to perform tactical routing effectively, a computer-aided navigation support system for safety using various sensors attached to the hull and onboard personal computer has been developed by the Ship Research Institute in Japan.<sup>(2)</sup> That system not only can display the wind/wave conditions, ship's motion data ( e.g. pitch, roll, vertical acceleration, hull distortion, etc. ) and speed performance data ( e.g. speed through the water, number of propeller revolutions, engine power, etc. ) but also can provide the

optimum speed and heading based on the risk of damage predicted for various speeds and headings.

Application of such a computer-aided navigation support system to the tactical routing will certainly improve the safety and efficiency of ship operations in rough seas.

In recent years, a high speed data communication system between weather routing offices and ships via communication satellites ( INMARSAT ) has been developed. In the near future, when the environmental forecasts are updated during the voyage, stochastic routing simulations based on the updated forecasts will be performed by a mainframe computer in the routing office and their results will be immediately shown on a display of a personal ( or mini ) computer on board a ship using that communication system.

On the other hand, the ship's speed performance data and ship's motion data as well as the ship's position, wind/wave conditions, etc. continuously monitored on board a ship will also be input to a mainframe computer ashore with a certain time-interval.

Although the rate of data transmission is comparatively low at present ( e.g. 2,400 bits per second in Oceanroutes Japan, Ltd. ), it will be increased in the near future. The cost for data transmission will be reduced as the transmission rate is increased, which will make it possible to perform frequent communications.

Such rapid and frequent information exchange between the routing office and the ship will certainly enhance the shipmaster's confidence to the routing office and greatly improve the economy of ship operations.



## APPENDICES

### Appendix I

#### Accuracy of arrival latitude

According to formulae (2.13), (2.14) and (2.15) (Mercator's sailing), the arrival latitude  $\phi_{i+1}$  at time  $t_{i+1}$  is given as

$$\phi_{i+1} = \phi_i + \{ V \cos(\theta_i + \alpha_i) + N_i \} \Delta t / R_M(\phi_i) \quad (\text{A.1})$$

This is, however, an approximate formula. Strictly speaking,  $\phi_{i+1}$  is determined as a solution of the following equation:

$$\int_{\phi_i}^{\phi_{i+1}} R_M(\phi) d\phi = \{ V \cos(\theta_i + \alpha_i) + N_i \} \Delta t \quad (\text{A.2})$$

Although the local radius of meridian of the earth  $R_M(\phi)$  given by (2.7) can not be integrated analytically, the left-hand side of equation (A.2) can be approximated with sufficient accuracy by [12]

$$\int_{\phi_i}^{\phi_{i+1}} R_M(\phi) d\phi = S(\phi_{i+1}) - S(\phi_i) \quad (\text{A.3})$$

where  $S(\phi) = a \{ A_0 \phi + A_2 \sin(2\phi) + A_4 \sin(4\phi) + A_6 \sin(6\phi) \}$

$$A_0 = 1 - (e^2/4) - (3e^4/64) - (5e^6/256)$$

$$A_2 = (3/8) \{ e^2 + (e^4/4) + (15e^6/128) \}$$

$$A_4 = (15/256) \{ e^4 + (3e^6/4) \}$$

$$A_6 = (35/3072) e^6$$

$a$  : radius of equator of the earth

$e$  : eccentricity of meridian of the earth

Letting the right-hand side of (A.2) be equal to the right-hand

side of (A.3), and applying Newton's method to that equation,  $\phi_{arr}$  can be numerically determined.

Now, we represent the right-hand side of (A.2) (i.e. northerly component of travelled distances for  $\Delta t$ ) by  $D_N$ . The comparisons of the exact  $\phi_{arr}$  computed by the above mentioned method with the approximate  $\phi_{arr}$  by (A.1) are shown in Table A.1 for six combinations of  $\phi_{dep}$  and  $D_N$ .

Table A.1 Comparison of exact arrival latitudes with approximate arrival latitudes

$\phi_{dep}$	$D_N$	Exact $\phi_{arr}$	Approximate $\phi_{arr}$	Relative error
0.6235988 (30°00'00")	555,600 m (300 n.m.)	0.6110417 (35°00'36")	0.6110759 (35°00'43")	- 0.0056 %
	1,111,200 m (600 n.m.)	0.6984123 (40°00'58")	0.6985530 (40°01'27")	- 0.0201 %
0.6981317 (40°00'00")	555,600 m (300 n.m.)	0.7854273 (45°00'06")	0.7854654 (45°00'14")	- 0.0049 %
	1,111,200 m (600 n.m.)	0.8726463 (49°59'56")	0.8727990 (50°00'28")	- 0.0175 %
0.8726646 (50°00'00")	555,600 m (300 n.m.)	0.9598683 (54°59'35")	0.9598456 (54°59'42")	- 0.0039 %
	1,111,200 m (600 n.m.)	1.0468817 (59°58'55")	1.0470257 (59°59'25")	- 0.0138 %

From Table A.1, it can be seen that the approximate  $\phi_{arr}$  by (A.1) are hardly different from the exact  $\phi_{arr}$  from a practical point of view. Since  $D_N$  seldom exceeds 300 n.m. in normal weather routing simulations, it can be said that  $\phi_{arr}$  calculated by (A.1) has sufficient accuracy.

The arrival longitude  $\lambda_{arr}$  given by (2.13), (2.14) and (2.15) is strictly exact provided  $\phi_{arr}$  is exact.

When the northerly component of the ship's speed over the ground,

i.e.,  $V \cos(\theta_i + \alpha_i) + N_{i+1}$  is very close to zero, the accuracy of  $\lambda_{i+1}$  given by (2.13), (2.14) and (2.15) deteriorates because of numerical instability. In that case, using middle latitude sailing instead of Mercator's sailing,  $\lambda_{i+1}$  is calculated by

$$\lambda_{i+1} = \lambda_i + [V \sin(\theta_i + \alpha_i) + B_i] \Delta t / R_\phi(\phi_m) \quad (A.4)$$

where  $\phi_m$  : middle latitude between  $\phi_i$  and  $\phi_{i+1}$

$$\phi_m = (\phi_i + \phi_{i+1}) / 2$$

$R_\phi(\phi_m)$  : local radius of parallel of latitude of the earth

## Appendix 2

### Accuracy of rhumbline distance

The formula (2.23) gives an approximate rhumbline distance  $D_r$  between  $\lambda_{n,r}$  and  $\lambda_r$ . An exact  $D_r$  is determined by

$$D_r = \sec \theta_{n,r} \int_{\phi_{n,r}}^{\phi_r} R_\phi(\phi) d\phi \quad (A.5)$$

Letting  $\theta_{n,r}$  be zero, the exact  $D_r$  were calculated by formulae (A.3) and (A.5) for three combinations of  $\phi_{n,r}$  and  $\phi_r$ , and they were compared with the approximate  $D_r$  calculated by (2.23). The results are shown in Table A.2.

From Table A.2, it is found that the approximate  $D_r$  by (2.23) almost coincide with the exact  $D_r$  by (A.5). In normal weather routing simulations, since the difference between  $\phi_{n,r}$  and  $\phi_r$  does not exceed 0.1745329 ( $\approx 10^\circ$ ), it can be said that  $D_r$  calculated by (2.23) has sufficient accuracy.

When  $\phi_{n,r}$  is very close to  $\phi_r$  (i.e.  $\theta_{n,r}$  is nearly equal to  $\pi/2$  or  $3\pi/2$ ), the accuracy of  $D_r$  given by (2.23) deteriorates because of numerical instability. In that case,  $D_r$  is calculated by the following formula instead of (2.23):



Table A.2 Comparison of exact rhumbline distances with approximate rhumbline distances

$\phi_{nr}$	$\phi_r$	Exact $D_r$	Approximate $D_r$	Relative error
0.5235988 ( 30° )	0.6981317 ( 40° )	1,109,415 m	1,109,405 m	0.0009 %
0.6981317 ( 40° )	0.8726646 ( 50° )	1,111,317 m	1,111,317 m	0.0000 %
0.8726646 ( 50° )	1.0471975 ( 60° )	1,113,212 m	1,113,232 m	- 0.0018 %

$$D_r = R_p(\phi_m) (\lambda_r - \lambda_{nr}) \operatorname{cosec} \theta_{nr} \quad (\text{A.6})$$

where  $\phi_m = (\phi_{nr} + \phi_r) / 2$

$R_p(\phi_m)$  : local radius of parallel of latitude of the earth

### Appendix 3

#### Comparison of geodetic distance with great circle distance

The geodetic distance  $D_{ge}$  between departure point  $(\phi_1, \lambda_1)$  and arrival point  $(\phi_2, \lambda_2)$  on the earth as a spheroid can be approximated with sufficient accuracy by the following Andoyer-Lambert's formula:<sup>(1)</sup>

$$D_{ge} = a \theta - (1/4) a f^2 (m u + n v) \quad (\text{A.7})$$

where  $a$  : radius of equator of the earth

$f$  : flattening of the earth (= 0.00335278 in WGS-72)

$$\theta = \cos^{-1} \{ \sin \beta_1 \sin \beta_2 + \cos \beta_1 \cos \beta_2 \cos(\lambda_2 - \lambda_1) \}$$

$$\beta_1 = \tan^{-1} \{ (b/a) \tan \phi_1 \}$$

$$\beta_2 = \tan^{-1} \{ (b/a) \tan \phi_2 \}$$

$$m = ( \sin \beta_1 + \sin \beta_2 )^2$$

$$n = ( \sin \beta_1 - \sin \beta_2 )^2$$

$$u = ( \theta - \sin \theta ) / ( 1 + \cos \theta )$$

$$v = ( \theta + \sin \theta ) / ( 1 - \cos \theta )$$

$$b = a ( 1 - f )$$

On the other hand, regarding the earth as a sphere, the great circle distance  $D_{gc}$  between  $(\phi_1, \lambda_1)$  and  $(\phi_2, \lambda_2)$  is given by

$$D_{gc} = r \cos^{-1} \{ \sin \phi_1 \sin \phi_2 + \cos \phi_1 \cos \phi_2 \cos(\lambda_2 - \lambda_1) \} \quad (A-8)$$

where  $r$  : radius of the earth (  $= 1652 \times 60 \times 180 / \pi$  meters )

Letting  $\phi_1$  and  $\lambda_1$  be  $0.8108652$  (  $= 35^\circ N$  ) and  $2.4434810$  (  $= 140^\circ E$  ),  $D_{ge}$  and  $D_{gc}$  were calculated for six arrival points. The results are shown in Table A.3. In Table A.3, Diff of  $D_{ge}$  and Diff of  $D_{gc}$  denote the difference of geodetic distances and the difference of great circle distances between departure point and nearby arrival points, respectively.

Table A.3 Comparison of geodetic distances with great circle distances

$\phi_2$	$\lambda_2$	$D_{ge}$		$D_{gc}$	
0.2617994 (15°N)	3.8397244 (140°W)	8,171,289 m	90,546 m	8,155,191 m	90,306 m
	3.8571776 (139°W)	8,281,837 m		8,245,437 m	
0.6108652 (35°N)	3.8397244 (140°W)	7,081,363 m	82,114 m	7,061,012 m	81,884 m
	3.8571776 (139°W)	7,163,477 m		7,142,896 m	
0.9569311 (55°N)	3.8397244 (140°W)	6,301,024 m	61,761 m	6,282,119 m	61,529 m
	3.8571776 (139°W)	6,362,785 m		6,343,646 m	

From Table A.3, it is found that  $D_{GE}$  are a bit larger than  $D_{GO}$ . This is because  $\phi_1$  and  $\phi_2$  used for calculating  $D_{GE}$  are the geographical latitudes, whereas those used for calculating  $D_{GO}$  correspond to the geocentric latitudes.

It can be seen that the difference of  $D_{GE}$  hardly differs from the difference of  $D_{GO}$  for three pairs of nearby arrival points. Thus, for computing the isochrone, great circle distances can be used as the substitutes for geodetic distances with sufficient accuracy.

#### Appendix 4

##### Reason for existence of the alternative route with a possibility to provide less fuel consumption

In the minimum fuel routing stated in 2.3.2, the number of propeller revolutions is kept constant during the voyage. As mentioned in 3.6, provided the number of propeller revolutions is constant, the fuel consumption per unit time decreases as the ship's speed increases. Thus, when the passage time is specified, the total fuel consumption during the voyage decreases as the total travelled distance increases ( i.e. as the average speed increases ).

Now, suppose that the double point of the final isochrone is located near the destination as shown in Fig.A.1, and the passage time on the alternative route is a bit larger than that on the calculated minimum fuel route.

In this case, if the total travelled distance on the alternative route is much longer than that on the calculated minimum fuel route, the total fuel consumption on the former route becomes considerably smaller than that on the latter route. Therefore, when we slightly increase the number of propeller revolutions so as to get the passage time on the alternative route equal to the specified passage time, that alternative route may provide less total fuel consumption than the calculated minimum fuel route.



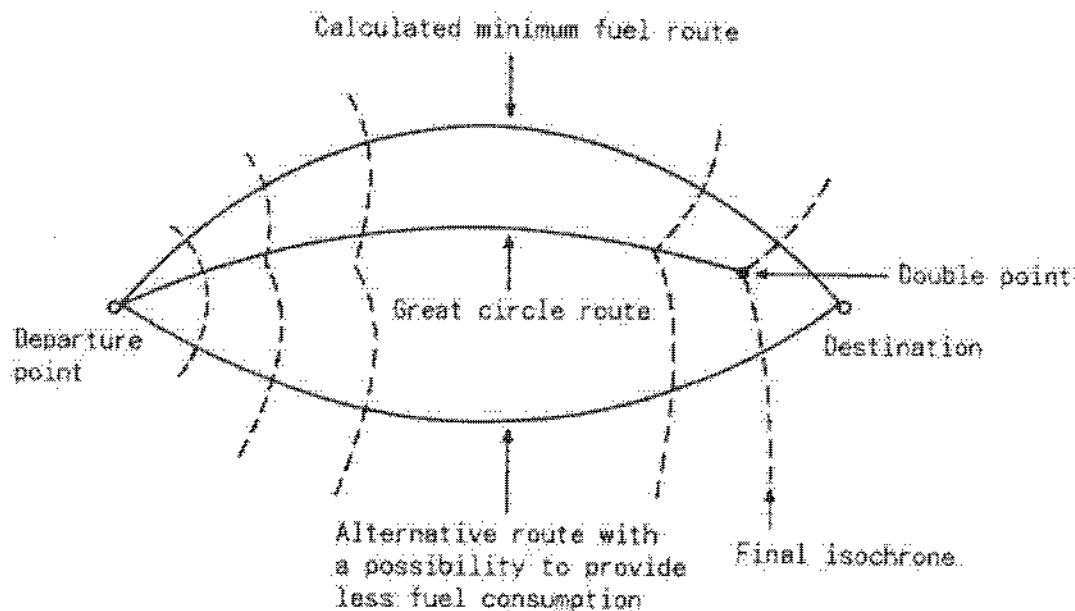


Fig. A.1 Alternative route with a possibility to provide less fuel consumption

## Appendix 5

### Calculation method of the great circle route

In each weather routing simulation, the track, passage time and fuel consumption of the 'great circle route' is calculated as follows.

- (i) Navigate the ship for sub-time-interval  $\Delta t'$  hours from the departure point  $\underline{X}_0$ , letting ship's heading be the initial course of the great circle route from  $\underline{X}_0$  to the destination  $\underline{X}_1$ , and calculate the arrival point  $\underline{X}_1$  by Mercator's sailing (2.13). ( For computing the initial course of the great circle route from  $\underline{X}_0$  to  $\underline{X}_1$ , the earth is assumed to be the sphere. ) At the same time, calculate the fuel consumption  $G_0$  between  $\underline{X}_0$  and  $\underline{X}_1$ .
- (ii) Navigate the ship for  $\Delta t'$  hours from  $\underline{X}_1$ , letting ship's heading be the initial course of the great circle route from  $\underline{X}_1$  to  $\underline{X}_1$ , and calculate the arrival point  $\underline{X}_2$  by Mercator's sailing (2.13). ( For computing the initial course of the great circle route from

$\underline{X}_1$  to  $\underline{X}_2$ , the earth is assumed to be the sphere. } At the same time, calculate the fuel consumption  $G_1$  between  $\underline{X}_1$  and  $\underline{X}_2$ .

(iii) Repeating the above procedures, compute the arrival points  $\underline{X}_3, \underline{X}_4, \dots$ , and the fuel consumptions  $G_2, G_3, \dots$ .

(iv) When the rhumbline distance  $D_r$  between  $\underline{X}_n$  and  $\underline{X}_1$  becomes smaller than  $V_{sg}\Delta t'$  (  $V_{sg}$  : ship's speed over the ground along that rhumbline ), navigate the ship along that rhumbline. The passage time  $T$  and the total fuel consumption  $F$  between  $\underline{X}_0$  and  $\underline{X}_1$  are given by

$$T = n \Delta t' + D_r / V_{sg} \quad (A.9)$$

$$F = \sum_{l=0}^{n-1} G_l + G_n \quad (A.10)$$

where  $G_n$  : fuel consumption between  $\underline{X}_n$  and  $\underline{X}_1$ .

The minimum distance route, i.e. geodesic line, between  $\underline{X}_0$  and  $\underline{X}_1$  is piecewise approximated by the above-mentioned sequence of rhumbines connecting  $\underline{X}_0, \underline{X}_1, \dots, \underline{X}_n$  and  $\underline{X}_1$ . When the sub-time-interval is around 12 hours, that sequence may be regarded as the geodesic line between  $\underline{X}_0$  and  $\underline{X}_1$ . From the practical point of view. In weather routing simulations of this study, we call the above-mentioned sequence of rhumbines 'great circle route'.

## Appendix E

### Calculation method of 39% error ellipse of the ship's position

The 39% error ellipse of the ship's position at time  $t_1$  is calculated by the following procedure.

The covariance matrix of the ship's position error  $P_x(i)$  at time  $t_1$  is defined as

$$P_x(1) = E \begin{bmatrix} \Delta\phi_1^2 & \Delta\phi_1\Delta\lambda_1 \\ \Delta\lambda_1\Delta\phi_1 & \Delta\lambda_1^2 \end{bmatrix} \quad (A.11)$$

where  $\Delta\phi_1$  : error of latitude of the ship's position (rad)  
 $\Delta\lambda_1$  : error of longitude of the ship's position (rad)

$P_x(1)$  can be obtained as the upper-left 2X2 partitioned matrix of  $P_1$  in (2.64).

Now, we set up the local Cartesian  $\Delta x$ - $\Delta y$  coordinates with the origin at the predicted ship's position  $\bar{X}_1 = [\bar{\phi}_1, \bar{\lambda}_1]^T$ ;  $\Delta x$  and  $\Delta y$  denote the easterly axis and northerly axis, respectively.

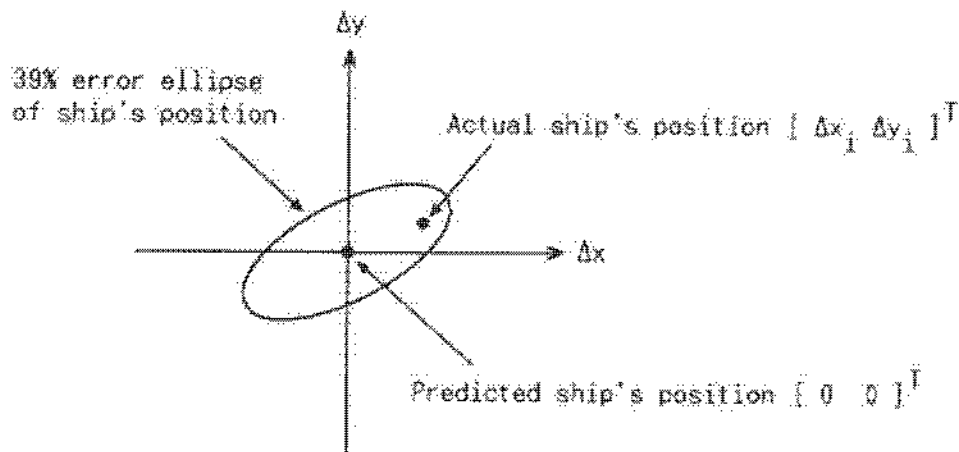


Fig. A.2 Local Cartesian  $\Delta x$ - $\Delta y$  coordinates.

The relation between ship's position error  $[\Delta\phi_1, \Delta\lambda_1]^T$  in  $\phi$ - $\lambda$  coordinates and ship's position error  $[\Delta x_1, \Delta y_1]^T$  in  $\Delta x$ - $\Delta y$  coordinates is given by

$$\begin{bmatrix} \Delta x_1 \\ \Delta y_1 \end{bmatrix} = \begin{bmatrix} 0 & R_p(\bar{\phi}_1) \\ R_M(\bar{\phi}_1) & 0 \end{bmatrix} \begin{bmatrix} \Delta\phi_1 \\ \Delta\lambda_1 \end{bmatrix} \quad (A.12)$$



where  $\Delta x_1$  : easterly component of ship's position error ( m )  
 $\Delta y_1$  : northerly component of ship's position error ( m )  
 $R_m(\bar{\phi}_1)$  : local radius of meridian of the earth ( m )  
 $R_p(\bar{\phi}_1)$  : local radius of parallel of latitude of the earth ( m )

In  $\Delta x$ - $\Delta y$  coordinates, the covariance matrix of ship's position error  $P_X(1)'$  is given by

$$P_X(1)' = E \begin{bmatrix} \Delta x_1^2 & \Delta x_1 \Delta y_1 \\ \Delta y_1 \Delta x_1 & \Delta y_1^2 \end{bmatrix} \\ = \begin{bmatrix} 0 & R_p(\bar{\phi}_1) \\ R_m(\bar{\phi}_1) & 0 \end{bmatrix} P_X(1) \begin{bmatrix} 0 & R_m(\bar{\phi}_1) \\ R_p(\bar{\phi}_1) & 0 \end{bmatrix} \quad (A.13)$$

Since the error vector  $[\Delta \phi, \Delta \lambda]^T$  has a Gaussian distribution, the error vector  $[\Delta x_1, \Delta y_1]^T$  also has a Gaussian distribution. Thus, the 39% error ellipse of the ship's position in  $\Delta x$ - $\Delta y$  local coordinates can be drawn by calculating the eigenvalues and eigenvectors of the covariance matrix  $P_X(1)'$ .

That is, the directions of the eigenvectors of  $P_X(1)'$  coincide with those of the major/minor axes of the 39% error ellipse; the square roots of the eigenvalues of  $P_X(1)'$  are equal to the lengths of the major/minor axes of the 39% error ellipse.

On the Mercator's chart, the 39% error ellipse is expanded by the scale factor  $M$ :

$$M = a / R_p(\bar{\phi}_1) \quad (A.14)$$

where  $a$  : radius of equator of the earth

## REFERENCES

### Chapter 1

- (1) James, R.W. (1957), Application of Wave Forecasts to Marine Navigation, U.S. Naval Oceanographic Office, SP-1.
- (2) Hagiwara, H. and Spaans, J.A. (1987), Practical Weather Routing of Sail-assisted Motor Vessels, Journal of the Royal Institute of Navigation, Vol.40, No.1.
- (3) Hagiwara, H. (1988), Advanced Weather Routing of Sail-assisted Motor Vessels, Proceedings of the International Congress of Institutes of Navigation, Sydney, February.

### Chapter 2

- (1) Spaans, J.A. (1988), Navigation IV, Part 1, Configuration of the Earth (in Dutch), Report No.845-K, Department of Maritime Technology, Delft University of Technology.
- (2) Faulkner, F.D. (1984), Numerical Methods for Determining Optimum Ship Routes, Journal of U.S. Institute of Navigation, Vol.10, No.4.
- (3) De Wit, C. (1974), Progress and Developments of Ocean Weather Routing, Report No.201 S, Netherlands Ship Research Center INQ.
- (4) Bijlsma, S.J. (1975), On Minimal-time Ship Routing, Report No.94, Royal Netherlands Meteorological Institute.
- (5) Hagiwara, H. (1983; 1985), A Study on the Minimum Fuel Consumption Route I, II (in Japanese), Journal of Japan Institute of Navigation, Vol.69; 72.
- (6) Frankel, E.G. and Chen, H.T. (1980), Optimization of Ship Routing, Report NMRC-KP-189, U.S. National Maritime Research Center.
- (7) Hagiwara, H. and Makishima, T. (1980), A Study on the Optimum Ship Routes (in Japanese), Journal of Japan Institute of Navigation.

Vol.82.

- (8) Motte, R. and Calvert, S. (1986), Operational Considerations and Constraints in Ship-based Weather Routing Procedures, Journal of the Royal Institute of Navigation, Vol.41, No.3.
- (9) James, R.W. (1957), Application of Wave Forecasts to Marine Navigation, U.S. Naval Oceanographic Office, SP-1.
- (10) Hagiwara, H., Shoji, K. and Sugisaki, A.M. (1981), On the Operation of Hybrid Power (Sails and Engines) Driven Ship I - A Method of Selecting the Optimum Route of Sailing Ship (in Japanese), Journal of Japan Institute of Navigation, Vol.84.
- (11) Hagiwara, H. and Spaans, J.A. (1987), Practical Weather Routing of Sail-assisted Motor Vessels, Journal of the Royal Institute of Navigation, Vol.40, No.1.
- (12) Spaans, J.A. and Hagiwara, H. (1987), Computation of Optimum Routes for Ship Weather Routing, Proceedings of the International Seminar on Ship Weather Routing, Tokyo, December.

### Chapter 3

- (1) Journée, J.M.J. (1984), Report on the Development of an On-board Energy Saving Device (in Dutch), Report No.808, Delft Shiphydrodynamics Laboratory, Delft University of Technology.
- (2) Walker, J.C. (1985), A High Performance Automatic Wingsail Auxiliary Propulsion System for Commercial Ships, Proceedings of the International Symposium on Windship Technology, Part B, Southampton, April.
- (3) Hagiwara, H. and Spaans, J.A. (1987), Practical Weather Routing of Sail-assisted Motor Vessels, Journal of the Royal Institute of Navigation, Vol.40, No.1.
- (4) Hagiwara, H. (1986), Advanced Weather Routing of Sail-assisted Motor Vessels, Proceedings of the International Congress of Institutes of Navigation, Sydney, February.
- (5) Isherwood, R.M. (1973), Wind Resistance of Merchant Ships, Transactions of Royal Institute of Naval Architects, Vol.115.



- (6) Inoue, S., Hirano, M., Kijima, K. and Takashina, J. (1981), A Practical Calculation Method of Ship Maneuvering Motion, International Shipbuilding Progress, September.
- (7) Hasegawa, K. (1980), On a Performance Criterion of Autopilot Navigation (in Japanese), Journal of West-Japan Society of Naval Architects, No.178.
- (8) Inoue, S., Hirano, M. and Kijima, K. (1981), Hydrodynamic Derivatives on Ship Manoeuvring, International Shipbuilding Progress, Vol.28, No.321.
- (9) Kose, K., Yumuro, A. and Yoshimura, Y. (1981), Embodiment of Mathematical Models for Ship Maneuvering Motion - Interaction between Hull, Propeller and Rudder and Its Representation (in Japanese), Proceedings of the 3rd Symposium on Ship Manoeuvrability, The Society of Naval Architects of Japan, December.
- (10) Hirano, M. (1980), On Calculation Method of Ship Maneuvering Motion at Initial Design Phase (in Japanese), Journal of Society of Naval Architects of Japan, Vol.147.
- (11) Journée, J.M.J., Rijke, R.J. and Verleg, G.J.H. (1987), Marine Performance Surveillance with a Personal Computer, Proceedings of Automation Days '87, Helsinki, May.
- (12) Sköglman, A. (1985), The Practical Meaning of Lateral Balance for a Sail-assisted Research Vessel, Proceedings of the International Symposium on Windship Technology, Part B, Southampton, April.
- (13) St. Denis, M. and Pierson, W.J. (1953), On the Motions of Ships in Confused Seas, Transactions of Society of Naval Architects and Marine Engineers, Vol.61.
- (14) Ochi, M.K. and Moiter, E. (1974), Prediction of Extreme Ship Responses in Rough Seas, International Symposium on Dynamics of Marine Vehicles, Paper 20, London.
- (15) Longuet-Higgins, M.S. (1952), On the Statistical Distribution of the Heights of Sea Waves, Journal of Marine Research, Vol.11, No.3.
- (16) Nakamura, S. (1973), On the Seakeeping Performance of a Ship (in Japanese), Symposium on Shiphandling in Rough Sea, Japan.

Institute of Navigation, February.

(17) Lewis, E.V. (1987), Principles of Naval Architecture, Chapter 9, The Motion of Ships in Waves, Society of Naval Architects and Marine Engineers.

(18) Aertsen, G. (1988), Laboring of Ships in Rough Seas with Special Emphasis on Fast Ship, Commemorative Proceedings of the Diamond Jubilee International Meeting, Society of Naval Architects and Marine Engineers.

(19) Kitazawa, T., et al. (1975), Critical Speed of a Container Ship in Rough Sea (in Japanese), Journal of Society of Naval Architects of Japan, Vol.138.

(20) Journée, J.M.J. (1987), PROGRAM : SEAWAY ( Motion Calculations of a Ship in a Seaway ), September.

#### Chapter 4

(1) Komen, G.J. (1987), Medium-range Forecast of Weather Conditions Including Wave Conditions, Proceedings of the International Seminar on Ship Weather Routing, Tokyo, December.

(2) Weinstein, A.I. (1980), NOGAPS in Navy's Entry into Field of Global Numerical Weather Prediction, NEPRF Meteor Report No.2.

(3) Pierson, W.J. (1982), The Spectral Ocean Wave Model ( SOWM ) - A Northern Hemisphere Computer Model for Specifying and Forecasting Ocean Wave Spectra, David W. Taylor Ship Research and Development Center, Report DTNSRDC-82/011.

(4) Makishima, T., Horigome, M., Kuwashima, S., Ohtsu, K. and Hagiwara, H. (1983; 1984; 1985), Report of the Basic Research on Ship Weather Routing I, II, III (in Japanese), Tokyo University of Mercantile Marine.

(5) Suda, K., Makishima, T., Horigome, M., Kuwashima, S., Ohtsu, K. and Hagiwara, H. (1981), An Approach to the Weather Routing over the North Pacific in Winter (in Japanese), Journal of Japan Institute of Navigation, Vol.65.

(6) Suda, K., Makishima, T., Horigome, K., Kuwashima, S., Ohtsu, K.

and Hagiwara, H. (1982), Ship Weather Routing over the North Pacific in Winter - Wave Pattern and Prediction Index (in Japanese), Journal of Japan Institute of Navigation, Vol.67.

(7) Suda, K., Makishima, T., Horigome, M., Kuwashima, S., Ohtsu, K. and Hagiwara, H. (1982), Ship Weather Routing Based on the Mean Atmospheric Circulation, Proceedings of the International Congress of Institutes of Navigation, Paris, September.

(8) Suda, K., Makishima, T., Kuwashima, S., and Hagiwara, H. (1984), Upper-air Circulation and Ocean Wave Distribution over the North Pacific in Winter (in Japanese), NAVIGATION ( Japan Institute of Navigation ), No.81.

(9) Hagiwara, H. (1987), Ship Weather Routing Based on the Mean Upper-air Circulation - Strategic Routing for the North Pacific Crossing in Winter (in Japanese), Proceedings of the International Seminar on Ship Weather Routing, Tokyo, December.

(10) Makishima, T. (1953), Turbulence of the Ocean Current and the Error of the Estimated Position (in Japanese), Journal of Japan Institute of Navigation, Vol.8.

#### Chapter 6

(1) Hagiwara, H. and Makishima, T. (1980), A Study on the Optimum Ship Routes (in Japanese), Journal of Japan Institute of Navigation, Vol.62.

(2) Hagiwara, H. (1983; 1985), A Study on the Minimum Fuel Consumption Route I, II (in Japanese), Journal of Japan Institute of Navigation, Vol.69; 72.

#### Chapter 7

(1) Frankel, E.G. and Chen, H.T. (1980), Optimization of Ship Routing, Report NMRC-KR-189, U.S. National Maritime Research Center.

(2) Sugai K. (1987), Research and Development of a Computer-aided Navigation Support System For Safety, Proceedings of the International



Seminar on Ship Weather Routing, Tokyo, December.

Appendices

- (1) Spaans, J.A. (1986), Navigation IV, Part 1, Configuration of the Earth (In Dutch), Report No.645-K, Department of Maritime Technology, Delft University of Technology.

## NOMENCLATURE

$A(\underline{X}, \underline{U}, t)$	quantity per unit time evaluated during the voyage
$A'(\underline{X}_n, \underline{U}_n, t_n)$	quantity evaluated between $\underline{X}_n$ and $\underline{X}_n$
$A_L$	lateral projected area of the above-water part ( excluding sails )
$A_R$	rudder area
$A_s(i)$	area of i-th sail
$A_{ST}$	total sail area
$A_T$	transverse projected area of the above-water part ( excluding sails )
$A_w$	amplitude of component wave
$A_{11}$	13X13 matrix comprised of the partial derivatives and the correlation matrices
$A_{12}$	12X13 matrix comprised of the partial derivatives and the correlation matrices
$a$	radius of equator of the earth
$\delta_{LR}$	ratio of lateral force induced on the hull by rudder action to the rudder lateral force
$B$	- breadth of ship - 13X10 ( or 12X10 ) constant matrix
$B(t_f, t_s)$	quantity evaluated at the destination
$C$	- sum of the costs during the voyage - fuel cost per unit weight
$\hat{C}(m, n)$	analyzed wind/wave data at grid point (m,n)
$\hat{\hat{C}}(m, n, t)$	forecasted wind/wave data at grid point (m,n) for t-hour forecast
$\bar{C}(m, n, t)$	unbiased wind/wave forecast data at grid point (m,n) for t-hour forecast
$C_b$	block coefficient
$C_{MK}$	yawing moment coefficient
$C_{MH}$	hydrodynamic yawing moment coefficient
$C_V$	still water resistance coefficient ( for no drift )
$C_{XA}$	fore and aft wind force coefficient
$C_{XH}$	added resistance coefficient for drift
$C_{XS}$	sail thrust coefficient
$C_{YA}$	lateral wind force coefficient

$C_{YH}$	hydrodynamic lateral force coefficient
$C_{Ys}$	sail lateral force coefficient
$C_i$	arrival course of the great circle route from $\underline{X}_0$ to each point of the isochrone $\underline{X}_k(i)$ at time $t_k$
$\underline{C}_i$	actual ( true ) value of wind/wave condition vector at time $t_i$
$\hat{\underline{C}}_i$	forecasted value of wind/wave condition vector at time $t_i$
$\bar{\underline{C}}_i$	unbiased wind/wave forecast vector at time $t_i$
$C_i(i,j)$	initial course of the great circle route from $\underline{X}_0$ to each arrival point $\underline{X}_k(i,j)$ at time $t_k$
$C_0$	Initial course of the great circle route from $\underline{X}_0$ to $\underline{X}_i$
$\Delta C$	increment of ship's heading
$\Delta \underline{C}(m,n,t)$	errors of $\underline{C}(m,n,t)$
$\Delta \underline{C}_r$	error of unbiased wind/wave forecast vector at the destination
$\Delta \underline{C}_{r,1}$	error vector to produce $\Delta \underline{C}_r$ in shaping filter
$\Delta \underline{C}_i$	error of unbiased wind/wave forecast vector
$\Delta \hat{\underline{C}}_i$	error of forecasted wind/wave condition vector
$\Delta \underline{C}_{i,1}$	error vector to produce $\Delta \hat{\underline{C}}_i$ in shaping filter
$E[\Delta \hat{\underline{C}}(m,n,t)]$	mean errors of $\hat{\underline{C}}(m,n,t)$
$E[\Delta \hat{\underline{C}}_i]$	mean error of forecasted wind/wave condition vector
$D$	- total travelled distance - propeller diameter - distance between 40°N and 60°N parallel
$\hat{D}$	predicted total travelled distance
$D_{GC}$	great circle distance
$D_{GE}$	geodetic distance
$D_{HN}$	horizontal distance from the center of gravity to the point on which the lateral force induced on the hull by rudder action acts
$D_N$	northerly component of travelled distance for $\Delta t$ hours
$\hat{D}_P$	- analyzed primary wave direction - predominant sea ( swell ) direction
$\hat{\underline{D}}_P$	forecasted primary wave direction
$\bar{\underline{D}}_P$	- 5-day mean primary wave direction - predicted primary wave direction
$D_R$	horizontal distance from the center of gravity to the



	center of water pressure acting on the rudder
$D_{Si}(i)$	horizontal distance from the center of gravity to the center of effort of $i$ -th sail
$D_{SE}$	predominant sea direction
$D_{SW}$	predominant swell direction
$D_W$	analyzed wind direction
$\hat{D}_W$	forecasted wind direction
$\bar{D}_W$	- 5-day mean wind direction - predicted wind direction
$D_{Wj}$	wind direction
$D_k(i,j)$	great circle distance between $\underline{X}_S$ and each arrival point $\underline{X}_k(i,j)$ at time $t_k$
$D_r$	rhumbline distance between $\underline{X}_{A_1}$ ( or $\underline{X}_A$ ) and $\underline{X}_r$
$\Delta D$	error of predicted total travelled distance
$d$	draught of ship
$d_1$	expected travelled distance after $1\Delta t$ hours
$\Delta d$	predetermined local sub-sector width ( resolution of the isochrone )
$E$	easterly component of the ocean current
$\bar{E}$	mean easterly component of the ocean current in each $5^\circ \times 5^\circ$ sub-area in each month
$E_i$	easterly component of the ocean current at time $t_i$
$e$	eccentricity of meridian of the earth
$F$	total fuel consumption during the voyage
$\bar{F}$	predicted total fuel consumption
$F_R$	rudder normal force
$F_i$	accumulated fuel consumption from $t_0$ to $t_i$
$\bar{F}_i$	predicted value of $F_i$
$\Delta F$	error of predicted total fuel consumption
$\Delta F_i$	error of $\bar{F}_i$
$f$	- freeboard at the bow - flattening of the earth
$\overline{GM}$	metacentric height
$G_i$	fuel consumption between $t_i$ and $t_{i+1}$
$G_n$	fuel consumption between $\underline{X}_n$ and $\underline{X}_r$
$g$	acceleration of gravity
$H_A$	vertical distance from the center of gravity to the center of lateral projected area of the above-water

	part excluding sails
$H_G$	vertical distance from the center of gravity to the center of water pressure acting on the hull
$H_{GR}$	vertical distance from the center of gravity to the point on which the lateral force induced on the hull by rudder action acts
$H_R$	vertical distance from the center of gravity to the center of water pressure acting on the rudder
$H_s$	analyzed significant wave height
$\hat{H}_s$	forecasted significant wave height
$\bar{H}_s$	- 5-day mean significant wave height - predicted significant wave height
$H_s(i)$	vertical distance from the center of gravity to the center of effort of i-th sail
$H_{SE}, H_{SEA}$	significant sea height
$H_{SW}, H_{SWELL}$	significant swell height
$H_W$	significant wave height
$\bar{H}_{40}$	zonal mean 500mb height for 40°N parallel
$\bar{H}_{60}$	zonal mean 500mb height for 60°N parallel
$J$	- objective function - advance ratio
$J(k)$	objective function for each route reaching $\underline{X}_k$ from $\underline{X}_0$ via $\underline{X}_n(k)$ of the final isochrone $\{\underline{X}_n(k)\}$
$J^*(n)$	minimum value of $J(k)$ as a function of the number of propeller revolutions $n$
$J^*_{min}$	minimum value of $J^*(n)$
$K$	specific fuel consumption
$K_{EP}(i)$	correlation coefficient between errors in the unbiased forecasts of primary wave direction at $t_i$ and $t_{i+1}$
$K_{OW}(i)$	correlation coefficient between errors in the unbiased forecasts of wind direction at $t_i$ and $t_{i+1}$
$K_{HS}(i)$	correlation coefficient between errors in the unbiased forecasts of significant wave height at $t_i$ and $t_{i+1}$
$K_Q$	torque coefficient
$K_{SW}(i)$	correlation coefficient between errors in the unbiased forecasts of wind speed at $t_i$ and $t_{i+1}$
$K_T$	thrust coefficient
$K_{TP}(i)$	correlation coefficient between errors in the unbiased forecasts of primary wave period at $t_i$ and $t_{i+1}$

$L$	waterline length of ship
$L_A$	aerodynamic heeling moment due to hull and superstructure
$L_B$	hydrostatic righting moment due to heel of the hull
$L_{BH}$	hydrodynamic heeling moment due to the hull under water
$L_{OA}$	length overall of ship
$L_{PP}$	length between perpendiculars
$L_S$	sail heeling moment
$M$	scale factor for Mercator's chart
$\underline{\dot{M}}$	ship's motion vector
$M_A$	aerodynamic yawing moment due to hull and superstructure
$\underline{M_A}$	admissible ship's motion vector
$M_H$	hydrodynamic yawing moment due to the hull under water
$\underline{M_H}$	hydrodynamic yawing moment induced by the rudder
$M_S$	sail yawing moment
$mp(\phi_1)$	meridional parts from equator to latitude $\phi_1$
$N$	northerly component of the ocean current
$\bar{N}$	mean northerly component of the ocean current in each $5^\circ \times 5^\circ$ sub-area in each month
$N_i$	northerly component of the ocean current at time $t_i$
$n$	- number of propeller revolutions ( per second ) - number of time-intervals - number of sails - number of observations of the ocean current
$n^*$	optimal number of propeller revolutions
$n_i$	number of propeller revolutions between $t_i$ and $t_{i+1}$
$n_0$	initial number of propeller revolutions
$\Delta n$	increment of the number of propeller revolutions
$P$	engine power
$P(z_A > f)$	probability that the shipping green water occurs
$P(z_A > z_{Ac})$	probability that the amplitude of ship's motion $z_A$ exceeds a critical value $z_{Ac}$
$P_e(i)$	covariance matrix of the error of the unbiased wind/wave forecast vector at time $t_i$
$P_e(m,n,t)$	covariance matrix of the errors in the unbiased wind/wave forecast data at grid point $(m,n)$ for $t$ -hour forecast



$P_e(m', n', t)$	averaged covariance matrix of the errors in the unbiased wind/wave forecast data in sub-area $(m', n')$ for t-hour forecast
$P_{EE}$	variance of easterly component of the ocean current in each $5^\circ \times 5^\circ$ sub-area in each month
$P_{NE}$	covariance between northerly component and easterly component of the ocean current in each $5^\circ \times 5^\circ$ sub-area in each month
$P_{NN}$	variance of northerly component of the ocean current in each $5^\circ \times 5^\circ$ sub-area in each month
$P_w(i)$	covariance matrix of the error of the unbiased ocean current forecast vector at time $t_i$
$P_x(i)$	covariance matrix of the ship's position error at time $t_i$
$P_x(i)'$	covariance matrix of the ship's position error at time $t_i$ in local Cartesian $\Delta x$ - $\Delta y$ coordinates
$P_y$	covariance matrix of the error vector $\Delta y$
$P_z$	covariance matrix of the error vector $\Delta z$
$p$	propeller pitch
$Q_z$	covariance matrix of the error vector $\Delta z^*$
$Q_{z^*}$	covariance matrix of the error vector $\Delta z^*$
$RAO(\omega, V, \mu)$	response amplitude operator of ship's motion in regular waves
$R_w(\phi)$	local radius of meridian of the earth
$R_p(\phi)$	local radius of parallel of latitude of the earth
$R_{SEA}$	added resistance due to sea
$(R_{SEA}/H_{SEA}^2)$	added resistance per unit significant sea height squared
$R_{SWELL}$	added resistance due to swell
$(R_{SWELL}/H_{SWELL}^2)$	added resistance per unit significant swell height squared
$[R_w(\omega, V, \mu)/\Delta_w^2]$	transfer function of added resistance due to waves
$R_{WAVE}$	mean added resistance in irregular waves
$S$	- wetted surface of ship's hull - propeller slip ratio
$S(\phi)$	function to approximate the integral of the local radius of meridian of the earth
$S(\omega)$	Bretschneider spectrum

$S(\omega, \chi)$	directional spectrum of irregular waves
$S_w$	analyzed wind speed
$\hat{S}_w$	forecasted wind speed
$\bar{S}_w$	- 5-day mean wind speed
	- predicted wind speed
$S_{wt}$	wind speed
$\underline{S}_i$	vector comprised of ship's speed through the water $V_i$ and drift angle $\alpha_i$
$\hat{\underline{S}}_i$	predicted value of $\underline{S}_i$
$\underline{S}_i(k)$	sub-sector at time $t_i$
$\{\underline{S}_i(k)\}$	sub-sector set at time $t_i$
$\Delta S_i$	sub-sector angle at time $t_i$
$\Delta \underline{S}_i$	error of $\hat{\underline{S}}_i$
$T$	passage time between $\underline{X}_0$ and $\underline{X}_i$
$\hat{T}$	predicted passage time
$T_D$	( predicted ) period of exposure to excessive ship's motions, shipping green water, slamming, etc.
$\hat{T}_D$	predicted period in which the probability of shipping green water at the bow exceeds 0.04
$T_p$	- analyzed primary wave period
	- average sea ( swell ) period
$\hat{T}_p$	forecasted primary wave period
$\bar{T}_p$	- 5-day mean primary wave period
	- predicted primary wave period
$T_{se}$	average sea period
$T_{sw}$	average swell period
$T_w$	average wave period
$T_{min}$	minimum passage time between $\underline{X}_0$ and $\underline{X}_i$
$T_0$	passage time between $\underline{X}_0$ and $\underline{X}_i$
$T_A(k)$	passage time between each point of the final isochrone $\underline{X}_w(k)$ and $\underline{X}_i$
$T_s$	specified passage time
$\Delta T$	error of predicted passage time
$t$	- time
	- thrust-deduction fraction
$t_i$	actual arrival time
$\hat{t}_i$	predicted arrival time
$t_i$	discretized time

$t_n$	time $t_n + r\Delta t$
$t_a$	scheduled ( or specified ) arrival time
$t_0$	departure time
$\Delta t$	time-interval
$\Delta t'$	sub-time-interval
$\underline{U}$	ship's control vector
$\bar{U}$	mean easterly component of the velocity of the upper-air westerlies between 40°N and 60°N parallel
$\underline{U}^*(t)$	optimum control ( $t_0 \leq t \leq t_a$ )
$U_A$	apparent wind speed
$\underline{U}_A$	admissible ship's control vector
$\underline{U}_i$	ship's control vector from $t_i$ to $t_{i+1}$
$\underline{U}^*_i$	optimum control ( $i = 0, 1, \dots, n$ )
$V$	ship's speed through the water
$\bar{V}$	predicted average speed
$V_R$	effective rudder inflow speed
$V_S$	service speed in knots
$V_i$	ship's speed through the water at time $t_i$
$\bar{V}_i$	predicted value of $V_i$
$V_{og}$	ship's speed over the ground at time $t_{og}$ ( or $t_a$ )
$\Delta V$	- error of predicted average speed - increment of ship's speed
$\Delta V_i$	error of $\bar{V}_i$
$W$	volume of displacement of the ship
$\underline{W}_i$	actual ( true ) value of ocean current vector at time $t_i$
$\hat{\underline{W}}_i$	forecasted value of ocean current vector at time $t_i$
$\bar{\underline{W}}_i$	unbiased ocean current forecast vector at time $t_i$
$\Delta \underline{W}_i$	error of unbiased ocean current forecast vector at the destination
$\Delta \underline{W}^*_i$	error vector to produce $\Delta \underline{W}_i$ in shaping filter
$\Delta \underline{W}_i$	error of unbiased ocean current forecast vector
$\Delta \hat{\underline{W}}_i$	error of forecasted ocean current vector
$\Delta \underline{W}^*_{i+1}$	error vector to produce $\Delta \underline{W}_{i+1}$ in shaping filter
$E[\Delta \hat{\underline{W}}_i]$	mean error of forecasted ocean current vector
$w$	- weighting coefficient
$w$	- wake fraction
$w_i$	weighting coefficient



$\underline{X}$	ship's position vector
$\underline{X}^*(t)$	optimum route ( $t_0 \leq t \leq t_1$ )
$X_A$	aerodynamic resistance due to hull and superstructure
$\underline{X}_A$	admissible ship's position vector
$X_H$	hydrodynamic resistance due to the hull under water
$X_P$	propeller thrust
$X_R$	hydrodynamic resistance induced by the rudder
$X_S$	sail thrust
$X_W$	added resistance due to waves
$\underline{X}_1$	destination
$\underline{X}_i$	ship's position at time $t_i$
$\underline{X}_i^*$	optimum route ( $i = 1, 2, \dots, n$ )
$\underline{X}_i(k)$	each point of the isochrone at time $t_i$
$\{\underline{X}_i(k)\}$	isochrone at time $t_i$
$\underline{X}_A(i, j)$	arrival point at time $t_i$
$\underline{X}_{n+1}$	ship's position at time $t_0 + i\Delta t$
$\underline{X}_0$	departure point
$\Delta \underline{X}_i$	error of predicted ship's position
$\Delta x_i$	easterly component of ship's position error at time $t_i$
$Y_A$	aerodynamic lateral force due to hull and superstructure
$Y_H$	hydrodynamic lateral force due to the hull under water
$Y_R$	hydrodynamic lateral force induced by the rudder
$Y_S$	sail lateral force
$\Delta \underline{Y}_i$	augmented error vector comprised of $\Delta T_i$ , $\Delta F_i$ , $\Delta C_i$ and $\Delta W_i$
$\underline{\Delta Y}_i$	augmented error vector comprised of $\Delta \underline{X}_i$ , $\Delta F_i$ , $\Delta C_i$ and $\Delta W_i$
$\Delta y_i$	northerly component of ship's position error at time $t_i$
$Z$	environmental condition
$ZI$	zonal index
$\Delta \underline{Z}^*$	augmented error vector comprised of $\Delta C^*$ and $\Delta W^*$
$\Delta \underline{Z}^*_{i+1}$	augmented error vector comprised of $\Delta C^*_{i+1}$ and $\Delta W^*_{i+1}$
$z(t)$	- ship's motion in irregular waves - relative vertical displacement of the bow to the local wave surface
$z_A$	amplitude of ship's motion
$\bar{z}_A$	mean value of $z_A$

$\bar{z}_{A(1/3)}$	1/3 highest mean of $z_A$
$\bar{z}_{A(1/10)}$	1/10 highest mean of $z_A$
$z_{AC}$	critical value of $z_A$
$\alpha$	drift angle ( leeway caused by wind )
$\alpha_i$	drift angle at time $t_i$
$\alpha_{n,r}$	drift angle at time $t_{n,r}$
$\beta$	true wind direction from the bow
$\beta_A$	apparent wind direction from the bow
$\delta$	rudder angle
$\delta^*$	effective rudder inflow angle
$\varepsilon$	heel angle
$\eta_M$	mechanical efficiency of shaft bearings
$\eta_R$	relative relative efficiency
$\theta$	ship's heading
$\theta_i$	ship's heading between $t_i$ and $t_{i+1}$
$\theta^*_i$	optimum ship's headings ( $i = 0, 1, \dots, n-1$ )
$\theta_{n,r}$	ship's heading at time $t_{n,r}$
$A$	aspect ratio of rudder
$\lambda$	longitude
$\lambda_i$	longitude of destination
$\lambda_i$	longitude at time $t_i$
$\lambda_{n,r}$	longitude at time $t_{n,r}$
$\Delta\lambda_i$	error of longitude of the ship's position at time $t_i$
$\mu$	direction of component wave from the bow
$\bar{\mu}$	predominant wave direction from the bow
$\rho_A$	density of air
$\rho_W$	density of sea water
$\sigma_T$	standard deviation of total fuel consumption
$\sigma_T(i)$	standard deviation of the accumulated fuel consumption between $t_0$ and $t_i$
$\sigma_t$	standard deviation of passage time
$\sigma_v$	standard deviation of average speed
$\sigma_{SEA}^2$	variance of ship's motion due to sea
$\sigma_{SWELL}^2$	variance of ship's motion due to swell
$\sigma_z^2$	variance of ship's motion $z(t)$ in ocean waves
$\tau$	time-interval
$\Phi_c(i)$	normalized correlation matrix between the error of the wind/wave conditions $\underline{AC}_i$ and $\underline{AC}_{i+1}$

## CURRICULUM VITAE

The author of this work was born in Tokyo on 12 January, 1954. The educational and occupational backgrounds of the author are as follows.

### Education

- 1972 - 1976 : Entered the Department of Navigation, Tokyo University of Mercantile Marine, and graduated from the same. Received the degree of Bachelor of Mercantile Marine Science and the license of Second Mate.
- 1977 - 1979 : Admitted to the Division of Navigation, Graduate School, Tokyo University of Mercantile Marine, and completed the two-year course of the same. Received the degree of Master of Mercantile Marine Science.
- 1981 - 1982 : Studied in the Department of Mathematical Engineering and Information Physics, Faculty of Engineering, University of Tokyo as a research fellow.

### Occupation

- 1979 - 1981 : Appointed assistant of the Department of Navigation, Tokyo University of Mercantile Marine.
- 1981 - 1984 : Appointed Lecturer of the Department of Navigation, Tokyo University of Mercantile Marine.
- 1984 to present : Appointed assistant professor of the Department of Navigation, Tokyo University of Mercantile Marine.
- 1989 to present : Appointed captain of the training ship of the Tokyo University of Mercantile Marine



## PROPOSITIONS

1. Modern optimization, estimation and control theory have been applied to ship operations with remarkable success in track keeping, heading/engine control, weather routing, etc.. Further computerization will increase their importance. These subjects should be compulsory for students specializing in Maritime Operations.
2. The development of remote sensing technology has changed the way of gathering meteorological and oceanographic data. In the near future, orbiting meteorological satellites will provide the mariner with global information on winds, waves, ocean currents, etc. on a quasi-real-time basis.
3. The global wave forecasting by ECMWF based on the new third generation forecast model WAM will be operated on a daily basis in the near future. This will certainly improve the efficiency of ship weather routing. Even in that case, however, statistical wave models to be used after the period of forecasts will still be indispensable for the routing procedure.
4. A ship's motion monitoring system, using various sensors attached to the hull, provides valuable information to the ship operator for avoiding damage to ship and cargo and for finding the optimum heading/speed in rough seas ( tactical routing ).
5. A high speed data communication system between the mainframe computer in a weather routing office and the onboard computer via communication satellite ( INMARSAT ) will greatly improve the economy of ship operations.
6. Modern vessels are complex systems. The onboard personnel has generally insufficient time to gain experience on these vessels.

Expert systems should be developed to support the bridge team in decision making as to collision avoidance, berthing, tactical routing, anchoring, etc..

7. For conducting a safe and efficient vessel traffic flow in congested waters, vessel traffic services (VTS) have been operated successfully in the last few decades. In view of complexing vessel traffic flows and increasing risk of disastrous accidents, not only technological improvements should be considered but also the competence of the VTS should be enhanced.

8. Training by simulators has occupied an important part of the education in maritime universities/academies. It is, however, dangerous to regard such training as the complete substitute for the onboard practice. A proper combination of training by simulators and onboard practice will yield maximum educational effect.

9. In the Japanese educational system, raising the level of creativeness of the students does not have a high priority. It would therefore be important for Japanese students to cooperate in projects with universities abroad or with research institutes/private companies.

10. When Japan was a closed country in the 17-19th centuries, only Dutch and Chinese ships were permitted to enter the specified port Nagasaki. Thus, for about four hundred years, Western culture and technology were introduced to Japan by the Dutch people. Based on such a long, friendly relation, fruitful results in various fields could be achieved by intensifying the cooperation between Japanese and Dutch researchers.

Hideki Hagiwara

7 November 1989